5-2015

Computational Fluid Dynamics Simulations of Oscillating Wings and Comparison to Lifting-Line Theory

Megan Keddington
Utah State University

COMPUTATIONAL FLUID DYNAMICS SIMULATIONS OF OSCILLATING WINGS AND COMPARISON TO LIFTING-LINE THEORY

by

Megan Keddington

A thesis submitted in partial fulfillment
of the requirements for the degree

of

MASTER OF SCIENCE

in

Aerospace Engineering

Approved:

_____	_____
Warren F. Phillips Major Professor	Steven L. Folkman Committee Member
_____	_____
Douglas F. Hunsaker Committee Member	Mark R. McLellan Vice President for Research and Dean of the School of Graduate Studies

UTAH STATE UNIVERSITY
Logan, Utah

2015

ABSTRACT

Computational Fluid Dynamics Simulations of Oscillating Wings

and Comparison to Lifting-Line Solution

by

Megan Keddington

Utah State University, 2015

Major Professor: Dr. Warren F. Phillips
Department: Mechanical and Aerospace Engineering

Computational fluid dynamics (CFD) analysis was performed in order to compare the solutions of oscillating wings with Prandtl's lifting-line theory. Quasi-steady and steady-periodic simulations were completed using the CFD software Star-CCM+. The simulations were performed for a number of frequencies in a pure plunging setup. Additional simulations were then completed using a setup of combined pitching and plunging at multiple frequencies. Results from the CFD simulations were compared to the quasi-steady lifting-line solution in the form of the axial-force, normal-force, power, and thrust coefficients, as well as the efficiency obtained for each simulation. The mean values were evaluated for each simulation and compared to the quasi-steady lifting-line solution. It was found that as the frequency of oscillation increased, the quasi-steady lifting-line solution was decreasingly accurate in predicting solutions.

(350 pages)

PUBLIC ABSTRACT

Computational Fluid Dynamics Simulations of Oscillating Wings and Comparison to Lifting-Line Theory

Megan Keddington

Computational fluid dynamics (CFD) analysis was performed in order to compare the solutions of oscillating wings with Prandtl's lifting-line theory. Quasi-steady and steady-periodic simulations were completed using the CFD software Star-CCM+. Quasi-steady simulations were completed for both two-dimensional and three-dimensional setups. The steady-periodic simulations were only performed using a three-dimensional setup. The simulations were performed for nine separate frequencies in a pure plunging setup. An additional four simulations were then completed using a setup of combined pitching and plunging at four separate frequencies. Results from the CFD simulations were compared to the quasi-steady lifting-line solution in the form of the axial-force, normal-force, power, and thrust coefficients, as well as the efficiency obtained for each simulation. The mean values were evaluated for each simulation and compared to the quasi-steady lifting-line solution.

It was found that as the frequency of oscillation increased, the quasi-steady lifting-line solution was decreasingly accurate in predicting solutions. It was also observed that the thrust was generated only by plunging, not pitching of the wing in the simulations.

ACKNOWLEDGMENTS

I would like to thank Dr. Warren Phillips for imparting to me a small portion of his vast knowledge. He expected the highest, and for that, I am grateful. I would also like to thank Dr. Douglas Hunsaker for his constant guidance, council, and assistance. I could have never completed this thesis without his support and encouragement. I am indebted to both Dr. Phillips and Dr. Hunsaker for the extensive work they have put into teaching me and helping me along in this process.

I am eternally grateful to my family, and especially my parents, for teaching me that I can do anything. Lastly, I'd like to thank my husband, for always being my rock, my champion, and my sanctuary. Words cannot express how grateful I am.

Megan Keddington Jensen

LIST OF TABLES

LIST OF FIGURES

CONTENTS

NOMENCLATURE

A = Fourier coefficient defined in Eq. (1.47)
A_n = coefficients in the infinite series solution
A_{x0-x2} = coefficients defined in Eq. (1.50)
A_{y1} = coefficient defined in Eq. (1.50)
A_{12-32} = correlation coefficients used in Eq. (1.61) and defined in Table 1
a = axial location of the axis of rotation nondimensionalized with respect to the airfoil half chord
a_n = planform coefficients in the decomposed Fourier-series solution to the lifting-line equation
B = Fourier coefficient defined in Eq. (1.47)
B_{x1-x2} = coefficient defined in Eq. (1.50)
B_{y1} = coefficient defined in Eq. (1.50)
B_{12-30} = correlation coefficients used in Eq. (1.62) and defined in Table 1
b = airfoil section half chord
b_n = washout coefficients in the decomposed Fourier-series solution to the lifting-line equation
C = complex Theodorsen function given in Eq. (1.4)
C_D = drag coefficient
C_{D_i} = induced drag coefficient
$\overline{C}_{D_i}$ = mean wing induced-drag coefficient averaged over a complete flapping cycle
C_{D_P} = wing parasitic-drag coefficient
C_L = instantaneous section lift coefficient
$\overline{C}_L$ = mean section lift coefficient
$C_{L,\alpha}$ = wing lift slope
$C_{L,1-3}$ = lift coefficient of the first, second, and third grid
$\widetilde{C}_{L,\alpha}$ = airfoil-section lift slope
$C_{m_{ac}}$ = section pitching moment coefficient about the airfoil aerodynamic center
$C_{m_{c/4}}$ = section pitching moment coefficient about the airfoil quarter chord
$\overline{C}_{m_{c/4}}$ = mean section pitching moment coefficient about the quarter chord
C_P = instantaneous section power-required coefficient
$\overline{C}_P$ = mean section power-required coefficient
$\overline{C}_{P_A}$ = mean available-power coefficient averaged over a complete flapping cycle
C_{P_f} = instantaneous flapping-power coefficient required to support the flapping rate
$\overline{C}_{P_f}$ = mean flapping-power coefficient averaged over a complete flapping cycle
C_T = instantaneous thrust coefficient
$\overline{C}_T$ = mean thrust coefficient
C_x = instantaneous section axial-force coefficient
$\overline{C}_x$ = mean section axial-force coefficient
C_{x0} = axial-force coefficient at the zero plunging velocity point in the cycle
C_y = instantaneous section normal-force coefficient
$\overline{C}_y$ = mean section normal-force coefficient
$C_{0-\infty}$ = coefficients in the Taylor series expansion given in Eq. (1.44)
c = airfoil section chord length
c_n = control coefficients in the decomposed Fourier-series solution to the lifting-line equation
d_n = plunging coefficients in the decomposed Fourier-series solution to the lifting-line equation
e_n = plunging coefficients in the Fourier-series solution for induced drag
F = real part of the complex Theodorsen function given in Eq. (1.5)

F_x = section axial force
F_y = section normal force
G = imaginary part of the complex Theodorsen function given in Eq. (1.6)
$g, g_{1\text{-}3}$ = cell size for Richardson extrapolation, defined in Eq. (2.3)
h, h_a = complex plunging displacement at the axis of rotation (positive downward)
$h_{c/4}$ = complex plunging displacement at the quarter chord (positive downward)
$h_{3c/4}$ = complex plunging displacement at the three-quarter chord (positive downward)
$\dot{h}_a$ = complex plunging velocity at the axis of rotation
$\ddot{h}_a$ = complex plunging acceleration at the axis of rotation
$\dot{h}_{c/4}$ = complex plunging velocity at the quarter chord
$\ddot{h}_{c/4}$ = complex plunging acceleration at the quarter chord
$\dot{h}_{3c/4}$ = complex plunging velocity at the three-quarter chord
i = square root of −1
J_0, J_1 = Bessel functions
k = reduced frequency used by Theodorsen based on the airfoil half chord, defined in Eq. (1.7)
L = instantaneous section lift
$\overline{L}$ = mean section lift
$M_a, M_{c/4}$ = complex section pitching moment about the axis of rotation and the quarter chord
$m_{ac}, m_{c/4}$ = section pitching moment about the aerodynamic center and the quarter chord
$\overline{m}_{c/4}$ = mean section pitching moment about the quarter chord
N = number of cells
P = complex section lift force (positive downward)
p = apparent order of convergence, defined in Eq. (2.7)
P_f = instantaneous power required to support the instantaneous flapping rate
$\hat{p}$ = dimensionless angular wing-tip rotation rate about the roll axis
$\hat{p}_{steady}$ = steady dimensionless rigid-body rolling rate, which produces a zero net rolling rate
$\hat{p}_{rms}$ = root mean square of the dimensionless flapping rate averaged over a complete flapping cycle
Q = variable used by Theodorsen, defined in Eq. (1.1)
q = logarithm of the difference of the grid ratios, defined in Eq. (2.11)
R_A = aspect ratio of the wing
R_{AL} = lift amplitude ratio, defined in Eq. (1.26)
R_{Am} = quarter-chord pitching-moment amplitude ratio, defined in Eq. (1.27)
R_T = wing taper ratio
R_τ = ratio of the current case to the original case
R_{y1} = amplitude of the sinusoidal terms A_{y1} and B_{y1}
r_{21} = ratio of the second grid to the first grid
r_{32} = ratio of the third grid to the second grid
S = wing planform area
s = sign of the ratio of the lift coefficients, defined in Eq. (2.12)
T = section thrust
$T_{A1\text{–}2}$ = correlation coefficients, used in Eq. (1.61) and defined in Table 1
$T_{B1\text{–}2}$ = correlation coefficients, used in Eq. (1.62) and defined in Table 1
t = time
V = freestream airspeed
V_y = y-velocity component of the airfoil aerodynamic center (positive upward)

V_s = start velocity
V_t = translational velocity
x, y, z = streamwise, upward normal, and spanwise coordinates relative to the section quarter chord
Y_0, Y_1 = Bessel functions
y_A = aerodynamic-center plunging amplitude
y_{A_0} = original aerodynamic-center plunging amplitude
y_{ac} = aerodynamic-center plunging displacement
α = pitching angle of attack
$\dot{\alpha}$ = angular velocity
$\ddot{\alpha}$ = angular acceleration
$\overline{\alpha}$ = mean pitching angle
α_A = pitching amplitude
α_g = geometric angle of attack
α_i = induced angle of attack
α_{L0} = zero-lift angle of attack
α_P = plunging angle of attack
α_{root} = root angle of attack
$\hat{\alpha}_y$ = aerodynamic-center geometric angle-of-attack ratio, defined in Eq. (1.22)
Γ = wing section circulation
$\Delta\widetilde{D}_i$ = local section induced-drag increments
ΔV_i = volume of the ith cell
$\Delta\alpha_p$ = spanwise variation in local angle of attack increment resulting from wing-section plunging
δ_c = control-surface deflection angle
ε_{21} = difference between the second and first grid solutions
ε_{32} = difference between the third and second grid solutions
ζ = dummy variable for z-integration
η = propulsive efficiency
$\overline{\eta}$ = mean propulsive efficiency averaged over a complete flapping cycle
θ = angular coordinate
θ = change of variables for the spanwise coordinate, defined in Eq. (1.64)
κ_a = planform coefficient in the lifting-line relation for required power, defined in Eq. (1.95)
κ_b = washout coefficient in the lifting-line relation for required power, defined in Eq. (1.96)
κ_D = planform coefficient in the lifting-line relation for induced drag, defined in Eq. (1.80)
κ_d = plunging coefficient in the lifting-line relation for required power, defined in Eq. (1.97)
κ_{DL} = washout-lift coefficient in the lifting-line relation for induced drag, defined in Eq. (1.81)
$\kappa_{D\Omega}$ = washout coefficient in the lifting-line relation for induced drag, defined in Eq. (1.82)
κ_{Lp} = plunging-lift coefficient in the lifting-line relation for induced drag, defined in Eq. (1.88)
κ_p = plunging coefficient in the lifting-line relation for induced drag, defined in Eq. (1.90)
$\overline{\kappa}_p$ = plunging coefficient in the lifting-line relation for induced drag, defined in Eq. (1.93)
$\kappa_{\Omega p}$ = plunging-washout coefficient in the lifting-line relation for induced drag, defined in Eq. (1.89)
$\lambda_{1\text{-}3}$ = solution for the first, second, and third grids
φ = phase shift
φ_{y1} = phase shift of the sinusoidal terms A_{y1} and B_{y1}
ρ = air density
τ = oscillation period

τ_0 = original oscillation period
χ = spanwise twist distribution function resulting from control-surface deflection
ψ = spanwise twist distribution function resulting from wing-section plunging
Ω = total symmetric wing washout angle, geometric plus aerodynamic
Ω_{opt} = optimum total symmetric wing washout angle, geometric plus aerodynamic
ω = oscillation frequency
ω = spanwise twist distribution function for symmetric wing washout
$\hat{\omega}_x$ = reduced frequency based on the airfoil chord, defined in Eq. (52)
$\hat{\omega}_y$ = reduced frequency based on the aerodynamic-center plunging amplitude, defined in Eq. (1.21)

CHAPTER I

INTRODUCTION

Flapping flight is of particular interest due to the recent boom in Unmanned Aerial Vehicles (UAVs), and more specifically, Micro Air Vehicles (MAVs) [1]. The development of MAVs has been driven by commercial, research, government, and military purposes. These MAVs allow remote observation of hazardous environments that are inaccessible to ground vehicles [2]. Flapping flight could greatly increase the efficiency and use of these MAVs, resulting in a greater ability for tagging, targeting, and communications for the military personnel in particular. Recently, the primary mission for MAVs has been identified as surveillance. In order to perform well for surveillance, maneuverability and sustained flights are desired. Flapping flight has therefore been researched in order to produce the wing motion that is energy-efficient and capable of providing the required aerodynamic performance for MAV flight [3].

Flapping flight is of interest because of the potential efficiency gained. Lift and propulsion can be combined into a single flapping motion, providing high efficiencies as well as keeping the vehicle at a lower weight [2]. A range of parameters has been discovered that contribute to this high propulsive efficiency [4], and great effort has been made to recreate the high efficiency of wildlife, such as fish and birds, in man-made machines [5].

There have been many studies in the area of flapping flight. Studies have been developed for both two-dimensional and three-dimensional models. In both of these areas, analytical, numerical, and experimental studies exist.

A. Two-Dimensional Studies

1. Analytical Studies

Knoller [6] and Betz [7] independently showed that thrust could be produced by flapping airfoils. Their studies focused on low frequency quasi-steady effects of flapping flight. Wagner [8] later focused on calculating the vorticity in the wake of an airfoil with non-uniform motion.

Theodore Theodorsen [9] was one of the first to study in depth oscillating airfoils. He used conformal mapping in order to produce his model. Expressions for the lift and pitching moment with three degrees of freedom were shown. However, the calculation for force in the streamwise direction was omitted. von Kármán and Burgers' [10] work on general aerodynamic theory was later extended by Garrick [11] using Theodorsen's model. Garrick was then able to present expressions for the propulsive efficiency and axial force of a flapping airfoil [11].

Several approximations were made, including that of a thin airfoil with small camber, small angles of attack, small-amplitude sinusoidal oscillations, and a planar wake with oscillating vorticity. However, reasonable results are obtained with conditions outside of these seemingly tight constraints.

For the case of both pitching and plunging, a thin symmetric airfoil of half chord b represented by the straight line shown in Fig. 1 was considered. A sinusoidal vertical displacement, $h(t)$, is undergone at the dimensionless distance $x/b = a$ aft of the half chord. This is referred to as the axis of rotation. The entire airfoil is also rotated with a small-angle sinusoidal rotation, $\alpha(t)$. Mean values of zero were assumed for both h and α, where h is positive downward, and α is positive clockwise relative to the constant freestream velocity V.

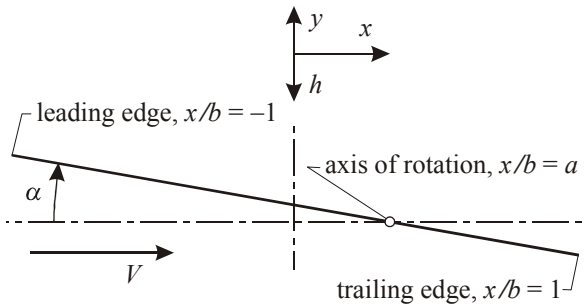

Fig. 1 Parameters used by Theodorsen [9] to describe plunging and pitching motion (from Hunsaker and Phillips [12] with permission).

The angle α is time dependent, so the instantaneous downward displacement is different for each point on the chord line. For clarification of which point is considered, the symbol h will be subscripted. $Q(t)$ is defined such that Q/V is the instantaneous small-angle geometric angle of attack at the airfoil section three-quarter chord point.

$$\frac{Q}{V} \equiv \frac{\dot{h}_{3c/4}}{V} + \alpha = \frac{\dot{h}_a}{V} + \left(\frac{1}{2} - a\right)\frac{b\dot{\alpha}}{V} + \alpha \tag{1.1}$$

Expressions for the complex lift and complex pitching moment were developed using potential flow and conformal mapping. These were shown to be

$$P(t) = -2\pi\rho V^2 b\left[\frac{Q}{V}C(k) + \frac{b\ddot{h}_a}{2V^2} - \frac{ab^2\ddot{\alpha}}{2V^2} + \frac{b\dot{\alpha}}{2V}\right] \tag{1.2}$$

$$M_a(t) = 2\pi\rho V^2 b^2\left[\left(a + \frac{1}{2}\right)\frac{Q}{V}C(k) + \frac{a}{2}\frac{b\ddot{h}_a}{V^2} - \left(\frac{1}{16} + \frac{a^2}{2}\right)\frac{b^2\ddot{\alpha}}{V^2} + \left(\frac{a}{2} - \frac{1}{4}\right)\frac{b\dot{\alpha}}{V}\right] \tag{1.3}$$

where

$$C(k) = F(k) + iG(k) \tag{1.4}$$

$$F(k) = \frac{J_1(k)[J_1(k)+Y_0(k)]+Y_1(k)[Y_1(k)-J_0(k)]}{[J_1(k)+Y_0(k)]^2+[Y_1(k)-J_0(k)]^2} \tag{1.5}$$

$$G(k) = -\frac{Y_1(k)Y_0(k)+J_1(k)J_0(k)}{[J_1(k)+Y_0(k)]^2+[Y_1(k)-J_0(k)]^2} \tag{1.6}$$

$$k \equiv \omega b/V \tag{1.7}$$

Equations (1.5) and (1.6) are fundamental for Theodorsen's [9] theory.

Currently, convention is to describe moments and rotations about the section aerodynamic center of the airfoil. Using Theodorsen's assumptions, the aerodynamic center is at the section quarter chord of the airfoil. Eqs. (1.1), (1.2), and (1.3) can then be transformed to

$$\frac{Q}{V} \equiv \frac{\dot{h}_{c/4}}{V} + \frac{b\dot{\alpha}}{V} + \alpha \tag{1.8}$$

$$P(t) = -2\pi\rho V^2 b\left[\frac{Q}{V}C(k) + \frac{b\ddot{h}_{c/4}}{2V^2} + \frac{b^2\ddot{\alpha}}{4V^2} + \frac{b\dot{\alpha}}{2V}\right] \tag{1.9}$$

$$M_{c/4}(t) = -2\pi\rho V^2 b^2\left(\frac{b\ddot{h}_{c/4}}{4V^2} + \frac{3b^2\ddot{\alpha}}{16V^2} + \frac{b\dot{\alpha}}{2V}\right) \tag{1.10}$$

using the relations

$$\dot{h}_{c/4} = \dot{h}_a - (a+1/2)b\dot{\alpha} \tag{1.11}$$

$$M_{c/4} = M_a + (a+1/2)bP \tag{1.12}$$

Theodorsen [9] defined a phase shift between pitching and plunging as the angle between the downward plunging displacement and the pitching rotation at the point *a*, defined as *x/b*. However, due to current convention, the phase shift will be defined here as the angle between the pitching rotation, $\alpha(t)$, and the quarter-chord *y*-velocity component, $V_y(t) = -\dot{h}_{c/4}(t)$. The position, velocity, and acceleration of the motion at the quarter-chord can then be found to be

$$h_{c/4}(t) = -y_A e^{i\omega t} = [-y_A\cos(\omega t)] + i\,[-y_A\sin(\omega t)] \tag{1.13}$$

$$\dot{h}_{c/4}(t) = -i\,\omega y_A e^{i\omega t} = [\omega y_A\sin(\omega t)] + i\,[-\omega y_A\cos(\omega t)] \tag{1.14}$$

$$\ddot{h}_{c/4}(t) \;=\; \omega^2 y_A e^{i\omega t} \;=\; [\omega^2 y_A \cos(\omega t)] + i\,[\omega^2 y_A \sin(\omega t)] \tag{1.15}$$

$$\alpha(t) \;=\; i\,\alpha_A e^{i(\omega t+\varphi)} \;=\; [-\alpha_A \sin(\omega t+\varphi)] + i\,[\alpha_A \cos(\omega t+\varphi)] \tag{1.16}$$

$$\dot{\alpha}(t) \;=\; -\omega\alpha_A e^{i(\omega t+\varphi)} \;=\; [-\omega\alpha_A \cos(\omega t+\varphi)] + i\,[-\omega\alpha_A \sin(\omega t+\varphi)] \tag{1.17}$$

$$\ddot{\alpha}(t) \;=\; -i\,\omega^2\alpha_A e^{i(\omega t+\varphi)} \;=\; [\omega^2\alpha_A \sin(\omega t+\varphi)] + i\,[-\omega^2\alpha_A \cos(\omega t+\varphi)] \tag{1.18}$$

The effects of mean lift and finite thickness can be added to the solution and the section lift coefficient is obtained to be

$$\begin{aligned} C_L(t) \;&\equiv\; \frac{\overline{L} - \text{imag}[P(t)]}{\frac{1}{2}\rho V^2 (2b)} \\ &=\; \overline{C}_L + \widetilde{C}_{L,\alpha}\ \text{imag}\left[\left(\frac{\dot{h}_{c/4}}{V} + \frac{b\dot{\alpha}}{V} + \alpha\right)(F + i\,G) + \frac{b\ddot{h}_{c/4}}{2V^2} + \frac{b^2\ddot{\alpha}}{4V^2} + \frac{b\dot{\alpha}}{2V}\right] \end{aligned} \tag{1.19}$$

Equations (1.13) through (1.18) can be substituted into Eq. (1.19) to obtain

$$\begin{aligned} C_L(t) \;=\; &\overline{C}_L - \widetilde{C}_{L,\alpha}\,\hat{\omega}_y[\cos(\omega t) + k\hat{\alpha}_y \sin(\omega t+\varphi) - \hat{\alpha}_y \cos(\omega t+\varphi)]F \\ &+ \widetilde{C}_{L,\alpha}\,\hat{\omega}_y[\sin(\omega t) - k\hat{\alpha}_y \cos(\omega t+\varphi) - \hat{\alpha}_y \sin(\omega t+\varphi)]G \\ &+ \widetilde{C}_{L,\alpha}\,\hat{\omega}_y(k/2)[\sin(\omega t) - (k\hat{\alpha}_y/2)\cos(\omega t+\varphi) - \hat{\alpha}_y \sin(\omega t+\varphi)] \end{aligned} \tag{1.20}$$

$$\hat{\omega}_y \;\equiv\; \omega y_A / V \tag{1.21}$$

$$\hat{\alpha}_y \;\equiv\; \alpha_A / \hat{\omega}_y \tag{1.22}$$

Observation of Eqs. (1.14) and (1.21) show that $\hat{\omega}_y$ is also the small-angle geometric angle-of-attack amplitude due to the aerodynamic-center plunging, as well as a reduced frequency based on the aerodynamic-center plunging amplitude. It can also be seen that $\hat{\alpha}_y$ is a geometric angle-of-attack ratio at the aerodynamic center of the airfoil. For flapping flight, $\hat{\alpha}_y$ is usually small due to the fact that thrust is only produced from plunging. When the upward quarter-chord y-velocity component is in phase with the pitching angle, the lift coefficient is

$$\begin{aligned} C_L(t) \;=\; &\overline{C}_L - \widetilde{C}_{L,\alpha}\,\hat{\omega}_y(1-\hat{\alpha}_y)[F\cos(\omega t) - G\sin(\omega t)] \\ &+ \widetilde{C}_{L,\alpha}\,\hat{\omega}_y(k/2)\{[1-\hat{\alpha}_y(1+2F)]\sin(\omega t) - \hat{\alpha}_y(2G + k/2)\cos(\omega t)\} \end{aligned} \tag{1.23}$$

Adding the effects of finite thickness and camber, Eq. (1.10) can be used to obtain an expression for the quarter-chord moment. Applying Eq. (1.13) – (1.18) to this expression gives

$$C_{m_{c/4}}(t) \;=\; \overline{C}_{m_{c/4}} - \widetilde{C}_{L,\alpha}\,\hat{\omega}_y(k/8)[\sin(\omega t) - (3k\hat{\alpha}_y/4)\cos(\omega t+\varphi) - 2\hat{\alpha}_y\sin(\omega t+\varphi)] \tag{1.24}$$

Again, examining when the upward y-velocity component is in phase with the pitching angle, Eq. (1.23) becomes

$$C_{m_{c/4}}(t) \;=\; \overline{C}_{m_{c/4}} - \widetilde{C}_{L,\alpha}\,\hat{\omega}_y(k/8)[(1-2\hat{\alpha}_y)\sin(\omega t) - (3k\hat{\alpha}_y/4)\cos(\omega t)] \tag{1.25}$$

It is advantageous to define the amplitude ratios

$$R_{AL} \;\equiv\; \text{amplitude}[C_L(t) - \overline{C}_L]\big/(\widetilde{C}_{L,\alpha}\,\hat{\omega}_y) \tag{1.26}$$

$$R_{Am} \;\equiv\; \text{amplitude}[C_{m_{c/4}}(t) - \overline{C}_{m_{c/4}}]\big/\widetilde{C}_{L,\alpha}\,\hat{\omega}_y \tag{1.27}$$

in order to compare numerical and experimental results with Eqs. (1.23) and (1.25). Observing when the upward quarter-chord y-velocity component is in phase with the pitching angle, Eqs. (1.23) and (1.25) can be used to obtain

$$R_{AL} \;=\; \sqrt{[(1-\hat{\alpha}_y)F + \hat{\alpha}_y(2G+k/2)(k/2)]^2 + [(1-\hat{\alpha}_y)G + (k/2) - \hat{\alpha}_y(1+2F)(k/2)]^2} \tag{1.28}$$

$$R_{Am} \;=\; (k/8)\sqrt{(1-2\hat{\alpha}_y)^2 + (3k\hat{\alpha}_y/4)^2} \tag{1.29}$$

For low frequencies (k approaching zero), Eq. (1.28) predicts an amplitude ratio approaching the quasi-steady solution of $(1-\hat{\alpha}_y)$. However, for high frequencies (k approaching infinity), Eq. (1.28) predicts an infinite amplitude ratio. This is not realistic. For low frequencies, Eq. (1.29) predicts an amplitude ratio approaching the quasi-steady solution of zero. Again, for high frequencies, Eq. (1.29) predicts an unrealistic infinite amplitude ratio.

The instantaneous power coefficient is found using the small angle approximation to be

$$C_P(t) \;\equiv\; \frac{-L(t)V_y(t) - m_{c/4}(t)\,\dot{\alpha}(t)}{\frac{1}{2}\rho V^3(2b)} \;=\; -C_L(t)\,\text{imag}\left(\frac{-\dot{h}_{c/4}(t)}{V}\right) - C_{m_{c/4}}(t)\,\text{imag}\left(\frac{2b\dot{\alpha}(t)}{V}\right) \tag{1.30}$$

Applying previous equations for when the upward y-velocity component is in phase with the pitching angle, Eq. (1.30) becomes

$$\begin{aligned} C_P(t) \;=\; & -\{\overline{C}_L\hat{\omega}_y - \widetilde{C}_{L,\alpha}\,\hat{\omega}_y^2(1-\hat{\alpha}_y)[F\cos(\omega t) - G\sin(\omega t)]\}\cos(\omega t) \\ & -\widetilde{C}_{L,\alpha}\,\hat{\omega}_y^2(k/2)\{[1-\hat{\alpha}_y(1+2F)]\sin(\omega t) - \hat{\alpha}_y(2G+k/2)\cos(\omega t)\}\cos(\omega t) \\ & +\{2\overline{C}_{m_{c/4}}\hat{\omega}_y k\hat{\alpha}_y - \widetilde{C}_{L,\alpha}\,\hat{\omega}_y^2(k^2\hat{\alpha}_y/4)[(1-2\hat{\alpha}_y)\sin(\omega t) \\ & -(3k\hat{\alpha}_y/4)\cos(\omega t)]\}\sin(\omega t) \end{aligned} \tag{1.31}$$

The mean power coefficient can be found by integrating Eq. (1.31) over a complete cycle and dividing by the period.

$$\overline{C}_P \;\equiv\; \frac{1}{\tau}\int_{t=0}^{\tau} C_P(t)dt \;=\; \widetilde{C}_{L,\alpha}\,\hat{\omega}_y^2\,[(1-\hat{\alpha}_y)F + k\hat{\alpha}_y(G + k\hat{\alpha}_y/2)]/2 \tag{1.32}$$

For low frequencies, Eq. (1.32) approaches the quasi-steady solution. However, for high frequencies, Eq. (1.32) approaches the unrealistic value of infinity.

Garrick [11] later developed a solution for the mean section axial-force coefficient for when the upward y-velocity component is in phase with the pitching angle

$$\overline{C}_x \;=\; -\widetilde{C}_{L,\alpha}\,\hat{\omega}_y^2\,\{(F^2+G^2)[(1-\hat{\alpha}_y)^2 + k^2\hat{\alpha}_y^2] + F(\hat{\alpha}_y - \hat{\alpha}_y^2 - k^2\hat{\alpha}_y^2) + k\hat{\alpha}_y(G + k\hat{\alpha}_y/2)\}/2 \tag{1.33}$$

For low frequencies, Eq. (1.33) approaches the quasi-steady solution. For high frequencies, Eq. (1.33) approaches an unrealistic value. The coefficient for the instantaneous propulsive power available is

$$\frac{-F_x V}{\frac{1}{2}\rho V^3(2b)} \;=\; -C_x(t) \tag{1.34}$$

Using Eqs. (1.32), (1.33), and (1.34), the efficiency when the upward y-velocity component is in phase with the pitching angle is found to be

$$\eta \;=\; \frac{-\overline{C}_x}{\overline{C}_P} \;=\; \frac{(F^2+G^2)[(1-\hat{\alpha}_y)^2 + k^2\hat{\alpha}_y^2] + F(\hat{\alpha}_y - \hat{\alpha}_y^2 - k^2\hat{\alpha}_y^2) + k\hat{\alpha}_y(G + k\hat{\alpha}_y/2)}{(1-\hat{\alpha}_y)F + k\hat{\alpha}_y(G + k\hat{\alpha}_y/2)} \tag{1.35}$$

For low frequencies, the efficiency approaches the quasi-steady solution of 1.0, while for high frequencies, the efficiency approaches 0.5. The results have correct behavior at low frequencies, but unrealistic values at high frequencies.

Other analytical studies have been performed in various aspects of flapping flight, such as the effect of wind gusts [13], pressure forces [14], and energy conservation [15]. Helicopters and hovering [16] have also been a large area of research. Brunton and Rowley [17] compared analytical models (including

Theodorsen's presented earlier) and numerical simulations to test where the analytical models broke down. Glauert [18] calculated the damping moment of oscillating airfoils, while von Ellenrieder, Parker, and Soria [19] developed and discussed a hypothesis for proper selection of the Strouhal number.

2. Experimental Studies

Katzmayr [20] was the first to experimentally show that the Knoller-Betz [6,7] model produces thrust. He produced a series of experiments, the first of which was the oscillation of an airfoil about an axis parallel to the span. He concluded that there was no improvement of the aerodynamic properties of an airfoil in this setup and in fact stated that periodic oscillations impair the aerodynamic properties. However, he then changed his experiment to oscillate the freestream while keeping the airfoil stationary. For his second experiment, he concluded that the oscillating freestream was extraordinarily favorable on airfoils [20].

The examination of the effect of vortices in flapping flight has been a large area of interest in experimental studies [21–30]. These studies aim to uncover the physics involved in flapping flight [25], as well as to understand how the vortices effect the aerodynamic forces [22]. Studying the wake of an oscillating airfoil is another large area of interest [31–36]. These studies differ from the vorticity studies by examining the entirety of the wake, including jets [35] and asymmetric wakes [33].

Several aspects of flapping flight have been experimentally studied such as hover [37], take off [38], and stall [39]. Adding an oscillatory in-line motion has also been studied [40] in order to examine whether it is a limitation or improvement for the animals that utilize this technique. Other aspects of animal flight have been studied as well, including fins [41,42] and insect models [43,44]. Spawning from the imitation of animals, flexible flapping foils has also been studied in order to determine the effects on the aerodynamic properties [45–48].

3. Numerical Studies

In a very recent study, Hunsaker and Phillips [12] performed a numerical simulation of Theodorsen's [9] model using computational fluid dynamics (CFD). In order to be consistent with Theodorsen [9], an inviscid solver was used. Other components of the setup of these simulations were that second-order upwinding was used and the implicit unsteady solver was used with second-order temporal discretization. A constant fluid density of 1.225 kg/m^3 and a freestream velocity of 14 m/s were chosen. A von Kármán Trefftz airfoil with a maximum thickness of 15%, a chord length of 0.25 m, and a zero-lift angle of attack of −5.0 degrees was the airfoil used throughout their computations. The analytical aerodynamic center of

the airfoil used is located at $x/c = 0.2757$ and $y/c = 0.0061$. The simulation used an overset grid over a background grid. The overset grid translated vertically (plunging) with motion described by $y_A \sin(\omega t)$, while it also rotated about the airfoil aerodynamic center (pitching) with motion described by $\alpha_A \cos(\omega t)$. Structured C-grids were used and were setup as shown in Fig. 2.

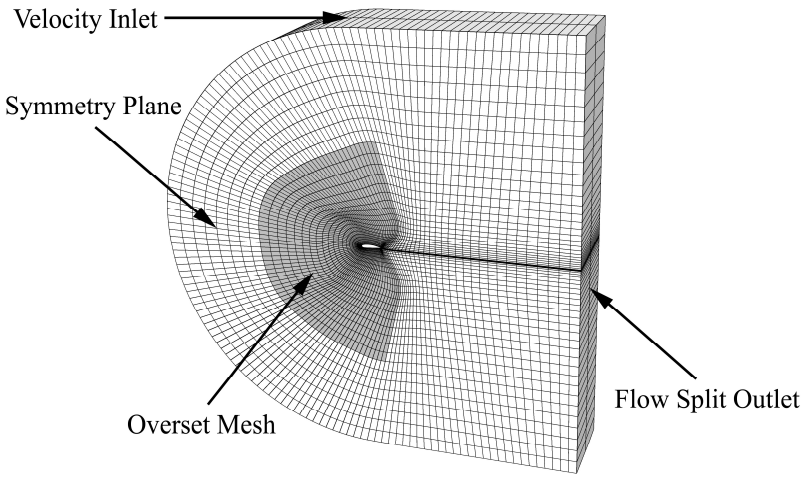

Fig. 2 Example coarse grid for computational fluid dynamics calculations (from Hunsaker and Phillips [12] with permission).

In order to obtain two-dimensional results while using a three-dimensional solver, three identical grid planes in the z-direction were set with the two outer z-planes set as symmetry boundaries. Grid convergence was studied by producing three similar grids from an initial fine grid. A medium grid was generated from the fine grid by removing every other node, and the coarse grid was generated from the medium grid by again removing every other node. Accuracy was evaluated by comparing the solutions of 16 steps in a quasi-steady flapping cycle to the analytical solution. In order to accomplish this, the overset grid was offset from the background grid by using the translation equation $y_A \sin(\omega t)$, and the overset grid was given a steady translational velocity using $\omega y_A \cos(\omega t)$. Values for y_A and ω were chosen to give geometric angles of attack ranging from -4.0 to 4.0 degrees.

The results of these 16 step cases compared to the analytical solution show grid convergence. The authors note that the increase in drag in the CFD solutions is due to numerical viscosity. For the lift and aerodynamic center pitching moment coefficients, the error was less than 0.5% of the mean values for the fine grid.

Transient CFD solutions were then obtained. 128 time steps per cycle for eight cycles using the same grid as the previous cases was determined to be both grid and time-step converged. The calculations used a

geometric angle of attack amplitude of $\hat{\omega}_y(1-\hat{\alpha}_y) = 4.29°$ and mean lift coefficient of $\overline{C}_L = 0.614$. Birds in forward flight typically have a reduced frequency range between $k \cong 0.015$ and $k \cong 0.2$. The reduced frequency range of this study was $0.05 < k < 0.42$.

Values for the mean axial-force coefficient and mean power required coefficient were obtained and are shown in Figs. 3 and 4 compared to Theodorsen's [9] model. The difference between the CFD and Theodorsen's model increased with increasing reduced frequency, with the differences for the mean axial-force coefficient ranging from -2.9% to 34% and for the mean power required coefficient ranging from -1.2% to 24%. The author remarks that this is remarkable considering the constraining approximations used by Theodorsen [9].

Hunsaker and Phillips [12] then propose an alternate approach for predicting the aerodynamic properties of a flapping airfoil using numerical solutions to experimental data to calibrate the frequency dependence of the unsteady aerodynamic coefficients. It is noted that this approach may be better for high flapping frequencies. To set up this new approach, a two-dimensional airfoil immersed in uniform flow and constant freestream velocity, V, is considered. Sinusoidal vertical displacement, $y_{ac}(t)$, with a zero mean and positive upward orientation, of the airfoil's aerodynamic center is combined with small-angle sinusoidal rotation, $\alpha(t)$, also about the airfoil's aerodynamic center. The rotation α has a mean value of $\overline{\alpha}$ and is oriented such that it is positive clockwise relative to the freestream velocity, which is approaching the airfoil from the left. This allows the vertical position of the aerodynamic center to be expressed as

$$y_{ac}(t) = y_A \sin(\omega t) \tag{1.36}$$

The normal-velocity component can then be shown to be

$$V_y(t) = \omega y_A \cos(\omega t) \tag{1.37}$$

The pitching angle is oscillating at the same frequency as the normal-velocity component, as well being in phase with the normal-velocity component. The pitching angle can then be expressed as

$$\alpha(t) = \overline{\alpha} + \alpha_A \cos(\omega t) \tag{1.38}$$

where the pitching amplitude is denoted as α_A. Using the small-angle approximation, the total geometric angle of attack is then shown to be

$$\alpha_g(t) = \overline{\alpha} - \hat{\omega}_y(1-\hat{\alpha}_y)\cos(\omega t) \tag{1.39}$$

The lift coefficient can be written as

$$C_L(t) = \widetilde{C}_{L,\alpha}[\alpha_g(t)+\alpha_i(t)-\alpha_{L0}] \tag{1.40}$$

where $\widetilde{C}_{L,\alpha}$ is the airfoil section lift slope, α_{L0} is the zero lift angle of attack, and $\alpha_i(t)$ is the time-dependent induced angle of attack. Eq. (1.39) can be applied to Eq. (1.40) with the result

$$C_L(t) = \widetilde{C}_{L,\alpha}[\overline{\alpha}-\hat{\omega}_y(1-\hat{\alpha}_y)\cos(\omega t)+\alpha_i(t)-\alpha_{L0}] \tag{1.41}$$

The axial and normal component of lift are found to be

$$C_x(t) = -\widetilde{C}_{L,\alpha}[\overline{\alpha}-\hat{\omega}_y(1-\hat{\alpha}_y)\cos(\omega t)+\alpha_i(t)-\alpha_{L0}][-\hat{\omega}_y\cos(\omega t)+\alpha_i(t)] \tag{1.42}$$

$$C_y(t) = C_L(t) = \widetilde{C}_{L,\alpha}[\overline{\alpha}-\hat{\omega}_y(1-\hat{\alpha}_y)\cos(\omega t)+\alpha_i(t)-\alpha_{L0}] \tag{1.43}$$

utilizing the small angle approximation.

The instantaneous induced angle of attack can depend on the oscillating component of the geometric angle of attack and all of the time derivatives

$$\alpha_i(t) = C_0[\alpha_g(t)-\overline{\alpha}]+\sum_{n=1}^{\infty}C_n\frac{d^n\alpha_g}{dt^n} \tag{1.44}$$

In order to evaluate the time derivatives,

$$\frac{d^n\alpha_g}{dt^n} = \hat{\omega}_y(1-\hat{\alpha}_y)\begin{cases}(-1)^{(n+3)/2}\omega^n\sin(\omega t), \text{ for } n \text{ odd}\\ (-1)^{(n+2)/2}\omega^n\cos(\omega t), \text{ for } n \text{ even}\end{cases} \tag{1.45}$$

can be used. Using Eqs. (1.39) and (1.45) in Eq. (1.44),

$$\alpha_i(t) = \hat{\omega}_y(1-\hat{\alpha}_y)[A\cos(\omega t)+B\sin(\omega t)] \tag{1.46}$$

is obtained, where

$$A \equiv \sum_{\substack{n=0\\ n \text{ even}}}^{\infty}(-1)^{(n+2)/2}C_n\omega^n, \quad B \equiv \sum_{\substack{n=1\\ n \text{ odd}}}^{\infty}(-1)^{(n+3)/2}C_n\omega^n \tag{1.47}$$

The coefficients A and B do not vary with time over the flapping cycle for this study.

Using Eq. (1.46) in (1.42), along with the trigonometric identities $\cos^2\theta=[1+\cos(2\theta)]/2$, $\sin^2\theta=[1-\cos(2\theta)]/2$, and $\cos\theta\sin\theta=\sin(2\theta)/2$, the following is obtained

$$C_x(t) \;=\; \overline{C}_L\,\hat{\omega}_y[A_{x1}\cos(\omega t)+B_{x1}\sin(\omega t)]-\widetilde{C}_{L,\alpha}\,\hat{\omega}_y^2(1-\hat{\alpha}_y)[A_{x0}+A_{x2}\cos(2\omega t)+B_{x2}\sin(2\omega t)] \quad (1.48)$$

The same can be done to Eq. (1.43) to obtain

$$C_y(t) \;=\; \overline{C}_L-\widetilde{C}_{L,\alpha}\,\hat{\omega}_y(1-\hat{\alpha}_y)[A_{y1}\cos(\omega t)+B_{y1}\sin(\omega t)] \quad (1.49)$$

where

$$\begin{aligned}
A_{x0} &\equiv [(1-A)(1-A+\hat{\alpha}_y A)+(1-\hat{\alpha}_y)B^2]\big/2,\\
A_{x1} &\equiv 1-(1-\hat{\alpha}_y)A, \quad B_{x1} \equiv -(1-\hat{\alpha}_y)B,\\
A_{x2} &\equiv [(1-A)(1-A+\hat{\alpha}_y A)-(1-\hat{\alpha}_y)B^2]\big/2,\\
B_{x2} &\equiv -[(1-A)(1-\hat{\alpha}_y)+\hat{\alpha}_y/2]B\\
A_{y1} &\equiv 1-A, \quad B_{y1} \equiv -B
\end{aligned} \quad (1.50)$$

and

$$\overline{C}_L \;=\; \widetilde{C}_{L,\alpha}(\overline{\alpha}-\alpha_{L0}) \quad (1.51)$$

It can be seen that the seven coefficients, A_{x0}, A_{x1}, B_{x1}, A_{x2}, B_{x2}, A_{y1}, and B_{y1}, depend on the plunging frequency. For steady sinusoidal oscillations, however, they are Fourier coefficients and do not vary over the flapping cycle. The axial- and normal-force coefficients depend on at least one reduced frequency, $\hat{\omega}_y$, as can be seen in Eqs. (1.42) and (1.43). It is expected that these force coefficients should depend on two reduced frequencies, the normal reduced frequency, $\hat{\omega}_y$, and axial reduced frequency,

$$\hat{\omega}_x \;\equiv\; \omega c/V \quad (1.52)$$

As the Fourier coefficients A and B are strong functions of $\hat{\omega}_y$, it is expected that they will be strong functions of $\hat{\omega}_x$ as well. The authors note that $\hat{\omega}_x$ is simply twice the reduced frequency that Theodorsen [9] defined.

For quasi-steady sinusoidal oscillations, the Fourier coefficients approach the low-frequency limit of

$$A_{x0} = 1/2, \quad A_{x1} = 1, \quad B_{x1} = 0, \quad A_{x2} = 1/2, \quad B_{x2} = 0, \quad A_{y1} = 1, \quad B_{y1} = 0 \quad (1.53)$$

while $\hat{\omega}_x$, α_i, A, and B all approach zero.

The instantaneous power coefficient for pitching and plunging motion is

$$C_P(t) \equiv \frac{-F_y(t)V_y(t) - m_{ac}\dot{\alpha}(t)}{\frac{1}{2}\rho V^3 c} = \frac{-C_y(t)V_y(t) - C_{m_{ac}} c\dot{\alpha}(t)}{V} \tag{1.54}$$

Using the small angle approximation, assuming the pitching angle is in phase with the upward y-velocity component, and applying Eqs. (1.21), (1.22), (1.37), (1.38), (1.43), and (1.52), the expression for the instantaneous power required can be found to be

$$\begin{aligned} C_P(t) = & -\{\overline{C}_L \hat{\omega}_y - \widetilde{C}_{L,\alpha} \hat{\omega}_y^2 (1-\hat{\alpha}_y)[(1-A)\cos(\omega t) - B\sin(\omega t)]\}\cos(\omega t) \\ & + C_{m_{ac}} \hat{\omega}_x \hat{\omega}_y \hat{\alpha}_y \sin(\omega t) \end{aligned} \tag{1.55}$$

Equations (1.55) and (1.48) can be integrated over a cycle and divided by the period to obtain the mean required-power coefficient and the mean axial-force coefficient

$$\overline{C}_P \equiv \frac{1}{\tau}\int_{t=0}^{\tau} C_P(t)dt = \widetilde{C}_{L,\alpha} \hat{\omega}_y^2 (1-\hat{\alpha}_y)(1-A)/2 \tag{1.56}$$

$$\overline{C}_x \equiv \frac{1}{\tau}\int_{t=0}^{\tau} C_x(t)dt = -\widetilde{C}_{L,\alpha} \hat{\omega}_y^2 (1-\hat{\alpha}_y)[(1-A)(1-A+\hat{\alpha}_y A) + (1-\hat{\alpha}_y)B^2]/2 \tag{1.57}$$

Continuing to assume the pitching angle is in phase with the upward y-velocity component, the propulsive efficiency is obtained to be

$$\overline{\eta} = -\overline{C}_x/\overline{C}_P = 1-(1-\hat{\alpha}_y)[A - B^2/(1-A)] \tag{1.58}$$

In order to determine the time-dependent wake-induced angle of attack, values for the Fourier coefficients A and B must be found. It can be seen that in Eq. (1.56), the mean required-power coefficient is independent of the Fourier coefficient B. Therefore, the A coefficient can be found to be

$$A = 1 - \frac{2\overline{C}_P}{\widetilde{C}_{L,\alpha} \hat{\omega}_y^2 (1-\hat{\alpha}_y)} \tag{1.59}$$

A similar process can be utilized to find the B coefficient from Eqs. (1.57) and (1.59).

$$B = \sqrt{\frac{-2\overline{C}_x}{\widetilde{C}_{L,\alpha}\hat{\omega}_y^2(1-\hat{\alpha}_y)^2} - \frac{(1-A)(1-A+\hat{\alpha}_y A)}{(1-\hat{\alpha}_y)}} \tag{1.60}$$

The wake-induced angle of attack can then be found from Eq. (1.46).

Using the CFD solutions previously described, $\hat{\omega}_x$ was varied from 0.10 to 0.84, while $\hat{\omega}_y$ was varied from 0.025 to 0.117, and $\hat{\alpha}_y$ was varied from -0.2 to 0.2. The solutions from the calculations were then used with Eqs. (1.59) and (1.60) to evaluate the Fourier coefficients A and B. The results were used to obtain algebraic correlation equations, relating A and B to the parameters $\hat{\omega}_x$, $\hat{\omega}_y$, and $\hat{\alpha}_y$. Values for the Fourier coefficients A and B obtained from the CFD solutions were correlated accurately using the piecewise continuous functions

$$A = (1+0.13\hat{\alpha}_y)\begin{cases} A_{15}\hat{\omega}_x^5 + A_{14}\hat{\omega}_x^4 + A_{13}\hat{\omega}_x^3 + A_{12}\hat{\omega}_x^2, & \hat{\omega}_x \le T_{A1} \\ A_{23}\hat{\omega}_x^3 + A_{22}\hat{\omega}_x^2 + A_{21}\hat{\omega}_x + A_{20}, & T_{A1} \le \hat{\omega}_x \le T_{A2} \\ A_{30} - A_{31}\exp(-A_{32}\hat{\omega}_x), & \hat{\omega}_x \ge T_{A2} \end{cases} \tag{1.61}$$

$$B = \{1-\exp[-(35.6-30.4\hat{\alpha}_y)\hat{\omega}_y]\}(1-0.71\hat{\alpha}_y^2)\begin{cases} B_{15}\hat{\omega}_x^5 + B_{14}\hat{\omega}_x^4 + B_{13}\hat{\omega}_x^3 + B_{12}\hat{\omega}_x^2, & \hat{\omega}_x \le T_{B1} \\ B_{23}\hat{\omega}_x^3 + B_{22}\hat{\omega}_x^2 + B_{21}\hat{\omega}_x + B_{20}, & T_{B1} \le \hat{\omega}_x \le T_{B2} \\ B_{30}, & \hat{\omega}_x \ge T_{B2} \end{cases} \tag{1.62}$$

The coefficients found in Eqs. (1.61) and (1.62) were found by forcing continuity of the functions and their first derivatives at the transition points and minimizing the RMS difference between the CFD solutions and the functions. The results of the comparison between Eqs. (1.61) and (1.62) and the CFD solutions are shown in Figs. 3 and 4. The authors note that the fact that there is significantly more deviation in the B coefficient could be due to the difference in uncertainty in the CFD solutions for the mean axial force and the mean required power. Comparison of the mean axial-force coefficient, mean required-power coefficient, and propulsive efficiency of the CFD solutions to both the Hunsaker and Phillips [12] results and the Theodorsen [9] results are shown in Figs. 5–7.

Table 1. Correlation coefficients for Eqs. (1.61) and (1.62).

A_{15} =	97.29135	A_{23} =	0.546031	A_{30} =	0.587284	B_{15} =	−544.4944	B_{23} =	−14.76825
A_{14} =	−43.97278	A_{22} =	−1.041703	A_{31} =	0.804087	B_{14} =	49.2633	B_{22} =	11.25173
A_{13} =	−17.06888	A_{21} =	0.961984	A_{32} =	2.611038	B_{13} =	109.3024	B_{21} =	−2.75989
A_{12} =	9.97222	A_{20} =	0.108206	B_{30} =	−0.265167	B_{12} =	−26.2319	B_{20} =	−0.05111
T_{A1} =	0.332091	T_{A2} =	0.728294	T_{B1} =	0.226322	T_{B2} =	0.300902		

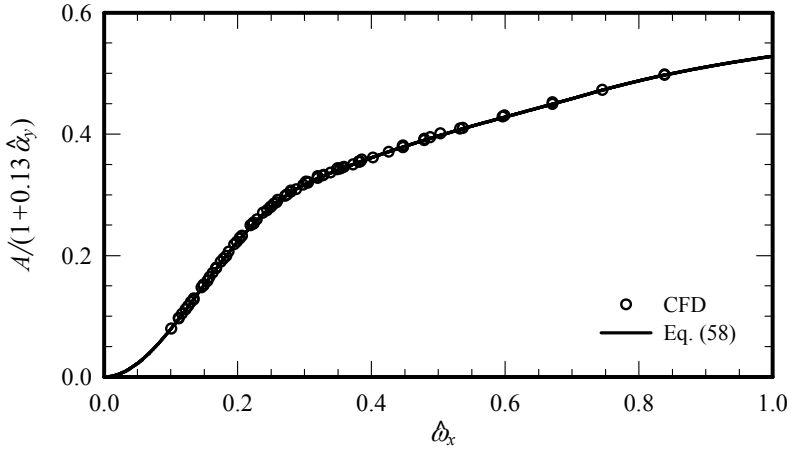

Fig. 3 Comparison between the CFD solutions and the correlation with Eq. (1.61) (from Hunsaker and Phillips [12] with permission).

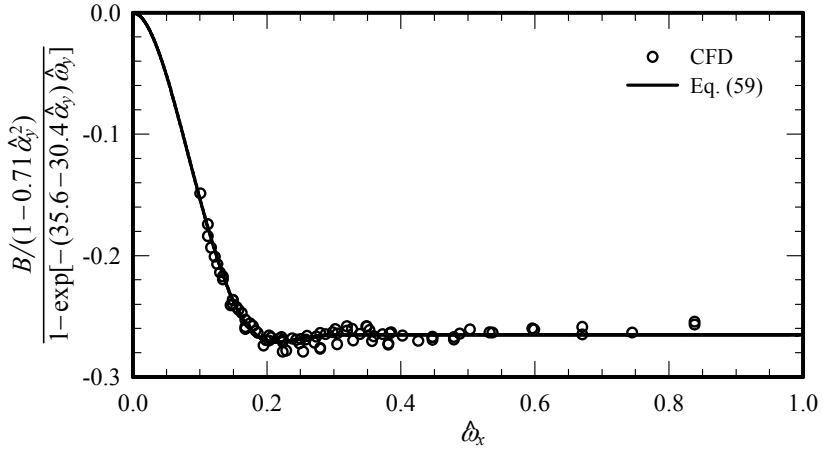

Fig. 4 Comparison between the CFD solutions and the correlation with Eq. (1.62) (from Hunsaker and Phillips [12] with permission).

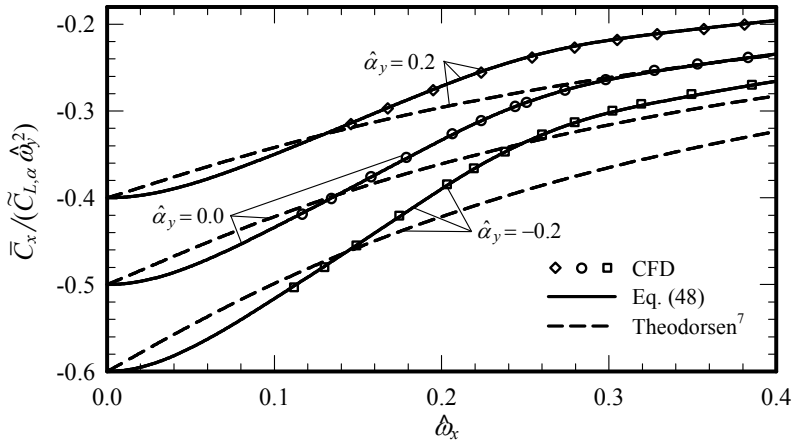

Fig. 5 Comparison of the mean axial-force coefficient predicted from the CFD solutions, Eq. (1.57), and the model first presented by Theodorsen [9] (from Hunsaker and Phillips [12] with permission).

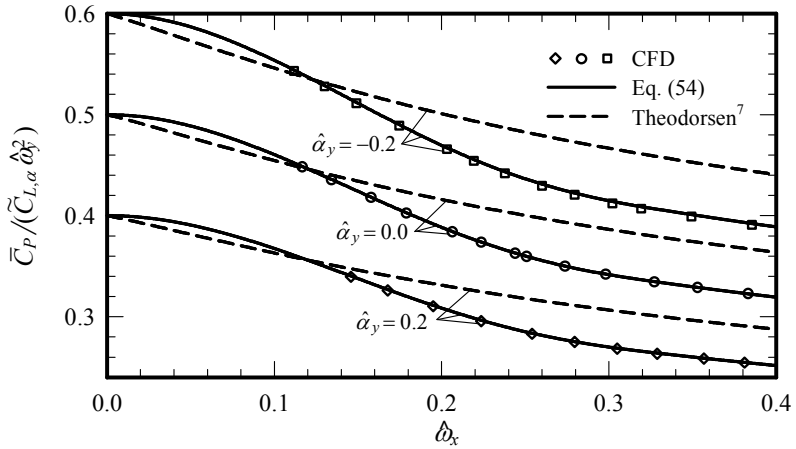

Fig. 6 Comparison of the mean required-power coefficient predicted from the CFD solutions, Eq. (1.56), and the model first presented by Theodorsen [9] (from Hunsaker and Phillips [12] with permission).

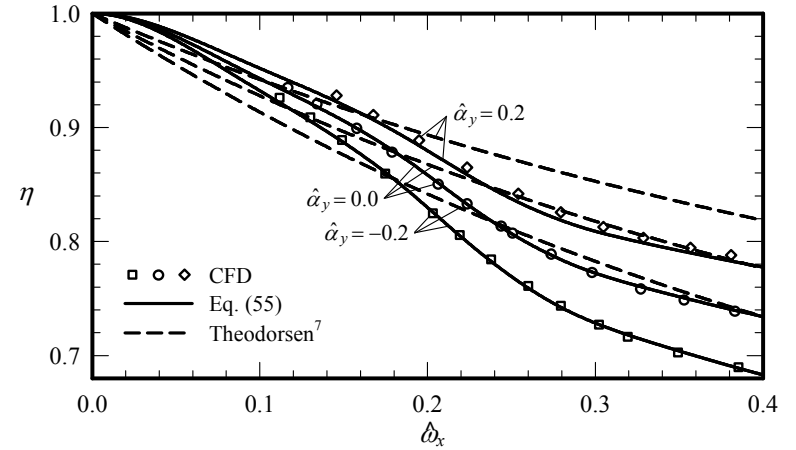

Fig. 7 Comparison of the propulsive efficiency predicted from the CFD solutions, Eq. (1.58), and the model first presented by Theodorsen [9] (from Hunsaker and Phillips [12] with permission).

It is noted that the correlations between the CFD solution and the Hunsaker and Phillips [12] results shows a noticeable improvement over the Theodorsen [9] model.

Hunsaker and Phillips [12] focused on the propulsive efficiency in their calculations, but other studies have focused on propulsive efficiency as well. Tuncer and Kaya [3] performed numerical calculations and found that efficiency was increased when plunging is decreased and pitching was increased. As was seen in Fig. 7, this was consistent with Hunsaker and Phillips' [12] findings. Kaya and Tuncer [49] found that a nonsinusoidal flapping cycle gave more thrust, but reduced efficiency and that the efficiency increased the closer to sinusoidal the flapping cycle was. The examination of sinusoidal and nonsinusoidal flapping motions was also studied by Sarkar and Venkatraman [50]. Young and Lai [51] studied the effect of flow separation on thrust and efficiency and found that flow separation, and therefore efficiency, was partially controlled by reduced frequency as well as the flapping motion.

As was of interest in experimental studies, flexibility [52–57], hover [58–64], and stall [65,66] have been areas of interest in numerical studies as well. Vorticity [4, 67–73] and investigation into the wakes [2, 74–77] of oscillating airfoils also are large areas of numerical study. Several aspects of the flapping cycle have been numerically investigated such as the effect of frequency [78,79], chord thickness [80], pitching and plunging ratio [81], and general dynamics [82]. Bi-plane configurations [83–86] have also been studied numerically in order to determine aerodynamic properties in comparison to a single airfoil.

There are multiple ways to study flapping foils numerically. Studies have ranged from using CFD analysis [48, 87], Duhamel Superposition [88], Finite Element analysis [89], immersed boundary methods [90], panel codes [91,92], and vortex-lattice methods [93]. Studies have investigated the materials and structure requirements [94] and the effects of channel flow [95] and placement near solid walls [96] on the aerodynamic properties.

Several studies have combined both numerical and experimental solutions to produce results. These studies cover a wide range of subjects. Toomey and Eldredge [97] studied the effect of flexible airfoils, while Jones, Dohring, and Platzer [98] studied the wake of a flapping airfoil. Ground effect [99] and hover [100] have also been studied in a combination of numerical and experimental solutions.

B. Three-Dimensional Studies

1. Analytical Studies

There have been many three-dimensional analytical studies examining the aerodynamic properties of flapping flight. Multiple studies discuss the interest for flapping flight [101], the problems that need to be

solved in order to produce an accurate model [102], as well as a discussion of different approaches that have been taken [103] and overall summaries of existing work [104,105]. Hover is also a large area of interest in three-dimensional analytical studies [106–113], including the study of conversion from hover to forward flight [114] and studies specific to helicopters [106].

Nature has been examined extensively in order to learn more about the aerodynamic properties associated with oscillating wings. Birds [115], bats [116], and insects [117,118] have all been analytically investigated. An extensive effort has been made into examining different effects of the wing motion [119], including bending moments [120], efficiency [121], rotation timing [122], twist [123], vortices [124,125], and wake effects [126].

Different techniques of modeling have been of large interest as well [127–139]. Many different approaches have been taken such as the continuous loading approach [131], a stream tube model [132], investigation into the effect of the Strouhal number [133], and adaptations of Prandtl's Lifting Line Theory [5,134–139].

Prandtl's classic lifting-line theory [140,141] shows that when the planform shape and other wing characteristics are known, the lift and drag of the wing can be found. Phillips [138] expanded this theory by breaking down the fundamental equation

$$\frac{2\Gamma(z)}{Vc(z)}+\frac{\widetilde{C}_{L,\alpha}}{4\pi V}\int_{\varsigma=-b/2}^{b/2}\frac{1}{z-\varsigma}\left(\frac{d\Gamma}{dz}\right)_{z=\varsigma}d\varsigma=\widetilde{C}_{L,\alpha}\left[\alpha(z)-\alpha_{L0}(z)\right] \tag{1.63}$$

and examining how each component of wing planform, washout distribution, surface deflection, and wing roll effects the lift and drag. Phillips has continued this examination to the application of flapping flight [134,135].

Phillips [134,135] begins from Prandtl's lifting-line theory's fundamental equation, Eq. (1.63). Assuming a wing with no sweep or dihedral, and using a Fourier series, change of variables,

$$\theta\equiv\cos^{-1}(-2z/b) \tag{1.64}$$

and the Kutta–Joukowski Law [142,143], Eq. (1.63) is solved and a lift coefficient is obtained as

$$C_L=\pi R_A A_1 \tag{1.65}$$

Downwash induced by the trailing vortex sheet causes the local section lift vectors to tilt aft, producing induced drag. Assuming no roll, the coefficient of induced drag is found to be

$$C_{D_i} = \pi R_A \sum_{n=1}^{N} n A_n{}^2 = \frac{C_L{}^2}{\pi R_A} + \pi R_A \sum_{n=2}^{N} n A_n{}^2 \tag{1.66}$$

If a wing has geometric or aerodynamic twist, the Fourier coefficients have to be re-evaluated at each point along the semispan because of the varying angles of attack, as well as for each operating condition. Using a change of variables, a more efficient equation for the Fourier coefficients can be determined

$$A_n = a_n \left(\alpha - \alpha_{L0}\right)_{root} - b_n \Omega + c_n \delta_c + d_n \hat{p} \tag{1.67}$$

where

$$\sum_{n=1}^{N} a_n \left[\frac{4b}{\widetilde{C}_{L,\alpha} c(\theta)} + \frac{n}{\sin(\theta)} \right] \sin(n\theta) = 1 \tag{1.68}$$

$$\sum_{n=1}^{N} b_n \left[\frac{4b}{\widetilde{C}_{L,\alpha} c(\theta)} + \frac{n}{\sin(\theta)} \right] \sin(n\theta) = \omega(\theta) \tag{1.69}$$

$$\sum_{n=1}^{N} c_n \left[\frac{4b}{\widetilde{C}_{L,\alpha} c(\theta)} + \frac{n}{\sin(\theta)} \right] \sin(n\theta) = \chi(\theta) \tag{1.70}$$

$$\sum_{n=1}^{N} d_n \left[\frac{4b}{\widetilde{C}_{L,\alpha} c(\theta)} + \frac{n}{\sin(\theta)} \right] \sin(n\theta) = \psi(\theta) \tag{1.71}$$

Rigid-body roll produces a linearly varying plunging distribution function

$$\psi(z) = -2z/b \qquad or \qquad \psi(\theta) = \cos(\theta) \tag{1.72}$$

A wing can be designed to decrease the amount of induced drag by including the optimum washout distribution. Information on how to do this, as well as prediction of rolling and yawing moments can be found in Phillips [138]. Aerodynamic forces depend on both translational and rotational acceleration and velocity components. The dependence on the acceleration components are for two reasons. The first reason is that as the surface of an object accelerates, some of the surrounding fluid accelerates as well, causing an equal and opposite force on the surface. If the weight of the object is much greater than the weight of the fluid, this force is small and can generally be ignored. The second reason is that the trailing vortex sheet has

a significant effect on the lift and drag. Therefore, the plunging acceleration has a significant effect on the lift and drag as well. There are two conditions that must be satisfied in order that the plunging acceleration and the effect it has on the trailing vortex sheet can be ignored. These two conditions are that the freestream airspeed must be high enough and that the rolling acceleration, along with the flapping frequency, must be low enough. This is because lifting-line solutions are quasi-steady solutions. In order to prevent boundary-layer separation, the local section geometric angle of attack, and therefore the component of wind normal to the flight path, must be small. If this is small and below stall, the lift coefficient can be modeled as a linear function. This gives

$$C_L = \pi R_A [a_1 (\alpha - \alpha_{L0})_{root} - b_1 \Omega + c_1 \delta_c + d_1 \hat{p}] \tag{1.73}$$

Rotation about the roll axis causes a change in the section lift vector, which changes the component of lift parallel to the freestream. Therefore, Eq. (1.66) cannot be used to compute the induced drag when there is rotation about the roll axis. The total section induced drag is caused by the tilting of the local section lift vector aft by $\Delta\alpha_i$ and forward by $\Delta\alpha_p$. The angular rotation rate about the roll axis is constant in rigid-body roll, positive on one semi-span and negative on the other in rigid-body flapping, and continuously varying for birds. How $\Delta\alpha_p$ varies in the spanwise direction is a product of the twist distribution and the dimensionless rotation rate. To obtain a function for the plunging distribution, it is assumed that the angular rotation rate distribution is constant across each semispan, and the flapping rate is spanwise symmetric about the midpoint.

$$\psi(z) = \begin{cases} -2z/b, & z < 0 \\ 2z/b, & z > 0 \end{cases} \tag{1.74}$$

From previous equations, an equation for induced drag as a function of the plunging distribution with rotation about the roll axis can be found.

$$C_{D_i} = \frac{{C_L}^2}{\pi R_A} + \pi R_A \sum_{n=2}^{N} n {A_n}^2 - \pi R_A \sum_{n=1}^{N} A_n e_n \hat{p} \tag{1.75}$$

where

$$e_n = \frac{2}{\pi} \int_{\theta=0}^{\pi} \psi(\theta) \sin(n\theta) \sin(\theta) d\theta \tag{1.76}$$

In Eq. (1.75), if the third term can become negative enough, the entire induced drag becomes negative, therefore actually being induced thrust. This is how flapping wings get forward flight. Induced thrust cannot exist without plunging, but induced thrust also depends on variations in chord length, twist, and aileron deflection. The periodic flapping motion is very complex, including twist, sweep, and plunging. An ornithopter can be designed to deflect ailerons to achieve certain objectives. Lifting-line theory allows it to be seen what exactly contributes to lift and drag so that this machine could be designed.

If a planform is spanwise symmetric along with the washout, the *a* and *b* coefficients are zero and all odd *c* and *d* coefficients are zero as well. With this, a simplified expression for the coefficient of induced drag with aileron deflection and rigid-body roll can be found.

$$C_{D_i} = \pi R_A \sum_{n=1}^{N} n\left[a_n\left(\alpha - \alpha_{L0}\right)_{root} - b_n\Omega\right]^2 + \pi R_A \sum_{n=1}^{N} n\left(c_n\delta_c + d_n\hat{p}\right)^2 + \frac{\pi R_A d_2}{2}\hat{p}_{steady}\hat{p} - \frac{\pi R_A d_2}{2}\hat{p}^2 \tag{1.77}$$

Using the small-angle approximation, we can find an equation for the rolling moment coefficient using the Fourier coefficients. An even simpler equation can be found if the planform and washout distribution are spanwise symmetric. An airplane quickly approaches a steady rolling rate when ailerons are deflected, caused by a net rolling moment of zero. This can be used to then simplify the coefficient of induced drag to see that the steady rigid-body roll causes no induced drag, but instantaneous roll before it reaches a steady rate increases induced drag. With no aileron deflection or roll, there is a set of equations for steady level flight.

$$C_{D_i} = \frac{\left(1+\kappa_D\right)C_L{}^2 - \kappa_{DL}C_L C_{L,\alpha}\Omega + \kappa_{D\Omega}\left(C_{L,\alpha}\Omega\right)^2}{\pi R_A} \tag{1.78}$$

$$C_{L,\alpha} = \pi R_A a_1 \tag{1.79}$$

$$\kappa_D = \sum_{n=2}^{N} n\frac{a_n{}^2}{a_1{}^2} \tag{1.80}$$

$$\kappa_{DL} = 2\frac{b_1}{a_1}\sum_{n=2}^{N} n\frac{a_n}{a_1}\left(\frac{b_n}{b_1} - \frac{a_n}{a_1}\right) \tag{1.81}$$

$$\kappa_{D\Omega} = \left(\frac{b_1}{a_1}\right)^2 \sum_{n=1}^{N} n\left(\frac{b_n}{b_1} - \frac{a_n}{a_1}\right)^2 \tag{1.82}$$

Rigid-body roll, in the absence of aileron deflection, always contributes negative induced drag, or induced thrust. In steady rigid-body roll, the induced drag from the aileron deflection is balanced out exactly by the induced thrust from the rolling rate. The local section lift can be written using Fourier coefficients to be a function of planform shape, washout, aileron deflection, and roll.

$$\begin{aligned}\frac{\tilde{L}}{\frac{1}{2}\rho V^2 b} &= 4\left(\alpha-\alpha_{L0}\right)_{root}\sum_{n=1}^{N}a_n\sin\left(n\theta\right)-4\Omega\sum_{n=1}^{N}b_n\sin\left(n\theta\right)\\ &+4\delta_c\sum_{n=1}^{N}c_n\sin\left(n\theta\right)+4\hat{p}\sum_{n=1}^{N}d_n\sin\left(n\theta\right)\end{aligned} \tag{1.83}$$

Plotting each contribution to the section lift separately as a distribution, it can be seen that when the aileron deflection term is tilted through $\alpha\Delta_p$, it is exactly balanced by the rolling rate term. Using the small angle approximation, Eq. (1.83) can be taken to determine the component of induced drag caused by tilting the local section lift through $\alpha\Delta_p$. If there is a left aileron deflection and left roll, it can be seen that the aileron term and the roll term will exactly cancel out in Eq. (1.84).

$$\begin{aligned}\frac{\Delta\tilde{D}_i}{\frac{1}{2}\rho V^2 b} &= -4\left(\alpha-\alpha_{L0}\right)_{root}\hat{p}\cos\left(\theta\right)\sum_{n=1}^{N}a_n\sin\left(n\theta\right)+4\Omega\hat{p}\cos\left(\theta\right)\sum_{n=1}^{N}b_n\sin\left(n\theta\right)\\ &-4\delta_c\hat{p}\cos\left(\theta\right)\sum_{n=1}^{N}c_n\sin\left(n\theta\right)-4\hat{p}^2\cos\left(\theta\right)\sum_{n=1}^{N}d_n\sin\left(n\theta\right)\end{aligned} \tag{1.84}$$

Washout and aileron deflection only change the magnitude of the section lift vector, while rotation about the roll axis changes both the magnitude and direction by tilting the vector through $\alpha\Delta_p$. By comparing Eq. (1.66) and Eq. (1.71) it can be seen that Eq. (1.66) does not account for this tilting. However, it holds for steady rigid-body roll or no roll because the induced drag and induced thrust produced exactly cancel out. For spanwise symmetric wings, there is no net effect on lift, but a small effect on induced drag from aileron deflection. Normally, the aileron deflection and roll terms of induced drag cancel out, but a yawning moment is produced. As seen in the previous discussion, there is a way to create induced thrust from rotation about the roll axis. If there is periodic rocking with no aileron deflection, induced thrust can be produced. In nature, the difficulty of this problem is overcome by rotating the semi-spans in opposite directions, or flapping.

Unlike rigid-body roll, flapping causes parallel effects on both semi-spans, producing significant changes in the lift and induced drag. The two-dimensional downstroke is well understood, but the upstroke

is not. Knoller [6] and Betz [7] described it as having positive thrust on both the upstroke and the downstroke in their cycle, but this description does not work for birds where there is not significant buoyancy. It is frequently said that birds fold their wings or separate their feathers on the upstroke to minimize the negative aerodynamic lift, but this can only be sustained for a few seconds and in forward flight, this is not necessary. It is not reasonable to use potential-flow analysis for all forms of flapping flight, but Prandtl's [140,141] lifting-line theory is a good way to analyze high-speed forward, or quasi-steady, flapping flight. In pure plunging, where there is no rotation in pitch, an expression for both the mean lift coefficient and the instantaneous lift coefficient using the small angle approximation in Prandtl's lifting-line theory can be found, as well as the observation that the periodic motion gives a mean flapping rate, $\hat{p}$, of zero.

$$\overline{C}_L = \pi R_A [a_1 (\alpha - \alpha_{L0})_{root} - b_1 \Omega] \tag{1.85}$$

$$C_L = \overline{C}_L + \pi R_A d_1 \hat{p} \tag{1.86}$$

Rather than having α_{root} and the washout remain fixed, it is more convenient to keep the lift coefficient fixed and let α_{root} and the washout vary over the cycle. After allowing the lift coefficient to remain fixed, an expression can be obtained for the induced drag coefficient.

$$C_{D_i} = \frac{(1+\kappa_D) {C_L}^2 - \kappa_{DL} C_L C_{L,\alpha} \Omega + \kappa_{D\Omega} (C_{L,\alpha} \Omega)^2}{\pi R_A} + \frac{(-\kappa_{Lp} C_L + \kappa_{\Omega p} C_{L,\alpha} \Omega - \kappa_p C_{L,\alpha} \hat{p}) C_{L,\alpha} \hat{p}}{\pi R_A} \tag{1.87}$$

where

$$\kappa_{Lp} \equiv \frac{e_1}{a_1} + \frac{d_1}{a_1} \sum_{n=2}^{N} \frac{a_n}{a_1} \left[\frac{e_n}{d_1} - 2n \left(\frac{d_n}{d_1} - \frac{a_n}{a_1} \right) \right] \tag{1.88}$$

$$\kappa_{\Omega p} \equiv \frac{b_1}{a_1} \frac{d_1}{a_1} \sum_{n=2}^{N} \left(\frac{b_n}{b_1} - \frac{a_n}{a_1} \right) \left[\frac{e_n}{d_1} - 2n \left(\frac{d_n}{d_1} - \frac{a_n}{a_1} \right) \right] \tag{1.89}$$

$$\kappa_p \equiv \left(\frac{d_1}{a_1} \right)^2 \sum_{n=2}^{N} \left(\frac{d_n}{d_1} - \frac{a_n}{a_1} \right) \left[\frac{e_n}{d_1} - n \left(\frac{d_n}{d_1} - \frac{a_n}{a_1} \right) \right] \tag{1.90}$$

An optimum value of washout as a function of the lift coefficient and rotation rate can be found. This is optimized over the entire cycle such that a flapping motion with maximum induced thrust results.

$$\Omega_{opt} = \frac{\kappa_{DL} C_L - \kappa_{\Omega p} C_{L,\alpha} \hat{p}}{2\kappa_{D\Omega} C_{L,\alpha}} \tag{1.91}$$

Equation (1.91) can be taken and made so there is optimum washout the entire cycle, yielding expressions for both the mean and instantaneous coefficient of induced drag. It can be rearranged to keep washout and the root aerodynamic angle of attack fixed, letting the coefficient of lift vary, and obtain and expression for the instantaneous drag coefficient. The mean induced drag coefficient has two components. The first is the same as induced drag without flapping. The second is parallel to the freestream and opposite the drag, causing induced thrust, as can be seen in Eq. (1.29).

$$\overline{C}_{D_i} = \frac{(1-\kappa_D)\overline{C}_L{}^2 - \kappa_{DL}\overline{C}_L C_{L,\alpha}\Omega + \kappa_{D\Omega}\left(C_{L,\alpha}\Omega\right)^2}{\pi R_A} - \frac{\overline{\kappa}_p\left(C_{L,\alpha}\hat{p}_{rms}\right)^2}{\pi R_A} \tag{1.92}$$

where

$$\overline{\kappa}_p \equiv \kappa_p + \kappa_{Lp}\left(\frac{d_1}{a_1}\right) - (1+\kappa_D)\left(\frac{d_1}{a_1}\right)^2 \tag{1.93}$$

On the downstroke, the local section lift vectors are tilted forward and the magnitude increases. On the upstroke, they are tilted aft and the magnitude decreases. This give induced thrust for pure plunging over a cycle. In order to get numerical results for the instantaneous drag coefficient, the plunging distribution function must be known. Assuming a small angle rotation about the midspan with no bending in the semispan, Fourier coefficients can be produced for this case.

When the left wing rolls up, the rolling moment is defined positive and an expression can be obtained for the left wing's effect on the rolling moment coefficient using the small angle approximation. If there is no aileron deflection with spanwise symmetric planform shape, washout, and flapping, the left wing's effect on the rolling moment coefficient can be simplified further. The left wing's moment coefficient is the root bending moment coefficient, and from that a flapping power coefficient can be defined. This is done using the fact that the instantaneous power is two times the left wing moment times the flapping rate.

$$C_{P_f} = \frac{P_f}{\frac{1}{2}\rho V^3 S} = 4\left(\kappa_a C_L - \kappa_b C_{L,\alpha}\Omega + \kappa_d C_{L,\alpha}\hat{p}\right)\hat{p} \tag{1.94}$$

where

$$\kappa_a \equiv \frac{1}{3\pi} + \frac{1}{\pi}\sum_{n=3}^{N} \frac{(-1)^{(n+1)/2}}{n^2-4}\frac{a_n}{a_1}\bigg|_{for \quad n \quad odd} \tag{1.95}$$

$$\kappa_b \equiv \frac{b_1}{\pi a_1}\sum_{n=3}^{N} \frac{(-1)^{(n+1)/2}}{n^2-4}\left(\frac{b_n}{b_1} - \frac{a_n}{a_1}\right)\bigg|_{for \quad n \quad odd} \tag{1.96}$$

$$\kappa_d \equiv \frac{d_1}{\pi a_1}\sum_{n=3}^{N} \frac{(-1)^{(n+1)/2}}{n^2-4}\left(\frac{d_n}{d_1} - \frac{a_n}{a_1}\right)\bigg|_{for \quad n \quad odd} \tag{1.97}$$

In order to maximize thrust, the Eq. (1.91) for optimum twist can be used in the flapping power coefficient. Keeping other variables fixed and letting the lift coefficient vary, an expression is found for the instantaneous flapping power coefficient in pure plunging. Seeing that under certain circumstances, the instantaneous power could be negative, an equation is obtained for the minimum possible mean flapping power coefficient. Finding the mean power available, simply the induced thrust times the freestream velocity, helps to find the ideal efficiency, showing that propulsive efficiency is independent of the flapping rate in pure plunging.

$$\overline{\eta} \equiv \frac{\overline{C}_{P_A}}{\overline{C}_{P_f}} = \frac{\overline{\kappa}_p a_1}{4\left(\kappa_d - \kappa_a d_1 / a_1\right)} \tag{1.98}$$

Phillips [134,135] finds that efficiencies of 95% or greater are possible with flapping flight. This is compared to traditional methods of propulsion that have a range of efficiency of 70-80% [144]. This shows that flapping flight has the potential to be much more efficient than traditional methods of propulsion.

If a rigid-semispan is considered, the washout and twist must remain constant. No bending can occur either. Using an elliptic planform shape in order to minimize induced drag without twist, yields solutions for the Fourier coefficients. Expressions can then be found for the lift coefficient, induced drag coefficient, and flapping power coefficient for small-angle flapping.

$$C_L = \overline{C}_L + \frac{4}{3\pi} C_{L,\alpha}\hat{p} \tag{1.99}$$

$$C_{P_f} = 4\left[\frac{\overline{C}_L}{3\pi} - \kappa_b C_{L,\alpha}\Omega + \left(\kappa_d + \frac{4}{9\pi^2}\right)C_{L,\alpha}\hat{p}\right]\hat{p} \tag{1.100}$$

$$\overline{C}_{D_i} = \frac{\overline{C}_L{}^2 + \kappa_{D\Omega}\left(C_{L,\alpha}\Omega\right)^2}{\pi R_A} - \frac{\overline{\kappa}_p\left(C_{L,\alpha}\hat{p}_{rms}\right)^2}{\pi R_A} \tag{1.101}$$

Looking at Eq. (1.101), it can be seen that in order to maintain steady periodic motion, the condition in Eq. (1.102) must be met.

$$\hat{p}_{rms} = \frac{1}{C_{L,\alpha}}\sqrt{\frac{\pi R_A}{\overline{\kappa}_p}\left[C_{D_P} + \frac{\overline{C}_L{}^2 + \kappa_{D\Omega}\left(C_{L,\alpha}\Omega\right)^2}{\pi R_A}\right]} \tag{1.102}$$

Assuming a sinusoidal flapping cycle, as well as a washout of zero, and therefore an untwisted wing, it can be seen that the lift, drag, and flapping-power coefficients are dependent on the wing aspect ratio. A sinusoidal flapping cycle causes a slightly negative power coefficient for a part of the cycle. For ideal efficiency, this power is recovered, but if this power is not recovered, the mean flapping power coefficient rises and efficiency decreases to roughly the values of traditional aircraft propulsion.

Assumptions of elliptic planforms and rigid semispans are made, but these assumptions may not be realistic. Therefore, the Fourier coefficients must be found numerically. This can be done using N nodes clustered at the wing tips equally spaced in theta. At the wing tips, l'Hospital's rule is used. Assuming characteristics of the wandering-albatross, 199 nodes, steady periodic flapping, a constant parasitic drag coefficient and a flight speed equal to the minimum dag airspeed without flapping, give a very good efficiency value. It can be seen that it is independent of wing twist and wing loading. These results are not optimized, but if the washout is optimized and the flapping rate changed, an increase in efficiency of 15% can be found. Recovering the power on the upstroke, an increase of another 15% can be obtained showing that significant increases in efficiency can be gained by careful design.

2. Experimental Studies

Three-dimensional experimental studies have covered a wide range of subjects. Some have focused on the study of animals [145–151], including fish [148] and insects [149–151]. Others have focused on different configurations of flight, including bi-planes [152], tandem-wings [153,154], flat plates [155–157], and propellers [158]. Flexibility [159], hover [160–164], and the study of the wake [165–171] and vortices [172–179] of oscillating wings have all been areas of interest in experimental studies as well.

Experimental studies are extremely useful to investigating different designs [180–183], models [184], and methods [185] of flapping flight, as well as testing previously built ornithopters [186]. It is also helpful in examining the many aspects of the wings stroke [187], including the flexibility of the wings [159], the

flapping frequency [188,189], and transition to forward flight [190]. These experimental studies give insight into how to handle the aerodynamic forces [191], especially lift [192].

3. Numerical Studies

There have been many approaches and techniques used to numerically study oscillating wings such as computational fluid dynamics (CFD) [193–195] (including the study of the mesh [196]), efficient multiobjective evolutionary algorithm (e-MOEA) [197], Euler solutions [198], finite element [199], panel codes [200,201], shape morphing [202], and a strong-coupling approach [1]. Some of these techniques have been compared and contrasted in order to determine which purposes each technique is best suited for [203]. These different approaches have also been used to study a variety of subjects including energy extraction [204,205], stall [206], power [207], and thrust [208].

Many different aspects of flight have been numerically studied such as hover [209–221], ground effect [222], and wind gusts [223]. Aspects and configurations of the flying machine have also been studied including flexibility [224,225] and stretching [226] of the wings, bi-wing [227] and tandem-wing [228] configurations, flat plate modeling [229–231], and high-frequency flapping [232]. Butterflies [233], MAVs [234], and the high-altitude long endurance (HALE) aircraft [235] have also been studied numerically.

As has been studied both analytically and experimentally, the vortices [236–243] and wake [244] of oscillating wings are of high interest. All of these studies help to create more accurate models [245–247], better designs [248,249], and optimize aerodynamic properties [250]. The summary of many experimental studies can be seen in Rozhdestvensky and Ryzhov [251].

One technique that has proven useful is an adaptation of Prandtl's [140,141] lifting-line theory [252]. A CFD validation of minimization of induced drag with wing twist using lifting-line theory has been accomplished by Phillips, Fugal, and Spall [253]. They show that the minimum induced drag for a tapered or rectangular wing occurs when

$$\omega(z) = 1 - \frac{\sqrt{1-(2z/b)^2}}{1-(1-R_T)\left|2z/b\right|} \tag{1.103}$$

describes the twist distribution and the total twist is specified by

$$\Omega_{opt} = [2(1+R_T)/\pi\widetilde{C}_{L,\alpha}]C_L \tag{1.104}$$

Their results show that induced drag can be reduced significantly by implementing the appropriate twist. They do find, however, that because the minimization of induced drag varies with the lift coefficient, the optimization can only be done for a single operating condition when using fixed twist. On the other hand, if variable twist is used, then the wing twist could be varied and optimized with the changing lift coefficient.

A number of additional three-dimensional studies have utilized a combination of analytical, numerical, and experimental techniques. Numerical and experimental has been combined most often. These study a range of subjects, including flexibility of the wings [254,255], ground effect [256], modeling using a flat plate [257], and a general summary of past studies [258]. Numerical and analytical techniques were combined to study the flexibility of the wings [259], as well as modeling using a flat plate [260]. It is observed that most work for three-dimensional flapping flight has been done using experimental and numerical studies. A relatively little amount of research has been studied analytically. The present research is aimed to support future analytical work on three-dimensional flapping flight.

C. Purpose of the Present Research

The work that will be presented here is a comparison of the propulsion theory presented by Phillips [134,135] with computational fluid dynamics (CFD). The purpose present research is to extend the CFD work of Hunsaker and Phillips [12] to a three-dimensional finite wing. These three-dimensional CFD results will be compared to results found using the quasi-steady lifting-line model presented by Phillips [134,135].

There are many options of methods that could be used to compare to the work of Phillips [134,135]. A numerical study was decided to be the best option for this comparison. Both panel codes and CFD analysis options were considered. Panel codes are advantageous because they are very fast and inexpensive solvers. However, panel codes cannot grid resolve, approaching a single value as the grid is refined. This makes it so that panel codes can give incorrect solutions very easily and often. Computational fluid dynamics is advantageous because of the wide range of settings and conditions for which it can be used, as well as having the ability to grid resolve. However, CFD analysis can be slower than other methods of numerical analysis, as well as some software can be very expensive. Even with these disadvantages, it was chosen that CFD would be the best option for this study due to the grid resolution.

There are still areas of research missing from the body of work described earlier. The major thing that is still missing from this body of a work is a highly detailed analytical model of flapping flight. Multiple models have been presented, but none have yet to be highly detailed and that can accurately describe

oscillating wings. Many assumptions are made, such as rigid wings, pure plunging, or thin airfoils. A model with very few constraining assumptions is yet to be developed.

Lifting-line theory was chosen to be compared with CFD because this comparison has yet to be made for three-dimensional flapping flight. Phillips [134,135] presented an analytical model using lifting-line theory applied to flapping flight, but no comparison of this model with experimental or numerical study has yet to be presented. As described above, CFD was determined to be the best option to present this comparison. This comparison is needed because lifting-line theory is a steady-state solution, while flapping flight is an unsteady problem. Phillips [134,135] has proposed a quasi-steady solution based on Prandtl's [140,141] steady-state lifting-line theory. This quasi-steady solution can be used to predict the propulsive thrust and required power from the plunging of the airfoil sections along the span of an oscillating finite wing. This model can be used for a wing with arbitrary time-dependent planform, twist distribution, control surface distribution, and plunging distribution. Applying a quasi-steady solution to an unsteady problem requires that a comparison be made either experimentally or numerically in order to observe how well the quasi-steady theory can accurately describe the unsteady problem. The work presented here will contribute to the body of work studying flapping flight by demonstrating the applicability of Prandtl's [140,141] lifting-line theory as has been applied to oscillating wings by Phillips [134,135].

The CFD grid generation software used by Hunsaker and Phillips [12] is capable of generating a three-dimensional wing grid from a two-dimensional airfoil grid. However, this software is not capable of generating a three-dimensional grid that can be used to study flapping wings. Considerable adaptation would need to be made to the grid generation software in order to produce a grid that could be used to study flapping wings. Therefore, as a starting point for the extension of Hunsaker and Phillips' [12] work, uniform sinusoidal plunging and pitching of a rigid rectangular wing with no twist or control surface deflection was chosen. This setup is consistent with both the grid generation software and the quasi-steady lifting-line model presented by Phillips [134,135].

The main objective of this work is to evaluate the analytical model presented by Phillips [134,135] in the ability it has to predict the thrust, power, and efficiency of oscillating wings in certain circumstances. Although Phillips [134,135] presented a relatively general model, the analytical relations presented were for two special cases, rigid-body roll with aileron deflection and small-angle wing flapping with no semispan bending or control surface deflection. Therefore, additional analytical relations will be developed for the lift coefficient, drag coefficient, axial-force coefficient, normal-force coefficient, required-power coefficient, thrust coefficient, and propulsive efficiency. These analytical relations will be for the present

research's special case of uniform sinusoidal plunging and pitching of a rigid wing with not twist or control surface deflection.

Study into how the model Phillips [134,135] presented differs from CFD and experimental results, especially at high frequencies, is of interest in the present work. In order to accomplish this objective, a range of simulations must be done to compare results to those predicted by Phillips [134,135]. These simulations must range in frequency of flapping and ratio of pitching to plunging, as well as fulfilling the requirements of quality CFD work such as being grid resolved, time step resolved, and cycle resolved.

Specific plunging and twist distributions were selected for this research. The twist distribution was selected to be a constant zero across the span for simplicity in later calculations. The plunging distribution of pure rigid-body plunging was studied extensively in four stages. First, a two-dimensional study was performed with steady-state assumptions. The analysis was then progressed to two-dimensional unsteady assumptions. Both of these analyses were compared to analytical conformal mapping results. Once that analysis was completed, three-dimensional analysis was carried out using steady-state settings. Finally, a three-dimensional analysis was completed using unsteady, time-varying settings. This progression allowed for comparison of the two-dimensional results to be compared to the analytical conformal mapping results at different stages and with different assumptions. The same could then be done for the comparison of the three-dimensional results to Phillips' [134,135] model. The research was also completed in this order so that the ultimate goal of simulating three-dimensional unsteady conditions could be reached. Because lifting-line theory is a state-state solution, the steady-state simulations performed at the beginning must compare very closely to lifting-line theory. This then allowed the research to progress with the knowledge that simulations were being performed correctly.

Pure plunging was chosen as the plunging distribution for the majority of the research, as it is a natural starting point for this type of research. Full flapping, and especially mimicking of birds' flapping is extremely complex. In order to start simply to eventually build up to a full flapping simulation in future research, pure plunging was decided to be the plunging distribution for the bulk of the present research.

Phillips [134,135] presentation of the decomposed Fourier coefficients a_n, b_n, c_n, and d_n were shown earlier in Eqs. (1.68), (1.69), (1.70), and (1.71). They are shown here again for reference.

$$\sum_{n=1}^{N} a_n \left[\frac{4b}{\widetilde{C}_{L,\alpha} c(\theta)} + \frac{n}{\sin(\theta)} \right] \sin(n\theta) = 1 \tag{1.68}$$

$$\sum_{n=1}^{N} b_n \left[\frac{4b}{\widetilde{C}_{L,\alpha} c(\theta)} + \frac{n}{\sin(\theta)} \right] \sin(n\theta) = \omega(\theta) \tag{1.69}$$

$$\sum_{n=1}^{N} c_n \left[\frac{4b}{\widetilde{C}_{L,\alpha} c(\theta)} + \frac{n}{\sin(\theta)} \right] \sin(n\theta) = \chi(\theta) \tag{1.70}$$

$$\sum_{n=1}^{N} d_n \left[\frac{4b}{\widetilde{C}_{L,\alpha} c(\theta)} + \frac{n}{\sin(\theta)} \right] \sin(n\theta) = \psi(\theta) \tag{1.71}$$

The present work does not include control surface deflection, therefore, the control surface distribution function $\chi(\theta)$ and the Fourier coefficients c_n are zero for the remainder of the work. In addition to the cases previously presented in Phillips [134,135], an additional special case will be presented. The special case considered will be uniform sinusoidal plunging and pitching of a rigid wing with no twist or control surface deflection. For this special case,

$$\omega(\theta) = 0 \tag{1.105}$$

because the wing used in this research has no washout, and with the entire wing pitching and plunging, there is no washout caused from the flapping cycle. This washout distribution gives a result of the b_n coefficients equal to zero. The plunging distribution for rigid-wing plunging is

$$\psi(\theta) = 1 \tag{1.106}$$

because the entire wing is pitching and plunging at the same time. There is no difference in how the wing is pitching and plunging across the span, and therefore the non-dimensional plunging distribution is Eq. (1.106). It is observed that $a_n = d_n$ with all even coefficients equal to zero. These distributions and coefficients will play a role in the analytical development for the special case of uniform sinusoidal plunging and pitching of a rigid wing with no twist or control surface deflection.

CHAPTER II

COMPUTATIONAL FLUID DYNAMICS METHODOLOGY

The case that this research is focusing on is a starting point for the comparison between CFD solutions and the lifting-line solution presented by Philips [134,135]. This study is focused on an oscillating wing. Because this is just a starting point for the comparison, a simple case of plunging and pitching is studied. The plunging motion is defined using Eq. (1.36)

$$y_{ac}(t) = y_A \sin(\omega t) \tag{2.1}$$

where y_A is the plunging amplitude and ω is the frequency. The pitching motion is defined using Eq. (1.38) and noting that the mean angle of attack is equal to zero

$$\alpha = \alpha_A \cos(\omega t) \tag{2.2}$$

where α_A is the pitching amplitude. These two equations help to define the motion as pure plunging, pure pitching, or a combination of both. In order to leave room for a case with some pitching to be analyzed in the future, both motions are specified. The period of the oscillation cycle is defined as $\tau = 2\pi/\omega$. The period of the cycle can be changed in order to create different cycle times, or different frequencies.

In order to simulate the above case using CFD, a C-O grid about one semispan of a finite wing was used. As can be seen in Figs. 8–10, the i, j, and k directions are defined as shown. A radius of ten chord lengths was used based on past experience. A radius of 20 chord lengths was also tested and it was found that the results were unaffected by the additional radius length.

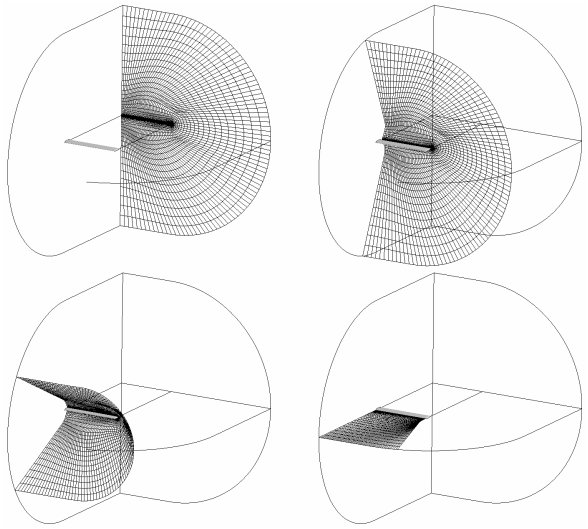

Fig. 8 Constant-i planes for a typical C-O grid (from Alley, Phillips, and Spall [262] with permission).

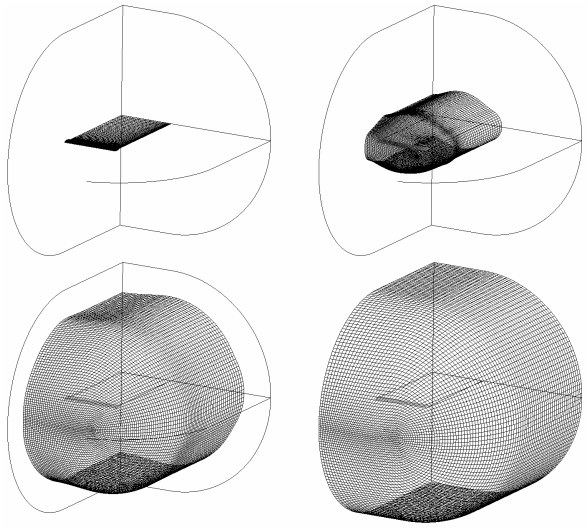

Fig. 9 Constant-j planes for a typical C-O grid (from Alley, Phillips, and Spall [262] with permission).

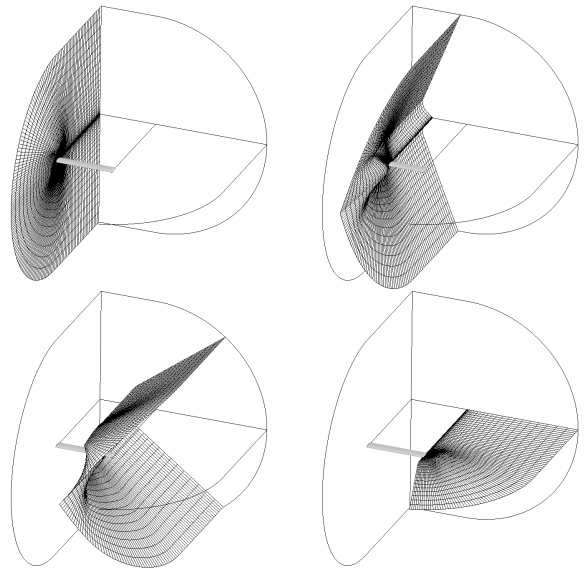

Fig. 10. Constant-k planes for a typical C-O grid (from Alley, Phillips, and Spall [262] with permission).

A. Software Selection

The CFD software to be used had to be selected before any research could be performed. The CFD software selection had multiple factors. The first factor considered was the familiarly with a specific CFD software package. As Star-CCM+ is the CFD software of choice for Utah State University, it is the software that is most familiar. Availability was another factor that was largely considered. Both Star-CCM+ and CFL3D are available through Utah State University resources. Lastly, the motion specification is a major aspect in this research, and therefore, the CFD software chosen needed to be able to easily specify motion so that the steady-periodic and fully unsteady analyses could be performed. All of these factors were considered when choosing the CFD software. Ultimately, version 8.06 of Star-CCM+ [261] by CD-adapco was selected due to the familiarity, availability, and most importantly, the ease of use of the motion specification within the software.

A software selection for the grid generation then had to be determined. Although Star-CCM+ has the ability to create grids, it was decided that separate grid generation software would be used. This was because the geometry being used for this research was very specific and would not be changed throughout the research. Another reason for choosing separate grid generation software was because there was a thoroughly validated grid generation software available for this problem that would create the needed grids very accurately and allowing many user inputs. The grid generation software allowed the user to specify the

wing aspect ratio, taper ratio, design lift coefficient, and root airfoil cross section. This specific grid generation software has been used to produce results for multiple publications [12,253].

The grid generation software allowed the user to create structured grids, while Star-CCM+ creates unstructured grids. Structured is advantageous because of the ability to specify the grid more evenly. Both structured and unstructured grids allow the clustering of nodes in specific areas, but a structured grid does this more efficiently and effectively. Unstructured grids are advantageous because it allows complex geometry to be simulated. However, in the present simulations, the geometry is relatively simple. Although there are advantages to both, it was determined to use a structured grid for the present research. This was because of the ability of the structured grid to cluster nodes in areas that were critical to this research.

B. Grid Generation

Once it was determined that a separate grid generation software was to be used, a grid then needed to be generated for the CFD work. The first step was to create a two-dimensional airfoil grid that was accurate when used in a generic quasi-steady CFD analysis. In order to know if the grid was accurate, an airfoil with a closed-form solution was chosen. Two airfoils were considered, a Joukowski airfoil and a von Kármán Trefftz airfoil. Ultimately, the von Kármán Trefftz airfoil was chosen due to the fact that a Joukowski airfoil has a zero trailing edge angle. Although this is not an issue for the CFD work, this airfoil is not desirable for experimental analysis. Future work may involve experimental analysis, and therefore, an airfoil with a finite trailing edge angle was desired. The original two-dimensional airfoil grid is of great importance to the accuracy of the research because of how the grid generation software works. A two-dimensional grid is created with a root airfoil section, as seen in the top left-hand corner of Fig. 10. This two-dimensional root airfoil section is then duplicated and transformed to create additional planes. These planes are then connected and a three-dimensional grid is created.

The grid was created for a von Kármán Trefftz airfoil with a maximum thickness of 15%, chord length of 0.25 meters, and a zero lift angle of attack of -5°. Nodes for the grid were clustered in four areas: near both the leading and the trailing edge of the airfoil in the chordwise direction, near the wing tip in the spanwise direction, and in the wake region, as shown in Figs. 11, 12, and 13. The software aligned the wake with the freestream, which was also aligned with the root angle of attack. The thick airfoil was chosen for ease of use in the CFD simulations. Many CFD software packages, including Star-CCM+, have difficulty solving the necessary equations when a thin airfoil is used and the thickness of the chosen airfoil allowed easier computations. Star-CCM+ does not have a two-dimensional solver, and therefore, the two-dimensional grid had to be modified to a three-dimensional grid. It was chosen to have three planes in the k

direction and the outer planes were set as symmetry boundaries to simulate a two-dimensional solution while using the three-dimensional solver in Star-CCM+. Figure 14 shows this grid.

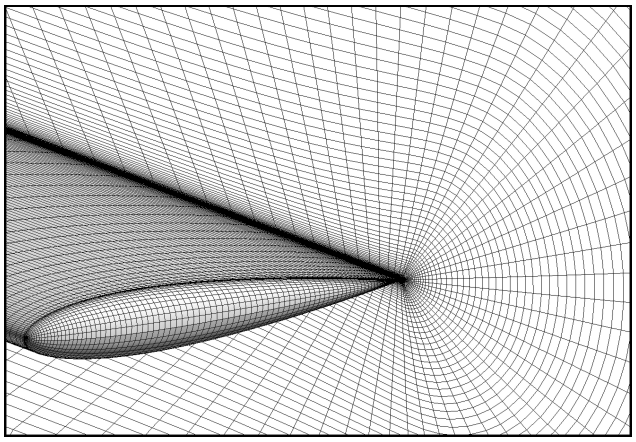

Fig. 11 Example of a constant-i plane at the trailing edge of the wingtip and constant-j plane on the wing surface of a three-dimensional grid (from Alley, Phillips, and Spall [262] with permission).

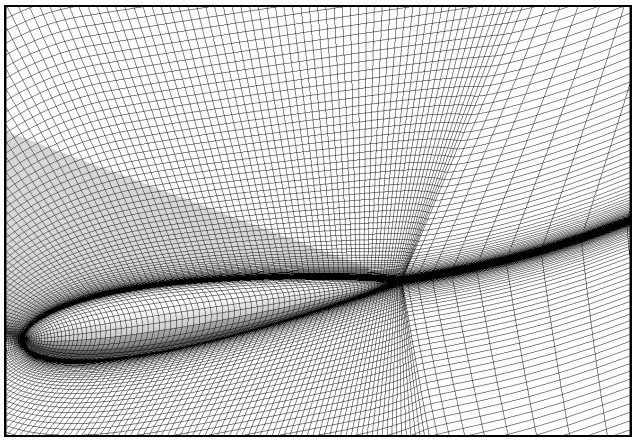

Fig. 12 Example of a constant-k plane at the base of the wing end cap and constant-j plane on the end cap surface of a three-dimensional grid (from Alley, Phillips, and Spall [262] with permission).

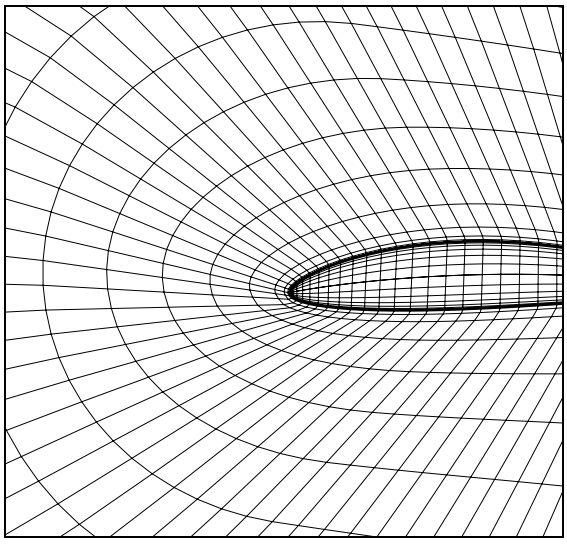

Fig. 13 Constant-k plane at the base of the wing end cap and constant-j plane on the wing surface near the leading edge of the three-dimensional coarse grid.

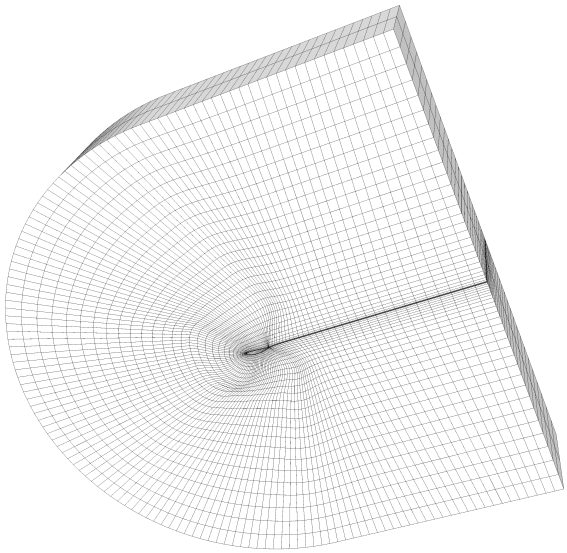

Fig. 14 Coarse grid for two-dimensional CFD calculations.

Once the two-dimensional grid had been created and validated as accurate, which will be shown in a later section, the grid then had to be converted to a three-dimensional grid. This was done using the grid generator and planes in the k direction were added to cover the entire span of the wing and the endcaps can be seen in Fig. 10. Grid resolution was then examined in order to determine the accuracy of the solution.

This grid resolution will be addressed in a following section. The wing was chosen as a rectangular wing with a taper ratio of 1, an aspect ratio, R_A, of 8, a chord length, c, of 0.25 m, and a planform area, S, of 0.5 m^2.

After the three-dimensional grid was created, an overset grid was also created. This overset grid was created in order for the motion of the wing to be simulated against the original, hereafter referred to as the background, grid. This overset grid was produced by taking a center section of the background grid and overlaying it on top of the background grid. The size of the section taken was varied to determine the optimal overset grid. How large of a section needed was determined by varying the number of nodes in the i and j directions and running a quasi-steady case to determine the accuracy. The nodes in the i direction were varied from 9 to 49 in increments of eight, while the nodes in the j direction were varied from 41 to 113, again in increments of eight. The results of each of these variations were then compared to the exact solution. This comparison will be shown in a later section. A two-dimensional view of the overset grid is shown in Fig. 15.

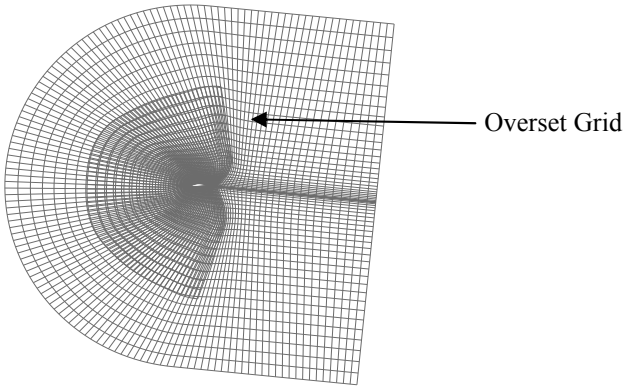

Fig. 15 Overset grid compared to the background grid.

Normally, when a grid generation occurs, there is a hole in the grid where the geometry is. This was the case for the present research. However, an update to the grid generation software was made in order to cover the geometry of the airfoil for the background grid. The hole was still present for the overset grid, as was desired. This grid over the airfoil was very coarse, but the overset grid covered this hole during the CFD analysis so this was not an issue.

C. Quasi-Steady Setup

Once the background and overset grids had been produced, the quasi-steady cases could be set up and the CFD analysis could be carried out. The physics models used were that of constant density, inviscid, segregated flow, three-dimensional, steady flow, and gradients. The gradient method used was the Green-Guass method. The constant density used was set at 1.225 kg/m^3. The reference pressure used was 1 atmosphere and the freestream velocity was 14 m/s in the x-direction. The overset grid velocity changed with each case, dependant upon the angle of attack of the simulation. The starting point velocity was 14 m/s in the x-direction at negative 4 degrees.

There were two regions used, a background region and a foreground region. The background region was a fluid region using the imported background grid from the grid generator described previously and the physics continuum as described in the previous paragraph. There were three boundaries in the background region. First was the farfield, which was set to be a velocity inlet with constant velocity as described above. The second boundary was the $i = 1$ plane, set to be a split outlet with a split ratio of 1. The final boundary in the background was the $k = 1$ plane, which was set as a symmetry plane. As can be seen in Fig. 16, the red region is the farfield, set as a velocity inlet. The blue region seen in Fig. 17, where the farfield region is hidden, is the symmetry plane, and the green region is the split outlet region. The interface to the foreground region and the airfoil can be seen in Fig. 17 as well.

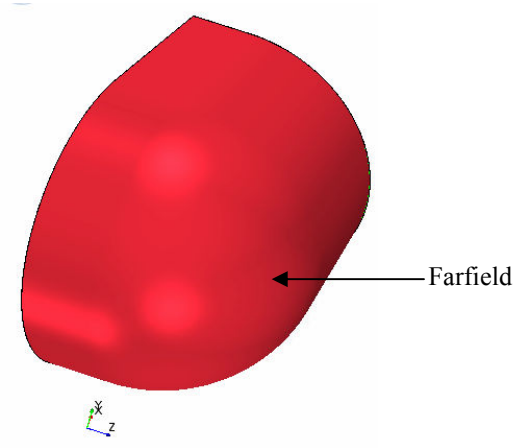

Fig. 16 Star-CCM+ farfield background region.

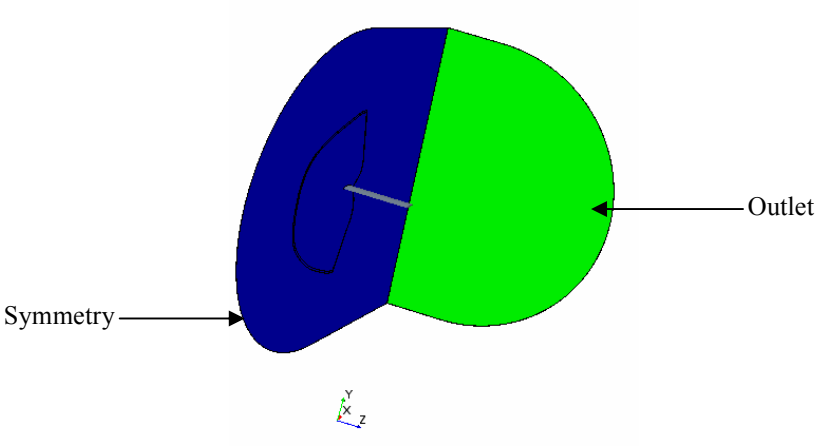

Fig. 17 Star-CCM+ symmetry plane and outlet background regions with the wing foreground region visible.

The foreground region was also a fluid region that used the physics continuum described above and used the imported overset grid from the grid generator. There were three boundaries as well. The first boundary was the wing, which was set to be a slip wall type. The second boundary was the overset grid, which was set as an overset mesh type and acts as the interface to the background grid. The final boundary was the $k = 1$ plane, set as a symmetry plane as in the background region. As seen in Fig. 18, the blue region is the symmetry plane and the grey region is the airfoil. The overset region cannot be seen. However, in Fig. 19, all regions in both the foreground and background can be seen.

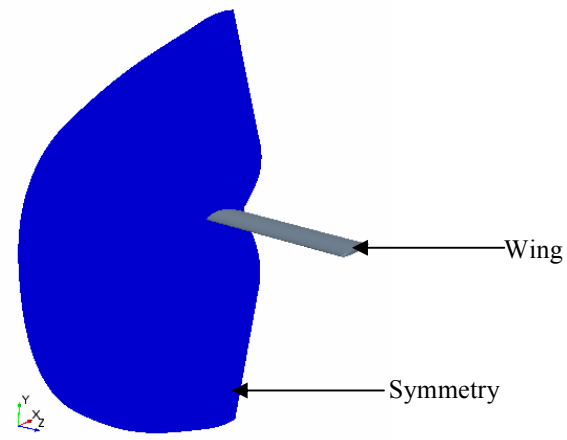

Fig. 18 Star-CCM+ foreground regions.

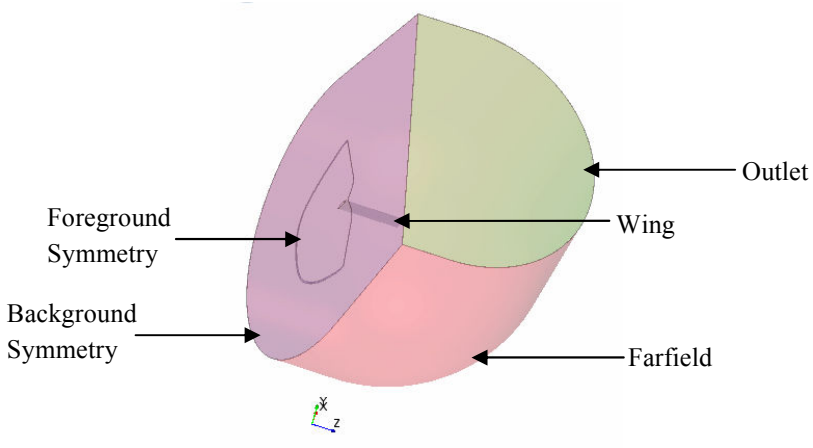

Fig. 19 Star-CCM+ foreground and background regions.

There was an interface created in order to correctly use the overset mesh in the foreground region. This interface was set to use the interpolation option of *distance weighted* in the physics conditions. It was also set as an overset mesh interface type to allow the motion of the overset grid to rotate and slide relative to the background grid.

There were two solvers used, the default partitioning, and also the segregated flow. The default partitioning method uses a per-region method and the default was not changed. The segregated flow solver for the velocity used a linear ramp for the under-relaxation factor and the under-relaxation factor was set to be 0.7. For the pressure, the under-relaxation factor was set to be 0.3, and a linear ramp was also used. The under-relaxation factors were periodically changed when the particular simulation was not converging well. Reducing the under-relaxation factors caused the solution to converge slower, but more effectively.

D. Grid Convergence and Resolution

The Richardson Extrapolation [263] is a widely used and accepted method to extrapolate grid-resolved solution from multiple solutions that are not grid resolved. The Richardson Extrapolation requires three grids to be produced and the results from all of the grids are used together to produce a better estimate of the true solution. A summary of the Richardson Extrapolation and how it was used in the present research will be presented here.

1. Richardson Extrapolation

The Richardson Extrapolation is a numerical method developed by Lewis Fry Richardson [263]. First, the average cell size, denoted as h, is computed as

$$h = \left[\frac{1}{N} \sum_{i=1}^{N} \Delta V_i \right]^{\frac{1}{3}} \tag{2.3}$$

where N is the number of cells and ΔV_i is the volume of the ith cell. The fine, intermediate, and coarse grids are represented by h_1, h_2, and h_3 respectively. Ratios are defined as

$$r_{21} = \frac{h_2}{h_1} \tag{2.4}$$

$$r_{32} = \frac{h_3}{h_2} \tag{2.5}$$

Resulting from the way the grids were created, by halving the number of nodes in each direction of the next finest grid, the ratios are equal

$$r_{21} = r_{32} = 2 \tag{2.6}$$

The apparent order of convergence, denoted as p, is computed as

$$p = \frac{\left| \ln \left| \frac{\varepsilon_{32}}{\varepsilon_{21}} \right| + q(p) \right|}{\ln(r_{21})} \tag{2.7}$$

where

$$\varepsilon_{32} = \phi_3 - \phi_2 \tag{2.8}$$

$$\varepsilon_{21} = \phi_2 - \phi_1 \tag{2.9}$$

and ϕ is the solution from the respective grids. The present research commonly used the lift coefficient as the solution. Therefore, the apparent order of convergence used was

$$p = \frac{\left| \ln \left| \frac{C_{L,3} - C_{L,2}}{C_{L,2} - C_{L,1}} \right| + q(p) \right|}{\ln(r_{21})} \tag{2.10}$$

where C_{L1}, C_{L2}, and C_{L3} represent the fine, medium and coarse grids respectively and

$$q(p) = \ln\left(\frac{r_{21}^{p} - s}{r_{32}^{p} - s}\right) \tag{2.11}$$

where

$$s = sign\left(\frac{C_{L,3} - C_{L,2}}{C_{L,2} - C_{L,1}}\right) \tag{2.12}$$

Note that because in the present research the ratios are constant and equal, $q(p) = 0$.

The first grid resolution that needed to be done was for the two-dimensional background grid. In order to utilize the Richardson Extrapolation [263] as just described, a coarse, medium, and fine grid were generated. The fine grid was first created, with the medium grid being produced by removing every other node from the fine grid. The coarse grid was then created by removing every other node from the medium grid. The Richardson Extrapolation [263] could then be used to extrapolate a grid-resolved solution. The two-dimensional background grid was used the quasi-steady setup previously described to simulate cycles at angles of attack ranging from negative four to positive four. The angle of attack was changed by rotating the direction of the freestream velocity appropriately. Figure 20 shows the results from this study. As can be seen, the Richardson Extrapolation breaks down at the higher angles of attack. This may be due to the fact that the coarse grids could have separated flow due to numerical viscocity.

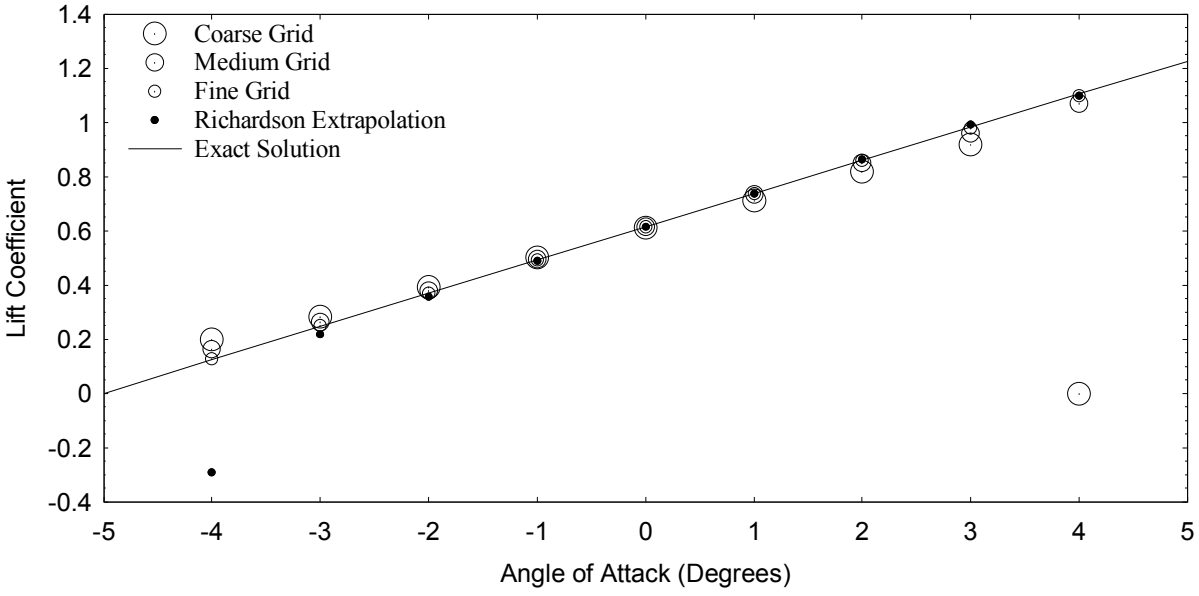

Fig. 20 Comparison of two-dimensional coarse-, medium-, and fine-grids with Richardson Extrapolation to exact lift coefficient.

The next grid that needed to be grid resolved was the three-dimensional grid that was created from the original two-dimensional grid. This was done using a coarse, medium, and fine grid and applying the Richardson Extrapolation as was described earlier. For perspective, the fine grid used had 12,096,000 cells, while the medium contained 1,512,000 cells, and the coarse grid contained 189,000 cells. The lift coefficient results from the quasi-steady cycle can be seen in Fig. 21. As can be seen, both the fine grid and the Richardson Extrapolation very closely follow the quasi-steady lifting-line solution. The error between the fine grid solution and the quasi-steady lifting-line solution was under 0.5%. From this, we can determine that when using the Richardson Extrapolation, the three-dimensional background grid is grid resolved.

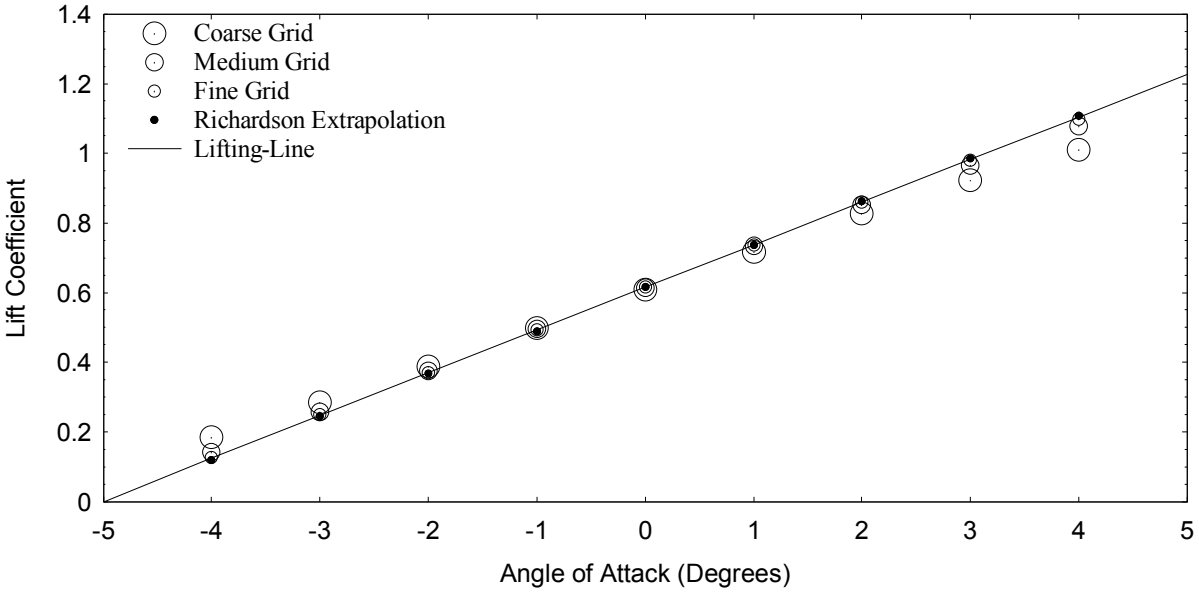

Fig. 21 Coarse-, medium-, and fine-grids compared to the quasi-steady lifting-line solution for the three-dimensional background grid.

The two-dimensional overset grid was the next grid that needed to be grid resolved. Due to the nature of the overset grid, it is possible to change the angle of attack of the airfoil in various ways. There were three options in how to vary the angle of attack. First, the direction of the freestream velocity could be changed to effectively change the angle of attack. Second, the overset grid could be physically rotated against the background grid. Lastly, a velocity could be imparted to the overset grid that would change the angle of attack. All three of these methods were tested, to evaluate the error associated with each method. This was determined by running a set of quasi-steady cases with each option and comparing the errors.

Determining if this method was accurate was critical due to the fact that this was the only possible method of changing the angle of attack for steady-periodic simulations in Star-CCM+. The results can be seen in Figs. 22 – 24 and the error in Fig. 25. It was noted that the error was extremely close for all three methods, which showed that all three methods of changing the angle of attack were equivalent.

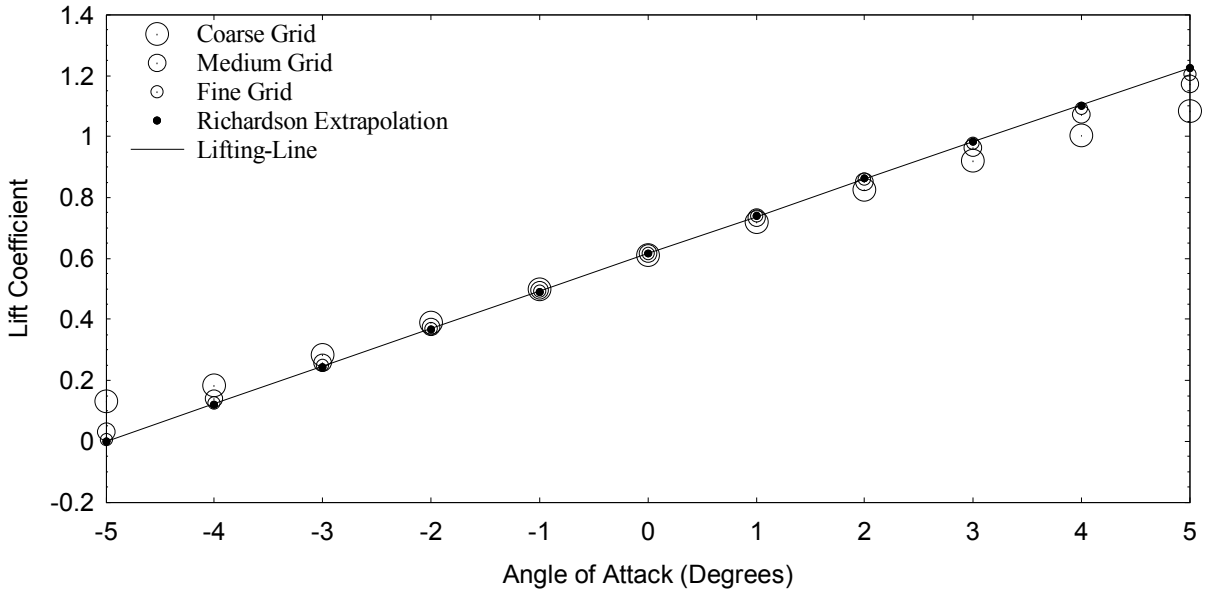

Fig. 22 Lift coefficient when rotating the overset grid.

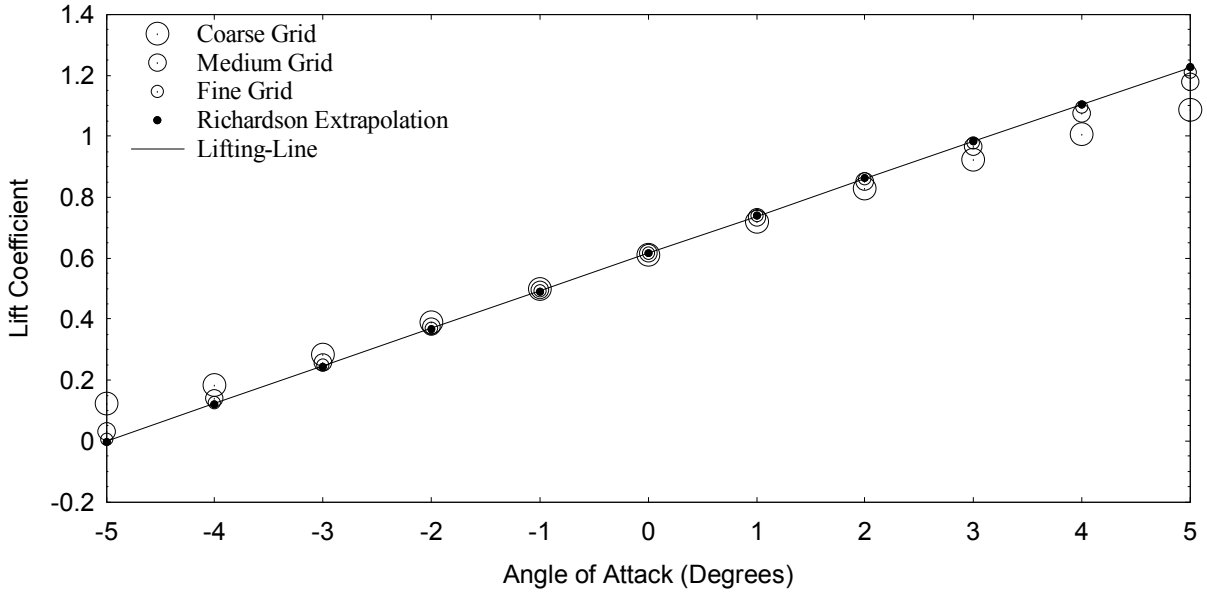

Fig. 23 Lift coefficient when rotating the freestream velocity.

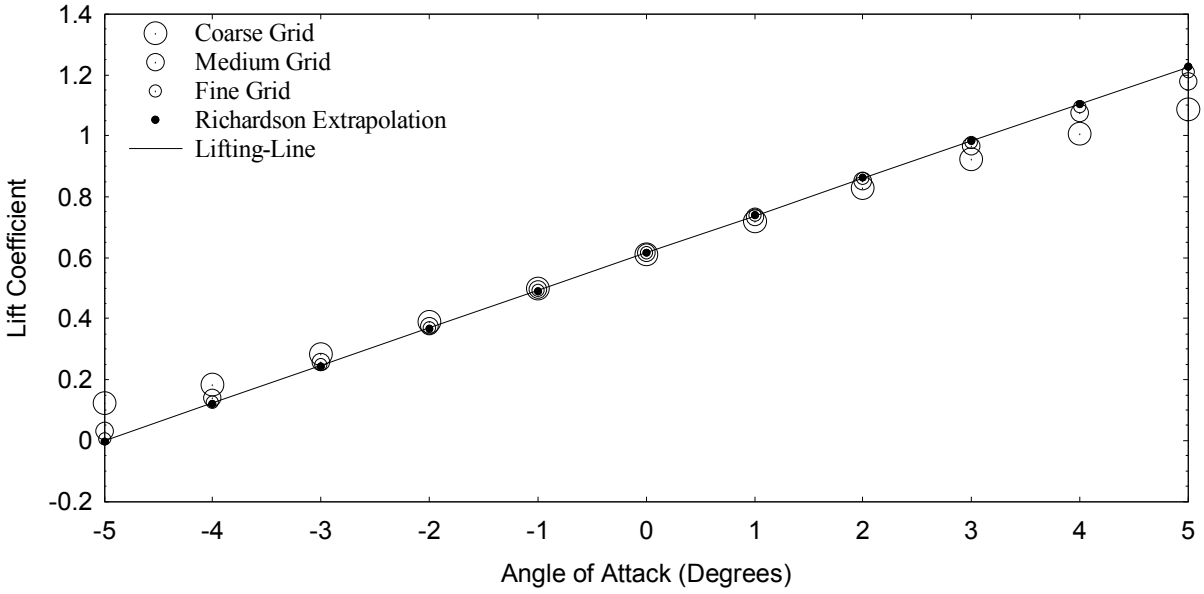

Fig. 24 Lift coefficient when imparting a velocity to the overset grid.

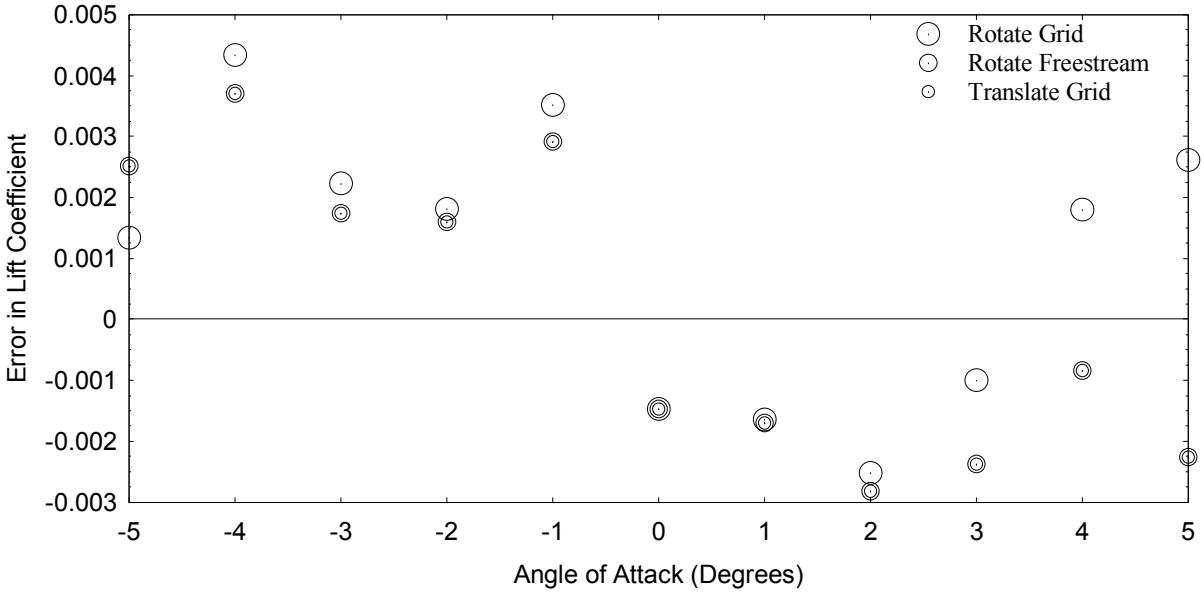

Fig. 25 Error for the Richardson Extrapolation for each angle of attack defining technique.

The overset grid that was chosen had 89 nodes in the j direction, 25 nodes in the i direction, and 337 nodes in the k direction. This gave a fine overset grid with 5,332,240 cells. This grid was determined to be the optimum grid for this research based on the results from the study described previously which varied the nodes in both the i and j directions. Figure 26 shows the comparison of the four overset grids that were the closest to the exact solution along with the overset grid chosen. Figures 27 and 28 show the lift and drag coefficients that were calculated from the overset grid chosen compared to the exact value. Figures 29 and 30 show the error in the axial- and normal-force coefficients. It can be seen in these two figures that the Richardson Extrapolation solution has much more error than the fine grid, especially in the normal-force coefficient. Due to this fact, as well as the earlier indication that at higher angles of attack, the Richardson Extrapolation breaks down with separated flow, the choice was made to discontinue using the Richardson Extrapolation because the Richardson Extrapolation would not be as accurate. The fine grid would be sufficient for this study, as could also be seen in Figs. 20 and 21and therefore the fine grid was used throughout the remainder of the research, and assumed to give grid-resolved results.

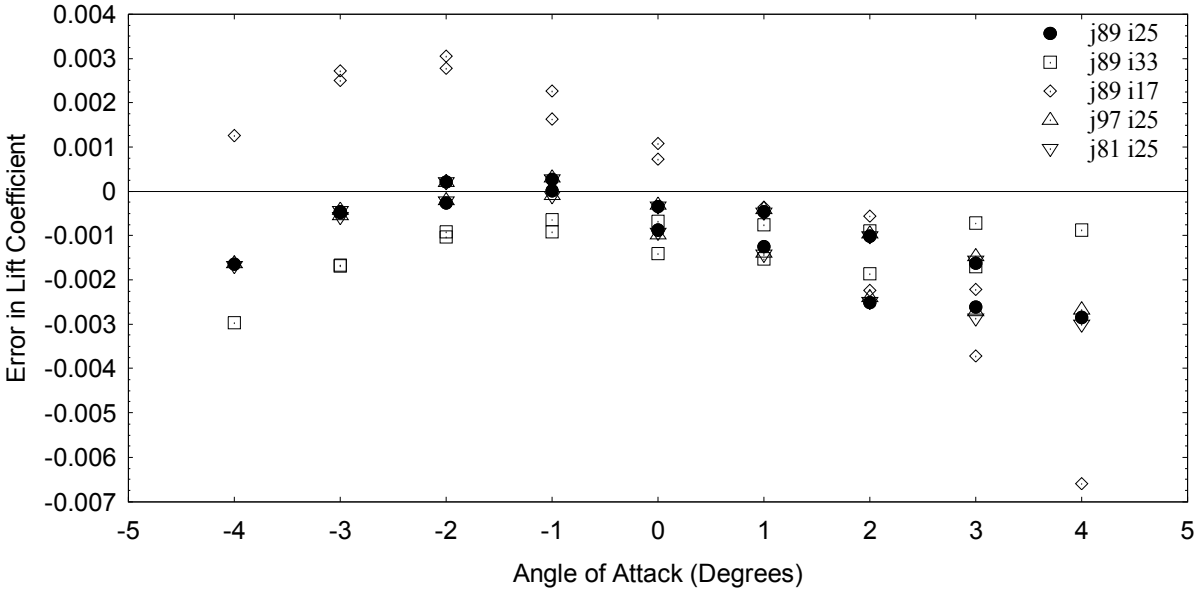

Fig. 26 Comparison of the error in the lift coefficient of the closest overset grids as well as the overset grid chosen, j=89, i=25.

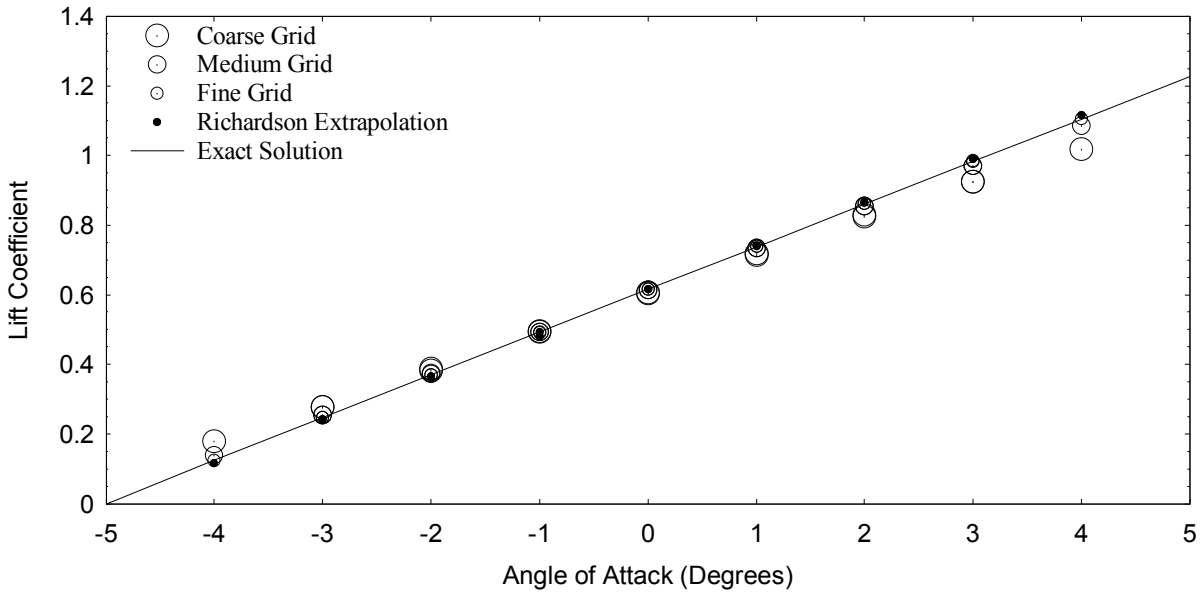

Fig. 27 Lift coefficient of the coarse-, medium-, and fine-grid CFD solutions compared to Richardson Extrapolation solution.

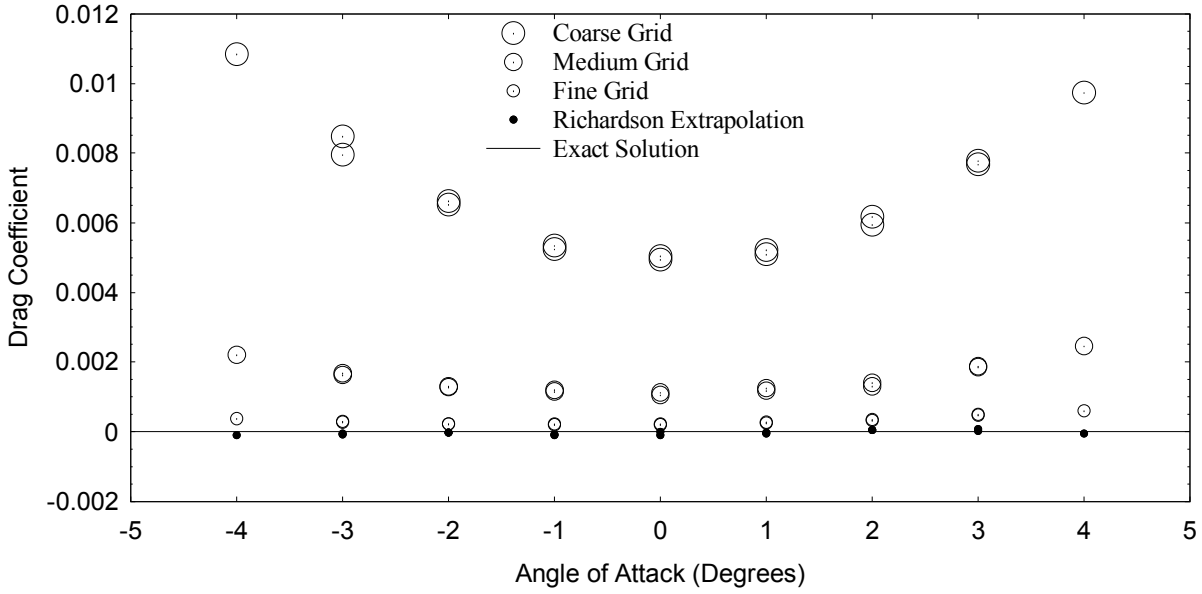

Fig. 28 Drag coefficient of the coarse-, medium-, and fine-grid CFD solutions compared to Richardson Extrapolation solution.

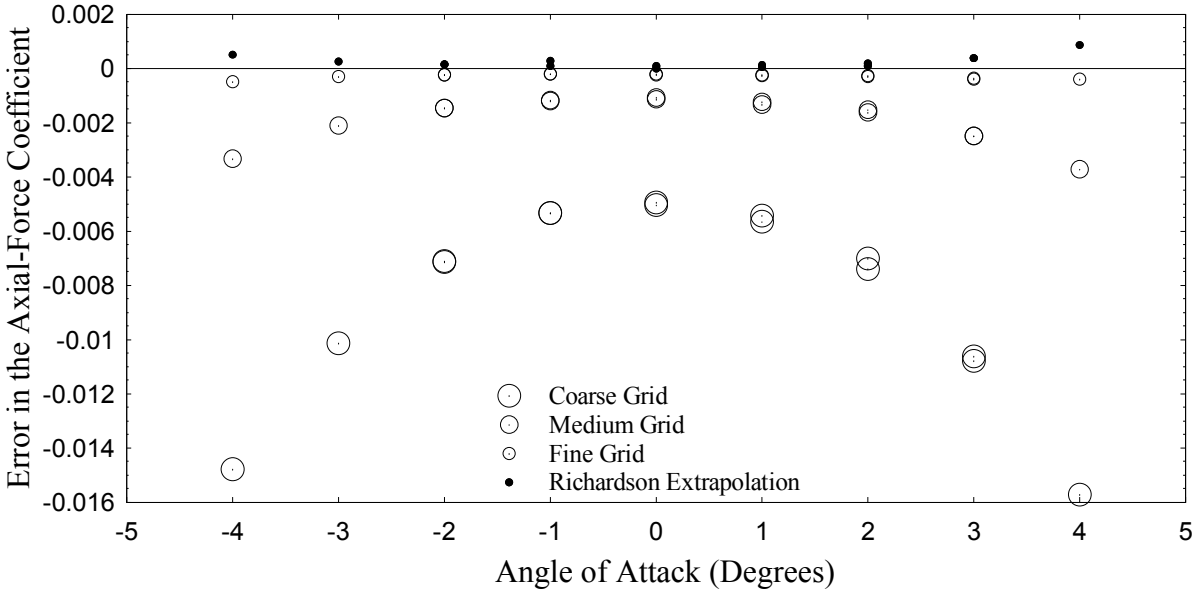

Fig. 29 Error in the axial-force coefficient of the coarse-, medium-, and fine-grid CFD solutions compared to Richardson Extrapolation solution.

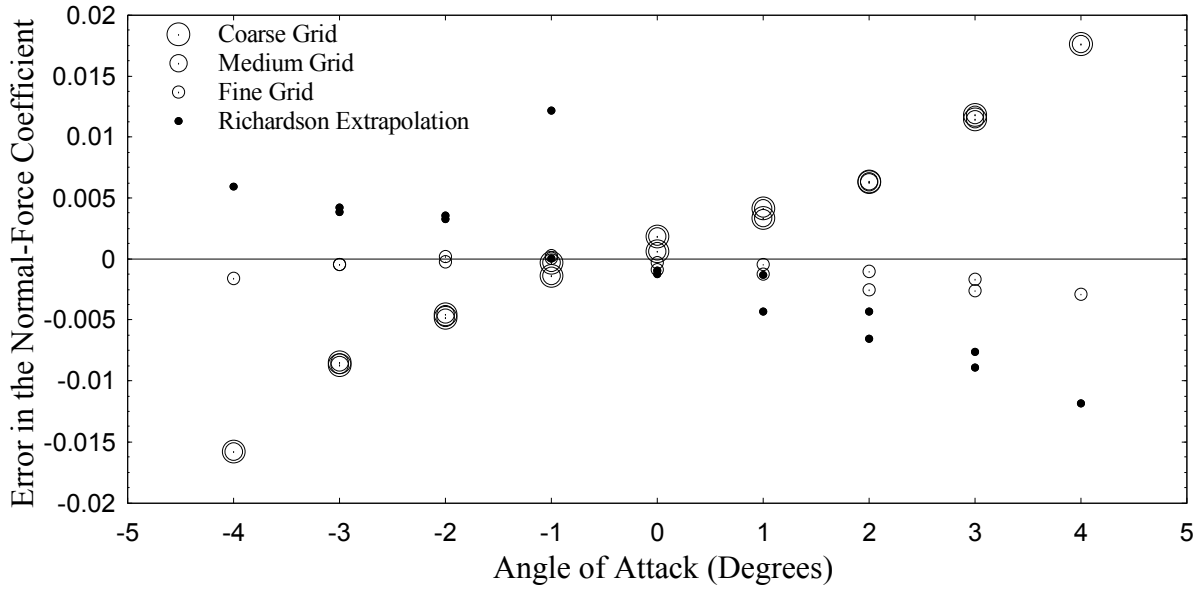

Fig. 30 Error in the normal-force coefficient of the course-,medium-, and fine-grid CFD solutions compared to Richardson Extrapolation Solution.

E. Steady-Periodic Case Setup

The quasi-steady case setup had to be updated to accommodate the next step of simulating a steady-periodic problem. The first setting that needed to be changed was the physics model. Previously, the steady flow model had been used, therefore the physics model needed to be updated to the implicit unsteady setting. The segregated flow solver with a linear ramp was again utilized, but the relaxation factors were adjusted to 0.4 for velocity and 0.1 for pressure.

There were multiple field functions that needed to be added to the simulation and defined. The first of the field functions added was π, equaling 3.141592653589793. It was chosen to define π out to 16 digits because that is the accuracy of machine precision and any digits past 16 would be lost. The next field functions that were defined were R_τ and $\hat{\alpha}_y$. R_τ is a ratio of the period of each new case to the original -5° to 5° case that was simulated. As defined in the previous chapter, $\hat{\alpha}_y$ is the ratio of pitching to plunging of the wing in the cycle. The period of the cycle, τ, is related to the frequency, ω, by

$$\tau = \frac{2\pi}{\omega} \tag{2.13}$$

Using Eqs. (2.13) and (1.21), the reduced frequency in relation to the plunging amplitude, $\hat{\omega}_y$, can be written as

$$\hat{\omega}_y = \frac{y_A 2\pi}{\tau V} \tag{2.14}$$

For the present research, $\overline{\alpha} = 0$. Using Eqs. (2.14) and (1.39), it can be seen the amplitude of the total geometric angle of attack can be shown as

$$\hat{\omega}_y\left(1-\hat{\alpha}_y\right) = \frac{y_A 2\pi}{\tau V}\left(1-\hat{\alpha}_y\right) \tag{2.15}$$

From Eq. (2.15), an original τ_0 and y_{A_0} can be defined. These were the original period and plunging amplitude from the -5° to 5° case that was simulated.

$$\tau_0 = 0.836396554819284 \; seconds \tag{2.16}$$

$$y_{A_0} = 0.139626340159546 \; meters \tag{2.17}$$

This amplitude was chosen to make the angle of attack large enough that the solutions are not dominated by the round off error, but small enough to keep the flow from separating. These constants give an amplitude that accomplishes this. Using the relations

$$\tau = \tau_0 R_\tau (1 - \hat{\alpha}_y) \tag{2.18}$$

$$y_A = y_{A_0} R_\tau \tag{2.19}$$

Which builds in the factor R_τ as the ratio of the new case in comparison to our original case, Eq. (2.15) becomes

$$\hat{\omega}_y \left(1 - \hat{\alpha}_y\right) = \frac{y_{A_0} 2\pi}{\tau_0 V} \tag{2.20}$$

Equations (2.18) and (2.19) were the equations used to define the field functions of τ and y_A in the simulations. From Eq. (1.21) and (1.22), α_A, which represents the amplitude of the pitching motion in the cycle, can be written as

$$\alpha_A = \frac{\hat{\alpha}_y y_A 2\pi}{V\tau} \tag{2.21}$$

Equation (2.21) was used to define the field function α_A in the simulations. The next field function that was defined was named “MyPosition” and defined the position of the airfoil in the simulation. It was defined as

$$MyPosition = y_A \sin\left(\frac{2\pi t}{\tau}\right) \tag{2.22}$$

Three velocities were then described as field functions, a vertical velocity, a rotational velocity, and a translational velocity. The vertical, or normal, velocity was previously defined in Eq. (1.37). The time period, τ, has been substituted in for ω using Eq. (2.13) in Eq. (2.23) below. These field functions were expressed as

$$V_y = \frac{y_A 2\pi}{\tau} \cos\left(\frac{2\pi t}{\tau}\right) \tag{2.23}$$

$$\dot{\alpha} = \frac{\alpha_A 2\pi}{\tau} \sin\left(\frac{2\pi t}{\tau}\right) \tag{2.24}$$

$$V_t = \begin{bmatrix} 0 & V_y & 0 \end{bmatrix} \tag{2.25}$$

Lastly, a start velocity was determined to define what the initial velocity of the wing would be.

$$V_s = \begin{bmatrix} 0 & \frac{y_A 2\pi}{\tau} & 0 \end{bmatrix} \tag{2.26}$$

All of the velocities specified in Eqs. (2.23) – (2.26) were using the reference frame specified by the background coordinates. However, an additional reference frame was needed in order to produce the correct results. This reference frame was set up as a rotating and translating reference frame and was attached to the overset mesh so that the airfoil could move against the background grid. The center of this reference frame was set as the aerodynamic center of the wing. This reference frame will be referred to as the overset reference frame.

A user defined vertex was defined in order to create the transient condition. This user defined vertex was specified as a linear displacement in the y-direction with the field function "MyPosition". This was done by creating both a translational motion using the translation velocity described and a superposing rotation using the rotational velocity described. These were both again attached to the overset grid. This method of specifying motion was chosen because it allowed the pitching and plunging to be more easily specified than other methods of specifying motion.

In conjunction with the transient condition, a time step needed to be defined. The time step that was specified was defined as $\tau/128$, giving 128 time steps per period. As will be shown later, this was determined to be time-step resolved. In order to get a good sampling, three periods were simulated so there was a total of 384 time steps taken. This was also tested to see if the analysis was cycle resolved and will be shown in the following section. The *y*-residual of each time step was required to resolve to not change by 1×10^{-8} for 100 iterations before the simulation would move on to the next time step in the cycle. This assured that each time step was sufficiently converged.

The output of the CFD simulation was forces in the *x* and *y* directions, as well as a moment about the aerodynamic center. These forces were aligned with the background reference frame. The forces were then converted to axial- and normal-force coefficients using the following equations.

$$C_x \equiv \frac{F_x}{\frac{1}{2}\rho V^2 S} \tag{2.27}$$

$$C_y \equiv \frac{F_y}{\frac{1}{2}\rho V^2 S} \tag{2.28}$$

where S is the planform area of 0.50 m^2. Once the axial- and normal-force coefficients were known, the power and thrust coefficients could then be calculated. The power and thrust coefficients are defined as

$$C_P \equiv \frac{-F_y V_y}{\frac{1}{2}\rho V^3 S} \tag{2.29}$$

$$C_T \equiv \frac{T}{\frac{1}{2}\rho V^2 S} \tag{2.30}$$

The power and thrust coefficient were effectively calculated using Eqs. (2.31) and (2.32).

$$C_P = \frac{-C_y V_y}{V} \tag{2.31}$$

$$C_T = -(C_x - C_{x0}) \tag{2.32}$$

where C_{x0} is the axial-force coefficient at the zero plunging velocity points in the cycle. This C_{x0} term is included because it is the induced drag on the wing.

From Eqs. (1.21) and (2.19), the relation between R_τ and ω can be seen to be

$$\omega = \frac{\hat{\omega}_y V}{y_{A_0} R_\tau} \tag{2.33}$$

From Eq. (2.33), it can be seen that ω, the frequency of the oscillation, will decrease as R_τ increases. This is because for a constant $\hat{\alpha}_y$, as is the case in the present research, $\hat{\omega}_y$ will be constant as well. Lifting-line theory has a small ω value, which gives a large R_τ value, and therefore, $\hat{\omega}_x = \omega c \to 0$.

F. Steady-Periodic Convergence

The first thing that needed to be resolved was the time step. As mentioned previously, 128 time steps was ultimately chosen as sufficiently resolved. This was determined by beginning with a cycle with 32 time steps. This time step was doubled to 64, again to 128, and again to 256. When evaluating the results of each of these cycles, it was found that the difference in the mean efficiency result between 128 time steps and 256 time steps was less than 0.26%, and therefore it was determined that the solution was sufficiently time-

step resolved with 128 time steps. Figures 30 and 31 show the power and thrust coefficients of the two cycles compared. The efficiency is defined as the propulsive power available divided by the propulsive power required. This is effectively

$$\eta = \frac{C_T}{C_P} \tag{2.34}$$

As can be seen in Figs. 31 and 32, the difference between the two cycles cannot be seen, and therefore, it can be determined that 128 time steps is time-step resolved.

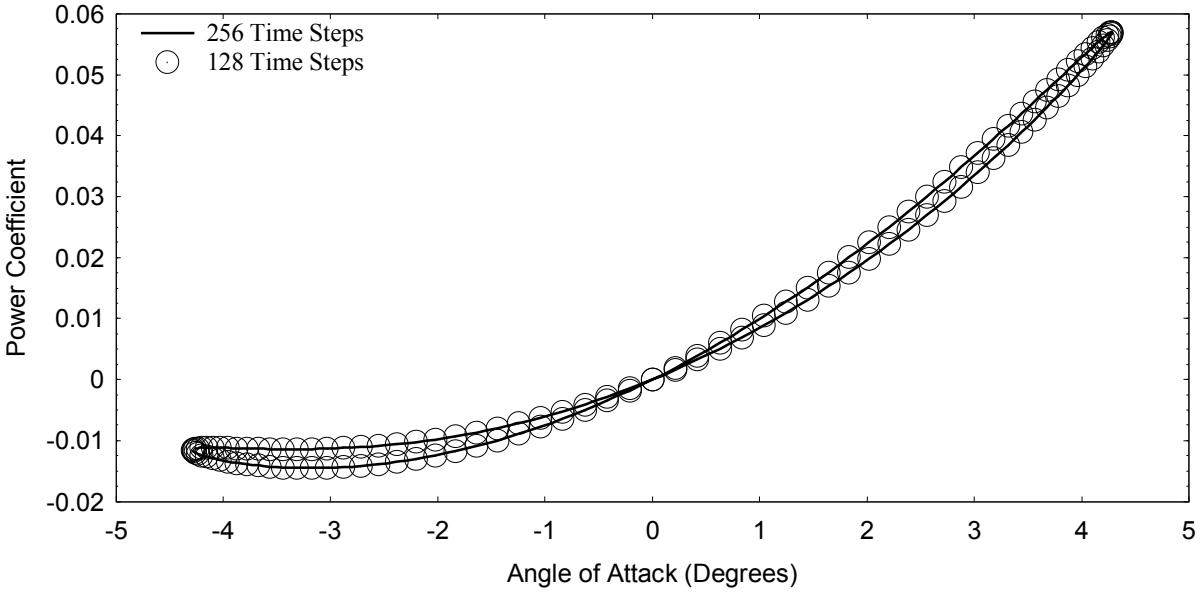

Fig. 31 Time step resolution shown with the comparison of the power coefficient using $\hat{\omega}_x \to 0$ and $\hat{\omega}_y = 0.07492$.

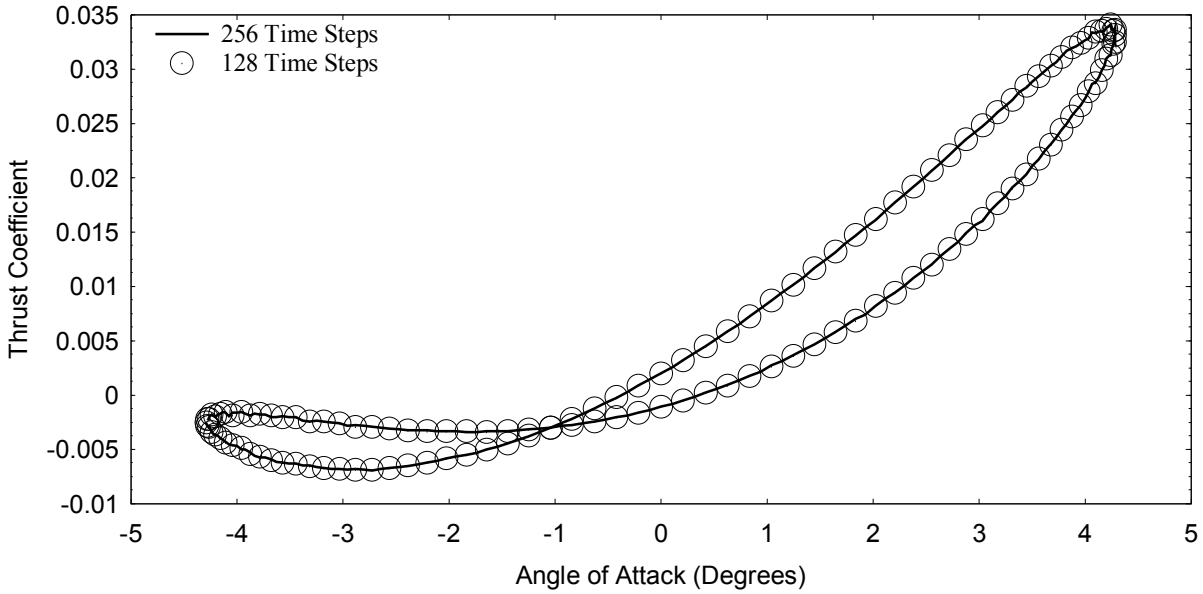

Fig. 32 Time step resolution shown with the comparison of the thrust coefficient using $\hat{\omega}_x \to 0$ and $\hat{\omega}_y = 0.07492$.

The next aspect of the steady-periodic case that needed to be resolved was the cycle. This was done by running the simulation out to eight cycles. Each cycle was compared to the previous cycle and the error was calculated. The mean efficiency error between the third and fourth cycle again was less than 0.30%, and therefore it was determined that the third cycle was resolved. For the remainder of the research, three cycles with 128 time steps per cycle was used. Figures 33 and 34 show the power and thrust coefficients of the two cycles compared. As can be seen in the figures, the difference between the two cycles cannot be seen, and therefore, it can be determined that three cycles is cycle resolved.

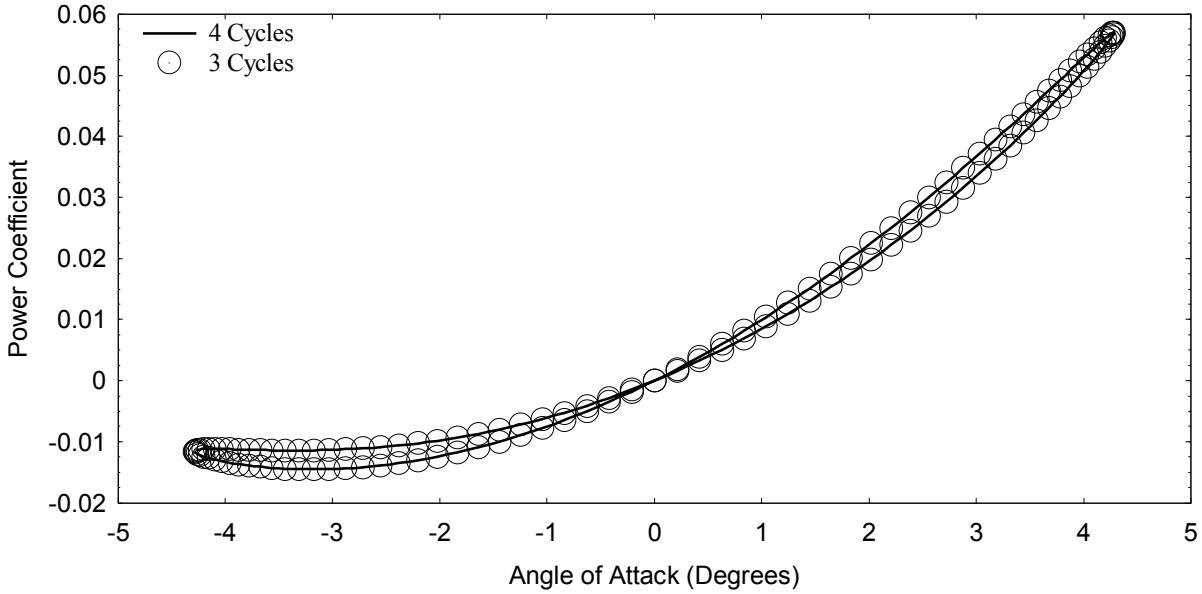

Fig. 33 Cycle resolution shown with the comparison of the power coefficient using $\hat{\omega}_x \to 0$ and $\hat{\omega}_y = 0.07492$.

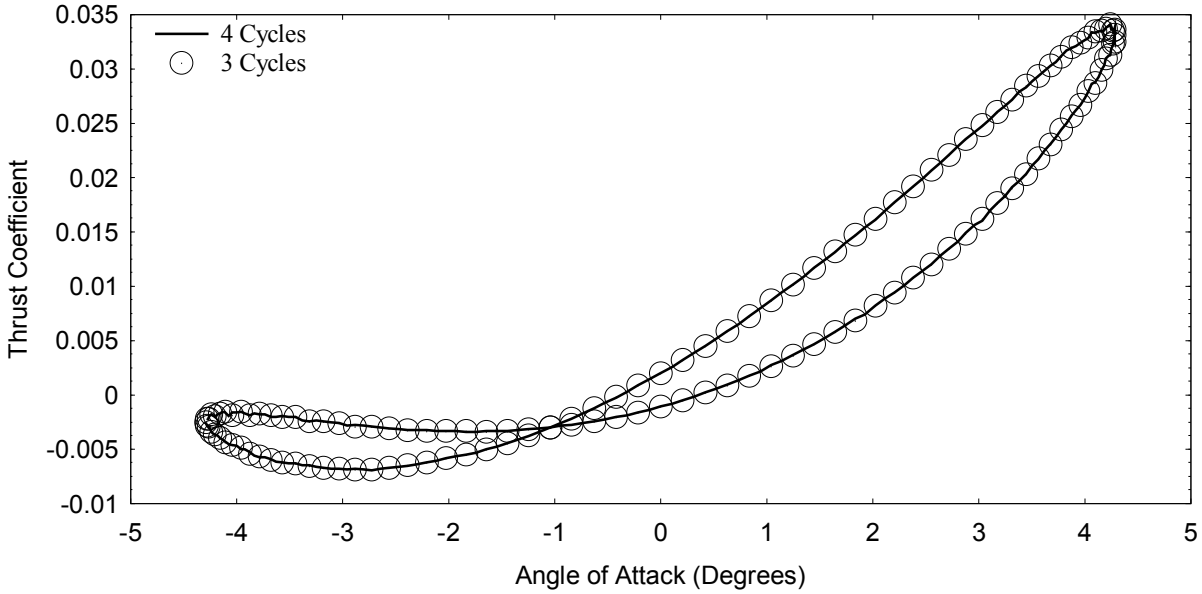

Fig. 34 Cycle resolution shown with the comparison of the thrust coefficient using $\hat{\omega}_x \to 0$ and $\hat{\omega}_y = 0.07492$.

Lastly, the number of iterations the time step could run before terminating needed to be determined. This was necessary because of the time limit on the simulations. The two-dimensional grid's residuals were at the $1x10^{-12}$ level, while the three-dimensional grids resolved at the $1x10^{-8}$ level. The error in the results from each case were compared and it was found that the additional convergence did not make a significant

difference in the solution. Therefore, residuals in the $1x10^{-8}$ level were determined to be acceptable. The simulations that resolved to this level were examined and it was found that all time steps had resolved to the acceptable level well within 2500 iterations. Consequently, each time step was given a maximum of 2500 iterations to converge before moving on automatically to the next time step.

CHAPTER III

RESULTS

A. Quasi-Steady Results

The quasi-steady CFD analysis was completed first. The analysis was done using 128 steps per cycle, equally spaced in angle of attack. Each angle of attack corresponded to a specific point in the cycle. As τ is the period of the cycle, the results are shown in increments of t/τ in order to show the cycle more clearly. The settings used in the quasi-steady analysis were described in a previous chapter. The exact solutions for the two-dimensional portion of the quasi-steady analysis were found using the conformal mapping solution for the von Kármán Trefftz airfoil.

A two-dimensional quasi-steady analysis was conducted first. This analysis included both a background and an overset grid, as described in the previous chapter. This was a large amplitude, low frequency simulation where $\hat{\omega}_x \to 0$, $\hat{\omega}_y = 0.07492$, and $\hat{\alpha}_y = 0.0$ and contained 16 steps per cycle. Figures 35 and 36 show the axial- and normal-force coefficients calculated from Eqs. (2.28) and (2.29), while Figs. 37 and 38 show the power and thrust coefficients calculated from Eqs. (2.32) and (2.33). Table 2 shows the comparison of the mean values of the CFD and the exact solution.

In order to determine the thrust coefficient, the opposite of the axial-force coefficient was added to the average of the two axial-force coefficients at zero plunging velocity in the cycle, which correspond to $t/\tau = 0.25$ and $t/\tau = 0.75$, as shown in Eqs. (3.1) and (3.2). The zero plunging velocity points in the cycle are equivalent to the induced drag for the wing.

$$C_T(t/\tau) = -C_x(t/\tau) + \left(\frac{C_x(0.25) + C_x(0.75)}{2} \right) \tag{3.1}$$

The mean thrust coefficient is then given by

$$\overline{C}_T = -\overline{C}_x + \left(\frac{C_x(0.25) + C_x(0.75)}{2} \right) \tag{3.2}$$

The mean value for the efficiency was obtained using Eq. (2.35), where the efficiency is equal to the propulsive power available divided by the power required. Therefore, the mean value for the efficiency becomes simply the mean propulsive power required divided by the mean power available. This is effectively

$$\overline{\eta} = \frac{\overline{C}_T}{\overline{C}_P} \tag{3.3}$$

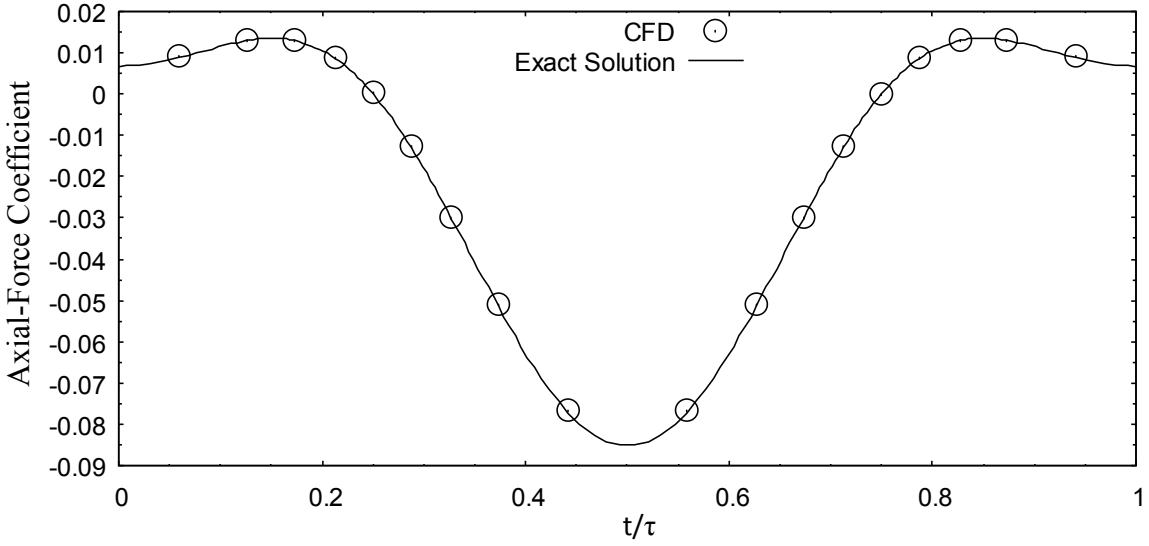

Fig. 35 Axial-force coefficient of the 2D quasi-steady cycle $\hat{\omega}_x \to 0$, $\hat{\omega}_y = 0.07492$, and $\hat{\alpha}_y = 0.0$ compared with the exact solution.

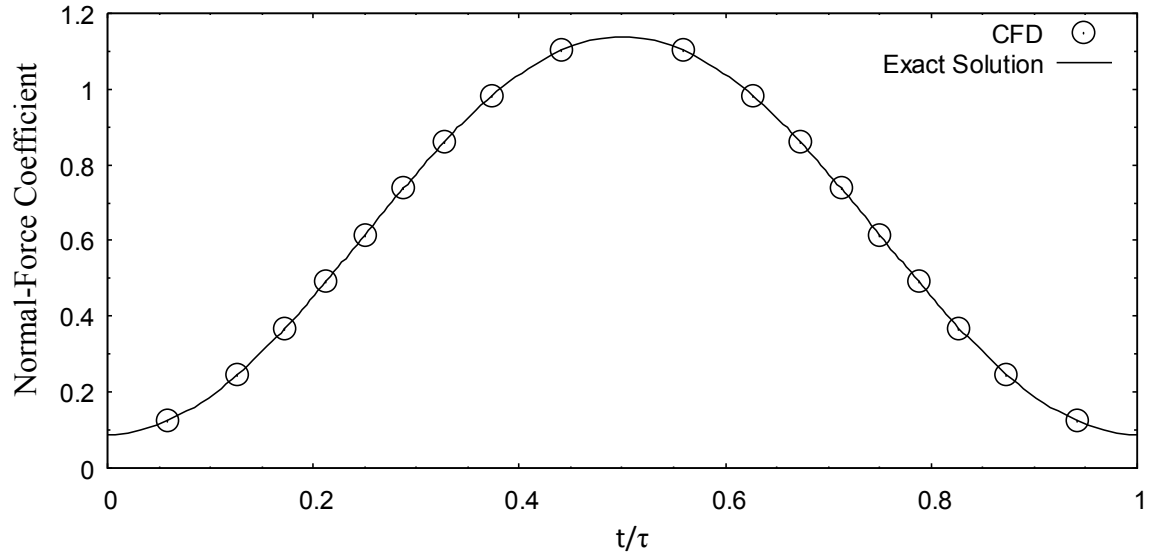

Fig. 36 Normal-force coefficient of the 2D quasi-steady cycle $\hat{\omega}_x \to 0$, $\hat{\omega}_y = 0.07492$, and $\hat{\alpha}_y = 0.0$ compared with the exact solution.

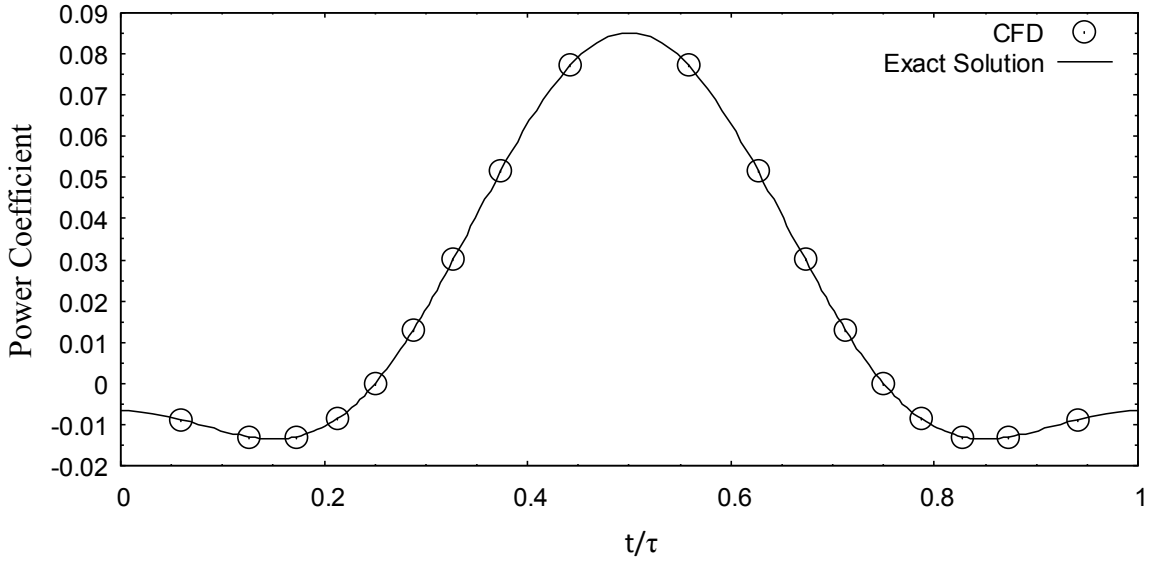

Fig. 37 Power coefficient of the 2D quasi-steady cycle $\hat{\omega}_x \to 0$, $\hat{\omega}_y = 0.07492$, and $\hat{\alpha}_y = 0.0$ compared with the exact solution.

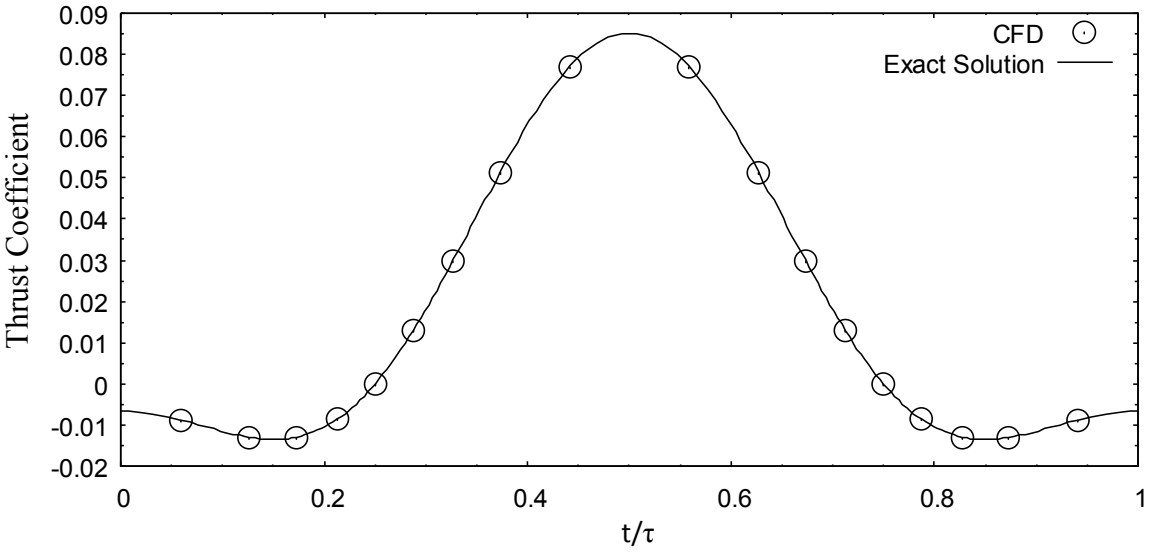

Fig. 38 Thrust coefficient of the 2D quasi-steady cycle $\hat{\omega}_x \to 0$, $\hat{\omega}_y = 0.07492$, and $\hat{\alpha}_y = 0.0$ compared with the exact solution.

Table 2 Mean values of 2D quasi-steady cycle $\hat{\omega}_x \to 0$, $\hat{\omega}_y = 0.07492$, and $\hat{\alpha}_y = 0.0$ compared with the exact solution

	$\hat{\omega}_x \to 0$, $\hat{\omega}_y = 0.07492$, $\hat{\alpha}_y = 0.0$	Exact Solution
Mean Axial-Force Coefficient	-0.013960167928051	-0.0146606046196942
Mean Normal-Force Coefficient	0.615172026114394	0.629625942947288
Mean Power Coefficient	0.0142933161790745	0.0146606046196942
Mean Thrust Coefficient	0.0141730152357757	0.0146606046196942
Mean Efficiency	0.991583412709015	1.0000000000000000

As can be seen in Figs. 35–38, the CFD analysis very closely follows the exact solution. The mean values in Table 2 are also very comparable. This is expected as this first case was a two-dimensional, quasi-steady setup, as the exact solution is.

Next, a three-dimensional case was evaluated. A three-dimensional background grid with an overset grid was analyzed using the quasi-steady setup described in the previous chapter. In order to simulate a full cycle, 128 steps of the full cycle were evaluated separately as quasi-steady cases, as in the two-dimensional quasi-steady case. This was again a large amplitude, low frequency simulation where $\hat{\omega}_x \to 0$ and $\hat{\omega}_y = 0.07492$. However, the pitching amplitude ratio was varied and evaluated at three values. The first simulation used a pitching amplitude ratio of $\hat{\alpha}_y = 0.0$. Figures 39 and 40 show the axial- and normal-force coefficients calculated using Eqs. (2.28) and (2.29), while Figs. 41 and 42 show the power and thrust coefficients calculated using Eqs. (2.32) and (2.33). Table 3 shows the comparison of the mean values of the CFD and the quasi-steady lifting-line solution.

The values for the quasi-steady lifting-line solution were found analytically. The angle of attack due to plunging is defined as

$$\alpha_p \equiv \tan^{-1}\left(\frac{-V_y}{V}\right) \tag{3.4}$$

As can be observed through observation of the airfoil geometry, the following is rotated through the angle of attack due to plunging,

$$C_x = -C_L \sin(\alpha_P) + C_D \cos(\alpha_P) \tag{3.5}$$

The small angle approximation can be used to find

$$C_x = -C_L \alpha_P + C_D \tag{3.6}$$

The small angle approximation can be used to show that

$$\alpha_p = -\frac{V_y}{V} \tag{3.7}$$

and Eq. (3.6) becomes

$$C_x = C_L \frac{V_y}{V} + C_D \tag{3.8}$$

The coefficient of lift is found using Eq. (1.73),

$$C_L = \pi R_A [a_1 (\alpha - \alpha_{L0})_{root} - b_1 \Omega + c_1 \delta_c + d_1 \hat{p}] \tag{3.9}$$

For the present research, there is no control surface deflection or washout. As also discussed earlier, the *d* coefficients are equal to the *a* coefficients. In the present research, the root angle of attack is the same as the angle of attack across the entire span as well. Therefore, substituting Eq. (1.79) into Eq. (3.9), the following is obtained

$$C_L = C_{L,\alpha} (\alpha - \alpha_{L0} + \hat{p}) \tag{3.10}$$

As $\hat{p}$ is the wingtip plunging rate,

$$\hat{p} = \frac{-V_y}{V} \tag{3.11}$$

and α is the angle of attack due to pitching, as shown in Eq. (1.38)

$$\alpha = \overline{\alpha} + \alpha_A \cos\left(\frac{2\pi t}{\tau}\right) \tag{3.12}$$

Eq. (3.10) becomes

$$C_L = C_{L,\alpha} \left(\overline{\alpha} + \alpha_A \cos\left(\frac{2\pi t}{\tau}\right) - \alpha_{L0} - \frac{V_y}{V} \right) \tag{3.13}$$

Using Eqs. (1.37) for the vertical velocity and (1.21) for the reduced frequency, Eq. (3.13) becomes

$$C_L(t) = C_{L,\alpha}\left(\overline{\alpha} + \alpha_A \cos\left(\frac{2\pi t}{\tau}\right) - \alpha_{L0} - \hat{\omega}_y \cos\left(\frac{2\pi t}{\tau}\right)\right) \tag{3.14}$$

For the present research, $\overline{\alpha} = 0$. Using Eq. (1.22) in Eq. (3.14), the following is obtained

$$C_L(t) = C_{L,\alpha}\left(-\hat{\omega}_y\left(1-\hat{\alpha}_y\right)\cos\left(\frac{2\pi t}{\tau}\right) - \alpha_{L0}\right) \tag{3.15}$$

From Eq. (1.78), the coefficient of drag can be found to be

$$C_D = \frac{\left(1+\kappa_D\right){C_L}^2 - \kappa_{DL} C_L C_{L,\alpha}\Omega + \kappa_{D\Omega}\left(C_{L,\alpha}\Omega\right)^2}{\pi R_A} \tag{3.16}$$

As shown in Eqs. (1.81) and (1.82),

$$\kappa_{DL} \equiv 2\frac{b_1}{a_1}\sum_{n=2}^{N} n\frac{a_n}{a_1}\left(\frac{b_n}{b_1} - \frac{a_n}{a_1}\right) \tag{3.17}$$

$$\kappa_{D\Omega} \equiv \left(\frac{b_1}{a_1}\right)^2 \sum_{n=2}^{N} n\left(\frac{b_n}{b_1} - \frac{a_n}{a_1}\right)^2 \tag{3.18}$$

For the present research,

$$\Omega = 0 \tag{3.19}$$

$$\kappa_{DL} = 0 \tag{3.20}$$

$$\kappa_{D\Omega} = 0 \tag{3.21}$$

Therefore, Eq. (3.16) becomes

$$C_D = \frac{\left(1+\kappa_D\right){C_L}^2}{\pi R_A} \tag{3.22}$$

Substituting in the previously determined equation for the lift coefficient, Eq. (3.15), and the equation for the wingtip plunging rate, Eq. (3.11), the following is produced

$$C_D(t) = \frac{(1+\kappa_D){C_{L,\alpha}}^2}{\pi R_A}\alpha_{L0}^2 + \left[\frac{2(1+\kappa_D){C_{L,\alpha}}^2}{\pi R_A}\alpha_{L0}\hat{\omega}_y(1-\hat{\alpha}_y)\right]\cos\left(\frac{2\pi t}{\tau}\right) + \left[\frac{(1+\kappa_D){C_{L,\alpha}}^2}{\pi R_A}\omega_y^2(1-\hat{\alpha}_y)^2\right]\cos^2\left(\frac{2\pi t}{\tau}\right) \tag{3.23}$$

Using Eqs. (3.15) and (3.23) in Eq. (3.8) yields

$$C_x(t) = \frac{(1+\kappa_D){C_{L,\alpha}}^2}{\pi R_A}\alpha_{L0}^2 + \left[\frac{2(1+\kappa_D){C_{L,\alpha}}^2}{\pi R_A}\alpha_{L0}\hat{\omega}_y(1-\hat{\alpha}_y) - C_{L,\alpha}\hat{\omega}_y\alpha_{L0}\right]\cos\left(\frac{2\pi t}{\tau}\right) + \left[\frac{(1+\kappa_D){C_{L,\alpha}}^2}{\pi R_A}\omega_y^2(1-\hat{\alpha}_y)^2 - C_{L,\alpha}\hat{\omega}_y^2(1-\hat{\alpha}_y)\right]\cos^2\left(\frac{2\pi t}{\tau}\right) \tag{3.24}$$

The mean value is then found by integrating Eq. (3.24)

$$\overline{C}_x = \int_0^1 C_x d\left(\frac{t}{\tau}\right) \tag{3.25}$$

resulting in Eq. (3.26)

$$\overline{C}_x = \left[\frac{(1+\kappa_D){C_{L,\alpha}}^2}{\pi R_A}\alpha_{L0}^2\right] + \frac{1}{2}\left[\frac{(1+\kappa_D){C_{L,\alpha}}^2}{\pi R_A}\omega_y^2(1-\hat{\alpha}_y)^2 - C_{L,\alpha}\hat{\omega}_y^2(1-\hat{\alpha}_y)\right] \tag{3.26}$$

The same approach was taken to find the analytical solution for the mean normal-force coefficient. By observation of the airfoil,

$$C_y = C_L\cos(\alpha_p) + C_D\sin(\alpha_p) \tag{3.27}$$

Using the small angle approximation for the both the normal-force coefficient and the plunging angle of attack,

$$C_y = C_L \tag{3.28}$$

Using the coefficients of lift defined in Eq. (3.15), the normal-force coefficient is found to be

$$C_y = C_{L,\alpha}\left(-\hat{\omega}_y\left(1-\hat{\alpha}_y\right)\cos\left(\frac{2\pi t}{\tau}\right)-\alpha_{L0}\right) \tag{3.29}$$

The mean value is then found by integrating Eq. (3.29)

$$\overline{C}_y = \int_0^1 C_y d\left(\frac{t}{\tau}\right) \tag{3.30}$$

which results in

$$\overline{C}_y = -C_{L,\alpha}\alpha_{L0} \tag{3.31}$$

The mean power coefficient could then be found using Eq. (2.32)

$$C_P = \frac{-C_y V_y}{V} \tag{3.32}$$

and substituting in Eq. (1.37) and (1.21) to find

$$C_P = -C_y\hat{\omega}_y\cos\left(\frac{2\pi t}{\tau}\right) \tag{3.33}$$

The previously found equation for the normal-force coefficient, Eq. (3.29) can then be used in Eq. (3.33) to obtain

$$C_P = C_{L,\alpha}\alpha_{L0}\hat{\omega}_y\cos\left(\frac{2\pi t}{\tau}\right)+C_{L,\alpha}\hat{\omega}_y^2\left(1-\hat{\alpha}_y\right)\cos^2\left(\frac{2\pi t}{\tau}\right) \tag{3.34}$$

The mean value could then be found by integrating Eq. (3.34)

$$\overline{C}_P = \int_0^1 C_P d\left(\frac{t}{\tau}\right) \tag{3.35}$$

The integration in Eq. (3.35) results in

$$\overline{C}_P = \frac{1}{2}\left[C_{L,\alpha}\hat{\omega}_y^2\left(1-\hat{\alpha}_y\right)\right] \tag{3.36}$$

Lastly, the thrust coefficient was found by using Eq. (2.33)

$$C_T = -(C_x - C_{x0}) \tag{3.37}$$

where C_{x0} is the axial-force coefficient at the points in the cycle with no plunging. Using Eqs. (3.8), (3.22) and recognizing that there is no plunging,

$$C_{x0} = C_D = \left.\frac{(1+\kappa_D)C_L^2}{\pi R_A}\right|_{\hat{p}=0} \tag{3.38}$$

and after applying Eqs. (3.10), (3.12), and (1.22)

$$C_{x0} = \frac{(1+\kappa_D)C_{L,\alpha}^2}{\pi R_A}\alpha_{L0}^2 \tag{3.39}$$

Substituting Eqs. (3.39) and Eq. (3.24) into Eq. (3.37), the following is obtained

$$\begin{aligned} C_T = &\left[C_{L,\alpha}\hat{\omega}_y\alpha_{L0} - \frac{2(1+\kappa_D)C_{L,\alpha}^2\alpha_{L0}\hat{\omega}_y(1-\hat{\alpha}_y)}{\pi R_A}\right]\cos\left(\frac{2\pi t}{\tau}\right) \\ &+\left[C_{L,\alpha}\hat{\omega}_y^2(1-\hat{\alpha}_y) - \frac{(1+\kappa_D)C_{L,\alpha}^2\hat{\omega}_y^2(1-\hat{\alpha}_y)^2}{\pi R_A}\right]\cos^2\left(\frac{2\pi t}{\tau}\right) \end{aligned} \tag{3.40}$$

The thrust coefficient is integrated to obtain the mean thrust coefficient

$$\overline{C}_T = \int_0^1 C_T\, d\left(\frac{t}{\tau}\right) \tag{3.41}$$

such that Eq. (3.42) is obtained when Eq. (3.40) is substituted in

$$\overline{C}_T = \frac{1}{2}\left[C_{L,\alpha}\hat{\omega}_y^2(1-\hat{\alpha}_y) - \frac{(1+\kappa_D)C_{L,\alpha}^2\hat{\omega}_y^2(1-\hat{\alpha}_y)^2}{\pi R_A}\right] \tag{3.42}$$

The mean efficiency was then calculated using Eq. (3.3) and substituting Eqs. (3.36) and (3.42)

$$\overline{\eta} = 1 - \frac{(1+\kappa_D) C_{L,\alpha} \left(1 - \hat{\alpha}_y\right)}{\pi R_A} \tag{3.43}$$

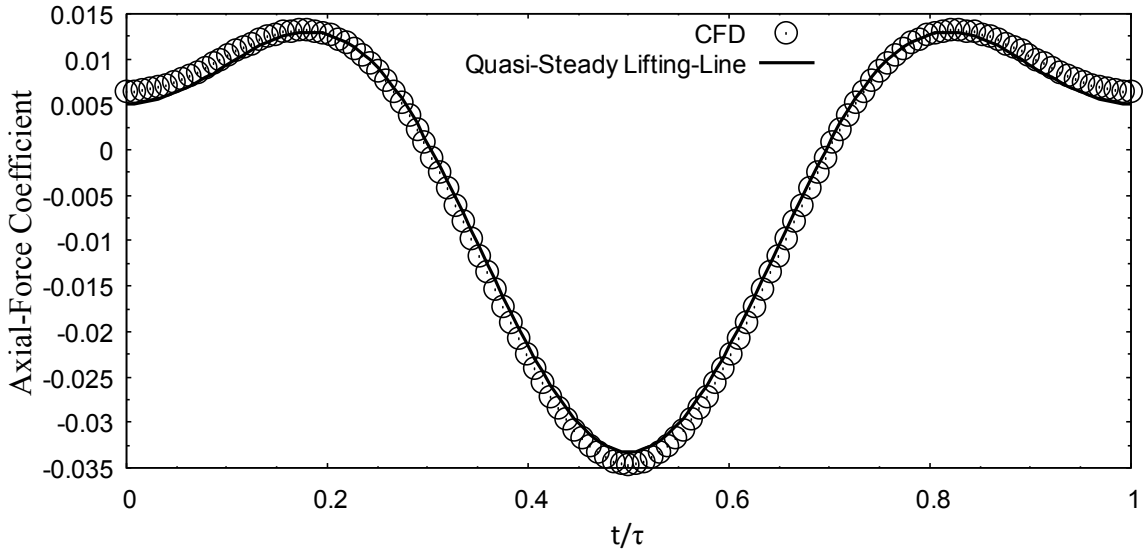

Fig. 39 Axial-force coefficient of the 3D quasi-steady cycle $\hat{\omega}_x \to 0$, $\hat{\omega}_y = 0.07492$, and $\hat{\alpha}_y = 0.0$ compared with the quasi-steady lifting-line solution, Eq. (3.24).

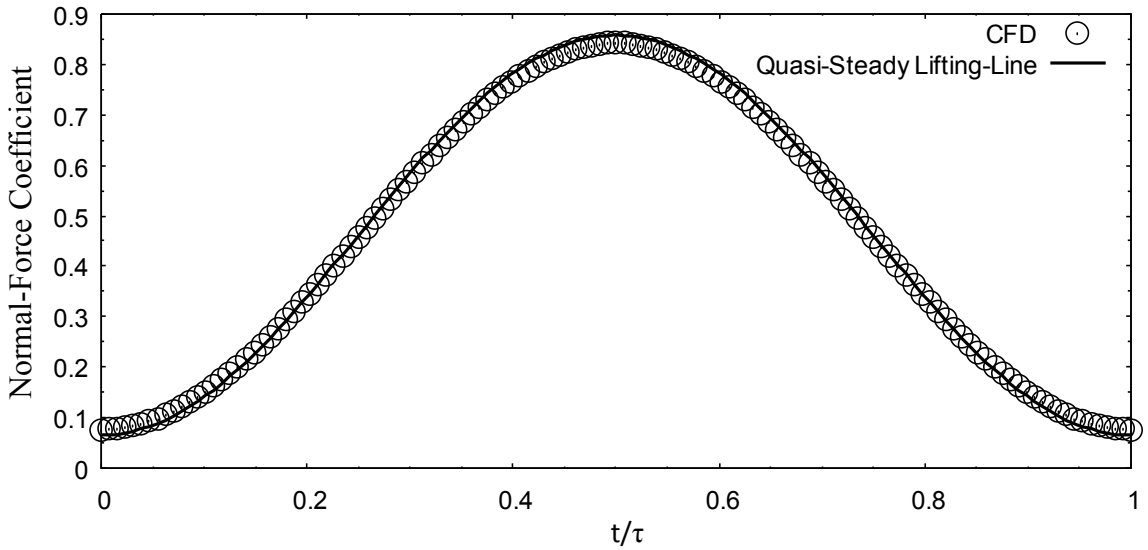

Fig. 40 Normal-force coefficient of the 3D quasi-steady cycle $\hat{\omega}_x \to 0$, $\hat{\omega}_y = 0.07492$, and $\hat{\alpha}_y = 0.0$ compared with the quasi-steady lifting-line solution, Eq. (3.29).

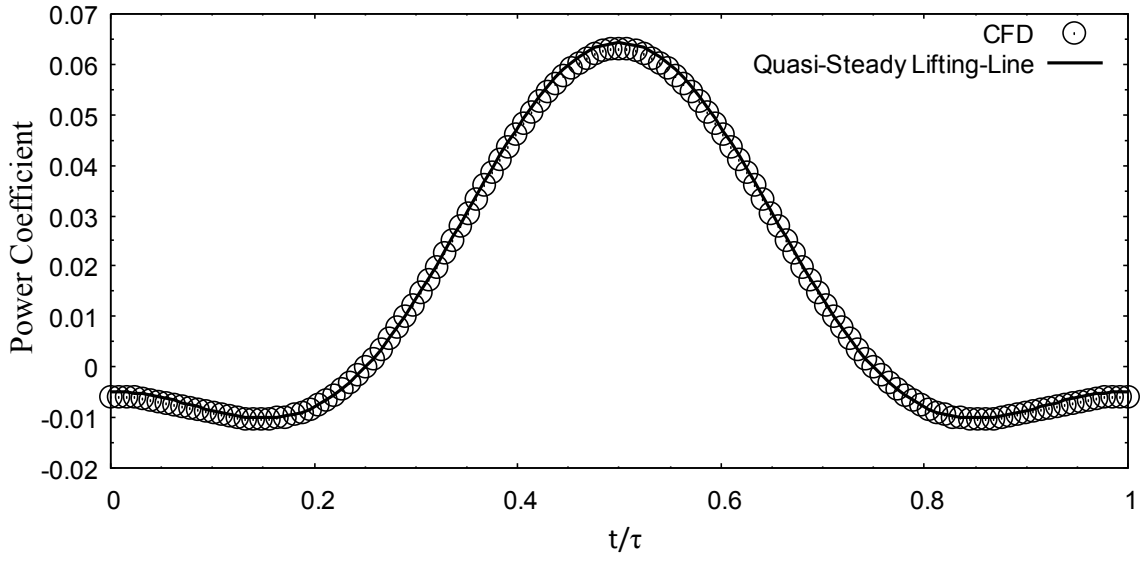

Fig. 41 Power coefficient of the 3D quasi-steady cycle $\hat{\omega}_x \to 0$, $\hat{\omega}_y = 0.07492$, and $\hat{\alpha}_y = 0.0$ compared with the quasi-steady lifting-line solution, Eq. (3.34).

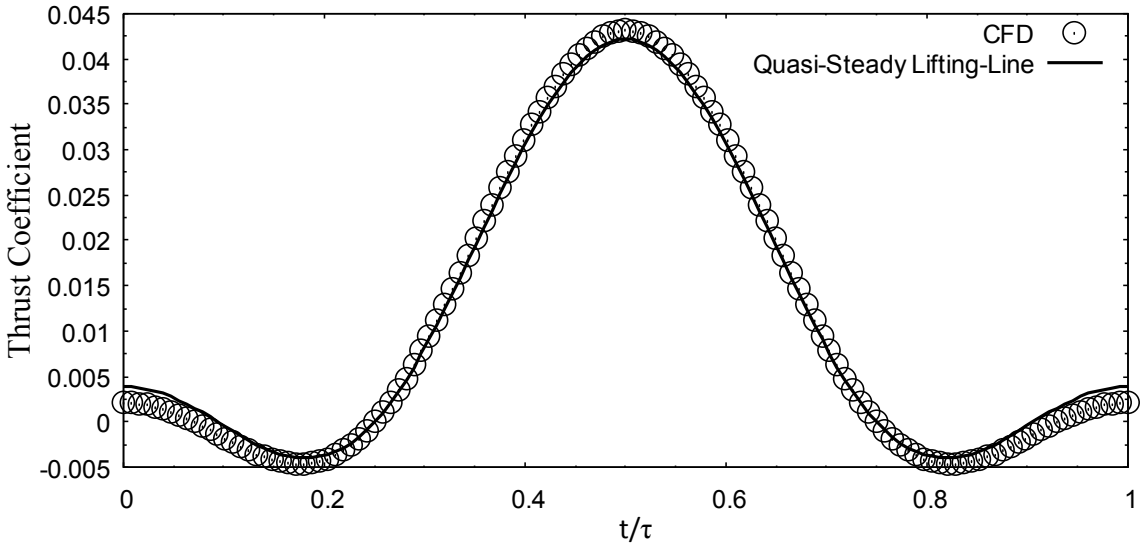

Fig. 42 Thrust coefficient of the 3D quasi-steady cycle $\hat{\omega}_x \to 0$, $\hat{\omega}_y = 0.07492$, and $\hat{\alpha}_y = 0.0$ compared with the quasi-steady lifting-line solution, Eq. (3.40).

Table 3 Mean values of 3D quasi-steady cycle $\hat{\omega}_x \to 0$, $\hat{\omega}_y = 0.07492$, and $\hat{\alpha}_y = 0.0$ compared with the quasi-steady lifting-line solution

	$\hat{\omega}_x \to 0$, $\hat{\omega}_y = 0.07492$, $\hat{\alpha}_y = 0.0$	Quasi-Steady Lifting-Line
Mean Axial-Force Coefficient	-0.002708695331591	-0.002556914522526
Mean Normal-Force Coefficient	0.458295820144760	0.461438397544391
Mean Power Coefficient	0.014339674260158	0.014840559242373
Mean Thrust Coefficient	0.011332766799852	0.011532618698595
Mean Efficiency	0.790308524046427	0.777101355160974

As can be seen in Figs. 39–42, the CFD solutions closely follow the quasi-steady lifting-line solution. However, it is noticed that it differs more than the two-dimensional quasi-steady CFD differed from the exact conformal mapping solution.

The next simulation was completed with $\hat{\omega}_x \to 0$, $\hat{\omega}_y = 0.09365$, and $\hat{\alpha}_y = 0.2$. Again, 128 time steps were used in order to evaluate a full cycle. Figures 43 and 44 show the axial- and normal-force coefficients, calculated using Eqs. (2.28) and (2.29), while Figs. 45 and 46 show the power and thrust coefficients calculated using Eqs. (2.32) and (2.33). Table 4 shows the comparison of the mean values of the CFD and the quasi-steady lifting-line solution.

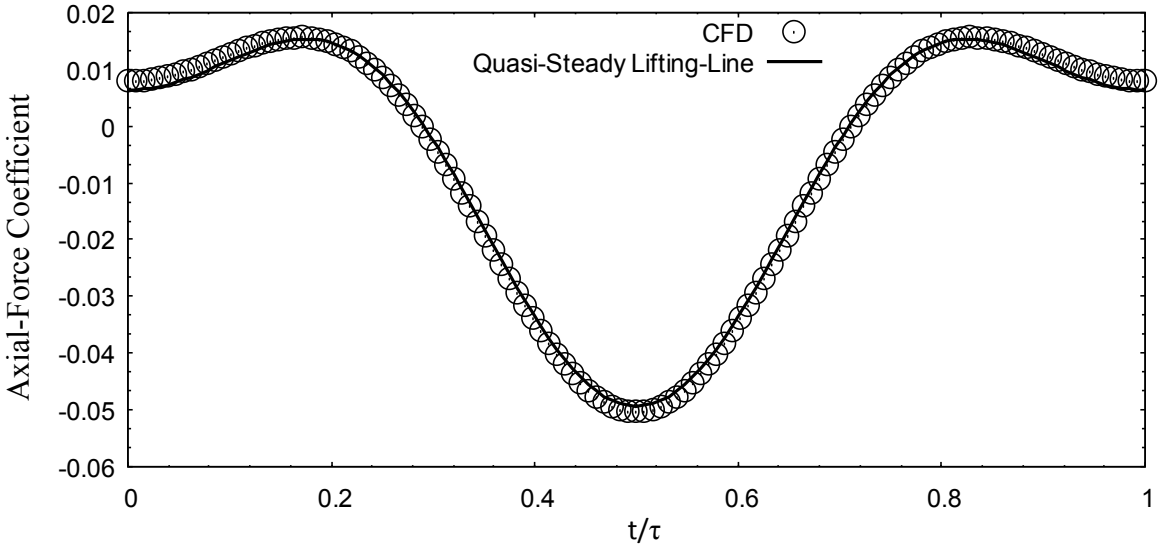

Fig. 43 Axial-force coefficient of the 3D quasi-steady cycle $\hat{\omega}_x \to 0$, $\hat{\omega}_y = 0.09365$, and $\hat{\alpha}_y = 0.2$ compared with the quasi-steady lifting-line solution, Eq. (3.24).

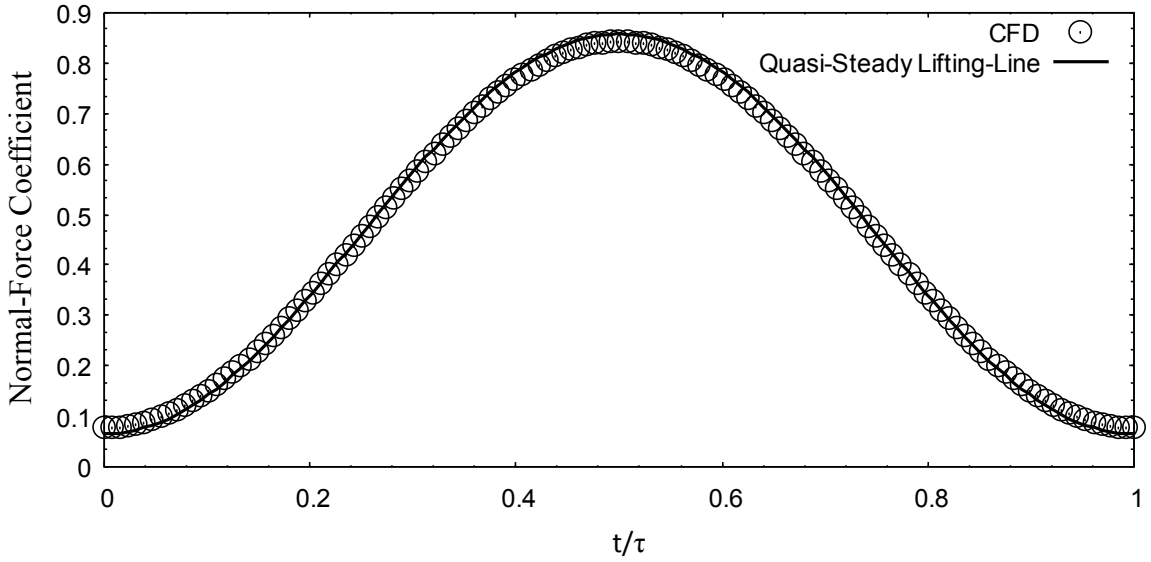

Fig. 44 Normal-force coefficient of the 3D quasi-steady cycle $\hat{\omega}_x \to 0$, $\hat{\omega}_y = 0.09365$, and $\hat{\alpha}_y = 0.2$ compared with the quasi-steady lifting-line solution, Eq. (3.29).

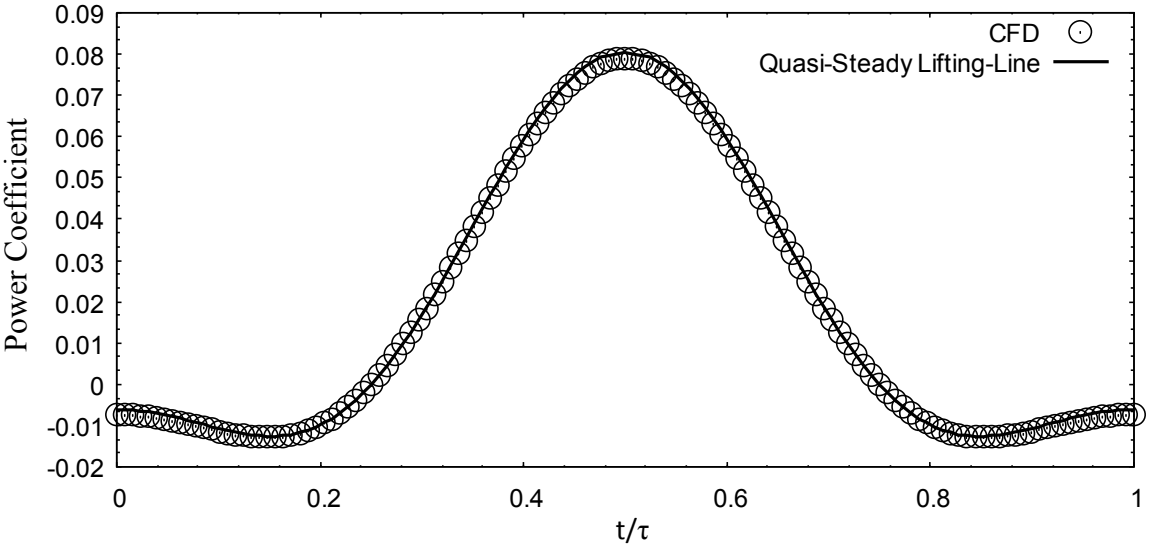

Fig. 45 Power coefficient of the 3D quasi-steady cycle $\hat{\omega}_x \to 0$, $\hat{\omega}_y = 0.09365$, and $\hat{\alpha}_y = 0.2$ compared with the quasi-steady lifting-line solution, Eq. (3.34).

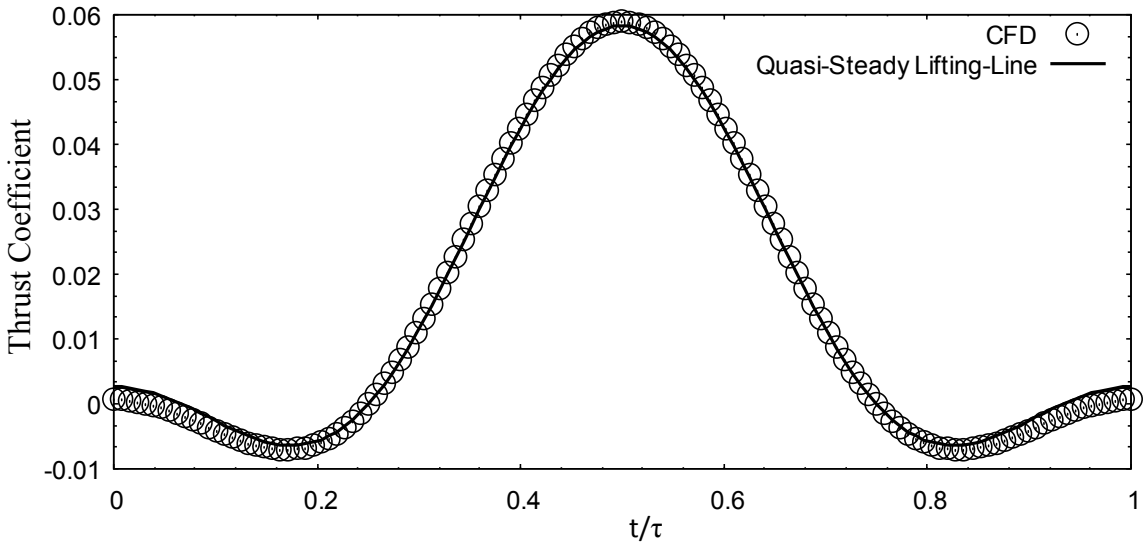

Fig. 46 Thrust coefficient of the 3D quasi-steady cycle $\hat{\omega}_x \to 0$, $\hat{\omega}_y = 0.09365$, and $\hat{\alpha}_y = 0.2$ compared with the quasi-steady lifting-line solution, Eq. (3.40).

Table 4 Mean values of 3D quasi-steady cycle $\hat{\omega}_x \to 0$, $\hat{\omega}_y = 0.09365$, and $\hat{\alpha}_y = 0.2$ compared with the quasi-steady lifting-line solution

	$\hat{\omega}_x \to 0$, $\hat{\omega}_y = 0.09365$, $\hat{\alpha}_y = 0.2$	Quasi-Steady Lifting-Line
Mean Axial-Force Coefficient	-0.006266960080557	-0.006267054333119
Mean Normal-Force Coefficient	0.458547645167638	0.461438397544391
Mean Power Coefficient	0.017939885711920	0.018550699052966
Mean Thrust Coefficient	0.014903433518451	0.015242758509188
Mean Efficiency	0.830742946625847	0.821681084128779

As can be seen in Figs. 43–46, the CFD solutions very closely follow the quasi-steady lifting-line solution. This difference between the CFD and the quasi-steady lifting-line solution using $\hat{\alpha}_y = 0.2$ is very comparable to the difference using $\hat{\alpha}_y = 0.0$.

The final three-dimensional quasi-steady simulation was completed using $\hat{\omega}_x \to 0$, $\hat{\omega}_y = 0.06243$, and $\hat{\alpha}_y = -0.2$. Figures 47 and 48 show the axial- and normal-force coefficients, calculated using Eqs. (2.28) and (2.29), while Figs. 49 and 50 show the power and thrust coefficients calculated using Eqs. (2.32) and (2.33). Table 5 shows the comparison of the mean values of the CFD and the quasi-steady lifting-line solution.

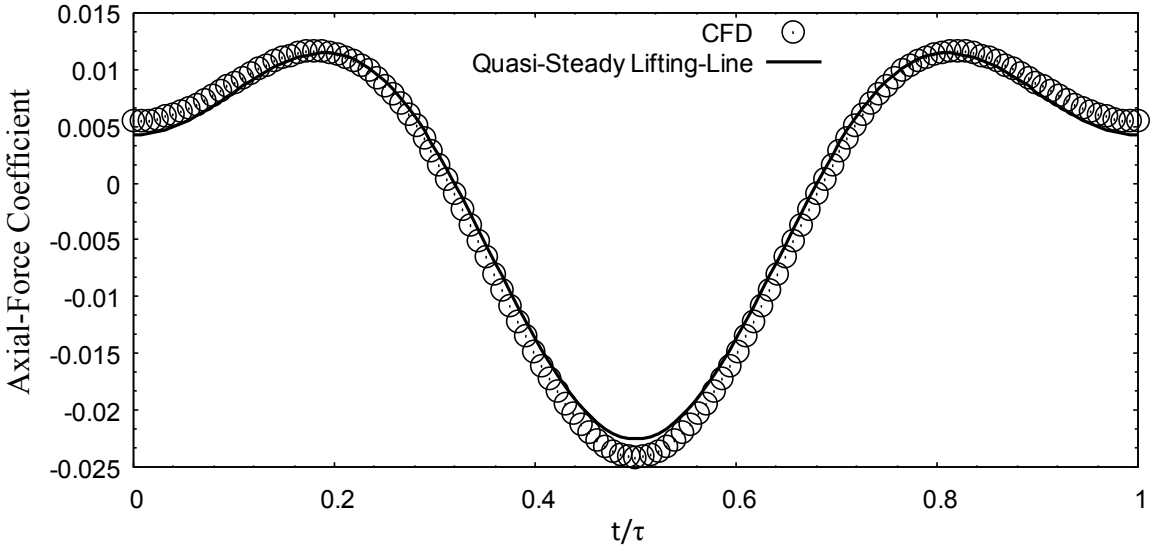

Fig. 47 Axial-force coefficient of the 3D quasi-steady cycle $\hat{\omega}_x \to 0$, $\hat{\omega}_y = 0.06243$, and $\hat{\alpha}_y = -0.2$ compared with the quasi-steady lifting-line solution, Eq. (3.24).

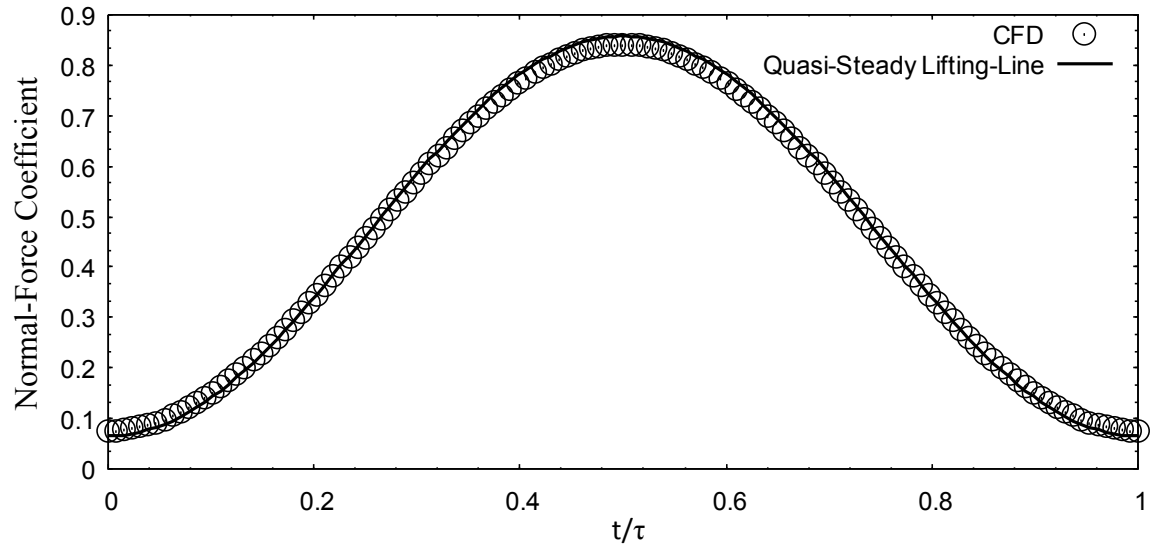

Fig. 48 Normal-force coefficient of the 3D quasi-steady cycle $\hat{\omega}_x \to 0$, $\hat{\omega}_y = 0.06243$, and $\hat{\alpha}_y = -0.2$ compared with the quasi-steady lifting-line solution, Eq. (3.29).

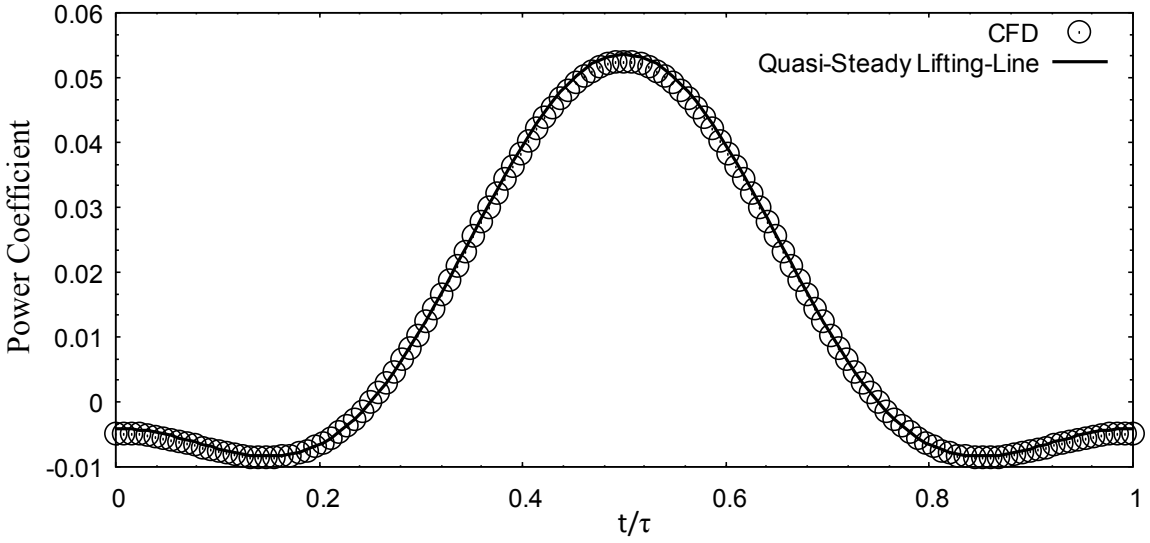

Fig. 49 Power coefficient of the 3D quasi-steady cycle $\hat{\omega}_x \to 0$, $\hat{\omega}_y = 0.06243$, and $\hat{\alpha}_y = -0.2$ compared with the quasi-steady lifting-line solution, Eq. (3.34).

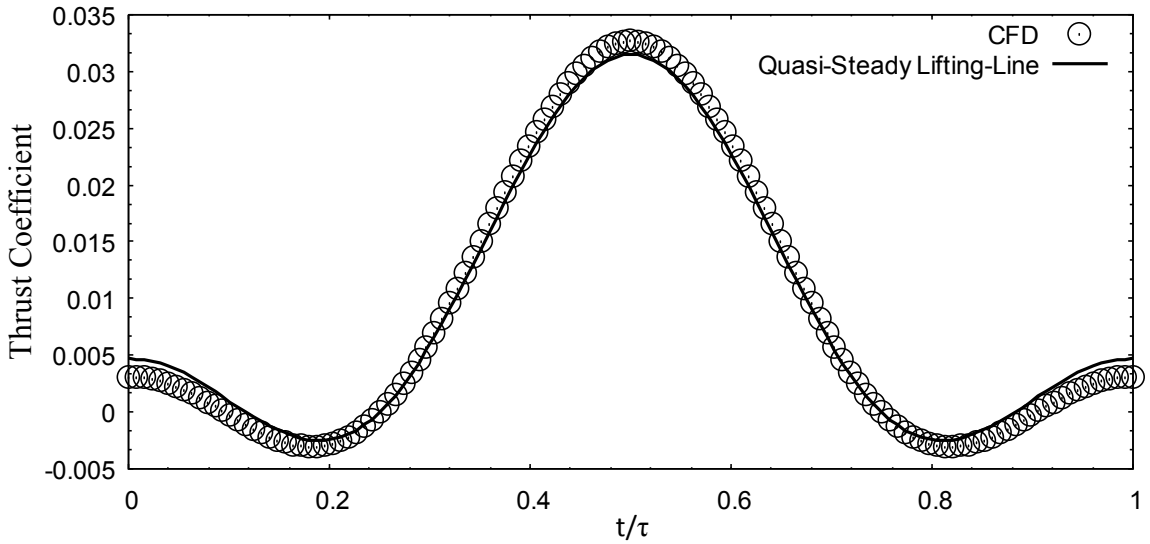

Fig. 50 Thrust coefficient of the 3D quasi-steady cycle $\hat{\omega}_x \to 0$, $\hat{\omega}_y = 0.06243$, and $\hat{\alpha}_y = -0.2$ compared with the quasi-steady lifting-line solution, Eq. (3.40).

Table 5 Mean values of 3D quasi-steady cycle $\hat{\omega}_x \to 0$, $\hat{\omega}_y = 0.06243$, and $\hat{\alpha}_y = -0.2$ compared with the quasi-steady lifting-line solution

	$\hat{\omega}_x \to 0$, $\hat{\omega}_y = 0.06243$, $\hat{\alpha}_y = -0.2$	Quasi-Steady Lifting-Line
Mean Axial-Force Coefficient	-0.000334324565370	-0.000083487982131
Mean Normal-Force Coefficient	0.457753349264002	0.461438397544391
Mean Power Coefficient	0.011927742884959	0.012367132701978
Mean Thrust Coefficient	0.008958396033631	0.009059192158199
Mean Efficiency	0.751055427672565	0.732521626193169

As can be seen in Figs. 47–50, the CFD solutions follow the quasi-steady lifting-line solution. However, it is noticed that it differs more than the previous three-dimensional quasi-steady CFD solution with a pitching amplitude ratio of $\hat{\alpha}_y = 0.2$ and much more than the original solution with $\hat{\alpha}_y = 0.0$.

B. Steady-Periodic Results

The steady-periodic CFD was completed using the three-dimensional and overset grid. The setup for the steady-periodic analysis was described in the previous chapter. The reduced frequency, $\hat{\omega}_x$, was varied in order to produce results showing how the solutions varied with these conditions. Both the pitching amplitude and reduced frequency $\hat{\omega}_y$ were held constant in order to hold a constant geometric angle of attack for all simulations. Each cycle shown was both cycle and time-step converged, as was discussed in a previous section. The cycles shown in the following results are all the third cycles of the applicable study.

1. Pure Plunging

Pure plunging was studied first, as it is a simple case of the oscillating wings. Therefore, the pitching amplitude ratio, $\hat{\alpha}_y$, was equal to zero. The first analysis in pure plunging was done using $\hat{\omega}_x = 0.13414$, $\hat{\omega}_y = 0.07492$, and $\hat{\alpha}_y = 0.0$. This was the lowest frequency oscillation that was studied. First, the axial- and normal-force coefficients, as calculated in Eqs. (2.28) and (2.29) were compared to lifting-line theory, as shown in Figs. 51 and 52. Figures 53 and 54 show the power and thrust coefficients, which were calculated from the Eqs. (2.32) and (2.33). Table 6 shows the comparison of the mean values from the CFD analysis to the quasi-steady lifting-line solution. The mean values were found using the trapezoidal rule.

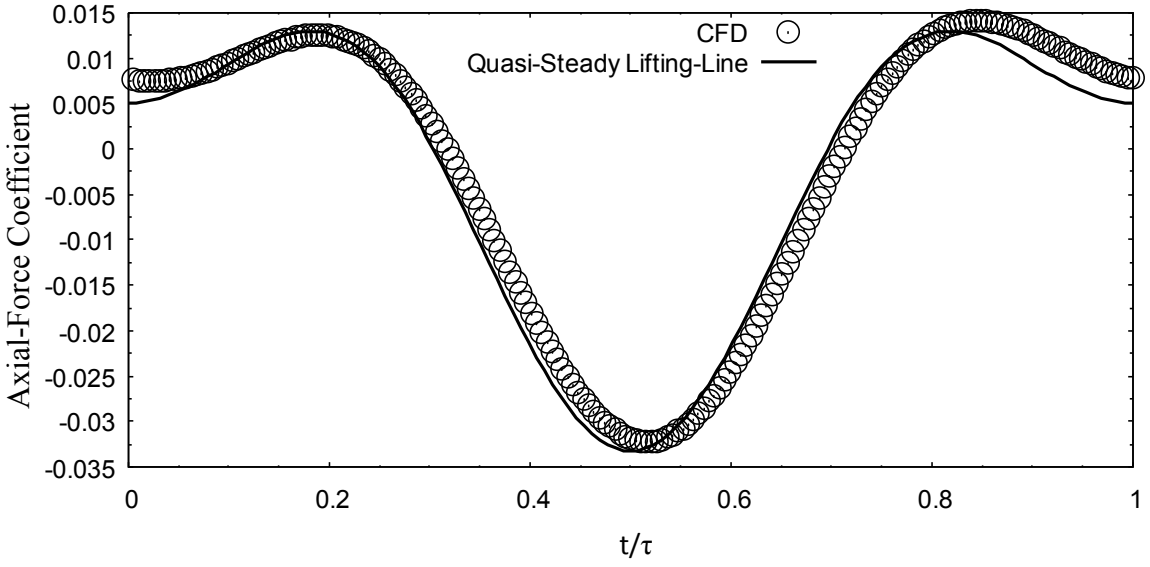

Fig. 51 Axial-force coefficient of oscillation cycle with $\hat{\omega}_x = 0.13414$, $\hat{\omega}_y = 0.07492$, and $\hat{\alpha}_y = 0.0$ compared to the quasi-steady lifting-line solution, Eq. (3.24).

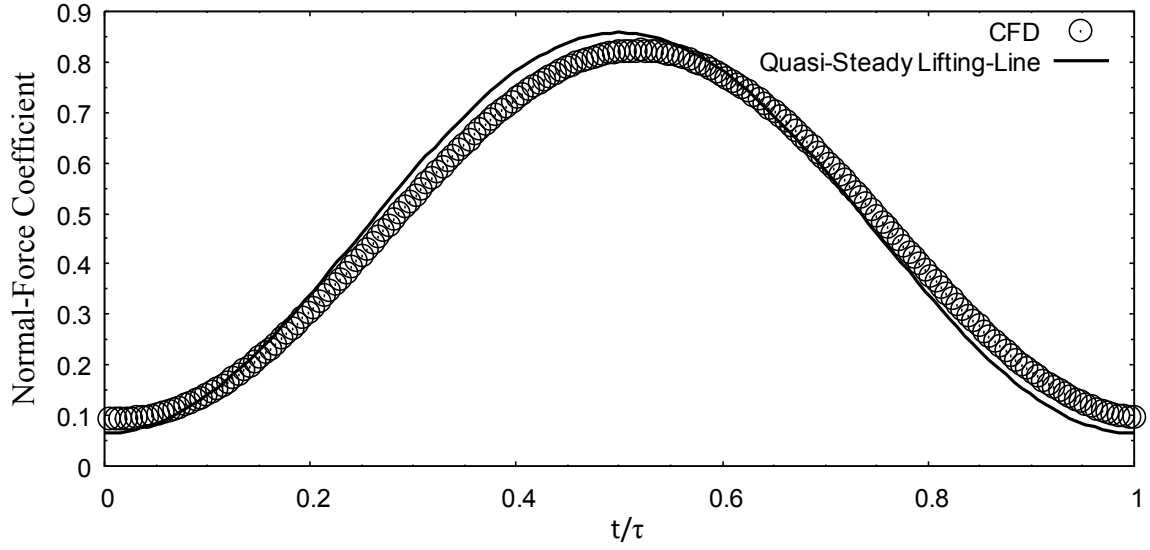

Fig. 52 Normal-force coefficient of oscillation cycle with $\hat{\omega}_x = 0.13414$, $\hat{\omega}_y = 0.07492$, and $\hat{\alpha}_y = 0.0$ compared to the quasi-steady lifting-line solution, Eq. (3.29).

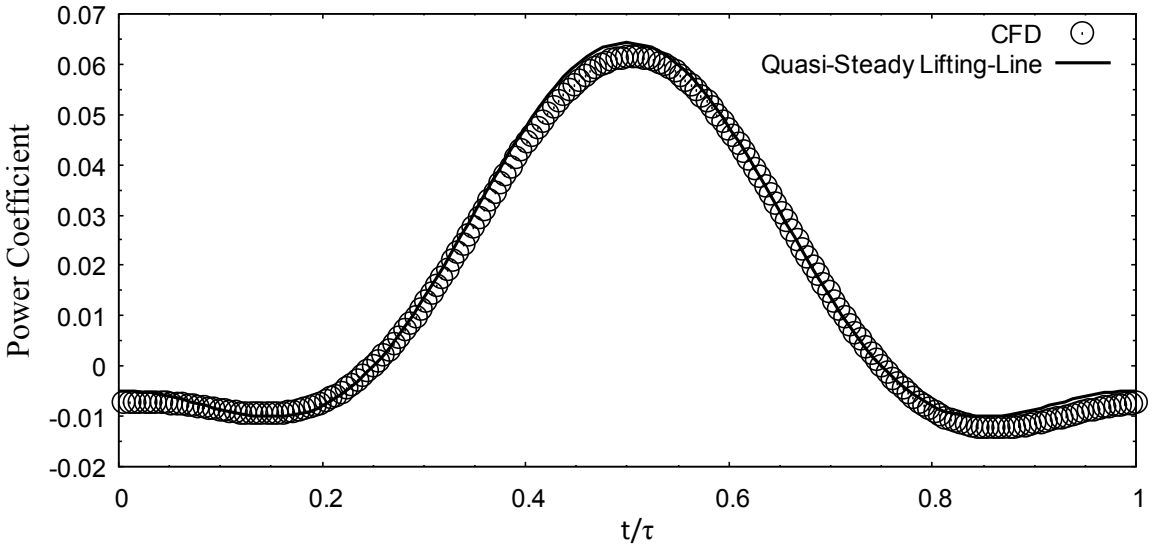

Fig. 53 Power coefficient of oscillation cycle with $\hat{\omega}_x = 0.13414$, $\hat{\omega}_y = 0.07492$, and $\hat{\alpha}_y = 0.0$ compared to the quasi-steady lifting-line solution, Eq. (3.34).

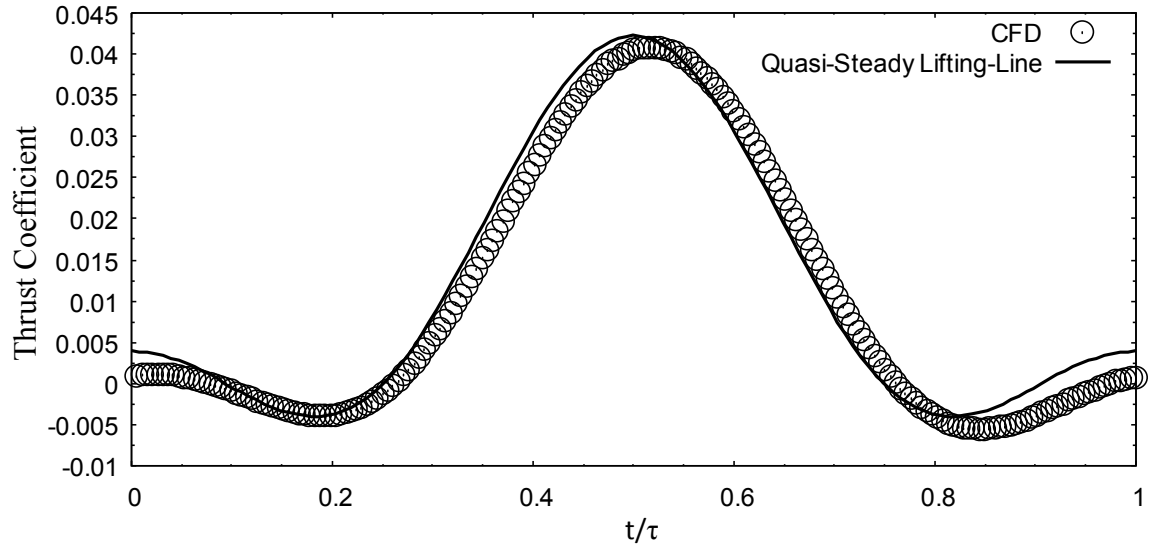

Fig. 54 Thrust coefficient of oscillation cycle with $\hat{\omega}_x = 0.13414$, $\hat{\omega}_y = 0.07492$, and $\hat{\alpha}_y = 0.0$ compared to the quasi-steady lifting-line solution, Eq. (3.40).

Table 6 Mean values of oscillation cycle with $\hat{\omega}_x = 0.13414$, $\hat{\omega}_y = 0.07492$, and $\hat{\alpha}_y = 0.0$ compared to the quasi-steady lifting-line solution

	$\hat{\omega}_x = 0.13414$, $\hat{\omega}_y = 0.07492$, $\hat{\alpha}_y = 0.0$	Quasi-Steady Lifting-Line
Mean Axial-Force Coefficient	-0.00186072320976934	-0.002556914522526
Mean Normal-Force Coefficient	0.457870601687481	0.461438397544391
Mean Power Coefficient	0.0135636877863321	0.014840559242373
Mean Thrust Coefficient	0.0104847946780306	0.011532618698595
Mean Efficiency	0.773004719896013	0.777101355160974

As can be seen in Figs. 51–54 and Table 6, the solution with $\hat{\omega}_x = 0.13414$, $\hat{\omega}_y = 0.07492$, and $\hat{\alpha}_y = 0.0$ is quite close to the quasi-steady lifting-line solution. This is the lowest frequency oscillation studied, so it most closely resembles lifting-line theory for all the steady-periodic cases.

The next oscillation frequency that was studied was with $\hat{\omega}_x = 0.14905$, $\hat{\omega}_y = 0.07492$, and $\hat{\alpha}_y = 0.0$. As can be seen, the frequency of the oscillation was higher than the previous case. Figures 55 and 56 show the axial- and normal-force coefficients calculated using Eqs. (2.28) and (2.29), while Figs. 57 and 58 show the power and thrust coefficients calculated using Eqs. (2.32) and (2.33). Table 5 shows the comparison of the mean values from the CFD analysis to the quasi-steady lifting-line solution.

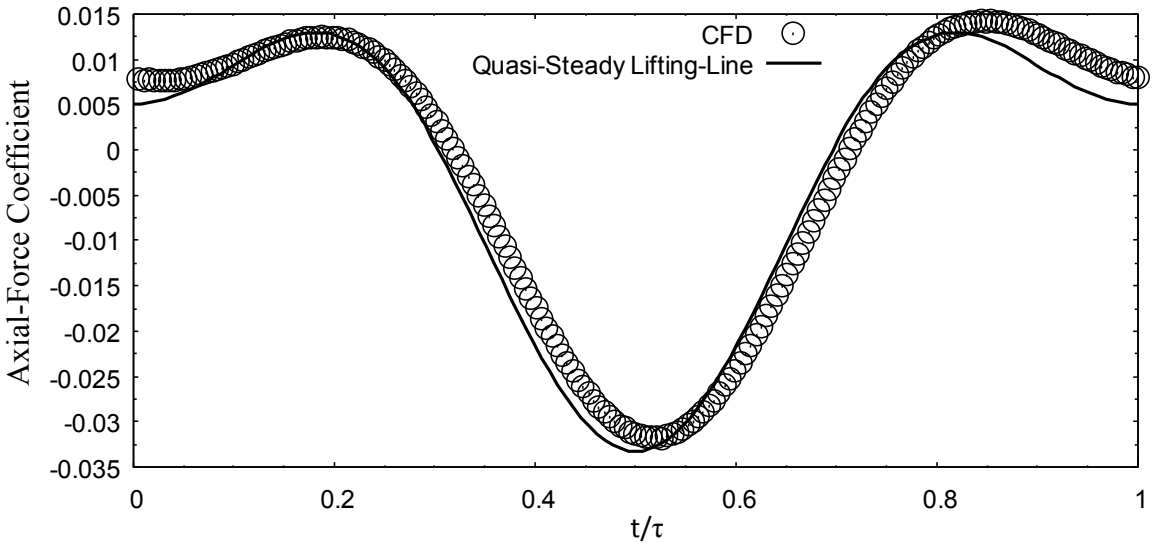

Fig. 55 Axial-force coefficient of oscillation cycle with $\hat{\omega}_x = 0.14905$, $\hat{\omega}_y = 0.07492$, and $\hat{\alpha}_y = 0.0$ compared to the quasi-steady lifting-line solution, Eq. (3.24).

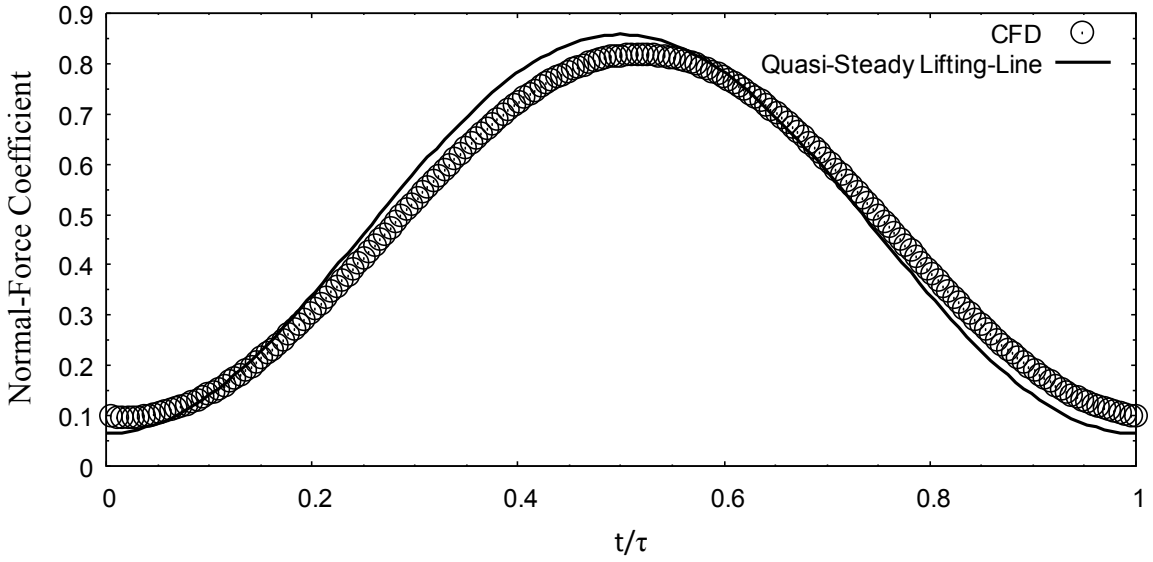

Fig. 56 Normal-force coefficient of oscillation cycle with $\hat{\omega}_x = 0.14905$, $\hat{\omega}_y = 0.07492$, and $\hat{\alpha}_y = 0.0$ compared to the quasi-steady lifting-line solution, Eq. (3.29).

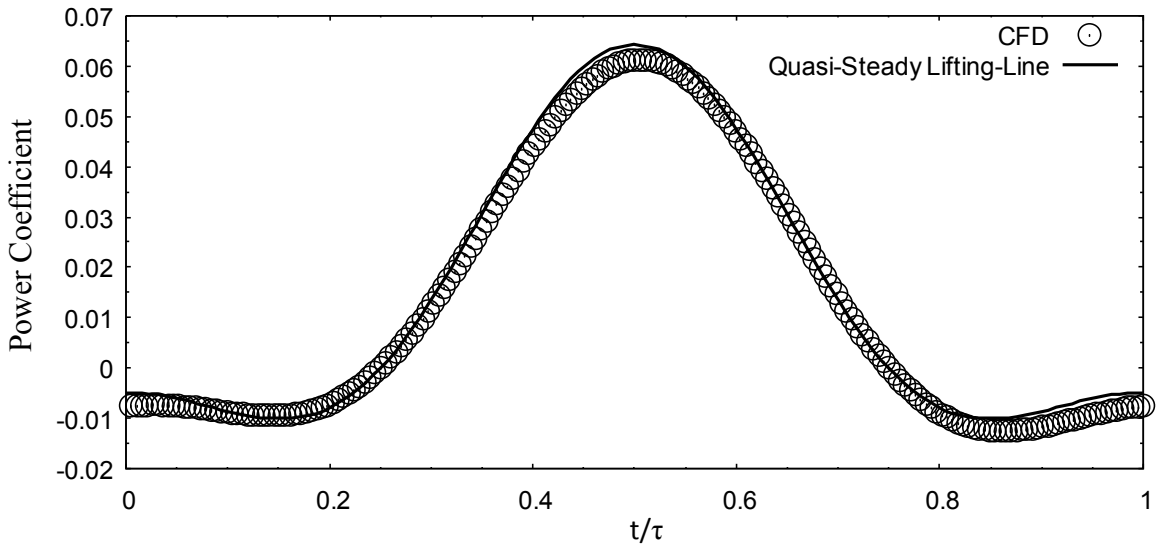

Fig. 57 Power coefficient of oscillation cycle with $\hat{\omega}_x = 0.14905$, $\hat{\omega}_y = 0.07492$, and $\hat{\alpha}_y = 0.0$ compared to the quasi-steady lifting-line solution, Eq. (3.34).

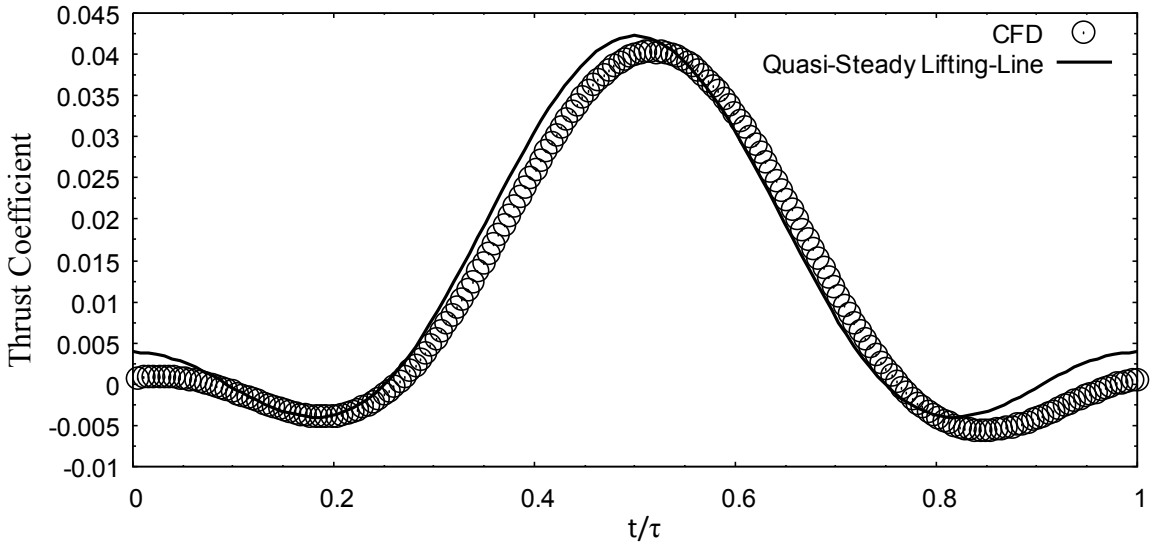

Fig. 58 Thrust coefficient of oscillation cycle with $\hat{\omega}_x = 0.14905$, $\hat{\omega}_y = 0.07492$, and $\hat{\alpha}_y = 0.0$ compared to the quasi-steady lifting-line solution, Eq. (3.40).

Table 7 Mean values of oscillation cycle with $\hat{\omega}_x = 0.14905$, $\hat{\omega}_y = 0.07492$, and $\hat{\alpha}_y = 0.0$ compared to the quasi-steady lifting-line solution

	$\hat{\omega}_x = 0.14905$, $\hat{\omega}_y = 0.07492$, $\hat{\alpha}_y = 0.0$	Quasi-Steady Lifting-Line
Mean Axial-Force Coefficient	-0.00169275920625829	-0.002556914522526
Mean Normal-Force Coefficient	0.45785913590994	0.461438397544391
Mean Power Coefficient	0.0134201124741529	0.014840559242373
Mean Thrust Coefficient	0.0103168306745195	0.011532618698595
Mean Efficiency	0.768758882937066	0.777101355160974

As can be seen in Figs. 55–58 and Table 5, the CFD solution still closely follows the quasi-steady lifting-line solution. However, the solution has diverged more than the previous solution with a lower frequency oscillation.

The next oscillation frequency that was studied was with $\hat{\omega}_x = 0.16162$, $\hat{\omega}_y = 0.07492$, and $\hat{\alpha}_y = 0.0$. As can be seen, the frequency of the oscillation was higher than the previous case. Figures 59 and 60 show the axial- and normal-force coefficients calculated using Eqs. (2.28) and (2.29), while Figs. 61 and 62 show the power and thrust coefficients calculated using Eqs. (2.32) and (2.33). Table 6 shows the comparison of the mean values from the CFD analysis to the quasi-steady lifting-line solution.

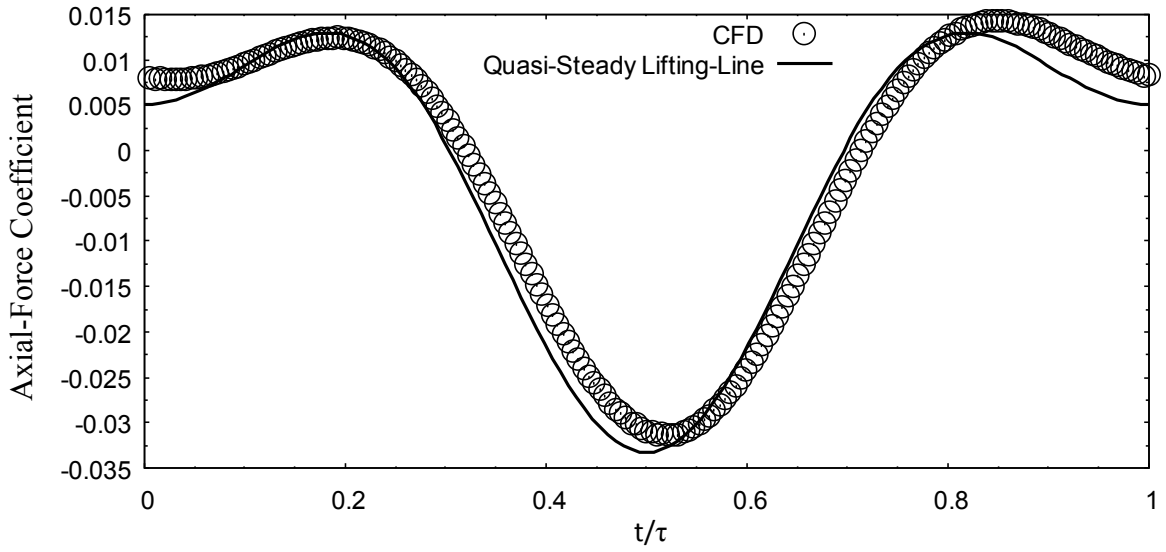

Fig. 59 Axial-force coefficient of oscillation cycle with $\hat{\omega}_x = 0.16162$, $\hat{\omega}_y = 0.07492$, and $\hat{\alpha}_y = 0.0$ compared to the quasi-steady lifting-line solution, Eq. (3.24).

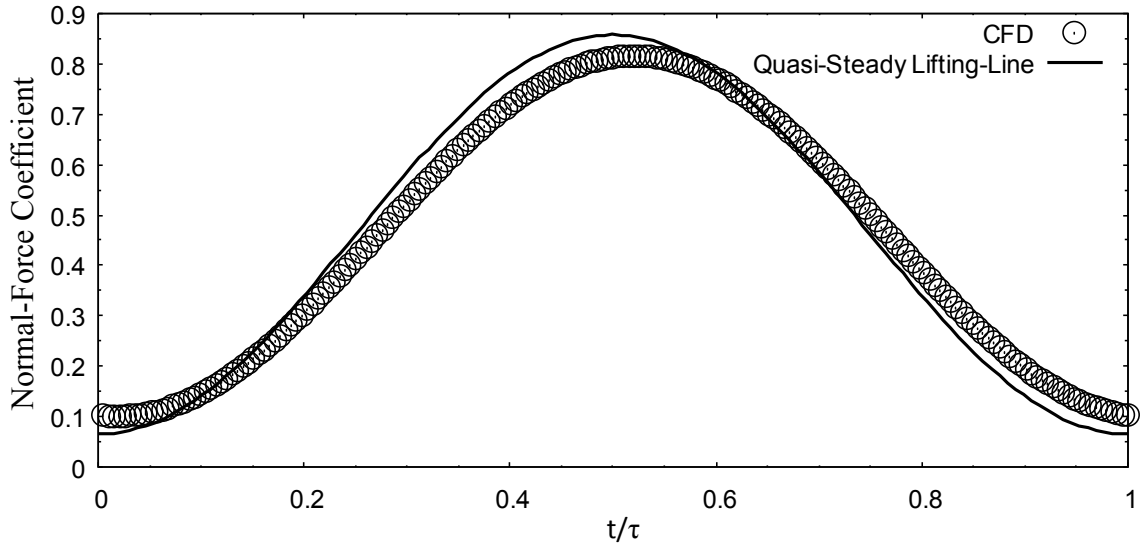

Fig. 60 Normal-force coefficient of oscillation cycle with $\hat{\omega}_x = 0.16162$, $\hat{\omega}_y = 0.07492$, and $\hat{\alpha}_y = 0.0$ compared to the quasi-steady lifting-line solution, Eq. (3.29).

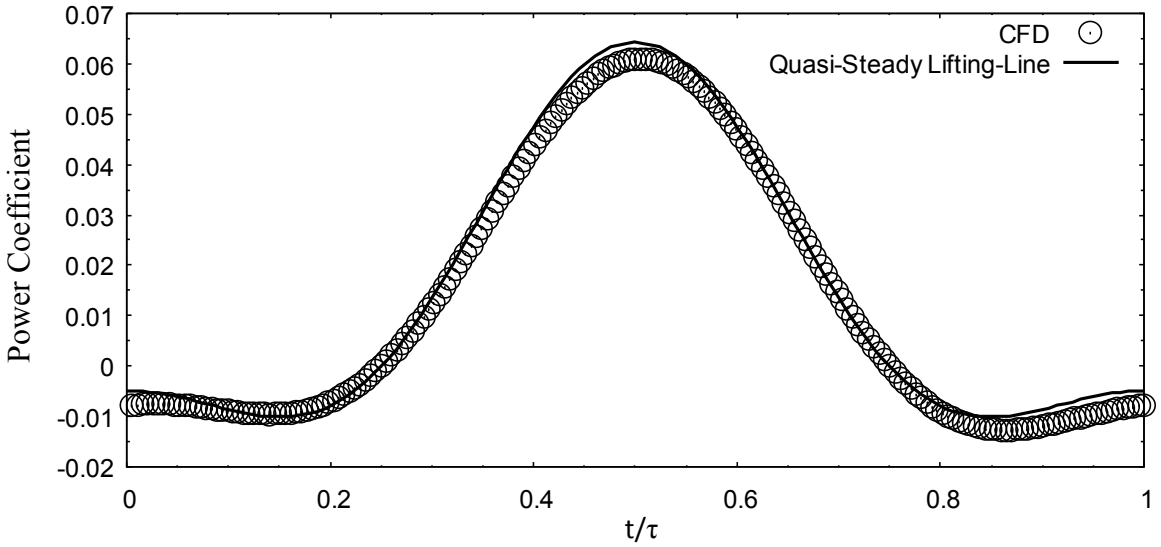

Fig. 61 Power coefficient of oscillation cycle with $\hat{\omega}_x = 0.16162$, $\hat{\omega}_y = 0.07492$, and $\hat{\alpha}_y = 0.0$ compared to the quasi-steady lifting-line solution, Eq. (3.34).

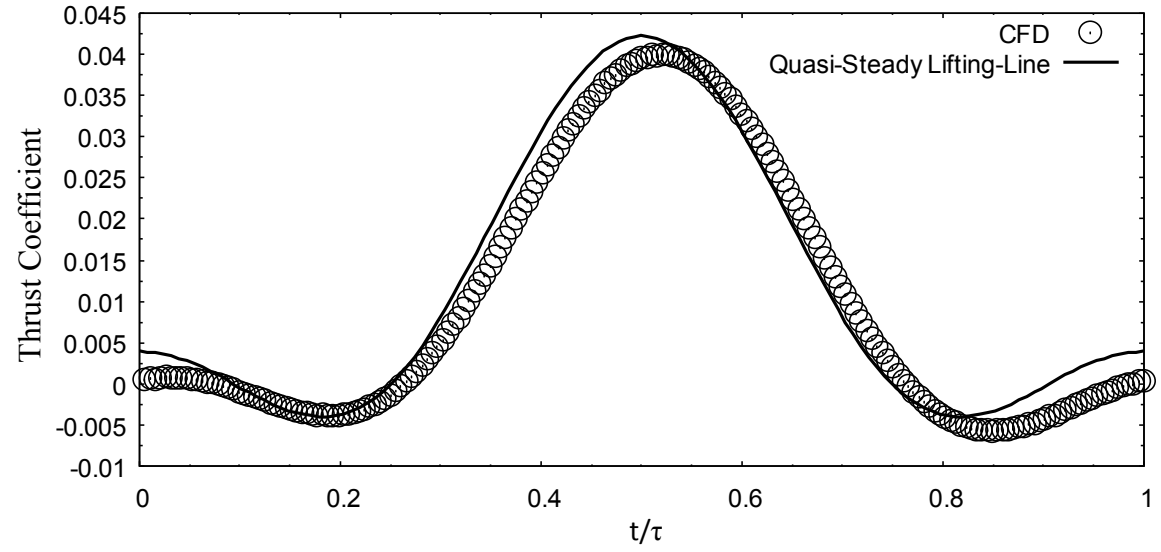

Fig. 62 Thrust coefficient of oscillation cycle with $\hat{\omega}_x = 0.16162$, $\hat{\omega}_y = 0.07492$, and $\hat{\alpha}_y = 0.0$ compared to the quasi-steady lifting-line solution, Eq. (3.40).

Table 8 Mean values of oscillation cycle with $\hat{\omega}_x = 0.16162$, $\hat{\omega}_y = 0.07492$, and $\hat{\alpha}_y = 0.0$ compared to the quasi-steady lifting-line solution

	$\hat{\omega}_x = 0.16162, \hat{\omega}_y = 0.07492, \hat{\alpha}_y = 0.0$	Quasi-Steady Lifting-Line
Mean Axial-Force Coefficient	-0.0015426630597719	-0.002556914522526
Mean Normal-Force Coefficient	0.457861112881205	0.461438397544391
Mean Power Coefficient	0.0132937832852906	0.014840559242373
Mean Thrust Coefficient	0.0101667345280332	0.011532618698595
Mean Efficiency	0.764773602055217	0.777101355160974

It can be seen more clearly in Figs. 59–62 and Table 8 that the CFD solutions continue to diverge from the quasi-steady lifting-line solution with increasing frequency. The divergence is most clearly seen in the axial-force and thrust coefficients in Figs. 59 and 62.

The next oscillation frequency that was studied was with $\hat{\omega}_x = 0.19163$, $\hat{\omega}_y = 0.07492$, and $\hat{\alpha}_y = 0.0$. As can be seen, the frequency of the oscillation was higher than the previous case. Figures 63 and 64 show the axial- and normal-force coefficients calculated using Eqs. (2.28) and (2.29), while Figs. 65 and 66 show the power and thrust coefficients calculated using Eqs. (2.32) and (2.33). Table 9 shows the comparison of the mean values from the CFD analysis to the quasi-steady lifting-line solution.

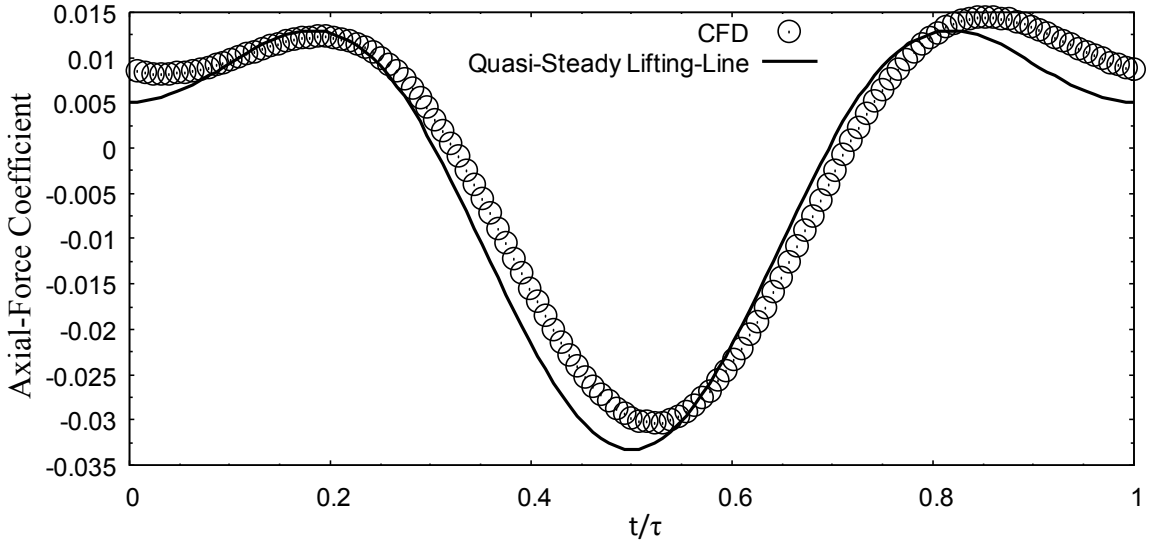

Fig. 63 Axial-force coefficient of oscillation cycle with $\hat{\omega}_x = 0.19163$, $\hat{\omega}_y = 0.07492$, and $\hat{\alpha}_y = 0.0$ compared to the quasi-steady lifting-line solution, Eq. (3.24).

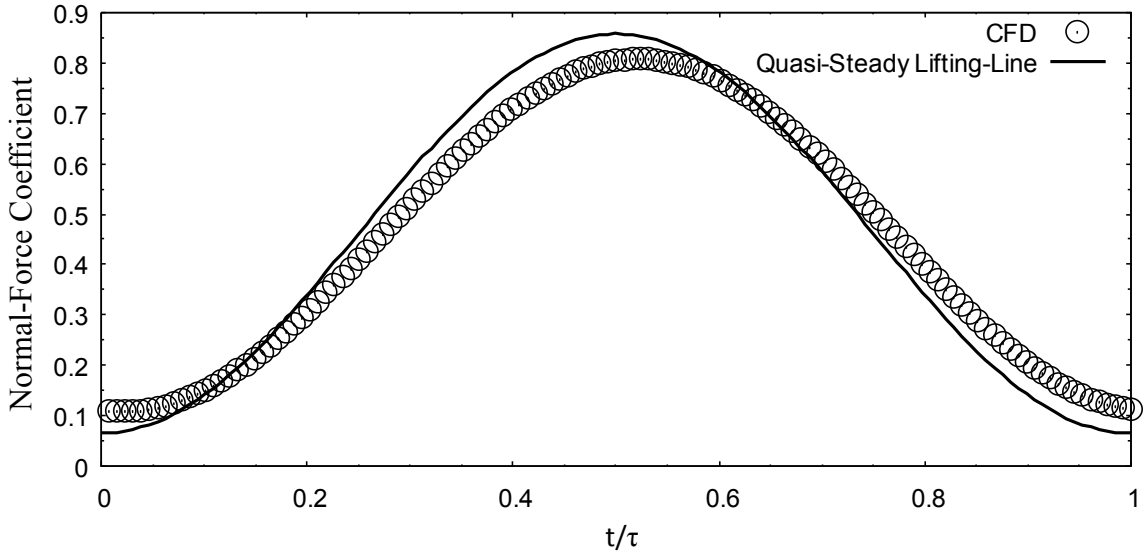

Fig. 64 Normal-force coefficient of oscillation cycle with $\hat{\omega}_x = 0.19163$, $\hat{\omega}_y = 0.07492$, and $\hat{\alpha}_y = 0.0$ compared to the quasi-steady lifting-line solution, Eq. (3.29).

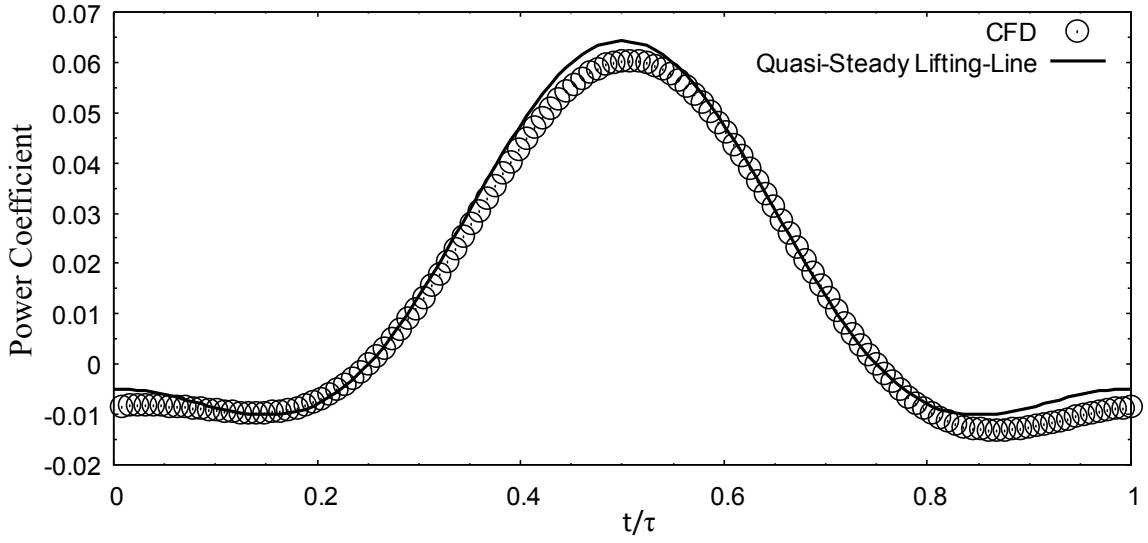

Fig. 65 Power coefficient of oscillation cycle with $\hat{\omega}_x = 0.19163$, $\hat{\omega}_y = 0.07492$, and $\hat{\alpha}_y = 0.0$ compared to the quasi-steady lifting-line solution, Eq. (3.34).

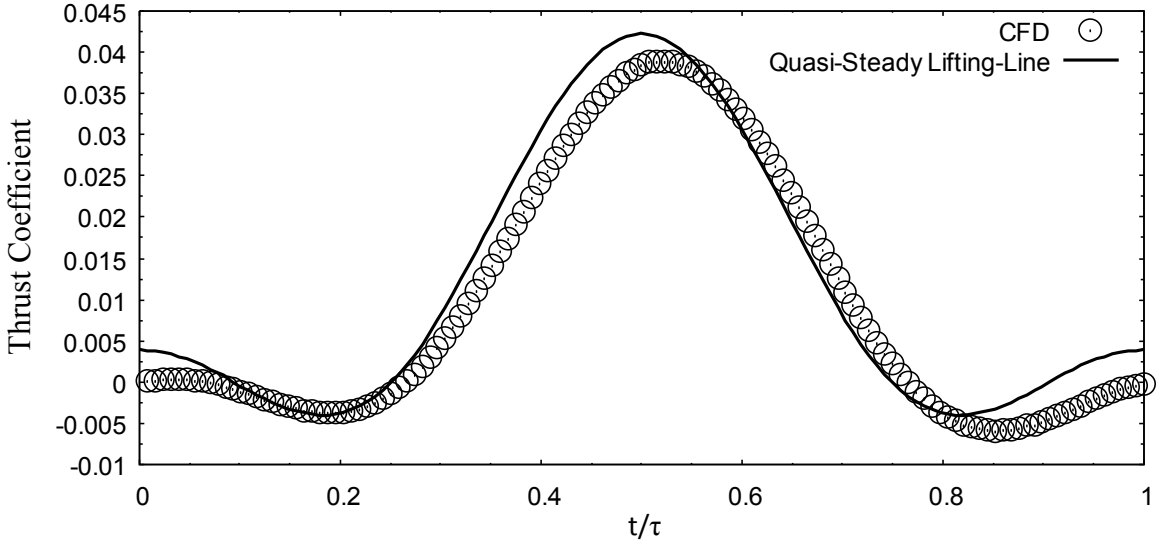

Fig. 66 Thrust coefficient of oscillation cycle with $\hat{\omega}_x = 0.19163$, $\hat{\omega}_y = 0.07492$, and $\hat{\alpha}_y = 0.0$ compared to the quasi-steady lifting-line solution, Eq. (3.40).

Table 9 Mean values of oscillation cycle with $\hat{\omega}_x = 0.19163$, $\hat{\omega}_y = 0.07492$, and $\hat{\alpha}_y = 0.0$ compared to the quasi-steady lifting-line solution

	$\hat{\omega}_x = 0.19163$, $\hat{\omega}_y = 0.07492$, $\hat{\alpha}_y = 0.0$	Quasi-Steady Lifting-Line
Mean Axial-Force Coefficient	-0.000977714879967232	-0.002556914522526
Mean Normal-Force Coefficient	0.457815309776183	0.461438397544391
Mean Power Coefficient	0.0128190718223785	0.014840559242373
Mean Thrust Coefficient	0.0096017863482285	0.011532618698595
Mean Efficiency	0.74902352379885	0.777101355160974

As seen in Figs. 63–66 and Table 9, and as has been previously observed, the CFD solutions with increasing frequency diverge further than the quasi-steady lifting-line solution.

The next oscillation frequency that was studied was with $\hat{\omega}_x = 0.20637$, $\hat{\omega}_y = 0.07492$, and $\hat{\alpha}_y = 0.0$. As can be seen, the frequency of the oscillation was higher than the previous case. Figures 67 and 68 show the axial- and normal-force coefficients calculated using Eqs. (2.28) and (2.29), while Figs. 69 and 70 show the power and thrust coefficients calculated using Eqs. (2.32) and (2.33). Table 10 shows the comparison of the mean values from the CFD analysis to the quasi-steady lifting-line solution.

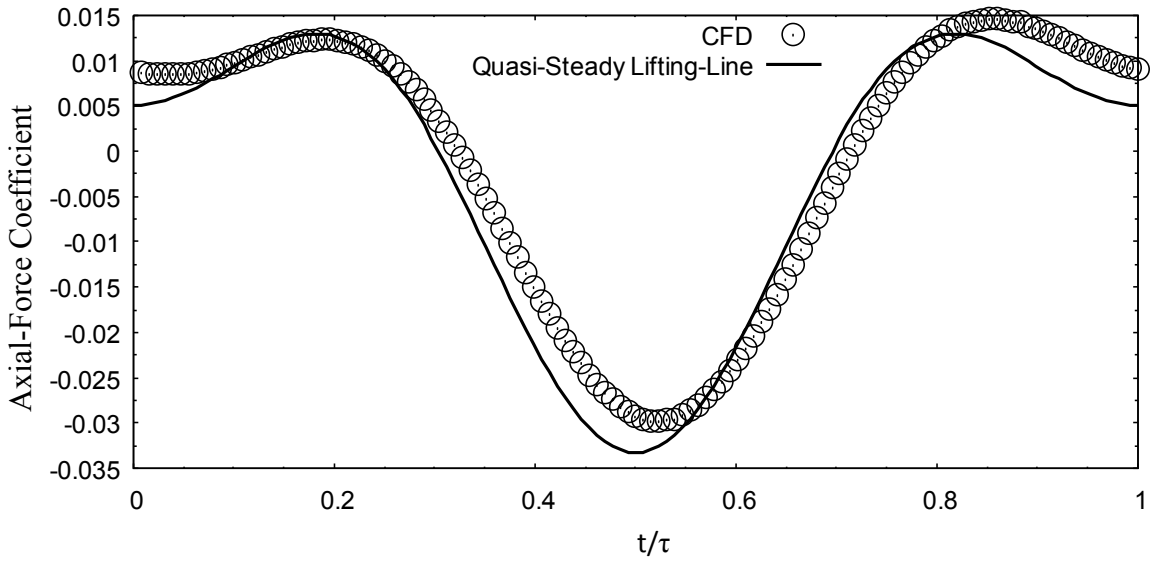

Fig. 67 Axial-force coefficient of oscillation cycle with $\hat{\omega}_x = 0.20637$, $\hat{\omega}_y = 0.07492$, and $\hat{\alpha}_y = 0.0$ compared to the quasi-steady lifting-line solution, Eq. (3.24).

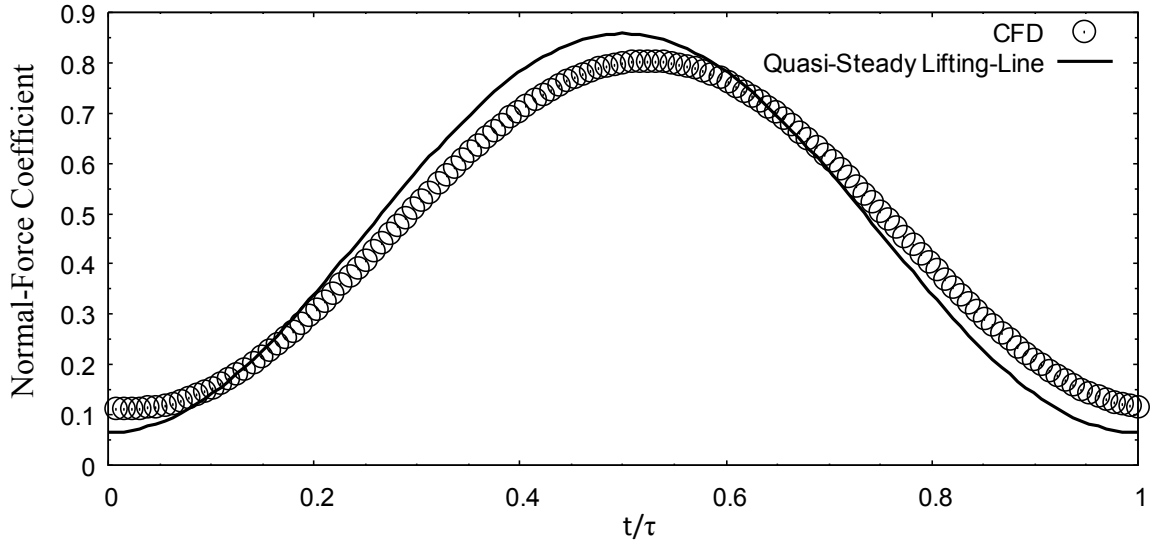

Fig. 68 Normal-force coefficient of oscillation cycle with $\hat{\omega}_x = 0.20637$, $\hat{\omega}_y = 0.07492$, and $\hat{\alpha}_y = 0.0$ compared to the quasi-steady lifting-line solution, Eq. (3.29).

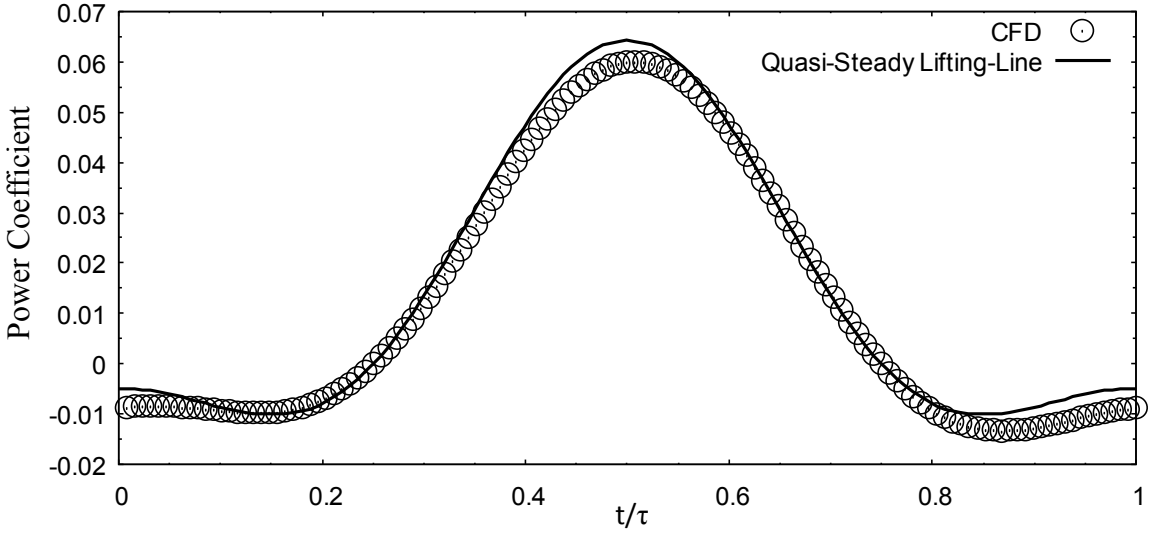

Fig. 69 Power coefficient of oscillation cycle with $\hat{\omega}_x = 0.20637$, $\hat{\omega}_y = 0.07492$, and $\hat{\alpha}_y = 0.0$ compared to the quasi-steady lifting-line solution, Eq. (3.34).

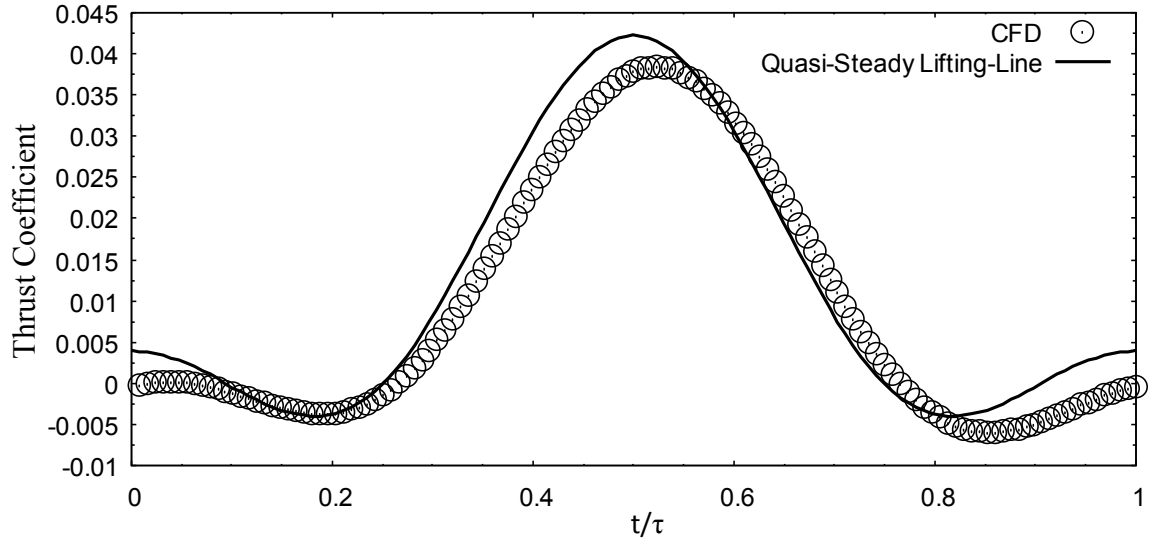

Fig. 70 Thrust coefficient of oscillation cycle with $\hat{\omega}_x = 0.20637$, $\hat{\omega}_y = 0.07492$, and $\hat{\alpha}_y = 0.0$ compared to the quasi-steady lifting-line solution, Eq. (3.40).

Table 10 Mean values of oscillation cycle with $\hat{\omega}_x = 0.20637$, $\hat{\omega}_y = 0.07492$, and $\hat{\alpha}_y = 0.0$ compared to the quasi-steady lifting-line solution

	$\hat{\omega}_x = 0.20637$, $\hat{\omega}_y = 0.07492$, $\hat{\alpha}_y = 0.0$	Quasi-Steady Lifting-Line
Mean Axial-Force Coefficient	-0.000977714879967232	-0.002556914522526
Mean Normal-Force Coefficient	0.457815309776183	0.461438397544391
Mean Power Coefficient	0.0128190718223785	0.014840559242373
Mean Thrust Coefficient	0.0096017863482285	0.011532618698595
Mean Efficiency	0.74902352379885	0.777101355160974

As seen in Figs. 67–70 and Table 10, the CFD solution differs from the quasi-steady lifting-line solution more than previously for lower frequencies of oscillation. This is still most clearly seen in the axial-force and thrust coefficients, Figs. 67 and 70.

The next oscillation frequency that was studied was with $\hat{\omega}_x = 0.24841$, $\hat{\omega}_y = 0.07492$, and $\hat{\alpha}_y = 0.0$. As can be seen, the frequency of the oscillation was higher than the previous case. Figures 71 and 72 show the axial- and normal-force coefficients calculated using Eqs. (2.28) and (2.29), while Figs. 73 and 74 show the power and thrust coefficients calculated using Eqs. (2.32) and (2.33). Table 11 shows the comparison of the mean values from the CFD analysis to the quasi-steady lifting-line solution.

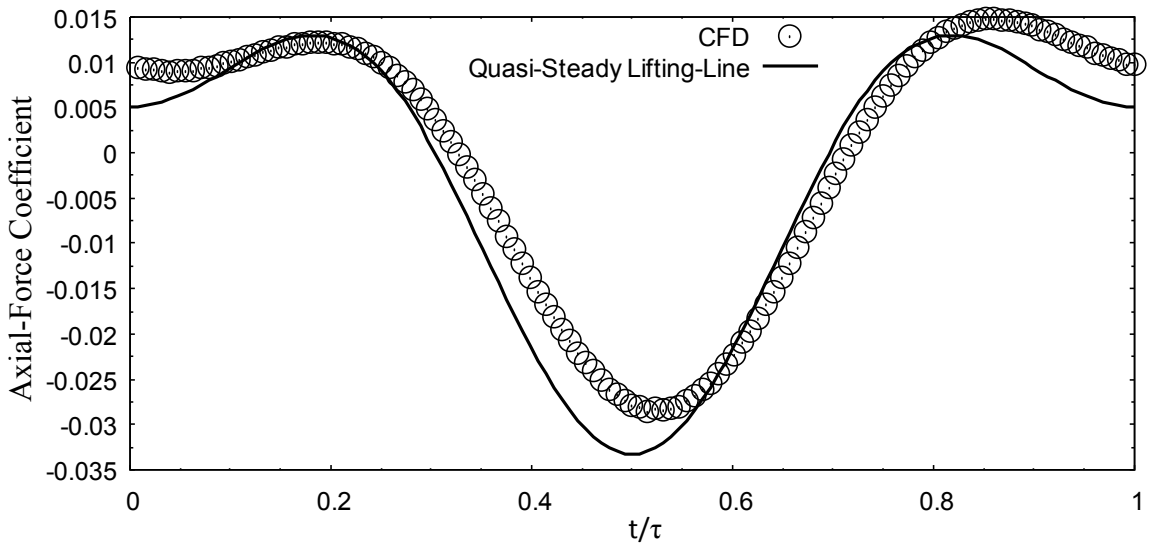

Fig. 71 Axial-force coefficient of oscillation cycle with $\hat{\omega}_x = 0.24841$, $\hat{\omega}_y = 0.07492$, and $\hat{\alpha}_y = 0.0$ compared to the quasi-steady lifting-line solution, Eq. (3.24).

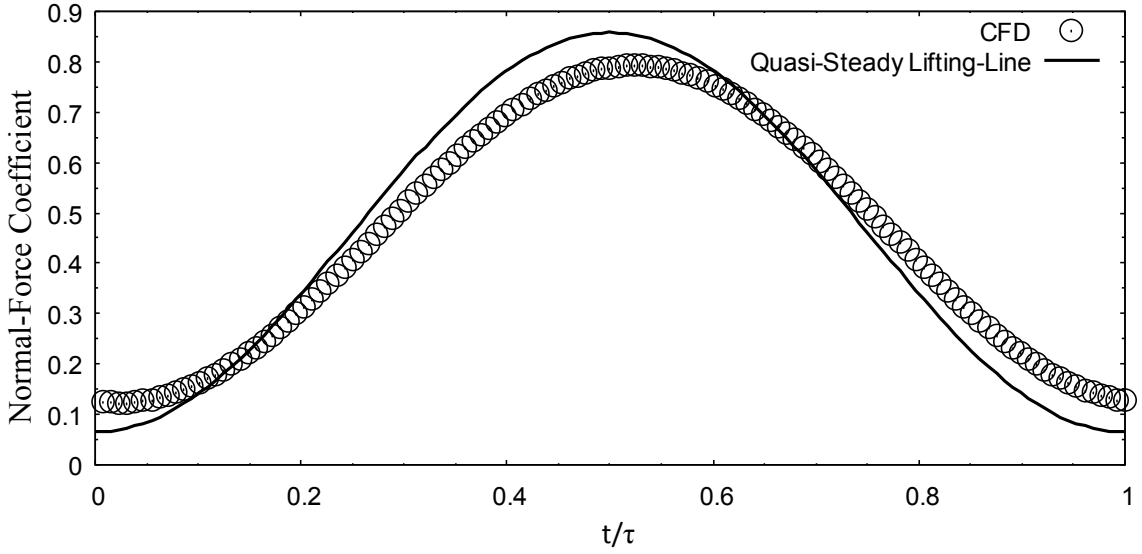

Fig. 72 Normal-force coefficient of oscillation cycle with $\hat{\omega}_x = 0.24841$, $\hat{\omega}_y = 0.07492$, and $\hat{\alpha}_y = 0.0$ compared to the quasi-steady lifting-line solution, Eq. (3.29).

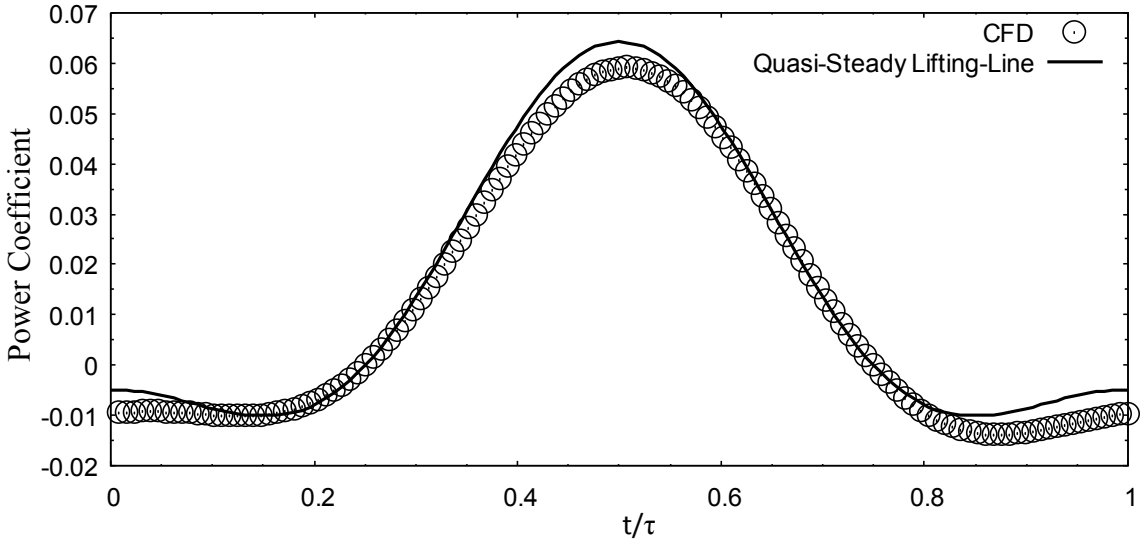

Fig. 73 Power coefficient of oscillation cycle with $\hat{\omega}_x = 0.24841$, $\hat{\omega}_y = 0.07492$, and $\hat{\alpha}_y = 0.0$ compared to the quasi-steady lifting-line solution, Eq. (3.34).

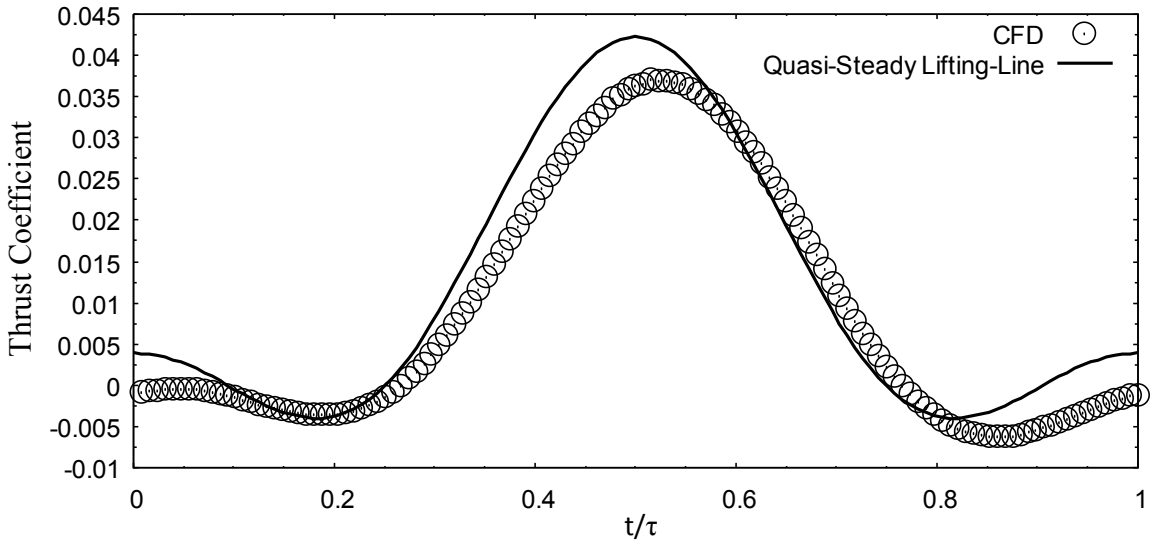

Fig. 74 Thrust coefficient of oscillation cycle with $\hat{\omega}_x = 0.24841$, $\hat{\omega}_y = 0.07492$, and $\hat{\alpha}_y = 0.0$ compared to the quasi-steady lifting-line solution, Eq. (3.40).

Table 11 Mean values of oscillation cycle with $\hat{\omega}_x = 0.24841$, $\hat{\omega}_y = 0.07492$, and $\hat{\alpha}_y = 0.0$ compared to the quasi-steady lifting-line solution

	$\hat{\omega}_x = 0.24841$, $\hat{\omega}_y = 0.07492$, $\hat{\alpha}_y = 0.0$	Quasi-Steady Lifting-Line
Mean Axial-Force Coefficient	-0.000464085694446977	-0.002556914522526
Mean Normal-Force Coefficient	0.457765765121338	0.461438397544391
Mean Power Coefficient	0.0123874307894113	0.014840559242373
Mean Thrust Coefficient	0.00908815716270823	0.011532618698595
Mean Efficiency	0.733659571319402	0.777101355160974

Figures 71–74 and Table 11 continue to support the trend that the CFD solution differs from the quasi-steady lifting-line solution more when the frequency of the oscillation is increased.

The next oscillation frequency that was studied was with $\hat{\omega}_x = 0.29162$, $\hat{\omega}_y = 0.07492$, and $\hat{\alpha}_y = 0.0$. As can be seen, the frequency of the oscillation was higher than the previous case. Figures 75 and 76 show the axial- and normal-force coefficients calculated using Eqs. (2.28) and (2.29), while Figs. 77 and 78 show the power and thrust coefficients calculated using Eqs. (2.32) and (2.33). Table 12 shows the comparison of the mean values from the CFD analysis to the quasi-steady lifting-line solution.

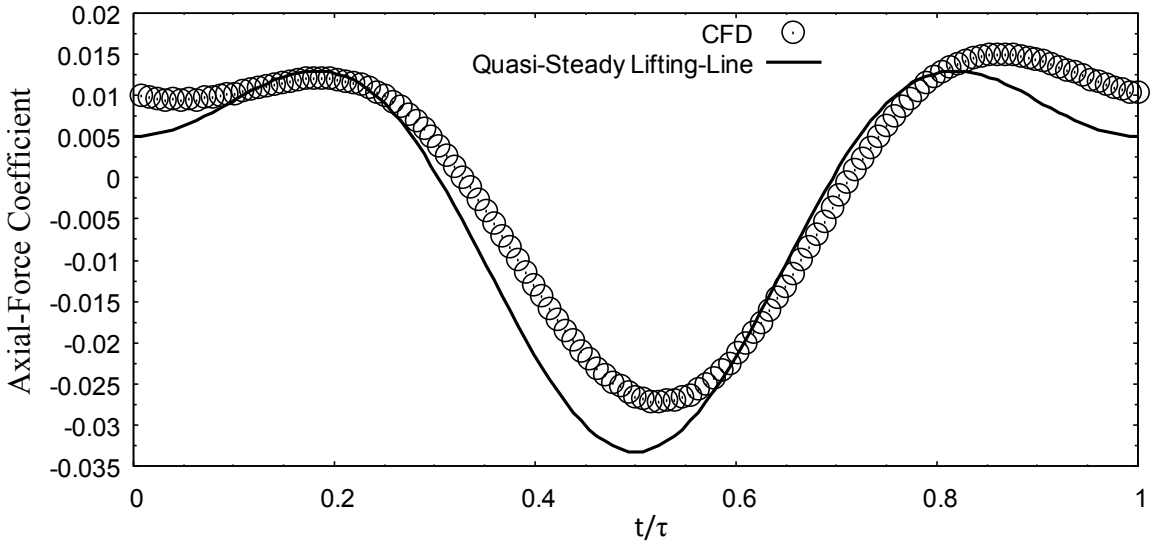

Fig. 75 Axial-force coefficient of oscillation cycle with $\hat{\omega}_x = 0.29162$, $\hat{\omega}_y = 0.07492$, and $\hat{\alpha}_y = 0.0$ compared to the quasi-steady lifting-line solution, Eq. (3.24).

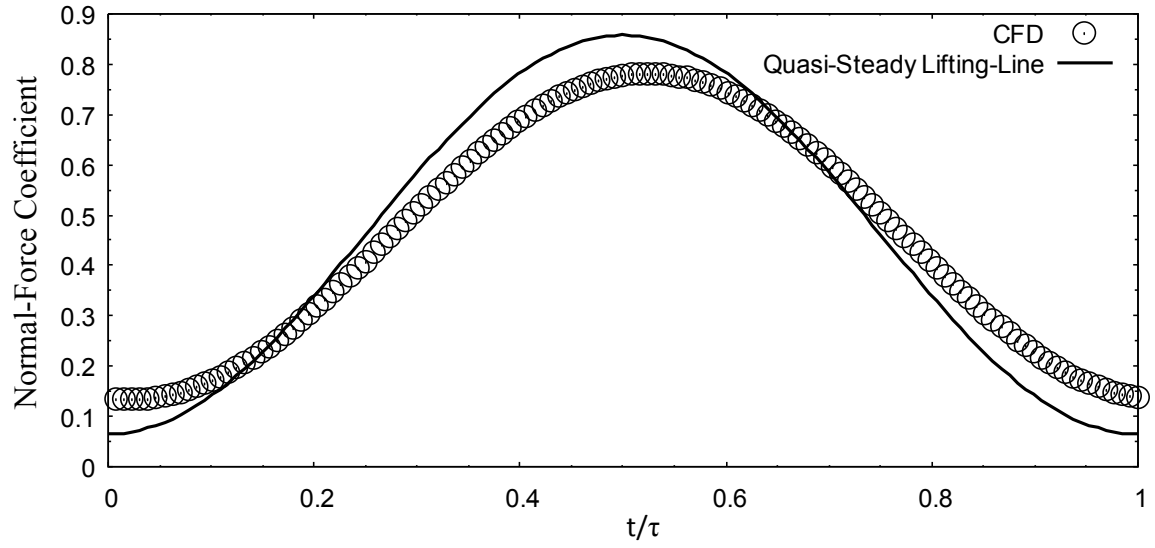

Fig. 76 Normal-force coefficient of oscillation cycle with $\hat{\omega}_x = 0.29162$, $\hat{\omega}_y = 0.07492$, and $\hat{\alpha}_y = 0.0$ compared to the quasi-steady lifting-line solution, Eq. (3.29).

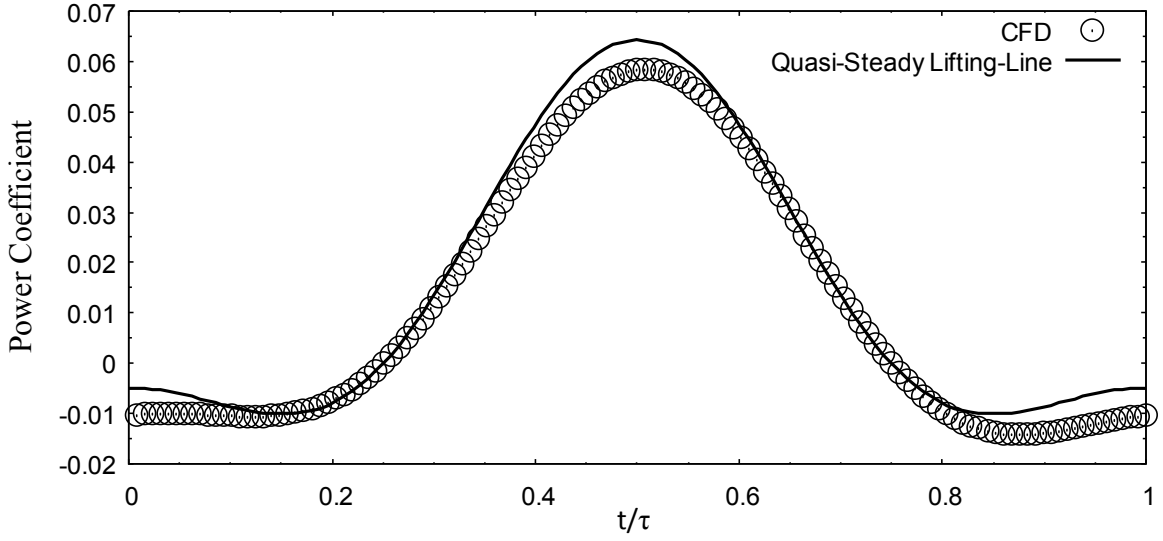

Fig. 77 Power coefficient of oscillation cycle with $\hat{\omega}_x = 0.29162$, $\hat{\omega}_y = 0.07492$, and $\hat{\alpha}_y = 0.0$ compared to the quasi-steady lifting-line solution, Eq. (3.34).

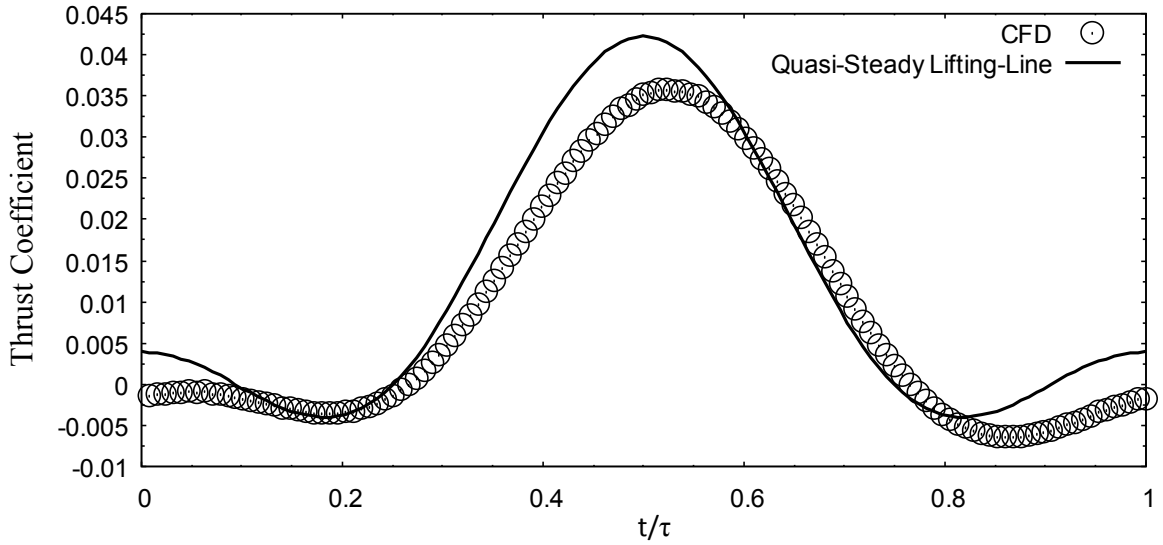

Fig. 78 Thrust coefficient of oscillation cycle with $\hat{\omega}_x = 0.29162$, $\hat{\omega}_y = 0.07492$, and $\hat{\alpha}_y = 0.0$ compared to the quasi-steady lifting-line solution, Eq. (3.40).

Table 12 Mean values of oscillation cycle with $\hat{\omega}_x = 0.29162$, $\hat{\omega}_y = 0.07492$, and $\hat{\alpha}_y = 0.0$ compared to the quasi-steady lifting-line theory

	$\hat{\omega}_x = 0.29162$, $\hat{\omega}_y = 0.07492$, $\hat{\alpha}_y = 0.0$	Quasi-Steady Lifting-Line
Mean Axial-Force Coefficient	-8.19059326594574E-08	-0.002556914522526
Mean Normal-Force Coefficient	0.457720039110048	0.461438397544391
Mean Power Coefficient	0.0119933123013147	0.014840559242373
Mean Thrust Coefficient	0.00862415337419392	0.011532618698595
Mean Efficiency	0.719080197156925	0.777101355160974

As can be seen in Figs. 75–78 and Table 12, the CFD solution differs more than the previous frequency studied. This continues to show that increasing frequency produces solutions that differ increasingly from the quasi-steady lifting-line solution.

The next oscillation frequency that was studied was with $\hat{\omega}_x = 0.33536$, $\hat{\omega}_y = 0.07492$, and $\hat{\alpha}_y = 0.0$. As can be seen, the frequency of the oscillation was higher than the previous case. Figures 79 and 80 show the axial- and normal-force coefficients calculated using Eqs. (2.28) and (2.29), while Figs. 81 and 82 show the power and thrust coefficients calculated using Eqs. (2.32) and (2.33). Table 13 shows the comparison of the mean values from the CFD analysis to the quasi-steady lifting-line solution.

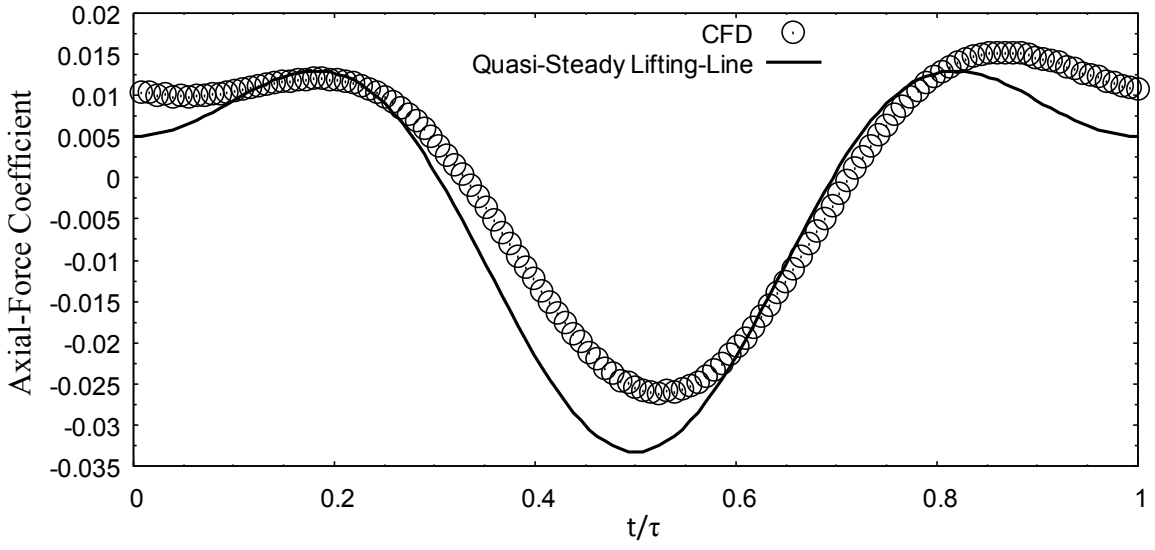

Fig. 79 Axial-force coefficient of oscillation cycle with $\hat{\omega}_x = 0.33536$, $\hat{\omega}_y = 0.07492$, and $\hat{\alpha}_y = 0.0$ compared to the quasi-steady lifting-line solution, Eq. (3.24).

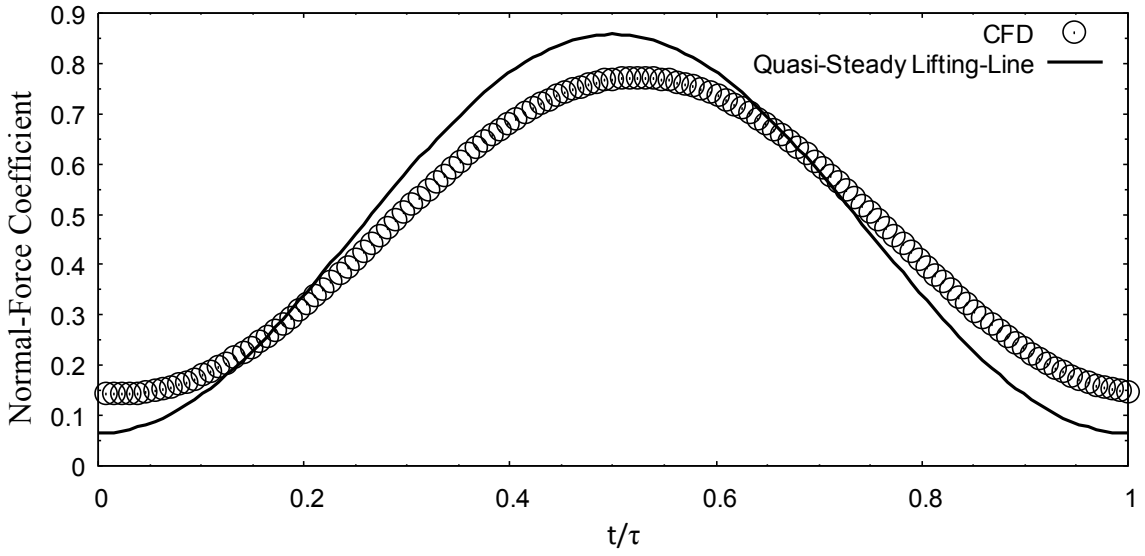

Fig. 80 Normal-force coefficient of oscillation cycle with $\hat{\omega}_x = 0.33536$, $\hat{\omega}_y = 0.07492$, and $\hat{\alpha}_y = 0.0$ compared to the quasi-steady lifting-line solution, Eq. (3.29).

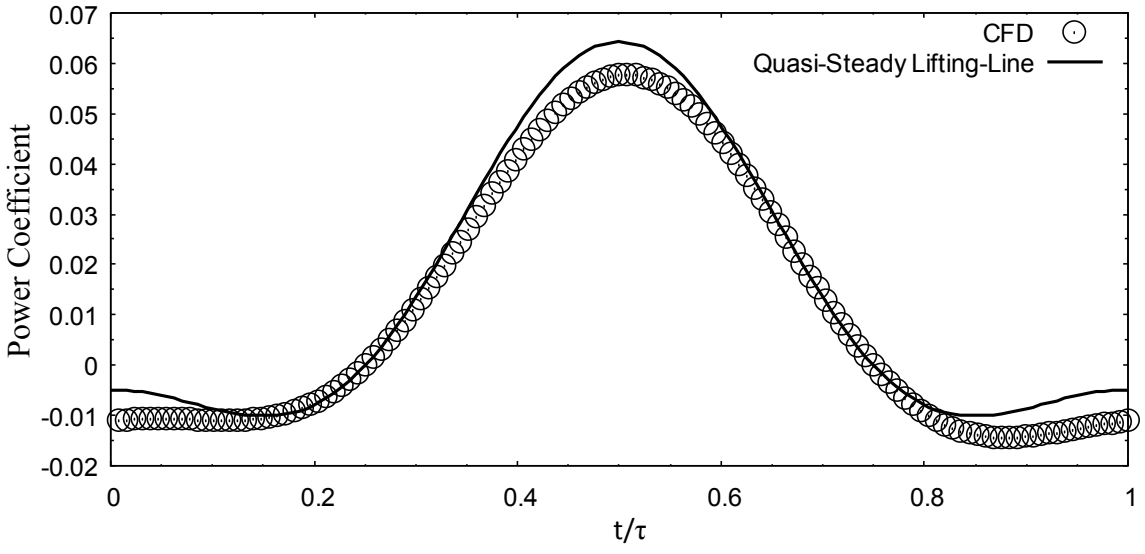

Fig. 81 Power coefficient of oscillation cycle with $\hat{\omega}_x = 0.33536$, $\hat{\omega}_y = 0.07492$, and $\hat{\alpha}_y = 0.0$ compared to the quasi-steady lifting-line solution, Eq. (3.34).

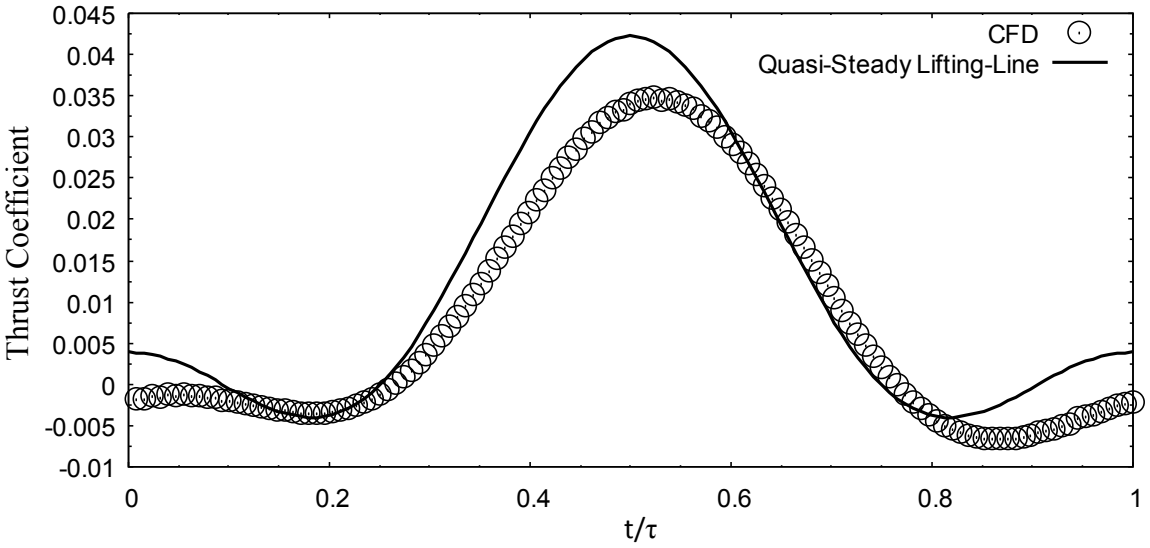

Fig. 82 Thrust coefficient of oscillation cycle with $\hat{\omega}_x = 0.33536$, $\hat{\omega}_y = 0.07492$, and $\hat{\alpha}_y = 0.0$ compared to the quasi-steady lifting-line solution, Eq. (3.40).

Table 13 Mean values of oscillation cycle with $\hat{\omega}_x = 0.33536$, $\hat{\omega}_y = 0.07492$, and $\hat{\alpha}_y = 0.0$ compared to the quasi-steady lifting-line solution

	$\hat{\omega}_x = 0.33536$, $\hat{\omega}_y = 0.07492$, $\hat{\alpha}_y = 0.0$	Quasi-Steady Lifting-Line
Mean Axial-Force Coefficient	0.000385261055126843	-0.002556914522526
Mean Normal-Force Coefficient	0.457687814622568	0.461438397544391
Mean Power Coefficient	0.0116557270524111	0.014840559242373
Mean Thrust Coefficient	0.00823881041313441	0.011532618698595
Mean Efficiency	0.706846546430594	0.777101355160974

As can be seen in Figs. 79–82, in particular Fig. 82, and Table 13, the CFD solution is diverging quite extensively from the quasi-steady lifting-line solution at the high frequency of $\hat{\omega}_x = 0.33536$.

The last analysis in pure plunging was done using $\hat{\omega}_x = 0.38327$, $\hat{\omega}_y = 0.07492$, and $\hat{\alpha}_y = 0.0$. This was the highest frequency oscillation that was studied. Figures 83 and 84 show the axial- and normal-force coefficients calculated using Eqs. (2.28) and (2.29), while Figs. 85 and 86 show the power and thrust coefficients calculated using Eqs. (2.32) and (2.33). Table 14 shows the comparison of the mean values from the CFD analysis to the quasi-steady lifting-line solution.

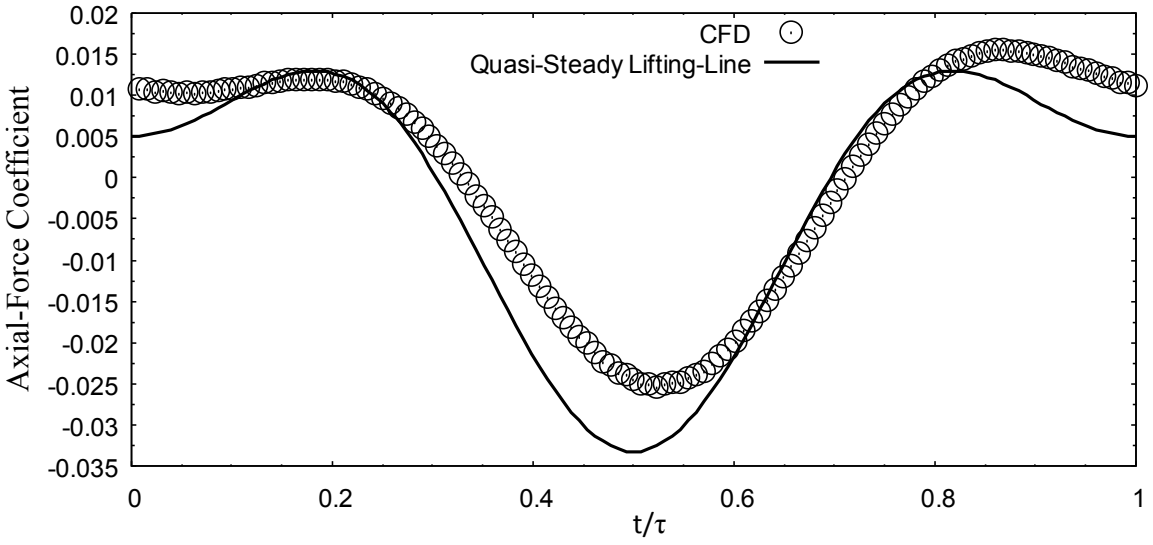

Fig. 83 Axial-force coefficient of oscillation cycle with $\hat{\omega}_x = 0.38327$, $\hat{\omega}_y = 0.07492$, and $\hat{\alpha}_y = 0.0$ compared to the quasi-steady lifting-line solution, Eq. (3.24).

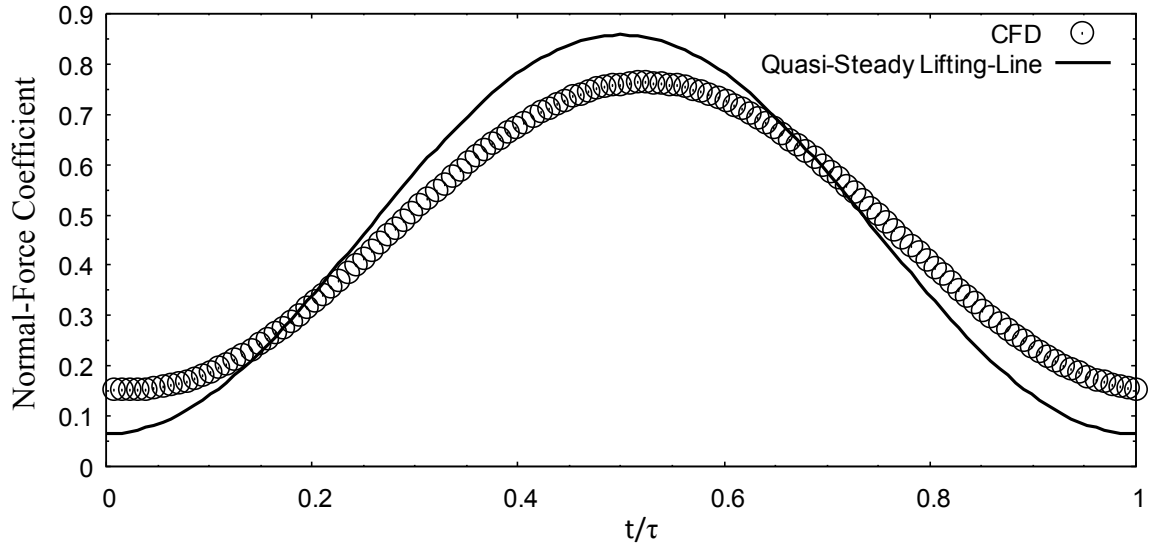

Fig. 84 Normal-force coefficient of oscillation cycle with $\hat{\omega}_x = 0.38327$, $\hat{\omega}_y = 0.07492$, and $\hat{\alpha}_y = 0.0$ compared to the quasi-steady lifting-line solution, Eq. (3.29).

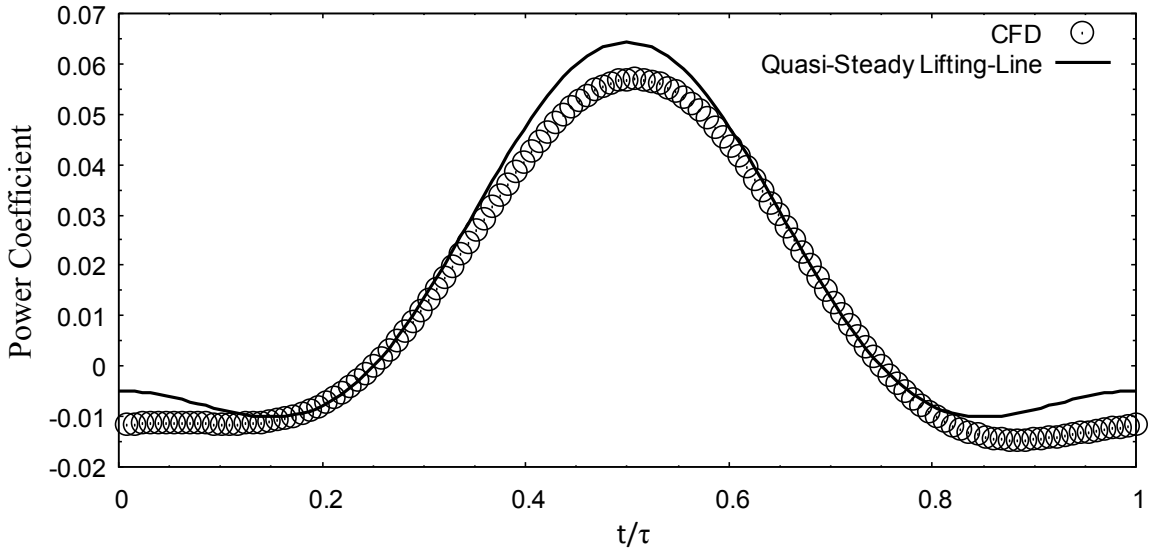

Fig. 85 Power coefficient of oscillation cycle with $\hat{\omega}_x = 0.38327$, $\hat{\omega}_y = 0.07492$, and $\hat{\alpha}_y = 0.0$ compared to the quasi-steady lifting-line solution, Eq. (3.34).

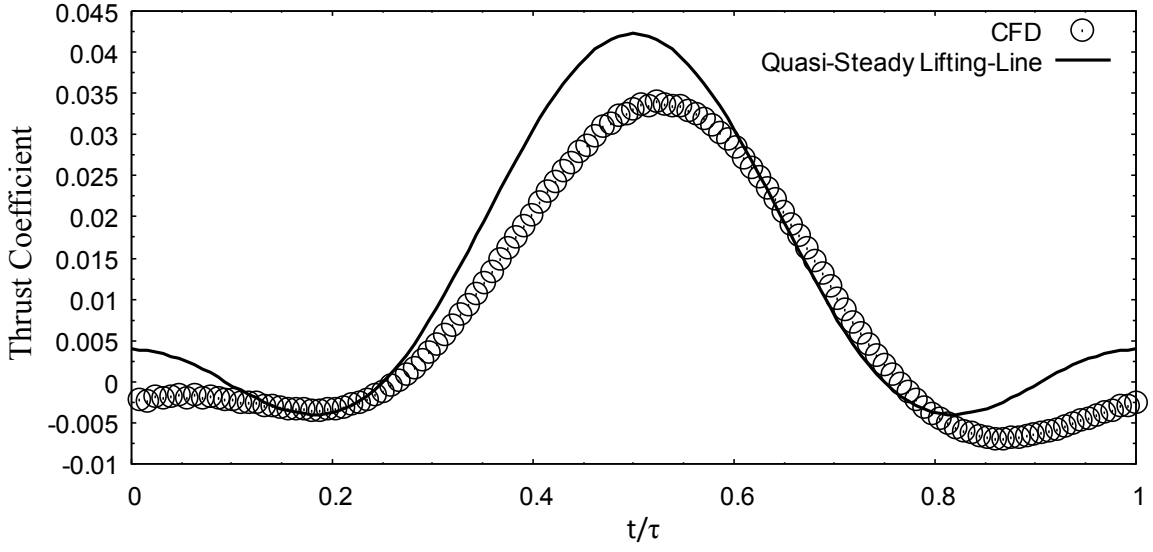

Fig. 86 Thrust coefficient of oscillation cycle with $\hat{\omega}_x = 0.38327$, $\hat{\omega}_y = 0.07492$, and $\hat{\alpha}_y = 0.0$ compared to the quasi-steady lifting-line solution, Eq. (3.40).

Table 14 Mean values of oscillation cycle with $\hat{\omega}_x = 0.38327$, $\hat{\omega}_y = 0.07492$, and $\hat{\alpha}_y = 0.0$ compared to the quasi-steady lifting-line solution

	$\hat{\omega}_x = 0.38327$, $\hat{\omega}_y = 0.07492$, $\hat{\alpha}_y = 0.0$	Quasi-Steady Lifting-Line
Mean Axial-Force Coefficient	0.000738117470188024	-0.002556914522526
Mean Normal-Force Coefficient	0.457668135908796	0.461438397544391
Mean Power Coefficient	0.011336641355661	0.014840559242373
Mean Thrust Coefficient	0.00788595399807323	0.011532618698595
Mean Efficiency	0.695616430887208	0.777101355160974

As can be seen in Figs. 83–86 and Table 14, this differed from the quasi-steady lifting-line solution the most from any of the previous CFD cases. As this was the highest frequency studied, this was expected, as the previous studied indicated that increasing frequency increasingly differs from the quasi-steady lifting-line solution.

2. Pitching and Plunging

Four cases were run for a combined pitching and plunging cycle. Two cases were run with a pitching amplitude of $\hat{\alpha}_y = 0.2$ and reduced frequency of $\hat{\omega}_y = 0.09365$, and two additional cases were run with $\hat{\alpha}_y = -0.2$, $\hat{\omega}_y = 0.06243$. The $\hat{\omega}_y$ for each pitching amplitude was found by keeping the maximum geometric angle of attack constant. The first two cases were run with $\hat{\alpha}_y = 0.2$, $\hat{\omega}_y = 0.09365$.

i. Pitching Amplitude $\hat{\alpha}_y = 0.2$, $\hat{\omega}_y = 0.09365$

The first analysis done was using $\hat{\omega}_x = 0.25797$, $\hat{\omega}_y = 0.09365$, and $\hat{\alpha}_y = 0.2$. Figures 87 and 88 show the axial- and normal-force coefficients calculated using Eqs. (2.28) and (2.29), while Figs. 89 and 90 show the power and thrust coefficients calculated using Eqs. (2.32) and (2.33). Table 15 shows the comparison of the mean values from the CFD analysis to the quasi-steady lifting-line solution.

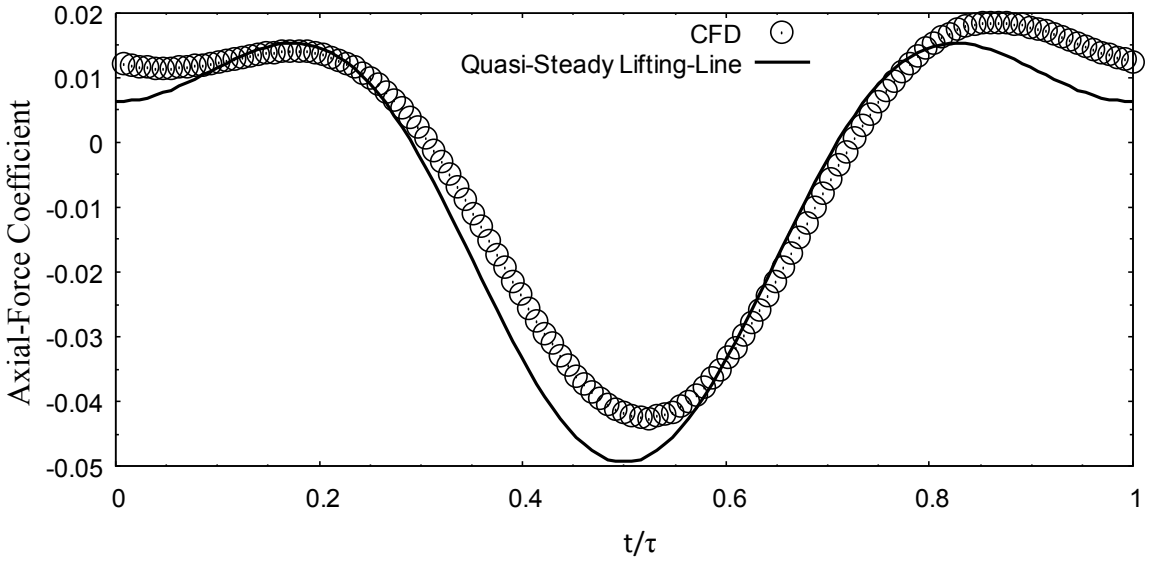

Fig. 87 Axial-force coefficient of oscillation cycle with $\hat{\omega}_x = 0.25797$, $\hat{\omega}_y = 0.09365$, and $\hat{\alpha}_y = 0.2$ compared to the quasi-steady lifting-line solution, Eq. (3.24).

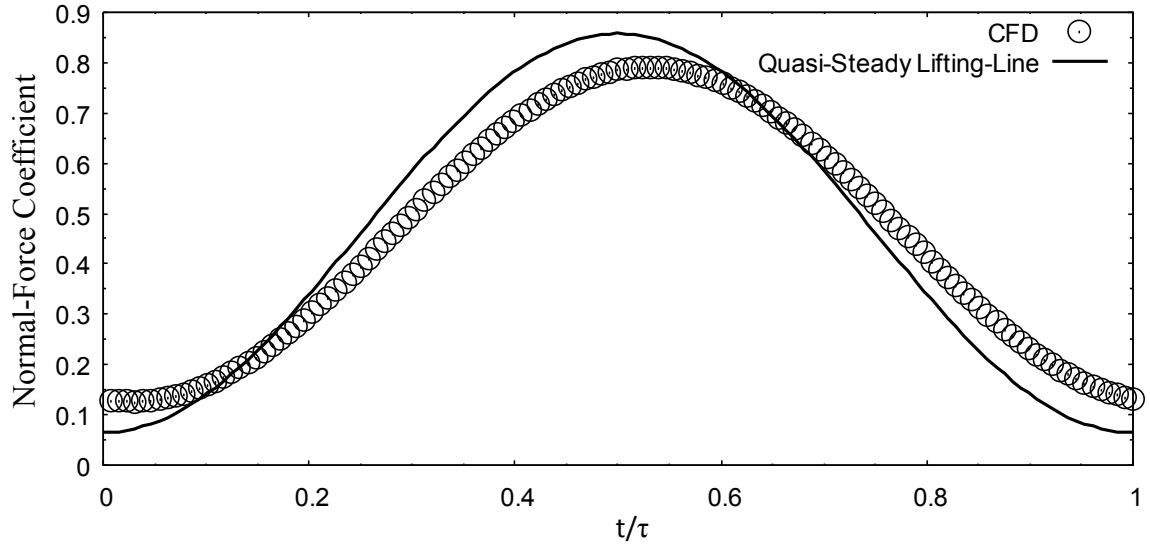

Fig. 88 Normal-force coefficient of oscillation cycle with $\hat{\omega}_x = 0.25797$, $\hat{\omega}_y = 0.09365$, and $\hat{\alpha}_y = 0.2$ compared to the quasi-steady lifting-line solution, Eq. (3.29).

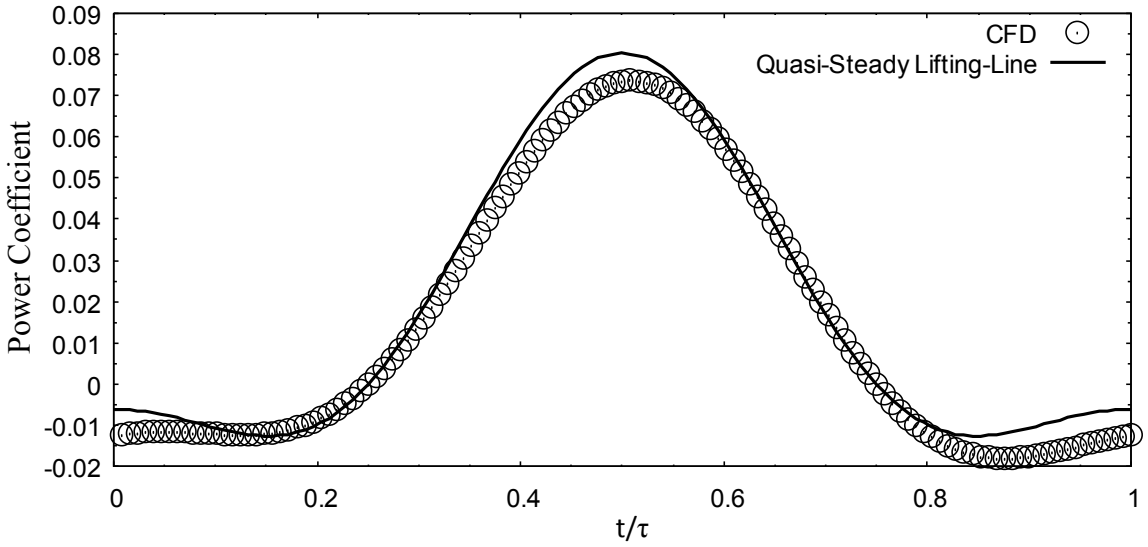

Fig. 89 Power coefficient of oscillation cycle with $\hat{\omega}_x = 0.25797$, $\hat{\omega}_y = 0.09365$, and $\hat{\alpha}_y = 0.2$ compared to the quasi-steady lifting-line solution, Eq. (3.34).

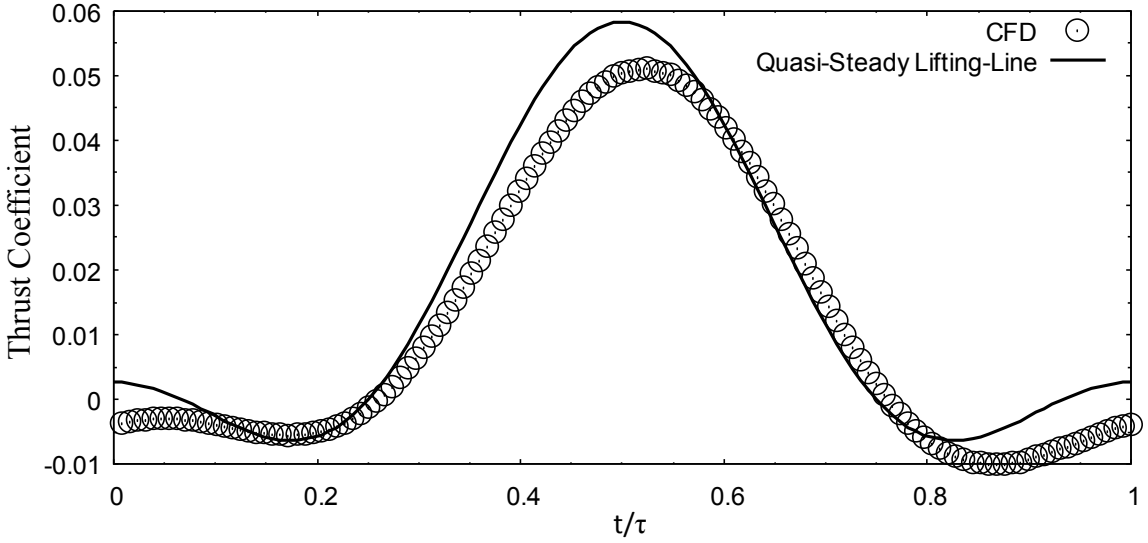

Fig. 90 Thrust coefficient of oscillation cycle with $\hat{\omega}_x = 0.25797$, $\hat{\omega}_y = 0.09365$, and $\hat{\alpha}_y = 0.2$ compared to the quasi-steady lifting-line solution, Eq. (3.40).

Table 15 Mean values of oscillation cycle with $\hat{\omega}_x = 0.25797$, $\hat{\omega}_y = 0.09365$, and $\hat{\alpha}_y = 0.2$ compared to the quasi-steady lifting-line solution

	$\hat{\omega}_x = 0.25797$, $\hat{\omega}_y = 0.09365$, $\hat{\alpha}_y = 0.2$	Quasi-Steady Lifting-Line
Mean Axial-Force Coefficient	-0.00330159388136112	-0.006267054333119
Mean Normal-Force Coefficient	0.458289344001795	0.461438397544391
Mean Power Coefficient	0.015269024411449	0.018550699052966
Mean Thrust Coefficient	0.0119256653496224	0.015242758509188
Mean Efficiency	0.781036497700554	0.821681084128779

As can be seen in Figs. 87–90 and Table 15, the CFD solution closely follows the quasi-steady lifting-line solution in the middle portion of the cycle. However, during the beginning and end of each cycle, the CFD solution differs quite extensively. It is also interesting to note that for the combined pitching and plunging, the normal-force coefficient differs more than the axial-force coefficient, as was the case in pure plunging.

The next oscillation frequency that was studied was with $\hat{\omega}_x = 0.47909$, $\hat{\omega}_y = 0.09365$, and $\hat{\alpha}_y = 0.2$. As can be seen, the frequency of the oscillation was higher than the previous case. Figures 91 and 92 show the axial- and normal-force coefficients calculated using Eqs. (2.28) and (2.29), while Figs. 93 and 94 show the power and thrust coefficients calculated using Eqs. (2.32) and (2.33). Table 16 shows the comparison of the mean values from the CFD analysis to the quasi-steady lifting-line solution.

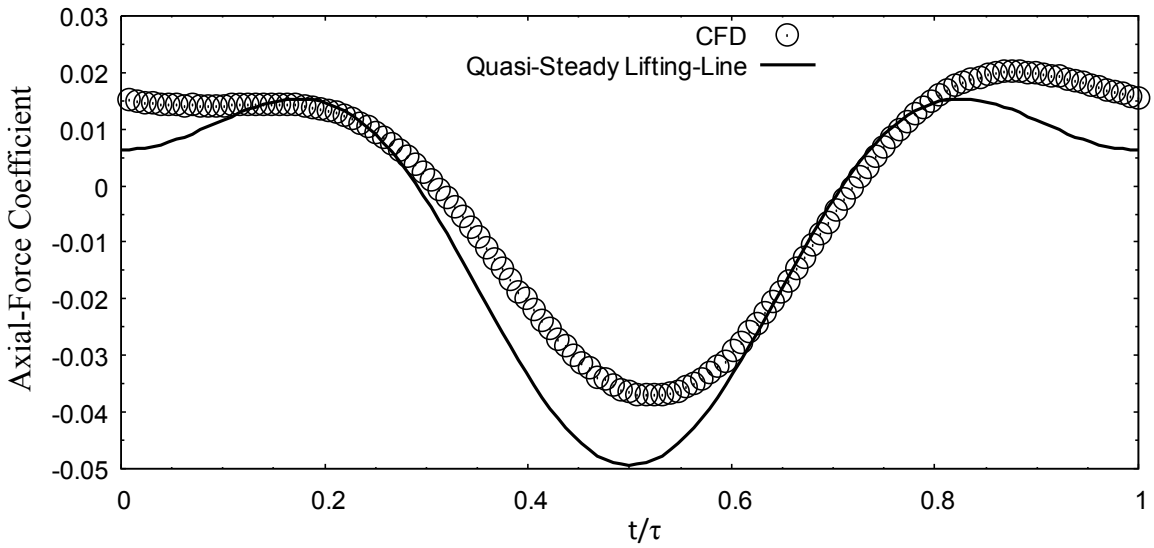

Fig. 91 Axial-force coefficient of oscillation cycle with $\hat{\omega}_x = 0.47909$, $\hat{\omega}_y = 0.09365$, and $\hat{\alpha}_y = 0.2$ compared to the quasi-steady lifting-line solution, Eq. (3.24).

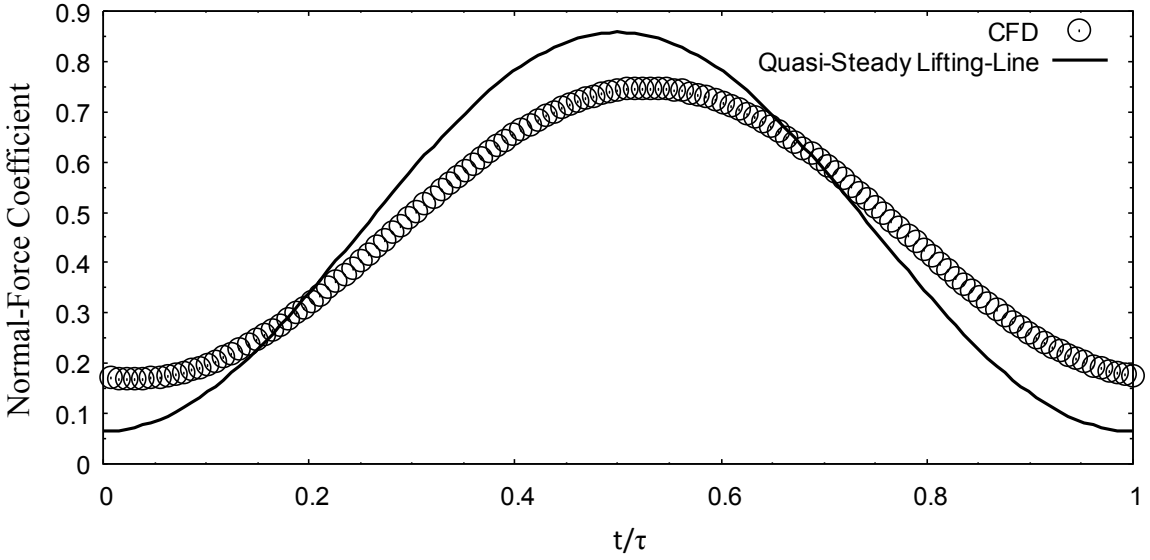

Fig. 92 Normal-force coefficient of oscillation cycle with $\hat{\omega}_x = 0.47909$, $\hat{\omega}_y = 0.09365$, and $\hat{\alpha}_y = 0.2$ compared to the quasi-steady lifting-line solution, Eq. (3.29).

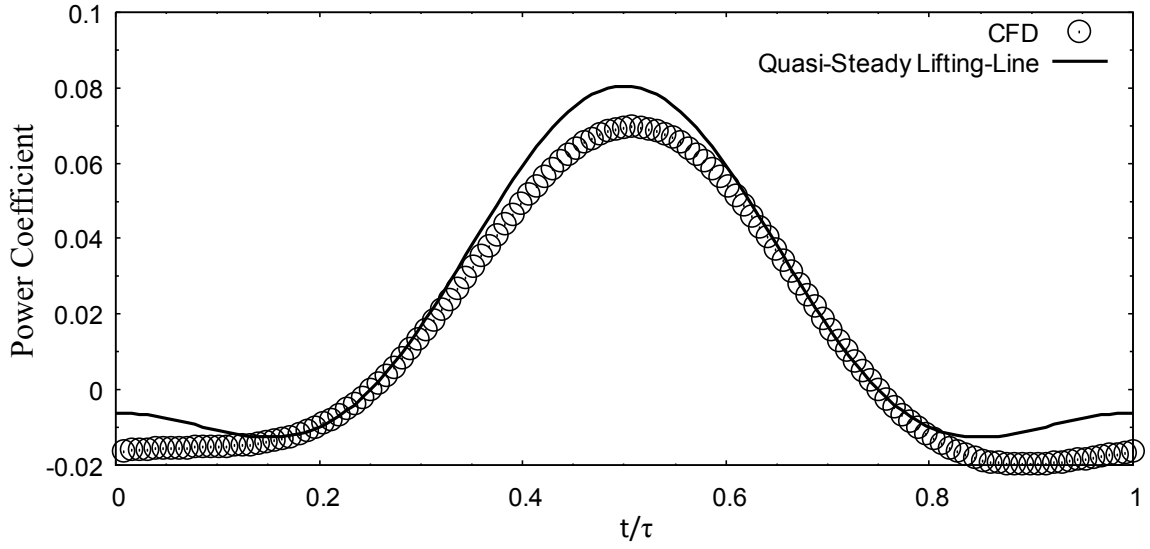

Fig. 93 Power coefficient of oscillation cycle with $\hat{\omega}_x = 0.47909$, $\hat{\omega}_y = 0.09365$, and $\hat{\alpha}_y = 0.2$ compared to the quasi-steady lifting-line solution, Eq. (3.34).

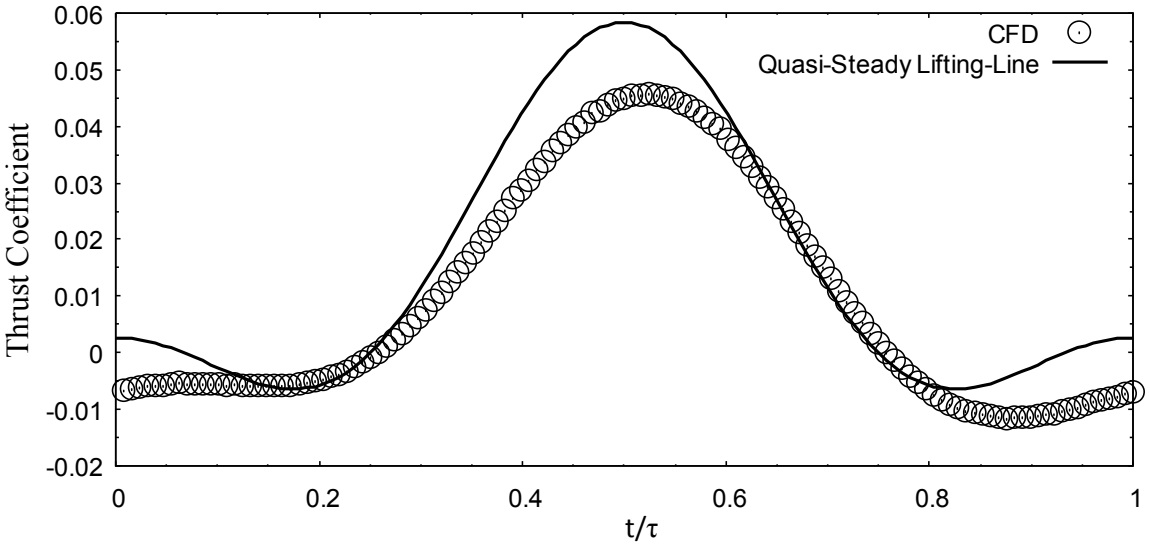

Fig. 94 Thrust coefficient of oscillation cycle with $\hat{\omega}_x = 0.47909$, $\hat{\omega}_y = 0.09365$, and $\hat{\alpha}_y = 0.2$ compared to the quasi-steady lifting-line solution, Eq. (3.40).

Table 16 Mean values of oscillation cycle with $\hat{\omega}_x = 0.47909$, $\hat{\omega}_y = 0.09365$, and $\hat{\alpha}_y = 0.2$ compared to the quasi-steady lifting-line solution

	$\hat{\omega}_x = 0.47909$, $\hat{\omega}_y = 0.09365$, $\hat{\alpha}_y = 0.2$	Quasi-Steady Lifting-Line
Mean Axial-Force Coefficient	-0.00112265642336803	-0.006267054333119
Mean Normal-Force Coefficient	0.458148614203382	0.461438397544391
Mean Power Coefficient	0.0132890173223486	0.018550699052966
Mean Thrust Coefficient	0.00974672789162928	0.015242758509188
Mean Efficiency	0.733442334764505	0.821681084128779

As can be seen in Figs. 91–94 and Table 16, this higher frequency case of combined pitching and plunging differs even more so from the quasi-steady lifting-line solution than the previous case. This higher frequency case differs not only at the beginning and end of the cycle, but all throughout the entire cycle. Again, the normal-force coefficient differs more than the axial-force coefficient for this case. However, the efficiencies are comparable for this case.

ii. Pitching Amplitude $\hat{\alpha}_y = -0.2$, $\hat{\omega}_y = 0.06243$

The pitching amplitude $\hat{\alpha}_y$ was then changed to be -0.2. The first case using this pitching amplitude used $\hat{\omega}_x = 0.17198$, $\hat{\omega}_y = 0.06243$, and $\hat{\alpha}_y = -0.2$. This was a lower frequency oscillation. Figures 95 and 96 show the axial- and normal-force coefficients calculated using Eqs. (2.28) and (2.29), while Figs. 97

and 98 show the power and thrust coefficients calculated using Eqs. (2.32) and (2.33). Table 17 shows the comparison of the mean values from the CFD analysis to the quasi-steady lifting-line solution.

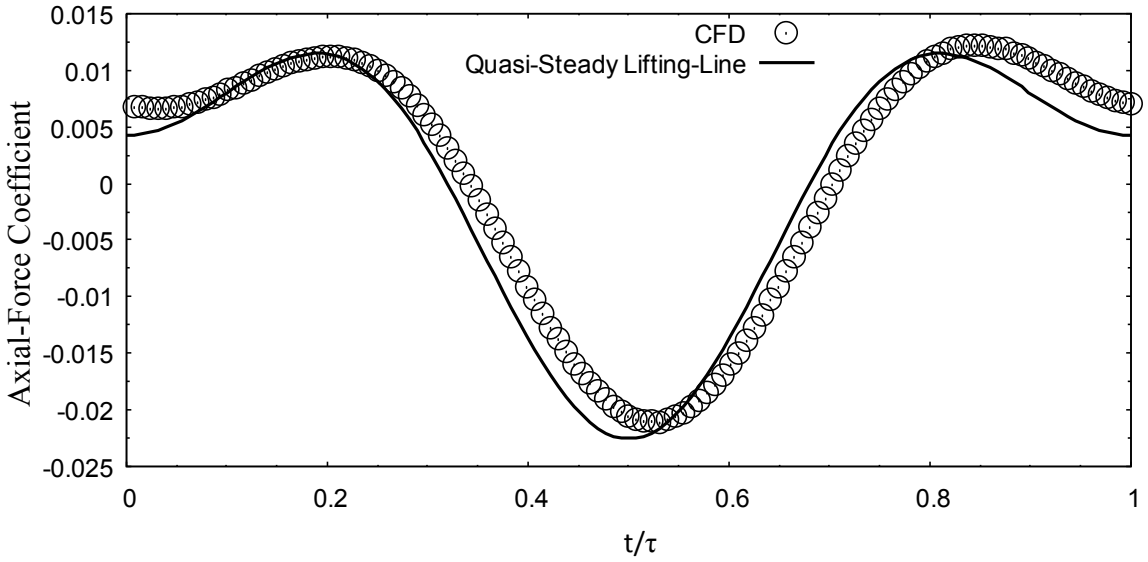

Fig. 95 Axial-force coefficient of oscillation cycle with $\hat{\omega}_x = 0.17198$, $\hat{\omega}_y = 0.06243$, and $\hat{\alpha}_y = -0.2$ compared to the quasi-steady lifting-line solution, Eq. (3.24).

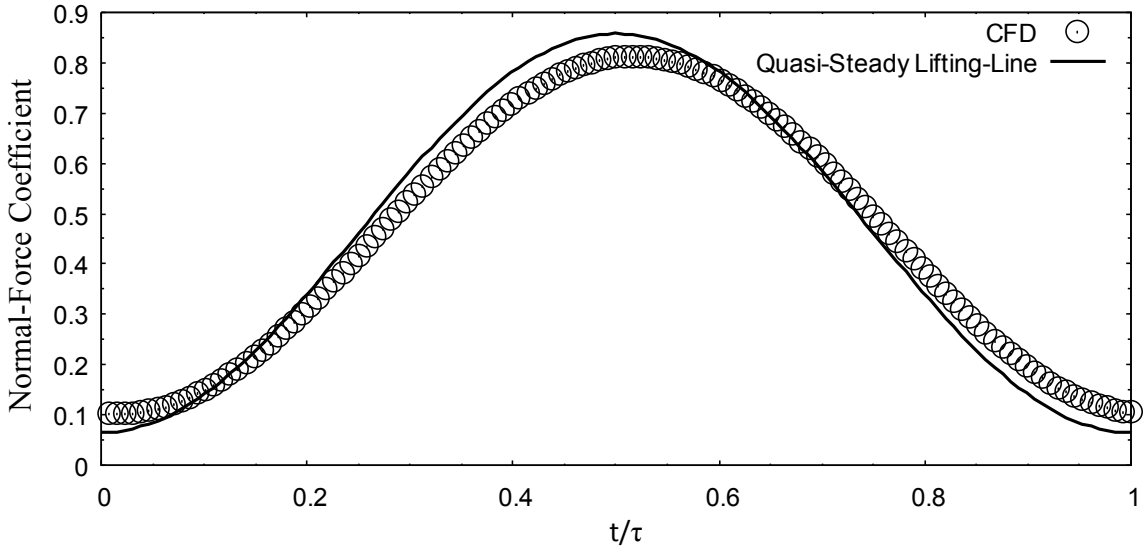

Fig. 96 Normal-force coefficient of oscillation cycle with $\hat{\omega}_x = 0.17198$, $\hat{\omega}_y = 0.06243$, and $\hat{\alpha}_y = -0.2$ compared to the quasi-steady lifting-line solution, Eq. (3.29).

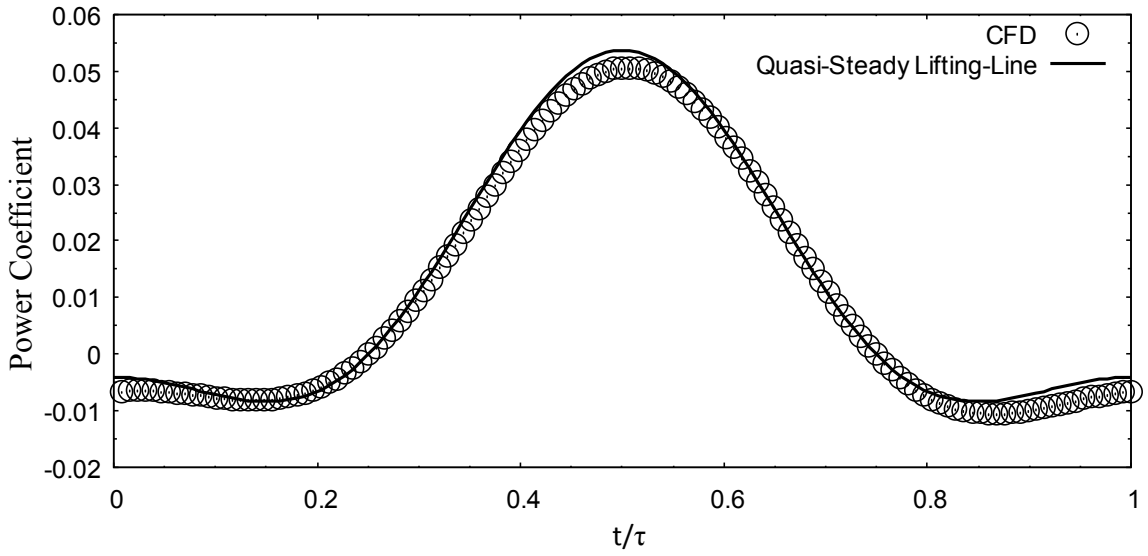

Fig. 97 Power coefficient of oscillation cycle with $\hat{\omega}_x = 0.17198$, $\hat{\omega}_y = 0.06243$, and $\hat{\alpha}_y = -0.2$ compared to the quasi-steady lifting-line solution, Eq. (3.34).

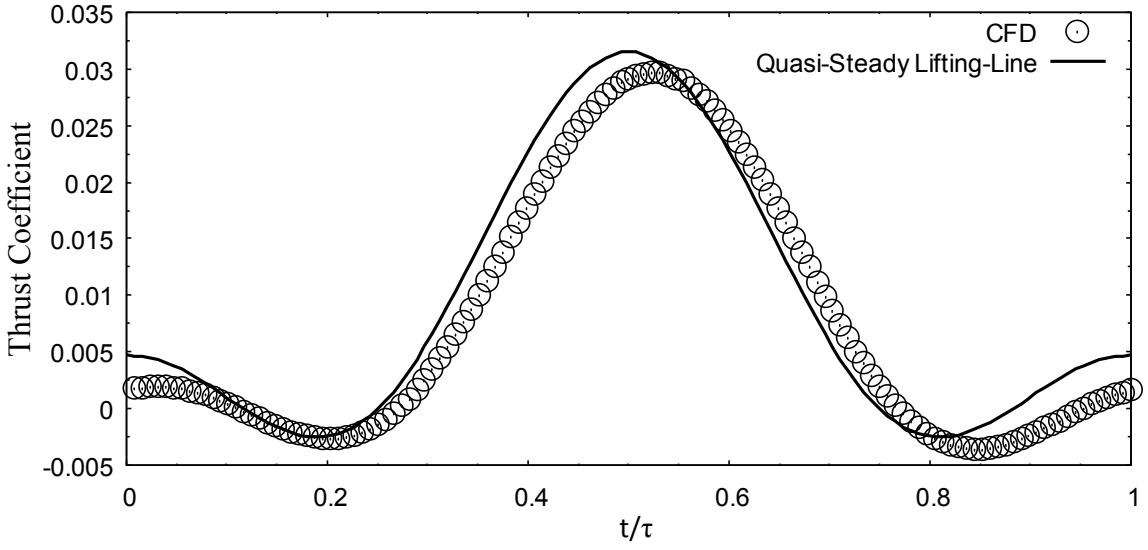

Fig. 98 Thrust coefficient of oscillation cycle with $\hat{\omega}_x = 0.17198$, $\hat{\omega}_y = 0.06243$, and $\hat{\alpha}_y = -0.2$ compared to the quasi-steady lifting-line solution, Eq. (3.40).

Table 17 Mean values of oscillation cycle with $\hat{\omega}_x = 0.17198$, $\hat{\omega}_y = 0.06243$, and $\hat{\alpha}_y = -0.2$ compared to the quasi-steady lifting-line solution

	$\hat{\omega}_x = 0.17198$, $\hat{\omega}_y = 0.06243$, $\hat{\alpha}_y = -0.2$	Quasi-Steady Lifting-Line
Mean Axial-Force Coefficient	0.000748896196075185	-0.000083487982131
Mean Normal-Force Coefficient	0.457571483483341	0.461438397544391
Mean Power Coefficient	0.0110089231760905	0.012367132701978
Mean Thrust Coefficient	0.00787517527218607	0.009059192158199
Mean Efficiency	0.715344738647067	0.732521626193169

As can be seen in Figs. 95–98 and Table 17, this particular combined pitching and plunging case very closely follows the quasi-steady lifting-line solution for normal-force and power coefficients. However, the axial-force and thrust coefficients differ significantly. It is also observed that as the previous combined pitching and plunging cases differed at the beginning and end of the cycle, this case differs most significantly in the middle of the cycle. It is also seen that the efficiency of the CFD cycle is much lower than the quasi-steady lifting-line solution.

The last oscillation frequency that was studied was with $\hat{\omega}_x = 0.31939$, $\hat{\omega}_y = 0.06243$, and $\hat{\alpha}_y = -0.2$. As can be seen, the frequency of the oscillation was higher than the previous case. Figures 99 and 100 show the axial- and normal-force coefficients calculated using Eqs. (2.28) and (2.29), while Figs. 101 and 102 show the power and thrust coefficients calculated using Eqs. (2.32) and (2.33). Table 18 shows the comparison of the mean values from the CFD analysis to the quasi-steady lifting-line solution.

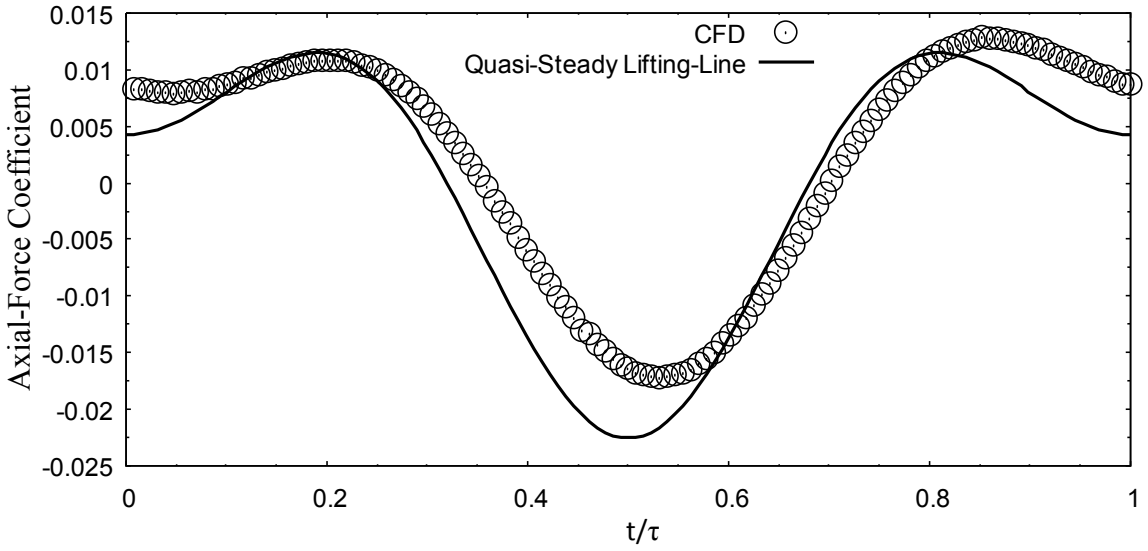

Fig. 99 Axial-force coefficient of oscillation cycle with $\hat{\omega}_x = 0.31939$, $\hat{\omega}_y = 0.06243$, and $\hat{\alpha}_y = -0.2$ compared to the quasi-steady lifting-line solution, Eq. (3.24).

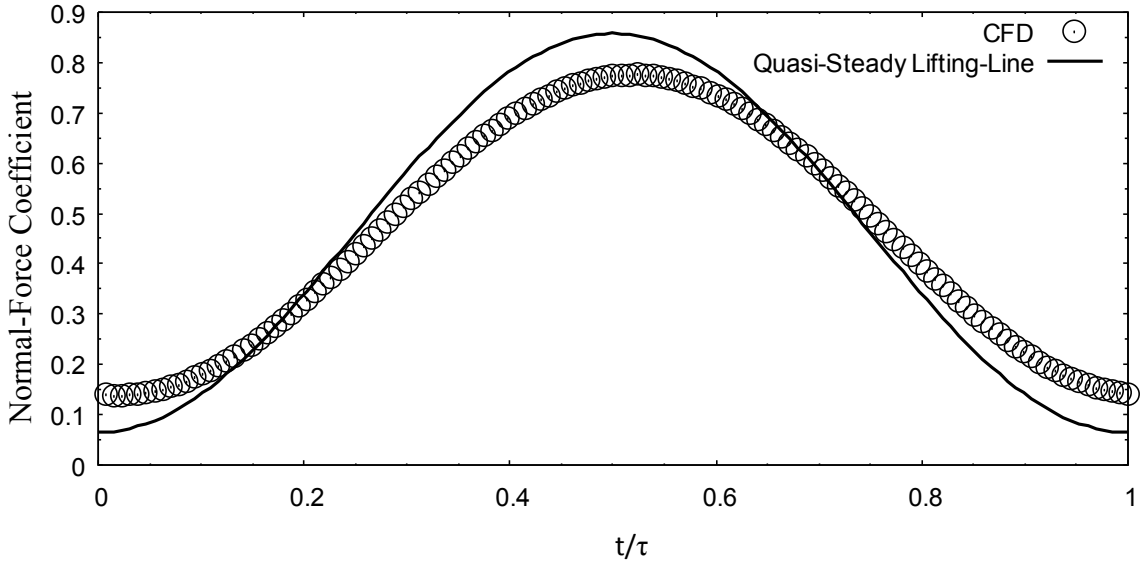

Fig. 100 Normal-force coefficient of oscillation cycle with $\hat{\omega}_x = 0.31939$, $\hat{\omega}_y = 0.06243$, and $\hat{\alpha}_y = -0.2$ compared to the quasi-steady lifting-line solution, Eq. (3.29).

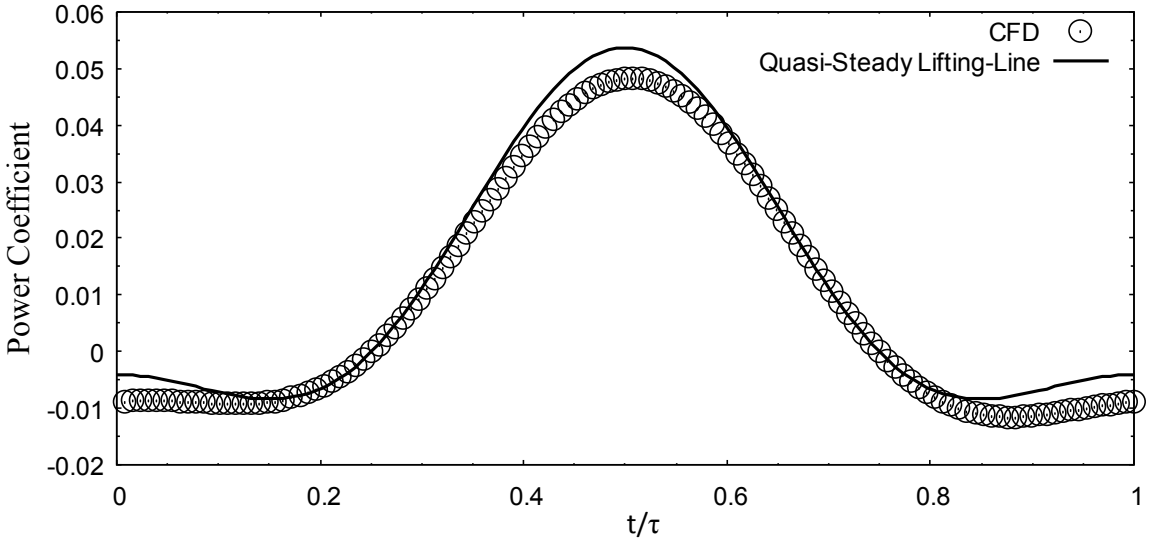

Fig. 101 Power coefficient of oscillation cycle with $\hat{\omega}_x = 0.31939$, $\hat{\omega}_y = 0.06243$, and $\hat{\alpha}_y = -0.2$ compared to the quasi-steady lifting-line solution, Eq. (3.34).

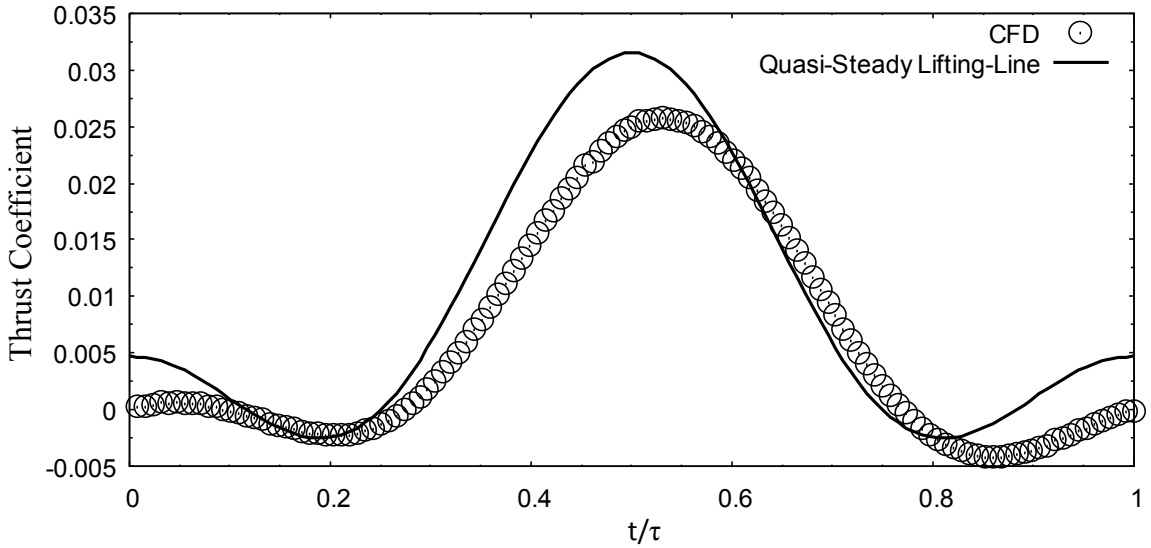

Fig. 102 Thrust coefficient of oscillation cycle with $\hat{\omega}_x = 0.31939$, $\hat{\omega}_y = 0.06243$, and $\hat{\alpha}_y = -0.2$ compared to the quasi-steady lifting-line solution, Eq. (3.40).

Table 18 Mean values of oscillation cycle with $\hat{\omega}_x = 0.31939$, $\hat{\omega}_y = 0.06243$, and $\hat{\alpha}_y = -0.2$ compared to the quasi-steady lifting-line solution

	$\hat{\omega}_x = 0.31939$, $\hat{\omega}_y = 0.06243$, $\hat{\alpha}_y = -0.2$	Quasi-Steady Lifting-Line
Mean Axial-Force Coefficient	0.00214490249202726	-0.000083487982131
Mean Normal-Force Coefficient	0.457396572013776	0.461438397544391
Mean Power Coefficient	0.0098643594051854	0.012367132701978
Mean Thrust Coefficient	0.006479168976234	0.009059192158199
Mean Efficiency	0.656826126269091	0.732521626193169

As can be seen in Figs. 99–102 and Table 18, this CFD case differs very significantly from the quasi-steady lifting-line solution in the axial-force and thrust coefficients. The difference is more severe than the previous case. It is also seen that the CFD efficiency is much lower than the quasi-steady lifting-line solution for this case.

C. Mean Results

The mean values for each of the $\hat{\omega}_x$ values simulated for both pure plunging and combined pitching and plunging is shown in Figs. 103–107. The quasi-steady lifting-line solutions are also shown for comparison.

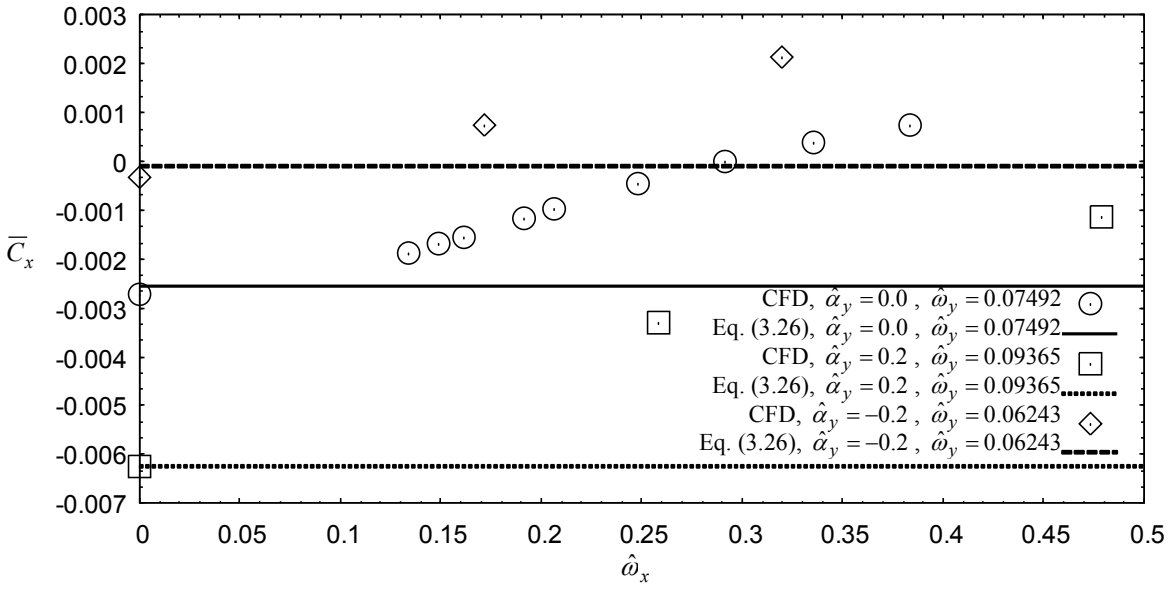

Fig. 103 Comparison of the CFD mean axial-force coefficients with quasi-steady lifting-line theory.

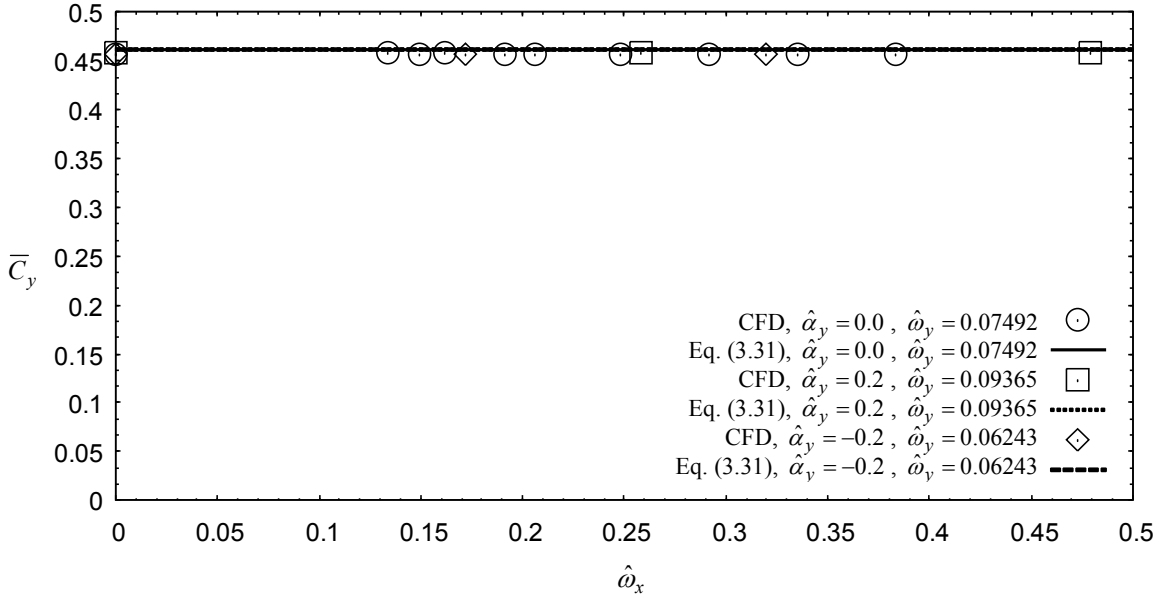

Fig. 104 Comparison of the CFD mean normal-force coefficients with quasi-steady lifting-line theory.

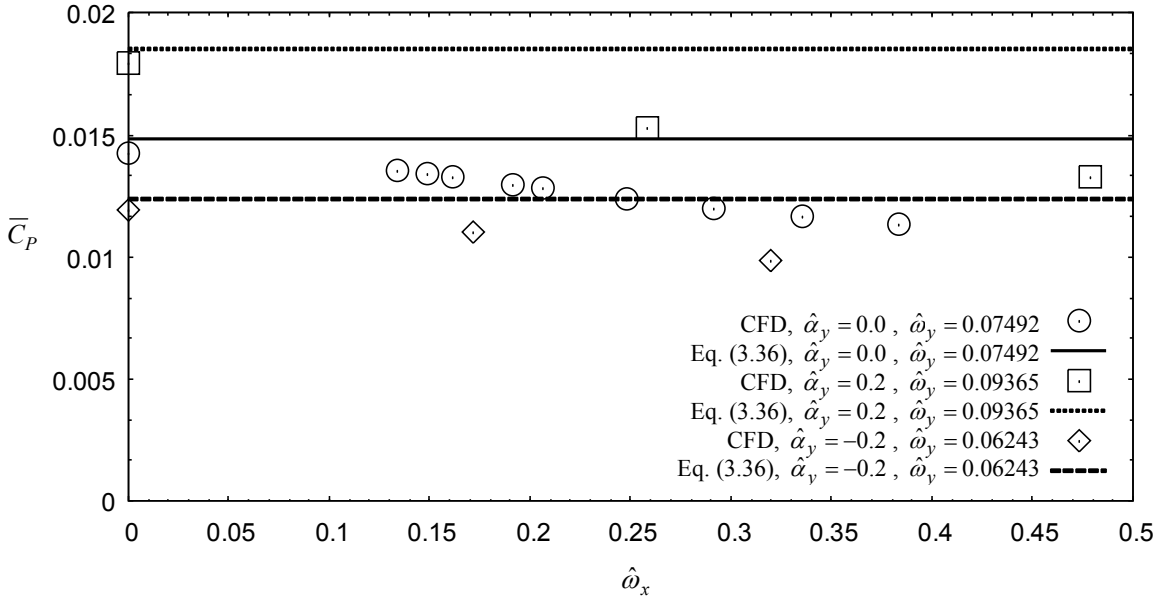

Fig. 105 Comparison of the CFD mean power coefficients with quasi-steady lifting-line theory.

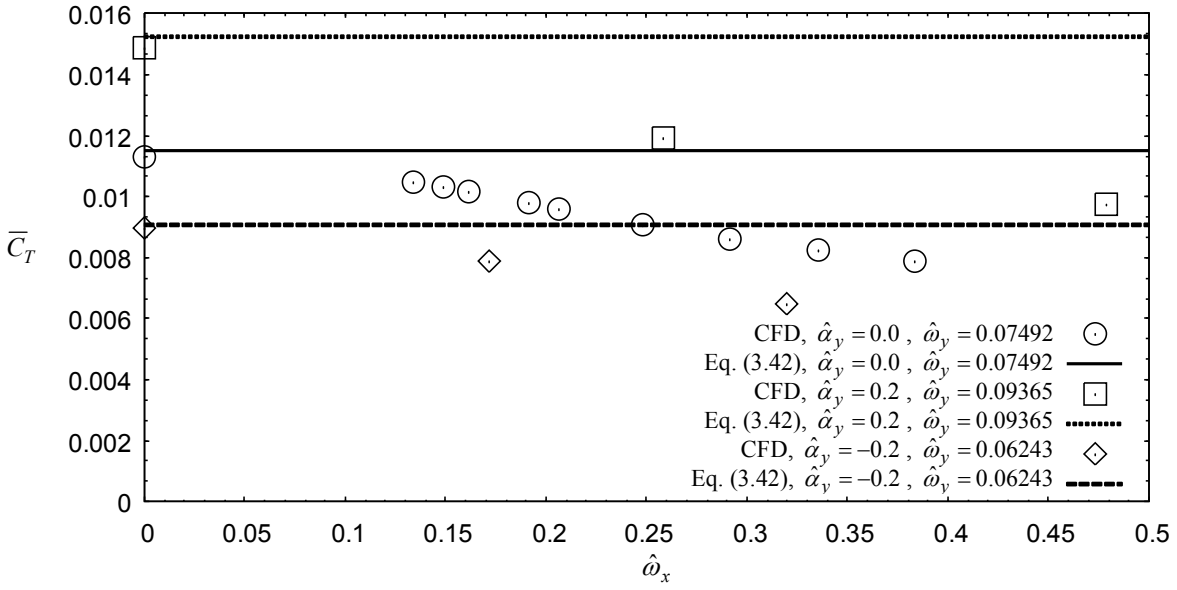

Fig. 106 Comparison of the CFD mean thrust coefficients with the quasi-steady lifting-line theory.

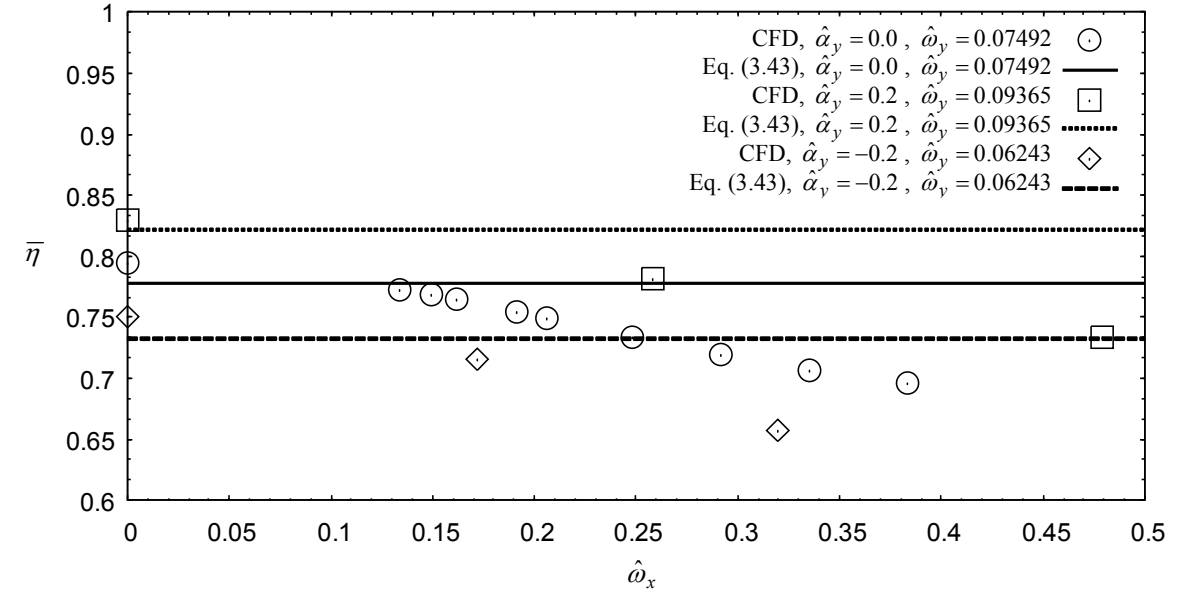

Fig. 107 Comparison of the CFD mean efficiency with the lifting-line theory.

The results from the CFD analysis clearly show that as the reduced frequency $\hat{\omega}_x$ is increased, lifting-line theory is decreasingly accurate in predicting solutions. This was most clearly seen in Figs. 35–81 for

pure plunging solutions. In the pure plunging simulations, both $\hat{\omega}_y$ and $\hat{\alpha}_y$ were held constant at $\hat{\omega}_y = 0.07492$ and $\hat{\alpha}_y = 0.0$. Therefore, the component that was varied was $\hat{\omega}_x$. Consistently, for all pure plunging and pitching and plunging simulations run, the normal-force, power, and thrust coefficients were lower than that predicted by lifting-line theory, as was seen in Figs. 104–106. However, the axial-force coefficient was consistently higher than that predicted by lifting-line theory, as shown in Fig. 103. This is as expected. As the reduced frequency $\hat{\omega}_x$ is increased, the axial-force coefficient increases due to the addition of drag from the wake. This drag is increasing because the faster the oscillating of the wings, the more the wake has an effect on the drag. This effect is an increase in the drag. This also is the reason for the decreasing thrust, as was shown in Fig. 106. This can easily be seen in the definitions for the axial-force and thrust coefficients. As was shown in Eq. (2.28) and (2.31), the axial-force and thrust coefficients are dependent on the force in the *x* direction. However, the thrust and the axial-force coefficients are opposite in sign. This is due to the defined direction of each the axial-force and thrust coefficients. Therefore, when the axial-force coefficient increases, the thrust coefficient decreases.

As can be seen in Eq. (1.43), using the small angle approximation, the lift vector is in line with the normal-force vector. This lift vector is rotated through the angle of attack due to plunging and the induced angle of attack, but not through the angle of attack due to pitching. This can be seen by the observation that the lift vector is perpendicular to the relative wind. This is also seen in Eq. (3.27) very clearly. Due to this, thrust is generated by plunging, not pitching, of the wing.

CHAPTER IV

CONCLUSIONS AND RECOMMENDATIONS FOR FUTURE WORK

A. Conclusion

Computational fluid dynamic simulations were desired to be performed in order to compare the solutions of oscillating wings with quasi-steady lifting-line theory. The first thing that was completed was software selection. Software for both the CFD simulations and the grid generation needed to be chosen. Ultimately, Star-CCM+ was chosen as the CFD software. One of the main reasons for choosing Star-CCM+ over other CFD software was its ability for easy motion specification, which was needed for this research. A separate grid generation software was chosen to create an acceptable grid. This software created a structured C-O grid that can be seen in Figs. 11–15. Nodes were clustered near the wing tip in the spanwise direction, at the leading and trailing edges of the airfoil in the chordwise direction, and in the wake region. A von Kármán Trefftz airfoil was chosen as the airfoil due to the fact that it has a closed-form solution. The grids created were a two-dimensional background grid, a three-dimensional background grid, and an overset grid. All of these grids were created using the grid generation software.

Grid convergence was then completed for the two-dimensional grid using quasi-steady simulations. The results from these simulations were then compared to the exact solution. When the difference between the two became acceptable, the grid was considered converged. Once grid convergence had been achieved for the two-dimensional grid, a grid convergence study was performed on the three-dimensional background grid. This was performed by comparing three-dimensional quasi-steady simulations to the quasi-steady lifting-line solution. These three-dimensional quasi-steady simulations were completed using 128 time steps per cycle, evenly spaced in angle of attack.

Once the grids were sufficiently converged, steady-periodic simulations could then be set up and completed using the three-dimensional background and overset grids. These simulations were determined to be both time-step and cycle resolved through another convergence study. The steady-periodic simulations used 128 time steps per cycle, equally spaced in t/τ, and completed a total of three cycles. The setup enabled a wing to oscillate at a range of frequencies, $\hat{\omega}_x$, and at multiple values of the pitching amplitude, $\hat{\alpha}_y$. These simulations were run for ten different values of $\hat{\omega}_x$ using $\hat{\alpha}_y = 0.0$, two values of $\hat{\omega}_x$ using $\hat{\alpha}_y = 0.2$, and two additional values of $\hat{\omega}_x$ using $\hat{\alpha}_y = -0.2$, totaling 14 steady-periodic simulations. The $\hat{\alpha}_y$ and $\hat{\omega}_y$ values were held constant while $\hat{\omega}_x$ was varied in order to keep a consistent maximum geometric angle of attack throughout all simulations performed. The simulations output values

for the forces in the x and y direction. These forces were converted to axial- and normal-force coefficients using Eqs. (2.28) and (2.29). Power and thrust coefficients were then calculated using Eqs. (2.32) and (2.33). Finally, the efficiency was computed using Eq. (3.3). The development for the quasi-steady lifting-line solutions for the coefficients were presented and can be seen in Eqs. (3.24), (3.29), (3.34), (3.40), and (3.43).

The results for these simulations presented as the axial-force, normal-force, power, and thrust coefficients were compared against the quasi-steady lifting-line solution and were shown in Figs. 43–94. It can easily be seen that as the reduced frequency $\hat{\omega}_x$ increased, the quasi-steady lifting-line solution was decreasingly accurate in predicting the response. The mean values for each quasi-steady simulation were calculated and presented as a function of the reduced frequency $\hat{\omega}_x$ in Figs. 95–99. It was observed that the axial-force coefficient increased as a function of $\hat{\omega}_x$, while the normal-force coefficient remained close to constant. This gave confidence that the CFD simulations were producing accurate results. Both the power and thrust coefficients decreased with $\hat{\omega}_x$, as was expected. It was noticed through Eq. (3.29) that thrust was generated only by plunging, not pitching, of the wing. Using the small angle approximation, the lift vector is in line with the normal-force vector. This lift vector is rotated through the angle of attack due to plunging and the induced angle of attack, but not through the angle of attack due to pitching. This can be seen by the observation that the lift vector is perpendicular to the relative wind. Therefore, thrust is generated by plunging, not pitching, of the wing.

Also noticed was that the mean normal-force coefficient was constant for all values of $\hat{\alpha}_y$. As seen in Eq. (3.28), the normal-force coefficient is equal to the lift coefficient. Equation (3.29) shows that this lift is dependent on both the plunging and the pitching in the combined expression $\hat{\omega}_y\left(1-\hat{\alpha}_y\right)$. Using Eqs. (1.21) and (1.22), this expression can be shown to be

$$\hat{\omega}_y\left(1-\hat{\alpha}_y\right)=\frac{\omega y_A}{V}-\alpha_A \tag{4.1}$$

It can be seen that all values on the right hand side of Eq. (4.1) are constants. Therefore, the expression used in Eq. (3.29), $\hat{\omega}_y\left(1-\hat{\alpha}_y\right)$, is a constant value. The zero-lift angle of attack and the wing lift slope are also constant values. The only variant in Eq. (3.29) is the term $\cos\left(2\pi t/\tau\right)$. The mean value of the cosine is zero, and therefore, the mean value of the normal-force coefficient for all values of $\hat{\alpha}_y$ is constant. This is also easily seen in Eq. (3.31).

B. Recommendations for Future Work

One of the first things that needs to be done in future work is the CFD study of additional $\hat{\omega}_x$ values for non-zero $\hat{\alpha}_y$ values. This will provide a fuller set of data and a better trend could then be seen. Additional studies also need to be completed for more values of $\hat{\alpha}_y$ to better identify the trend for each individual $\hat{\alpha}_y$ during combined pitching and plunging.

Experimental studies mimicking and comparing to the present research would also be beneficial. A von Kármán Trefftz airfoil was chosen due to it having a finite trailing edge angle, as opposed to a Joukowski airfoil. This finite trailing edge angle allows for experimental studies to be performed.

Once more insight is gained into the properties of a simple setup, such as the one in the present research, additional simulations with an increased number of complicating factors need to be explored. This includes CFD analysis of wing setup with a more traditional flyer with two wings hinged in the center. As the nature of oscillating wings is better understood, a correction to Prandtl's lifting-line theory to include the effects of oscillating wings could eventually be found.

REFERENCES

[1] Yang, T., and Wei, M., "A Fully-Coupled Approach to Simulate Three-Dimensional Flexible Flapping Wings," AIAA Paper 2013-0864, Jan. 2013.

[2] Young, J., "Numerical Simulation of the Unsteady Aerodynamics of Flapping Airfoils," Ph.D. Dissertation, The University of New South Wales, at the Australian Defense Force Academy, May 2005.

[3] Tuncer, I., and Kaya, M., "Optimization of Flapping Airfoils for Maximum Thrust and Propulsive Efficiency," *AIAA Journal*, Vol. 43, No. 11, 2005, pp. 2329–2336.

[4] Guglielmini, L., and Blondeaux, P., "Propulsive Efficiency of Oscillating Foils," *European Journal of Mechanics B Fluids*, Vol. 23, No. 2, 2004, pp. 255–278.

[5] Phlips, P. J., East, R. A., and Pratt, N. H., "An Unsteady Lifting Line Theory of Flapping Wings with Application to the Forward Flight of Birds," *Journal of Fluid Mechanics*, Vol. 112, Nov., 1981, pp. 97–125.

[6] Knoller, R., "Die Gesetze des Luftwiderstandes," *Flug- und Motortechnik (Wien)*, Vol. 3, No. 21, 1909, pp. 1–7.

[7] Betz, A., "Ein Beitrag zur Erklärung des Segelfluges," *Zeitschrift für Flugtechnik und Motorluftschiffahrt*, Vol. 3, Nov. 1912, pp. 269–272.

[8] Wagner, H. "Über die Entstehung des dynamischen Auftriebs von Tragflügeln," *Zeitschrift für Angewandte Mathematic und Mechanik*, Vol. 5, No. 1, 1925, pp. 17–35.

[9] Theodorsen, T., "General Theory of Aerodynamic Instability and the Mechanism of Flutter," NACA TR-496, Feb. 1935.

[10] von Kármán, T., and Burgers, J. M., "General Aerodynamic Theory — Perfect Fluids," *Aerodynamic Theory*, edited by Durand, W. F., Vol. 2, Springer, Berlin, 1935, pp. 293–310.

[11] Garrick, I. E., "Propulsion of a Flapping and Oscillating Airfoil," NACA TR-567, May 1936.

[12] Hunsaker, D. F., and Phillips, W. F., "Propulsion Theory of Flapping Airfoils, Comparison with Computational Fluid Dynamics," AIAA Paper 2015-0257, Jan. 2015.

[13] Jones, R. T., "The Unsteady Lift of a Wing of Finite Aspect Ratio," NACA TR-681, Jan. 1940.

[14] Minotti, F. O., "Determination of the Instantaneous Forces on Flapping Wings from a Localized Fluid Velocity Field," *Physics of Fluids*, Vol. 23, No. 11, 2011, pp. 111902-1–111902-10.

[15] Patil, M. J., "From Fluttering Wings to Flapping Flight: The Energy Connection," *Journal of Aircraft*, Vol. 40, No. 2, 2003, pp. 270–276.

[16] Johnson, W., "A Perturbation Solution of Helicopter Rotor Flapping Stability," *Journal of Aircraft*, Vol. 10, No. 5, 1973, pp. 257–258.

[17] Brunton, S. L. and Rowley, C. W., "Modeling the Unsteady Aerodynamic Forces on Small-Scale Wings," AIAA Paper 2009-1127, Jan. 2009.

[18] Glauert, H., "The Force and Moment on an Oscillating Aerofoil," Aeronautical Research Council R&M-1242, Mar. 1929, pp. 742–762.

[19] von Ellenrieder, K. D., Parker, K. and Soria, J., "Fluid Mechanics of Flapping Wings," *Experimental Thermal and Fluid Science*, Vol. 32, No. 8 2008, pp. 1578–1589.

[20] Katzmayr, R., "Effect of Periodic Changes of Angle of Attack on Behavior of Airfoils," NACA TR-147, Oct. 1922.

[21] Sunada, S., Kawachi, K., Matsumoto, A., and Sakaguchi, A., "Unsteady Forces on a Two-Dimensional Wing in Plunging and Pitching Motions," *AIAA Journal*, Vol. 39, No. 7, 2001, pp. 1230–1239.

[22] Birch, J. M., and Dickinson, M. H., "The Influence of Wing-Wake Interactions on the Production of Aerodynamic Forces in Flapping Flight," *Journal of Experimental Biology*, Vol. 206, July 2003, pp. 2257–2272.

[23] Lai, J. C., and Platzer, M. F., "Characteristics of a Plunging Airfoil at Zero Freestream Velocity," *AIAA Journal*, Vol. 39, No. 3, 2001, pp. 531–534.

[24] Godoy-Diana, R., Marais, C., Aider, J. L., and Wesfreid, J. E., "A Model for the Symmetry Breaking of the Reverse Bénard–von Kármán Vortex Street Produced by a Flapping Foil," *Journal of Fluid Mechanics*, Vol. 622, Mar. 2009, pp. 23–32.

[25] Milano, M., and Gharib, M., "Uncovering the Physics of Flapping Flat Plates with Artificial Evolution," *Journal of Fluid Mechanics*, Vol. 534, July 2005, pp. 403–409.

[26] Baik, Y. S., Bernal, L. P., Granlund, K., and Ol, M. V., "Unsteady Force Generation and Vortex Dynamics of Pitching and Plunging Aerofoils," *Journal of Fluid Mechanics*, Vol. 709, Oct. 2012, pp. 37–68.

[27] Chen, A. L., Jacob, J. D., and Savas, Ö., "Dynamics of Corotating Vortex Pairs in the Wakes of Flapped Airfoils," *Journal of Fluid Mechanics*, Vol. 382, Mar. 1999, pp. 155–193.

[28] Gopalkrishnan, R., Triantafyllou, M. S., Triantafyllou, G. S., and Barrett, D., "Active Vorticity Control in a Shear Flow Using a Flapping Foil," *Journal of Fluid Mechanics*, Vol. 274, Sept. 1994, pp. 1–21.

[29] Lua, K. B., Lim, T. T., Yeo, K. S., and Oo, G. Y., "Wake-Structure Formation of a Heaving Two-Dimensional Elliptic Airfoil," *AIAA Journal*, Vol. 45, No. 7, 2007, pp. 1571–1583.

[30] Pitt Ford, C. W., and Babinsky, H., "Lift and the Leading-Edge Vortex," *Journal of Fluid Mechanics*, Vol. 720, Apr. 2013, pp. 280–313.

[31] Anderson, J. M., Streitlien, K., Barrett, D. S., and Triantafyllou M. S., "Oscillating Foils of High Propulsive Efficiency," *Journal of Fluid Mechanics*, Vol. 360, Apr. 1998, pp. 41–72.

[32] Schnipper, T., Andersen, A., and Bohr, T., "Vortex Wakes of a Flapping Foil," *Journal of Fluid Mechanics*, Vol. 633, Aug. 2009, pp. 411–423.

[33] von Ellenrieder, K. D., and Pothos, S., "PIV Measurements of the Asymmetric Wake of a Two Dimensional Heaving Hydrofoil," *Experiments in Fluids*, Vol. 44, No. 5, 2008, pp. 733–745.

[34] Koochesfahani, M. M., "Vortical Patterns in the Wake of an Oscillating Airfoil," *AIAA Journal*, Vol. 27, No. 9, 1989, pp. 1200–1205.

[35] Lai, J. C., and Platzer, M. F., "Jet characteristics of a plunging airfoil," *AIAA Journal*, Vol. 37, No. 12, 1999, pp. 1529–1537.

[36] Bratt, J. B., "Flow Patterns in the Wake of an Oscillating Airfoil," Aeronautical Research Council R&M-2773, Mar. 1953, pp. 17–24.

[37] Freymuth, P., "Thrust Generation by an Airfoil in Hover Modes," *Experiments in Fluids*, Vol. 9, No. 1, 1990, pp. 17–24.

[38] Dickinson, M. H., and Goetz, K. G., "Unsteady Aerodynamic Performance of Model Wings at Low Reynolds Numbers," *Journal of Experimental Biology*, Vol. 174, Jan. 1993, pp. 45–64.

[39] Maresca, C., Favier, D. and Rebont, J., "Experiments on an Aerofoil at High Angle of Incidence in Longitudinal Oscillations," *Journal of Fluid Mechanics*, Vol. 92, June 1979, pp. 671–690.

[40] Izraelevitz, J. S., and Triantafyllou, M. S., "Adding In-Line Motion and Model-Based Optimization Offers Exceptional Force Control Authority in Flapping Foils," *Journal of Fluid Mechanics*, Vol. 742, Mar. 2014, pp. 5–34.

[41] Alben, S., "Flapping Propulsion Using a Fin Ray," *Journal of Fluid Mechanics*, Vol. 705, Aug. 2012, pp. 149–164.

[42] Bandyopadhyay, P. R., Beal, D. N., Hrubes, J. D., and Mangalam, A., "Relationship of Roll and Pitch Oscillations in a Fin Flapping at Transitional to High Reynolds Numbers," *Journal of Fluid Mechanics*, Vol. 702, July 2012, pp. 298–331.

[43] Sane, S. P., and Dickinson, M. H., "The Control of Flight Force by a Flapping Wing: Lift and Drag Production," *Journal of Experimental Biology*, Vol. 204, Aug. 2001, pp. 2607–2626.

[44] Seshadri, P., Benedict, M., and Chopra, I., "Understanding Micro Air Vehicle Flapping-Wing Aerodynamics Using Force and Flowfield Measurements," *Journal of Aircraft*, Vol. 50, No. 4, 2013, pp. 1070–1087.

[45] Heathcote, S. and Gursul, I., "Flexible Flapping Airfoil Propulsion at Low Reynolds Numbers," *AIAA Journal*, Vol. 45, No. 5, 2007, pp. 1066–1079.

[46] Yang, L. J., Ko, A. F., and Hsu, C. K., "Wing Stiffness on Light Flapping Micro Aerial Vehicles," *Journal of Aircraft*, Vol. 49, No. 2, 2012, pp. 423–431.

[47] Heathcote, S., and Gursul, I., "Jet Switching Phenomenon for a Periodically Plunging Airfoil," *Physics of Fluids*, Vol. 19, No. 2, 2007, pp. 027104-1–027104-12.

[48] Marais, C., Thiria, B., Wesfreid, J. E., and Godoy-Diana, R., "Stabilizing Effect of Flexibility in the Wake of a Flapping Foil," *Journal of Fluid Mechanics*, Vol. 710, Nov. 2012, pp. 659–669.

[49] Kaya, M., and Tuncer, I. H., "Nonsinusoidal Path Optimization of a Flapping Airfoil," *AIAA Journal*, Vol. 45, No. 8, 2007, pp. 2075–2082.

[50] Sarkar S., and Venkatraman, K., "Numerical Simulation of Incompressible Viscous Flow Past a Heaving Airfoil," *International Journal for Numerical Methods in Fluids*, Vol. 51, No. 1, 2006, pp. 1–29.

[51] Young, J., and Lai, J. C. S., "Mechanisms Influencing the Efficiency of Oscillating Airfoil Propulsion," *AIAA Journal*, Vol. 45, No. 7, 2007, pp. 1695–1702.

[52] Lee, K. B., Kim, J. H., and Kim, C., "Aerodynamic Effects of Structural Flexibility in Two-Dimensional Insect Flapping Flight," *Journal of Aircraft*, Vol. 48, No. 3, 2011, pp. 894–909.

[53] Miao, J. M., Sun, W. H., and Tai, C. H., "Numerical Analysis on Aerodynamic Force Generation of Biplane Counter-Flapping Flexible Airfoils," *Journal of Aircraft*, Vol. 46, No. 5, 2009, pp. 1785–1794.

[54] Yang, T., Wei, M., and Zhao, H., "Numerical Study of Flexible Flapping Wing Propulsion," *AIAA Journal*, Vol. 48, No. 12, 2010, pp. 2909–2915.

[55] Zhu, Q., "Numerical Simulation of a Flapping Foil with Chordwise or Spanwise Flexibility," *AIAA Journal*, Vol. 45, No. 10, 2007, pp. 2448–2457.

[56] Lian, Y., and Shyy, W., "Laminar-Turbulent Transition of a Low Reynolds Number Rigid or Flexible Airfoil," AIAA Paper 2006-3051, June 2006.

[57] Gulcat, U., "Propulsive Force of a Flexible Flapping Thin Airfoil," *Journal of Aircraft*, Vol. 46, No. 2, 2009, pp. 465–473.

[58] Blondeaux, P., Guglielmini, L., and Triantafyllou, M. S., "Chaotic Flow Generated by an Oscillating Foil," *AIAA Journal*, Vol. 43, No. 4, 2005, pp. 918–921.

[59] Eldredge, J. D., Toomey, J., and Medina, A., "On the Roles of Chord-wise Flexibility in a Flapping Wing with Hovering Kinematics," *Journal of Fluid Mechanics*, Vol. 659, Sep. 2010, pp. 94–115.

[60] Wang, Z. J., "Two Dimensional Mechanism for Insect Hovering," *Physical Review Letters*, Vol. 85, No. 10, 2000, pp. 2216–2219.

[61] Kurtulus, D. F., Farcy, A., and Alemdaroglu, N., "Unsteady Aerodynamics of Flapping Airfoil in Hovering Flight at Low Reynolds Numbers," AIAA Paper 2005-1356, Jan. 2005.

[62] Kurtulus, D. F., Farcy, A., and Alemdaroglu, N., "Aerodynamic Characteristics of Flapping Motion in Hover," *Experiments in Fluids*, Vol. 44, No. 1, 2008, pp. 23–26.

[63] Tang, J., Viieru, D., and Shyy, W., "Effects of Reynolds Number and Flapping Kinematics on Hovering Aerodynamics," *AIAA Journal*, Vol. 46, No. 4, 2008, pp. 967–976.

[64] Yin, B., and Luo, H., "Effect of Wing Inertia on Hovering Performance of Flexible Flapping Wings," *Physics of Fluids*, Vol. 22, No. 11, 2010, pp. 111902-1–111902-10.

[65] Isogai, K., Shinmoto, Y., and Watanabe, Y., "Effects of Dynamic Stall on Propulsive Efficiency and Thrust of Flapping Airfoil," *AIAA Journal*, Vol. 37, No. 10, 1999, pp. 1145–1151.

[66] Tuncer, I. H., Walz, R., and Platzer, M. F., "A Computational Study of the Dynamic Stall of a Flapping Airfoil," AIAA Paper 1998-2519, June 1998.

[67] Zheng, Z. C., and Wei, Z., "Study of Mechanisms and Factors that Influence the Formation of Vortical Wake of a Heaving Airfoil," *Physics of Fluids*, Vol. 24, No. 10, 2012, pp. 103601-1–103601-12.

[68] Liang, C. L., Ou, K., Premasuthan, S., Jameson, A., and Wang, Z. J., "High-order accurate simulations of unsteady flow past plunging and pitching airfoils," *Computers & Fluids*, Vol. 40, No. 1, 2011, pp. 236–248.

[69] Dong, H., Mittal, R., and Najjar, F. M., "Wake Topology and Hydrodynamic Performance of Low-Aspect-Ratio Flapping Foils," *Journal of Fluid Mechanics*, Vol. 566, Nov. 2006, pp. 309–343.

[70] Pan, Y., Dong, X., Zhu, Q., and Yue, D. K. P., "Boundary-Element Method for the Prediction of Performance of Flapping Foils with Leading-edge Separation," *Journal of Fluid Mechanics*, Vol. 698, May 2012, pp. 446–467.

[71] Ramesh, K., Gopalarathnam, A., Granlund, K., Ol, M. V., and Edwards, J. R., "Discrete-Vortex Method with Novel Shedding Criterion for Unsteady Aerofoil Flows with Intermittent Leading-Edge Vortex Shedding," *Journal of Fluid Mechanics*, Vol. 751, July 2014, pp. 500–538.

[72] Zhu, Q., and Peng, Z., "Mode Coupling and Flow Energy Harvesting by a Flapping Foil," *Physics of Fluids*, Vol. 21, No. 3, 2009, pp. 033601-1–033601-10.

[73] Lee, J., Kim, J., and Kim, C., "Numerical Study on the Unsteady-Force-Generation Mechanism of Insect Flapping Motion," *AIAA Journal*, Vol. 46, No. 7, 2008, pp. 1835–1848.

[74] Tuncer, I. H., and Platzer, M. F., "Computational Study of Flapping Airfoil Aerodynamics," *Journal of Aircraft*, Vol. 37, No. 2, 2000, pp. 514–520.

[75] Young, J., and Lai, J. C. S., "Oscillation Frequency and Amplitude Effects on the Wake of a Plunging Airfoil," *AIAA Journal*, Vol. 42, No. 10, 2004, pp. 2042–2052.

[76] Young, J., and Lai, J. C. S., "Vortex Lock-in Phenomenon in the Wake of a Plunging Airfoil," *AIAA Journal*, Vol. 45, No. 2, 2007, pp. 485–490.

[77] Zhu, Q., "Optimal Frequency for Flow Energy Harvesting of a Flapping Foil," *Journal of Fluid Mechanics*, Vol. 675, May 2011, pp. 495–517.

[78] Lewin, G. C., and Haj-Hariri, H., "Modelling Thrust Generation of a Two-Dimensional Heaving Airfoil in a Viscous Flow," *Journal of Fluid Mechanics*, Vol. 492, Oct. 2003, pp. 339–362

[79] Wang, Z. J., "Vortex Shedding and Frequency Selection in Flapping Flight," *Journal of Fluid Mechanics*, Vol. 410, May 2000, pp. 323–341.

[80] Zhang, X., Ni, S., Wang, S., and He, G., "Effects of Geometric Shape on the Hydrodynamics of a Self-Propelled Flapping Foil," *Physics of Fluids*, Vol. 21, No. 10, 2009, pp. 103302-1–103302-7.

[81] Gopalan, H., and Povitsky, A., "Lift Enhancement of Flapping Airfoils by Generalized Pitching Motion," *Journal of Aircraft*, Vol. 47, No. 6, 2010, pp. 1884–1897.

[82] Lu, X. Y., and Liao, Q., "Dynamic Responses of a Two-Dimensional Flapping Foil Motion," *Physics of Fluids*, Vol. 18, No. 9, 2006, pp. 098104-1–098104-4.

[83] Tuncer, I. H., and Platzer, M. F., "Thrust Generation Due to Airfoil Flapping," *AIAA Journal*, Vol. 34, No. 2, 1996, pp. 324–331.

[84] Tuncer, I. H., and Kaya, M., "Thrust Generation Caused by Flapping Airfoils in a Biplane Configuration," *Journal of Aircraft*, Vol. 40, No. 2, 2003, pp. 509–515.

[85] Kaya, M., Tuncer, I. H., Jones, K. D., and Platzer, M. F., "Optimization of Flapping Motion Parameters for Two Airfoils in a Biplane Configuration," *Journal of Aircraft*, Vol. 46, No. 2, 2009, pp. 583–592.

[86] Tay, W. B., Bijl, H., and van Oudheusden, B. W., "Biplane and Tail Effects in Flapping Flight," *AIAA Journal*, Vol. 51, No. 9, 2013, pp. 2133–2146.

[87] Choi, J. S., Kim, J. W., Park, G. J., and Lee, D. H., "Kinematic Optimization of a Flapping Motion for Maneuverability and Sustainability Flights," *Journal of Aircraft*, Vol. 50, No. 4, 2013, pp. 1027–1037.

[88] Leishman, J. G., "Unsteady Lift of a Flapped Airfoil by Indicial Concepts," *Journal of Aircraft*, Vol. 31, No. 2, 1994, pp. 288–297.

[89] Ramamurti, R., and Sandberg, W., "Simulation of Flow about Flapping Airfoils Using Finite Element Incompressible Flow Solver," *AIAA Journal*, Vol. 39, No. 2, 2001, pp. 253–260.

[90] Zhu, L., and Peskin, C. S., "Simulation of a Flapping Flexible Filament in a Flowing Soap Film by the Immersed Boundary Method," *Journal of Computational Physics*, Vol. 179, No. 2, 2002, pp. 452–468.

[91] Platzer, M. F., Neace, K. S., and Pang, K. C., "Aerodynamic Analysis of Flapping Wing Propulsion," AIAA Paper 1993-0484, Jan. 1993.

[92] Jones, K. D., and Platzer, M. F., "Time-Domain Analysis of Low-Speed Airfoil Flutter," *AIAA Journal*, Vol. 34, No. 5, 1996, pp. 1027–1033.

[93] Hall, K. C., and Hall, S. R., "A Rational Engineering Analysis of the Efficiency of Flapping Flight," *Fixed and Flapping Wing Aerodynamics for Micro Air Vehicles*, AIAA, Danvers, MA, 2001, pp. 249–274.

[94] Chae, E. J., Akcabay, D. T., and Young, Y. L., "Dynamic Response and Stability of a Flapping Foil in a Dense and Viscous Fluid," *Physics of Fluids*, Vol. 25, No. 10, 2013, pp. 104106-1–104106-27.

[95] Battaglia, F., Kulkarni, A. K., Feng, J., and Merkle, C. L., "Simulations of Planar Flapping Jets in Confined Channels," *AIAA Journal*, Vol. 36, No. 8, 1998, pp. 1425–1431.

[96] Wu, J., Qiu, Y. L., Shu, C., and Zhao, N., "Pitching-Motion-Activated Flapping Foil Near Solid Walls for Power Extraction: A Numerical Investigation," *Physics of Fluids*, Vol. 26, No. 8, 2014, pp. 083601-1–083601-19.

[97] Toomey, J., and Eldredge, J. D., "Numerical and Experimental Study of the Fluid Dynamics of a Flapping Wing with Low Order Flexibility," *Physics of Fluids*, Vol. 20, No. 7, 2008, pp. 073603-1–073603-10.

[98] Jones, K. D., Dohring, C. M., and Platzer, M. F., "Experimental and Computational Investigation of the Knoller-Betz Effect," *AIAA Journal*, Vol. 36, No. 7, 1998, pp. 1240–1246.

[99] Quinn, D. B., Moored, K. W., Dewey, P. A., and Smits, A. J., "Unsteady Propulsion Near a Solid Boundary," *Journal of Fluid Mechanics*, Vol. 742, Mar. 2014, pp. 152–170.

[100] Wang, Z. J., Birch, J. M., and Dickinson, M. H., "Unsteady Forces and Flows in Low Reynolds Number Hovering Flight: Two-Dimensional Computations vs Robotic Wing Experiments," *Journal of Experimental Biology*, Vol. 207, Jan. 2004, pp. 449–460.

[101] Ho, S., Nassef, H., Pornsinsirirak, N., Tai, Y. C., and Ho, C. M., "Unsteady Aerodynamics and Flow Control for Flapping Wing Flyers," *Progress in Aerospace Sciences*, Vol. 39, No. 8, 2003, pp. 635–681.

[102] von Holst, and Küchemann, D., "Biological and Aerodynamical Problems of Animal Flight," *Journal of the Royal Aeronautical Society*, Vol. 46, Jan. 1942, pp. 39–56.

[103] Ansari, S. A., Zbikowski, R., and Knowles, K., "Aerodynamic Modelling of Insect-like Flapping Flight for Micro Air Vehicles," *Progress in Aerospace Sciences*, Vol. 42, No. 2, 2006, pp. 129–172.

[104] Brown, R. J. H., "The flight of birds: II. Wing Function in Relation to Flight Speed," *Journal of Experimental Biology*, Vol. 30, Mar, 1953, pp. 90–103.

[105] Platzer, M. F., Jones, K. D., Young, J., and Lai, J. C. S., "Flapping-Wing Aerodynamics: Progress and Challenges," *AIAA Journal*, Vol. 46, No. 9, 2008, pp. 2136–2149.

[106] Chen, R. T. N., "Effects of Primary Rotor Parameters on Flapping Dynamics," NASA-TP-1431, Jan. 1980.

[107] Ellington, C. P., "The Aerodynamics of Hovering Insect Flight. V. A Vortex Theory," *Philosophical Transactions of the Royal Society of London*, Vol. 305, No. 1122, 1984, pp. 115–144.

[108] Weis-Fogh, T., "Quick Estimates of Flight Fitness in Hovering Animals Including Novel Mechanisms for Lift Production," *Journal of Experimental Biology*, Vol. 59, Aug. 1973, pp. 169–230.

[109] Ansari, S. A., Knowles, K., and Zbikowski, R., "Insectlike Flapping Wings in the Hover Part I: Effect of Wing Kinematics," *Journal of Aircraft*, Vol. 45, No. 6, 2008, pp. 1945–1954.

[110] Ansari, S. A., Knowles, K., and Zbikowski, R., "Insectlike Flapping Wings in the Hover Part II: Effect of Wing Geometry," *Journal of Aircraft*, Vol. 45, No. 6, 2008, pp. 1976–1990.

[111] Ansari, S. A., Zbikowski, R., and Knowles, K., "Nonlinear Unsteady Aerodynamic Model for Insect-like Flapping Wings in the Hover Part 1: Methodology and Analysis," *Proceedings of the Institute of Mechanical Engineering, Part G: Journal of Aerospace Engineering*, Vol. 220, No. 2, 2006, pp. 61–83.

[112] Gogulapati, A., Friedmann, P. P., Kheng, E., and Shyy, Wei, "Approximate Aeroelastic Modeling of Flapping Wings in Hover," *AIAA Journal*, Vol. 51, No. 3, 2013, pp. 567–583.

[113] Zbikowski, R., "On Aerodynamic Modelling of an Insect-like Flapping Wing in Hover for Micro Air Vehicles," *Philosophical Transactions of the Royal Society of London, Series A: Mathematical and Physical Sciences*, Vol. 360, No. 1791, 2002, pp. 273–290.

[114] Gogulapati, A., and Friedmann, P. P., "Approximate Aerodynamic and Aeroelastic Modeling of Flapping Wings in Forward Flight," *AIAA Journal*, Vol. 52, No. 1, 2014, pp. 212–218.

[115] Wilding, J., "Bird Flight and the Aeroplane," *Journal of the Royal Aeronautical Society*, Vol. 65, July 1961, pp. 796–799.

[116] Norberg, U. M., "Aerodynamics, Kinematics, and Energetics of Horizontal Flapping Flight in the Long-Eared bat Plecotus auritus," *Journal of Experimental Biology*, Vol. 65, Aug. 1976, pp. 179–212.

[117] Osborne, M. F. M., "Aerodynamics of Flapping Flight with Application to Insects," *Journal of Experimental Biology*, Vol. 28, June 1951, pp. 221–245.

[118] Wootton, R. J., and Kukalova-Peck, J., "Flight Adaptations in Palaeozoic Palaeoptera," *Biological Reviews of the Cambridge Philosophical Society*, Vol. 75, No. 1, 2000, pp. 129–167.

[119] Dickinson, M. H., Lehmann, F. O., and Sane, S. P., "Wing Rotation and the Aerodynamic Basis of Insect Flight," *Science*, Vol. 284, June 1999, pp. 1954–1960.

[120] Klemin, A., "Rotor Bending Moments in a Plane of Flapping," *Journal of the Aeronautical Sciences*, Vol. 9, No. 11, 1942, pp. 411–418.

[121] Betteridge, D. S. and Archer, R. D., "A Study of the Mechanics of Flapping Flight," *Aeronautical Quarterly*, Vol. 25, May 1974, pp. 129–142.

[122] Gopalakrishnan, P., and Tafti, D. K., "Effect of Rotation Kinematics and Angle of Attack on Flapping Flight," *AIAA Journal*, Vol. 47, No. 11, 2009, pp. 2505–2519.

[123] Truong, T. Q., Phan, V. H., Park, H. C., and Ko, J. H., "Effect of Wing Twisting on Aerodynamic Performance of Flapping Wing System," *AIAA Journal*, Vol. 51, No. 7, 2013, pp. 1612–1620.

[124] Li, G. J., and Lu, X. Y., "Force and Power of Flapping Plates in a Fluid," *Journal of Fluid Mechanics*, Vol. 712, Dec. 2012, pp. 598–613.

[125] Rayner, J. M. V., "A New Approach to Animal Flight Mechanics," *Journal of Experimental Biology*, Vol. 80, June 1979, pp. 17–54.

[126] Michelson, I., "Flapping Propulsion Wake Analysis," *AIAA Journal*, Vol. 1. No. 11, 1963, pp. 2658–2659.

[127] DeLaurier, J. D., "An aerodynamic model for flapping-wing flight," *Aeronautical Journal*, Vol. 97, Apr. 1993, pp. 125–130.

[128] Deng, X., Schenato, L., Wu, W. C., and Sastry, S. S., "Flapping Flight for Biomimetic Robotic Insects: Part I - System Modeling," *IEEE Transactions on Robotics*, Vol. 22, No. 4, 2006, pp. 776–788.

[129] Orlowski, C. T., and Girard, A. R., "Longitudinal Flight Dynamics of Flapping-Wing Micro Air Vehicles," *Journal of Guidance, Control, and Dynamics*, Vol. 35, No. 4, 2012, pp. 1115–1131.

[130] Shyy, W., Berg, M., and Ljungqvist, D., "Flapping and Flexible Wings for Biological and Micro Air Vehicles," *Progress in Aerospace Sciences*, Vol. 35, No. 5, 1999, pp. 455–505.

[131] Lan, C. E., "The Unsteady Quasi-Vortex-Lattice Method with Applications to Animal Propulsion," *Journal of Fluid Mechanics*, Vol. 93, Aug. 1979, pp. 747–765.

[132] Liu, T., "Time-Area-Averaged Momentum Stream Tube Model for Flapping Flight," *Journal of Aircraft*, Vol. 44, No. 2, 2007, pp. 459–466.

[133] Taylor, G. K., Nudds, R. L., and Thomas, A. L. R., "Flying and Swimming Animals Cruise at a Strouhal Number Tuned for High Power Efficiency," *Nature*, Vol. 425, Oct. 2003, pp. 707–711.

[134] Phillips, W. F., "Analytical Decomposition of Wing Roll and Flapping Using Lifting-Line Theory," AIAA Paper 2013-2918, June 2013.

[135] Phillips, W. F., "Analytical Decomposition of Wing Roll and Flapping Using Lifting-Line Theory," *Journal of Aircraft*, Vol. 51, No. 3, 2014, pp. 761–778.

[136] Phillips, W. F., Miller, R. A., and Hunsaker, D. F., "Decomposed Lifting-Line Predictions and Optimization for Propulsive Efficiency of Flapping Wings," AIAA Paper 2013-2921, June 2013.

[137] Phillips, W. F., "Lifting-Line Analysis for Twisted Wings and Washout-Optimized Wings," *Journal of Aircraft*, Vol. 41, No. 1, 2004, pp. 128–136.

[138] Phillips, W. F., "Incompressible Flow over Finite Wings," *Mechanics of Flight, 2nd ed.*, Wiley, Hoboken, NJ, 2010, pp. 46–94.

[139] Phillips, W. F., Alley, N. R., and Goodrich, W. D., "Lifting-Line Analysis of Roll Control and Variable Twist," *Journal of Aircraft*, Vol. 41, No. 5, 2004, pp. 1169–1176.

[141] Prandtl, L., "Tragflügel Theorie," *Nachricten von der Gesellschaft der Wissenschaften zu Göttingen*, Geschäeftliche Mitteilungen, Klasse, 1918, pp. 451–477.

[140] Prandtl, L., "Applications of Modern Hydrodynamics to Aeronautics," NACA TR-116, June 1921.

[142] Kutta, M. W., "Auftriebskräfte in Strömenden Flüssigkeiten," *Illustrierte Aeronautische Mitteilungen*, Vol. 6, No. 133, 1902, pp. 133–135.

[143] Joukowski, N. E., "Sur les Tourbillons Adjionts," *Traraux de la Section Physique de la Societé Imperiale des Amis des Sciences Naturales*, Vol. 13, No. 2, 1906, pp. 261–284.

[144] Phillips, W. F., Anderson, E. A., and Kelly, Q. J., "Predicting the Contribution of Running Propellers to Aircraft Stability Derivatives," *Journal of Aircraft*, Vol. 40, No. 6, 2003, pp. 1107–1114.

[145] Lighthill, M. J., "Aerodynamic Aspects of Animal Flight," *Bulletin of the Institute of Mathematics and its Applications*, Vol. 10, No. 3 1974, pp. 369–393.

[146] Pennycuick, C. J., "Power Requirements for Horizontal Flight in the Pigeon, Columba Livia," *Journal of Experimental Biology*, Vol. 49, Dec. 1968, pp. 527–555.

[147] Saharon, D., and Luttges, M., "Three-Dimensional Flow Produced by a Pitching-Plunging Model Dragonfly Wing," AIAA Paper 1987-0121, Jan. 1987.

[148] Childress, S., and Dudley, R., "Transition from Ciliary to Flapping Mode in a Swimming Mollusc: Flapping Flight as a Bifurcation in Re_{ω}," *Journal of Fluid Mechanics*, Vol. 498, Jan. 2004, pp. 257–288.

[149] Whitney, J. P., and Wood, R. J., "Aeromechanics of Passive Rotation in Flapping Flight," *Journal of Fluid Mechanics*, Vol. 660, Oct. 2010, pp. 197–220.

[150] Cloupeau, M., Devillers, J. and & Devezeaux, D., "Direct Measurements of Instantaneous Lift in Desert Locust; Comparison with Jensen's Experiments on Detached Wings," *Journal of Experimental Biology*, Vol. 80, June 1979, pp. 1–15.

[151] Sane, S. P., and Dickinson, M. H., "The Aerodynamic Effects of Wing Rotation and a Revised Quasi-Steady Model of Flapping Flight," *Journal of Experimental Biology*, Vol. 205, Jan. 2002, pp. 1087–1096.

[152] Warkentin, J., and DeLaurier, J., "Experimental Aerodynamic Study of Tandem Flapping Membrane Wings," *Journal of Aircraft*, Vol. 44, No. 5, 2007, pp. 1653–1661.

[153] Saharon, D., and Luttges, M., "Visualization of Unsteady Separated Flow Produced by Mechanically Driven Dragonfly Wing Kinematics Model," AIAA Paper 1988-0569, Jan. 1988.

[154] Saharon, D., and Luttges, M., "Dragonfly Unsteady Aerodynamic: The Role of the Wing Phase Relations in Controlling the Produced Flows," AIAA Paper 1989-0832, Jan. 1989.

[155] Ozen, C. A., and Rockwell, D., "Control of Vortical Structures on a Flapping Wing Via a Sinusoidal Leading-Edge," *Physics of Fluids*, Vol. 22, No. 2, 2010, pp. 021701-1–021701-3

[156] Hong, Y., and Altman, A., "Lift from Spanwise Flow in Simple Flapping Wings," *Journal of Aircraft*, Vol. 45, No. 3, 2008, pp. 1206–1216.

[157] Peng, D., and Milano, M., "Lift Generation with Optimal Elastic Pitching for a Flapping Plate," *Journal of Fluid Mechanics*, Vol. 717, Feb. 2013, pp. R1-1–R1-13.

[158] Schmidt, W., "Der Wellpropeller, ein Neuer Antrieb fuer Wasser-Land-, und Luftfahrzeuge," *Zeitschrift fur Flugwissenschaften*, Vol. 13, Oct. 1965, pp. 427–479.

[159] Heathcote, S., Wang, Z., and Gursul, I., "Effect of Spanwise Flexibility on Flapping Wing Propulsion," *Journal of Fluids and Structures,* Vol. 24, No. 2, 2008, pp. 182–199.

[160] Ellington, C. P., and Usherwood, J. R., "Lift and Drag Characteristics of Rotary and Flapping Wings," *Fixed and Flapping Wing Aerodynamics for Micro Air Vehicles*, AIAA, Danvers, MA, 2001, pp. 231–248.

[161] Heathcote, S., Martin, D., and Gursul, I., "Flexible Flapping Airfoil Propulsion at Zero Freestream Velocity," *AIAA Journal*, Vol. 42, No. 11, 2004, pp. 2196–2204.

[162] Norberg, R. A., "Hovering Flight of the Dragonfly Aeschna Juncea: Kinematics and Aerodynamics," *Swimming and Flying in Nature*, Plenum Press, New York, 1975, pp. 763–781.

[163] Sunada, S., Hatayama, Y., and Tokutake, H., "Pitch, Roll, and Yaw Damping of a Flapping Wing," *AIAA Journal*, Vol. 48, No. 6, 2010, pp. 1261–1265.

[164] Tarascio, M. J., Ramasamy, M., Chopra, I., and Leishman, J. G., "Flow Visualization of Micro Air Vehicle Scaled Insect-Based Flapping Wings," *Journal of Aircraft*, Vol. 42, No. 2, 2005, pp. 385–390.

[165] Goldschmidt, V. W., and Bradshaw, P., "Flapping of a Plane Jet," *Physics of Fluids*, Vol. 16, No. 3, 1973, pp. 397.

[166] Shinde, S. Y., and Arakeri, J. H., "Flexibility in Flapping Foil Suppresses Meandering of Induced Jet in Absence of Free Stream," *Journal of Fluid Mechanics*, Vol. 757, Oct. 2014, pp. 231–250.

[167] Hu, H., Clemons, L. and Igarashi, H., "An Experimental Study of the Unsteady Vortex Structures in the Wake of a Root-Fixed Flapping wing," *Experiments in Fluids*, Vol. 51, No. 2, 2011, pp. 347–359.

[168] Kokshaysky, N. V., "Tracing the Wake of a Flying Bird," *Nature*, Vol. 279, May 1979, pp. 146–148.

[169] Ren, W., Hu, H., Liu, H., and Wu, J. C., "An Experimental Investigation on the Asymmetric Wake Formation of an Oscillating Airfoil," AIAA Paper 2013-0794, Jan. 2013.

[170] Spedding, G. R., "The Wake of a Kestrel (Falco Tinnunculus) in Flapping Flight," *Journal of Experimental Biology*, Vol. 127, Jan. 1987, pp. 59–78.

[171] von Ellenrieder, K. D., Parker, K, and Soria, J., "Flow Structures Behind a Heaving and Pitching Finite-Span Wing," *Journal of Fluid Mechanics*, Vol. 490, Sep. 2003, pp. 129–138.

[172] Bandyopadhyay, P. R., and Leinhos, H. A., "Propulsion Efficiency of Bodies Appended with Multiple Flapping Fins: When More Is Less," *Physics of Fluids*, Vol. 25, No. 4, 2013, pp. 041902-1–041902-23.

[173] Wood, C. J., and Kirmani, S. F. A., "Visualization of Heaving Aerofoil Wakes Including the Effect of a Jet Flap," *Journal of Fluid Mechanics*, Vol. 41, Apr. 1970, pp. 627–640.

[174] Birch, J. M., Dickson, W. B., and Dickinson, M. H., "Force Production and Flow Structure of the Leading Edge Vortex on Flapping Wings at High and Low Reynolds Numbers," *Journal of Experimental Biology*, Vol. 207, Mar. 2004, pp. 1063–1072.

[175] Hong, Y., and Altman, A., "Streamwise Vorticity in Simple Mechanical Flapping Wings," *Journal of Aircraft*, Vol. 44, No. 5, 2007, pp. 1588–1597.

[176] Parker, K., Soria, J., and von Ellenrieder, K., "Thrust Measurements from a Finite-Span Flapping Wing," *AIAA Journal*, Vol. 45, No. 1, 2007, pp. 58–70.

[177] Parker, K., von Ellenrieder, K. D., and Soria, J., "Using Stereo Multigrid DPIV (SMDPIV) Measurements to Investigate the Vertical Skeleton Behind a Finite-Span Flapping Wing," *Experiments in Fluids*, Vol. 39, No. 2, 2005, pp. 281–298.

[178] Ramasamy, M., and Leishman, J. G., "Phase-Locked Particle Image Velocimetry Measurements of a Flapping Wing," *Journal of Aircraft*, Vol. 43, No. 5, 2006, pp. 1867–1876.

[179] Triantaflyllou, M. S., Techet, A. H. and Hover, F. S., "Review of Experimental Work in Biomimetic Foils," *IEEE Journal of Oceanic Engineering*, Vol. 29, No. 3, 2004, pp. 585–594.

[180] Grauer, J., Ulrich, E., Hubbard, J., Pines, D., and Humbert J. S., "Testing and System Identification of an Ornithopter in Longitudinal Flight," *Journal of Aircraft*, Vol. 48, No. 2, 2011, pp. 660–667.

[181] Lin, C. S., Hwu, C., and Young, W. B., "The Thrust and Lift of an Ornithopter's Membrane Wings with Simple Flapping Motion," *Aerospace Science and Technology*, Vol. 10, No. 2, 2006, pp. 111–119.

[182] Yang, L. J., Hsu, C. K., Han, H. C., and Miao, J. M., "Light Flapping Micro Aerial Vehicle Using Electrical-Discharge Wire-Cutting Technique," *Journal of Aircraft*, Vol. 46, No. 5, 2009, pp. 1866–1874.

[183] Zdunich, P., Bilyk, D., MacMaster, M., Loewen, D., DeLaurier, J., Kornbluh, R., Low, T., Stanford, S., and Holeman, D., "Development and Testing of the Mentor Flapping-Wing Micro Air Vehicle," *Journal of Aircraft*, Vol. 44, No. 5, 2007, pp. 1701–1711.

[184] Archer, R. D., Sapuppo, J. and Betteridge, D. S., "Propulsion Characteristics of Flapping Wings," *Aeronautical Journal*, Vol. 83, Sep. 1979, pp. 355–371.

[185] Yeo, D., Atkins, E. M., Bernal, L. P., and Shyy, W., "Experimental Characterization of Lift on a Rigid Flapping Wing," *Journal of Aircraft*, Vol. 50, No. 6, 2013, pp. 1806–1821.

[186] Jones, K. D., Bradshaw, C. J., Papadopoulos, J., and Platzer, M. F., "Bio-Inspired Design of Flapping-Wing Micro Air Vehicles," *Aeronautical Journal*, Vol. 109, Aug. 2005, pp. 385–393.

[187] Dickinson, M. H., "The Effects of Wing Rotation on Unsteady Aerodynamic Performance at Low Reynolds Numbers," *Journal of Experimental Biology*, Vol. 192, July 1994, pp. 179–206.

[188] Vandenberghe, N., Zhang, J., and Childress, S., "Symmetry Breaking Leads to Forward Flapping Flight," *Journal of Fluid Mechanics*, Vol. 506, May 2004, pp. 147–155.

[189] Birnbaum, W., "Das ebene Problem des Schlagenden Fluegels," *Zeitschrift fuer Angewandte Mathematik und Mechanik*, Vol. 4, No. 4, 1924, pp. 277–292.

[190] Vandenberghe, N., Childress, S., and Zhang, J., "On Unidirectional Flight of a Free Flapping Wing," *Physics of Fluids*, Vol. 18, No. 1, 2006, pp. 014102-1–014102-8.

[191] Lua, K. B., Lim, T. T., and Yeo, K. S., "Scaling of Aerodynamic Forces of Three-Dimensional Flapping Wings," *AIAA Journal*, Vol. 52, No. 5, 2014, pp. 1095–1101.

[192] Fejtek, I. and Nehera, J., "Experimental Study of Flapping Wing Lift and Propulsion," *Aeronautical Journal*, Vol. 84, Jan. 1980, pp. 28–33.

[193] Batina, J. T., "Unsteady Euler Algorithm with Unstructured Dynamic Mesh for Complex-Aircraft Aerodynamic Analysis," *AIAA Journal*, Vol. 29, No. 3, 1991, pp. 327–333.

[194] Roget, B., Sitaraman, J., Harmon, R., Grauer, J., Hubbard, J., and Humbert, S., "Computational Study of Flexible Wing Ornithopter Flight," *Journal of Aircraft*, Vol. 46, No. 6, 2009, pp. 2016–2031.

[195] Shkarayev, S., Maniar, G., and Shekhovtsov, A. V., "Experimental and Computational Modeling of the Kinematics and Aerodynamics of Flapping Wing," *Journal of Aircraft*, Vol. 50, No. 6, 2013, pp. 1734–1747.

[196] Cizmas, P., and Gargoloff, J., "Mesh Generation and Deformation Algorithm for Aeroelasticity Simulations," *Journal of Aircraft*, Vol. 45, No. 3, 2008, pp. 1062–1066.

[197] Hamdaoui, M., Chaskalovic, J., Doncieux, S., and Sagaut, P., "Using Multiobjective Evolutionary Algorithms and Data-Mining Methods to Optimize Ornithopters' Kinematics," *Journal of Aircraft*, Vol. 47, No. 5, 2010, pp. 1504–1516.

[198] Neef, M. F., and Hummel, D., "Euler Solutions for a Finite-Span Flapping Wing," *Fixed and Flapping Wing Aerodynamics for Micro Air Vehicles*, AIAA, Danvers, MA, 2001, pp. 429–451.

[199] Ramamurti, R., and Sandberg, W. C., "Computational Study of 3-D Flapping Foil Flows," AIAA Paper 2001-0605, Jan. 2001.

[200] Smith, M., "Simulating Moth Wing Aerodynamics: Towards the Development of Flapping-Wing Technology," *AIAA Journal*, Vol. 34, No. 7, 1996, pp. 1348–1355.

[201] Teng, N. H., "The Development of a Computer Code for the Numerical Solution of Unsteady Inviscid and Incompressible Flow Over an Airfoil," M.S. Thesis, Naval Postgraduate School, Monterey, CA, June 1987.

[202] Stanford, B. K., and Beran, P. S., "Analytical Sensitivity Analysis of an Unsteady Vortex-Lattice Method for Flapping-Wing Optimization," *Journal of Aircraft*, Vol. 47, No. 2, 2010, pp. 647–662.

[203] Fitzgerald, T., Valdez, M., and Balachandran, B., "A comparison of computational models for fluid-structure interaction studies of flexible flapping wing systems," AIAA Paper 2011-1115, Jan. 2011.

[204] Deng, J., Caulfield, C. P., and Shao, X., "Effect of Aspect Ratio on the Energy Extraction Efficiency of Three-Dimensional Flapping Foils," *Physics of Fluids*, Vol. 26, No. 4, 2014, pp. 043102-1–043102-24.

[205] Tucker, V. A., "Bird Metabolism During Flight, Evaluation of a Theory," *Journal of Experimental Biology*, Vol. 58, June 1973, pp. 689–709.

[206] Spentzos, A., Barakos, G. N., Badcock, K. J., Richards, B. E., Coton, F. N., Galbraith, R. A. McD., Berton, E., and Favier, D., "Computational Fluid Dynamics Study of Three-Dimensional Dynamic Stall of Various Planform Shapes," *Journal of Aircraft*, Vol. 44, No. 4, 2007, pp. 1118–1128.

[207] Hall, K. C., Pigott, S. A., and Hall, S. R., "Power Requirements for Large-Amplitude Flapping Flight," *Journal of Aircraft*, Vol. 35, No. 3, 1998, pp. 352–361.

[208] Buchmann, N., and Radespiel, R., "Computational Three-Dimensional Flapping-Wing Analysis," AIAA Journal, Vol. 52, No. 1, 2014, pp. 203–206.

[209] Rayner, J. M. V., "A Vortex Theory of Animal Flight. Part 1. The Vortex Wake of a Hovering Animal," *Journal of Fluid Mechanics*, Vol. 91, Apr. 1979, pp. 697–730.

[210] Ansari, S. A., Zbikowski, R., and Knowles, K., "Nonlinear Unsteady Aerodynamic Model for Insect-like Flapping Wings in the Hover Part 2: Implementation and Validation," *Proceedings of the Institute of Mechanical Engineering, Part G: Journal of Aerospace Engineering*, Vol. 220, No. 3, 2006, pp. 169–186.

[211] Gogulapati, A., Friedmann, P. P., and Martins, J. R. R. A., "Optimization of Flexible Flapping-Wing Kinematics in Hover," *AIAA Journal*, Vol. 52, No. 10, 2014, pp. 2342–2354.

[212] Isogai, K., and Shinmoto, Y., "Study on Aerodynamic Mechanism of Hovering Insects," AIAA Paper 2001-2470, June 2001.

[213] Jardin, T., Farcy, A., and David, L., "Three-Dimensional Effects in Hovering Flapping Flight," *Journal of Fluid Mechanics*, Vol. 702, July 2012, pp. 102–125.

[214] Kweon, J., and Choi, H., "Sectional Lift Coefficient of a Flapping wing in Hovering Motion," *Physics of Fluids*, Vol. 22, No. 7, 2010, pp. 071703-1–071703-4.

[215] Liu, H., Ellington, C. P., Kawachi, K., Van Den Berg, C., and Willmott, A. P., "A Computational Fluid Dynamic Study of Hawk-Moth Hovering," *Journal of Experimental Biology*, Vol. 201, Feb. 1998, pp. 461–477.

[216] Rosenfeld, N. C., and Wereley, N. M., "Time-Periodic Stability of a Flapping Insect Wing Structure in Hover," *Journal of Aircraft*, Vol. 46, No. 2, 2009, pp. 450–464.

[217] Stanford, B., Kurdi, M., Beran, P., and McClung, A., "Shape, Structure, and Kinematic Parameterization of a Power-Optimal Hovering Wing," *Journal of Aircraft*, Vol. 49, No. 6, 2012, pp. 1687–1699.

[218] Sun, M., and Tang, J., "Unsteady Aerodynamic Force Generation by a Model Fruit Fly Wing in Flapping Motion," *Journal of Experimental Biology*, Vol. 205, Jan. 2002, pp. 55–77.

[219] Young, J., Lai, J. C. S., and Germain, C., "Numerical Simulation and Parameter Variation of Insect Wing Motion based on Dragonfly Hovering," AIAA Paper 2006-0038, Jan. 2006.

[220] Zheng, L., Hedrick, T. L., and Mittal, R., "A Multi-Fidelity Modelling Approach for Evaluation and Optimization of Wing Stroke Aerodynamics in Flapping Flight," *Journal of Fluid Mechanics*, Vol. 721, Apr. 2013, pp. 118–154.

[221] Isogai, K., Fujishoro, S., Saitoh, T., Yamamoto, M., Yamasaki, M., and Matsubara, M., "Unsteady Three-Dimensional Viscous Flow Simulation of a Dragonfly Hovering," *AIAA Journal*, Vol. 42, No. 10, 2004, pp. 2053–2059.

[222] Su, J. Y., Tang, J. H., Wang, C. H., and Yang, J. T., "A Numerical Investigation on the Ground Effect of a Flapping-Flying Bird," *Physics of Fluids*, Vol. 25, No. 9, 2013, pp. 093101-1–093101-13.

[223] Viswanath, K., and Tafti, D. K., "Effect of Frontal Gusts on Forward Flapping Flight," *AIAA Journal*, Vol. 48, No. 9, 2010, pp. 2049–2062.

[224] Hua, R. N., Zhu, L., and Lu, X. Y., "Locomotion of a Flapping Flexible Plate," *Physics of Fluids*, Vol. 25, No. 12, 2013, pp. 121901-1–121901-17.

[225] Kang, C. K., Aono, H., Cesnik, C. E. S., and Shyy, W., "Effects of Flexibility on the Aerodynamic Performance of Flapping Wings," *Journal of Fluid Mechanics*, Vol. 689, Dec. 2011, pp. 32–74.

[226] Wang, S., Zhang, X., He, G., and Liu, T., "Lift Enhancement by Dynamically Changing Wingspan in Forward Flapping Flight," *Physics of Fluids*, Vol. 26, No. 6, 2014, pp. 061903-1–061903-19.

[227] Rakotomamonjy, T., Ouladsine, M., and Le Moing, T., "Modelization and Kinematics Optimization for a Flapping-Wing Microair Vehicle," *Journal of Aircraft*, Vol. 44, No. 1, 2007, pp. 217–231.

[228] Broering, T. M., Yongsheng, L., and Henshaw, W., "Numerical Investigation of Energy Extraction in a Tandem Flapping Wing Configuration," *AIAA Journal*, Vol. 50, No. 11, 2012, pp. 2295–2307.

[229] Viswanath, K., and Tafti, D. K., "Effect of Stroke Deviation on Forward Flapping Flight," *AIAA Journal*, Vol. 51, No. 1, 2013, pp. 145–160.

[230] Wu, J., and Shu, C., "Numerical Study of Flow Characteristics Behind a Stationary Circular Cylinder with a Flapping Plate," *Physics of Fluids*, Vol. 23, No. 7, 2011, pp. 073601-1–073601-17.

[231] Zhang, J., Liu, N. S., and Lu, X. Y., "Locomotion of a Passively Flapping Flat Plate," *Journal of Fluid Mechanics*, Vol. 659, Sep. 2010, pp. 43–68.

[232] Fritz, T. E., and Long, L. N., "Object-Oriented Unsteady Vortex Lattice Method for Flapping Flight," *Journal of Aircraft*, Vol. 41, No. 6, 2004, pp. 1275–1290.

[233] Yokoyama, N., Senda, K., Iima, M., and Hirai, N., "Aerodynamic Forces and Vortical Structures in Flapping Butterfly's Forward Flight," *Physics of Fluids*, Vol. 25, No. 2, 2013, pp. 021902-1–021902-24.

[234] Ramamurti, R., Sandberg, W., Valana, P., Kellogg, J., and Cylinder, D., "Computational Fluid Dynamics Study of Unconventional Air Vehicle Configurations," *Aeronautical Journal*, Vol. 109, July 2005. pp. 337–347.

[235] Ashraf, M. A., Young, J., Lai, J.C.S., and Platzer, M. F., "Aerodynamic Analysis of Flapping-Wing Propellers For HALE Aircraft," AIAA Paper 2009-0092, Jan. 2009.

[236] Liu H., and Kawachi, K., "Leading-Edge Vortices of Flapping and Rotary Wings at Low Reynolds Number," *Fixed and Flapping Wing Aerodynamics for Micro Air Vehicles*, AIAA, Danvers, MA, 2001, pp. 275–285.

[237] Blondeaux, P., Fornarelli, F., Guglielmini, L., Triantafyllou, M. S., and Verzicco, R., "Numerical Experiments on Flapping Foils Mimicking Fish-like Locomotion," *Physics of Fluids*, Vol. 17, No. 11, 2005, pp. 113601-1–113601-12.

[238] Chandar, D. D. J., and Damodaran, M., "Computation of Unsteady Low Reynolds Number Free-Flight Aerodynamics of Flapping Wings," *Journal of Aircraft*, Vol. 47, No. 1, 2010, pp. 141–150.

[239] Harbig, R. R., Sheridan, J., and Thompson, M. C., "The Role of Advance Ratio and Aspect Ratio in Determining Leading-Edge Vortex Stability for Flapping Flight," *Journal of Fluid Mechanics*, Vol. 751, July 2014, pp. 71–105.

[240] Rayner, J. M. V., "A Vortex Theory of Animal Flight. Part 2. The Forward Flight of Birds," *Journal of Fluid Mechanics*, Vol. 91, Apr. 1979, pp. 731–763.

[241] Shyy, W., Aono, H., Chimakurthi, S. K., Trizila, P., Kang, C. K., Cesnik, C. E. S., Liu, H., "Recent Progress in Flapping Wing Aerodynamics and Aeroelasticity," *Progress in Aerospace Sciences*, Vol. 46, No. 7, 2010, pp. 284–327.

[242] Smith, M., Wilkin, P., and Williams, M., "The advantages of an unsteady panel method in modelling the aerodynamic forces on rigid flapping wings," *Journal of Experimental Biology*, Vol. 199, May 1996, pp. 1073–1083.

[243] Wang, X. X., and Wu, Z. N., "Stroke-Averaged Lift Forces Due to Vortex Rings and Their Mutual Interactions for a Flapping Flight Model," *Journal of Fluid Mechanics*, Vol. 654, July 2010, pp. 453–472.

[244] Zhu, Q., Wolfgang, M. J., Yue, D. K. P., and Triantafyllou, M. S., "Three-Dimensional Flow Structures and Vorticity Control in Fish-like Swimming," *Journal of Fluid Mechanics*, Vol. 468, Oct. 2002, pp. 1–28.

[245] Vest, M., and Katz, J., "Unsteady Aerodynamic Model of Flapping Wings," *AIAA Journal*, Vol. 34, No. 7, 1996, pp. 1435–1440.

[246] Liu, H., "Computational Biological Fluid Dynamics: Digitizing and Visualizing Animal Swimming and Flying," *Integrative and Comparative Biology*, Vol. 42, No. 5, 2002, pp. 1050–1059.

[247] Brunton, S. L., Rowley, C. W., and Williams, D. R., "Reduced-Order Unsteady Aerodynamic Models at Low Reynolds Numbers," *Journal of Fluid Mechanics*, Vol. 724, June 2013, pp. 203–233.

[248] Isogai, K., and Harino, Y., "Optimum Aeroelastic Design of a Flapping Wing," *Journal of Aircraft*, Vol. 44, No. 6, 2007, pp. 2040–2048.

[249] Willis, D. J., and Persson, P. O., "Multiple-Fidelity Computational Framework for the Design of Efficient Flapping Wings," *AIAA Journal*, Vol. 52, No. 12, 2014, pp. 2840–2854.

[250] Hall, K. C., and Hall, S. R., "Minimum Induced Power Requirements for Flapping Flight," *Journal of Fluid Mechanics*, Vol. 323, Sep. 1996, pp. 285–315.

[251] Rozhdestvensky, K. V., and Ryzhov, V. A., "Aerohydrodynamics of Flapping-wing Propulsors," *Progress in Aerospace Sciences*, Vol. 39, No. 8, 2003, pp. 585–633.

[252] Phillips, W. F., and Snyder, D. O., "Modern Adaptation of Prandtl's Classic Lifting-Line Theory," *Journal of Aircraft*, Vol. 37, No. 4, 2000, pp. 662–670.

[253] Phillips, W. F., Fugal, S. R., and Spall, R. E., "Minimizing Induced Drag with Wing Twist, Computational-Fluid-Dynamics Validation," *Journal of Aircraft*, Vol. 43, No. 2, 2006, pp. 437–444.

[254] Moore, M. N. J., "Analytical Results on the Role of Flexibility in Flapping Propulsion," *Journal of Fluid Mechanics*, Vol. 757, Oct. 2014, pp. 599–612.

[255] Spagnolie, S. E., Moret, L., Shelley, M. J., and Zhang, J., "Surprising Behaviors in Flapping Locomotion with Passive Pitching," *Physics of Fluids*, Vol. 22, No. 4, 2010, pp. 041903-1–041903-20.

[256] Jones, K. D., Castro, B. M., Mahmoud, O., and Platzer, M. F., "A Numerical and Experimental Investigation of Flapping Wing Propulsion in Ground Effect," AIAA Paper 2002-0866, Jan. 2002.

[257] Isaac, K. M., Rolwes, J., and Colozza, A., "Aerodynamics of a Flapping and Pitching Wing Using Simulations and Experiments," *AIAA Journal*, Vol. 46, No. 6, 2008, pp. 1505–1515.

[258] Jones, K. D., Lund, T. C., and Platzer, M. F., "Experimental and Computational Investigation of Flapping Wing Propulsion for Micro Air Vehicles," *Fixed and Flapping Wing Aerodynamics for Micro Air Vehicles*, AIAA, Danvers, MA, 2001, pp. 307–339.

[259] Alben, S., "Optimal Flexibility of a Flapping Appendage in an Inviscid Fluid," *Journal of Fluid Mechanics*, Vol. 614, Nov. 2008, pp. 355–380.

[260] Orchini, A., Mazzino, A., Guerrero, J., Festa, R., and Boragno, C., "Flapping States of an Elastically Anchored Plate in a Uniform Flow with Applications to Energy Harvesting by Fluid-Structure Interaction," *Physics of Fluids*, Vol. 25, No. 9, 2013, pp. 097105-1–097105-17.

[261] CD-adapco, "User Guide: Star-CCM+ Version 8.06," 2013, pp. 1–13268.

[262] Alley, N. R., Phillips, W. F., and Spall, R. E., "Predicting Maximum Lift Coefficient for Twisted Wings Using Computational Fluid Dynamics," *Journal of Aircraft*, Vol. 44, No. 3, pp. 911–917.

[263] Richardson, L.F., "The Approximate Arithmetical Solution by Finite Differences of Physical Problems Involving Differential Equations, with an Application to the Stresses in a Masonry Dam," *Philosophical Transactions of the Royal Society A*, Vol. 210, Jan. 1911, pp. 307–357.

APPENDICES

APPENDIX A

TWO DIMENSIONAL SCRIPTS

Star-CCM+ Scripts

The following scripts were used to setup the simulations in Star-CCM+. These were in .java format.

```
// STAR-CCM+ macro: Setup.java
// Written by STAR-CCM+ 8.06.007
package macro;

import java.util.*;

import star.material.*;
import star.common.*;
import star.base.neo.*;
import star.base.report.*;
import star.flow.*;
import star.motion.*;
import star.metrics.*;
import star.segregatedflow.*;

public class A_Setup extends StarMacro {

  public void execute() {
    execute0();
  }

  private void execute0() {

    Simulation simulation_0 =
      getActiveSimulation();

    PhysicsContinuum physicsContinuum_0 =
      ((PhysicsContinuum)
simulation_0.getContinuumManager().getContinuum("Physics 1"));

    physicsContinuum_0.enable(SteadyModel.class);

    physicsContinuum_0.enable(SingleComponentGasModel.class);

    physicsContinuum_0.enable(SegregatedFlowModel.class);

    physicsContinuum_0.enable(ConstantDensityModel.class);

    physicsContinuum_0.enable(InviscidModel.class);

    SingleComponentGasModel singleComponentGasModel_0 =

physicsContinuum_0.getModelManager().getModel(SingleComponentGasModel.c
lass);
```

```
    Gas gas_0 =
      ((Gas) singleComponentGasModel_0.getMaterial());

    ConstantMaterialPropertyMethod constantMaterialPropertyMethod_0 =
      ((ConstantMaterialPropertyMethod)
gas_0.getMaterialProperties().getMaterialProperty(ConstantDensityProper
ty.class).getMethod());

    constantMaterialPropertyMethod_0.getQuantity().setValue(1.225);

    GradientsModel gradientsModel_0 =

physicsContinuum_0.getModelManager().getModel(GradientsModel.class);


gradientsModel_0.getGradientMethodOption().setSelected(GradientMethodOp
tion.GAUSS_GRADIENTS);

    Units units_0 =
      ((Units) simulation_0.getUnitsManager().getObject("atm"));


physicsContinuum_0.getReferenceValues().get(ReferencePressure.class).se
tUnits(units_0);


physicsContinuum_0.getReferenceValues().get(ReferencePressure.class).se
tValue(1.0);

    VelocityProfile velocityProfile_0 =

physicsContinuum_0.getInitialConditions().get(VelocityProfile.class);


velocityProfile_0.getMethod(ConstantVectorProfileMethod.class).getQuant
ity().setComponents(14.0, 0.0, 0.0);

    Region region_0 =
      simulation_0.getRegionManager().getRegion("Background");

    Boundary boundary_0 =
      region_0.getBoundaryManager().getBoundary("Farfield");

    boundary_0.setBoundaryType(InletBoundary.class);


boundary_0.getConditions().get(InletVelocityOption.class).setSelected(I
nletVelocityOption.COMPONENTS);

    VelocityProfile velocityProfile_1 =
      boundary_0.getValues().get(VelocityProfile.class);


velocityProfile_1.getMethod(ConstantVectorProfileMethod.class).getQuant
ity().setComponents(14.0, 0.0, 0.0);
```

```
    Boundary boundary_1 =
      region_0.getBoundaryManager().getBoundary("Outlet");

    boundary_1.setBoundaryType(OutletBoundary.class);

    Boundary boundary_2 =
      region_0.getBoundaryManager().getBoundary("Symmetry");

    boundary_2.setBoundaryType(SymmetryBoundary.class);

    Region region_1 =
      simulation_0.getRegionManager().getRegion("Foreground");

    Boundary boundary_3 =
      region_1.getBoundaryManager().getBoundary("Overset");

    boundary_3.setBoundaryType(OversetMeshBoundary.class);

    Boundary boundary_4 =
      region_1.getBoundaryManager().getBoundary("Symmetry");

    boundary_4.setBoundaryType(SymmetryBoundary.class);

    IndirectRegionInterface indirectRegionInterface_0 =

simulation_0.getInterfaceManager().createIndirectRegionInterface(region
_0, region_1, "Overset Mesh");

    SegregatedFlowSolver segregatedFlowSolver_0 =
      ((SegregatedFlowSolver)
simulation_0.getSolverManager().getSolver(SegregatedFlowSolver.class));

    VelocitySolver velocitySolver_0 =
      segregatedFlowSolver_0.getVelocitySolver();


velocitySolver_0.getRampCalculatorManager().getRampCalculatorOption().s
etSelected(RampCalculatorOption.LINEAR_RAMP);

    LinearRampCalculator linearRampCalculator_0 =
      ((LinearRampCalculator)
velocitySolver_0.getRampCalculatorManager().getCalculator());

    linearRampCalculator_0.setEndIteration(1000);

    PressureSolver pressureSolver_0 =
      segregatedFlowSolver_0.getPressureSolver();


pressureSolver_0.getRampCalculatorManager().getRampCalculatorOption().s
etSelected(RampCalculatorOption.LINEAR_RAMP);

    LinearRampCalculator linearRampCalculator_1 =
      ((LinearRampCalculator)
pressureSolver_0.getRampCalculatorManager().getCalculator());
```

```
    linearRampCalculator_1.setEndIteration(1000);

    StepStoppingCriterion stepStoppingCriterion_0 =
      ((StepStoppingCriterion)
simulation_0.getSolverStoppingCriterionManager().getSolverStoppingCrite
rion("Maximum Steps"));

    stepStoppingCriterion_0.setMaximumNumberSteps(5000);

    ResidualMonitor residualMonitor_0 =
      ((ResidualMonitor)
simulation_0.getMonitorManager().getMonitor("Y-momentum"));

    MonitorIterationStoppingCriterion
monitorIterationStoppingCriterion_0 =
      residualMonitor_0.createIterationStoppingCriterion();

    ((MonitorIterationStoppingCriterionOption)
monitorIterationStoppingCriterion_0.getCriterionOption()).setSelected(M
onitorIterationStoppingCriterionOption.ASYMPTOTIC);

    MonitorIterationStoppingCriterionAsymptoticType
monitorIterationStoppingCriterionAsymptoticType_0 =
      ((MonitorIterationStoppingCriterionAsymptoticType)
monitorIterationStoppingCriterion_0.getCriterionType());


monitorIterationStoppingCriterionAsymptoticType_0.getMaxWidth().setValu
e(1.0E-15);


monitorIterationStoppingCriterionAsymptoticType_0.setNumberSamples(300)
;

    LabCoordinateSystem labCoordinateSystem_0 =

simulation_0.getCoordinateSystemManager().getLabCoordinateSystem();

    CartesianCoordinateSystem cartesianCoordinateSystem_0 =

labCoordinateSystem_0.getLocalCoordinateSystemManager().createLocalCoor
dinateSystem(CartesianCoordinateSystem.class, "Cartesian");

    Coordinate coordinate_0 =
      cartesianCoordinateSystem_0.getOrigin();

    Units units_1 =
      ((Units) simulation_0.getUnitsManager().getObject("m"));

    coordinate_0.setCoordinate(units_1, units_1, units_1, new
DoubleVector(new double[] {0.0625, 0.0, 0.0}));

    UserRotatingAndTranslatingReferenceFrame
userRotatingAndTranslatingReferenceFrame_0 =

simulation_0.get(ReferenceFrameManager.class).createReferenceFrame(User
```

```
RotatingAndTranslatingReferenceFrame.class, "Rotating And
Translating");

    ForceReport forceReport_0 =
      simulation_0.getReportManager().createReport(ForceReport.class);

    forceReport_0.setPresentationName("Fx");

    forceReport_0.setCoordinateSystem(cartesianCoordinateSystem_0);

    Boundary boundary_5 =
      region_1.getBoundaryManager().getBoundary("Airfoil");

    forceReport_0.getParts().setObjects(boundary_5);

    ForceReport forceReport_1 =
      simulation_0.getReportManager().createReport(ForceReport.class);

    forceReport_1.setPresentationName("Fy");

    forceReport_1.getDirection().setComponents(0.0, 1.0, 0.0);

    forceReport_1.setCoordinateSystem(cartesianCoordinateSystem_0);

    forceReport_1.getParts().setObjects(boundary_5);

    MomentReport momentReport_0 =
      simulation_0.getReportManager().createReport(MomentReport.class);

    momentReport_0.setPresentationName("Mz");

    momentReport_0.setCoordinateSystem(cartesianCoordinateSystem_0);

    momentReport_0.getParts().setObjects(boundary_5);

    simulation_0.getMonitorManager().createMonitorAndPlot(new
NeoObjectVector(new Object[] {forceReport_0, forceReport_1,
momentReport_0}), false, "%1$s Plot");

    ReportMonitor reportMonitor_0 =
      ((ReportMonitor) simulation_0.getMonitorManager().getMonitor("Fx
Monitor"));

    MonitorPlot monitorPlot_0 =
      simulation_0.getPlotManager().createMonitorPlot(new
NeoObjectVector(new Object[] {reportMonitor_0}), "Fx Monitor Plot");

    ReportMonitor reportMonitor_1 =
      ((ReportMonitor) simulation_0.getMonitorManager().getMonitor("Fy
Monitor"));

    MonitorPlot monitorPlot_1 =
      simulation_0.getPlotManager().createMonitorPlot(new
NeoObjectVector(new Object[] {reportMonitor_1}), "Fy Monitor Plot");

    ReportMonitor reportMonitor_2 =
```

```
      ((ReportMonitor) simulation_0.getMonitorManager().getMonitor("Mz
Monitor"));

    MonitorPlot monitorPlot_2 =
      simulation_0.getPlotManager().createMonitorPlot(new
NeoObjectVector(new Object[] {reportMonitor_2}), "Mz Monitor Plot");
  }
}

// STAR-CCM+ macro: blub.java
package macro;

import java.util.*;

import star.common.*;
import star.base.neo.*;

public class B_AltCutting extends StarMacro {

  public void execute() {
    execute0();
  }

  private void execute0() {

    Simulation simulation_0 =
      getActiveSimulation();

      for (Interface iface :
simulation_0.get(InterfaceManager.class).getObjects()) {
         if (iface instanceof IndirectRegionInterface)
           {
            System.out.println("interface:
"+iface.getPresentationName());
            NeoSystemOut.println("interface:
"+iface.getPresentationName());

            IndirectRegionInterface indirectInterface =
(IndirectRegionInterface) iface;
            indirectInterface.setUseAlternateHoleCutting(true);

           }
      }

}
}

// STAR-CCM+ macro: AdjustFore.java
// Written by STAR-CCM+ 8.06.007
package macro;

import java.util.*;

import star.common.*;
import star.base.neo.*;
import star.flow.*;
```

```
import star.motion.*;

public class C_AdjustFore extends StarMacro {

  public void execute() {
    execute0();
  }

  private void execute0() {

    double Vx=blank; //m/s
    double Vy=blank; //m/s
    double Vgridy=blank; //m/s
    double dy=blank; //m
    double rot_grid=blank; //rad

    Simulation simulation_0 =
      getActiveSimulation();

    Region region_0 =
      simulation_0.getRegionManager().getRegion("Background");

    Boundary boundary_0 =
      region_0.getBoundaryManager().getBoundary("Farfield");

    VelocityProfile velocityProfile_1 =
      boundary_0.getValues().get(VelocityProfile.class);


velocityProfile_1.getMethod(ConstantVectorProfileMethod.class).getQuant
ity().setComponents(Vx, Vy, 0.0);

    Units units_2 =
      simulation_0.getUnitsManager().getPreferredUnits(new
IntVector(new int[] {0, 0, 0, 0, 0, 0, 0, 1, 0, 0, 0, 0, 0, 0, 0, 0, 0,
0, 0, 0, 0, 0, 0, 0}));

    Units units_1 =
      simulation_0.getUnitsManager().getPreferredUnits(new
IntVector(new int[] {0, 1, 0, 0, 0, 0, 0, 0, 0, 0, 0, 0, 0, 0, 0, 0, 0,
0, 0, 0, 0, 0, 0, 0}));

    Region region_1 =
      simulation_0.getRegionManager().getRegion("Foreground");

    LabCoordinateSystem labCoordinateSystem_0 =

simulation_0.getCoordinateSystemManager().getLabCoordinateSystem();

    CartesianCoordinateSystem cartesianCoordinateSystem_0 =
      ((CartesianCoordinateSystem)
labCoordinateSystem_0.getLocalCoordinateSystemManager().getObject("Cart
esian 1"));

    simulation_0.getRepresentationManager().rotateMesh(new
NeoObjectVector(new Object[] {region_1}), new DoubleVector(new double[]
```

```
{0.0, 0.0, 1.0}), new NeoObjectVector(new Object[] {units_1, units_1,
units_1}), rot_grid, cartesianCoordinateSystem_0);

    simulation_0.getRepresentationManager().translateMesh(new
NeoObjectVector(new Object[] {region_1}), new DoubleVector(new double[]
{0.0, dy, 0.0}), new NeoObjectVector(new Object[] {units_1, units_1,
units_1}), cartesianCoordinateSystem_0);

    UserRotatingAndTranslatingReferenceFrame
userRotatingAndTranslatingReferenceFrame_0 =
      ((UserRotatingAndTranslatingReferenceFrame)
simulation_0.get(ReferenceFrameManager.class).getObject("Rotating And
Translating"));


userRotatingAndTranslatingReferenceFrame_0.getTranslationVelocity().set
Components(0.0, Vgridy, 0.0);

    MotionSpecification motionSpecification_0 =
      region_1.getValues().get(MotionSpecification.class);


motionSpecification_0.setReferenceFrame(userRotatingAndTranslatingRefer
enceFrame_0);

    simulation_0.getInterfaceManager().initialize();
  }
}

// STAR-CCM+ macro: D_SaveResults.java
// Written by STAR-CCM+ 8.06.007
package macro;

import java.util.*;

import star.common.*;
import star.base.neo.*;
import star.base.report.*;
import star.flow.*;

public class D_SaveResults extends StarMacro {

  public void execute() {
    execute0();
  }

  private void execute0() {

    Simulation simulation_0 =
      getActiveSimulation();

    ForceReport forceReport_0 =
      ((ForceReport) simulation_0.getReportManager().getReport("Fx"));

    ForceReport forceReport_1 =
      ((ForceReport) simulation_0.getReportManager().getReport("Fy"));
```

```
    MomentReport momentReport_0 =
      ((MomentReport) simulation_0.getReportManager().getReport("Mz"));

    simulation_0.getMonitorManager().createMonitorAndPlot(new
NeoObjectVector(new Object[] {forceReport_0, forceReport_1,
momentReport_0}), true, "Reports Plot");



    ReportMonitor reportMonitor_0 =
      ((ReportMonitor) simulation_0.getMonitorManager().getMonitor("Fx
Monitor 2"));

    ReportMonitor reportMonitor_1 =
      ((ReportMonitor) simulation_0.getMonitorManager().getMonitor("Fy
Monitor 2"));

    ReportMonitor reportMonitor_2 =
      ((ReportMonitor) simulation_0.getMonitorManager().getMonitor("Mz
Monitor 2"));

    MonitorPlot monitorPlot_0 =
      simulation_0.getPlotManager().createMonitorPlot(new
NeoObjectVector(new Object[] {reportMonitor_0, reportMonitor_1,
reportMonitor_2}), "Reports Plot");


//Take 1 step
    simulation_0.getSimulationIterator().step(1);

    monitorPlot_0.export(resolvePath("ReportResults.csv"), ",");

    ResidualPlot residualPlot_0 =
      ((ResidualPlot)
simulation_0.getPlotManager().getPlot("Residuals"));

    residualPlot_0.export(resolvePath("Residuals.csv"), ",");
    residualPlot_0.encode(resolvePath("Result_Residuals.png"), "png",
600, 600);
  }
}
```

Fortran Scripts

The following script was written in the Fortran programming language in order to obtain results from multiple simulations.

```
PROGRAM datamine
    IMPLICIT NONE

    CHARACTER*(20)::rec
    CHARACTER(40):: fin,fout
```

```
integer :: ts,icycle,i,ierror
real :: pi,Rtau,Tau,RPhia,PhiA,denom,divisor,chord,alpha_hat
real,allocatable,dimension(:,:):: time,Fx,Fy,Mz,Py

!---------- Set Defaults ------------
pi = 3.1415926535897932384
divisor = 1.0
Rtau = 1.0
alpha_hat = 0.2
RPhia = 1.0
ts = 128
icycle = 8
denom = 0.5*1.225*14.0*14.0*0.25
chord = 0.25


write(*,*) 'Enter Divisor (',divisor,' ):'
read(5,'(a)') rec
if(rec .ne. ' ') read(rec,*) divisor

write(*,*) 'Enter Rtau (',Rtau,' ):'
read(5,'(a)') rec
if(rec .ne. ' ') read(rec,*) Rtau

write(*,*) 'Enter Alpha_hat (',alpha_hat,' ):'
read(5,'(a)') rec
if(rec .ne. ' ') read(rec,*) alpha_hat
Tau = Rtau*0.836396554819284/divisor*(1.0-alpha_hat)
PhiA = Rtau*0.139626340159546

write(*,*) 'Enter timesteps/cycle (',ts,' ):'
read(5,'(a)') rec
if(rec .ne. ' ') read(rec,*) ts

write(*,*) 'Enter desired cycle (',icycle,' ):'
read(5,'(a)') rec
if(rec .ne. ' ') read(rec,*) icycle

allocate(time(ts+1,3))
allocate(Fx(ts+1,3))
allocate(Fy(ts+1,3))
allocate(Mz(ts+1,3))
allocate(Py(ts+1,3))


fin = 'input.txt'
write(*,*) 'Enter filename (',fin,' ):'
read(5,'(a)') rec
if(rec .ne. ' ') read(rec,*) fin
open(1,FILE=fin,status='old',iostat=ierror)
if(ierror.eq.0) then !Case completed successfully
    read(1,*) !header line
    do i=1,ts*(icycle-2)-1
        read(1,*)
    end do
    do i=1,ts+1
```

```
            read(1,*) time(i,1), Fx(i,1), Fy(i,1), Mz(i,1), Py(i,1)
        end do
        time(1,2) = time(ts+1,1)
        Fx(1,2) = Fx(ts+1,1)
        Fy(1,2) = Fy(ts+1,1)
        Mz(1,2) = Mz(ts+1,1)
        Py(1,2) = Py(ts+1,1)
        do i=2,ts+1
            read(1,*) time(i,2), Fx(i,2), Fy(i,2), Mz(i,2), Py(i,2)
        end do
    end if
    close(1)

    time(:,3) = time(:,2) - time(:,1)
    Fx(:,3) = Fx(:,2) - Fx(:,1)
    Fy(:,3) = Fy(:,2) - Fy(:,1)
    Mz(:,3) = Mz(:,2) - Mz(:,1)
    Py(:,3) = Py(:,2) - Py(:,1)


    fout = trim(adjustl(fin))//'_results.txt'
    open(2,FILE=fout,status='replace')
    write(2,*) '   Time(s)                  Fx(N)
Fy(N)                    Mz_ac(N-m)              &
                  &MaxY(m)                 Time(s)                  Cx
Cy                       &
                  &Y(m)                    abs(Delta_Cx)
abs(Delta_Cy)            abs(Delta_Y)            &
                  &abs(%_Delta_Cx)         abs(%_Delta_Cy)          &
                  &Cm_ac                   abs(Delta_Cm_ac)
abs(%_Delta_Cm_ac)'
    do i=1,ts+1
        write(2,'(17e25.15)') time(i,2), Fx(i,2), Fy(i,2), Mz(i,2),
Py(i,2),&
                              &time(i,2), Fx(i,2)/denom,
Fy(i,2)/denom,PhiA*sin(2.0*pi*time(i,2)/Tau),&

&abs(Fx(i,3)/denom),abs(FY(i,3)/denom),abs(Py(i,3)),abs(Fx(i,3)/Fx(i,2)
),abs(Fy(i,3)/Fy(i,2)),&
                              &-
Mz(i,2)/denom/chord,abs(Mz(i,3)/denom/chord),abs(Mz(i,3)/Mz(i,2))
    end do
    close(2)
    stop
end program
```

APPENDIX B

THREE DIMENSIONAL SCRIPTS

The following scripts were used to setup the simulations in Star-CCM+. These were in .java format.

Quasi-Steady Setup

```
// STAR-CCM+ macro: Setup_2.java
// Written by STAR-CCM+ 8.06.007
package macro;

import java.util.*;

import star.material.*;
import star.common.*;
import star.base.neo.*;
import star.flow.*;
import star.motion.*;
import star.metrics.*;
import star.segregatedflow.*;

public class Setup_2 extends StarMacro {

  public void execute() {
    execute0();
  }

  private void execute0() {

    Simulation simulation_0 =
      getActiveSimulation();

    PhysicsContinuum physicsContinuum_0 =
      ((PhysicsContinuum)
simulation_0.getContinuumManager().getContinuum("Physics 1"));

    physicsContinuum_0.enable(SteadyModel.class);

    physicsContinuum_0.enable(SingleComponentGasModel.class);

    physicsContinuum_0.enable(SegregatedFlowModel.class);

    physicsContinuum_0.enable(ConstantDensityModel.class);

    physicsContinuum_0.enable(InviscidModel.class);

    SingleComponentGasModel singleComponentGasModel_0 =

physicsContinuum_0.getModelManager().getModel(SingleComponentGasModel.c
lass);

    Gas gas_0 =
      ((Gas) singleComponentGasModel_0.getMaterial());
```

```
    ConstantMaterialPropertyMethod constantMaterialPropertyMethod_0 =
      ((ConstantMaterialPropertyMethod)
gas_0.getMaterialProperties().getMaterialProperty(ConstantDensityProper
ty.class).getMethod());

    constantMaterialPropertyMethod_0.getQuantity().setValue(1.225);

    GradientsModel gradientsModel_0 =

physicsContinuum_0.getModelManager().getModel(GradientsModel.class);


gradientsModel_0.getGradientMethodOption().setSelected(GradientMethodOp
tion.GAUSS_GRADIENTS);

    Units units_0 =
      ((Units) simulation_0.getUnitsManager().getObject("atm"));


physicsContinuum_0.getReferenceValues().get(ReferencePressure.class).se
tUnits(units_0);


physicsContinuum_0.getReferenceValues().get(ReferencePressure.class).se
tValue(1.0);

    VelocityProfile velocityProfile_0 =

physicsContinuum_0.getInitialConditions().get(VelocityProfile.class);


velocityProfile_0.getMethod(ConstantVectorProfileMethod.class).getQuant
ity().setComponents(14.0, 0.0, 0.0);

    Region region_0 =
      simulation_0.getRegionManager().getRegion("Background");

    Boundary boundary_0 =
      region_0.getBoundaryManager().getBoundary("Farfield");

    boundary_0.setBoundaryType(InletBoundary.class);

    Boundary boundary_1 =
      region_0.getBoundaryManager().getBoundary("Outlet");

    boundary_1.setBoundaryType(OutletBoundary.class);

    Boundary boundary_2 =
      region_0.getBoundaryManager().getBoundary("Symmetry");

    boundary_2.setBoundaryType(SymmetryBoundary.class);


boundary_0.getConditions().get(InletVelocityOption.class).setSelected(I
nletVelocityOption.COMPONENTS);
```

```
    VelocityProfile velocityProfile_1 =
      boundary_0.getValues().get(VelocityProfile.class);


velocityProfile_1.getMethod(ConstantVectorProfileMethod.class).getQuant
ity().setComponents(14.0, 0.0, 0.0);

    Region region_1 =
      simulation_0.getRegionManager().getRegion("Foreground");

    Boundary boundary_3 =
      region_1.getBoundaryManager().getBoundary("Overset");

    boundary_3.setBoundaryType(OversetMeshBoundary.class);

    Boundary boundary_4 =
      region_1.getBoundaryManager().getBoundary("Symmetry");

    boundary_4.setBoundaryType(SymmetryBoundary.class);

    SegregatedFlowSolver segregatedFlowSolver_0 =
      ((SegregatedFlowSolver)
simulation_0.getSolverManager().getSolver(SegregatedFlowSolver.class));

    VelocitySolver velocitySolver_0 =
      segregatedFlowSolver_0.getVelocitySolver();


velocitySolver_0.getRampCalculatorManager().getRampCalculatorOption().s
etSelected(RampCalculatorOption.LINEAR_RAMP);

    LinearRampCalculator linearRampCalculator_0 =
      ((LinearRampCalculator)
velocitySolver_0.getRampCalculatorManager().getCalculator());

    linearRampCalculator_0.setEndIteration(10000);

    linearRampCalculator_0.setInitialRampValue(0.08);

    PressureSolver pressureSolver_0 =
      segregatedFlowSolver_0.getPressureSolver();


pressureSolver_0.getRampCalculatorManager().getRampCalculatorOption().s
etSelected(RampCalculatorOption.LINEAR_RAMP);

    LinearRampCalculator linearRampCalculator_1 =
      ((LinearRampCalculator)
pressureSolver_0.getRampCalculatorManager().getCalculator());

    linearRampCalculator_1.setEndIteration(10000);

    linearRampCalculator_1.setInitialRampValue(0.02);

    velocitySolver_0.setUrf(0.4);
```

```
    pressureSolver_0.setUrf(0.1);

// Alternate Hole Cutting
   for (Interface iface :
simulation_0.get(InterfaceManager.class).getObjects()) {
         if (iface instanceof IndirectRegionInterface)
           {
            System.out.println("interface:
"+iface.getPresentationName());
            NeoSystemOut.println("interface:
"+iface.getPresentationName());

            IndirectRegionInterface indirectInterface =
(IndirectRegionInterface) iface;
            indirectInterface.setUseAlternateHoleCutting(true);
  }
}


// Field Functions

    //Pi
    UserFieldFunction userFieldFunction_0 =
      simulation_0.getFieldFunctionManager().createFieldFunction();

    userFieldFunction_0.setPresentationName("Pi");

    userFieldFunction_0.setFunctionName("Pi");

    userFieldFunction_0.setDefinition("3.141592653589793");


// These change for each run
// ----------------------------------------------------------------------
----------------------------------

    //Divisor
    UserFieldFunction userFieldFunction_D =
      simulation_0.getFieldFunctionManager().createFieldFunction();

    userFieldFunction_D.setPresentationName("Divisor");

    userFieldFunction_D.setFunctionName("Divisor");

    userFieldFunction_D.setDefinition("1.0");
// If this value = 1.0, then ag=4.29
// If this value = 0.75, then ag=3.22
// If this value = 1.25, then ag=5.37

    //Rtau
    UserFieldFunction userFieldFunction_1 =
      simulation_0.getFieldFunctionManager().createFieldFunction();

    userFieldFunction_1.setPresentationName("Rtau");

    userFieldFunction_1.setFunctionName("Rtau");
```

```
    userFieldFunction_1.setDefinition("0.35");
//
    //Alpha_hat
    UserFieldFunction userFieldFunction_a =
      simulation_0.getFieldFunctionManager().createFieldFunction();

    userFieldFunction_a.setPresentationName("Alpha_hat");

    userFieldFunction_a.setFunctionName("Alpha_hat");

    userFieldFunction_a.setDefinition("0.0");



    double rotategrid = 0.0;
// This number comes from the excel sheet.

// ------------------------------------------------------------------------
---------------------------------------


    //Tau
    UserFieldFunction userFieldFunction_2 =
      simulation_0.getFieldFunctionManager().createFieldFunction();

    userFieldFunction_2.setPresentationName("Tau");

    userFieldFunction_2.setFunctionName("Tau");

    userFieldFunction_2.setDefinition("0.836396554819284*$Rtau*(1.0-
$Alpha_hat)/$Divisor");

    //PhiA
    UserFieldFunction userFieldFunction_3 =
      simulation_0.getFieldFunctionManager().createFieldFunction();

    userFieldFunction_3.setPresentationName("PhiA");

    userFieldFunction_3.setFunctionName("PhiA");

    userFieldFunction_3.setDefinition("$Rtau*0.139626340159546");

    //MyPosition
    UserFieldFunction userFieldFunction_4 =
      simulation_0.getFieldFunctionManager().createFieldFunction();

    userFieldFunction_4.setPresentationName("MyPosition");

    userFieldFunction_4.setFunctionName("MyPosition");

    userFieldFunction_4.setDefinition("$PhiA*sin(2.0*$Pi*$Time/$Tau)");

    //Alpha_A
    UserFieldFunction userFieldFunction_6 =
      simulation_0.getFieldFunctionManager().createFieldFunction();
```

```
    userFieldFunction_6.setPresentationName("Alpha_A");

    userFieldFunction_6.setFunctionName("Alpha_A");


userFieldFunction_6.setDefinition("$Alpha_hat*$PhiA*2.0*$Pi/14.0/$Tau")
;

    //VerticalVelocity
    UserFieldFunction userFieldFunction_7 =
      simulation_0.getFieldFunctionManager().createFieldFunction();

    userFieldFunction_7.setPresentationName("VerticalVelocity");

    userFieldFunction_7.setFunctionName("VerticalVelocity");


userFieldFunction_7.setDefinition("$PhiA*2.0*$Pi/$Tau*cos(2.0*$Pi*$Time
/$Tau)");

    //RotationalVelocity
    UserFieldFunction userFieldFunction_8 =
      simulation_0.getFieldFunctionManager().createFieldFunction();

    userFieldFunction_8.setPresentationName("RotationalVelocity");

    userFieldFunction_8.setFunctionName("RotationalVelocity");


userFieldFunction_8.setDefinition("2.0*$Pi*$Alpha_A/$Tau*sin(2.0*$Pi*$T
ime/$Tau)");

    //TranslationalVelocity
    UserFieldFunction userFieldFunction_9 =
      simulation_0.getFieldFunctionManager().createFieldFunction();

    userFieldFunction_9.setPresentationName("TranslationalVelocity");

    userFieldFunction_9.setFunctionName("TranslationalVelocity");


userFieldFunction_9.getTypeOption().setSelected(FieldFunctionTypeOption
.VECTOR);

    userFieldFunction_9.setDefinition("[0.0, $VerticalVelocity, 0.0]");

    //StartVelocity
    UserFieldFunction userFieldFunction_10 =
      simulation_0.getFieldFunctionManager().createFieldFunction();

    userFieldFunction_10.setPresentationName("StartVelocity");

    userFieldFunction_10.setFunctionName("StartVelocity");
```

```
userFieldFunction_10.getTypeOption().setSelected(FieldFunctionTypeOptio
n.VECTOR);

    userFieldFunction_10.setDefinition("[0.0, $PhiA*2.0*$Pi/$Tau,
0.0]");


//End of field functions

    LabCoordinateSystem labCoordinateSystem_0 =

simulation_0.getCoordinateSystemManager().getLabCoordinateSystem();

    CartesianCoordinateSystem cartesianCoordinateSystem_0 =

labCoordinateSystem_0.getLocalCoordinateSystemManager().createLocalCoor
dinateSystem(CartesianCoordinateSystem.class, "Cartesian");

    Coordinate coordinate_0 =
      cartesianCoordinateSystem_0.getOrigin();

    Units units_1 =
      ((Units) simulation_0.getUnitsManager().getObject("m"));

    coordinate_0.setCoordinate(units_1, units_1, units_1, new
DoubleVector(new double[] {0.06891727606, 0.0015142592350, 0.0}));

    UserRotatingAndTranslatingReferenceFrame
userRotatingAndTranslatingReferenceFrame_0 =

simulation_0.get(ReferenceFrameManager.class).createReferenceFrame(User
RotatingAndTranslatingReferenceFrame.class, "Rotating And
Translating");

    Units units_2 =
      simulation_0.getUnitsManager().getInternalUnits(new IntVector(new
int[] {0, 0, 0, 0, 0, 0, 0, 0, 0, 0, 0, 0, 0, 0, 1, 0, 0, 0, 0, 0, 0,
0, 0, 0}));



userRotatingAndTranslatingReferenceFrame_0.getTranslationVelocity().set
Definition("$$StartVelocity");

    IndirectRegionInterface indirectRegionInterface_0 =

simulation_0.getInterfaceManager().createIndirectRegionInterface(region
_0, region_1, "Overset Mesh");


indirectRegionInterface_0.getConditions().get(OversetMeshInterpolationO
ption.class).setSelected(OversetMeshInterpolationOption.LINEAR);

    MotionSpecification motionSpecification_0 =
      region_1.getValues().get(MotionSpecification.class);
```

```
motionSpecification_0.setReferenceFrame(userRotatingAndTranslatingRefer
enceFrame_0);

   StepStoppingCriterion stepStoppingCriterion_0 =
      ((StepStoppingCriterion)
simulation_0.getSolverStoppingCriterionManager().getSolverStoppingCrite
rion("Maximum Steps"));

    stepStoppingCriterion_0.setMaximumNumberSteps(5000);

    ResidualMonitor residualMonitor_0 =
      ((ResidualMonitor)
simulation_0.getMonitorManager().getMonitor("Y-momentum"));

    MonitorIterationStoppingCriterion
monitorIterationStoppingCriterion_0 =
      residualMonitor_0.createIterationStoppingCriterion();

    ((MonitorIterationStoppingCriterionOption)
monitorIterationStoppingCriterion_0.getCriterionOption()).setSelected(M
onitorIterationStoppingCriterionOption.ASYMPTOTIC);

    MonitorIterationStoppingCriterionAsymptoticType
monitorIterationStoppingCriterionAsymptoticType_0 =
      ((MonitorIterationStoppingCriterionAsymptoticType)
monitorIterationStoppingCriterion_0.getCriterionType());


monitorIterationStoppingCriterionAsymptoticType_0.getMaxWidth().setValu
e(1.0E-15);


monitorIterationStoppingCriterionAsymptoticType_0.setNumberSamples(300)
;

    ForceReport forceReport_0 =
      simulation_0.getReportManager().createReport(ForceReport.class);

    forceReport_0.setPresentationName("Fx");

    forceReport_0.setCoordinateSystem(cartesianCoordinateSystem_0);

    Boundary boundary_5 =
      region_1.getBoundaryManager().getBoundary("Airfoil");

    forceReport_0.getParts().setObjects(boundary_5);

    ForceReport forceReport_1 =
      simulation_0.getReportManager().createReport(ForceReport.class);

    forceReport_1.setPresentationName("Fy");

    forceReport_1.getDirection().setComponents(0.0, 1.0, 0.0);
```

```
    forceReport_1.setCoordinateSystem(cartesianCoordinateSystem_0);

    forceReport_1.getParts().setObjects(boundary_5);

    MomentReport momentReport_0 =
      simulation_0.getReportManager().createReport(MomentReport.class);

    momentReport_0.setPresentationName("Mz");

    momentReport_0.setCoordinateSystem(cartesianCoordinateSystem_0);

    momentReport_0.getParts().setObjects(boundary_5);

    simulation_0.getMonitorManager().createMonitorAndPlot(new
NeoObjectVector(new Object[] {forceReport_0, forceReport_1,
momentReport_0}), false, "%1$s Plot");

    AutoSave autoSave_0 =
      simulation_0.getSimulationIterator().getAutoSave();

    StarUpdate starUpdate_0 =
      autoSave_0.getStarUpdate();


starUpdate_0.getUpdateModeOption().setSelected(StarUpdateModeOption.ITE
RATION);

    IterationUpdateFrequency iterationUpdateFrequency_0 =
      starUpdate_0.getIterationUpdateFrequency();

    iterationUpdateFrequency_0.setIterations(500);
  }
}

// STAR-CCM+ macro: Reports.java
// Written by STAR-CCM+ 8.06.007
package macro;

import java.util.*;

import star.common.*;
import star.base.neo.*;
import star.base.report.*;

public class Reports extends StarMacro {

  public void execute() {
    execute0();
  }

  private void execute0() {

    Simulation simulation_0 =
      getActiveSimulation();

    ReportMonitor reportMonitor_0 =
```

```
      ((ReportMonitor) simulation_0.getMonitorManager().getMonitor("Fx
Monitor"));

    MonitorPlot monitorPlot_0 =
      simulation_0.getPlotManager().createMonitorPlot(new
NeoObjectVector(new Object[] {reportMonitor_0}), "Fx Monitor Plot");

    ReportMonitor reportMonitor_1 =
      ((ReportMonitor) simulation_0.getMonitorManager().getMonitor("Fy
Monitor"));

    MonitorPlot monitorPlot_1 =
      simulation_0.getPlotManager().createMonitorPlot(new
NeoObjectVector(new Object[] {reportMonitor_1}), "Fy Monitor Plot");

    ReportMonitor reportMonitor_2 =
      ((ReportMonitor) simulation_0.getMonitorManager().getMonitor("Mz
Monitor"));

    MonitorPlot monitorPlot_2 =
      simulation_0.getPlotManager().createMonitorPlot(new
NeoObjectVector(new Object[] {reportMonitor_2}), "Mz Monitor Plot");
  }
}
```

Steady-Periodic Setup

```
// STAR-CCM+ macro: Steady_State_To_Transient.java
// Written by STAR-CCM+ 8.06.007
package macro;

import java.util.*;

import star.common.*;
import star.base.neo.*;

public class Steady_State_To_Transient extends StarMacro {

  public void execute() {
    execute0();
  }

  private void execute0() {

    Simulation simulation_0 =
      getActiveSimulation();

    PhysicsContinuum physicsContinuum_0 =
      ((PhysicsContinuum)
simulation_0.getContinuumManager().getContinuum("Physics 1"));

    SteadyModel steadyModel_0 =
      physicsContinuum_0.getModelManager().getModel(SteadyModel.class);

    physicsContinuum_0.disableModel(steadyModel_0);
```

```
    physicsContinuum_0.enable(ImplicitUnsteadyModel.class);

    Units units_0 =
      simulation_0.getUnitsManager().getInternalUnits(new IntVector(new
int[] {0, 0, 1, 0, 0, 0, 0, 0, 0, 0, 0, 0, 0, 0, 0, 0, 0, 0, 0, 0,
0, 0, 0}));

    ImplicitUnsteadySolver implicitUnsteadySolver_0 =
      ((ImplicitUnsteadySolver)
simulation_0.getSolverManager().getSolver(ImplicitUnsteadySolver.class)
);

    implicitUnsteadySolver_0.getTimeStep().setDefinition("$Tau/128.0");


implicitUnsteadySolver_0.getTimeDiscretizationOption().setSelected(Time
DiscretizationOption.SECOND_ORDER);

// Alternate Hole Cutting
   for (Interface iface :
simulation_0.get(InterfaceManager.class).getObjects()) {
         if (iface instanceof IndirectRegionInterface)
           {
            System.out.println("interface:
"+iface.getPresentationName());
            NeoSystemOut.println("interface:
"+iface.getPresentationName());

            IndirectRegionInterface indirectInterface =
(IndirectRegionInterface) iface;
            indirectInterface.setUseAlternateHoleCutting(true);
  }
}
  }
}

// STAR-CCM+ macro: Motion.java
// Written by STAR-CCM+ 8.06.007
package macro;

import java.util.*;

import star.common.*;
import star.base.neo.*;
import star.motion.*;

public class Motion extends StarMacro {

  public void execute() {
    execute0();
  }

  private void execute0() {

    Simulation simulation_0 =
      getActiveSimulation();
```

```
    TranslatingMotion translatingMotion_0 =

simulation_0.get(MotionManager.class).createMotion(TranslatingMotion.cl
ass, "Translation");

    Units units_0 =
      simulation_0.getUnitsManager().getInternalUnits(new IntVector(new
int[] {0, 0, 0, 0, 0, 0, 0, 0, 0, 0, 0, 0, 0, 0, 1, 0, 0, 0, 0, 0, 0,
0, 0, 0}));


translatingMotion_0.getTranslationVelocity().setDefinition("$$Translati
onalVelocity");

    LabCoordinateSystem labCoordinateSystem_0 =

simulation_0.getCoordinateSystemManager().getLabCoordinateSystem();

    CartesianCoordinateSystem cartesianCoordinateSystem_0 =
      ((CartesianCoordinateSystem)
labCoordinateSystem_0.getLocalCoordinateSystemManager().getObject("Cart
esian 1"));


translatingMotion_0.getManagedCoordinateSystems().setObjects(cartesianC
oordinateSystem_0);

    SuperposingRotatingMotion superposingRotatingMotion_0 =

translatingMotion_0.getSuperposingMotionManager().createSuperposingMoti
on(SuperposingRotatingMotion.class, "Superposing Rotation");


superposingRotatingMotion_0.setCoordinateSystem(cartesianCoordinateSyst
em_0);

    Units units_1 =
      simulation_0.getUnitsManager().getInternalUnits(new IntVector(new
int[] {0, 0, 0, 0, 0, 0, 0, 0, 0, 0, 0, 0, 0, 0, 1, 0, 0, 0, 0, 0, 0,
0, 0, 0}));


superposingRotatingMotion_0.getRotationRate().setDefinition("$Rotationa
lVelocity");

    superposingRotatingMotion_0.getAxisDirection().setComponents(0.0,
0.0, 1.0);

    Region region_0 =
      simulation_0.getRegionManager().getRegion("Foreground");

    MotionSpecification motionSpecification_0 =
      region_0.getValues().get(MotionSpecification.class);

    motionSpecification_0.setMotion(superposingRotatingMotion_0);
```

```
  }
}

// STAR-CCM+ macro: Stopping_Criteria.java
// Written by STAR-CCM+ 8.06.007
package macro;

import java.util.*;

import star.common.*;
import star.base.neo.*;
import star.base.report.*;
import star.flow.*;

public class Stopping_Criteria extends StarMacro {

  public void execute() {
    execute0();
  }

  private void execute0() {

    Simulation simulation_0 =
      getActiveSimulation();

    InnerIterationStoppingCriterion innerIterationStoppingCriterion_0 =
      ((InnerIterationStoppingCriterion)
simulation_0.getSolverStoppingCriterionManager().getSolverStoppingCrite
rion("Maximum Inner Iterations"));


innerIterationStoppingCriterion_0.setMaximumNumberInnerIterations(2500)
;

    Units units_0 =
      simulation_0.getUnitsManager().getInternalUnits(new IntVector(new
int[] {0, 0, 1, 0, 0, 0, 0, 0, 0, 0, 0, 0, 0, 0, 0, 0, 0, 0, 0, 0,
0, 0, 0}));

    PhysicalTimeStoppingCriterion physicalTimeStoppingCriterion_0 =
      ((PhysicalTimeStoppingCriterion)
simulation_0.getSolverStoppingCriterionManager().getSolverStoppingCrite
rion("Maximum Physical Time"));


physicalTimeStoppingCriterion_0.getMaximumTime().setDefinition("$Tau*2.
5");

    StepStoppingCriterion stepStoppingCriterion_0 =
      ((StepStoppingCriterion)
simulation_0.getSolverStoppingCriterionManager().getSolverStoppingCrite
rion("Maximum Steps"));

    stepStoppingCriterion_0.setMaximumNumberSteps(162000);
```

```
    MonitorIterationStoppingCriterion
monitorIterationStoppingCriterion_0 =
      ((MonitorIterationStoppingCriterion)
simulation_0.getSolverStoppingCriterionManager().getSolverStoppingCrite
rion("Y-momentum Criterion"));

    MonitorIterationStoppingCriterionAsymptoticType
monitorIterationStoppingCriterionAsymptoticType_0 =
      ((MonitorIterationStoppingCriterionAsymptoticType)
monitorIterationStoppingCriterion_0.getCriterionType());


monitorIterationStoppingCriterionAsymptoticType_0.getMaxWidth().setValu
e(1.0E-8);


monitorIterationStoppingCriterionAsymptoticType_0.setNumberSamples(100)
;

    MaxReport maxReport_0 =
      simulation_0.getReportManager().createReport(MaxReport.class);

    maxReport_0.setPresentationName("MaxPosY");

    PrimitiveFieldFunction primitiveFieldFunction_0 =
      ((PrimitiveFieldFunction)
simulation_0.getFieldFunctionManager().getFunction("Position"));

    LabCoordinateSystem labCoordinateSystem_0 =

simulation_0.getCoordinateSystemManager().getLabCoordinateSystem();

    CartesianCoordinateSystem cartesianCoordinateSystem_0 =
      ((CartesianCoordinateSystem)
labCoordinateSystem_0.getLocalCoordinateSystemManager().getObject("Cart
esian 1"));

    VectorComponentFieldFunction vectorComponentFieldFunction_0 =
      ((VectorComponentFieldFunction)
primitiveFieldFunction_0.getFunctionInCoordinateSystem(cartesianCoordin
ateSystem_0).getComponentFunction(1));

    maxReport_0.setScalar(vectorComponentFieldFunction_0);

    VectorComponentFieldFunction vectorComponentFieldFunction_1 =
      ((VectorComponentFieldFunction)
primitiveFieldFunction_0.getComponentFunction(1));

    maxReport_0.setScalar(vectorComponentFieldFunction_1);

    Region region_0 =
      simulation_0.getRegionManager().getRegion("Foreground");

    Boundary boundary_0 =
      region_0.getBoundaryManager().getBoundary("Airfoil");
```

```
    maxReport_0.getParts().setObjects(boundary_0);

    ForceReport forceReport_0 =
      ((ForceReport) simulation_0.getReportManager().getReport("Fx"));

    forceReport_0.setCoordinateSystem(labCoordinateSystem_0);

    ForceReport forceReport_1 =
      ((ForceReport) simulation_0.getReportManager().getReport("Fy"));

    forceReport_1.setCoordinateSystem(labCoordinateSystem_0);

    simulation_0.getMonitorManager().createMonitorAndPlot(new
NeoObjectVector(new Object[] {maxReport_0}), true, "%1$s Plot");

    ReportMonitor reportMonitor_0 =
      ((ReportMonitor)
simulation_0.getMonitorManager().getMonitor("MaxPosY Monitor"));

    MonitorPlot monitorPlot_0 =
      simulation_0.getPlotManager().createMonitorPlot(new
NeoObjectVector(new Object[] {reportMonitor_0}), "MaxPosY Monitor
Plot");

    ReportMonitor reportMonitor_1 =
      ((ReportMonitor) simulation_0.getMonitorManager().getMonitor("Fx
Monitor"));

    StarUpdate starUpdate_0 =
      reportMonitor_1.getStarUpdate();


starUpdate_0.getUpdateModeOption().setSelected(StarUpdateModeOption.TIM
ESTEP);

    ReportMonitor reportMonitor_2 =
      ((ReportMonitor) simulation_0.getMonitorManager().getMonitor("Fy
Monitor"));

    StarUpdate starUpdate_1 =
      reportMonitor_2.getStarUpdate();


starUpdate_1.getUpdateModeOption().setSelected(StarUpdateModeOption.TIM
ESTEP);

    ReportMonitor reportMonitor_3 =
      ((ReportMonitor) simulation_0.getMonitorManager().getMonitor("Mz
Monitor"));

    StarUpdate starUpdate_2 =
      reportMonitor_3.getStarUpdate();


starUpdate_2.getUpdateModeOption().setSelected(StarUpdateModeOption.TIM
ESTEP);
```

```
  }
}

// STAR-CCM+ macro: Relaxation.java
// Written by STAR-CCM+ 8.06.007
package macro;

import java.util.*;

import star.common.*;
import star.base.neo.*;
import star.segregatedflow.*;

public class Relaxation extends StarMacro {

  public void execute() {
    execute0();
  }

  private void execute0() {

    Simulation simulation_0 =
      getActiveSimulation();

    SegregatedFlowSolver segregatedFlowSolver_0 =
      ((SegregatedFlowSolver)
simulation_0.getSolverManager().getSolver(SegregatedFlowSolver.class));

    VelocitySolver velocitySolver_0 =
      segregatedFlowSolver_0.getVelocitySolver();

    velocitySolver_0.setUrf(0.4);

    PressureSolver pressureSolver_0 =
      segregatedFlowSolver_0.getPressureSolver();

    pressureSolver_0.setUrf(0.1);
  }
}

// STAR-CCM+ macro: Reports.java
// Written by STAR-CCM+ 8.06.007
package macro;

import java.util.*;

import star.common.*;
import star.base.neo.*;
import star.base.report.*;

public class Reports extends StarMacro {

  public void execute() {
    execute0();
  }
```

```
  private void execute0() {

    Simulation simulation_0 =
      getActiveSimulation();

    ReportMonitor reportMonitor_0 =
      ((ReportMonitor) simulation_0.getMonitorManager().getMonitor("Fx
Monitor"));

    MonitorPlot monitorPlot_0 =
      simulation_0.getPlotManager().createMonitorPlot(new
NeoObjectVector(new Object[] {reportMonitor_0}), "Fx Monitor Plot");

    ReportMonitor reportMonitor_1 =
      ((ReportMonitor) simulation_0.getMonitorManager().getMonitor("Fy
Monitor"));

    MonitorPlot monitorPlot_1 =
      simulation_0.getPlotManager().createMonitorPlot(new
NeoObjectVector(new Object[] {reportMonitor_1}), "Fy Monitor Plot");

    ReportMonitor reportMonitor_2 =
      ((ReportMonitor) simulation_0.getMonitorManager().getMonitor("Mz
Monitor"));

    MonitorPlot monitorPlot_2 =
      simulation_0.getPlotManager().createMonitorPlot(new
NeoObjectVector(new Object[] {reportMonitor_2}), "Mz Monitor Plot");
  }
}

// STAR-CCM+ macro: Transient_Reports.java
// Written by STAR-CCM+ 8.06.007
package macro;

import java.util.*;

import star.common.*;
import star.base.neo.*;
import star.base.report.*;

public class Transient_Reports extends StarMacro {

  public void execute() {
    execute0();
  }

  private void execute0() {

    Simulation simulation_0 =
      getActiveSimulation();

    MonitorPlot monitorPlot_0 =
      ((MonitorPlot) simulation_0.getPlotManager().getPlot("Reports
Plot"));
```

```
    simulation_0.getPlotManager().deletePlots(new NeoObjectVector(new
Object[] {monitorPlot_0}));

    ReportMonitor reportMonitor_0 =
      ((ReportMonitor) simulation_0.getMonitorManager().getMonitor("Fx
Monitor 2"));

    ReportMonitor reportMonitor_1 =
      ((ReportMonitor) simulation_0.getMonitorManager().getMonitor("Fy
Monitor 2"));

    ReportMonitor reportMonitor_2 =
      ((ReportMonitor)
simulation_0.getMonitorManager().getMonitor("MaxPosY Monitor"));

    ReportMonitor reportMonitor_3 =
      ((ReportMonitor) simulation_0.getMonitorManager().getMonitor("Mz
Monitor 2"));

    MonitorPlot monitorPlot_1 =
      simulation_0.getPlotManager().createMonitorPlot(new
NeoObjectVector(new Object[] {reportMonitor_0, reportMonitor_1,
reportMonitor_2, reportMonitor_3}), "Monitors Plot");

    monitorPlot_1.open();

    ReportMonitor reportMonitor_4 =
      ((ReportMonitor) simulation_0.getMonitorManager().getMonitor("Fx
Monitor"));

    ReportMonitor reportMonitor_5 =
      ((ReportMonitor) simulation_0.getMonitorManager().getMonitor("Fy
Monitor"));

    ReportMonitor reportMonitor_6 =
      ((ReportMonitor) simulation_0.getMonitorManager().getMonitor("Mz
Monitor"));

    MonitorPlot monitorPlot_2 =
      simulation_0.getPlotManager().createMonitorPlot(new
NeoObjectVector(new Object[] {reportMonitor_4, reportMonitor_5,
reportMonitor_2, reportMonitor_6}), "Monitors Plot");
  }
}
```

APPENDIX C

REFERENCES, KEYWORDS, AND ABSTRACTS

[1] Yang, T., and Wei, M., "A Fully-Coupled Approach to Simulate Three-Dimensional Flexible Flapping Wings," AIAA Paper 2013-0864, Jan. 2013.

Keywords: 3-D, Numerical, Strong-Coupling Approach

Abstract: In this study, a fully-coupled approach is used to simulate three-dimensional highly-flexible flapping wings interacting with the surrounding fluid flow. In this approach, the elastic body and its interaction with the fluid are implemented as body/surface force terms. In this way, the fluid and solid can be solved by a combined and modified form of typical Navier-Stokes equations. The motion trajectory is defined similarly by adding another bodyforce term using direct-forcing type of Immersed Boundary method. The advantage of solving a combined fluid-solid equation in a global Eulerian framework is that the solution of fluid, solid, and their interaction can be obtained in a monolithic manner and we avoid any sub-step iterations. The current extension of algorithm to three-dimensional configuration is based on our earlier work in two-dimensional setup. After extensive benchmarks in 2D and 3D, rigid and flexible cases, we eventually apply the algorithm on solving three-dimensional flexible flapping wings.

[2] Young, J., "Numerical Simulation of the Unsteady Aerodynamics of Flapping Airfoils," Ph.D. Dissertation, The University of New South Wales, at the Australian Defense Force Academy, May 2005.

Keywords: 2-D, Numerical, Wake

Abstract: There is currently a great deal of interest within the aviation community in the design of small, slow-flying but maneuverable uninhabited vehicles for reconnaissance, surveillance, and search and rescue operations in urban environments. Inspired by observation of birds, insects, fish and cetaceans, flapping wings are being actively studied in the hope that they may provide greater propulsive efficiencies than propellers and rotors at low Reynolds numbers for such Micro-Air Vehicles (MAVs). Researchers have posited the Strouhal number (combining flapping frequency, amplitude and forward speed) as the parameter controlling flapping wing aerodynamics in cruising flight, although there is conflicting evidence. This thesis explores the effect of flapping frequency and amplitude on forces and wake structures, as well as physical mechanisms leading to optimum propulsive efficiency. Two-dimensional rigid airfoils are considered at Reynolds number 2,000 – 40,000. A compressible Navier-Stokes simulation is combined with numerical and analytical potential flow techniques to isolate and evaluate the effect of viscosity, leading and trailing edge vortex separation, and wake vortex dynamics. The wake structures of a plunging airfoil are shown to be sensitive to the flapping frequency independent of the Strouhal number. For a given frequency, the wake of the airfoil exhibits 'vortex lock-in' as the amplitude of motion is increased, in a manner analogous to an oscillating circular cylinder. This is caused by interaction between the flapping frequency and the 'bluff-body' vortex shedding frequency apparent even for streamlined airfoils at low Reynolds number. The thrust and propulsive efficiency of a plunging airfoil are also shown to be sensitive to the flapping frequency independent of Strouhal number. This dependence is the result of vortex shedding from the leading edge, and an interaction between the flapping frequency and the time for vortex formation, separation and convection over the airfoil surface. The observed propulsive efficiency peak for a pitching and plunging airfoil is shown to be the result of leading edge vortex shedding at low flapping frequencies (low Strouhal numbers), and high power requirements at large flapping amplitudes (high Strouhal numbers). The efficiency peak is governed by flapping frequency and amplitude separately, rather than the Strouhal number directly.

[3] Tuncer, I., and Kaya, M., "Optimization of Flapping Airfoils for Maximum Thrust and Propulsive Efficiency," *AIAA Journal*, Vol. 43, No. 11, 2005, pp. 2329–2336.

Keywords: 2-D, Numerical, Efficiency

Abstract: The thrust and/or propulsive efficiency of a single flapping airfoil is maximized by using a numerical optimization method based on the steepest ascent. The flapping motion of the airfoil is described by a combined sinusoidal plunge and pitching motion. Optimization parameters are taken to be the amplitude of the plunge and pitching motions and the phase shift between them at a fixed flapping frequency. Two-dimensional, unsteady, low-speed, laminar, and turbulent flows are computed by using a Navier-Stokes solver on moving overset grids. Computations are performed in parallel in a computer cluster. The optimization data show that high thrust values may be obtained at the expense of propulsive efficiency. For a high propulsive efficiency, the effective angle of attack of the airfoil is reduced, and large-scale vortex formations at the leading edge are prevented.

[4] Guglielmini, L., and Blondeaux, P., "Propulsive Efficiency of Oscillating Foils," *European Journal of Mechanics B Fluids*, Vol. 23, No. 2, 2004, pp. 255–278.

Keywords: 2-D, Numerical, Vortices

Abstract: The dynamics of the vortex structures generated by a foil in steady forward motion, plus a combination of harmonic heaving and pitching oscillations, is determined by means of the numerical solution of the vorticity equation. The force and the torque acting on the foil are also computed. The investigation extends a previous study of the phenomenon (J. Fluid Mech. 410 (2000) 323–341), where only heaving oscillations were considered. The pitching motion turns out to be the only means to produce thrust when the forward motion of the foil vanishes, i.e., for foils operating in the hovering mode. Moreover pitching oscillations added to the heaving motion of the foil produce much larger values of the thrust and better efficiencies. Results are obtained for many combinations of the parameters characterizing the phenomenon and the investigation allows us to identify the range of the parameters providing high propulsive efficiency. The numerical results agree well with previous experimental measurements and, in addition, allow access to the velocity and vorticity fields as functions of space and time, which in turn allows us to identify the underlying thrust production mechanisms more easily.

[5] Phlips, P. J., East, R. A., and Pratt, N. H., "An Unsteady Lifting Line Theory of Flapping Wings with Application to the Forward Flight of Birds," *Journal of Fluid Mechanics*, Vol. 112, Nov., 1981, pp. 97–125.

Keywords: 3-D, Analytical, Lifting-Line, Vortices

Abstract: A lifting line theory of flapping wings in steady forward flight is presented in which the unsteady features of the flow are modelled. A detailed three-dimensional model of the vortex wake is used to evaluate the unsteadiness to first order. The method gives satisfactory agreement with well-known limiting cases. Relationships between the geometric and the kinematic parameters, and the forces and the power are predicted which are compatible with the limited experimental evidence. The theory is applied to the calculation of the power curve of specific birds. Important similarities and differences are observed between the present results and those of Pennycuick (1975) and Rayner (1979*c*).

[6] Knoller, R., "Die Gesetze des Luftwiderstandes," *Flug- und Motortechnik (Wien)*, Vol. 3, No. 21, 1909, pp. 1–7.

Keywords: 2-D, Analytical

[7] Betz, A., "Ein Beitrag zur Erklärung des Segelfluges," *Zeitschrift für Flugtechnik und Motorluftschiffahrt*, Vol. 3, Nov. 1912, pp. 269–272.

Keywords: 2-D, Analytical, Gliding

[8] Wagner, H. "Über die Entstehung des dynamischen Auftriebs von Tragflügeln," *Zeitschrift für Angewandte Mathematic und Mechanik*, Vol. 5, No. 1, 1925, pp. 17–35.

Keywords: 2-D, Analytical

[9] Theodorsen, T., "General Theory of Aerodynamic Instability and the Mechanism of Flutter," NACA TR-496, Feb. 1935.

Keywords: 2-D, Analytical, Oscillating Foils, Conformal Mapping

Abstract: The aerodynamic forces on an oscillating airfoil or airfoil-aileron combination of three independent degrees of freedom have been determined. The problem resolves itself into the solution of certain definite integrals, which have been identified as Bessel functions of the first and second kind and of zero and first order. The theory, being based on potential flow and the Kutta condition, is fundamentally equivalent to the conventional wing-section theory relating to the steady case. The air forces being known, the mechanism of aerodynamic instability has been analyzed in detail. An exact solution, involving potential flow and the adoption of the Kutta condition, has been arrived at. The solution is of a simple form and is expressed by means of an auxiliary parameter k. The mathematical treatment also provides a convenient cyclic arrangement permitting a uniform treatment of all subcases of two degrees of freedom. The flutter velocity, defined as the air velocity at which flutter starts, and which is treated as the unknown quantity, is determined as a function of a certain ratio of the frequencies in the separate degrees of freedom for any magnitudes and combinations of the airfoil-aileron parameters. For those interested solely or particularly in the numerical solutions Appendix I has been prepared. The routine procedure in solving numerical examples is put down detached from the theoretical background of the paper. It first is necessary to determine a certain number of constants pertaining to the case, then to perform a few routine calculations as indicated. The result is readily obtained in the form of a plot of flutter velocity against frequency for any values of the other parameters chosen. The numerical work of

calculating the constants is simplified by referring to a number of tables, which are included in Appendix I. A number of illustrative examples and experimental results are given in Appendix II.

[10] von Kármán, T., and Burgers, J. M., "General Aerodynamic Theory — Perfect Fluids," *Aerodynamic Theory*, edited by Durand, W. F., Vol. 2, Springer, Berlin, 1935, pp. 293–310.
Keywords: 2-D, Analytical

[11] Garrick, I. E., "Propulsion of a Flapping and Oscillating Airfoil," NACA TR-567, May 1936.
Keywords: 2-D, Analytical, Conformal Mapping
Abstract: Formulas are given for the propelling or drag force experience in a uniform air stream by an airfoil or an airfoil-aileron combination, oscillating in any of three degrees of freedom; vertical flapping, torsional oscillations about a fixed axis parallel to the span, and angular oscillations of the aileron about a hinge.

[12] Hunsaker, D. F., and Phillips, W. F., "Propulsion Theory of Flapping Airfoils, Comparison with Computational Fluid Dynamics," AIAA Paper 2015-0257, Jan. 2015.
Keywords: 2-D, Numerical, Lifting-line, CFD
Abstract: The thrust, required power, and propulsive efficiency of a flapping airfoil as predicted by the well-known Theodorsen model are compared with solutions obtained from grid-resolved inviscid computational fluid dynamics. A straight-forward summary of Theodorsen's flapping airfoil model is presented using updated terminology and symbols. This shows that both axial and normal reduced frequencies are of significant importance. The axial reduced frequency is based on the chord length and the normal reduced frequency is based on the plunging amplitude. Computational fluid dynamics solutions are presented over the range of both reduced frequencies typically encountered in the forward flight of birds. It is shown that computational results agree reasonably well with those predicted by Theodorsen's model at low flapping frequencies. An alternate model is also developed, which shows that the time-dependent aerodynamic forces acting on a flapping airfoil can be related to two unknown Fourier coefficients. The computational results are correlated with algebraic relations for these Fourier coefficients, which can be used to predict the thrust, required power, and propulsive efficiency for airfoils with sinusoidal pitching and plunging motion.

[13] Jones, R. T., "The Unsteady Lift of a Wing of Finite Aspect Ratio," NACA TR-681, Jan. 1940.
Keywords: 2-D, Analytical, Gusts
Abstract: Unsteady-lift functions for wings of finite aspect ratio have been calculated by correcting the aerodynamic inertia and the angle of attack of the infinite wing. The calculations are based on the operational method. The starting lift of the finite wing is found to be only slightly less than that of the infinite wing; whereas the final lift may be considerably less. The theory indicates that the initial distribution of lift is similar to the final distribution. Curves showing the variation of lift after a sudden unit change in angle of attack, during penetration of a sharp-edge gust, and during a continuous oscillation are given. Operational equivalents of these functions have been devised to facilitate the calculation of lift under various conditions of motion. As an application of these formulas, the vertical accelerations of a loaded wing caused by penetrating a gust has been calculated.

[14] Minotti, F. O., "Determination of the Instantaneous Forces on Flapping Wings from a Localized Fluid Velocity Field," *Physics of Fluids*, Vol. 23, No. 11, 2011, pp. 111902-1–111902-10.
Keywords: 2-D, Analytical, Pressure
Abstract: Expressions are derived to relate the instantaneous pressure force on a flapping wing to the velocity field on a plane at the trailing edge and on a highly localized region around and near the wing, valid when the vortex sheet is thin. In its more practical version, the formalism is applicable to wings with close to two-dimensional geometry and has the advantage of not using spatial derivatives, but only a time derivative of a surface integral of the velocity. In the purely two-dimensional case, the expression obtained is used to justify a much simpler one that only requires the evaluation of the time derivative of the wing circulation. A comparison with a numerical simulation in a two-dimensional case shows a good representation of the forces, even with the most simplified expression, when the condition of a thin wake is met. Other examples are shown in which the wake is not thin in order to explore the limitations of the formalism. It is found in these cases that the thrust is sometimes not so well reproduced, with a tendency to be overestimated, while the lift is generally better reproduced. Remarkably, the simpler expression reproduces rather acceptably the phase and amplitude of both thrust and lift in all cases.

[15] Patil, M. J., "From Fluttering Wings to Flapping Flight: The Energy Connection," *Journal of Aircraft*, Vol. 40, No. 2, 2003, pp. 270–276.

Keywords: 2-D, Analytical, Energy

Abstract: A new paradigm is presented for understanding flutter and flapping flight. The framework for the investigation is based on conservation of energy. Energy produced, energy lost and/or work done due to structural vibration, aerodynamic wake, and propulsion are taken into account. It is shown that there exist three types of modes in an aeroelastic system, namely 1) unstable mode producing drag (flutter mode), 2) stable mode producing drag, and 3)stable mode producing thrust (flapping flight mode). The type of mode can be determined from the mode shape for a given reduced frequency. The regions (in the modal vector space) corresponding to the three types of modes are presented for a two-dimensional airfoil. It is shown that the flutter region is separate from the thrust-producing region and the boundaries of these regions are tangential to one another at a common neutral point. The neutral point corresponds to no energy transfer between the energy sources. The efficiency of flapping flight and occurrence of flutter is further investigated. Finally, the possibility of a limit-cycle oscillations due to constant thrust flight is presented.

[16] Johnson, W., "A Perturbation Solution of Helicopter Rotor Flapping Stability," *Journal of Aircraft*, Vol. 10, No. 5, 1973, pp. 257–258.

Keywords: 2-D, Analytical, Helicopters

Abstract: A solution for the flapping stability of a helicopter blade, including the influence of a periodic coefficients due to the rotor forward velocity, is obtained using the techniques of perturbation theory.

[17] Brunton, S. L. and Rowley, C. W., "Modeling the Unsteady Aerodynamic Forces on Small-Scale Wings," AIAA Paper 2009-1127, Jan. 2009.

Keywords: 2-D, Analytical, Theories

Abstract: The goal of this work is to develop low order dynamical systems models for the unsteady aerodynamic forces on small wings and to better understand the physical characteristics of unsteady laminar separation. Reduced order models for a fixed, high angle of attack flat plate are obtained through Galerkin projection of the governing Navier-Stokes equations onto POD modes. Projected models are compared with direct numerical simulation (DNS) to show that they preserve qualitative behavior such as coherent structures. It is shown that in flows with Reynolds number 100, even a two degree of freedom model is sufficient to capture high angle of attack laminar vortex shedding. Next, the classical theories of Theodorsen and Wagner are compared with DNS for a number of pitch and plunge maneuvers of varying Strouhal number, reduced frequency, pitch amplitude and center. In addition to determining when these theories break down, the flow field structures are investigated to determine how the theories break down. This is an important first step toward combining and extending classical unsteady aerodynamic models to include high angle of attack effects. Theodorsen's model for the lift of a sinusoidally pitching or plunging plate is shown to agree moderately well with DNS for reduced frequencies $k<2.0$. One major observation is that the classical aerodynamic models all begin to disagree when the effective angle of attack, either determined by Strouhal number in the plunging case or angle of attack excursion in the pitching case, exceeds the critical stall angle where vortex shedding and laminar separation become prominent. Velocity field and body force data for a flat plate are generated by 2D direct numerical simulation using an immersed boundary method for Reynolds number 100-300, and regions of separated flow and wake structures are visualized using Finite Time Lyapunov Exponents (FTLE) fields , the range of which are Legrangian coherent structures.

[18] Glauert, H., "The Force and Moment on an Oscillating Aerofoil," Aeronautical Research Council R&M-1242, Mar. 1929, pp. 742–762.

Keywords: 2-D, Analytical, Damping Moment

Abstract: In an interesting paper[1], published early in 1925 in the Zeitschrift für angewandte Mathematik und Mechanik, Dr. H. Wagner has developed a method of calculating the lift and pitching moment of an aerofoil in accelerated motion. Dr. Wagner's paper is confined mainly to linear motion at a constant angle of incidence, but towards the end of the paper the analysis is extended to include the effects of an angular velocity also. Towards the end of last year I became interested in the problem of an oscillating aerofoil and wished to calculate the aerodynamic damping moment experienced by the aerofoil, since certain wind tunnel experiments had suggested that this damping moment increased with the frequency of the oscillation. If the amplitude of the oscillation is small, Dr. Wagner's equations may by applied directly to the problem of the oscillating aerofoil, and the following paper is a brief account of my calculations, full details of which are contained in two reports[2] of the R. and M. Series. In passing I may mention

that I derived the expressions for the force and moment on the aerofoil by suitable transformations of the fundamental hydrodynamical equations on lines differing from those followed by Dr. Wagner, and so obtained an independent check on his equations.

[19] von Ellenrieder, K. D., Parker, K. and Soria, J., "Fluid Mechanics of Flapping Wings," *Experimental Thermal and Fluid Science*, Vol. 32, No. 8 2008, pp. 1578–1589.

Keywords: 2-D, Analytical, Strouhal Number

Abstract: Based on the results of two-dimensional flapping wing studies, the selection of Strouhal number for steady cruising is explored. The hypothesis that Strouhal number selection in natural flapping wing propulsion is a limit cycle process is proposed and the implications of this hypothesis for the design, control and computational/experimental modeling of freely flying systems are explored. It is suggested that the steady-state propulsive efficiency of man-made systems that use flapping propulsion must be designed-in, rather than actively controlled and that sensory feedback may be more important for control during maneuvering/acceleration and play only a minor role in the regulation of a flying/swimming system's steady forward motion. A brief literature review of the structure of the flow around three-dimensional translating and revolving wings is also presented. In the case of translating wings the flow structure consists of a chain of interconnected vortex loops and has a strong Strouhal number dependence. For revolving wings the leading edge vortex is especially important for the development of lift and thrust. The stability of this leading edge vortex is strongly dependent on the development of a spanwise flow that creates a balance between the creation of vorticity at the leading edge of the wing and the transport of vorticity into the wake.

[20] Katzmayr, R., "Effect of Periodic Changes of Angle of Attack on Behavior of Airfoils," NACA TR-147, Oct. 1922.

Keywords: 2-D, Experimental

[21] Sunada, S., Kawachi, K., Matsumoto, A., and Sakaguchi, A., "Unsteady Forces on a Two-Dimensional Wing in Plunging and Pitching Motions," *AIAA Journal*, Vol. 39, No. 7, 2001, pp. 1230–1239.

Keywords: 2-D, Experimental, Vortices

Abstract: Unsteady fluid dynamic forces acting on a two-dimensional wing in sinusoidal plunging and pitching motions in still water were measured. The measured fluid dynamic forces were larger than those estimated by quasi-steady analysis, where the effect of unsteady separated vortices on the fluid dynamic forces is not considered. Vortex capture is a phenomenon related to the larger fluid dynamic forces in wing motion that is similar to wing motion of real insects. By using the measured fluid dynamic forces, we identified combinations of plunging and pitching motions for maximum time-averaged thrust and for maximum efficiency.

[22] Birch, J. M., and Dickinson, M. H., "The Influence of Wing-Wake Interactions on the Production of Aerodynamic Forces in Flapping Flight," *Journal of Experimental Biology*, Vol. 206, July 2003, pp. 2257–2272.

Keywords: 2-D, Experimental, Vortices

Abstract: We used two-dimensional digital particle image velocimetry (DPIV) to visualize flow patterns around the flapping wing of a dynamically scaled robot for a series of reciprocating strokes starting from rest. The base of the wing was equipped with strain gauges so that the pattern of fluid motion could be directly compared with the time history of force production. The results show that the development and shedding of vortices throughout each stroke are highly stereotyped and influence force generation in subsequent strokes. When a wing starts from rest, it generates a transient force as the leading edge vortex (LEV) grows. This early peak, previously attributed to added-mass acceleration, is not amenable to quasi-steady models but corresponds well to calculations based on the time derivative of the first moment of vorticity within a sectional slice of fluid. Forces decay to a stable level as the LEV reaches a constant size and remains attached throughout most of the stroke. The LEV grows as the wing supinates prior to stroke reversal, accompanied by an increase in total force. At stroke reversal, both the LEV and a rotational starting vortex (RSV) are shed into the wake, forming a counter-rotating pair that directs a jet of fluid towards the underside of the wing at the start of the next stroke. We isolated the aerodynamic influence of the wake by subtracting forces and flow fields generated in the first stroke, when the wake is just developing, from those produced during the fourth stroke, when the pattern of both the forces and wake dynamics has reached a limit cycle. This technique identified two effects of the wake on force production by the wing: an early augmentation followed by a small attenuation. The later decrease in force is consistent with the influence of a decreased aerodynamic angle of attack on translational forces caused by downwash within the wake and is well explained by a quasi-steady model. The early effect of the wake is not well approximated by a quasi-steady model, even when the magnitude and orientation of the instantaneous velocity

field are taken into account. Thus, the wake capture force represents a truly unsteady phenomenon dependent on temporal changes in the distribution and magnitude of vorticity during stroke reversal.

[23] Lai, J. C., and Platzer, M. F., "Characteristics of a Plunging Airfoil at Zero Freestream Velocity," *AIAA Journal*, Vol. 39, No. 3, 2001, pp. 531–534.

Keywords: 2-D, Experimental, Vortices

[24] Godoy-Diana, R., Marais, C., Aider, J. L., and Wesfreid, J. E., "A Model for the Symmetry Breaking of the Reverse Bénard–von Kármán Vortex Street Produced by a Flapping Foil," *Journal of Fluid Mechanics*, Vol. 622, Mar. 2009, pp. 23–32.

Keywords: 2-D, Experimental, Vortices

Abstract: The vortex streets produced by a flapping foil of span to chord aspect ratio of 4:1 are studied in a hydrodynamic tunnel experiment. In particular, the mechanisms giving rise to the symmetry breaking of the reverse Bénard–von Kármán (BvK) vortex street that characterizes fishlike swimming and forward flapping flight are examined. Two-dimensional particle image velocimetry (PIV) measurements in the midplane perpendicular to the span axis of the foil are used to characterize the different flow regimes. The deflection angle of the mean jet flow with respect to the horizontal observed in the average velocity field is used as a measure of the asymmetry of the vortex street. Time series of the vorticity field are used to calculate the advection velocity of the vortices with respect to the free stream, defined as the phase velocity U_{phase}, as well as the circulation Γ of each vortex and the spacing ξ between consecutive vortices in the near wake. The observation that the symmetry-breaking results from the formation of a dipolar structure from each couple of counter-rotating vortices shed on each flapping period serves as the starting point to build a model for the symmetry-breaking threshold. A symmetry-breaking criterion based on the relation between the phase velocity of the vortex street and an idealized self-advection velocity of two consecutive counter-rotating vortices in the near wake is established. The predicted threshold for symmetry breaking accounts well for the deflected wake regimes observed in the present experiments and may be useful to explain other experimental and numerical observations of similar deflected propulsive vortex streets reported in the literature.

[25] Milano, M., and Gharib, M., "Uncovering the Physics of Flapping Flat Plates with Artificial Evolution," *Journal of Fluid Mechanics*, Vol. 534, July 2005, pp. 403–409.

Keywords: 2-D, Experimental, Vortices, Flat Plate

Abstract: We consider an experiment in which a rectangular flat plate is flapped with two degrees of freedom, and a genetic algorithm tunes its trajectory parameters so as to achieve maximum average lift force, thus evolving a population of trajectories all yielding optimal lift forces. We cluster the converged population by defining a dynamical formation number for a flapping flat plate, thus showing that optimal unsteady force generation is linked to the formation of a leading-edge vortex with maximum circulation. Force and digital particle image velocimetry measurements confirm this result.

[26] Baik, Y. S., Bernal, L. P., Granlund, K., and Ol, M. V., "Unsteady Force Generation and Vortex Dynamics of Pitching and Plunging Aerofoils," *Journal of Fluid Mechanics*, Vol. 709, Oct. 2012, pp. 37–68.

Keywords: 2-D, Experimental, Vortices

Abstract: Experimental studies of the flow topology, leading-edge vortex dynamics and unsteady force produced by pitching and plunging flat-plate aerofoils in forward flight at Reynolds numbers in the range 5000–20 000 are described. We consider the effects of varying frequency and plunge amplitude for the same effective angle-of-attack time history. The effective angle-of-attack history is a sinusoidal oscillation in the range -6 to 22 with mean of 8 and amplitude of 14. The reduced frequency is varied in the range 0.314–1.0 and the Strouhal number range is 0.10–0.48. Results show that for constant effective angle of attack, the flow evolution is independent of Strouhal number, and as the reduced frequency is increased the leading-edge vortex (LEV) separates later in phase during the downstroke. The LEV trajectory, circulation and area are reported. It is shown that the effective angle of attack and reduced frequency determine the flow evolution, and the Strouhal number is the main parameter determining the aerodynamic force acting on the aerofoil. At low Strouhal numbers, the lift coefficient is proportional to the effective angle of attack, indicating the validity of the quasi-steady approximation. Large values of force coefficients (-6) are measured at high Strouhal number. The measurement results are compared with linear potential flow theory and found to be in reasonable agreement. During the downstroke, when the LEV is present, better agreement is found when the wake effect is ignored for both the lift and drag coefficients.

[27] Chen, A. L., Jacob, J. D., and Savas, Ö., "Dynamics of Corotating Vortex Pairs in the Wakes of Flapped Airfoils," *Journal of Fluid Mechanics*, Vol. 382, Mar. 1999, pp. 155–193.

Keywords: 2-D, Experimental, Vortices

Abstract: The behaviour of a pair of corotating vortices in the wake of a flapped airfoil is experimentally studied in a water towing tank. Reynolds numbers based on total circulation of the vortices range from 1.0×10^4 to 6.4×10^4. Planar velocity vector fields and their gradients are derived from PIV images using an adaptive Lagrangian parcel tracking algorithm. Isovorticity surfaces are extracted from time series of planar vorticity data. The behaviour of the vortices is tracked by using various moments of both the probability density distribution and the spatial distribution of their streamwise vorticity. All vortices show a Lamb–Oseen circulation distribution when they are clearly identifiable. Further, vortices from the apless wing exhibit Lamb–Oseen velocity and vorticity distributions with slow growth. All corotating vortex pairs are observed to merge at about 0.8 orbit periods. First-order statistics of the flow field remain invariant during the merger. The higher-order moments of the vorticity distribution show strong time dependence, which implies three-dimensionality of the flow resulting from vortex stretching. The strengths of the individual vortices before merger are constant, and the total circulation before and after merger remains constant within the range of observations. The trajectory of the centre of vorticity remains unaffected by the merger process. The merger is preceded by a splitting of the weaker vortex into filaments which, depending on the relative strengths of the vortices, can occur in the radial direction, the axial direction, or a combination of the two. Mechanisms contributing to the merger dynamics are discussed.

[28] Gopalkrishnan, R., Triantafyllou, M. S., Triantafyllou, G. S., and Barrett, D., "Active Vorticity Control in a Shear Flow Using a Flapping Foil," *Journal of Fluid Mechanics*, Vol. 274, Sept. 1994, pp. 1–21.

Keywords: 2-D, Experimental, Vortices

Abstract: It is shown experimentally that free shear flows can be substantially altered through direct control of the large coherent vortices present in the flow. First, flow-visualization experiments are conducted in Kalliroscope fluid at Reynolds number 550. A foil is placed in the wake of a D-section cylinder, sufficiently far behind the cylinder so that it does not interfere with the vortex formation process. The foil performs a heaving and pitching oscillation at a frequency close to the Strouhal frequency of the cylinder, while cylinder and foil also move forward at constant speed. By varying the phase of the foil oscillation, three basic interaction modes are identified. (i) Formation of a street of pairs of counter-rotating vortices, each pair consisting of one vortex from the initial street of the cylinder and one vortex shed by the foil. The width of the wake is then substantially increased. (ii) Formation of a street of vortices with reduced or even reverse circulation compared to that of oncoming cylinder vortices, through repositioning of cylinder vortices by the foil and interaction with vorticity of the opposite sign shed from the trailing edge of the foil. (iii) Formation of a street of vortices with circulation increased through merging of cylinder vortices with vortices of the same sign shed by the foil. In modes (ii) and (iii) considerable repositioning of the cylinder vortices takes place immediately behind the foil, resulting in a regular or reverse Kármán street. The formation of these three interaction patterns is achieved only for specific parametric values; for different values of the parameters no dominant stable pattern emerges. Subsequently, the experiments are repeated in a different facility at larger scale, resulting in Reynolds number 20000, in order to obtain force and torque measurements. The purpose of the second set of experiments is to assess the impact of flow control on the efficiency of the oscillating foil, and hence investigate the possibility of energy extraction. It is found that the efficiency of the foil depends strongly on the phase difference between the oscillation of the foil and the arrival of cylinder vortices. Peaks in foil efficiency are associated with the formation of a street of weakened vortices and energy extraction by the foil from the vortices of the vortex street.

[29] Lua, K. B., Lim, T. T., Yeo, K. S., and Oo, G. Y., "Wake-Structure Formation of a Heaving Two-Dimensional Elliptic Airfoil," *AIAA Journal*, Vol. 45, No. 7, 2007, pp. 1571–1583.

Keywords: 2-D, Experimental, Vortices

Abstract: This paper is prompted by a recent numerical study (Lew, G. C., and Haj-Hariri, H., "Modelling Thrust Generation of a Two-Dimensional Heaving Airfoil in Viscous Flow," Journal of Fluid Mechanics, Vol. 492, Oct. 2003, pp. 339-362) that shows that for a two-dimensional elliptic airfoil undergoing prescribed heaving motion in a viscous fluid, both leading-edge vortices and trailing-edge vortices contributed to the formation of the wake structures. However, an earlier dye-visualization study (Lai, J. C. S., and Platzer, M. F., "Jet Characteristics of a Plunging Airfoil," AIAA Journal, Vol. 37, No. 12, 1999, pp. 1529-1537) on a heaving NACA 0012 airfoil appears to show that the wake structures were derived from trailing-edge vortices only. The dissimilarity in the two studies remains unclear because there is no corresponding experimental data on a 2-D heaving elliptic airfoil. In this study,

digital particle image velocimetry technique was used to investigate the wake-structure formation of a 2-D elliptic airfoil undergoing simple harmonic heaving motion. For the range of flow conditions investigated here, our results show that the type of wake structures produced is controlled by when and how the leading-edge vortices interact with the trailing-edge vortices.

[30] Pitt Ford, C. W., and Babinsky, H., "Lift and the Leading-Edge Vortex," *Journal of Fluid Mechanics*, Vol. 720, Apr. 2013, pp. 280–313.

Keywords: 2-D, Experimental, Vortices

Abstract: Flapping wings often feature a leading-edge vortex (LEV) that is thought to enhance the lift generated by the wing. Here the lift on a wing featuring a leading-edge vortex is considered by performing experiments on a translating flat-plate aerofoil that is accelerated from rest in a water towing tank at a fixed angle of attack of 15°. The unsteady flow is investigated with dye flow visualization, particle image velocimetry (PIV) and force measurements. Leading- and trailing-edge vortex circulation and position are calculated directly from the velocity vectors obtained using PIV. In order to determine the most appropriate value of bound circulation, a two-dimensional potential flow model is employed and flow fields are calculated for a range of values of bound circulation. In this way, the value of bound circulation is selected to give the best fit between the experimental velocity field and the potential flow field. Early in the trajectory, the value of bound circulation calculated using this potential flow method is in accordance with Kelvin's circulation theorem, but differs from the values predicted by Wagner's growth of bound circulation and the Kutta condition. Later the Kutta condition is established but the bound circulation remains small; most of the circulation is contained instead in the LEVs. The growth of wake circulation can be approximated by Wagner's circulation curve. Superimposing the non-circulatory lift, approximated from the potential flow model, and Wagner's lift curve gives a first-order approximation of the measured lift. Lift is generated by inertial effects and the slow buildup of circulation, which is contained in shed vortices rather than bound circulation.

[31] Anderson, J. M., Streitlien, K., Barrett, D. S., and Triantafyllou M. S., "Oscillating Foils of High Propulsive Efficiency," *Journal of Fluid Mechanics*, Vol. 360, Apr. 1998, pp. 41–72.

Keywords: 2-D, Experimental, Wake

Abstract: Thrust-producing harmonically oscillating foils are studied through force and power measurements, as well as visualization data, to classify the principal characteristics of the flow around and in the wake of the foil. Visualization data are obtained using digital particle image velocimetry at Reynolds number 1100, and force and power data are measured at Reynolds number 40 000. The experimental results are compared with theoretical predictions of linear and nonlinear inviscid theory and it is found that agreement between theory and experiment is good over a certain parametric range, when the wake consists of an array of alternating vortices and either very weak or no leading-edge vortices form. High propulsive efficiency, as high as 87%, is measured experimentally under conditions of optimal wake formation. Visualization results elucidate the basic mechanisms involved and show that conditions of high efficiency are associated with the formation on alternating sides of the foil of a moderately strong leading-edge vortex per half-cycle, which is convected downstream and interacts with trailing-edge vorticity, resulting eventually in the formation of a reverse Kármán street. The phase angle between transverse oscillation and angular motion is the critical parameter affecting the interaction of leading-edge and trailing-edge vorticity, as well as the efficiency of propulsion.

[32] Schnipper, T., Andersen, A., and Bohr, T., "Vortex Wakes of a Flapping Foil," *Journal of Fluid Mechanics*, Vol. 633, Aug. 2009, pp. 411–423.

Keywords: 2-D, Experimental, Wake

Abstract: We present an experimental study of a symmetric foil performing pitching oscillations in a vertically flowing soap film. By varying the frequency and amplitude of the oscillation we visualize a variety of wakes with up to 16 vortices per oscillation period, including von Kármán vortex street, inverted von Kármán vortex street, 2P wake, 2P+2S wake and novel wakes ranging from 4P to 8P. We map out the wake types in a phase diagram spanned by the width-based Strouhal number and the dimensionless amplitude. We follow the time evolution of the vortex formation near the round leading edge and the shedding process at the sharp trailing edge in detail. This allows us to identify the origins of the vortices in the 2P wake, to understand that two distinct 2P regions are present in the phase diagram due to the timing of the vortex shedding at the leading edge and the trailing edge and to propose a simple model for the vorticity generation. We use the model to describe the transition from 2P wake to 2S wake with increasing oscillation frequency and the transition from the von Kármán wake, typically associated with drag, to the inverted von Kármán wake, typically associated with thrust generation.

[33] von Ellenrieder, K. D., and Pothos, S., "PIV Measurements of the Asymmetric Wake of a Two Dimensional Heaving Hydrofoil," *Experiments in Fluids*, Vol. 44, No. 5, 2008, pp. 733–745.

Keywords: 2-D, Experimental, Wake

Abstract: Particle image velocimetry is used to examine the flow behind a two-dimensional heaving hydrofoil of NACA 0012 cross section, operating with heave amplitude to chord ratio of 0.215 at Strouhal numbers between 0.174 and 0.781 and a Reynolds number of 2,700. The measurements show that for Strouhal numbers larger than 0.434, the wake becomes deflected such that the average velocity profile is asymmetric about the mean heave position of the hydrofoil. The deflection angle of the wake, which is related to the average lift and drag on the hydrofoil, is found to lie between 13° and 18°. An examination of the swirl strength of the vortices generated by the hydrofoil motion reveal that the strongest vortices, which are created at the higher Strouhal numbers, dissipate most rapidly.

[34] Koochesfahani, M. M., "Vortical Patterns in the Wake of an Oscillating Airfoil," *AIAA Journal*, Vol. 27, No. 9, 1989, pp. 1200–1205.

Keywords: 2-D, Experimental, Wake

Abstract: The vortical flow patterns in the wake of a NACA 0012 airfoil pitching at small amplitudes are studied in a low-speed water channel. It is shown that a great deal of control can be exercised on the structure of the wake by the control of the frequency, amplitude, and also the shape of the oscillation waveform. An important observation in this study is the existence of an axial flow in the cores of the wake vortices. Estimates of the magnitude of the axial flow suggest a linear dependence on the oscillation frequency and amplitude.

[35] Lai, J. C., and Platzer, M. F., "Jet characteristics of a plunging airfoil," *AIAA Journal*, Vol. 37, No. 12, 1999, pp. 1529–1537.

Keywords: 2-D, Experimental, Wake

Abstract: Water-tunnel tests of a NACA 0012 airfoil that was oscillated sinusoidally in plunge are described. The flowfield downstream of the airfoil was explored by dye flow visualization and single-component laser Doppler velocimetry (LDV) measurements for a range of freestream speeds, frequencies, and amplitudes of oscillation. The dye visualizations show that the vortex patterns generated by the plunging airfoil change from drag-producing wake flows to thrust-producing jet flows as soon as the ratio of maximum plunge velocity to freestream speed, i.d., the nondimensional plunge velocity, exceeds approximately 0.4. The LDV measurements show that the nondimensional plunge velocity is the appropriate parameter to collapse the maximum streamwise velocity data covering a nondimensional plunge velocity range from 0.18 to 9.3. The maximum streamwise velocity at a given streamwise distance downstream starts to exceed the freestream speed as soon as the nondimensional plunge velocity exceeds 0.25. Furthermore, this maximum jet velocity has been shown to be a linear function of the nondimensional plunge velocity.

[36] Bratt, J. B., "Flow Patterns in the Wake of an Oscillating Airfoil," Aeronautical Research Council R&M-2773, Mar. 1953, pp. 17–24.

Keywords: 2-D, Experimental, Wake

[37] Freymuth, P., "Thrust Generation by an Airfoil in Hover Modes," *Experiments in Fluids*, Vol. 9, No. 1, 1990, pp. 17–24.

Keywords: 2-D, Experimental, Hover

Abstract: A small airfoil is operated in combined harmonic plunging and pitching motions to generate thrust in a still air environment. By full utilization of dynamic stall vortices large thrust coefficients were attained. The vortical signature of thrust is a simple vortex street with the character of a jet stream.

[38] Dickinson, M. H., and Goetz, K. G., "Unsteady Aerodynamic Performance of Model Wings at Low Reynolds Numbers," *Journal of Experimental Biology*, Vol. 174, Jan. 1993, pp. 45–64.

Keywords: 2-D, Experimental, Take-off

Abstract: The synthesis of a comprehensive theory of force production in insect flight is hindered in part by the lack of precise knowledge of unsteady forces produced by wings. Data are especially sparse in the intermediate Reynolds number regime ($10<Re<1000$) appropriate for the flight of small insects. This paper attempts to fill this deficit by quantifying the time-dependence of aerodynamic forces for a simple yet important motion, rapid acceleration from rest to a constant velocity at a fixed angle of attack. The study couples the measurement of lift and drag on a two-dimensional model with simultaneous flow visualization. The results of these experiments are summarized below. 1. At angles of attack below 13.5°, there was virtually no evidence of a delay in the generation of lift, in contrast to similar

studies made at higher Reynolds numbers. 2. At angles of attack above 13.5°, impulsive movement resulted in the production of a leading edge vortex that stayed attached to the wing for the first 2 chord lengths of travel, resulting in an 80 % increase in lift compared to the performance measured 5 chord lengths later. It is argued that this increase is due to the process of detached vortex lift, analogous to the method of force production in delta-wing aircraft. 3. As the initial leading edge vortex is shed from the wing, a second vortex of opposite vorticity develops from the trailing edge of the wing, correlating with a decrease in lift production. This pattern of alternating leading and trailing edge vortices generates a von Karman street, which is stable for at least 7.5 chord lengths of travel. 4. Throughout the first 7.5 chords of travel the model wing exhibits a broad lift plateau at angles of attack up to 54°, which is not significantly altered by the addition of wing camber or surface projections. 5. Taken together, these results indicate how the unsteady process of vortex generation at large angles of attack might contribute to the production of aerodynamic forces in insect flight. Because the fly wing typically moves only 2–4 chord lengths each half-stroke, the complex dynamic behavior of impulsively started wing profiles is more appropriate for models of insect flight than are steady-state approximations.

[39] Maresca, C., Favier, D. and Rebont, J., "Experiments on an Aerofoil at High Angle of Incidence in Longitudinal Oscillations," *Journal of Fluid Mechanics*, Vol. 92, June 1979, pp. 671–690.

Keywords: 2-D, Experimental, Stall

Abstract: Details of flow visualization, aerodynamic forces and pitching moment, static pressure and skin friction measurements have been carried out on a symmetrical aerofoil at fixed angle of incidence in longitudinal oscillations parallel to the uniform airstream of a wind-tunnel. This investigation shows weak unsteady effects at incidences below that of static stall. For higher incidences, strong unsteady effects appear and depend on the frequency and amplitude of the oscillations. The measurements indicate an overshoot of the instantaneous lift and drag which is explained by a strong vortex shedding process occurring during the dynamic stall encountered by the aerofoil in decelerated motion, as observed for profiles oscillating in pitch through stall. When the aerofoil is going forward in accelerated motion dynamic reattachment may be observed at very high incidence over a short part of the period of oscillation. Dynamic stall and dynamic reattachment contribute to a favourable effect of unsteadiness on the mean lift coefficient, which increases as compared to the steady state one, and which is expressed through an empirical formula involving incidence, frequency and amplitude of oscillations. At given incidence, optimization of this feature is achieved by matching the frequency and the amplitude of oscillation, respectively with the frequency linked with the highest peak of energy in the wake, and with the distance between two consecutive vortices in the mean wake when modelled as a von Kármán's vortex street.

[40] Izraelevitz, J. S., and Triantafyllou, M. S., "Adding In-Line Motion and Model-Based Optimization Offers Exceptional Force Control Authority in Flapping Foils," *Journal of Fluid Mechanics*, Vol. 742, Mar. 2014, pp. 5–34.

Keywords: 2-D, Experimental, In-Line Motion

Abstract: We study experimentally the effect of adding an in-line oscillatory motion to the oscillatory heaving and pitching motion of flapping foils that use a power downstroke. We show that far from being a limitation imposed by the muscular structure of certain animals, in-line motion can be a powerful means to either substantially augment the mean lift, or reduce oscillatory lift and increase thrust; propulsive efficiency can also be increased. We also show that a model-based optimization scheme that is used to drive an iterative sequence of experimental runs provides exceptional ability for flapping foils to tightly vector and keep the force in a desired direction, hence improving performance in locomotion and manoeuvring. Flow visualization results, using particle image velocimetry, establish the connection of distinct wake patterns with flapping modes associated with high lift forces, or modes of high thrust and low lift forces.

[41] Alben, S., "Flapping Propulsion Using a Fin Ray," *Journal of Fluid Mechanics*, Vol. 705, Aug. 2012, pp. 149–164.

Keywords: 2-D, Experimental, Fins

Abstract: We calculate optimal driving motions for a fin ray in a two-dimensional inviscid fluid, which is a model for caudal fin locomotion. The driving is sinusoidal in time, and consists of heaving, pitching and a less-studied motion called 'shifting'. The optimal phases of shifting relative to heaving and pitching for maximum thrust power and efficiency are calculated. The optimal phases undergo jumps at resonant combinations of fin ray bending and shear moduli, and are nearly constant in regions between resonances. In two examples, pitching- and heaving-based motions converge with the addition of optimal shifting. Shifting provides an order-one increase in output power and efficiency.

[42] Bandyopadhyay, P. R., Beal, D. N., Hrubes, J. D., and Mangalam, A., "Relationship of Roll and Pitch Oscillations in a Fin Flapping at Transitional to High Reynolds Numbers," *Journal of Fluid Mechanics*, Vol. 702, July 2012, pp. 298–331.

Keywords: 2-D, Experimental, Fins

Abstract: Hydrodynamic effects of the relationship between the roll and pitch oscillations in low-aspect-ratio fins, with a laminar section and a rounded leading edge, flapping at transitional to moderately high Reynolds numbers, are considered. The fin is hinged at one end and its roll amplitude is large. Also examined is how this relationship is affected by spanwise twist, which alters the pitch oscillation amplitude and its phase relative to the roll motion. Force, efficiency and surface hot-film-anemometry measurements, and flow visualization are carried out in a tow tank. A fin of an abstracted penguin-wing planform and a NACA 0012 cross-section is used, and the chord Reynolds number varies from 3558 to 150 000 based on total speed. The fin is forced near the natural shedding frequency. Strouhal number and pitch amplitude are directly related when thrust is produced, and efficiency is maximized in narrow combinations of Strouhal number and pitch amplitude when oscillation of the leading-edge stagnation point is minimal. Twist makes the angle of attack uniform along the span and enhances thrust by up to 24 %, while maintaining high efficiency. Only 5 % of the power required to roll is spent to pitch, and yet roll and pitch are directly related. During hovering, dye visualization shows that a diffused leading-edge vortex is produced in rigid fins, which enlarges along the span; however, twist makes the vortex more uniform and the fin in turn requires less power to roll. Low-order phase maps of the measurements of force oscillation versus its derivative are modelled as due to van der Pol oscillators; the higher-order maps show trends in the sub-regimes of the transitional Reynolds number. Fin oscillation imparts a chordwise fluid motion, yielding a Stokes wave in the near-wall vorticity layer. When the roll and pitch oscillations are directly related, the wave is optimized: causing vorticity lift-up as the fin is decelerated at the roll extremity; the potential energy at the stagnation point is converted into kinetic energy; a vortex is produced as the lifted vorticity is wrapped around the leading edge; and free-stream reattachment keeps the vortex trapped. When the twist oscillation is phased along the span, this vortex becomes self-preserving at all amplitudes of twist, indicating the most stable (low-bandwidth) tuned nature.

[43] Sane, S. P., and Dickinson, M. H., "The Control of Flight Force by a Flapping Wing: Lift and Drag Production," *Journal of Experimental Biology*, Vol. 204, Aug. 2001, pp. 2607–2626.

Keywords: 2-D, Experimental, Insect

Abstract: We used a dynamically scaled mechanical model of the fruit fly Drosophila melanogaster to study how changes in wing kinematics influence the production of unsteady aerodynamic forces in insect flight. We examined 191 separate sets of kinematic patterns that differed with respect to stroke amplitude, angle of attack, flip timing, flip duration and the shape and magnitude of stroke deviation. Instantaneous aerodynamic forces were measured using a two-dimensional force sensor mounted at the base of the wing. The influence of unsteady rotational effects was assessed by comparing the time course of measured forces with that of corresponding translational quasi-steady estimates. For each pattern, we also calculated mean stroke-averaged values of the force coefficients and an estimate of profile power. The results of this analysis may be divided into four main points. (i) For a short, symmetrical wing flip, mean lift was optimized by a stroke amplitude of 180° and an angle of attack of 50°. At all stroke amplitudes, mean drag increased monotonically with increasing angle of attack. Translational quasi-steady predictions better matched the measured values at high stroke amplitude than at low stroke amplitude. This discrepancy was due to the increasing importance of rotational mechanisms in kinematic patterns with low stroke amplitude. (ii) For a 180° stroke amplitude and a 45° angle of attack, lift was maximized by short-duration flips occurring just slightly in advance of stroke reversal. Symmetrical rotations produced similarly high performance. Wing rotation that occurred after stroke reversal, however, produced very low mean lift. (iii) The production of aerodynamic forces was sensitive to changes in the magnitude of the wing's deviation from the mean stroke plane (stroke deviation) as well as to the actual shape of the wing tip trajectory. However, in all examples, stroke deviation lowered aerodynamic performance relative to the no deviation case. This attenuation was due, in part, to a trade-off between lift and a radially directed component of total aerodynamic force. Thus, while we found no evidence that stroke deviation can augment lift, it nevertheless may be used to modulate forces on the two wings. Thus, insects might use such changes in wing kinematics during steering maneuvers to generate appropriate force moments. (iv) While quasi-steady estimates failed to capture the time course of measured lift for nearly all kinematic patterns, they did predict with reasonable accuracy stroke-averaged values for the mean lift coefficient. However, quasi-steady estimates grossly underestimated the magnitude of the mean drag coefficient under all conditions. This discrepancy was due to the contribution of rotational effects that steady-state

estimates do not capture. This result suggests that many prior estimates of mechanical power based on wing kinematics may have been grossly underestimated.

[44] Seshadri, P., Benedict, M., and Chopra, I., "Understanding Micro Air Vehicle Flapping-Wing Aerodynamics Using Force and Flowfield Measurements," *Journal of Aircraft*, Vol. 50, No. 4, 2013, pp. 1070–1087.

Keywords: 2-D, Experimental, Insect

Abstract: Experimental studies were conducted by flapping a rigid rectangular wing with a mechanism that is capable of emulating complex insect wing kinematics, including figure-of-eight motions, in order to explore the fundamental unsteady flow on a flapping wing at micro-air-vehicle-scale Reynolds numbers. Force and moment measurements were obtained from a miniature six-component force transducer installed at the wing root. The wing was flapped in air and vacuum at the same frequency, and wing kinematics, and the resultant forces, were subtracted in order to obtain the pure aerodynamic forces. In the first part of this paper, the forces produced on the wing undergoing single-degree-of-freedom fixed-pitch pure flapping motions (no pitching or out-of-the-plane coning motions) were determined for a variety of pitch angles. The unsteady aerodynamic coefficients measured during these tests were almost six times the steady-state values measured in the wind tunnel. Flow visualization and particle image velocimetry tests were also conducted, which showed that the key reason for the force increase on the flapping wing is due to a strong leading-edge vortex for which the strength varied throughout the flapping cycle. In the second part of this paper, complete three-degree-of-freedom (flapping, pitching, and coning) insect wing kinematics were investigated for different pitching and coning variations. The aerodynamic forces obtained in these tests were compared with coefficients obtained from the single-degree-of-freedom flapping tests and wind-tunnel tests.

[45] Heathcote, S. and Gursul, I., "Flexible Flapping Airfoil Propulsion at Low Reynolds Numbers," *AIAA Journal*, Vol. 45, No. 5, 2007, pp. 1066–1079.

Keywords: 2-D, Experimental, Flexibility

Abstract: Water tunnel experiments on chordwise-flexible airfoils heaving with constant amplitude have been carried out for Reynolds numbers of 9,000 to 27,000. A degree of flexibility was found to increase both thrust coefficient and propulsive efficiency. Measurements of the flow field revealed stronger trailing-edge vortices corresponding to higher thrust coefficients, and weaker leading-edge vortices corresponding to higher efficiencies. By analogy with a rigid airfoil in coupled heave and pitch, thrust coefficient and propulsive efficiency were found to be functions of the Strouhal number and pitch phase angle. Propulsive efficiency peaks at a pitch phase angle of 95-100 deg (consistent with experimental and computational simulations of rigid airfoils in coupled heave and pitch), and a Strouhal number of 0.29, which lies in the middle of the range observed in nature. Thrust peaks at pitch phase angles in the region of 110-120 deg, but at higher Strouhal numbers. The results suggest the effect of chordwise flexibility is beneficial for purely heaving airfoils at low Reynolds numbers.

[46] Yang, L. J., Ko, A. F., and Hsu, C. K., "Wing Stiffness on Light Flapping Micro Aerial Vehicles," *Journal of Aircraft*, Vol. 49, No. 2, 2012, pp. 423–431.

Keywords: 2-D, Experimental, Flexibility

Abstract: In an effort to develop micro aerial vehicles of 10-cm-span with a successful flight record, this study aims to investigate the influences of wing configuration and foil stiffness on the aerodynamic forces via wind-tunnel testing. These wings with the same wing skeleton structures are made of polyethylene, polyethyleneterephthalate, and polyxylene (parylene). The foil thickness ranges from 17 to 43 micrometers, which corresponds to the varying stiffness of the membrane. The tests showed that the lift coefficients have little importance with the wing foil thickness. Inspection on the relations between power consumption and the flexural stiffness of tested flapping wings reveals that the larger lift force and greater power consumption is associated with the 35 and 43 micrometer thick parylene. Therefore, the present study demonstrated that the flight test of a micro aerial vehicle with the vest wing foil of 24 micrometer thick PET resulted in the longest endurance time of 8 min. Several innovative aspects of developing this work are also summarized.

[47] Heathcote, S., and Gursul, I., "Jet Switching Phenomenon for a Periodically Plunging Airfoil," *Physics of Fluids*, Vol. 19, No. 2, 2007, pp. 027104-1–027104-12.

Keywords: 2-D, Experimental, Flexibility

Abstract: An experimental investigation has been carried out on rigid and flexible airfoils oscillating in still fluid. It was found that the vortex pairs generated by the oscillating airfoil move at an angle to the chordwise direction. The deflection angle of the induced jet was observed to change periodically in time. The switching period was found to

increase with increasing airfoil stiffness and to decrease with increasing heave frequency and increasing amplitude. Over the range of frequency, amplitude, and stiffness tested, the switching period was found to be two orders of magnitude greater than the heave period. The development of the vorticity field for upward and downward deflected jets, as well as the transition between the two modes, was captured with the particle image velocimetry measurements. The deflection of the jet, and thus the jet switching effect, was found to diminish with increasing free stream velocity (decreasing Strouhal number).

[48] Marais, C., Thiria, B., Wesfreid, J. E., and Godoy-Diana, R., "Stabilizing Effect of Flexibility in the Wake of a Flapping Foil," *Journal of Fluid Mechanics*, Vol. 710, Nov. 2012, pp. 659–669.

Keywords: 2-D, Experimental, Flexibility

Abstract: The wake of a flexible foil undergoing pitching oscillations in a low-speed hydrodynamic tunnel is used to examine the effect of chordwise foil flexibility in the dynamical features of flapping-based propulsion. We compare the regime transitions in the wake with respect to the case of a rigid foil and show that foil flexibility inhibits the symmetry breaking of the reverse Bénard–von Kármán wake reported in the literature. A momentum balance calculation shows the average thrust to be up to three times greater for the flexible foil than for the rigid foil. We explain both of these observations by analyzing the vortex dynamics in the very near wake.

[49] Kaya, M., and Tuncer, I. H., "Nonsinusoidal Path Optimization of a Flapping Airfoil," *AIAA Journal*, Vol. 45, No. 8, 2007, pp. 2075–2082.

Keywords: 2-D, Numerical, Efficiency, Optimization

Abstract: The path of a flapping airfoil undergoing a combined, nonsinusoidal pitching and plunging motion is optimized for maximum thrust and/or propulsive efficiency. The nonsinusoidal, periodic flapping motion is described using nonuniform rational B splines. A gradient based algorithm is then employed for the optimization of the nonuniform rational B-spline parameters. Unsteady, low speed laminar flows are computed using a Navier-Stokes solver in a parallel computing environment. The numerical evaluation of the gradient vector components, which requires unsteady flow solutions, is also performed in parallel. It is shown that the thrust generation may significantly be increased in comparison to the sinusoidal flapping motion. For a maximum thrust generation, the airfoil stays at about a constant angle of attack during the upstroke and the downstroke, and may reach very high effective angle of attack values. The pitching motion mostly occurs at the minimum and maximum plunge positions.

[50] Sarkar S., and Venkatraman, K., "Numerical Simulation of Incompressible Viscous Flow Past a Heaving Airfoil," *International Journal for Numerical Methods in Fluids*, Vol. 51, No. 1, 2006, pp. 1–29.

Keywords: 2-D, Numerical, Sinusoidal vs Non Sinusoidal

Abstract: Numerical simulations of a heaving airfoil undergoing non-sinusoidal motions in an incompressible viscous flow is presented. In particular, asymmetric sinusoidal motions, constant heave rate oscillations, and sinusoidal motions with a quiescent gap, are considered. The wake patterns, thrust force coefficients, and propulsive efficiency at various values of non-dimensional heave velocity are computed. These have been compared with those of corresponding sinusoidal heaving motions of the airfoil. It is shown that for a given non-dimensional heave velocity and reduced frequency of oscillation, asymmetric sinusoidal motions give better thrust and propulsive efficiencies in comparison to pure harmonic motion. On the other hand, constant rate heave motion do not compare favourably with harmonic motion. A train of sinusoidal pulses separated by a quiescent gap compares favourably with a pure sinusoidal motion, but with the notable exception that the quiescent gap induces a discontinuity that induces large impulses to the wake pattern.

[51] Young, J., and Lai, J. C. S., "Mechanisms Influencing the Efficiency of Oscillating Airfoil Propulsion," *AIAA Journal*, Vol. 45, No. 7, 2007, pp. 1695–1702.

Keywords: 2-D, Numerical, Efficiency

Abstract: A NACA 0012 airfoil undergoing pitching and plunging motion at Re=20,000-40,000 was simulated using a two-dimensional Navier-Stokes flow solver. Results were compared with experimental measurements in the literature and those from an inviscid analytical method and an unsteady panel method code. Although the peak in propulsive efficiency with Strouhal number demonstrated in the experimental results was predicted by the inviscid methods, it was found to be significantly modified by leading-edge vortex shedding and viscous drag at low Strouhal numbers. The occurrence and influence of vortex shedding is controlled by both the motion of the airfoil (amplitudes and phases of plunging and pitching) and the flapping frequency, which limits the

time available for vortex formation and convection over the airfoil surface. Thus, Strouhal number alone is insufficient to characterize the efficiency of flapping-foil propulsion.

[52] Lee, K. B., Kim, J. H., and Kim, C., "Aerodynamic Effects of Structural Flexibility in Two-Dimensional Insect Flapping Flight," *Journal of Aircraft*, Vol. 48, No. 3, 2011, pp. 894–909.

Keywords: 2-D, Numerical, Flexibility

Abstract: Interaction between a flexible flapping wing and the ambient fluid is of considerable importance in realistic flapping flight. In this paper, two-dimensional fluid-structure interaction simulations are conducted to examine realistic flow features of insects' flapping motion and to investigate aerodynamic change due to structural flexibility of insect wings under a forward-flight condition. Three types of airfoils are considered to reflect structural deformation. Compared with earlier studies regarding two-dimensional rigid-airfoil simulations, the same key physical phenomena and flow patterns could be observed in the flexible case. For example, lift is mainly generated during downstroke by effective angle of attack and leading-edge vortex, while a large amount of thrust is impulsively generated at the end of the upstroke by vortex pairing and vortex staying. On the other hand, the quantitative aspect of flowfields is somewhat different. Structural deformation does affect aerodynamic force generation pattern, and thus structural flexibility has a significant impact on aerodynamic performance. Aerodynamic force coefficient and propulsive efficiency are enhanced compared with the case of a rigid airfoil. In addition, numerical simulations are performed to inspect effects of aerodynamic parameters such as the Reynolds number and reduced frequency. From extensive numerical comparisons, it is observed that key physical phenomena such as vortex pairing and vortex staying are still observed in other flow conditions.

[53] Miao, J. M., Sun, W. H., and Tai, C. H., "Numerical Analysis on Aerodynamic Force Generation of Biplane Counter-Flapping Flexible Airfoils," *Journal of Aircraft*, Vol. 46, No. 5, 2009, pp. 1785–1794.

Keywords: 2-D, Numerical, Flexibility

Abstract: This study explores the effect of chordwise flexible deformation on unsteady aerodynamic characteristics for biplane counter-flapping dual NACA 0014 airfoils with various combinations of Reynolds number and reduced frequency. Unsteady laminar viscous flows over duel rigid and flexible airfoils executing counter-plunge motion are computed with time-dependent two-dimensional laminar Reynolds-averaged Navier-Stokes equations coupled with conformal hybrid meshes. The tested Reynolds number with an airfoil characteristic chord length is 10^2, 10^2, and 10^4, and the reduced frequency ranges from 0.5 to 3.5. The dynamic mesh technique is applied to illustrate the flapping deformation modes of the flexible airfoils. To investigate the influence of the chordwise flexure extent on the aerodynamic performance of the flapping airfoils, the present study considers various different curvature deformations of flapping foils with flexture extent ranging from 0 to 0.3 times the chord length at 0.05 intervals. The visualized particle-tracing paths clearly revealed the formation and evolution of leading-edge vortices along the body of the flexible airfoil as it undergoes biplane counter-plunge motion. The generation of thrust-indicative wake structure or the drag-indicated wake structure behind the flexible airfoils depended on the degree of flexure extent of the airfoil at a fixed range of reduced frequency. The thrust force for each airfoil with biplane counter-flapping mode will be enhanced 6.32% more than that for a rigid single flapping airfoil. Present results show that flexible airfoils with flexure extent 0.25 times the chord length in counter-plunge flapping motion could get maximum propulsive efficiency and produce about 64.65% more than that of a biplane rigid airfoils. The outcome indicates that appropriate flexible biplane flapping flight could not only increase the thrust force, but also boost the propulsive performance.

[54] Yang, T., Wei, M., and Zhao, H., "Numerical Study of Flexible Flapping Wing Propulsion," *AIAA Journal*, Vol. 48, No. 12, 2010, pp. 2909–2915.

Keywords: 2-D, Numerical, Flexibility

Abstract: In this study, a strong-coupling approach is applied to simulate highly flexible flapping wings interacting with fluid flows. Here, the fluid motion, solid motion, and their interaction are solved together by a single set of equations of motion on a fixed Eulerian mesh. To provide necessary flapping mechanism, control cells are implemented in solid area (i.e., the wing) as "skeleton." The moving trajectory of the skeleton is therefore prescribed by a conventional direct-forcing type of immersed boundary method, while the rest of the wing moves passively through elasticity and fluid-structure interaction. This is combined algorithm is then used to study the propulsion characteristics of flexible flapping wings with different elastic moduli and at different flapping frequencies and amplitudes. A two-dimensional NACA 0012 airfoil is chosen as a model wing, and it is under active plunging defined by control cells and corresponding passive pitching motion. With different elastic moduli and at different flapping frequencies and amplitudes. A two-dimensional NACA 0012 airfoil is chosen as a model wing, and it is under active plunging defined

by control cells and corresponding passive pitching motion. With different input parameters, very large different wake structures can be observed. As a result, the coupled plunging-pitching motion can be either drag-producing or thrust-producing. Finally, passive pitching angle theta and nominal angle of attach alpha for flexible wings are defined to characterize the flapping motion. It is found that theta needs to be greater than 0.26 and alpha needs to be greater than 0.3 to generate thrust instead of drag for the flapping motion within the current parametric matrix.

[55] Zhu, Q., "Numerical Simulation of a Flapping Foil with Chordwise or Spanwise Flexibility," *AIAA Journal*, Vol. 45, No. 10, 2007, pp. 2448–2457.

Keywords: 2-D, Numerical, Flexibility

Abstract: Motivated by the discovery that living creatures may be able to enhance their locomotion capability through passive or active deformations of their wings or fins, we carry out a fully coupled fluid-structure interaction study to investigate the flapping motion of a foil with either chordwise or spanwise flexibility. We employ a fluid-structure interaction model, which accounts for fluid dynamics using the boundary-element method and structural dynamics using a two-dimensional nonlinear thin-plate model. With this approach, we numerically investigate the effect of structural deformation on the performance of the foil when it is immersed in two different fluids, a low-density fluid (e.g. air) in which the deformation is determined primarily by the inertia of the foil, and a high-density fluid (e.g. water), in which the fluid loading has a significant impact. In the first scenario, we find that the chordwise flexibility reduces both the thrust and the propulsion efficiency and the spanwise flexibility increases the thrust without efficiency reduction within a small range of structural parameters. In the second scenario, we find that the chordwise flexibility increases the efficiency. The spanwise flexibility, on the other hand, compromises the performance of the foil by diminishing both the thrust and the efficiency. Possible applications of these findings and their relation to designs in aquatic animals are discussed.

[56] Lian, Y., and Shyy, W., "Laminar-Turbulent Transition of a Low Reynolds Number Rigid or Flexible Airfoil," AIAA Paper 2006-3051, June 2006.

Keywords: 2-D, Numerical, Flexibility

Abstract: Laminar-turbulent transition can affect the aerodynamic performance of low Reynolds number flyers, such as micro air vehicles that operate at the Reynolds number of 10^4-10^5. To gain better understanding of the fluid physics and the associated aerodynamics characteristics, we coupled a Navier-Stokes solver, the e^N transition model, and a Reynolds-averaged two-equation closure to study the low Reynolds number flow characterized with the laminar separation bubble and transition. A new intermittency function suitable for low Reynolds number transitional flow incurred by laminar separation is proposed and tested. With the method, we investigate the performance of a rigid airfoil and a flexible airfoil, mounted with a flexible membrane structure on the upper surface, using SD7003 as the configuration. Good agreement is obtained between the prediction and experimental measurements regarding the transition location, aerodynamic coefficients, and overall flow structures. We also examine the impact of a gust on the transition process and airfoil performance. We further investigate the effect of the flexible surface on the transition. We find that the self-excited flexible surface vibration affects the separation and transition positions; however, the time-averaged lift and drag coefficients are close to those of the rigid airfoil.

[57] Gulcat, U., "Propulsive Force of a Flexible Flapping Thin Airfoil," *Journal of Aircraft*, Vol. 46, No. 2, 2009, pp. 465–473.

Keywords: 2-D, Numerical, Flexibility

Abstract: The propulsive force generated by the leading-edge suction of a flapping thin airfoil can be obtained using unsteady aerodynamic notions based on the potential flow theory. Because the potential theory fails to predict the viscous forces, for flapping airfoils, in general there exists a net propulsive force generation. For low Reynolds numbers and for oscillations at low reduced frequencies, however, the viscous forces overcome the propulsive forces to give a net force against the flight direction. In the case of higher Reynolds numbers, flapping with large amplitudes, and high frequencies, the leading-edge suction force generated by the airfoil overcomes the viscous forces. In this study, the critical Reynolds number, the amplitude, and the reduced frequency values that yield the net propulsive force for an oscillating airfoil are predicted with unsteady viscous-inviscid interaction. The airfoil motions are modeled as 1) a thin rigid plate in vertical oscillation, that is, a heaving-plunging motion; 2) a flexibly cambered airfoil whose camber is changing periodically; and 3) the heaving-plunging motion of a flexibly cambered airfoil. The leading-edge suction force for all cases is predicted by means of the well-known Blasius theorem, and the time dependent surface velocity distribution of the airfoil is determined by unsteady aerodynamic considerations. This surface velocity distribution is used as the edge velocity of the unsteady boundary layer to predict the viscous effects.

The coefficient of the propulsive force predicted with the present method agrees well with the values given in the literature up to the effective angles of attack at which the dynamic stall takes place.

[58] Blondeaux, P., Guglielmini, L., and Triantafyllou, M. S., "Chaotic Flow Generated by an Oscillating Foil," *AIAA Journal*, Vol. 43, No. 4, 2005, pp. 918–921.
Keywords: 2-D, Numerical, Hover

[59] Eldredge, J. D., Toomey, J., and Medina, A., "On the Roles of Chord-wise Flexibility in a Flapping Wing with Hovering Kinematics," *Journal of Fluid Mechanics*, Vol. 659, Sep. 2010, pp. 94–115.
Keywords: 2-D, Numerical, Hover
Abstract: The aerodynamic performance of a flapping two-dimensional wing section with simplified chord-wise flexibility is studied computationally. Bending stiffness is modelled by a torsion spring connecting two or three rigid components. The leading portion of the wing is prescribed with kinematics that are characteristic of biological hovering, and the aft portion responds passively. Coupled simulations of the Navier–Stokes equations and the wing dynamics are conducted for a wide variety of spring stiffnesses and kinematic parameters. Performance is assessed by comparison of the mean lift, power consumption and lift per unit power, with those from an equivalent rigid wing, and two cases are explored in greater detail through force histories and vorticity snapshots. From the parametric survey, four notable mechanisms are identified through which flexible wings behave differently from rigid counterparts. Rigid wings consistently require more power than their flexible counterparts to generate the same kinematics, as passive deflection leads to smaller drag and torque penalties. Aerodynamic performance is degraded in very flexible wings undergoing large heaving excursions, caused by a premature detachment of the leading-edge vortex. However, a mildly flexible wing has consistently good performance over a wide range of phase differences between pitching and heaving – in contrast to the relative sensitivity of a rigid wing to this parameter – due to better accommodation of the shed leading-edge vortex into the wake during the return stroke, and less tendency to interact with previously shed trailing-edge vortices. Furthermore, a flexible wing permits lift generation even when the leading portion remains nearly vertical, as the wing passively deflects to create an effectively smaller angle of attack, similar to the passive pitching mechanism recently identified for rigid wings. It is found that an effective pitch angle can be defined that accounts for wing deflection to align the results with those of the equivalent rigid wing.

[60] Wang, Z. J., "Two Dimensional Mechanism for Insect Hovering," *Physical Review Letters*, Vol. 85, No. 10, 2000, pp. 2216–2219.
Keywords: 2-D, Numerical, Hover
Abstract: Resolved computation of two dimensional insect hovering shows for the first time that a two dimensional hovering motion can generate enough lift to support a typical insect weight. The computation reveals a two dimensional mechanism of creating a downward dipole jet of counter rotating vortices, which are formed from leading and trailing edge vortices. The vortex dynamics further elucidates the role of the phase relation between the wing translation and rotation in lift generation and explains why the instantaneous forces can reach a periodic state after only a few strokes. The model predicts the lower limits in Reynolds number and amplitude above which the averaged forces are sufficient.

[61] Kurtulus, D. F., Farcy, A., and Alemdaroglu, N., "Unsteady Aerodynamics of Flapping Airfoil in Hovering Flight at Low Reynolds Numbers," AIAA Paper 2005-1356, Jan. 2005.
Keywords: 2-D, Numerical, Hover
Abstract: The major aim of flapping motion research is based on the understanding of the relation between the temporal and the spatial changes of the wake structure and the resulting instantaneous aerodynamic forces over the flapping wings. The essential physics of non-steady airfoil problems can be observed from simplified two-dimensional experiments, and the interpretations of the behavior can be supported by theoretical or numerical models. The aim of this study is to find optimum parameters to generate maximum lift during this motion, by using numerical methods and analytical models. A great number of cases are investigated involving the changes in the parameters such as angle of attack, location of start of change of incidence, location of start of change of velocity, axis of rotation, and Re number. In addition to the instantaneous aerodynamic forces, pressure distributions and vorticity contours, the average lift and drag coefficient values are also calculated. Positive lift values along the motion are obtained for angle of attack greater than 30 deg. The vortices shed during the flapping motion generate the lift. A modelization program is developed by use of Duhamel integral in order to compare with DNS results.

[62] Kurtulus, D. F., Farcy, A., and Alemdaroglu, N., "Aerodynamic Characteristics of Flapping Motion in Hover," *Experiments in Fluids*, Vol. 44, No. 1, 2008, pp. 23–26.

Keywords: 2-D, Numerical, Hover

Abstract: The aim of the present work is to understand the aerodynamic phenomena and the vortex topology of an unsteady flapping motion by means of numerical and experimental methods. Instead of the use of real insect/bird wing geometries and kinematics which are highly complex and difficult to imitate by an exact modeling, a simplified model is used in order to understand the unsteady aerodynamics and vortex formation mechanisms during the different phases of the flapping motion. The flow is assumed to be laminar with a Reynolds number of 1,000. Direct numerical simulations, laser sheet visualizations and particle image velocimetry (PIV) measurements are performed for the phenomenological analysis of the flow. The vortex dynamics and their identification are put in evidence with PIV measurements by considering velocity magnitude, streamlines, second invariant of velocity gradient (*Q*-criteria), vorticity contours and Eulerian accelerations.

[63] Tang, J., Viieru, D., and Shyy, W., "Effects of Reynolds Number and Flapping Kinematics on Hovering Aerodynamics," *AIAA Journal*, Vol. 46, No. 4, 2008, pp. 967–976.

Keywords: 2-D, Numerical, Hover

Abstract: Motivated by our interest in micro and biological air vehicles, Navier-Stokes simulations for fluid flow around a hovering elliptic airfoil have been conducted to investigate the effects of Reynolds number, reduced frequency, and flapping kinematics on the flow structure and aerodynamics. The Reynolds number investigated ranges from 75 to 1700, and the reduced frequency from 0.36 to 2.0. Two flapping modes are studied, namely, the "water-treading" hovering mode, and the normal hovering mode. Although the delayed-stall mechanisms is found to be responsible for generating the maximum lift peaks in both hovering modes, the wake-capturing mechanism is identified only in the normal hovering mode. In addition to the strong role played by the kinematics, the Reynolds number's role has also been clearly identified. In the low Reynolds number regime, O(100), the viscosity dissipates the vortex structures quickly and leads to essentially symmetric flow structure and aerodynamics force between the forward stroke and backward strokes. At higher Reynolds numbers (300 and larger), the history effect is influential, resulting in distinctly asymmetric phenomena between the forward and backward strokes.

[64] Yin, B., and Luo, H., "Effect of Wing Inertia on Hovering Performance of Flexible Flapping Wings," *Physics of Fluids*, Vol. 22, No. 11, 2010, pp. 111902-1–111902-10.

Keywords: 2-D, Numerical, Hover

Abstract: Insect wings in flight typically deform under the combined aerodynamic force and wing inertia; whichever is dominant depends on the mass ratio defined as $m_*=\rho_{sh}/(\rho_f c)$, where ρ_{sh} is the surface density of the wing, ρ_f is the density of the air, and c is the characteristic length of the wing. To study the differences that the wing inertia makes in the aerodynamic performance of the deformable wing, a two-dimensional numerical study is applied to simulate the flow-structure interaction of a flapping wing during hovering flight. The wing section is modeled as an elastic plate, which may experience nonlinear deformations while flapping. The effect of the wing inertia on lift production, drag resistance, and power consumption is studied for a range of wing rigidity. It is found that both inertia-induced deformation and flow-induced deformation can enhance lift of the wing. However, the flow-induced deformation, which corresponds to the low-mass wing, produces less drag and leads to higher aerodynamic power efficiency. In addition, the wing deformation has a significant effect on the unsteady vortices around the wing. The implication of the findings on insect flight is discussed.

[65] Isogai, K., Shinmoto, Y., and Watanabe, Y., "Effects of Dynamic Stall on Propulsive Efficiency and Thrust of Flapping Airfoil," *AIAA Journal*, Vol. 37, No. 10, 1999, pp. 1145–1151.

Keywords: 2-D, Numerical, Stall

Abstract: Numerical simulations of dynamic stall phenomena around an airfoil oscillating in a coupled mode, in which the pitching and heaving oscillations have some phase difference, have been performed with a Navier-Stokes code. The propulsive efficiency and the thrust have been calculated for various combinations of the phase difference and the reduced frequency for two different amplitude ratios. The effects of the dynamic stall phenomena on the behaviors of the propulsive efficiency and thrust are discussed in detail by examination of each flow pattern obtained. Highest efficiency has been observed for the case in which the pitching oscillation advances 90 degrees ahead of the heaving oscillation and the reduced frequency is at some optimum value, for which there appears no appreciable flow separation in spite of large-amplitude oscillations. For phase angles and reduced frequency other than this best condition, efficiency is rapidly degraded by the occurrence of the large-scale leading-edge separation.

[66] Tuncer, I. H., Walz, R., and Platzer, M. F., "A Computational Study of the Dynamic Stall of a Flapping Airfoil," AIAA Paper 1998-2519, June 1998.

Keywords: 2-D, Numerical, Stall

Abstract: The dynamic stall boundaries of a NACA 0012 airfoil oscillating in either the pure plunge mode or in the combined pitch and plunge mode is computed using a thin-layer Navier-Stokes solver. Unsteady flowfields are computed at the free-stream Mach number of 0.3, the Reynolds number of 10^6, and the Baldwin-Lomax turbulence model is employed. It is found that a pure plunge oscillation leads to dynamic stall as soon as the non-dimensional plunge velocity exceeds the approximate value of 0.35. In addition, the power extraction capability of the airfoil operating in the wingmill mode is studied by computing the dynamic stall boundary for a combined pitch and plunge motion at the reduced frequency values of 0.1, 0.25, and 0.5.

[67] Zheng, Z. C., and Wei, Z., "Study of Mechanisms and Factors that Influence the Formation of Vortical Wake of a Heaving Airfoil," *Physics of Fluids*, Vol. 24, No. 10, 2012, pp. 103601-1–103601-12.

Keywords: 2-D, Numerical, Vortices

Abstract: A two-dimensional numerical study is performed to investigate the relation between the direction of a deflected wake and the vortex pairing mechanisms. The deflection angle can be correlated with two effective phase velocities defined to represent the trends of symmetry breaking and symmetry holding, respectively. The deflection angle increases with the strength of the vortex pairs, which is associated with the heaving amplitude, frequency, and the free stream Reynolds number. Furthermore, not only the influence of Strouhal number but also those of the two heaving motion components – amplitude and frequency – are studied individually under different Reynolds numbers. The study shows that the deflection angle consistently increases with the difference between the symmetry-breaking phase velocity and symmetry-holding phase velocity.

[68] Liang, C. L., Ou, K., Premasuthan, S., Jameson, A., and Wang, Z. J., "High-order accurate simulations of unsteady flow past plunging and pitching airfoils," *Computers & Fluids*, Vol. 40, No. 1, 2011, pp. 236–248.

Keywords: 2-D, Numerical, Vortices

Abstract: This paper presents simulations of unsteady flow past plunging and pitching airfoils using a high-order spectral difference (SD) method. Both third-order and fourth-order SD methods are employed on unstructured quadrilateral grids for the plunging airfoil at a low Reynolds number. The vortex shedding pattern of an airfoil in an oscillating plunge motion becomes asymmetric at a sufficiently high frequency. The SD method is able to capture this effect and reveal a fine structure that closely replicates the experimental photograph. Interestingly, our simulations also predict that the degree of this asymmetry increases with Reynolds number. Unsteady flow at a higher Reynolds number past a pitching airfoil is studied using the fifth-order SD method. Our predictions show very good agreements with the available experimental data. The developed high-order accurate SD algorithms could enable high-order accurate simulations of unsteady flow past flapping Micro-Air-Vehicles (MAVs).

[69] Dong, H., Mittal, R., and Najjar, F. M., "Wake Topology and Hydrodynamic Performance of Low-Aspect-Ratio Flapping Foils," *Journal of Fluid Mechanics*, Vol. 566, Nov. 2006, pp. 309–343.

Keywords: 2-D, Numerical, Vortices, Thrust

Abstract: Numerical simulations are used to investigate the effect of aspect ratio on the wake topology and hydrodynamic performance of thin ellipsoidal flapping foils. The study is motivated by the quest to understand the hydrodynamics of fish pectoral fins. The simulations employ an immersed boundary method that allows us to simulate flows with complex moving boundaries on fixed Cartesian grids. A detailed analysis of the vortex topology shows that the wake of low-aspect-ratio flapping foils is dominated by two sets of interconnected vortex loops that evolve into distinct vortex rings as they convect downstream. The flow downstream of these flapping foils is characterized by two oblique jets and the implications of this characteristic on the hydrodynamic performance are examined. Simulations are also used to examine the thrust and propulsive efficiency of these foils over a range of Strouhal and Reynolds numbers as well as pitch-bias angles.

[70] Pan, Y., Dong, X., Zhu, Q., and Yue, D. K. P., "Boundary-Element Method for the Prediction of Performance of Flapping Foils with Leading-edge Separation," *Journal of Fluid Mechanics*, Vol. 698, May 2012, pp. 446–467.

Keywords: 2-D, Numerical, Vortices

Abstract: A numerical model based on a boundary-element method is developed to predict the performance of flapping foils for the general cases where vorticities are shed near the leading edge as well as from the trailing edge. The shed vorticities are modelled as desingularized thin shear layers which propagate with the local flow velocity. Special treatments are developed to model the unsteady and alternating leading-edge separation (LES), which is a main

element of difficulty for theoretical and numerical analyses of general flapping foils. The present method is compared with existing experiments where it is shown that the inclusion of LES significantly improves the prediction of thrust and efficiency, obtaining excellent agreement with measurements over a broad range of flapping frequencies (Strouhal number) and motion amplitudes (maximum angle of attack). It is found that the neglect of LES leads to substantial over-prediction of the thrust (and efficiency). The effects of LES on thrust generation in terms of the circulation around the foil, the steady and unsteady thrust components, and the vortex-induced pressure on the foil are elucidated. The efficiency and robustness of the method render it suitable for design optimization which generally requires large numbers of performance evaluations. To illustrate this, we present a sample problem of designing the flapping motion, with the inclusion of higher harmonic components, to maximize the efficiency under specified thrust. When optimal higher harmonic motions are included, the performance of the flapping foil is appreciably improved, mitigating the adverse effects of LES vortex on the performance.

[71] Ramesh, K., Gopalarathnam, A., Granlund, K., Ol, M. V., and Edwards, J. R., "Discrete-Vortex Method with Novel Shedding Criterion for Unsteady Aerofoil Flows with Intermittent Leading-Edge Vortex Shedding," *Journal of Fluid Mechanics*, Vol. 751, July 2014, pp. 500–538.

Keywords: 2-D, Numerical, Vortices

Abstract: Unsteady aerofoil flows are often characterized by leading-edge vortex (LEV) shedding. While experiments and high-order computations have contributed to our understanding of these flows, fast low-order methods are needed for engineering tasks. Classical unsteady aerofoil theories are limited to small amplitudes and attached leading-edge flows. Discrete-vortex methods that model vortex shedding from leading edges assume continuous shedding, valid only for sharp leading edges, or shedding governed by *ad-hoc* criteria such as a critical angle of attack, valid only for a restricted set of kinematics. We present a criterion for intermittent vortex shedding from rounded leading edges that is governed by a maximum allowable leading-edge suction. We show that, when using unsteady thin aerofoil theory, this leading-edge suction parameter (LESP) is related to the A0 term in the Fourier series representing the chordwise variation of bound vorticity. Furthermore, for any aerofoil and Reynolds number, there is a critical value of the LESP, which is independent of the motion kinematics. When the instantaneous LESP value exceeds the critical value, vortex shedding occurs at the leading edge. We have augmented a discrete-time, arbitrary-motion, unsteady thin aerofoil theory with discrete-vortex shedding from the leading edge governed by the instantaneous LESP. Thus, the use of a single empirical parameter, the critical-LESP value, allows us to determine the onset, growth, and termination of LEVs. We show, by comparison with experimental and computational results for several aerofoils, motions and Reynolds numbers, that this computationally inexpensive method is successful in predicting the complex flows and forces resulting from intermittent LEV shedding, thus validating the LESP concept.

[72] Zhu, Q., and Peng, Z., "Mode Coupling and Flow Energy Harvesting by a Flapping Foil," *Physics of Fluids*, Vol. 21, No. 3, 2009, pp. 033601-1–033601-10.

Keywords: 2-D, Numerical, Vortices

Abstract: As demonstrated in recent studies, the bioinspired flapping foils are capable of harvesting kinetic energy from incoming wind or current. A practical measure to achieve this is via the coupling between different modes in a system with multiple degrees of freedom. A typical scenario includes external activation of one motion mode and extracting the mechanical energy from other modes that follow. In this study we create a numerical model based upon the Navier–Stokes equations to investigate the performance of such a system in low Reynolds numbers. The effects of both the mechanical design and the operational parameters are examined. Specifically, we concentrate on the vorticity control mechanisms involved in the process, and demonstrate that through vortex-body interactions energy of the leading-edge vortices can be partially recovered to enhance the energy harvesting capacity.

[73] Lee, J., Kim, J., and Kim, C., "Numerical Study on the Unsteady-Force-Generation Mechanism of Insect Flapping Motion," *AIAA Journal*, Vol. 46, No. 7, 2008, pp. 1835–1848.

Keywords: 2-D, Numerical, Vortices

Abstract: Detailed numerical simulations are conducted to investigate aerodynamic characteristics of unsteady-force generation by a two-dimensional flapping motion under a forward-flight condition. A realistic wing trajectory called the figure-eight motion is extracted from a blowfly's tethered flight under freestream. Computed results show complex vortical flowfields that exhibit very interesting and distinctive unsteady characteristics. Lift is mainly generated during downstroke motion by a high effective angle of attack due to translational and lagging motion. On the other hand, a large amount of thrust is abruptly generated at the end of upstroke motion. Vortical structure in the wake and the pressure field shows that vortex-pairing and vortex-staying mechanisms can be presented as strong

evidence for the abrupt large thrust generation, which is fundamentally different from the inverse Karman vortex that is used to explain thrust generation by sinusoidal oscillating airfoil. Additional numerical simulations are conducted to examine the effects of motion components of figure-eight motion. From numerical results and comparisons, it is observed that wing rotational motion at the end of upstroke is crucial in generating the pairing and staying of vortices, which eventually leads to the abrupt thrust generation.

[74] Tuncer, I. H., and Platzer, M. F., "Computational Study of Flapping Airfoil Aerodynamics," *Journal of Aircraft*, Vol. 37, No. 2, 2000, pp. 514–520.

Keywords: 2-D, Numerical, Wake

Abstract: Unsteady, viscous, low-speed flows over a NACA 0012 airfoil oscillated in plunge and/or pitch at various reduced frequency, amplitude, and phase shift are computed. Vortical wake formations, boundary-layer flows at the leading edge, the formation of leading-edge vortices and their downstream convection are presented in terms of unsteady particle traces. Flow separation characteristics and thrust-producing wake profiles are identified. Computed results compare well with water tunnel flow visualization and force data and other computational data. The maximum propulsive efficiency is obtained for cases where the flow remains mostly attached over the airfoil oscillated in a combined pitch and plunge.

[75] Young, J., and Lai, J. C. S., "Oscillation Frequency and Amplitude Effects on the Wake of a Plunging Airfoil," *AIAA Journal*, Vol. 42, No. 10, 2004, pp. 2042–2052.

Keywords: 2-D, Numerical, Wake

Abstract: The flow over a NACA 0012 airfoil, oscillated sinusoidally in plunge, is simulated numerically using a compressible two-dimensional Navier-Stokes solver at a Reynolds number of 2x10^4. The wake of the airfoil is visualized using a numerical particle tracing method. Close agreement is obtained between numerically simulated wake structures and experimental wake visualizations in the literature, when the flow is assumed to be fully laminar. The wake structures, and the lift and thrust of the airfoil are shown to be strongly dependent on both the Strouhal number and the reduced frequency k of the plunge oscillation at this Reynolds number. Leading-edge separation appears to dominate the generation of aerodynamic forces for reduced frequencies below approximately k=4 but becomes secondary for higher frequencies. Wake structures appear to be controlled primarily by trailing-edge effects at all frequencies tested up to k=20. Aerodynamic force results obtained at this Reynolds number show marked differences from those predicted by potential flow analyses at low plunge frequency and high amplitude but are similar and high frequency and low amplitude, consistent with the effect of leading-edge separation.

[76] Young, J., and Lai, J. C. S., "Vortex Lock-in Phenomenon in the Wake of a Plunging Airfoil," *AIAA Journal*, Vol. 45, No. 2, 2007, pp. 485–490.

Keywords: 2-D, Numerical, Wake

Abstract: The flow over a NACA 0012 airfoil, oscillated sinusoidally in plunge, is simulated numerically using a two-dimensional Navier-Stokes solver at a Reynolds number of 20,000. The wake of the airfoil is visualized using a numerical particle tracing method for high reduced frequencies ($1.0<k<10.0$) and small nondimensional amplitudes ($h<0.1$). Anomalous vortex shedding modes (involving multiple vortices shed per half-cycle of airfoil motion) observed experimentally in the literature are reproduced numerically and are shown to be the result of interaction between the plunging frequency and a natural bluff-body shedding frequency. This results in a vortex lock-in phenomenon analogous to that seen for oscillating cylinders. However, the lock-in boundary is not symmetric about the natural shedding frequency, due to the sharp trailing edge forcing the flow to separate at the trailing edge on the windward side of the airfoil for the majority of the plunge cycle at higher frequencies and amplitudes.

[77] Zhu, Q., "Optimal Frequency for Flow Energy Harvesting of a Flapping Foil," *Journal of Fluid Mechanics*, Vol. 675, May 2011, pp. 495–517.

Keywords: 2-D, Numerical, Wake

Abstract: Inspired by the correlation between the propulsion efficiency of a flapping foil propeller and stability of the wake behind it (which leads to the optimal Strouhal number for propulsion), we numerically simulated a heaving/pitching foil in energy harvesting regime, and investigated the relation between wake stability and the energy harvesting efficiency. The base flow is computed using a Navier–Stokes algorithm and the stability analysis is performed via the Orr–Sommerfeld equation. The wake is found to be convectively unstable and the frequency of the most unstable mode f_w is determined. The case when $f_w \sim f$ coincides with maximum energy harvesting efficiency of the system (f is the frequency of foil oscillation), suggesting that flow energy extraction is closely related to efficient

evolution of the wake. This occurs at a frequency of $f \sim 0.15$ (f is normalized by the chord length and the flow speed), under the constraint that there is significant vortex shedding from the leading edge at sufficiently large effective angles of attack. Indeed, this 'foil–wake resonance' is usually associated with multi-vortex shedding from the leading edge. Furthermore, detailed examination of energy extractions from the heaving and the pitching motions indicates that near the optimal performance point the average energy extraction from the pitching motion is close to zero. This suggests the feasibility of achieving high-efficient energy harvesting through a simple fully passive system we proposed earlier in which no activation is needed.

[78] Lewin, G. C., and Haj-Hariri, H., "Modelling Thrust Generation of a Two-Dimensional Heaving Airfoil in a Viscous Flow," *Journal of Fluid Mechanics*, Vol. 492, Oct. 2003, pp. 339–362.

Keywords: 2-D, Numerical, Frequency

Abstract: A numerical model for two-dimensional flow around an airfoil undergoing prescribed heaving motions in a viscous flow is presented. The model is used to examine the flow characteristics and power coefficients of a symmetric airfoil heaving sinusoidally over a range of frequencies and amplitudes. Both periodic and aperiodic solutions are found. Additionally, some flows are asymmetric in that the upstroke is not a mirror image of the downstroke. For a given Strouhal number – defined as the product of dimensionless frequency and heave amplitude – the maximum efficiency occurs at an intermediate heaving frequency. This is in contrast to ideal flow models, in which efficiency increases monotonically as frequency decreases. In accordance with Wang (2000), the separation of the leading-edge vortices at low heaving frequencies leads to diminished thrust and efficiency. At high frequencies, the efficiency decreases similarly to inviscid theory. Interactions between leading- and trailing-edge vortices are categorized, and the effects of this interaction on efficiency are discussed. Additionally, the efficiency is related to the proximity of the heaving frequency to the frequency of the most spatially unstable mode of the average velocity profile of the wake; the greatest efficiency occurs when the two frequencies are nearly identical. The importance of viscous effects for low-Reynolds-number flapping flight is discussed.

[79] Wang, Z. J., "Vortex Shedding and Frequency Selection in Flapping Flight," *Journal of Fluid Mechanics*, Vol. 410, May 2000, pp. 323–341.

Keywords: 2-D, Numerical, Frequency

Abstract: Motivated by our interest in unsteady aerodynamics of insect flight, we devise a computational tool to solve the Navier–Stokes equation around a two-dimensional moving wing, which mimics biological locomotion. The focus of the present work is frequency selection in forward flapping flight. We investigate the time scales associated with the shedding of the trailing- and leading-edge vortices, as well as the corresponding time-dependent forces. We present a generic mechanism of the frequency selection as a result of unsteady aerodynamics.

[80] Zhang, X., Ni, S., Wang, S., and He, G., "Effects of Geometric Shape on the Hydrodynamics of a Self-Propelled Flapping Foil," *Physics of Fluids*, Vol. 21, No. 10, 2009, pp. 103302-1–103302-7.

Keywords: 2-D, Numerical, Chord Thickness

Abstract: The hydrodynamics of a free flapping foil is studied numerically. The foil undergoes a forced vertical oscillation and is free to move horizontally. The effect of chord-thickness ratio is investigated by varying this parameter while fixing other ones such as the Reynolds number, the density ratio, and the flapping amplitude. Three different flow regimes have been identified when we increase the chord-thickness ratio, i.e., left-right symmetry, back-and-forth chaotic motion, and unidirectional motion with staggered vortex street. It is observed that the chord-thickness ratio can affect the symmetry-breaking bifurcation, the arrangement of vortices in the wake, and the terminal velocity of the foil. The similarity in the symmetry-breaking bifurcation of the present problem to that of a flapping body under constraint is discussed. A comparison between the dynamic behaviors of an elliptic foil and a rectangular foil at various chord-thickness ratios is also presented.

[81] Gopalan, H., and Povitsky, A., "Lift Enhancement of Flapping Airfoils by Generalized Pitching Motion," *Journal of Aircraft*, Vol. 47, No. 6, 2010, pp. 1884–1897.

Keywords: 2-D, Numerical, Pitch/Plunge

Abstract: The pitching and plunging motions of airfoils have received a lot of attention recently, due to the increased interest in the design of micro air vehicles. The use of combined pitch-plunge motion with phase difference between them has often been used for the generation of thrust and lift. These aerodynamic forces could be significantly enhanced under similar operating conditions by using generalized pitch motion with variable center of wing rotation. The current study investigated the flowfield and aerodynamic forces for this generalized pitching motion. Two-

dimensional rigid airfoils were taken as prototypes of micro air vehicle wings. First, the computational results were compared with the available measurements for an SD 7003 airfoil in pure-pitch and pure-plunge motions at Re=10,000. Good agreement was observed between the numerical computations and the experimental results in terms of streamwise velocity, location of the vorticity contours, and wake profiles. Next, the pure-pitch case was considered with the stationary centers of rotation located at different positions along the chord of the airfoil. It was found that the maximum value of the computed average coefficient of lift was obtained when the pitching axis was positioned at either the leading edge or the trailing edge. The generalized pitching motion computations were performed next. It was observed that a phase difference of 90 deg between the pitching motion and the motion of the axis caused a twofold increase of the mean coefficient of lift compared to the pitching about leading edge and combined pitch-plunge motion with a 90 deg phase difference. The stability of the leading-edge vortex was found to be responsible for the enhancement of lift by reduction in pressure at the upper surface of the airfoil. However, thrust force was not generated by applying the generalized pitching alone, whereas it was generated by the combined pitch-plunge motion. Finally a generalized pitching motion combined with a superimposed plunging motion was studied. It was found that for this motion, thrust was generated and the generated lift was higher than that for the generalized pitching motion. This result may help in the use of superposition of kinematic motions of wings to produce the desired amount of lift and thrust.

[82] Lu, X. Y., and Liao, Q., "Dynamic Responses of a Two-Dimensional Flapping Foil Motion," *Physics of Fluids*, Vol. 18, No. 9, 2006, pp. 098104-1–098104-4.

Keywords: 2-D, Numerical, Dynamics

Abstract: The investigation of a flapping foil, which is used as a basic mode of the flapping-based locomotion in insects, birds, and fish, is performed by solving the Navier-Stokes equations numerically. In this Brief Communication we provide insight into the understanding of dynamics of a flapping foil. A critical flapping Reynolds number based on the flapping frequency and amplitude, above which a forward flapping movement occurs, is predicted. The dynamics of the flapping foil are analyzed in two dynamic responses, i.e., an oscillatory movement and a steady movement, which depend on the density ratio between the foil and the surrounded fluid. The steady movement response is related to the forward flapping motion. The Strouhal number that governs a vortex shedding for the forward flapping foil is calculated and lies in the range where flying and swimming animals will be likely to tune for high propulsive efficiency.

[83] Tuncer, I. H., and Platzer, M. F., "Thrust Generation Due to Airfoil Flapping," *AIAA Journal*, Vol. 34, No. 2, 1996, pp. 324–331.

Keywords: 2-D, Numerical, Biplane

Abstract: Thrust generation on a single flapping airfoil and a flapping/stationary airfoil combination in tandem is studied parametrically. A multiblock Navier-Stokes solver is employed to compute unsteady flowfields. The unsteady flow-field around a single flapping airfoil is also computed by an unsteady potential flow code. The numerical solutions predict thrust generation in flapping airfoils and a significant augmentation of thrust in flapping/stationary airfoil combined in tandem. The propulsive efficiency is found to be a strong function of reduced frequency and the amplitude of the flapping motion. At a flapping amplitude of 0.40 chord lengths and a reduced frequency of 0.10, the propulsive efficiency of a single NACA 0012 airfoil was computed to be more than 70%. For the airfoil combination in tandem, the propulsive efficiency was augmented more than 40% at a reduced frequency of 0.75 and a flapping amplitude of 0.20 chord lengths when the airfoils are separated by about two chord lengths.

[84] Tuncer, I. H., and Kaya, M., "Thrust Generation Caused by Flapping Airfoils in a Biplane Configuration," *Journal of Aircraft*, Vol. 40, No. 2, 2003, pp. 509–515.

Keywords: 2-D, Numerical, Biplane

Abstract: Unsteady, viscous flows over flapping airfoils in a biplane configuration are computed on moving overset grids. The overset grid solutions are obtained in parallel in a distributed memory environment. Unsteady flowfields are described by particle traces. Time-averaged thrust values are obtained from the integration of the unsteady drag coefficient. It is shown that airfoils in a biplane configuration and oscillating in a combined pitch and plunge motion with a proper phase shift between them produce 20-40% more thrust than a single flapping airfoil. Turbulence in the flow further augments the thrust generation. For a maximum thrust at a given flapping frequency, an optimization of the flapping motion parameters is needed.

[85] Kaya, M., Tuncer, I. H., Jones, K. D., and Platzer, M. F., "Optimization of Flapping Motion Parameters for Two Airfoils in a Biplane Configuration," *Journal of Aircraft*, Vol. 46, No. 2, 2009, pp. 583–592.

Keywords: 2-D, Numerical, Biplane

Abstract: Flapping motion parameters of airfoils in a biplane configuration are optimized for maximum thrust and/or propulsive efficiency. Unsteady, viscous flowfields over airfoils flapping in a combined plunge and pitch are computed with a parallel flow solver on moving and deforming overset grids. The amplitudes of the sinusoidal pitch and plunge motions and the phase shift between them are optimized for a range of flapping frequencies. A gradient-based optimization algorithm is implemented in a parallel computing environment. The deforming overset grids employed remove the restriction on the flapping motion of airfoils, and improve the optimization results obtained earlier. In the Strouhal number range $0.17>Sr<0.25$, an airfoil in a biplane configuration produces more thrust than a single airfoil. Yet, at a higher Strouhal number, the airfoil in a biplane configuration produced less thrust at a significantly lower efficiency than a single flapping airfoil.

[86] Tay, W. B., Bijl, H., and van Oudheusden, B. W., "Biplane and Tail Effects in Flapping Flight," *AIAA Journal*, Vol. 51, No. 9, 2013, pp. 2133–2146.

Keywords: 2-D, Numerical, Biplane

Abstract: A numerical investigation is performed on the interference effects in single or biplane flapping airfoil propulsion in the presence of a stationary downstream tail. At a Reynolds number of 1000, this corresponds to the regime of small micro aerial vehicles. The objective of this study is to provide insight into the complex wing–tail interaction effects occurring in flapping-wing propulsion configurations. The effect of the relative distance between the airfoils, as well as the positioning and incidence angle of the tail, is investigated. Adding a tail behind a single flapping airfoil increases the efficiency and average thrust by up to 10 and 25%, respectively. For the biplane flapping airfoils without tail, overall efficiency and average thrust per airfoil increase up to 17 and 126%, respectively, with respect to the single airfoil due to the formation of a strong momentum jet. The effect of adding a tail behind the biplane flapping airfoils depends on the tail's orientation and location. Increasing the incidence angle of the tail generates higher lift, although at the expense of decreased efficiency and thrust. Lastly, shifting the vertical position of the tail to have it coincide with the middle heaving position of the leading top airfoil gives the best overall performance.

[87] Choi, J. S., Kim, J. W., Park, G. J., and Lee, D. H., "Kinematic Optimization of a Flapping Motion for Maneuverability and Sustainability Flights," *Journal of Aircraft*, Vol. 50, No. 4, 2013, pp. 1027–1037.

Keywords: 2-D, Numerical, CFD, Kinematics

Abstract: The design of a biomimetic micro air vehicle with flapping wings is an essential challenge in the military/civilian field to conduct various missions. The success of a micro-air-vehicle flight is strongly related to the maneuverability and sustainability of an unsteady aerodynamic performance of the flapping motion. Appropriate flapping kinematics need to be established that are amenable to various flight purposes under a fluctuating environment. In this research, kinematics of flapping motion are determined by the study of aerodynamic performance of a flapping airfoil for appropriate maneuverability and sustainability. The flapping motion of an airfoil is formulated by a combined sinusoidal plunging and pitching motion in various angles of the stroke plane. The optimization process is carried out to determine the efficient motions based on a well-defined surrogate model that is made from the results of two-dimensional computational-fluid-dynamics analysis. The kriging method and genetic algorithm are used for the kinematic-optimization problems. The optimization results present appropriate flapping motions for forward flight, hovering flight, and high-thrust flight, respectively. The numerical results of the optimized cases show how the unsteady aerodynamic mechanisms efficiently maximize lift and thrust-force generation.

[88] Leishman, J. G., "Unsteady Lift of a Flapped Airfoil by Indicial Concepts," *Journal of Aircraft*, Vol. 31, No. 2, 1994, pp. 288–297.

Keywords: 2-D, Numerical, Duhamel Superposition

Abstract: A practical method is described for computing the unsteady lift on an airfoil due to arbitrary motion of a trailing-edge flap. The result for the incompressible case is obtained in state-space form by means of Duhamel superposition and employing an improved exponential approximation to Wagner's indicial lift function. For subsonic compressible flow, the indicial lift at small values of time due to impulsive trailing-edge flap deflection is obtained from linear theory in conjunction with the aerodynamic reciprocal theorems. These results are used with experimental results for the oscillating case to obtain complete exponential approximations for the indicial response due to impulsive flap deflection. The final result for the unsteady lift due to an arbitrary flap motion in subsonic flow is obtained in state-space form. Numerical results and comparisons with experimental data are shown.

[89] Ramamurti, R., and Sandberg, W., "Simulation of Flow about Flapping Airfoils Using Finite Element Incompressible Flow Solver," *AIAA Journal*, Vol. 39, No. 2, 2001, pp. 253–260.

Keywords: 2-D, Numerical, Finite Element

Abstract: A finite element flow solver based on unstructured grids is employed for studying the unsteady flow past oscillating airfoils. The viscous flow past a NACA 0012 airfoil at various pitching frequencies is simulated. The variation of the force coefficient with reduced frequency is compared to experimental and other numerical studies. The effect of variation of the amplitude of the pitching motion on the force coefficient shows that the critical parameter for thrust generation is not the reduced frequency but the Strouhal number based on the maximum excursion of the trailing edge. The flow about the airfoil in a combined pitching and heaving motion, a mode found in many insects, is also simulated. The effects of varying the phase angle between the pitch and the heave motions is studied. The thrust coefficient was compared with experimental studies and good agreement is obtained. It is found that the maximum thrust coefficient is obtained for when the pitch motion leads the heave motion for 120 deg and maximum propulsive efficiency occurs at a phase angle of 90 deg.

[90] Zhu, L., and Peskin, C. S., "Simulation of a Flapping Flexible Filament in a Flowing Soap Film by the Immersed Boundary Method," *Journal of Computational Physics*, Vol. 179, No. 2, 2002, pp. 452–468.

Keywords: 2-D, Numerical, Immersed Boundary

Abstract: This paper reports the computer simulation of a flapping flexible filament in a flowing soap film using the immersed boundary method. Our mathematical formulation includes filament mass and elasticity, gravity, air resistance, and the two wires that bound the flowing soap film. The incompressible viscous Navier–Stokes equations, which are used to describe the motion of the soap film and filament in our formulation, are discretized on a fixed uniform Eulerian lattice while the filament equations are discretized on a moving Lagrangian array of points which do not necessarily coincide with the fixed Eulerian mesh points of the fluid computation. The interaction between the filament and the soap film is handled by a smoothed approximation to the Dirac delta function. This delta function approximation is used not only to interpolate the fluid velocity and to apply force to the fluid (as is commonly done in immersed boundary computations), but also to handle the mass of the filament, which is represented in our calculation as delta function layer of fluid mass density supported along the immersed filament. Because of this nonuniform density, we need to use a multigrid method for solving the discretized fluid equations. This replaces the FFT-based method that is commonly used in the uniform-density case. Our main results are as follows. (i) The sustained flapping of the filament only occurs when filament mass is included in the formulation of the model; within a certain range of mass, the more the mass of the filament, the bigger the amplitude of the flapping. (ii) When the length of filament is short enough (below some critical length), the filament always approaches its straight (rest) state, in which the filament points downstream; but when the length is larger, the system is bistable, which means that it can settle into either state (rest state or sustained flapping) depending on the initial conditions. This numerical result we observed in computer simulation is the same as that of the laboratory experiment even though the Reynolds number of the computations is lower than that of the laboratory experiment by two orders of magnitude.

[91] Platzer, M. F., Neace, K. S., and Pang, K. C., "Aerodynamic Analysis of Flapping Wing Propulsion," AIAA Paper 1993-0484, Jan. 1993.

Keywords: 2-D, Numerical, Panel Code

Abstract: In this paper a panel code is described which allows the systematic study of the thrust and lift characteristics produced by oscillating airfoils and airfoil combinations in incompressible inviscid flow. Results are presented for plunging or pitching airfoils and airfoil combinations. An assessment is made of the propulsive efficiencies and of the interference effects. Comparisons with flat-plate theory and with experiments by Schmidt, Mckinney and DeLaurier, and Freymuth show favorable agreement.

[92] Jones, K. D., and Platzer, M. F., "Time-Domain Analysis of Low-Speed Airfoil Flutter," *AIAA Journal*, Vol. 34, No. 5, 1996, pp. 1027–1033.

Keywords: 2-D, Numerical, Panel Code

Abstract: A time-domain aeroelastic analysis code is described for single airfoils and two-foil systems in incompressible, inviscid flow. Flow solutions are obtained using a time-stepping panel code, and airfoil motions are computed using a two-degree-of-freedom spring/mass model. The time-stepping aeroelastic code is evaluated through comparisons with several classical frequency-domain studies for single-degree-of-freedom pitching motion. Results show excellent agreement with past studies and provide a look into the evolution of the motion in time. Additionally, using a two-foil system, it is shown that flutter of a trailing airfoil can be controlled by proper oscillation and phasing

of a leading airfoil. Three applications of the aeroelastic code are presented, including a feedback loop to actively stabilize flutter of a trailing airfoil, simulations of wake interference in rotary-wing flowfields, and simulations of flutter in ground effect.

[93] Hall, K. C., and Hall, S. R., "A Rational Engineering Analysis of the Efficiency of Flapping Flight," *Fixed and Flapping Wing Aerodynamics for Micro Air Vehicles*, AIAA, Danvers, MA, 2001, pp. 249–274.
Keywords: 2-D, Numerical, Vortex-Lattice

[94] Chae, E. J., Akcabay, D. T., and Young, Y. L., "Dynamic Response and Stability of a Flapping Foil in a Dense and Viscous Fluid," *Physics of Fluids*, Vol. 25, No. 10, 2013, pp. 104106-1–104106-27.
Keywords: 2-D, Numerical, Structure
Abstract: It is important to understand and accurately predict the static and dynamic response and stability of flexible hydro/aero lifting bodies to ensure their structural safety, to facilitate the design/optimization of new/existing concepts, and to test the feasibility of using advanced materials. The present study investigates the influence of solid-to-fluid added mass ratio ($\sqrt{\mu_b}$) and viscous effects on the fluid-structure interaction (FSI) response and stability of a flapping foil in incompressible and turbulent flows using a recently presented efficient and stable numerical algorithm in time-domain, which couples an unsteady Reynolds Average Navier-Stokes solver with a two degrees-of freedom structural model. The new numerical coupling method is able to stably and accurately simulate the FSI behavior of light foils in dense fluids: a limit which is known to be numerically difficult to study with classical FSI coupling methods. The studied FSI responses include static/dynamic divergence and flutter instabilities, which are compared with inviscid, linear potential theory predictions obtained with both time and frequency domain formulations, as well as with several published experimental data. In general, the results show that the critical reduced flutter velocities and reduced divergence velocities both decrease as $\sqrt{\mu_b}$ decreases, and are captured with good accuracy using the viscous FSI solver for a wide range of relative mass ratios that are typical to air/hydrofoils. The comparative analyses showed that the classic frequency-domain linear potential theory is severely unconservative for predicting the flutter velocity for cases with $\sqrt{\mu_b}<3$: this includes the typical operating conditions of most marine and biomedical lifting devices, where the fluid forces are comparable to the solid forces, and strong nonlinear interactions may develop. In addition, the viscous FSI solver is shown to correctly predict the experimentally reported critical divergence speed of a light foil in a dense fluid for a case where the classical potential theory predicts an infinite divergence speed as the foil's elastic axis (E.A.) coincided with the aerodynamic center. The results show that static/dynamic divergence will occur before flutter for light hydrofoils with an E.A. downstream of the center of pressure. However, for high solid-to-fluid added mass ratios ($\sqrt{\mu_b}>2$), flutter tends to occur prior to divergence. In addition, in between the regions governed by static divergence ($\sqrt{\mu_b}<1$) and flutter ($\sqrt{\mu_b}>2$), there is a dynamic divergence region, where the foil deformations oscillate with an increasing mean amplitude, and the oscillation frequency decreases toward zero as the deformation increases; this region could only be captured by using a viscous FSI solver.

[95] Battaglia, F., Kulkarni, A. K., Feng, J., and Merkle, C. L., "Simulations of Planar Flapping Jets in Confined Channels," *AIAA Journal*, Vol. 36, No. 8, 1998, pp. 1425–1431.
Keywords: 2-D, Numerical, Channel Flow
Abstract: Computational analyses are used to provide a more complete understanding of the mechanisms that contribute to the development of oscillating planar jets. The geometry considered is a two-dimensional jet exhausting into a blind channel, whose open end is opposite to the initial direction such that the jet must turn through 180 degrees to exit. The resulting flowfields exhibit three distinct characters that depend on the channel expansion ratio and the Reynolds number. At low Reynolds numbers the flow is steady and symmetric. A symmetry-breaking bifurcation at intermediate Reynolds numbers produces steady asymmetric flows. A Hopf bifurcation at higher Reynolds numbers yields unsteady flows. Predicted critical Reynolds numbers and oscillation frequencies are presented for different expansion ratios. Solutions are obtained from the time-dependent Navier-Stokes equations by means of an incompressible formulation based on dual-time stepping via artificial compressibility.

[96] Wu, J., Qiu, Y. L., Shu, C., and Zhao, N., "Pitching-Motion-Activated Flapping Foil Near Solid Walls for Power Extraction: A Numerical Investigation," *Physics of Fluids*, Vol. 26, No. 8, 2014, pp. 083601-1–083601-19.
Keywords: 2-D, Numerical, Power
Abstract: A numerical investigation on the power extraction of a pitching-motion-activated flapping foil near solid walls is performed by using an immersed boundary-lattice Boltzmann method in this study. The flapping motions of the foil include a forced pitching component and an induced plunging component. The foil is placed either near a

solid wall or between two parallel plane walls. Compared to previous work on the flapping foil for power extraction, the effect of the walls is first considered in this work. At a Reynolds number of 1100 and with the position of the foil pitching axis at third chord, the influences of the mechanical parameters (such as damping coefficient and spring constant) of the foil, the amplitude and frequency of the pitching motion and the clearance between the foil pitching axis and the wall on the power extraction performance of the flapping foil are systematically evaluated. Compared to the situation of free stream, the power extraction performance of the foil near the wall is improved. For given amplitude and frequency, as the clearance decreases the net power extraction efficiency improves. Moreover, as the foil is placed near one wall, there is a transverse shift to the plunging motion that consequently weakens the improvement of net power extraction efficiency. In contrast, the shift can be significantly eliminated as the foil is placed between two walls, which can further improve the net power extraction efficiency. In addition, it is found that the efficiency improvement is essentially from the increased power extraction, which is due to the generation of high lift force.

[97] Toomey, J., and Eldredge, J. D., "Numerical and Experimental Study of the Fluid Dynamics of a Flapping Wing with Low Order Flexibility," *Physics of Fluids*, Vol. 20, No. 7, 2008, pp. 073603-1–073603-10.

Keywords: 2-D, Numerical and Experimental, Flexibility

Abstract: A simple canonical problem for understanding the role of flexibility in flapping wing flight is investigated numerically and experimentally. The problem consists of a two-dimensional two-component wing structure connected by a single hinge with a damped torsion spring. One component of the wing is driven with hovering flapping wing kinematics, while the other component responds passively to the fluid dynamic and inertial/elastic forces. Numerical simulations are carried out with the viscous vortex particle method with strongly coupled body dynamics. The experiments are conducted in a water tank with suspended particles for flow visualization. The system is analyzed in several different kinematic test cases that are designed to span a broad parametric range of flapping. Hinge deflection is used as the primary metric for comparison; the agreement between computation and experiment is very good in all cases. The trajectories of shed vortices are also compared, again with favorable agreement. Fluid forces and moments are computed in the numerical simulation at two different Reynolds numbers. It is found that the rate and timing of wing rotation primarily controls the generation of lift; in contrast, the translational acceleration has little effect. Likewise, kinematics with rotation transition well separated from translation transition are captured utilizing rotation-only kinematics. Reynolds number has little effect on the wing deflection but does influence the mean lift generated by the wing.

[98] Jones, K. D., Dohring, C. M., and Platzer, M. F., "Experimental and Computational Investigation of the Knoller-Betz Effect," *AIAA Journal*, Vol. 36, No. 7, 1998, pp. 1240–1246.

Keywords: 2-D, Numerical and Experimental, Wake

Abstract: The ability of a sinusoidally plunging airfoil to produce thrust, known as the Knoller-Betz or Katzmayr effect, is investigated experimentally and numerically. Water-tunnel experiments are performed providing flow visualization and laser Doppler velocimetry data of the unsteady wakes formed by the plunging foils. Vortical structures and time-averaged velocity profiles in the wake are compared with numerical computations from a previously developed inviscid, unsteady panel code that utilizes a nonlinear wake model. Qualitative and quantitative comparisons are excellent over a broad range of reduced frequencies and Strouhal numbers, indicating that the formation and evolution of the thrust-indicative wake structures are primarily inviscid phenomena. Results at Strouhal numbers greater than about 1.0 (based on plunge amplitude) demonstrate nonsymmetric, deflected wake patterns, where both an average thrust and an average lift are produced. These highly nonlinear wake formations are generated reproducibly, both experimentally and numerically.

[99] Quinn, D. B., Moored, K. W., Dewey, P. A., and Smits, A. J., "Unsteady Propulsion Near a Solid Boundary," *Journal of Fluid Mechanics*, Vol. 742, Mar. 2014, pp. 152–170.

Keywords: 2-D, Numerical and Experimental, Ground Effect

Abstract: Experimental and computational results are presented on an aerofoil undergoing pitch oscillations in ground effect, that is, close to a solid boundary. The time-averaged thrust is found to increase monotonically as the mean position of the aerofoil approaches the boundary while the propulsive efficiency stays relatively constant, showing that ground effect can enhance thrust at little extra cost for a pitching aerofoil. Vortices shed into the wake form pairs rather than vortex streets, so that in the mean a momentum jet is formed that angles away from the boundary. The time-averaged lift production is found to have two distinct regimes. When the pitching aerofoil is between 0.4 and 1 chord lengths from the ground, the lift force pulls the aerofoil towards the ground. In contrast, for wall proximities between 0.25 and 0.4 chord lengths, the lift force pushes the aerofoil away from the ground. Between

these two regimes there is a stable equilibrium point where the time-averaged lift is zero and thrust is enhanced by approximately 40%.

[100] Wang, Z. J., Birch, J. M., and Dickinson, M. H., "Unsteady Forces and Flows in Low Reynolds Number Hovering Flight: Two-Dimensional Computations vs Robotic Wing Experiments," *Journal of Experimental Biology*, Vol. 207, Jan. 2004, pp. 449–460.

Keywords: 2-D and 3-D, Numerical and Experimental, Hover

Abstract: We compare computational, experimental and quasi-steady forces in a generic hovering wing undergoing sinusoidal motion along a horizontal stroke plane. In particular, we investigate unsteady effects and compare two-dimensional (2D) computations and three-dimensional (3D) experiments in several qualitatively different kinematic patterns. In all cases, the computed drag compares well with the experiments. The computed lift agrees in the cases in which the sinusoidal changes in angle of attack are symmetrical or advanced with respect to stroke positions, but lags behind the measured 3D lift in the delayed case. In the range of amplitudes studied here, 3–5 chords, the force coefficients have a weak dependence on stroke amplitude. As expected, the forces are sensitive to the phase between stroke angle and angle of attack, a result that can be explained by the orientation of the wing at reversal. This dependence on amplitude and phase suggests a simple maneuver strategy that could be used by a flapping wing device. In all cases the unsteady forces quickly reach an almost periodic state with continuous flapping. The fluid forces are dominated by the pressure contribution. The force component directly proportional to the linear acceleration is smaller by a factor proportional to the ratio of wing thickness and stroke amplitude; its net contribution is zero in hovering. The ratio of wing inertia and fluid force is proportional to the product of the ratio of wing and fluid density and the ratio of wing thickness and stroke amplitude; it is negligible in the robotic wing experiment, but need not be in insect flight. To identify unsteady effects associated with wing acceleration, and coupling between rotation and translation, as well as wake capture, we examine the difference between the unsteady forces and the estimates based on translational velocities, and compare them against the estimate of the coupling between rotation and translation, which have simple analytic forms for sinusoidal motions. The agreement and disagreement between the computed forces and experiments offer further insight into when the 3D effects are important. A main difference between a 3D revolving wing and a 2D translating wing is the absence of vortex shedding by a revolving wing over a distance much longer than the typical stroke length of insects. No doubt such a difference in shedding dynamics is responsible in part for the differences in steady state force coefficients measured in 2D and 3D. On the other hand, it is unclear whether such differences would have a significant effect on transient force coefficients before the onset of shedding. While the 2D steady state force coefficients under predict 3D forces, the transient 2D forces measured prior to shedding are much closer to the 3D forces. In the cases studied here, the chord is moving between 3 to 5 chords, typical of hovering insect stroke length, and the flow does not appear to separate during each stroke in the cases of advanced and symmetrical rotation. In these cases, the wing reverses before the leading edge vortex would have time to separate even in 2D. This suggests that the time scale for flow separation in these strokes is dictated by the flapping frequency, which is dimensionally independent. In such cases, the 2D unsteady forces turn out to be good approximations of 3D experiments.

[101] Ho, S., Nassef, H., Pornsinsirirak, N., Tai, Y. C., and Ho, C. M., "Unsteady Aerodynamics and Flow Control for Flapping Wing Flyers," *Progress in Aerospace Sciences*, Vol. 39, No. 8, 2003, pp. 635–681.

Keywords: 3-D, Analytical, Discussion, Design/Control

Abstract: The creation of micro air vehicles (MAVs) of the same general sizes and weight as natural fliers has spawned renewed interest in flapping wing flight. With a wingspan of approximately 15 cm and a flight speed of a few meters per second, MAVs experience the same low Reynolds number (10^4–10^5) flight conditions as their biological counterparts. In this flow regime, rigid fixed wings drop dramatically in aerodynamic performance while flexible flapping wings gain efficacy and are the preferred propulsion method for small natural fliers. Researchers have long realized that steady-state aerodynamics does not properly capture the physical phenomena or forces present in flapping flight at this scale. Hence, unsteady flow mechanisms must dominate this regime. Furthermore, due to the low flight speeds, any disturbance such as gusts or wind will dramatically change the aerodynamic conditions around the MAV. In response, a suitable feedback control system and actuation technology must be developed so that the wing can maintain its aerodynamic efficiency in this extremely dynamic situation; one where the unsteady separated flow field and wing structure are tightly coupled and interact nonlinearly. For instance, birds and bats control their flexible wings with muscle tissue to successfully deal with rapid changes in the flow environment. Drawing from their example, perhaps MAVs can use lightweight actuators in conjunction with adaptive feedback control to shape the wing and achieve active flow control. This article first reviews the scaling laws and unsteady flow regime constraining both

biological and man-made fliers. Then a summary of vortex dominated unsteady aerodynamics follows. Next, aeroelastic coupling and its effect on lift and thrust are discussed. Afterwards, flow control strategies found in nature and devised by man to deal with separated flows are examined. Recent work is also presented in using microelectromechanical systems (MEMS) actuators and angular speed variation to achieve active flow control for MAVs. Finally, an explanation for aerodynamic gains seen in flexible versus rigid membrane wings, derived from an unsteady three-dimensional computational fluid dynamics model with an integrated distributed control algorithm, is presented.

[102] von Holst, and Küchemann, D., "Biological and Aerodynamical Problems of Animal Flight," *Journal of the Royal Aeronautical Society*, Vol. 46, Jan. 1942, pp. 39–56.
Keywords: 3-D, Analytical, Discussion

[103] Ansari, S. A., Zbikowski, R., and Knowles, K., "Aerodynamic Modelling of Insect-like Flapping Flight for Micro Air Vehicles," *Progress in Aerospace Sciences*, Vol. 42, No. 2, 2006, pp. 129–172.
Keywords: 3-D, Analytical, Discussion
Abstract: Insect-like flapping flight offers a power-efficient and highly maneuverable basis for a micro air vehicle capable of indoor flight. The development of such a vehicle requires a careful wing aerodynamic design. This is particularly true since the flapping wings will be responsible for lift, propulsion and maneuvers, all at the same time. It sets the requirement for an aerodynamic tool that will enable study of the parametric design space and converge on one (or more) preferred configurations. In this respect, aerodynamic modelling approaches are the most attractive, principally due to their ability to iterate rapidly through various design configurations. In this article, we review the main approaches found in the literature, categorizing them into steady-state, quasi-steady, semi-empirical and fully unsteady methods. The unsteady aerodynamic model of Ansari et al. seems to be the most satisfactory to date and is considered in some detail. Finally, avenues for further research in this field are suggested.

[104] Brown, R. J. H., "The flight of birds: II. Wing Function in Relation to Flight Speed," *Journal of Experimental Biology*, Vol. 30, Mar, 1953, pp. 90–103.
Keywords: 3-D, Analytical, Summary
Abstract: 1. The changes in the form of the wing movement of different birds with change of air speed are described. 2. The aerodynamic properties of various configurations of the wing are discussed. 3. Reconciliation of various contradictory accounts in the literature is attempted. 4. Improvements in photographic methods are described.

[105] Platzer, M. F., Jones, K. D., Young, J., and Lai, J. C. S., "Flapping-Wing Aerodynamics: Progress and Challenges," *AIAA Journal*, Vol. 46, No. 9, 2008, pp. 2136–2149.
Keywords: 3-D, Analytical, Summary
Abstract: It is the objective of this paper to review recent developments in the understanding and prediction of flapping-wing aerodynamics. To this end, several flapping-wing configurations are considered. First, the problem of single flapping wings is treated with special emphasis on the dependence of thrust, lift, and propulsive efficiency on flapping mode, amplitude, frequency, and wing shape. Second, the problem of hovering flight is studied for single flapping wings. Third, the aerodynamic phenomena and benefits produced by the flapping-wing interactions on tandem wings or biplane configurations are discussed. Such interactions occur on dragonflies or on a recently developed micro air vehicle. The currently available two- and three-dimensional inviscid and viscous flapping-wing flow solutions are presented. It is shown that the results are strongly dependent on flapping frequency, amplitude, and Reynolds number. These findings are substantiated by comparison with the available experimental data.

[106] Chen, R. T. N., "Effects of Primary Rotor Parameters on Flapping Dynamics," NASA-TP-1431, Jan. 1980.
Keywords: 3-D, Analytical, Helicopters
Abstract: The effects of flapping dynamics of four main rotor design features that influence the agility, stability, and operational safety of helicopters are studied. The parameters include flapping hinge offset, flapping hinge restraint, pitch-flap coupling, and blade lock number. First, the flapping equations of motion are derived that explicitly contain the design parameters. The dynamic equations are then developed for the tip-path plane, and the influence of individual and combined variations in the design parameters determined. The steady state flapping response is examined with respect to control input and aircraft angular rate which leads to a feedforward control law for control decoupling through cross feed, and a feedback control law to decouple the steady state flapping response. The condition for achieving perfect decoupling of the flapping response due to aircraft pitch and roll rates without using

feedback control is also found for the hover case. It is indicated that the frequency of the regressing flapping mode of the rotor system can become low enough to require consideration in the assessment of handling characteristics.

[107] Ellington, C. P., "The Aerodynamics of Hovering Insect Flight. V. A Vortex Theory," *Philosophical Transactions of the Royal Society of London*, Vol. 305, No. 1122, 1984, pp. 115–144.
Keywords: 3-D, Analytical, Hover

[108] Weis-Fogh, T., "Quick Estimates of Flight Fitness in Hovering Animals Including Novel Mechanisms for Lift Production," *Journal of Experimental Biology*, Vol. 59, Aug. 1973, pp. 169–230.
Keywords: 3-D, Analytical, Hover
Abstract: 1. On the assumption that steady-state aerodynamics applies, simple analytical expressions are derived for the average lift coefficient, Reynolds number, the aerodynamic power, the moment of inertia of the wing mass and the dynamic efficiency in animals which perform normal hovering with horizontally beating wings. 2. The majority of hovering animals, including large lamellicorn beetles and sphingid moths, depend mainly on normal aerofoil action. However, in some groups with wing loading less than 10 N m-2 (1 kgf m-2), non-steady aerodynamics must play a major role, namely in very small insects at low Reynolds number, in true hover-flies (Syrphinae), in large dragonflies (Odonata) and in many butterflies (Lepidoptera Rhopalocera). 3. The specific aerodynamic power ranges between 1.3 and 4.7 WN-1 (11-40 cal h-1 gf-1) but power output does not vary systematically with size, inter alia because the lift/drag ratio deteriorates at low Reynolds number. 4. Comparisons between metabolic rate, aerodynamic power and dynamic efficiency show that the majority of insects require and depend upon an effective elastic system in the thorax which counteracts the bending moments caused by wing inertia. 5. The free flight of a very small chalcid wasp Encarsia formosa has been analyzed by means of slow-motion films. At this low Reynolds number (10-20), the high lift co-efficient of 2 or 3 is not possible with steady-state aerodynamics and the wasp must depend almost entirely on non-steady flow patterns. 6. The wings of Encarsia are moved almost horizontally during hovering, the body being vertical, and there are three unusual phases in the wing stroke: the clap, the fling and the flip. In the clap the wings are brought together at the top of the morphological upstroke. In the fling, which is a pronation at the beginning of the morphological downstroke, the opposed wings are flung open like a book, hinging about their posterior margins. In the flip, which is a supination at the beginning of the morphological upstroke, the wings are rapidly twisted through about 180°. 7. The fling is a hitherto undescribed mechanism for creating lift and for setting up the appropriate circulation over the wing in anticipation of the downstroke. In the case of Encarsia the calculated and observed wing velocities at which lift equals body weight are in agreement, and lift is produced almost instantaneously from the beginning of the downstroke and without any Wagner effect. The fling mechanism seems to be involved in the normal flight of butterflies and possibly of Drosophila and other small insects. Dimensional and other considerations show that it could be a useful mechanism in birds and bats during take-off and in emergencies. 8. The flip is also believed to be a means of setting up an appropriate circulation around the wing, which has hitherto escaped attention; but its operation is less well understood. It is not confined to Encarsia but operates in other insects, not only at the beginning of the upstroke (supination) but also at the beginning of the downstroke where a flip (pronation) replaces the clap and fling of Encarsia. A study of freely flying hover-flies strongly indicates that the Syrphinae (and Odonata) depend almost entirely upon the flip mechanism when hovering. In the case of these insects a transient circulation is presumed to be set up before the translation of the wing through the air, by the rapid pronation (or supination) which affects the stiff anterior margin before the soft posterior portions of the wing. In the flip mechanism vortices of opposite sense must be shed, and a Wagner effect must be present. 9. In some hovering insects the wing twistings occur so rapidly that the speed of propagation of the elastic torsional wave from base to tip plays a significant role and appears to introduce beneficial effects. 10. Non-steady periods, particularly flip effects, are present in all flapping animals and they will modify and become superimposed upon the steady-state pattern as described by the mathematical model presented here. However, the accumulated evidence indicates that the majority of hovering animals conform reasonably well with that model. 11. Many new types of analysis are indicated in the text and are now open for future theoretical and experimental research.

[109] Ansari, S. A., Knowles, K., and Zbikowski, R., "Insectlike Flapping Wings in the Hover Part I: Effect of Wing Kinematics," *Journal of Aircraft*, Vol. 45, No. 6, 2008, pp. 1945–1954.
Keywords: 3-D, Analytical, Hover
Abstract: The aerodynamic design of a flapping-wing micro air vehicle requires a careful study of the wing-design space to ascertain the best combination of parameters. Here, such wing design for hovering insectlike flapping flight is studied using a nonlinear unsteady aerodynamic model developed by the authors. The work is characterized, in particular, by the insights it provides into flapping-wing flows and the use it makes of these insights for aerodynamic

design. This is the first of a two-part paper. The effects of wing kinematics on the aerodynamic performance of such flapping wings are investigated in this part by varying one parameter at a time; the effects of wing geometry are considered in part 2. It is found here that there are benefits in increasing flapping frequency and stroke amplitude and in advancing wing pitching rotation. Other important trends are also identified and practical considerations are noted. When possible, comparisons are also drawn with quasi-steady expectations and discrepancies are explained.

[110] Ansari, S. A., Knowles, K., and Zbikowski, R., "Insectlike Flapping Wings in the Hover Part II: Effect of Wing Geometry," *Journal of Aircraft*, Vol. 45, No. 6, 2008, pp. 1976–1990.

Keywords: 3-D, Analytical, Hover

Abstract: The aerodynamic design of a flapping-wing micro air vehicle requires a careful study of the wing-design space to ascertain the best combination of parameters. A nonlinear unsteady aerodynamic model developed by the authors is used to make such a study for hovering insectlike flapping wings. The work is characterized, in particular, by the insights it provides into flapping-wing flows and the use of these insights for aerodynamic design. The effects of wing geometry on the aerodynamic performance of such flapping wings are investigated by comparing the influence on a number of synthetic planform shapes while varying only one parameter at a time. Best performance appears to be for wing shapes that have nearly straight leading edges and more area outboard, where flow velocities are higher. Other important trends are also identified and practical considerations are noted. When possible, comparisons are also drawn with quasi-steady expectations and discrepancies are explained.

[111] Ansari, S. A., Zbikowski, R., and Knowles, K., "Nonlinear Unsteady Aerodynamic Model for Insect-like Flapping Wings in the Hover Part 1: Methodology and Analysis," *Proceedings of the Institute of Mechanical Engineering, Part G: Journal of Aerospace Engineering*, Vol. 220, No. 2, 2006, pp. 61–83.

Keywords: 3-D, Analytical, Hover

Abstract: The essence of this two-part paper is the analytical, aerodynamic modelling of insect-like flapping wings in the hover for micro air vehicle applications. A key feature of such flapping-wing flows is their unsteadiness and the formation of a leading-edge vortex in addition to the conventional wake shed from the trailing edge. What ensues is a complex interaction between the shed wakes which, in part, determines the forces and moments on the wing. In an attempt to describe such a flow, two-novel coupled, non-linear, wake-integral equations are developed in this first part of the paper, and these form the foundation upon which the rest of the work stands. The circulation-based model thus developed is unsteady and inviscid in nature and essentially two-dimensional. It is converted to a 'quasi-three-dimensional' model using a blade-element-type method, but with radial chords. The main results from the model are force and moment data for the flapping wing and are derived as part of this article using the method of impulses. These forces and moments have been decomposed into constituent elements. The governing equations developed in the study are exact, but do not have a closed analytic form. Therefore, solutions are found by numerical methods. These are described in the second part of this paper.

[112] Gogulapati, A., Friedmann, P. P., Kheng, E., and Shyy, Wei, "Approximate Aeroelastic Modeling of Flapping Wings in Hover," *AIAA Journal*, Vol. 51, No. 3, 2013, pp. 567–583.

Keywords: 3-D, Analytical, Hover

Abstract: A nonlinear aeroelastic model suitable for flexible insectlike flapping wings in hover is presented. The aeroelastic model is obtained by coupling a nonlinear structural dynamic model based on MARC, with a potential-flow-based approximate aerodynamic model that consists of leading-edge vortices and a wake model. The aeroelastic response is obtained using an updated Lagrangian method. The paper describes validation studies conducted on the structural dynamic model, aerodynamic comparisons, and aeroelastic studies conducted on isotropic and anisotropic Zimmerman wings. The results demonstrate the suitability of MARC for modeling anisotropic wings undergoing insectlike wing kinematics. For the aeroelastic cases considered, the approximate model shows acceptable agreement with computational-fluid-dynamics-based and experimental results. The approximate model captured several important trends correctly.

[113] Zbikowski, R., "On Aerodynamic Modelling of an Insect-like Flapping Wing in Hover for Micro Air Vehicles," *Philosophical Transactions of the Royal Society of London, Series A: Mathematical and Physical Sciences*, Vol. 360, No. 1791, 2002, pp. 273–290.

Keywords: 3-D, Analytical, Hover

Abstract: This theoretical paper discusses recent advances in the fluid dynamics of insect and micro air vehicle (MAV) flight and considers theoretical analyses necessary for their future development. The main purpose is to propose a new conceptual framework and, within this framework, two analytic approaches to aerodynamic modelling

of an insect–like flapping wing in hover in the context of MAVs. The motion involved is periodic and is composed of two half–cycles (downstroke and upstroke) which, in hover, are mirror images of each other. The downstroke begins with the wing in the uppermost and rearmost position and then sweeps forward while pitching up and plunging down. At the end of the half–cycle, the wing flips, so that the leading edge points backwards and the wing's lower surface becomes its upper side. The upstroke then follows by mirroring the downstroke kinematics and executing them in the opposite direction. Phenomenologically, the interpretation of the flow dynamics involved, and adopted here, is based on recent experimental evidence obtained by biologists from insect flight and related mechanical models. It is assumed that the flow is incompressible, has low Reynolds number and is laminar, and that two factors dominate: (i) forces generated by the bound leading–edge vortex, which models flow separation; and (ii) forces due to the attached part of the flow generated by the periodic pitching, plunging and sweeping. The first of these resembles the analogous phenomenon observed on sharp–edged delta wings and is treated as such. The second contribution is similar to the unsteady aerodynamics of attached flow on helicopter rotor blades and is interpreted accordingly. Theoretically, the fluid dynamic description is based on: (i) the superposition of the unsteady contributions of wing pitching, plunging and sweeping; and (ii) adding corrections due to the bound leading–edge vortex and wake distortion. Viscosity is accounted for indirectly by imposing the Kutta condition on the trailing edge and including the influence of the vortical structure on the leading edge. Mathematically, two analytic approaches are proposed. The first derives all the quantities of interest from the notion of circulation and leads to tractable integral equations. This is an application of the von Kármán–Sears unsteady wing theory and its nonlinear extensions due to McCune and Tavares; the latter can account for the bound leading–edge vortex and wake distortion. The second approach uses the velocity potential as the central concept and leads to relatively simple ordinary differential equations. It is a combination of two techniques: (i) unsteady aerodynamic modelling of attached flow on helicopter rotor blades; and (ii) Polhamus's leading edge suction analogy. The first of these involves both frequency–domain (Theodorsen style) and time–domain (indicial) methods, including the effects of wing sweeping and returning wake. The second is a nonlinear correction accounting for the bound leading–edge vortex. Connections of the proposed framework with control engineering and aeroelasticity are pointed out.

[114] Gogulapati, A., and Friedmann, P. P., "Approximate Aerodynamic and Aeroelastic Modeling of Flapping Wings in Forward Flight," *AIAA Journal*, Vol. 52, No. 1, 2014, pp. 212–218.

Keywords: 3-D, Analytical, Hover to Forward Flight

[115] Wilding, J., "Bird Flight and the Aeroplane," *Journal of the Royal Aeronautical Society*, Vol. 65, July 1961, pp. 796–799.

Keywords: 3-D, Analytical, Animals

[116] Norberg, U. M., "Aerodynamics, Kinematics, and Energetics of Horizontal Flapping Flight in the Long-Eared bat Plecotus auritus," *Journal of Experimental Biology*, Vol. 65, Aug. 1976, pp. 179–212.

Keywords: 3-D, Analytical, Animals

Abstract: The kinematics, aerodynamics, and energetics of Plecotus auritus in slow horizontal flight, 2–35 m s-1, are analyzed. At this speed the inclination of the stroke path is ca. 58 degrees to the horizontal, the stroke angle ca. 91 degrees, and the stroke frequency ca. 11-9 Hz. A method, based on steady-state aerodynamic and momentum theories, is derived to calculate the lift and drag coefficients as averaged over the whole wing the whole wing-stroke for horizontal flapping flight. This is a further development of Pennycuick's (1968) and Weis-Fogh's (1972) expressions for calculating the lift coefficient. The lift coefficient obtained varies between 1-4 and 1-6, the drag coefficient between 0-4 and 1-2, and the lift/drag ratio between 1-2 and 4-0. The corresponding, calculated, total specific mechanical power output of the wing muscles varies between 27-0 and 40-4 W kg-1 body mass. A maximum estimate of mechanical efficiency is 0–26. The aerodynamic efficiency varies between 0–07 and 0–10. The force coefficient, total mechanical power output, and mechanical and aerodynamic efficiencies are all plausible, demonstrating that the slow flapping flight of Plecotus is thus explicable by steady-state aerodynamics. The downstroke is the power stroke for the vertical upward forces and the upstroke for the horizontal forward forces.

[117] Osborne, M. F. M., "Aerodynamics of Flapping Flight with Application to Insects," *Journal of Experimental Biology*, Vol. 28, June 1951, pp. 221–245.

Keywords: 3-D, Analytical, Insects

Abstract: 1. General formulae are derived giving the lift, thrust and power when the wing motion is specified. The formulae are applied to twenty-five insects for which quantitative data are available. Average values for lift and

drag coefficients, CL and CD, are derived by equating the weight to the vertical force and the thrust to the horizontal drag of the body. 2. The large drag and lift coefficients obtained for insect flight are attributed to acceleration effects. There is a distinct correlation between (C2L,+ C2)D)½ and the ratio of the flapping velocity of the wings to the linear velocity of flight. When this ratio and therefore the accelerations are small, the force coefficients do not exceed those to be expected for flat plates. Owing to the nature of the assumptions and approximations made, the values derived for CD, CL and CD/CL are minimum values. 3. Other characteristics of insect flight are discussed. In general, insects fly in such a way as to minimize the mechanical power required. In most, but not all cases, the useful force is the one perpendicular rather than parallel to the relative wind. The wing tips should move in a figure 8, the down beat should be slower than the upbeat, and the majority of the necessary force must be supplied on the down beat. 4. Figures are given using the data from the twenty-five insects considered, showing average relations between power, specific power, mass, acceleration forces, force coefficients and geometrical dimensions. The power per gram, the 'wasted power', and the force coefficients all increase as the importance of the acceleration forces increases. 5. When plotted as functions of mass, quantities involving the power show much less dispersion than quantities involving the geometrical dimensions. This is taken to mean that despite the diversity of insect form, as 'power plants', they are all essentially similar. 6. A table of the observed or adopted flight parameters (frequency of beating, mass, wing area, velocity of flight, amplitude and orientation of wing motion) is appended.

[118] Wootton, R. J., and Kukalova-Peck, J., "Flight Adaptations in Palaeozoic Palaeoptera," *Biological Reviews of the Cambridge Philosophical Society*, Vol. 75, No. 1, 2000, pp. 129–167.

Keywords: 3-D, Analytical, Insects

Abstract: The use of available morphological characters in the interpretation of the flight of insects known only as fossils is reviewed, and the principles are then applied to elucidating the flight performance and techniques of Palaeozoic palaeopterous insects. Wing-loadings and pterothorax mass/total mass ratios are estimated and aspect ratios and shape-descriptors are derived for a selection of species, and the functional significance of wing characters discussed. Carboniferous and Permian ephemeropteroids ('mayflies') show major differences from modern forms in morphology and presumed flight ability, whereas Palaeozoic odonatoids ('dragonflies') show early adaptation to aerial predation on a wide size-range of prey, closely paralleling modern dragonflies and damselflies in shape and wing design but lacking some performance-related structural refinements. The extensive adaptive radiation in form and flight technique in the haustellate orders Palaeodictyoptera, Megasecoptera, Diaphanopterodea and Permothemistida is examined and discussed in the context of Palaeozoic ecology.

[119] Dickinson, M. H., Lehmann, F. O., and Sane, S. P., "Wing Rotation and the Aerodynamic Basis of Insect Flight," *Science*, Vol. 284, June 1999, pp. 1954–1960.

Keywords: 3-D, Analytical, Wing Motion

Abstract: The enhanced aerodynamic performance of insects results from an interaction of three distinct yet interactive mechanisms: delayed stall, rotational circulation, and wake capture. Delayed stall functions during the translational portions of the stroke, when the wings sweep through the air with a large angle of attack. In contrast, rotational circulation and wake capture generate aerodynamic forces during stroke reversals, when the wings rapidly rotate and change direction. In addition to contributing to the lift required to keep an insect aloft, these two rotational mechanisms provide a potent means by which the animal can modulate the direction and magnitude of flight forces during steering maneuvers. A comprehensive theory incorporating both translational and rotational mechanisms may explain the diverse patterns of wing motion displayed by different species of insects.

[120] Klemin, A., "Rotor Bending Moments in a Plane of Flapping," *Journal of the Aeronautical Sciences*, Vol. 9, No. 11, 1942, pp. 411–418.

Keywords: 3-D, Analytical, Bending Moments

Abstract: The present paper, a problem in autogiro rotor stress analysis, can be outlined as follows: 1. Calculation of the characteristics of a typical autogiro employed for illustrative purposes. 2. Derivation of formulas for bending moments in the plane of flapping taking into account the effects of the weight of the blade, centrifugal force, inertia forces in flapping and aerodynamic thrust. 3. Examination of the effect of the azimuth angle on bending moments at a given point on the blade. 4. Effect of variations in (mu), the tip speed ratio, on the bending moment at a given point on the blade. 5. Examination of the effect of the ratio r/R on bending moments. 6. Formulas for the centrifugal relief of bending moments. 7. Comparison of bending moments obtained by the use of empirical formulas available hitherto.

[121] Betteridge, D. S. and Archer, R. D., "A Study of the Mechanics of Flapping Flight," *Aeronautical Quarterly*, Vol. 25, May 1974, pp. 129–142.
Keywords: 3-D, Analytical, Efficiency

[122] Gopalakrishnan, P., and Tafti, D. K., "Effect of Rotation Kinematics and Angle of Attack on Flapping Flight," *AIAA Journal*, Vol. 47, No. 11, 2009, pp. 2505–2519.
Keywords: 3-D, Analytical, Rotation
Abstract: Unsteady aerodynamics of a rigid flapping wing at a Reynolds number of 10,000 for forward flight with an advance ratio of 0.5 is analyzed. A spiral leading-edge vortex with a strong spanwise flow along its core is formed during the downstroke, resulting in a peak lift and thrust. A negative spanwise flow formed due to the tip vortex prevents the removal of vorticity from the leading-edge vortex, leading to instability and separation of the leading-edge vortex. Analysis of different rotation timings shows that supination results in the leading-edge vortex formation near the base and its strength depends on the flapping velocity. A stronger vortex is formed for advanced rotation and it generates high lift. Delayed rotation affects thrust production during translation and results in low propulsive efficiency. Analysis of rotation duration shows that shorter rotation results in high instantaneous lift values, whereas continuous long-duration rotation results in high thrust and propulsive efficiency. Analysis of different angles of attack show that a moderate angle of attack, which results in a high thrust-to-lift ratio and complete shedding of the leading-edge vortex at the end of translation, is required for high propulsive efficiency.

[123] Truong, T. Q., Phan, V. H., Park, H. C., and Ko, J. H., "Effect of Wing Twisting on Aerodynamic Performance of Flapping Wing System," *AIAA Journal*, Vol. 51, No. 7, 2013, pp. 1612–1620.
Keywords: 3-D, Analytical, Twist
Abstract: In this paper, a simple but effective design for implementing a negative wing twist in a beetle-mimicking wing system is presented. The effectiveness of the design in terms of force generation and power consumption is confirmed by both experiment and calculation. An unsteady blade-element-theory model is used to estimate the aerodynamic forces produced by two different wing kinematics of a flapping-wing system. The model was first validated with the measurement data and two three-dimensional computational-fluid-dynamics results from the literature. The difference between the estimated average lift and the measured lift is 5.6%, which proves that the unsteady blade-element-theory model provides reasonable aerodynamic force estimation. The time history of the current estimation is also close to the measured data and is in between the two computational-fluid-dynamics results. The forces generated by the flapping wings with and without wing twist are estimated using the unsteady blade-element theory to investigate effect of the wing twist on the force generation. The result shows that the flapping-wing system with wing twist produces a 9.5% larger average vertical force or thrust while consuming 37% less power than the flapping-wing system without wing twist. The measured thrust by the swing test also shows 13.2% increase for the flapping wing with wing twist. Thus, by the estimation and measurement, it is confirmed that the wing twist improves the thrust generation.

[124] Li, G. J., and Lu, X. Y., "Force and Power of Flapping Plates in a Fluid," *Journal of Fluid Mechanics*, Vol. 712, Dec. 2012, pp. 598–613.
Keywords: 3-D, Analytical, Vortices
Abstract: The force and power of flapping plates are studied by vortex dynamic analysis. Based on the dynamic analysis of the numerical results of viscous flow past three-dimensional flapping plates, it is found that the force and power are strongly dominated by the vortical structures close to the body. Further, the dynamics of the flapping plate is investigated in terms of viscous vortex-ring model. It is revealed that the model can reasonably reflect the essential properties of the ring-like vortical structure in the wake, and the energy of the plate transferred to the flow for the formation of each vortical structure possesses a certain relation. Moreover, simplified formulae for the thrust and efficiency are proposed and verified to be reliable by the numerical solutions and experimental measurements of animal locomotion. The results obtained in this study provide physical insight into the understanding of the dynamic mechanisms relevant to flapping locomotion.

[125] Rayner, J. M. V., "A New Approach to Animal Flight Mechanics," *Journal of Experimental Biology*, Vol. 80, June 1979, pp. 17–54.
Keywords: 3-D, Analytical, Vortices
Abstract: The mechanics of lift and thrust generation by flying animals are studied by considering the distribution of vorticity in the wake. As wake generation is not continuous, the momentum jet theory, which has previously been used, is not satisfactory, and the vortex theory is a more realistic model. The vorticity shed by the

wings in the course of each powered stroke deforms into a small-cored vortex ring; the wake is a chain of such rings. The momentum of each ring sustains and propels the animal; induced power is calculated as the rate of increase of wake kinetic energy. A further advantage of the vortex theory is that lift and induced drag coefficients are not required; estimated instantaneous values of these coefficients are generally too large for steady state aerodynamic theory to be appropriate to natural flapping flight. The vortex theory is applied to hovering of insects and to avian forward flight. A simple expression for induced power in hovering is found. Induced power is always greater than simple momentum jet estimates, and the discrepancy becomes substantial as body mass increases. In hovering the wake is composed of a stack of horizontal, coaxial, circular vortex rings. In forward flight of birds the rings are elliptic; they are neither horizontal nor coaxial because the momentum of each ring balances the vector sum of parasite and profile drag and the bird's weight. Total power consumption as a function of flight velocity is calculated and compared for several species. Power reduction is one of the major factors influencing the choice of flight style. A large body of data is used to obtain an approximate scaling between stroke period and the body mass for birds. Together with relations between other morphological parameters, this is used to estimate the variation of flight speed and power with body mass for birds, and on this basis deviations from allometric scaling can be related to flight proficiency and to the use of such strategies as the bounding flight of small passerines.

[126] Michelson, I., "Flapping Propulsion Wake Analysis," *AIAA Journal*, Vol. 1. No. 11, 1963, pp. 2658–2659.
Keywords: 3-D, Analytical, Wake

[127] DeLaurier, J. D., "An aerodynamic model for flapping-wing flight," *Aeronautical Journal*, Vol. 97, Apr. 1993, pp. 125–130.
Keywords: 3-D, Analytical, Model
Abstract: A design-oriented model for the unsteady aerodynamics of a flapping wing has been developed using a modified strip theory approach. Within this constraint, vortex-wake effects are accounted for as well as partial leading edge suction and post stall behavior. Also, the contributions of sectional mean angle of attack, camber, and friction drag are added, which allows this model to be used for the calculation of the average lift, as well as the thrust, power required, and propulsive efficiency of a flapping wing in equilibrium flight. An example of such calculations is presented in the performance prediction of a mechanical flying pterosaur replica.

[128] Deng, X., Schenato, L., Wu, W. C., and Sastry, S. S., "Flapping Flight for Biomimetic Robotic Insects: Part I - System Modeling," *IEEE Transactions on Robotics*, Vol. 22, No. 4, 2006, pp. 776–788.
Keywords: 3-D, Analytical, Dynamic Models
Abstract: This paper presents the mathematical modeling of flapping flight inch-size micro aerial vehicles (MAVs), namely micromechanical flying insects (MFIs). The target robotic insects are electromechanical devices propelled by a pair of independent flapping wings to achieve sustained autonomous flight, thereby mimicking real insects. In this paper, we describe the system dynamic models which include several elements that are substantially different from those present in fixed or rotary wing MAVs. These models include the wing-thorax dynamics, the flapping flight aerodynamics at a low Reynolds number regime, the body dynamics, and the biomimetic sensory system consisting of ocelli, halteres, magnetic compass, and optical flow sensors. The mathematical models are developed based on biological principles, analytical models, and experimental data. They are presented in the Virtual Insect Flight Simulator (VIFS) and are integrated together to give a realistic simulation for MFI and insect flight. VIFS is a software tool intended for modeling flapping flight mechanisms and for testing and evaluating the performance of different flight control algorithms.

[129] Orlowski, C. T., and Girard, A. R., "Longitudinal Flight Dynamics of Flapping-Wing Micro Air Vehicles," *Journal of Guidance, Control, and Dynamics*, Vol. 35, No. 4, 2012, pp. 1115–1131.
Keywords: 3-D, Analytical, Dynamics
Abstract: The multibody flight dynamics of flapping-wing micro air vehicles are inherently complex. Stability analyses and control algorithms are best applied to equations of motion in first-order form. This paper presents a method for approximating the first-order equations of motion for a flapping-wing micro air vehicle. The first-order equations of motion are derived from a coupled, multibody representation of the system. The first-order equations are analyzed using an approximation method called quarter-cycle averaging. The quarter-cycle averaging method is necessary because the classical averaging techniques are not available. The quarter-cycle approximation method is applied to representations of hovering flight and forward flight. The method enables the calculation of equilibrium

points for the averaged system. For both flight regimes, the quarter-cycle approximation method provides an order of magnitude improvement in accuracy when compared to local averaging.

[130] Shyy, W., Berg, M., and Ljungqvist, D., "Flapping and Flexible Wings for Biological and Micro Air Vehicles," *Progress in Aerospace Sciences*, Vol. 35, No. 5, 1999, pp. 455–505.

Keywords: 3-D, Analytical, MAV Modeling

Abstract: Micro air vehicles (MAVs) with wing spans of 15 cm or less, and flight speed of 30–60 kph are of interest for military and civilian applications. There are two prominent features of MAV flight: (i) low Reynolds number (10^4–10^5), resulting in unfavorable aerodynamic conditions to support controlled flight, and (ii) small physical dimensions, resulting in certain favorable scaling characteristics including structural strength, reduced stall speed, and low inertia. Based on observations of biological flight vehicles, it appears that wing motion and flexible airfoils are two key attributes for flight at low Reynolds number. The small size of MAVs corresponds in nature to small birds, which do not glide like large birds, but instead flap with considerable change of wing shape during a single flapping cycle. With flapping and flexible wings, birds overcome the deteriorating aerodynamic performance under steady flow conditions by employing unsteady mechanisms. In this article, we review both biological and aeronautical literatures to present salient features relevant to MAVs. We first summarize scaling laws of biological and micro air vehicles involving wing span, wing loading, vehicle mass, cruising speed, flapping frequency, and power. Next we discuss kinematics of flapping wings and aerodynamic models for analyzing lift, drag and power. Then we present issues related to low Reynolds number flows and airfoil shape selection. Recent work on flexible structures capable of adjusting the airfoil shape in response to freestream variations is also discussed.

[131] Lan, C. E., "The Unsteady Quasi-Vortex-Lattice Method with Applications to Animal Propulsion," *Journal of Fluid Mechanics*, Vol. 93, Aug. 1979, pp. 747–765.

Keywords: 3-D, Analytical, Continuous Loading Approach

Abstract: In the early theoretical study of aquatic animal propulsion either the two-dimensional theory or the large aspect-ratio theory has been generally used. Only recently has the unsteady lifting-surface theory with the continuous loading approach been applied to the study of this problem by Chopra & Kambe (1977). Since it is well known that the continuous loading approach is difficult to extend to general configurations, a new quasi-continuous loading method, applicable to general configurations and yet accurate enough for practical applications, is developed in this paper. The method is an extension of the steady version of Lan (1974) and is particularly suitable for predicting the unsteady lead-edge suction during harmonic motion. The method is applied to the calculation of the propulsive efficiency and thrust for some swept and rectangular planforms by varying the phase angles between the pitching and heaving motions. It is found that with the pitching axis passing through the trailing edge of the root chord and the reduced frequency k equal to 0·75 the rectangular planform is quite sensitive in performance to the phase angles and may produce drag instead of thrust. These characteristics are not shared by the swept planforms simulating the lunate tails. In addition, when the pitching leads the heaving motion by 90°, the phase angle for nearly maximum efficiency, the planform inclination caused by pitching contributes to the propulsive thrust over a large portion of the swept planform, while, for the rectangular planform, only drag is produced from the planform normal force at k = 0·75. It is also found that the maximum thrust is not produced with maximum efficiency for all planforms considered. The theory is then applied to the study of dragonfly aerodynamics. It is shown that the aerodynamically interacting tandem wings of the dragonfly can produce high thrust with high efficiency if the pitching is in advance of the flapping and the hindwing leads the forewing with some optimum phase angle. The responsible mechanism allows the hindwing to extract wake energy from the forewing.

[132] Liu, T., "Time-Area-Averaged Momentum Stream Tube Model for Flapping Flight," *Journal of Aircraft*, Vol. 44, No. 2, 2007, pp. 459–466.

Keywords: 3-D, Analytical, Stream Tube Model, Lifting-line

Abstract: This paper formulates a time-area-averaged momentum stream tube model to provide the useful functional relations for the cruise velocity, power, and propulsive efficiency in forward flapping flight. This model is a direct generalization of the classical actuator disk theory by taking into account the effects of the unsteadiness and spatial nonuniformity of velocity in a momentum stream tube. It is found that the functional relation for the time-area-averaged power required in flapping flight is almost the same as that given by the classical lifting-line theory for a fixed wing. The flapping span efficiency is introduced, and its physical meaning and significant role in the power relation are interpreted. The flapping propulsive efficiency is related to the flapping span efficiency, normalized total fluctuating

kinetic energy, and wing aspect ratio. The use of this model to fit the collected data for birds allows estimating the flapping span efficiency, parasite, and induced drag coefficients and propulsive efficiency.

[133] Taylor, G. K., Nudds, R. L., and Thomas, A. L. R., "Flying and Swimming Animals Cruise at a Strouhal Number Tuned for High Power Efficiency," *Nature*, Vol. 425, Oct. 2003, pp. 707–711.

Keywords: 3-D, Analytical, Strouhal Number

Abstract: Dimensionless numbers are important in biomechanics because their constancy can imply dynamic similarity between systems, despite possible differences in medium or scale[1]. A dimensionless parameter that describes the tail or wing kinematics of swimming and flying animals is the Strouhal number[1], St = fA/U, which divides stroke frequency (f) and amplitude (A) by forward speed (U)[2, 3, 4, 5, 6, 7, 8]. St is known to govern a well-defined series of vortex growth and shedding regimes for airfoils undergoing pitching and heaving motions[6, 8]. Propulsive efficiency is high over a narrow range of St and usually peaks within the interval $0.2 < St < 0.4$ (refs 3–8). Because natural selection is likely to tune animals for high propulsive efficiency, we expect it to constrain the range of St that animals use. This seems to be true for dolphins[2, 3, 4, 5], sharks[3, 4, 5] and bony fish[3, 4, 5], which swim at $0.2 < St < 0.4$. Here we show that birds, bats and insects also converge on the same narrow range of St, but only when cruising. Tuning cruise kinematics to optimize St therefore seems to be a general principle of oscillatory lift-based propulsion.

[134] Phillips, W. F., "Analytical Decomposition of Wing Roll and Flapping Using Lifting-Line Theory," AIAA Paper 2013-2918, June 2013.

Keywords: 3-D, Analytical, Lifting-line

Abstract: A decomposed Fourier-series solution to Prandtl's classical lifting-line theory is used to examine the effects of rigid-body roll and small-angle wing flapping on the lift, induced-drag, and power coefficients developed by a finite wing. This solution shows that, if the flapping rate for any wing is large enough, the mean induced drag averaged over a complete flapping cycle will be negative, that is, the wing flapping produces net induced thrust. For quasi-steady flapping in pure plunging, the solution predicts that wing flapping has no net effect on the mean lift. A significant advantage of this analytical solution over commonly used numerical methods is the utility provided for optimizing wing-flapping cycles. The analytical solution involves five time-dependent functions that could all be optimized to maximize thrust, propulsive efficiency, and/or other performance measures. Results show that, by optimizing only one of these five functions, propulsive efficiencies exceeding 90% can be attained. For the case of an elliptic planform with linear twist, closed-form relations are presented for the decomposed Fourier coefficients and the flapping rate that produces mean induced thrust that balances the mean drag in the absence of wing flapping.

[135] Phillips, W. F., "Analytical Decomposition of Wing Roll and Flapping Using Lifting-Line Theory," *Journal of Aircraft*, Vol. 51, No. 3, 2014, pp. 761–778.

Keywords: 3-D, Analytical, Lifting-line

Abstract: A decomposed Fourier-series solution to Prandtl's classical lifting-line theory is used to examine the effects of rigid-body roll and small-angle wing flapping on the lift, induced-drag, and power coefficients developed by a finite wing. This solution shows that, if the flapping rate for any wing is large enough, the mean induced drag averaged over a complete flapping cycle will be negative, that is, the wing flapping produces net induced thrust. For quasi-steady flapping in pure plunging, the solution predicts that wing flapping has no net effect on the mean lift. A significant advantage of this analytical solution over commonly used numerical methods is the utility provided for optimizing wing-flapping cycles. The analytical solution involves five time-dependent functions that could all be optimized to maximize thrust, propulsive efficiency, and/or other performance measures. Results show that, by optimizing only one of these five functions, propulsive efficiencies exceeding 90% can be attained. For the case of an elliptic planform with linear twist, closed-form relations are presented for the decomposed Fourier coefficients and the flapping rate that produces mean induced thrust that balances the mean drag in the absence of wing flapping.

[136] Phillips, W. F., Miller, R. A., and Hunsaker, D. F., "Decomposed Lifting-Line Predictions and Optimization for Propulsive Efficiency of Flapping Wings," AIAA Paper 2013-2921, June 2013.

Keywords: 3-D, Analytical, Lifting-line

Abstract: A decomposed Four series solution to Prandtl's classical lifting-line theory is used to predict the lift, inducted-thrust, and power coefficients developed by a flapping wing. A significant advantage of this quasi-steady analytical solution over commonly used numerical methods is the utility provided for optimizing wing flapping cycles. The analytical solution involves five time-dependent functions that could all be optimized to maximize thrust, propulsive efficiency, and/or other performance measures. Results show that by optimizing only two of these five

functions, propulsive efficiencies exceeding 97% can be obtained. Results are presented for untwisted rectangular wings in pure plunging, rectangular wings with linear washout and the minimum-power washout magnitude, and rectangular wings with the minimum-power washout distribution and magnitude.

[137] Phillips, W. F., "Lifting-Line Analysis for Twisted Wings and Washout-Optimized Wings," *Journal of Aircraft*, Vol. 41, No. 1, 2004, pp. 128–136.
Keywords: 3-D, Analytical, Lifting-line
Abstract: A more practical form of the analytical solution for the effects of geometric and aerodynamic twist (washout) on the low-Mach-number performance of a finite wing of arbitrary planform is presented. This infinite series solution is based on Prandtl's classical lifting-line theory and the Fourier coefficients are presented in a form that only depends on wing geometry. The solution shows that geometric and aerodynamic washout do not affect the lift slope for a wing of any planform shape. This solution also shows that any wing with washout always produces induced drag at zero lift. Expect for the special case of an elliptic planform, washout can be used to reduce the induced drag for a wing producing finite lift. A relation describing the optimum spanwise distribution of washout for a wing of arbitrary planform is presented. If this optimum washout distribution is used, a wing of any planform shape can be designed for a given lift coefficient to produce induced drag at the same minimum level as an elliptic wing with the same aspect ratio and no washout.

[138] Phillips, W. F., "Incompressible Flow over Finite Wings," *Mechanics of Flight, 2nd ed.*, Wiley, Hoboken, NJ, 2010, pp. 46–94.
Keywords: 3-D, Analytical, Lifting-line

[139] Phillips, W. F., Alley, N. R., and Goodrich, W. D., "Lifting-Line Analysis of Roll Control and Variable Twist," *Journal of Aircraft*, Vol. 41, No. 5, 2004, pp. 1169–1176.
Keywords: 3-D, Analytical, Lifting-line
Abstract: A more practical form of an analytical solution that can be used to predict the roll response for a wing of arbitrary planform with arbitrary spanwise variation of control surface deflection and wing twist is presented. This infinite series solution is based on Prandtl's classical lifting-line theory, and the Fourier coefficients are presented in a form that depends only on wing geometry. The solution can be used to predict rolling and yawing moments as well as the lift and induced rag, which result from control surface deflection, rolling rate, and wing twist. The analytical solution can be applied to wings with conventional ailerons or to wings utilizing wing-warping control. The method is also applied to full-span twisting control surfaces, named "twisterons," which can be simultaneously used to provide roll control, high-lift, and minimum induced drag.

[141] Prandtl, L., "Tragflügel Theorie," *Nachricten von der Gesellschaft der Wissenschaften zu Göttingen*, Geschäeftliche Mitteilungen, Klasse, 1918, pp. 451–477.
Keywords: 3-D, Analytical, Lifting-line

[140] Prandtl, L., "Applications of Modern Hydrodynamics to Aeronautics," NACA TR-116, June 1921.
Keywords: 3-D, Analytical, Lifting-line

[142] Kutta, M. W., "Auftriebskräfte in Strömenden Flüssigkeiten," *Illustrierte Aeronautische Mitteilungen*, Vol. 6, No. 133, 1902, pp. 133–135.
Keywords: 2-D, Analytical

[143] Joukowski, N. E., "Sur les Tourbillons Adjionts," *Traraux de la Section Physique de la Societé Imperiale des Amis des Sciences Naturales*, Vol. 13, No. 2, 1906, pp. 261–284.
Keywords: 2-D, Analytical

[144] Phillips, W. F., Anderson, E. A., and Kelly, Q. J., "Predicting the Contribution of Running Propellers to Aircraft Stability Derivatives," *Journal of Aircraft*, Vol. 40, No. 6, 2003, pp. 1107–1114.
Keywords: 3-D, Analytical, Propeller
Abstract: Running propellers can have a profound effect on the trim and static stability of an airplane. The method most commonly used for determining propeller stability derivatives is based on blade element theory with the axial component of induced velocity taken to be that predicted from classical propeller momentum theory. The induced flow predicted from propeller momentum theory is not consistent with the actual induced flow in the vicinity of a rotating propeller. In the present paper an alternative method for predicting propeller stability derivatives is proposed.

This method is based on blade element theory with the induced velocity predicted from propeller vortex theory. Results are compared with other analytical predictions and experimental data for specific propeller blade geometry.

[145] Lighthill, M. J., "Aerodynamic Aspects of Animal Flight," *Bulletin of the Institute of Mathematics and its Applications*, Vol. 10, No. 3 1974, pp. 369–393.

Keywords: 3-D, Experimental, Animals

Abstract: A lecture or a course of lectures on 'Aircraft' would put approximately equal emphasis on aerodynamic, structural and power-plant aspects; whereas lectures on 'Aerodynamics of Aircraft' would concentrate principally on aerodynamic matters while referring to just the basic elements of what limitations are imposed by structural and power-plant considerations. Similarly this lecture on the 'Aerodynamic Aspects of Animal Flight' will concentrate on the aerodynamic forces, and the resulting dynamic interactions, between the movements of a flying animal relative to the air and the associated air movements; and include only brief references to fundamental limitations imposed by the strength and stiffness of the skeleton of the animal and other structural considerations, or by the power-plant capabilities of the animal's musculature and metabolism. Equally it will give only a highly condensed account (see section on Evolution) of the biologically fundamental questions of how systems for animal flight evolved in response to environmental demands and opportunities.

[146] Pennycuick, C. J., "Power Requirements for Horizontal Flight in the Pigeon, Columba Livia," *Journal of Experimental Biology*, Vol. 49, Dec. 1968, pp. 527–555.

Keywords: 3-D, Experimental, Animals

Abstract: 1. Certain measurements made on pigeons flying horizontally in a wind-tunnel are described. 2. A method, based on helicopter theory, for calculating the power required to fly at any given speed is explained. Induced, profile and parasite power are calculated separately. 3. It is concluded that the pigeon can fly horizontally without incurring an oxygen debt at speeds from 3 to 16 m./sec. The minimum power speed is 8-9 m./sec. The maximum continuous power output is estimated to be 10.5 W., and the corresponding oxygen consumption about 170 ml./min. The maximum (sprint) power is estimated to be 20.4 W., from observations of vertical climb after take-off. 4. The estimated best lift: drag ratio in horizontal flight is 5.9, giving a range of 11.8 km./g. of fat oxidized for a 400 g. pigeon. 5. It is argued from considerations of structural strength that the early part of the downstroke is used mainly to impart angular velocity to the wing, and that air loads are only developed after most of the angular acceleration has taken place. The tension in the pectoralis insertion may exceed 60% of the breaking tension in fast horizontal flight. 6. The power calculation was repeated for the ruby-throated hummingbird, using published data. Estimated best range is about 900 km./g. of fat oxidized, achieved at 9 m./sec. The corresponding effective lift/drag ratio is 4.1. 7. The variation of power required and power available with size is considered, and the effect on hovering and take-off performance of different birds deduced. 8. Performance estimates for the pigeon and ruby-throated hummingbird are very poor by engineering standards, but consistent with these birds' known abilities, and are in general agreement with estimates of effective lift/drag ratio derived from published data on other species.

[147] Saharon, D., and Luttges, M., "Three-Dimensional Flow Produced by a Pitching-Plunging Model Dragonfly Wing," AIAA Paper 1987-0121, Jan. 1987.

Keywords: 3-D, Experimental, Dragonfly

[148] Childress, S., and Dudley, R., "Transition from Ciliary to Flapping Mode in a Swimming Mollusc: Flapping Flight as a Bifurcation in Re_ω," *Journal of Fluid Mechanics*, Vol. 498, Jan. 2004, pp. 257–288.

Keywords: 3-D, Experimental, Fish

Abstract: From observations of swimming of the shell-less pteropod mollusc *Clione antarctica* we compare swimming velocities achieved by the organism using ciliated surfaces alone with velocities achieved by the same organism using a pair of flapping wings. Flapping dominates locomotion above a swimming Reynolds number *Re* in the range 5–20. We test the hypothesis that $Re \approx 5\text{–}20$ marks the onset of 'flapping flight' in these organisms. We consider the proposition that forward, reciprocal flapping flight is impossible for locomoting organisms whose motion is fully determined by a body length L and a frequency ω below some finite critical value of the Reynolds number $Re\omega=\omega L2/\nu$. For a self-similar family of body shapes, the critical Reynolds number should depend only upon the geometry of the body and the cyclic movement used to locomote. We give evidence of such a critical Reynolds number in our data, and study the bifurcation in several simplified theoretical models. We argue further that this bifurcation marks the departure of natural locomotion from the low Reynolds number or Stokesian realm and its entry into the high Reynolds number or Eulerian realm. This occurs because the equilibrium swimming or flying

speed *Uf* obtained at the instability is determined by the mechanics of a viscous fluid at a value of *Ref=UfL/v* that is not small.

[149] Whitney, J. P., and Wood, R. J., "Aeromechanics of Passive Rotation in Flapping Flight," *Journal of Fluid Mechanics*, Vol. 660, Oct. 2010, pp. 197–220.

Keywords: 3-D, Experimental, Insect

Abstract: Flying insects and robots that mimic them flap and rotate (or 'pitch') their wings with large angular amplitudes. The reciprocating nature of flapping requires rotation of the wing at the end of each stroke. Insects or flapping-wing robots could achieve this by directly exerting moments about the axis of rotation using auxiliary muscles or actuators. However, completely passive rotational dynamics might be preferred for efficiency purposes, or, in the case of a robot, decreased mechanical complexity and reduced system mass. Herein, the detailed equations of motion are derived for wing rotational dynamics, and a blade-element model is used to supply aerodynamic force and moment estimates. Passive-rotation flapping experiments with insect-scale mechanically driven artificial wings are conducted to simultaneously measure aerodynamic forces and three-degree-of-freedom kinematics (flapping, rotation and out-of-plane deviation), allowing a detailed evaluation of the blade-element model and the derived equations of motion. Variations in flapping kinematics, wing-beat frequency, stroke amplitude and torsional compliance are made to test the generality of the model. All experiments showed strong agreement with predicted forces and kinematics, without variation or fitting of model parameters.

[150] Cloupeau, M., Devillers, J. and & Devezeaux, D., "Direct Measurements of Instantaneous Lift in Desert Locust; Comparison with Jensen's Experiments on Detached Wings," *Journal of Experimental Biology*, Vol. 80, June 1979, pp. 1–15.

Keywords: 3-D, Experimental, Insect

Abstract: Instantaneous values of lift in the locust Schistocerca gregaria, flying in a wind tunnel, were measured by means of a piezo-electric probe. The airflow velocity was adjusted to be equal to that which would have been experienced by the freely flying insect. In order to obtain the true aerodynamic forces, the inertial forces must be subtracted from the gross forces measured. These inertial forces were calculated from the movement of the centre of gravity and from the mass of the different wing sections. The lift curves obtained have a shape similar to the curves deduced by Jensen from measurements on isolated wings in steady flows, but an approximately doubled amplitude. These amplitude differences appear to be caused by the existence of significant unsteady effects.

[151] Sane, S. P., and Dickinson, M. H., "The Aerodynamic Effects of Wing Rotation and a Revised Quasi-Steady Model of Flapping Flight," *Journal of Experimental Biology*, Vol. 205, Jan. 2002, pp. 1087–1096.

Keywords: 3-D, Experimental, Insect

Abstract: We used a dynamically scaled model insect to measure the rotational forces produced by a flapping insect wing. A steadily translating wing was rotated at a range of constant angular velocities, and the resulting aerodynamic forces were measured using a sensor attached to the base of the wing. These instantaneous forces were compared with quasi-steady estimates based on translational force coefficients. Because translational and rotational velocities were constant, the wing inertia was negligible, and any difference between measured forces and estimates based on translational force coefficients could be attributed to the aerodynamic effects of wing rotation. By factoring out the geometry and kinematics of the wings from the rotational forces, we determined rotational force coefficients for a range of angular velocities and different axes of rotation. The measured coefficients were compared with a mathematical model developed for two-dimensional motions in inviscid fluids, which we adapted to the three-dimensional case using blade element theory. As predicted by theory, the rotational coefficient varied linearly with the position of the rotational axis for all angular velocities measured. The coefficient also, however, varied with angular velocity, in contrast to theoretical predictions. Using the measured rotational coefficients, we modified a standard quasi-steady model of insect flight to include rotational forces, translational forces and the added mass inertia. The revised model predicts the time course of force generation for several different patterns of flapping kinematics more accurately than a model based solely on translational force coefficients. By subtracting the improved quasi-steady estimates from the measured forces, we isolated the aerodynamic forces due to wake capture.

[152] Warkentin, J., and DeLaurier, J., "Experimental Aerodynamic Study of Tandem Flapping Membrane Wings," *Journal of Aircraft*, Vol. 44, No. 5, 2007, pp. 1653–1661.

Keywords: 3-D, Experimental, Biplane

Abstract: A systematic series of wind-tunnel tests was conducted on an ornithopter configuration consisting of two sets of symmetrically flapping wings, located one behind the other in tandem. It was discovered that the tandem

arrangement can give thrust and efficiency increases over a single set of flapping wings for certain relative phase angles and longitudinal spacing between the wing sets. In particular, close spacing on the order of 1 chord length is generally best, and phase angles of approximately 0 +- 50 deg give the highest thrusts and propulsive efficiencies. Asymmetrical flapping was also studied, which consists of the two sets of wings rocking relative to one another 180 deg out of phase. It was found that the performance of such an arrangement is poor, relative to the best performing symmetrical tandem flapping.

[153] Saharon, D., and Luttges, M., "Visualization of Unsteady Separated Flow Produced by Mechanically Driven Dragonfly Wing Kinematics Model," AIAA Paper 1988-0569, Jan. 1988.

Keywords: 3-D, Experimental, Tandem-Wing

Abstract: Visualizations of three-dimensional unsteady separated flow produced by mechanically modeled dragonfly wing kinematics were obtained using wing motions that closely resemble those of live dragonflies. Tandem wing effects were gauged by individual effects of fore and aft wings tested alone. The effects of altered wing motions were studied by small changes in wing beat frequency. Full tandem wing models were used for these tests. Vortex structures produce by the mechanical model wings were quite similar to those elicited by the tethered dragonflies in the wing tunnel tests. The characteristic eight major vortex structure produced by the tandem wings during each wing beat cycle could be traced to similar structure produced about each wing tested individually. Wing-vortex interactions were evaluated in terms of initiation, development, and utilization. Changing parameter combinations altered the observed interactions between flow and wings largely due to differences in flow structure interference. Much of the interference was detrimental to maximized flow – wing interactions. And, constructive interference was limited to a narrow range of parameter combinations where the resulting flow fields were typically characterized by downwash pattern of streaklines. The delineated multi-oscillating wing beat cycle may be a comprehensive model of lift enhancement mechanisms used by many insect. The mechanism would enable many insects to use unsteady separated flows.

[154] Saharon, D., and Luttges, M., "Dragonfly Unsteady Aerodynamic: The Role of the Wing Phase Relations in Controlling the Produced Flows," AIAA Paper 1989-0832, Jan. 1989.

Keywords: 3-D, Experimental, Tandem-Wing

Abstract: Visualizations of three-dimensional unsteady separated flow produced by a mechanically driven dragonfly wing kinematics model were collected and analyzed. Tandem wing effects were evaluated by comparison with effects produced by fore and aft wings tested individually. The effects of wing kinematics were studied with an emphasis on changes in the phase relations between fore and aft wings. Vortex structures produced by the mechanical model were quite similar to those elicited from tethered dragonflies in wind tunnel tests. The eight kinematic elements of the model wing beat were short lived such that each yielded a specific transitional flow structure. Fore and aft wing phase differences produced flow structures that interacted, one with another, in differing wings. Flow interactions were either constructive or destructive and yielded different wing-flow interaction. Constructive flow interactions were evaluated in terms of integrating and fusing of vortex structures. Destructive flow interactions were evaluated in terms of vortex disruption, splitting, and deflecting. The net results of these interactions were to enhance lift and thrust as seen in downwash and downstream flow structures.

[155] Ozen, C. A., and Rockwell, D., "Control of Vortical Structures on a Flapping Wing Via a Sinusoidal Leading-Edge," *Physics of Fluids*, Vol. 22, No. 2, 2010, pp. 021701-1–021701-3.

Keywords: 3-D, Experimental, Flat Plate

Abstract: The flow structure generated by a flapping wing in the form of a plate is fundamentally altered if the leading-edge has a sinusoidal shape. It is possible to attenuate both the positive and negative spanwise flows along the plate surface, as well as the onset and development of large-scale concentrations of positive and negative streamwise vorticities at inboard locations. These alterations of the inboard flow structure have an insignificant influence on the structure of the tip vortex.

[156] Hong, Y., and Altman, A., "Lift from Spanwise Flow in Simple Flapping Wings," *Journal of Aircraft*, Vol. 45, No. 3, 2008, pp. 1206–1216.

Keywords: 3-D, Experimental, Flat Plate

Abstract: Spanwise flow contributes to lift in thin flat-plate zero-pitch-angle flapping wings in quiescent air. It is reasonable to maintain only the kinematics and mechanical complexity absolutely necessary in developing flapping-wing micro air vehicles. This study continues the quantification of the lift generated from a flapping motion of absolute minimum complexity thought to be capable of generating lift. A flapping-wing micro air vehicle with rectangular planform wings fabricated in-house (semispan aspect ratios from 1.5 to 4.0) was used to quantify the contributions to lift from flow along the span of wings at numerous points throughout the flapping cycle under a variety of operating conditions (3-6 Hz and Reynolds number of 6,000 - 15,000). These experiments were performed for

several aspect ratios for flat-plate and spanwise-cambered wings. The lift force was quantified experimentally using a force transducer and a high-speed camera. Digital particle image velocimetry was used to determine the lift contributions of spanwise flow to the total measured lift. Additionally, the presence of spanwise camber was shown to affect the transient lift behavior.

[157] Peng, D., and Milano, M., "Lift Generation with Optimal Elastic Pitching for a Flapping Plate," *Journal of Fluid Mechanics*, Vol. 717, Feb. 2013, pp. R1-1–R1-13.

Keywords: 3-D, Experimental, Flat Plate

Abstract: The lift-generating capabilities of a translating and passively pitching rectangular plate are assessed experimentally. The plate pitch dynamics are generated by a rotational spring, and a genetic algorithm isolates a set of spring parameters maximizing the average lift. Our experiments identified a range of parameters that produce kinematic trajectories associated with optimal lift production. The stroke length and the dynamic response of the spring at the driving frequency are revealed to play crucial roles in the generation of such trajectories. Measurements taken with digital particle image velocimetry are used to analyze the results.

[158] Schmidt, W., "Der Wellpropeller, ein Neuer Antrieb fuer Wasser-Land-, und Luftfahrzeuge," *Zeitschrift fur Flugwissenschaften*, Vol. 13, Oct. 1965, pp. 427–479.

Keywords: 3-D, Experimental, Propeller

[159] Heathcote, S., Wang, Z., and Gursul, I., "Effect of Spanwise Flexibility on Flapping Wing Propulsion," *Journal of Fluids and Structures,* Vol. 24, No. 2, 2008, pp. 182–199.

Keywords: 3-D, Experimental, Flexibility

Abstract: A water tunnel study of the effect of spanwise flexibility on the thrust, lift and propulsive efficiency of a rectangular wing oscillating in pure heave has been performed. The thrust and lift forces were measured with a force balance, and the flow field was measured with a Particle Image Velocimetry system. Introducing a degree of spanwise flexibility was found to be beneficial. For Strouhal numbers greater than 0.2, a degree of spanwise flexibility was found to yield a small increase in thrust coefficient, and a small decrease in power-input requirement, resulting in higher efficiency. In this case, a moderately stronger trailing-edge vortex system was observed. Introducing a far greater degree of spanwise flexibility, however, was found to be detrimental. A large phase delay of the wing tip displacement was observed, leading to the root and tip moving in opposite directions for a significant portion of the flapping stroke. Vorticity of opposing sign was observed to be shed from the root and tip, resulting in a weak and fragmented vorticity pattern. The thrust coefficient was observed to be significantly reduced, and the efficiency diminished. It is noted that the range of Strouhal numbers for which spanwise flexibility was found to offer benefits overlaps the range found in nature, of $0.2<Sr<0.4$. From a design aspect, flexibility may benefit flapping-wing Micro Air Vehicles both aerodynamically and in the inherent lightness of flexible structures.

[160] Ellington, C. P., and Usherwood, J. R., "Lift and Drag Characteristics of Rotary and Flapping Wings," *Fixed and Flapping Wing Aerodynamics for Micro Air Vehicles*, AIAA, Danvers, MA, 2001, pp. 231–248.

Keywords: 3-D, Experimental, Hover

[161] Heathcote, S., Martin, D., and Gursul, I., "Flexible Flapping Airfoil Propulsion at Zero Freestream Velocity," *AIAA Journal*, Vol. 42, No. 11, 2004, pp. 2196–2204.

Keywords: 3-D, Experimental, Hover

Abstract: Thrust generation for an airfoil plunging at zero freestream velocity, the case relevant to hovering birds and insects, has been studied. The objective was to investigate the effect of airfoil stiffness. Particle image velocimetry and force measurements were taken for three airfoils of relative bending stiffness 1:8:512 in a water tank. The deformation of the flexible airfoils produces an angle of attack that varies periodically with a phase angle with respect to the plunging motion. Amplitude and phase of this combined plunging/pitching motion play a major role in the flowfield and thrust generation. Vortex pairs or alternating vortex streets were observed depending on the amplitude and phase lag of the trailing edge. The strength of the vortices, their lateral spacing, and the time-averaged velocity of the induced jet were found to depend on the airfoil flexibility, plunge frequency, and amplitude. Direct force measurements confirmed that at high plunge frequencies the thrust coefficient of the airfoil with intermediate stiffness was greatest, although the least stiff airfoil can generate larger thrust at low frequencies. It is suggested that there is an optimum airfoil stiffness for a given plunge frequency and amplitude. The thrust/input-power ratio was found to be greater for the flexible airfoils than for the rigid airfoil.

[162] Norberg, R. A., "Hovering Flight of the Dragonfly Aeschna Juncea: Kinematics and Aerodynamics," *Swimming and Flying in Nature*, Plenum Press, New York, 1975, pp. 763–781.

Keywords: 3-D, Experimental, Hover

Abstract: The kinematics of free unimpeded hovering flight of Aeschna juncea L. was analyzed from films taken in the field with 80 frames sec^{-1}, and from still pictures taken with a motorized camera. The body is held almost horizontal, and the wing stroke plane is tilted 60° relative to the horizontal. In these respects the dragonfly differs strongly from most other hovering animals. The wing beats essentially in the same plane on the downstroke and upstroke. All wings are strongly supinated (pitched-up) during the upstroke. The stroke angle is ca. 60° and the wing beat frequency ca. 36 Hz. Average, minimum force coefficients were calculated with use of steady-state aerodynamic theory. Calculations were made under several alternative assumptions and gave lift coefficients of 3.5 to 6.1, which are all far too large to be explainable with steady-state aerodynamics. At least 60% of the force generated in hovering flight are due to non-steady-state aerodynamics. The pitching rotations of the wings at top and bottom of the stroke are believed to contribute much force, although the exact mechanism is not clear. At the leading edge of the wing of dragonflies there is a unique morphological arrangement, the node. It permits elastic tension of the leading edge and seems to be an adaptation permitting strong wing twistings. The node may also function as a shock absorber.

[163] Sunada, S., Hatayama, Y., and Tokutake, H., "Pitch, Roll, and Yaw Damping of a Flapping Wing," *AIAA Journal*, Vol. 48, No. 6, 2010, pp. 1261–1265.

Keywords: 3-D, Experimental, Hover

[164] Tarascio, M. J., Ramasamy, M., Chopra, I., and Leishman, J. G., "Flow Visualization of Micro Air Vehicle Scaled Insect-Based Flapping Wings," *Journal of Aircraft*, Vol. 42, No. 2, 2005, pp. 385–390.

Keywords: 3-D, Experimental, Hover

Abstract: A flow-visualization experiment was conducted on an insect-based flapping-wing mechanism. This enabled greater understanding and insight to be gained on the unsteady aerodynamic phenomena that are responsible for the enhanced lift of wing operating at low Reynolds numbers in hovering flapping flight. Flow-visualization images were acquired with a strobbed laser sheet to illuminate the flow, which was seeded with a mineral oil fog. The general flowfield structure was found to consist of a folded wake, with a relatively large starting vortex and the end of each half-stroke. A large flow recirculation region was generated in the plane of flapping, which was centered around the two extreme flapping displacements. These general flowfield features were enhanced by detailed observations of the local flowfield around the wing section. One observation was the presence of multiple vortices on the top surface of the wing as it underwent translation. Furthermore, the local flowfield images clearly showed the growth of the leading-edge vortex as a function of span and identified the presence of separated flow on the outboard regions of the wing. These experimental results were supported by a free vortex modeling of the wake developments. The model was found to predict similar wake flowfield dynamics to that found in the experiments. This research has contributed to a better understanding of the unsteady aerodynamic mechanisms that are responsible for the enhanced lift of insect-based flapping wings in hover.

[165] Goldschmidt, V. W., and Bradshaw, P., "Flapping of a Plane Jet," *Physics of Fluids*, Vol. 16, No. 3, 1973, pp. 397.

Keywords: 3-D, Experimental, Wake

Abstract: Correlations of the instantaneous velocity fluctuations on opposite sides of a subsonic plane jet have been measured. These indicate that there is a measurable flapping of the jet. The frequency of the flapping is estimated by taking the correlation with one signal delayed in time.

[166] Shinde, S. Y., and Arakeri, J. H., "Flexibility in Flapping Foil Suppresses Meandering of Induced Jet in Absence of Free Stream," *Journal of Fluid Mechanics*, Vol. 757, Oct. 2014, pp. 231–250.

Keywords: 3-D, Experimental, Wake

Abstract: Thrust-generating flapping foils are known to produce jets inclined to the free stream at high Strouhal numbers $St=fA/U\infty$, where f is the frequency and A is the amplitude of flapping and $U\infty$ is the free-stream velocity. Our experiments, in the limiting case of $St\rightarrow\infty$ (zero free-stream speed), show that a purely oscillatory pitching motion of a chordwise flexible foil produces a coherent jet composed of a reverse Bénard–Kármán vortex street along the centerline, albeit over a specific range of effective flap stiffnesses. We obtain flexibility by attaching a thin flap to the trailing edge of a rigid NACA0015 foil; length of flap is $0.79c$ where c is rigid foil chord length. It is the time-varying deflections of the flexible flap that suppress the meandering found in the jets produced by a pitching rigid

foil for zero free-stream condition. Recent experiments (Marais *et al.*, *J. Fluid Mech.*, vol. 710, 2012, p. 659) have also shown that the flexibility increases the *St* at which non-deflected jets are obtained. Analyzing the near-wake vortex dynamics from flow visualization and particle image velocimetry (PIV) measurements, we identify the mechanisms by which flexibility suppresses jet deflection and meandering. A convenient characterization of flap deformation, caused by fluid–flap interaction, is through a non-dimensional 'effective stiffness', $EI*=8EI/(\rho V2TEmaxsfc3f/2)$, representing the inverse of the flap deflection due to the fluid-dynamic loading; here, *EI* is the bending stiffness of flap, ρ is fluid density, *VTEmax* is the maximum velocity of rigid foil trailing edge, *sf* is span and *cf* is chord length of the flexible flap. By varying the amplitude and frequency of pitching, we obtain a variation in $EI*$ over nearly two orders of magnitude and show that only moderate $EI*$ ($0.1\lesssim EI*\lesssim 1$) generates a sustained, coherent, orderly jet. Relatively 'stiff' flaps ($EI*\gtrsim 1$), including the extreme case of no flap, produce meandering jets, whereas highly 'flexible' flaps ($EI*\lesssim 0.1$) produce spread-out jets. Obtained from the measured mean velocity fields, we present values of thrust coefficients for the cases for which orderly jets are observed.

[167] Hu, H., Clemons, L. and Igarashi, H., "An Experimental Study of the Unsteady Vortex Structures in the Wake of a Root-Fixed Flapping wing," *Experiments in Fluids*, Vol. 51, No. 2, 2011, pp. 347–359.

Keywords: 3-D, Experimental, Wake

Abstract: An experimental study was conducted to characterize the evolution of the unsteady vortex structures in the wake of a root-fixed flapping wing with the wing size, stroke amplitude, and flapping frequency within the range of insect characteristics for the development of novel insect-sized nano-air-vehicles (NAVs). The experiments were conducted in a low-speed wing tunnel with a miniaturized piezoelectric wing (i.e., chord length, $C = 12.7$ mm) flapping at a frequency of 60 Hz (i.e., $f = 60$ Hz). The non-dimensional parameters of the flapping wing are chord Reynolds number of $Re = 1{,}200$, reduced frequency of $k = 3.5$, and non-dimensional flapping amplitude at wingtip $h = A/C = 1.35$. The corresponding Strouhal number (Str) is 0.33, which is well within the optimal range of $0.2 < \text{Str} < 0.4$ used by flying insects and birds and swimming fishes for locomotion. A digital particle image velocimetry (PIV) system was used to achieve phased-locked and time-averaged flow field measurements to quantify the transient behavior of the wake vortices in relation to the positions of the flapping wing during the upstroke and down stroke flapping cycles. The characteristics of the wake vortex structures in the chordwise cross planes at different wingspan locations were compared quantitatively to elucidate underlying physics for a better understanding of the unsteady aerodynamics of flapping flight and to explore/optimize design paradigms for the development of novel insect-sized, flapping-wing-based NAVs.

[168] Kokshaysky, N. V., "Tracing the Wake of a Flying Bird," *Nature*, Vol. 279, May 1979, pp. 146–148.

Keywords: 3-D, Experimental, Wake

Abstract: Study of the classical problem concerning "the way of an eagle in the air", when applied to flapping bird flight, offers many difficulties. All dynamic interactions between an object and a fluid medium in which it moves are ciphered in the structure of its wake, but the wake behind a flying bird is difficult to work with because it is an invisible and very short-lived formation; moreover, its structure must be complicated as the bird's wings are working in a constantly changing manner. I report here the results of wake visualization experiments carried out during short flights of a chaffinch (*Fringilla coelebs*) and a brambling (*F. montifringilla*) in enclosures. The general configuration of a wake is given, but no measurements have been made: in general, to extract some quantitative information from the wake structure, a more precisely documented picture of the dynamics of its formation is needed.

[169] Ren, W., Hu, H., Liu, H., and Wu, J. C., "An Experimental Investigation on the Asymmetric Wake Formation of an Oscillating Airfoil," AIAA Paper 2013-0794, Jan. 2013.

Keywords: 3-D, Experimental, Wake

Abstract: Bio-inspired aerodynamic designs have been mutually promoted by the studies on flapping wings in the past decades. Among the tons of researches topics, the wake formation/structure of an oscillating airfoil is more attractive, and it results in the development of both numerical methods and flow diagnostics techniques. In this paper, wake formation behind a sinusoidally pitching NACA 0012 has been studied with PIV measurements. The evolution of wake structures with increasing Strouhal number was reproduced successfully. With further experiments, the effect of Strouhal number, the amplitude and mean value of AOA on the asymmetric wake formation were also investigated. Results showed that the distance between vortex street became larger with increasing amplitude, while mean strength of vortices declined. Besides, the asymmetric wake formation was strongly dependent on the mean. Specifically, based on our experiments, the direction of wake asymmetry was changed at alpha_bar=5 deg and St=0.37.

[170] Spedding, G. R., "The Wake of a Kestrel (Falco Tinnunculus) in Flapping Flight," *Journal of Experimental Biology*, Vol. 127, Jan. 1987, pp. 59–78.

Keywords: 3-D, Experimental, Wake

Abstract: The structure of the wake behind a kestrel in medium-speed flight down a 36 m length of corridor was analyzed qualitatively and quantitatively by stereophotogrammetry of multiple flash photographs of the motion of small soap-covered helium bubbles. The wake consists of a pair of continuous, undulating trailing vortices. The upstroke is therefore aerodynamically active and the circulation appears to remain constant along the wing whose geometry is altered during the course of the wingstroke. It is argued that the flight kinematics, and so the wake structure, of the kestrel may be typical of flapping flight at medium speeds and a flight model based on this wake geometry is presented. Rough estimates of the rate of momentum generated in the wake balance the weight almost exactly and a direct estimate of the induced power requirement from the wake measurements is obtained. The significance of these results for the various alternative aerodynamic descriptions and energetic predictions of models of flapping animal flight is briefly assessed.

[171] von Ellenrieder, K. D., Parker, K, and Soria, J., "Flow Structures Behind a Heaving and Pitching Finite-Span Wing," *Journal of Fluid Mechanics*, Vol. 490, Sep. 2003, pp. 129–138.

Keywords: 3-D, Experimental, Wake

Abstract: The three-dimensional structure of the flow behind a heaving and pitching finite-span wing is investigated using dye flow visualization at a Reynolds number of 164. Phase-locked image sequences, which are obtained from two orthogonal views, are combined to create a set of composite images that give an overall sense of the three-dimensional structure of the flow. A model of the vortex system behind the wing is constructed from the image sequences. Variations of the Strouhal number, pitch amplitude and heave/pitch phase angle are qualitatively shown to affect the structure of the wake.

[172] Bandyopadhyay, P. R., and Leinhos, H. A., "Propulsion Efficiency of Bodies Appended with Multiple Flapping Fins: When More Is Less," *Physics of Fluids*, Vol. 25, No. 4, 2013, pp. 041902-1–041902-23.

Keywords: 3-D, Experimental, Vortices

Abstract: Underwater animals propel themselves by flapping their pectoral and caudal fins in a narrow range of frequencies, given by Strouhal number *St*, to produce transitional vortex jets (*St* is generally expressed non-dimensionally as the product of flapping frequency and stroke (arc) length divided by forward speed). The organized nature of the selection of *St* and of the vortex jet is thought to maximize hydrodynamic efficiency, although the exact mechanism is not known. Our recent Stuart-Landau equation models, which have self-regulation properties, indicate that the fin and its jet vortices couple. Temporal maps of forces in single isolated fins show a bimodal behavior in certain ranges of the transitional Reynolds number; this behavior bears resemblance to neural bifurcation properties that owe their origin to the self-regulation mechanism. In view of our theoretical and biorobotic evidence of self-regulation in single flapping fins, we explore if this property is altered in a fin-appended body, the goal being to understand how the narrow selection of *St*, self-regulation, and maximization of hydrodynamic efficiency are related. Swimming vehicles of 1-m scale have been built where a rigid cylindrical body is appended with six flapping fins, three at each end. The fins are rigid, have a rounded leading edge and a laminar section (NACA 0012), and are hinged at one end. The planform is an abstracted version of the penguin wing; it has low aspect ratio and a chord Reynolds number that varies in the transitional range from 10 000 to 60 000. The fin geometry, Reynolds number range, and the nonflexible nature of the main body are in common with those in penguins, and the length and displacement volume are similar to those of sharks. The maximum hydrodynamic efficiency of the fin-appended body (0.40) is lower than that of the single fin (0.57), but is close to that of a fish using several fins. The propulsion density (kW/m^3 of displacement volume) of the fin-appended cylinder is similar to that of a cruising shark. If we allow comparison of electrical versus thermal measurements, the total efficiency of the fin-appended body is similar to that of the damselfly and dragonfly, which are also based on vortex propulsion. The fin force fluctuations are modeled by a van der Pol oscillator. Measured phase maps of force fluctuation versus its time derivative correlate with the Strouhal numbers. Until stabilization, the maximum hydrodynamic efficiency of the fin-appended body increases with fin Reynolds number in a staircase pattern whose boundaries correlate with similar transitional sub-regimes in single fins, including the bimodal sub-regimes, thereby relating efficiency with the self-regulating jet vortex oscillators. At low Reynolds numbers, the peak of hydrodynamic efficiency remains flat over a wide range of *St*, becoming steeper at higher Reynolds numbers with the maximum occurring at lower values of *St*. The modeling shows that for self-regulation, future biorobotic design should focus on the reduction of structural damping and on a fin-body assembly that has reciprocal energetic interaction with the shed vortex.

[173] Wood, C. J., and Kirmani, S. F. A., "Visualization of Heaving Aerofoil Wakes Including the Effect of a Jet Flap," *Journal of Fluid Mechanics*, Vol. 41, Apr. 1970, pp. 627–640.

Keywords: 3-D, Experimental, Vortices

Abstract: Theoretical solutions exist for the flow about aerofoils in various modes of unsteady motion. This is also true for aerofoils whose lift is augmented by a jet flap. A common feature of these theories is the assumption of small amplitude displacements from the mean path and the generation of a continuous vortex sheet wake. However, in practice when the motion is oscillatory and of finite amplitude, an alternating trail of individual vortices is often found. The present visual investigation includes the measurement of some vortex street parameters associated with heaving aerofoils. The results are compared with those of conventional thin aerofoil theory in order to assess the significance of this departure from the conventional small displacement flow model.

[174] Birch, J. M., Dickson, W. B., and Dickinson, M. H., "Force Production and Flow Structure of the Leading Edge Vortex on Flapping Wings at High and Low Reynolds Numbers," *Journal of Experimental Biology*, Vol. 207, Mar. 2004, pp. 1063–1072.

Keywords: 3-D, Experimental, Vortices

Abstract: The elevated aerodynamic performance of insects has been attributed in part to the generation and maintenance of a stable region of vorticity known as the leading edge vortex (LEV). One explanation for the stability of the LEV is that spiraling axial flow within the vortex core drains energy into the tip vortex, forming a leading-edge spiral vortex analogous to the flow structure generated by delta wing aircraft. However, whereas spiral flow is a conspicuous feature of flapping wings at Reynolds numbers (Re) of 5000, similar experiments at Re=100 failed to identify a comparable structure. We used a dynamically scaled robot to investigate both the forces and the flows created by a wing undergoing identical motion at Re of~ 120 and ~1400. In both cases, motion at constant angular velocity and fixed angle of attack generated a stable LEV with no evidence of shedding. At Re=1400, flow visualization indicated an intense narrow region of spanwise flow within the core of the LEV, a feature conspicuously absent at Re=120. The results suggest that the transport of vorticity from the leading edge to the wake that permits prolonged vortex attachment takes different forms at different Re.

[175] Hong, Y., and Altman, A., "Streamwise Vorticity in Simple Mechanical Flapping Wings," *Journal of Aircraft*, Vol. 44, No. 5, 2007, pp. 1588–1597.

Keywords: 3-D, Experimental, Vortices

Abstract: The presence of streamwise vorticity in the vicinity of the wing tip contributes to lift in thin flat plate zero pitch angle flapping wings in quiescent air. In creating flapping wing micro air vehicles it is desirable to maintain only the mechanical and kinematic complexity absolutely necessary to artificially duplicate flapping wing flight. This study quantifies the lift generated from a flapping motion of absolute minimum complexity thought to be capable of generating lift. Using a flapping wing micro air vehicle with wings fabricated in-house, streamwise vortices were identified along the span of wings of various aspect ratios and at numerous different points throughout the flapping cycle under a variety of operating conditions. The lift generated by the flapping mechanism was quantified experimentally using a force transducer and a high speed camera. Digital particle image velocimetry was used to determine the contributions of streamwise vorticity to the total measured lift. Further evidence was found of the importance of the relationship between wing span and flapping frequency in the nature of the formation and shedding of vortices.

[176] Parker, K., Soria, J., and von Ellenrieder, K., "Thrust Measurements from a Finite-Span Flapping Wing," *AIAA Journal*, Vol. 45, No. 1, 2007, pp. 58–70.

Keywords: 3-D, Experimental, Vortices

Abstract: The thrust per unit length behind a flapping NACA 0030 airfoil with an aspect ratio of three is measured and presented. Aspects of the evolution of vorticity behind the thrust-producing wing are discussed based on quantitative experiments. Multiple planes of stereoscopic particle image velocimetry measurements are conducted at several locations along the span of the wing at a Strouhal number of 0.35. Of particular interest is the effect of wingtip vortices on the structure of the flow behind the oscillating wing. Wing kinematics is responsible for the flow structure in the 2-D airfoil case. Here, the spanwise distribution of vorticity is found to be dominated, in the large scale, by a single pair of intense counter-rotating vortices. Each member of the large-scale vortex pair is constituted by two smaller corotating vortices that constructively merge in the initial stages of flow separation. Toward the wingtips, three-dimensional effects are more significant. The spatiotemporal variations of transverse and spanwise vorticity in these regions suggest sever local flow deformation. Measurements reveal that flow morhpology is highly complex and three-

dimensional, unlike any previously observed 2-D wing-based vortex sheets. Furthermore, using 2-D particle image velocimetry data, a sinusoidal variation in thrust force, 90 deg out of phase with the airfoil motion, is measured in the midspan region of the airfoil. The largest measured thrust occurs at the maximum angles of attack, corresponding to the creation of strong leading-edge vortices.

[177] Parker, K., von Ellenrieder, K. D., and Soria, J., "Using Stereo Multigrid DPIV (SMDPIV) Measurements to Investigate the Vertical Skeleton Behind a Finite-Span Flapping Wing," *Experiments in Fluids*, Vol. 39, No. 2, 2005, pp. 281–298.

Keywords: 3-D, Experimental, Vortices

Abstract: The structure of the flow behind wings with finite span (3D) is significantly more complex than the flow behind infinite span (2D) wings. It has been shown that the presence of wingtip vortices behind finite span wings significantly modifies the geometry of the wake flow. It is felt that this modification alters the dynamics of interaction between leading and trailing edge vorticity in a manner that affects the ability of 2D flapping wings to produce thrust. A model of the mean flow skeleton has been proposed from qualitative flow visualization experiments. An unambiguous quantitative representation of the actual flow is required for comparison to the proposed model. To accomplish this full 3D 3C velocity is required in the volume behind the 3D flapping wing. It is proposed to use stereoscopic multigrid digital particle image velocimetry (SMDPIV) measurements to investigate this unsteady oscillatory flow. This paper reports preliminary SMDPIV measurements along the plane of a symmetrical NACA-profile wing at a Strouhal number of 0.35. Phase averaged measurements are used to investigate the complex flow topology and the influence of the forcing flow on the evolution of the large scale structure of a jet-flow. This paper focuses on optimizing the SMDPIV experimental methodology applied to liquid flows. By refining the 2D 3C technique, the 3D topology of the flow can be investigated with a high degree of accuracy and repeatability. Preliminary results show that the flow is characterized by two pairs of coherent structures of positive and negative vorticity. The arrangement of these structures in the flow is controlled by the motion of the wing. Vorticity of opposite rotation is shed at the extreme heave and pitch positions of the aerofoil to set up a thrust indicative vortex street in support of the suggested topological model.

[178] Ramasamy, M., and Leishman, J. G., "Phase-Locked Particle Image Velocimetry Measurements of a Flapping Wing," *Journal of Aircraft*, Vol. 43, No. 5, 2006, pp. 1867–1876.

Keywords: 3-D, Experimental, Vortices

Abstract: The unsteady aerodynamics of a biomimetic inspired flapping-wing mechanism has been analyzed by performing detailed phase-locked diagnostics of its flow field. Flow visualization and particle image velocimetry results have shown the presence of a shed dynamic stall vortex that spans across most of the wing span. The shedding of this type of leading-edge vortex was accompanied by the formation of another leading-edge vortex before the first vortex reached the midchord, resulting in multiple shedding leading-edge vortices on the top surface of the wing during each wing stroke. A strong startling vortex was also formed at the trailing edge of the wing during the early part of its translational stroke. This vortex continuously gained strength from shed vorticity as the wing accelerated into its stroke. The startling vortex remained close to the trailing edge until the wing reached midstroke. A pair of vortices that continuously trailed from the root and tip of the wing were identified, both of which induced a significant downwash velocity over the wing surface. These trailed vortices were found to exhibit a contracting wake structure as they convected into the wake below the wing, consistent with an increase in slipstream velocity. The evolution of the tip and root vortex pair showed rapid diffusive characteristics with an increase in time (wake age).

[179] Triantaflyllou, M. S., Techet, A. H. and Hover, F. S., "Review of Experimental Work in Biomimetic Foils," *IEEE Journal of Oceanic Engineering*, Vol. 29, No. 3, 2004, pp. 585–594.

Keywords: 3-D, Experimental, Vortices

Abstract: Significant progress has been made in understanding some of the basic mechanisms of force production and flow manipulation in oscillating foils for underwater use. Biomimetic observations, however, show that there is a lot more to be learned, since many of the functions and details of fish fins remain unexplored. This review focuses primarily on experimental studies on some of the, at least partially understood, mechanisms, which include 1) the formation of streets of vortices around and behind two- and three-dimensional propulsive oscillating foils; 2) the formation of vortical structures around and behind two- and three-dimensional foils used for maneuvering, hovering, or fast-starting; 3) the formation of leading-edge vortices in flapping foils, under steady flapping or transient conditions; 4) the interaction of foils with oncoming, externally generated vorticity; multiple foils, or foils operating near a body or wall.

[180] Grauer, J., Ulrich, E., Hubbard, J., Pines, D., and Humbert J. S., "Testing and System Identification of an Ornithopter in Longitudinal Flight," *Journal of Aircraft*, Vol. 48, No. 2, 2011, pp. 660–667.

Keywords: 3-D, Experimental, Design

Abstract: There is currently a large effort underway to understand the flight dynamics of avian-based flapping-wing vehicles, or ornithopters, as they represent a critical intersection between existing biological flyers and the need for small aerial robots to conduct a variety of mission scenarios. Efforts to model the flight dynamics of these vehicles for feedback control have been complicated by a number of factors including nonlinear flight motions, unsteady aerodynamics at low Reynolds numbers, and limited sensor payload capacity. This paper presents data for a 0.45 kg ornithopter research planform, flown in straight and level mean flight. A visual tracking system was employed to follow retroreflective markers on the ornithopter and reconstruct state measurements. A multibody model of the flight dynamics was used to investigate the spacial distribution of kinematic variables over the duration of a wing stroke, and system identification techniques were employed to extract models for the lift, thrust, and pitching moment coefficients. Two methods of parameter estimation showed good results for relatively simple aerodynamic models that can be used for feedback control.

[181] Lin, C. S., Hwu, C., and Young, W. B., "The Thrust and Lift of an Ornithopter's Membrane Wings with Simple Flapping Motion," *Aerospace Science and Technology*, Vol. 10, No. 2, 2006, pp. 111–119.

Keywords: 3-D, Experimental, Design

Abstract: Human beings flying with the help of aircrafts of various kinds have been able to fly for about one century. Although the flapping wings of animals served as an inspiration to pioneers of human flight, we don't really understand how they work. In this study, we employ the concept of four-bar linkage to design a flapping mechanism which simulates a flapping motion of a bird. Wind tunnel tests were performed to measure the lift and thrust of the mechanical membrane flapping wing under different frequency, speed, and angle of attack. It is observed that the flexibility of the wing structure will affect the thrust and lift force due to its deformation at high flapping frequency. The lift force will increase with the increase of the flapping frequency under the corresponding flying speed. For the same flapping frequency, the flying speed can be increased by decrease of the angle of attack with the trade of losing some lift force. An angle of attack is necessary in a simple flapping motion in order to derive a lift force. The flapping motion generates the thrust to acquire the flying speed. The flying speed and angle of attack combine to generate the lift force for flying.

[182] Yang, L. J., Hsu, C. K., Han, H. C., and Miao, J. M., "Light Flapping Micro Aerial Vehicle Using Electrical-Discharge Wire-Cutting Technique," *Journal of Aircraft*, Vol. 46, No. 5, 2009, pp. 1866–1874.

Keywords: 3-D, Experimental, Design

Abstract: Electrical-discharge wire cutting is a promising technique that provides flexibility and lightness for a flapping micro aerial vehicle. Electrical-discharge wire cutting is used to fabricate the high-aspect-ratio structure of the four-bar linkage gear transmission module made of aluminum-alloy 7075. Aluminum-alloy 7075 has excellent specific strength (yield strength/density) good for durability of the transmission module in a micro aerial vehicle's tuff operation. A new flapping micro aerial vehicle of 21.6 cm wing span consequently has a minimum body mass of 5.9 g after installing the transmission module and a flexible wing frame made of carbon fibers and polyethylene terephthalate film. This micro aerial vehicle can endure a flight time of 6 min 7 s with the wingbeat frequency of 10-20 Hz. The lift and thrust coefficients of the micro aerial vehicle have been investigated through wind-tunnel testing. The proposed flapping micro aerial vehicle also exhibits the improved characteristic in the scaling law with respect to wingbeat frequency versus body mass.

[183] Zdunich, P., Bilyk, D., MacMaster, M., Loewen, D., DeLaurier, J., Kornbluh, R., Low, T., Stanford, S., and Holeman, D., "Development and Testing of the Mentor Flapping-Wing Micro Air Vehicle," *Journal of Aircraft*, Vol. 44, No. 5, 2007, pp. 1701–1711.

Keywords: 3-D, Experimental, Design and Development

Abstract: In 1997 the Defense Advanced Research Projects Agency initiated a program to explore the possibility of micro air vehicles for the purpose of individually portable surveillance systems for close-range operations. The various contractors approached the problem in several ways, such as developing tiny fixed-wing airplanes, rotary-wing aircraft, and ornithopters mimicking animal flight. This paper describes one such flapping-wing aircraft, which drew upon the clap-fling phenomenon that is exploited by many flying animals and insects for lift generation. Essentially this aircraft was a mechanical simulation of hummingbird flight, though with two sets of wings to eliminate the unbalanced side-to-side flapping forces. Two flying demonstration models were built, one with an

internal-combustion engine and another with an electric motor. In both cases, these incorporated a drive train to reduce the high rpm rotary shaft motion to lower-frequency oscillation for flapping. Also required was a programmable logic board for stabilization. Successful hovering flight was achieved with both models, and initial studies of transition to horizontal flight were also explored.

[184] Archer, R. D., Sapuppo, J. and Betteridge, D. S., "Propulsion Characteristics of Flapping Wings," *Aeronautical Journal*, Vol. 83, Sep. 1979, pp. 355–371.

Keywords: 3-D, Experimental, Dominant Parameters, Model

Abstract: In moving from the realm of stationary wing flight towards the complexity of flapping wing flight as evolved in birds, we wish to introduce the simplest means of flapping as a first step in an attempt to simplify as much as possible our wind tunnel model and also to confine our attention to the dominant thrust producing mechanism. Our model half wings flap only in the plane normal to flight. The flapping motion is sinusoidal with time and symmetrical about the mid position. No wing bending was allowed. The wing section shape had no camber and also was rigid in shape but free to twist in torsion about its shear center. However, the model root support was fixed and therefore could not simulate vertical plunging of a bird associated with ideal elliptic span loading. Our models were of simple construction such that aeroelastic response generated an unspecified but substantial spanwise twist, which varied in time with the flapping velocity.

[185] Yeo, D., Atkins, E. M., Bernal, L. P., and Shyy, W., "Experimental Characterization of Lift on a Rigid Flapping Wing," *Journal of Aircraft*, Vol. 50, No. 6, 2013, pp. 1806–1821.

Keywords: 3-D, Experimental, Methods, Comparison

Abstract: Measurements of aerodynamic forces over flapping wings are challenging due to unsteady flowfields and rapidly changing structural loads. This represents an important limitation to the aerodynamic data currently available to researchers working on the aerodynamics of bioinspired flapping wings. This paper proposes the use of pressure-based instrumentation for flapping-wing testing and documents the comparison of two experimental methods to measure the aerodynamic lift generated during the stroke of a rigid flapping wing. The first approach uses a force transducer to measure the forces in air and vacuum, and the second approach uses pressure measurements taken on the surfaces of the wing. The results from both methods are used to validate each other and provide experimental data for a test case with easily simulated conditions. This paper describes the design of the test hardware required, including a custom flap stand, flap mechanics, and instrumented wing construction techniques. A series of flap tests were conducted with pressures measured only in air and force measurements taken both in air and in a vacuum. The data are evaluated with respect to noise, repeatability, and expected scaling trends. The pressure sensor and force transducer measurement strategies are compared based on their accuracy and flexibility.

[186] Jones, K. D., Bradshaw, C. J., Papadopoulos, J., and Platzer, M. F., "Bio-Inspired Design of Flapping-Wing Micro Air Vehicles," *Aeronautical Journal*, Vol. 109, Aug. 2005, pp. 385–393.

Keywords: 3-D, Experimental, MAV Test

Abstract: The development and flight testing of flapping-wing propelled, radio-controlled micro air vehicles are described. The unconventional vehicles consist of a low aspect ratio fixed-wing with a trailing pair of higher aspect ratio flapping wings which flap in counterphase. The symmetric flapping-wing pair provides a mechanically and aerodynamically balanced platform, increases efficiency by emulating flight in ground effect, and suppresses stall over the main wing by entraining flow. The models weigh as little as 11g, with a 23cm span and 18cm length and will fly for about 20 minutes on a rechargeable battery. Stable flight at speeds between 2 and 5ms^{-1} has been demonstrated, and the models are essentially stall-proof while under power. The static-thrust figure of merit for the device is 60% higher than propellers with a similar scale and disk loading.

[187] Dickinson, M. H., "The Effects of Wing Rotation on Unsteady Aerodynamic Performance at Low Reynolds Numbers," *Journal of Experimental Biology*, Vol. 192, July 1994, pp. 179–206.

Keywords: 3-D, Experimental, Wing Stroke

Abstract: The downstroke-to-upstroke transition of many insects is characterized by rapid wing rotation. The aerodynamic consequences of these rapid changes in angle of attack have been investigated using a mechanical model dynamically scaled to the Reynolds number appropriate for the flight of small insects such as Drosophila. Several kinematic parameters of the wing flip were examined, including the speed and axis of rotation, as well as the duration and angle of attack during the wing stroke preceding rotation. Alteration of these kinematic parameters altered force generation during the subsequent stroke in a variety of ways. 1. When the rotational axis was close to the trailing edge,

the model wing could capture vorticity generated during rotation and greatly increase aerodynamic performance. This vortex capture was most clearly manifested by the generation of lift at an angle of attack of 0 deg. Lift at a 0 deg angle of attack was also generated following rotation about the leading edge, but only if the downstroke angle was large enough to generate a von Karman street. The lift may be due to an alteration in the effective angle of attack caused by the inter-vortex stream in the downstroke wake. 2. The maximum lift attained (over all angles of attack) was substantially elevated if the wing translated backwards through a wake generated by the previous stroke. Transient lift coefficient values of nearly 4 were obtained when the wing translated back through a von Karman street generated at a 76.5 deg angle of attack. This effect might also be explained by the influence of the inter-vortex stream, which contributes a small component to fluid velocity in the direction of translation. 3. The growth of lift with angle of attack was significantly elevated following a 7.5 chord stroke with a 76.5 deg angle of attack, although it was relatively constant under all other kinematic conditions. 4. The results also indicate the discrepancies between transient and time-averaged measures of performance that arise when unsteady mechanisms are responsible for force generation. Although the influence of wing rotation was strong during the first few chords of translation, averaging the performance over as little as 6.5 chords of motion greatly attenuated the effects of rotation. 5. Together, these modeling results suggest that the unsteady mechanisms generated by simple wing flips could provide an important source for the production of aerodynamic forces in insect flight. Furthermore, the extreme sensitivity to small variations in almost all kinematic parameters could provide a foundation for understanding the aerodynamic mechanisms underlying active flight control.

[188] Vandenberghe, N., Zhang, J., and Childress, S., "Symmetry Breaking Leads to Forward Flapping Flight," *Journal of Fluid Mechanics*, Vol. 506, May 2004, pp. 147–155.

Keywords: 3-D, Experimental, Frequency

Abstract: Flapping flight is ubiquitous in Nature, yet cilia and flagella, not wings, prevail in the world of micro-organisms. This paper addresses this dichotomy. We investigate experimentally the dynamics of a wing, flapped up and down and free to move horizontally. The wing begins to move forward spontaneously as a critical frequency is exceeded, indicating that 'flapping flight' occurs as a symmetry-breaking bifurcation from a pure flapping state with no horizontal motion. A dimensionless parameter, the Reynolds number based on the flapping frequency, characterizes the point of bifurcation. Above this bifurcation, we observe that the forward speed increases linearly with the flapping frequency. Visualization of the flow field around the heaving and plunging foil shows a symmetric pattern below transition. Above threshold, an inverted von Kármán vortex street is observed in the wake of the wing. The results of our model experiment, namely the critical Reynolds number and the behavior above threshold, are consistent with observations of the flapping-based locomotion of swimming and flying animals.

[189] Birnbaum, W., "Das ebene Problem des Schlagenden Fluegels," *Zeitschrift fuer Angewandte Mathematik und Mechanik*, Vol. 4, No. 4, 1924, pp. 277–292.

Keywords: 3-D, Experimental, Reduced Frequency

[190] Vandenberghe, N., Childress, S., and Zhang, J., "On Unidirectional Flight of a Free Flapping Wing," *Physics of Fluids*, Vol. 18, No. 1, 2006, pp. 014102-1–014102-8.

Keywords: 3-D, Experimental, Forward Flight

Abstract: We study the dynamics of a rigid, symmetric wing that is flapped vertically in a fluid. The motion of the wing in the horizontal direction is not constrained. Above a critical flapping frequency, forward flight arises as the wing accelerates to a terminal state of constant speed. We describe a number of measurements which supplement our previous work. These include (a) a study of the initial transition to forward flight near the onset of the instability, (b) the separate effects of flapping amplitude and frequency, (c) the effect of wing thickness, (d) the effect of asymmetry of the wing planform, and (e) the response of the wing to an added resistance. Our results emphasize the robustness of the mechanisms determining the forward-flight speed as observed in our previous study.

[191] Lua, K. B., Lim, T. T., and Yeo, K. S., "Scaling of Aerodynamic Forces of Three-Dimensional Flapping Wings," *AIAA Journal*, Vol. 52, No. 5, 2014, pp. 1095–1101.

Keywords: 3-D, Experimental, Velocity Scaling

[192] Fejtek, I. and Nehera, J., "Experimental Study of Flapping Wing Lift and Propulsion," *Aeronautical Journal*, Vol. 84, Jan. 1980, pp. 28–33.

Keywords: 3-D, Experimental, Lift

[193] Batina, J. T., "Unsteady Euler Algorithm with Unstructured Dynamic Mesh for Complex-Aircraft Aerodynamic Analysis," *AIAA Journal*, Vol. 29, No. 3, 1991, pp. 327–333.

Keywords: 3-D, Numerical, CFD

Abstract: An Euler solution algorithm is presented for unsteady aerodynamic analysis of complex-aircraft configurations. The flow solver involves a multistage Runge-Kutta time-stepping scheme that uses a finite-volume spatial discretization on an unstructured grid made up of tetrahedra. A significant contribution of the research is the development and implementation of a moving mesh algorithm that is employed for problems involving static or dynamic deformation of the aircraft. The mesh algorithm is a general procedure that can treat realistic motions and deformations of complex-aircraft configurations. Steady and unsteady results are presented for a supersonic fighter configuration to demonstrate applications of the Euler solver and dynamic mesh algorithm. The unsteady flow results were obtained for the aircraft oscillating harmonically in a complete-vehicle bending mode. Effects of the angle of attack and reduced frequency on instantaneous pressures and force responses were investigated. The paper presents descriptions of the Euler solver and dynamic mesh algorithm along with results that assess the capability.

[194] Roget, B., Sitaraman, J., Harmon, R., Grauer, J., Hubbard, J., and Humbert, S., "Computational Study of Flexible Wing Ornithopter Flight," *Journal of Aircraft*, Vol. 46, No. 6, 2009, pp. 2016–2031.

Keywords: 3-D, Numerical, CFD

Abstract: This paper presents the development and evaluation of a computational fluid dynamics based methodology to predict the aerodynamic forces produced by a flexible flapping wing. The computational fluid dynamics analysis code solves the compressible Reynolds-averaged form of the Navier-Stokes equations on structured curvilinear grids. A grid deformation algorithm is devised that deforms the body-conforming volume grid at each time step consistent with the measured wing motions. This algorithm is based on geometric considerations and is both computationally efficient and capable of handling very large deformations. This methodology is validated using experimental data obtained from a test on an ornithopter with flexible wings. Test data include measurements of the wing surface deformations as well as the generated forces in the horizontal and vertical directions. Correlation with test data shows good agreement with measured vertical force and satisfactory agreement with measured horizontal force at low flapping frequencies. However, the prediction accuracy degrades with an increase in flapping frequency. Evidence of resonance in the vehicle system was detected from the analysis of the experimental data. Unmodeled inertial effects from the vehicle body and support mounts may be one of the contributors to disagreement between the data and analysis.

[195] Shkarayev, S., Maniar, G., and Shekhovtsov, A. V., "Experimental and Computational Modeling of the Kinematics and Aerodynamics of Flapping Wing," *Journal of Aircraft*, Vol. 50, No. 6, 2013, pp. 1734–1747.

Keywords: 3-D, Numerical, CFD

Abstract: High-speed videography is used in measuring the kinematic and deformation parameters of the flapping wing. Based on these data, a theoretical analysis of the underlying physics is performed using computational fluid dynamics simulations. The time varying of the pitching angle in the chordwise directions exhibits a significant second harmonic. Results suggest the mechanics of membrane deformations during a flapping cycle is analogous to the buckling of a bistable structure. Noticeably, with an increase in the freestream speed, the downstroke duration increases. The solution to the three-dimensional fluid dynamics problem is constructed using two-dimensional solutions obtained for several sections of the wing by the improved discrete vortex method. The inertial component is dominant in the normal force coefficient, and hence, added mass is the main mechanism in aerodynamic force production for the studied problem. A normal component of the acceleration of the wing's trailing edge taken with a negative sign is introduced as a kinematic parameter that is essential in flapping-wing aerodynamics. The results show a satisfactory agreement in trends of the acceleration and force coefficients. From the analysis of kinematical changes, it follows that synchronization of acceleration and of the pitching angle is important for achieving maximum values of the vertical force coefficients.

[196] Cizmas, P., and Gargoloff, J., "Mesh Generation and Deformation Algorithm for Aeroelasticity Simulations," *Journal of Aircraft*, Vol. 45, No. 3, 2008, pp. 1062–1066.

Keywords: 3-D, Numerical, Mesh

[197] Hamdaoui, M., Chaskalovic, J., Doncieux, S., and Sagaut, P., "Using Multiobjective Evolutionary Algorithms and Data-Mining Methods to Optimize Ornithopters' Kinematics," *Journal of Aircraft*, Vol. 47, No. 5, 2010, pp. 1504–1516.

Keywords: 3-D, Numerical, e-MOEA

Abstract: The aim of this work is to present a method to find and analyze maximum propulsive efficiency kinematics for a birdlike flapping-wing unmanned aerial vehicle using multiobjective evolutionary optimization and data-mining tools. For the sake of clarity and simplicity, simple geometry (rectangular wings with the same profile along the span) and simple kinematics (symmetrical harmonic dihedral motion) are used. In addition, it is assumed that the birdlike aerial vehicle (for which the span and surface area are, respectively, 1 m and 0.15 m2) is in horizontal motion at low cruise speed (6 m/s). The aerodynamic performances of the flapping-wing vehicle are evaluated with a semi-empirical flight physics model and the problem is solved using an efficient multiobjective evolutionary algorithm called e-MOEA. Groups of attractive solutions are defined on the Pareto surface, and the most efficient solutions within these groups are characterized. Given the high dimensionality of the Pareto surface in the kinematic parameters space, data-mining techniques are used to conduct the study. First, it is shown that these groups can be qualified versus the whole Pareto surface by accurate mathematical relations on the kinematic parameters. Second, the inner structure of each group is studied and highly accurate mathematical relations are found on the optimized parameters describing the most efficient solutions.

[198] Neef, M. F., and Hummel, D., "Euler Solutions for a Finite-Span Flapping Wing," *Fixed and Flapping Wing Aerodynamics for Micro Air Vehicles*, AIAA, Danvers, MA, 2001, pp. 429–451.

Keywords: 3-D, Numerical, Euler

[199] Ramamurti, R., and Sandberg, W. C., "Computational Study of 3-D Flapping Foil Flows," AIAA Paper 2001-0605, Jan. 2001.

Keywords: 3-D, Numerical, Finite Element

Abstract: A finite element flow solver based on unstructured grids is employed for studying the unsteady flow past oscillating wings. In order to understand the basis of lift and thrust generation mechanisms, we have performed computational studies on the flapping wing of the fruit fly, Drosophila. The computational model is based on the experimental setup of Dickinson et al. Computations are performed for various phase angles between the rotation and translation motions and the time history of the unsteady forces are compared with the experiments. Good agreement is obtained for the thrust and drag forces. Also, a grid refinement study is performed to validate the computational results. The unsteady flow is discussed in detail.

[200] Smith, M., "Simulating Moth Wing Aerodynamics: Towards the Development of Flapping-Wing Technology," *AIAA Journal*, Vol. 34, No. 7, 1996, pp. 1348–1355.

Keywords: 3-D, Numerical, Panel Code

Abstract: The mechanization of flapping-wing flight is addressed. A tethered moth's flapping wings are simulated using an unsteady aerodynamic panel method and accounts for wing flexibility using a finite element model. The resultant simulation code delineates both the aerodynamic and inertial forces acting on flapping, flexible wings undergoing arbitrary motion in the presence of large-scale vortices and establishes the importance of including the wake in the unsteady analysis of flapping flexible wings. A switching pattern is discovered where the magnitude and direction of the aerodynamic force are decoupled, thereby pointing to a means whereby control is achieved. Overall, important groundwork necessary for the establishment of the principles of flapping-wing flight is laid, leading to the development of a highly agile, alternative flight technology.

[201] Teng, N. H., "The Development of a Computer Code for the Numerical Solution of Unsteady Inviscid and Incompressible Flow Over an Airfoil," M.S. Thesis, Naval Postgraduate School, Monterey, CA, June 1987.

Keywords: 3-D, Numerical, Panel Code

Abstract: A numerical technique is formulated, in a computer program U2DIIF, for the solution of flow over an airfoil executing an arbitrary unsteady motion in an inviscid and incompressible medium. The technique extends the well-known Panel Methods for steady flow into solving a non-linear unsteady flow problem arising from the continuous vortex shedding into the trailing wake due to the unsteady motion of the airfoil. Numerous case-runs are presented to verify U2DIIF computer code against other theoretical and/or numerical methods as well as in cases where limited experimental data are obtainable in literatures. These case-runs include airfoils undergoing a step change or a modified ramp change of angle-of-attack, airfoils executing harmonic oscillation in pitching and plunging motions and airfoils penetrating a sharp edge gust.

[202] Stanford, B. K., and Beran, P. S., "Analytical Sensitivity Analysis of an Unsteady Vortex-Lattice Method for Flapping-Wing Optimization," *Journal of Aircraft*, Vol. 47, No. 2, 2010, pp. 647–662.

Keywords: 3-D, Numerical, Shape Morphing

Abstract: This work considers the design optimization of a flapping wing in forward flight with active shape morphing, aimed at maximizing propulsive efficiency under lift and thrust constraints. This is done with an inviscid three-dimensional unsteady vortex-lattice method, for which the moderate level of fidelity is offset by a relatively inexpensive computational cost. The design is performed with a gradient-based optimization, where gradients are computed with an analytical sensitivity analysis. Wake terms provide the only connection between the forces generated at disparate time steps and must be included to compute the derivative of the aerodynamic state at a time step with respect to the wing shape at all previous steps. The cyclic wing morphing, superimposed upon the flapping motions, is defined by a series of spatial and temporal approximation. The generalized coordinates of a finite number of twisting and bending modes are approximated by cubic splines. The amplitudes at the control points provide design variables; increasing the number of variables (providing the wing morphing with a greater degree of spatial and temporal freedom) is seen to provide increasingly superior designs, with little increase in computational cost.

[203] Fitzgerald, T., Valdez, M., and Balachandran, B., "A comparison of computational models for fluid-structure interaction studies of flexible flapping wing systems," AIAA Paper 2011-1115, Jan. 2011.

Keywords: 3-D, Numerical, Comparison

Abstract: In this article, the authors examine two computational approaches that can be used to study the motions of flexible flapping systems. For illustration, a fully coupled interaction of a fluid system with a flapping profile performing harmonic flapping kinematics is studied. In one approach, the fluid model is based on the Navier-Stokes equations for viscous incompressible flow, where all spatio-temporal scales are directly resolved by means of Direct Numerical Simulations (DNS). In the other approach, the fluid model is an inviscid, potential flow model, based on the unsteady vortex lattice method (UVLM). In the UVLM model, the focus is on the vortex structures and the fluid dynamics is treated as a problem of vortex kinematics, whereas with the DNS model, the focus is on forming a detailed picture of the flapping physics. The UVLM based approach, although coarse from a modeling standpoint, is computationally inexpensive compared to the DNS based approach. This comparative study is motivated by the hypothesis that flapping related phenomena are primarily determined by vortex interactions and viscous effects plays a secondary role, which could mean that a UVLM based approach could be suitable for design purposes, and/or constructing a predictive tool. In most of the cases studied in this work, the UVLM based approach produces a good approximation for Cl/Cd. Apart from comparisons of the aerodynamic loads, comparisons are also made of the features of the system dynamics generated by using the two computational approaches. Limitations of both approaches are also discussed.

[204] Deng, J., Caulfield, C. P., and Shao, X., "Effect of Aspect Ratio on the Energy Extraction Efficiency of Three-Dimensional Flapping Foils," *Physics of Fluids*, Vol. 26, No. 4, 2014, pp. 043102-1–043102-24.

Keywords: 3-D, Numerical, Energy

Abstract: Numerical simulations are used to investigate the effect of variation of the aspect ratio and the structure of pitching motions on the energy extraction efficiency and wake topology of flapping foils. The central aim is to predict the energy extraction performance and efficiency of a flapping-foil-based energy harvesting system (EHS) in realistic working conditions with finite aspect ratios. A sinusoidal heaving motion is imposed upon the foil, as well as both a sinusoidal pitching motion and a variety of trapezoidal-like periodic pitching motions. The simulations employ a finite-volume method with body-fitted moving grids, allowing the capture of flow structure near the foil surface. A detailed analysis of the hydrodynamic performance shows two peaks per periodic cycle in the lift force time histories or equivalently, the energy extraction time histories. The first primary peak corresponds to an effective angle of attack around 15.4°, indicating good attachment of the flow on the foil surface without significant flow separation. The secondary peak corresponds to a leading edge vortex (LEV) travelling on the foil surface. The shape of the LEV is altered markedly as the aspect ratio varies, and consequently the secondary peak in the lift force time history is strongly affected by the effects of three-dimensionality for foils with smaller aspect ratios. By examining the relationship between energy extraction efficiency and aspect ratio, a critical aspect ratio of $AR = 4$ is identified for sinusoidal pitching motions, below which the three-dimensional low-aspect-ratio characteristics dominate the flow evolution. Therefore, the compromise between higher energy extraction efficiency and lower costs of manufacturing and installation suggests that an aspect ratio around $AR = 4$ is the most appropriate choice for a real EHS. Furthermore, although trapezoidal-like pitching motions are known to improve the efficiency in flows restricted to two dimensions, particularly for non-optimal angle of attack, the efficiency of such flows is even more strongly affected by three-dimensional motions, with substantial efficiency loss even for $AR = 8$. This suggests that the implementation of

efficiency improvement strategies obtained by two-dimensional studies should be treated with caution when extended to real three-dimensional flows.

[205] Tucker, V. A., "Bird Metabolism During Flight, Evaluation of a Theory," *Journal of Experimental Biology*, Vol. 58, June 1973, pp. 689–709.

Keywords: 3-D, Numerical, Energy

1. Pennycuick's (1969) theory for the energetic requirements of avian flight predicts the metabolic rates of budgerigars and laughing gulls flying level at intermediate speeds in a wind tunnel with an accuracy of 10% or better. However, its predictions appear to be low for most birds with masses less than 0·1 kg and high for most birds with masses greater than 0·5 kg. 2. Four modifications are made to Pennycuick's theory: (1) a different computation of induced power; (2) a different estimate of equivalent flat plate area that includes Reynolds number effects, and is based on additional measurements; (3) a different estimate of profile power that includes Reynolds number effects; and (4) the addition of power terms for respiration and circulation. These modifications improve the agreement between the theoretical predictions and existing measurements for flying birds and bats. 3. The metabolic rates of birds and bats in level flight at various speeds can be estimated by the modified theory if body mass alone is measured. Improved estimates can be made if wing span is measured as well. In the latter case the theory predicts measured values with a mean absolute error of 8·3%. 4. The results of the modified theory are presented by approximate equations that can be solved quickly for metabolic rate and flight speed with a slide rule.

[206] Spentzos, A., Barakos, G. N., Badcock, K. J., Richards, B. E., Coton, F. N., Galbraith, R. A. McD., Berton, E., and Favier, D., "Computational Fluid Dynamics Study of Three-Dimensional Dynamic Stall of Various Planform Shapes," *Journal of Aircraft*, Vol. 44, No. 4, 2007, pp. 1118–1128.

Keywords: 3-D, Numerical, Stall

Abstract: Numerical simulation of 3D dynamic stall has been undertaken using computational fluid dynamics. As a first step, validation calculations have been performed for cases in which experimental data were available. Although the amount and quality of the experimental data available for 3D dynamic stall does not match what is available for 2D cases, the computational fluid dynamics was found capable of predicting this complex 3D flow with good accuracy. Once confidence on the computational fluid dynamics method was established, further calculations were conducted for several wing planforms. The calculations revealed the detailed structure of the 3D dynamic stall vortex and its interaction with the tip vortex. Remarkably, strong similarities in the flow topology were identified for wings of very different planforms.

[207] Hall, K. C., Pigott, S. A., and Hall, S. R., "Power Requirements for Large-Amplitude Flapping Flight," *Journal of Aircraft*, Vol. 35, No. 3, 1998, pp. 352–361.

Keywords: 3-D, Numerical, Power

Abstract: In this paper, a method is presented for computing the circulation distribution along the span of a flapping wing that minimizes the power required to generate a prescribed lift and thrust. The power is composed of three parts: useful thrust power, induced power, and profile power. Here, the thrust and induced power are expressed in terms of the Kelvin impulse and kinetic energy associated with the sheet of trailing and shed vorticity left behind the flapping wing. The profile power is computed using a quasisteady approximation of the two-dimensional viscous drag polar at each spanwise station of the wing. A variational principle, which is essentially the viscous extension of the well-known Betz criterion for optimal propellers, is discretized using a vortex-lattice model of the wake, and the optimum solution is computed numerically. The present method is used to analyze a conventional propeller as well as a rigid wing in forward-flight flapping about a hinge point on the longitudinal axis.

[208] Buchmann, N., and Radespiel, R., "Computational Three-Dimensional Flapping-Wing Analysis," AIAA Journal, Vol. 52, No. 1, 2014, pp. 203–206.

Keywords: 3-D, Numerical, Thrust, Efficiency

[209] Rayner, J. M. V., "A Vortex Theory of Animal Flight. Part 1. The Vortex Wake of a Hovering Animal," *Journal of Fluid Mechanics*, Vol. 91, Apr. 1979, pp. 697–730.

Keywords: 3-D, Numerical, Hover, Vortices

Abstract: The distribution of vorticity in the wake of a hovering bird or insect is considered. The wake is modelled by a chain of coaxial small-cored circular vortex rings stacked one upon another; each member of the chain is generated by a single wing-stroke. Circulation is determined by the animal's weight and the time for which a single ring must provide lift; ring size is calculated from the circulation distribution on the animal's wing. The theory is equally

applicable to birds and insects, although the mechanism of ring formation differs. This approach avoids the use of lift and drag coefficients and is not bound by the constraints of steady-state aerodynamics; it gives a wake configuration in agreement with experimental observations. The classical momentum jet approach has steady momentum flux in the wake, and is difficult to relate to the wing motions of a hovering bird or insect; the vortex wake can be related to the momentum jet, but adjacent vortex elements are disjoint and momentum flux is periodic. The evolution of the wake starting from rest is considered by releasing vortex rings at appropriate time intervals and allowing them to interact in their own velocity fields. The resulting configuration depends on the feathering parameter f (which depends on the animal's morphology); f increases with body size. At the lower end of the wake rings coalesce to form a single large vortex, which breaks away from the rest of the wake at intervals. Wake contraction depends on f; the minimum areal contraction of one-half (as in momentum-jet theory) occurs only in the limit f [rightward arrow] 0, but values calculated for smaller insects of just over one-half suggest that the momentum jet may be a good approximation to the wake when f is small. Induced power in hovering is calculated as the limit of the mean rate of increase of wake kinetic energy as time progresses. It can be related to the classical momentum-jet induced power by a simple conversion factor. For an insect or hummingbird the usual momentum-jet estimate may be between 10 and 15% too low, but for a bird it may be as much as 50% too low. This suggests that few, if any, birds are able to sustain aerobic hovering, and that as small a value of f as possible would be necessary if the bird were to hover. Tip losses (energy cost of the vortex-ring wake compared with the equivalent momentum jet) are negligible for insects, but can be in the range 15–20% for birds.

[210] Ansari, S. A., Zbikowski, R., and Knowles, K., "Nonlinear Unsteady Aerodynamic Model for Insect-like Flapping Wings in the Hover Part 2: Implementation and Validation," *Proceedings of the Institute of Mechanical Engineering, Part G: Journal of Aerospace Engineering*, Vol. 220, No. 3, 2006, pp. 169–186.

Keywords: 3-D, Numerical, Hover

Abstract: The essence of this two-part paper is the analytical, aerodynamic modelling of insect-like flapping wings in the hover for micro-air-vehicle applications. A key feature of such flapping-wing flows is their unsteadiness and the formation of a leading-edge vortex in addition to the conventional wake shed from the trailing edge. What ensues is a complex interaction between the shed wakes, which, in part, determines the forces and moments on the wing. In an attempt to describe such a flow, two novel coupled, non-linear, wake integral equations were developed in the first part of the paper. The governing equations derived were exact, but did not have a closed analytical form. Solutions were, therefore, to be found by numerical methods and implemented in Fortran. This is the theme of the second part of the paper. The problem is implemented by means of vortex methods, whereby discrete point vortices are used to represent the wing and its wake. A number of numerical experiments are run to determine the best values for numerical parameters. The calculation is performed using a time-marching algorithm and the evolution of the wakes is tracked. In this way, both flow field and force data are generated. The model is then validated against existing experimental data and very good agreement is found both in terms of flow field representation and force prediction. The temporal accuracy of the simulations is also noteworthy, implying that the underlying flow features are well captured, especially the unsteadiness. The model also shows the similarity between two-dimensional and three-dimensional flows for insect-like flapping wings at low Reynolds numbers of the order of $Re \varepsilon 200$.

[211] Gogulapati, A., Friedmann, P. P., and Martins, J. R. R. A., "Optimization of Flexible Flapping-Wing Kinematics in Hover," *AIAA Journal*, Vol. 52, No. 10, 2014, pp. 2342–2354.

Keywords: 3-D, Numerical, Hover

Abstract: Hover-capable flapping-wing micro air vehicles are well suited for missions in confined spaces. The best design practices for flapping wings and their kinematics are largely unknown, especially for flexible wings. To address this issue, numerical optimization is applied to the design of the kinematics and structural sizing of a flapping wing using a surrogate-based approach. The surrogates are generated using kriging interpolation of the time-averaged thrust generated and power required by the wings. The thrust and power data are computed using a nonlinear approximate aeroelastic model developed in previous studies by the authors. A numerical optimization algorithm is used to identify designs that produce the desired combination of thrust and power. The design variables consist of parameters describing the flap–pitch kinematics and the stiffness of the flexible wings. A trend study of thrust and power indicate that the phase angle between flap and pitch motions significantly affects the wing performance when the stroke amplitudes and the frequency are fixed. Smaller amounts of pitch actuation produced peak thrust in flexible wings when compared to the rigid wings. Several flexible configurations produce higher thrust when compared to the best thrust-producing rigid configuration. However, rigid wings have higher propulsive efficiency when compared to

flexible wings for the same amount of generated thrust. Thus, the actual design of a flapping wing will depend on the relative importance given to thrust production and propulsive efficiency.

[212] Isogai, K., and Shinmoto, Y., "Study on Aerodynamic Mechanism of Hovering Insects," AIAA Paper 2001-2470, June 2001.

Keywords: 3-D, Numerical, Hover

[213] Jardin, T., Farcy, A., and David, L., "Three-Dimensional Effects in Hovering Flapping Flight," *Journal of Fluid Mechanics*, Vol. 702, July 2012, pp. 102–125.

Keywords: 3-D, Numerical, Hover

Abstract: This paper aims at understanding the influence of three-dimensional effects in hovering flapping flight. Numerical simulations at a Reynolds number of 1000 are performed to compare two types of flapping kinematics whose plunging phase is characterized by either a rectilinear translation or a revolving motion. In this way, we are able to isolate the three-dimensional effects induced by the free end condition from that induced by the spanwise incident velocity gradient (and the associated implicit Coriolis and centrifugal effects). In the rectilinear translation case, the analysis of the wake and of the aerodynamic loads reveals that the wingspan can be compartmented into three distinct regions whether it is predominantly subjected to an unstable two-dimensional flow, a stable three-dimensional flow or both two-dimensional and three-dimensional effects. It is found that this partitioning exhibits common features for three different aspect ratios of the wing. In conjunction with the previous results of Ringuette, Milano & Gharib (*J. Fluid Mech.*, vol. 581, 2007, pp. 453–468), this suggests that the influence of the tip vortex over the wingspan is driven by a characteristic length scale. In addition, this length scale matches the position of the connecting point between leading and tip vortices observed in the revolving case, providing insight into the connecting process. In both translating and revolving cases, leading edge vortex attachment and strong spanwise velocities are found to be strongly correlated phenomena. Spanwise velocities (that mostly confine at the periphery of the vortices), together with downward velocities, do not only affect the leading edge vortex but also act as an inhibitor for the trailing edge vortex growth. As a consequence, cross-wake interactions between leading and trailing edge vortices are locally limited, hence contributing to flow stabilization.

[214] Kweon, J., and Choi, H., "Sectional Lift Coefficient of a Flapping wing in Hovering Motion," *Physics of Fluids*, Vol. 22, No. 7, 2010, pp. 071703-1–071703-4.

Keywords: 3-D, Numerical, Hover

Abstract: We investigate the behavior of sectional lift coefficient of a flapping wing of a fruit-fly in hovering motion. Through three-dimensional numerical simulations, we show that during the stroke, the sectional lift coefficient significantly varies in time as well as in the spanwise direction owing to complex interactions between the wing and vortices in the wake. However, the time-averaged sectional lift force coefficient is inversely proportional to the spanwise distance from the rotation center except very near the wing-tip region. This is because the wing-tip vortex significantly decreases the lift force on the wing-tip region during and after midstroke.

[215] Liu, H., Ellington, C. P., Kawachi, K., Van Den Berg, C., and Willmott, A. P., "A Computational Fluid Dynamic Study of Hawk-Moth Hovering," *Journal of Experimental Biology*, Vol. 201, Feb. 1998, pp. 461–477.

Keywords: 3-D, Numerical, Hover

Abstract: A computational fluid dynamic (CFD) modelling approach is used to study the unsteady aerodynamics of the flapping wing of a hovering hawkmoth. We use the geometry of a Manduca sexta-based robotic wing to define the shape of a three-dimensional 'virtual' wing model and 'hover' this wing, mimicking accurately the three-dimensional movements of the wing of a hovering hawkmoth. Our CFD analysis has established an overall understanding of the viscous and unsteady flow around the flapping wing and of the time course of instantaneous force production, which reveals that hovering flight is dominated by the unsteady aerodynamics of both the instantaneous dynamics and also the past history of the wing. <P> A coherent leading-edge vortex with axial flow was detected during translational motions of both the up- and downstrokes. The attached leading-edge vortex causes a negative pressure region and, hence, is responsible for enhancing lift production. The axial flow, which is derived from the spanwise pressure gradient, stabilizes the vortex and gives it a characteristic spiral conical shape. <P> The leading-edge vortex created during previous translational motion remains attached during the rotational motions of pronation and supination. This vortex, however, is substantially deformed due to coupling between the translational and rotational motions, develops into a complex structure, and is eventually shed before the subsequent translational motion. <P> Estimation of the forces during one complete flapping cycle shows that lift is produced mainly during the downstroke

and the latter half of the upstroke, with little force generated during pronation and supination. The stroke plane angle that satisfies the horizontal force balance of hovering is 23.6 degrees, which shows excellent agreement with observed angles of approximately 20-25 degrees . The time-averaged vertical force is 40 % greater than that needed to support the weight of the hawkmoth.

[216] Rosenfeld, N. C., and Wereley, N. M., "Time-Periodic Stability of a Flapping Insect Wing Structure in Hover," *Journal of Aircraft*, Vol. 46, No. 2, 2009, pp. 450–464.

Keywords: 3-D, Numerical, Hover

Abstract: The wings of insectlike flapping-wing micro air vehicles experience time-periodic inertial stiffnesses during flapping motion. By modeling the wing structure as a thin beam, a linear time-periodic assumed-model analysis is developed. The equations of motion of a flapping wing undergoing out-of-plane bending and torsion are derived. The homogeneous assumed-model equations are nondimensionalized. It is shown that the nondimensional strain stiffness varies with the ratio of the wing's nonrotating natural frequencies to the flapping frequency, whereas the nondimensional, time-periodic inertial stiffnesses vary with the amplitudes of flapping and feathering motion. The parametric stability of a representative wing is assessed by applying Floquet analysis to the nondimensional equations of motion, and a scalable stability diagram is presented. Parametric instabilities of the wing structure, caused by time-periodic stiffnesses, are characterized and plotted in the time domain. The effects of important structural design properties on parametric stability are examined.

[217] Stanford, B., Kurdi, M., Beran, P., and McClung, A., "Shape, Structure, and Kinematic Parameterization of a Power-Optimal Hovering Wing," *Journal of Aircraft*, Vol. 49, No. 6, 2012, pp. 1687–1699.

Keywords: 3-D, Numerical, Hover

Abstract: In this paper, we investigate the aeroelastic hovering motions of a highly flexible flapping wing. It is desired to parameterize the wing shape, structural composition, and kinematic hovering motions, and then minimize the peak power required during the stroke, subject to trim and mechanical failure constraints. The aeroelastic model couples a nonlinear three-dimensional beam model to a quasi-steady blade element aerodynamic model, which is then solved in an implicit time-marching manner until the response becomes time-periodic. Sub-iterations are used within each time step to accommodate various physical nonlinearities. Gradients of the response with respect to the disparate design variables are computed analytically for optimization. Power-optimal flapping configurations are found to exploit interdependencies among the three types of design variables to effectively tailor the aeroelastic response.

[218] Sun, M., and Tang, J., "Unsteady Aerodynamic Force Generation by a Model Fruit Fly Wing in Flapping Motion," *Journal of Experimental Biology*, Vol. 205, Jan. 2002, pp. 55–77.

Keywords: 3-D, Numerical, Hover

Abstract: A computational fluid-dynamic analysis was conducted to study the unsteady aerodynamics of a model fruit fly wing. The wing performs an idealized flapping motion that emulates the wing motion of a fruit fly in normal hovering flight. The Navier–Stokes equations are solved numerically. The solution provides the flow and pressure fields, from which the aerodynamic forces and vorticity wake structure are obtained. Insights into the unsteady aerodynamic force generation process are gained from the force and flow-structure information. Considerable lift can be produced when the majority of the wing rotation is conducted near the end of a stroke or wing rotation precedes stroke reversal (rotation advanced), and the mean lift coefficient can be more than twice the quasi-steady value. Three mechanisms are responsible for the large lift: the rapid acceleration of the wing at the beginning of a stroke, the absence of stall during the stroke and the fast pitching-up rotation of the wing near the end of the stroke. When half the wing rotation is conducted near the end of a stroke and half at the beginning of the next stroke (symmetrical rotation), the lift at the beginning and near the end of a stroke becomes smaller because the effects of the first and third mechanisms above are reduced. The mean lift coefficient is smaller than that of the rotation-advanced case, but is still 80 % larger than the quasi-steady value. When the majority of the rotation is delayed until the beginning of the next stroke (rotation delayed), the lift at the beginning and near the end of a stroke becomes very small or even negative because the effect of the first mechanism above is cancelled and the third mechanism does not apply in this case. The mean lift coefficient is much smaller than in the other two cases.

[219] Young, J., Lai, J. C. S., and Germain, C., "Numerical Simulation and Parameter Variation of Insect Wing Motion based on Dragonfly Hovering," AIAA Paper 2006-0038, Jan. 2006.

Keywords: 3-D, Numerical, Hover

Abstract: The flapping motion of a wing based on the hind-wing of the Aeschna juncea dragonfly is simulated using a 3D incompressible Navier Stokes solver. The performance of the wing is investigated by variation of a number of kinematic parameters. Flapping amplitudes of between 10 deg to 60 deg (half-angle) and frequencies of 1 to 300 Hz are considered, resulting in a Reynolds number range of 100 to 50,000. The flapping amplitude observed for Aeschna juncea is shown to maximize the ratio of mean vertical force produced to power required.

[220] Zheng, L., Hedrick, T. L., and Mittal, R., "A Multi-Fidelity Modelling Approach for Evaluation and Optimization of Wing Stroke Aerodynamics in Flapping Flight," *Journal of Fluid Mechanics*, Vol. 721, Apr. 2013, pp. 118–154.

Keywords: 3-D, Numerical, Hover

Abstract: The aerodynamics of hovering flight in a hawkmoth (*Manduca sexta*) are examined using a computational modelling approach which combines a low-fidelity blade-element model with a high-fidelity Navier–Stokes-based flow solver. The focus of the study is on understanding the optimality of the hawkmoth-inspired wingstrokes with respect to lift generation and power consumption. The approach employs a tight coupling between the computational models and experiments; the Navier–Stokes model is validated against experiments, and the blade-element model is calibrated with the data from the Navier–Stokes modelling. In the first part of the study, blade-element and Navier–Stokes modelling are used concurrently to assess the predictive capabilities of the blade-element model. Comparisons between the two modelling approaches also shed insights into specific flow features and mechanisms that are lacking in the lower-fidelity model. Subsequently, we use blade-element modelling to explore a large kinematic parameter space of the flapping wing, and Navier–Stokes modelling is used to assess the performance of the wing-stroke identified as optimal by the blade-element parameter survey. This multi-fidelity optimization study indicates that even within a parameter space constrained by the animal's natural flapping amplitude and frequency, it is relatively easy to synthesize a wing stroke that exceeds the aerodynamic performance of the hawkmoth wing stroke. Within the prescribed constraints, the optimal wing stroke closely approximates the condition of normal hover, and the implications of these findings on hawkmoth flight capabilities as well as on the issue of biomimetic versus bioinspired design of flapping wing micro-aerial vehicles, are discussed.

[221] Isogai, K., Fujishoro, S., Saitoh, T., Yamamoto, M., Yamasaki, M., and Matsubara, M., "Unsteady Three-Dimensional Viscous Flow Simulation of a Dragonfly Hovering," *AIAA Journal*, Vol. 42, No. 10, 2004, pp. 2053–2059.

Keywords: 3-D, Numerical, Hover

Abstract: To clarify the basic aerodynamic mechanisms of the hovering flight of the dragonfly, numerical simulations of the unsteady viscous flow around a tandem wing configuration have been performed using a three-dimensional Navier-Stokes codes. The flow simulations are conducted for Anax parthenope julius as a typical dragonfly model. The total lifting force and specific necessary power predicted by the present simulation show close agreement with those observed experimentally for the present dragonfly model. The present code is further validated by comparing the results of the simulation with the experimental values of total lift and stroke-plane angle obtained using a robot.

[222] Su, J. Y., Tang, J. H., Wang, C. H., and Yang, J. T., "A Numerical Investigation on the Ground Effect of a Flapping-Flying Bird," *Physics of Fluids*, Vol. 25, No. 9, 2013, pp. 093101-1–093101-13.

Keywords: 3-D, Numerical, Ground Effect

Abstract: The flight of a small bird under the influence of the ground effect is numerically investigated with a complete three-dimensional model including the bird's body and wings. The flight mode is not the conventional steady gliding flight but an unsteady flight consisting of flapping, twisting, and folding motions. As the bird approaches the ground, the average lift force gradually increases while the average drag force decreases. At a particular distance, the average lift force increases by approximately 47%, whereas the average drag force decreases by nearly 20%, relative to the absence of the ground effect. Because of the ground, the improved aerodynamic performance in flapping flight is much more significant than in steady flight, in which the modification of the lift-drag ratio is typically less than 10%. On the basis of the flow field, regardless of the presence or absence of the ground, there exists no evidence for an obstruction of a wing-tip vortex, which is a remarkable phenomenon and accounts for the improved performance in steady flight. The extent of the region of high pressure beneath the wing in the near-ground case seems to surpass that in the far-ground case, accounting for the greater lift and thrust forces in the near-ground case. This air cushion beneath the wing, known as the cram effect, is the dominant factor of the ground effect on a flapping bird.

[223] Viswanath, K., and Tafti, D. K., "Effect of Frontal Gusts on Forward Flapping Flight," *AIAA Journal*, Vol. 48, No. 9, 2010, pp. 2049–2062.

Keywords: 3-D, Numerical, Gusts

Abstract: The response of a rigid flapping wing in forward flight, at Re=10,000, subjected to frontal gusts has been investigated. The phasing and duration of the gusts and their impact on the various unsteady mechanisms are analyzed within a single flapping cycle. The gust is characterized by a step function with integral length scale much larger than that of the physical dimension of the micro air vehicle and with time scale much smaller than the flapping time period. The instantaneous lift and thrust profiles were observed to be influenced by a combination of the effective angle of attack, wing rotation, and the leading-edge vortices on the wing surface that increased the lift and thrust, illustrating the importance of the leading-edge vortex dynamics to force production. The effect of the gust is observed to be diminished when it occurs during rapid supination of the wing. The lift and thrust profiles are found to react in a similar fashion for gusts applied during the downstroke, whereas they experienced opposite effects during the upstroke. During the upstroke, force characteristics are shown to primarily react to effective angle-of-attack changes more than to changes in flow structures.

[224] Hua, R. N., Zhu, L., and Lu, X. Y., "Locomotion of a Flapping Flexible Plate," *Physics of Fluids*, Vol. 25, No. 12, 2013, pp. 121901-1–121901-17.

Keywords: 3-D, Numerical, Flexibility

Abstract: The locomotion of a flapping flexible plate in a viscous incompressible stationary fluid is numerically studied by an immersed boundary-lattice Boltzmann method for the fluid and a finite element method for the plate. When the leading-edge of the flexible plate is forced to heave sinusoidally, the entire plate starts to move freely as a result of the fluid-structure interaction. Mechanisms underlying the dynamics of the plate are elucidated. Three distinct states of the plate motion are identified and can be described as forward, backward, and irregular. Which state to occur depends mainly on the heaving amplitude and the bending rigidity of the plate. In the forward motion regime, analysis of the dynamic behaviors of the flapping flexible plate indicates that a suitable degree of flexibility can improve the propulsive performance. Moreover, there exist two kinds of vortex streets in the downstream of the plate which are normal and deflected wake. Further the forward motion is compared with the flapping-based locomotion of swimming and flying animals. The results obtained in the present study are found to be consistent with the relevant observations and measurements and can provide some physical insights into the understanding of the propulsive mechanisms of swimming and flying animals.

[225] Kang, C. K., Aono, H., Cesnik, C. E. S., and Shyy, W., "Effects of Flexibility on the Aerodynamic Performance of Flapping Wings," *Journal of Fluid Mechanics*, Vol. 689, Dec. 2011, pp. 32–74.

Keywords: 3-D, Numerical, Flexibility

Abstract: Effects of chordwise, spanwise, and isotropic flexibility on the force generation and propulsive efficiency of flapping wings are elucidated. For a moving body immersed in viscous fluid, different types of forces, as a function of the Reynolds number, reduced frequency (k), and Strouhal number (St), acting on the moving body are identified based on a scaling argument. In particular, at the Reynolds number regime of O(10^3-10^4) and the reduced frequency of O(1), the added mass force, related to the acceleration of the wing, is important. Based on the order of magnitude and energy balance arguments, a relationship between the propulsive force and the maximum relative wing-tip deformation parameter (gamma) is established. The parameter depends on the density ratio, St, k, natural and flapping frequency ratio, and flapping amplitude. The lift generation, and the propulsive efficiency can be deduced by the same scaling procedures. It seems that the maximum propulsive force is obtained when flapping near the resonance, whereas the optimal propulsive efficiency is reached when flapping at about half of the natural frequency; both are supported by the reported studies. The established scaling relationships can offer direct guidance for micro air vehicle design and performance analysis.

[226] Wang, S., Zhang, X., He, G., and Liu, T., "Lift Enhancement by Dynamically Changing Wingspan in Forward Flapping Flight," *Physics of Fluids*, Vol. 26, No. 6, 2014, pp. 061903-1–061903-19.

Keywords: 3-D, Numerical, Stretching Wing

Abstract: Dynamically stretching and retracting wingspan has been widely observed in the flight of birds and bats, and its effects on the aerodynamic performance particularly lift generation are intriguing. The rectangular flat-plate flapping wing with a sinusoidally stretching and retracting wingspan is proposed as a simple model for biologically inspired dynamic morphing wings. Numerical simulations of the low-Reynolds-number flows around the flapping morphing wing are conducted in a parametric space by using the immersed boundary method. It is found that

the instantaneous and time-averaged lift coefficients of the wing can be significantly enhanced by dynamically changing wingspan in a flapping cycle. The lift enhancement is caused by both changing the lifting surface area and manipulating the flow structures responsible to the vortex lift generation. The physical mechanisms behind the lift enhancement are explored by examining the three-dimensional flow structures around the flapping wing.

[227] Rakotomamonjy, T., Ouladsine, M., and Le Moing, T., "Modelization and Kinematics Optimization for a Flapping-Wing Microair Vehicle," *Journal of Aircraft*, Vol. 44, No. 1, 2007, pp. 217–231.

Keywords: 3-D, Numerical, Bi-wing

Abstract: OSCAB, a flight-dynamics-oriented simulation model of a flapping-wing micro air vehicle, is presented here. This concept is based on flapping flight performed in nature by insects or hummingbirds. The model features two independent wings and integrates the aerodynamic forces computed along each wing to determine the global motion of the micro air vehicle with respect to an inertial reference frame. A comparison between our simulation model and previous experimental measurements is presented, showing that it can reproduce the influence of the wing rotation phasing on the total lift. An optimization of the flapping kinematics of the wing has also been conducted to maximize the mean lift. A neural network has been designed to reproduce various function shapes modeling the wing movements. The parameters of this network have been optimized with a genetic algorithm to avoid local extrema. Results show a lift gain from 30 to 40%, corroborating previous experiments.

[228] Broering, T. M., Yongsheng, L., and Henshaw, W., "Numerical Investigation of Energy Extraction in a Tandem Flapping Wing Configuration," *AIAA Journal*, Vol. 50, No. 11, 2012, pp. 2295–2307.

Keywords: 3-D, Numerical, Tandem-Wing

Abstract: A number of flying insects make use of tandem-wing configurations, suggesting that such a setup may have potential advantages over a single wing at low Reynolds numbers. Dragonflies, which are fast and highly maneuverable, demonstrate well the potential performance of such a design. In this paper, a tandem-wing flapping configuration is simulated at a Reynolds number of 10,000 using an incompressible Navier-Stokes solver and an overlapping grid method. The flapping motion consists of a simple sinusoidal pitch and plunge motion with a spacing of one chord length between both wings. The arrangement was tested at a Strouhal number of 0.3 for three different phase angles: 0, 90, and 180 deg. The aerodynamics of the hind wing was compared in detail to a single wing, with the same geometry and undergoing the same flapping kinematics, to determine the effect of vortex shedding from the forewing on the hindwing, as well as how the phase angle affects the interaction. The average lift, thrust, and power coefficients and the average efficiency of the fore-and hindwings were compared with a single wing to determine how the tandem-wing interaction affects performance. The results show that adjusting the phase angle allows the tandem wing to change the flight mode. At 0 deg phase lag, the tandem wing produces high thrust at high propulsive efficiency, but low lift efficiency. Switching to 90/180 deg phase lag decreases the thrust production and propulsive efficiency but greatly increases the lift efficiency. At 90/180 deg, the power coefficient is much lower than at 0 deg due to the hindwing extracting energy from the wake of the forewing.

[229] Viswanath, K., and Tafti, D. K., "Effect of Stroke Deviation on Forward Flapping Flight," *AIAA Journal*, Vol. 51, No. 1, 2013, pp. 145–160.

Keywords: 3-D, Numerical, Flat Plate

Abstract: The performance of a rigid, thin surface flat-plate flapping wing in forward flight, at Re=10,000 using different stroke deviation trajectories, has been investigated to assess the different capabilities that such kinematics might offer. The instantaneous lift and thrust profiles were observed to be influenced by a combination of the leading-edge vortex and the trailing-edge vortex structures existing in the flow at any given time. Unlike regular no-deviation flapping cycles, the trailing-edge vortex is shown to be significant for out-of-plane trajectories. Both clockwise and anticlockwise variations for trajectory choice are analyzed for their efficacy as an improved kinematic choice over a no-deviation base case. The power requirements for the different cases, based on the fluid torques, are used as an index of the cost of performance across all cases. The anticlockwise eight-cycle deviation is shown to be very complex with high power costs albeit having better performance. The clockwise O cycle holds promise with being used as a viable stroke deviation trajectory for forward flight over the base case.

[230] Wu, J., and Shu, C., "Numerical Study of Flow Characteristics Behind a Stationary Circular Cylinder with a Flapping Plate," *Physics of Fluids*, Vol. 23, No. 7, 2011, pp. 073601-1–073601-17.

Keywords: 3-D, Numerical, Flat Plate

Abstract: The laminar flow over a stationary circular cylinder with a flapping plate is simulated in this study to investigate the flow characteristics by using our recently developed boundary condition-enforced immersed boundary-lattice Boltzmann method [Wu and Shu, J. Comput. Phys.228, 1963 (2009); Wu *et al.*, Int. J. Numer. Methods Fluids62, 327 (2010); Wu and Shu, Comm. Comp. Phys.7, 793 (2010)]. The purpose of this work is to study the flow control behind a bluff body by an alternative way different from the rotationally oscillating motion. The idea is in fact from the tadpole locomotion, where the bluff head-body is modeled by a circular cylinder, and the thin tail is simplified by a rigid plate with flapping motion. In this work, only the laminar flow is considered and thus the Reynolds number is chosen as 100. Similar to the case of rotationally oscillating cylinder, the flow wake behind the cylinder and flapping plate is strongly affected by the flapping amplitude and frequency of plate. On the other hand, because of the existence of flapping plate, the length of plate can also modify the flow structures. Due to flapping motion of plate, some typical flow patterns and drag reduction are found, and two different vortex interaction modes, known as constructive interaction and destructive interaction, are observed.

[231] Zhang, J., Liu, N. S., and Lu, X. Y., "Locomotion of a Passively Flapping Flat Plate," *Journal of Fluid Mechanics*, Vol. 659, Sep. 2010, pp. 43–68.

Keywords: 3-D, Numerical, Flat Plate

Abstract: Locomotion of a passively flapping flat plate has been studied numerically by means of a multiblock lattice Boltzmann method. A flexible plate is modelled by a rigid plate with a torsion spring acting about the pivot at the leading edge of the plate. A dynamic model of this kind is called a lumped-torsional-flexibility model. When the leading edge is forced to heave sinusoidally, the plate pitches passively and propels itself in the horizontal direction as a result of the fluid–plate interaction. We have investigated various aspects of the mechanics behind the behavior of the flapping plate, including the periodic- and non-periodic-flow states, the spontaneous motion of the plate, vortical structure and how they compare to similar propulsion systems in animals. In the periodic-flow regime, two dynamical responses of the passively pitching plate (forward and backward movements) are observed. Which movement will occur depends only on the frequency ratio F of the natural frequency of the system and the heaving frequency associated with the lumped torsional flexibility. It is found that the plate will select the forward movement when $F > 1$ and the backward movement when $F \leq 1$. In the forward-movement regime, analysis of the dynamical behaviors and propulsive properties of the passively pitching plate indicates that the torsional flexibility can remarkably improve the propulsive performance. In addition, four kinds of vortex structures in the near wake are identified, which mainly depend on the forward speed of the plate. Finally the forward movement is compared to the flapping-based locomotion of swimming and flying animals. The results obtained in this study are consistent with the observations and measurements of swimming and flying animals; thus, they may provide physical insights into understanding of the propulsive mechanisms of the flapping wings and fins of animals.

[232] Fritz, T. E., and Long, L. N., "Object-Oriented Unsteady Vortex Lattice Method for Flapping Flight," *Journal of Aircraft*, Vol. 41, No. 6, 2004, pp. 1275–1290.

Keywords: 3-D, Numerical, High-frequency

Abstract: The unsteady vortex lattice method is used to model the oscillating plunging, pitching, twisting, and flapping motions of a finite-aspect-ratio wing. Its potential applications include design and analysis of small unmanned air vehicles and in the study of the high-frequency flapping flight of birds and other small flyers. The results are verified by theory and, in the plunging and pitching cases, by experimental data. The model includes free-wake relaxation, vortex stretching, and vortex dissipation effects and is implemented using object-oriented computing techniques. The results show that the method is capable of accurately simulating many of the features of complex flapping flight.

[233] Yokoyama, N., Senda, K., Iima, M., and Hirai, N., "Aerodynamic Forces and Vortical Structures in Flapping Butterfly's Forward Flight," *Physics of Fluids*, Vol. 25, No. 2, 2013, pp. 021902-1–021902-24.

Keywords: 3-D, Numerical, Butterfly

Abstract: Forward flights of a bilaterally symmetrically flapping butterfly modeled as a four-link rigid-body system consisting of a thorax, an abdomen, and left and right wings are numerically simulated. The joint motions of the butterflies are adopted from experimental observations. Three kinds of the simulations, distinguished by ways to determine the position and attitude of the thorax, are carried out: a tethered simulation, a prescribed simulation, and free-flight simulations. The upward and streamwise forces as well as the wake structures in the tethered simulation, where the thorax of the butterfly is fixed, reasonably agree with those in the corresponding tethered experiment. In the prescribed simulation, where the thoracic trajectories as well as the joint angles are given by those observed in a free-

flight experiment, it is confirmed that the butterfly can produce enough forces to achieve the flapping flights. Moreover, coherent vortical structures in the wake and those on the wings are identified. The generation of the aerodynamic forces due to the vortical structures are also clarified. In the free-flight simulation, where only the joint angles are given as periodic functions of time, it is found that the free flight is longitudinally unstable because the butterfly cannot maintain the attitude in a proper range. Focusing on the abdominal mass, which largely varies owing to feeding and metabolizing, we have shown that the abdominal motion plays an important role in periodic flights. The necessity of control of the thoracic attitude for periodic flights and maneuverability is also discussed.

[234] Ramamurti, R., Sandberg, W., Valana, P., Kellogg, J., and Cylinder, D., "Computational Fluid Dynamics Study of Unconventional Air Vehicle Configurations," *Aeronautical Journal*, Vol. 109, July 2005. pp. 337–347.

Keywords: 3-D, Numerical, MAV

Abstract: Two unconventional micro air vehicles developed by the Naval Research Laboratory are described. One of the vehicles employs flapping wings which is inspired by the flight of birds or insects but does not copy it directly. The second vehicle is a stop-rotor hybrid vehicle employing a pair of single blade, rotary/fixed wing panels, attached at their roots to separate coaxial shafts. An unstructured grid based incompressible flow solver, called feflo, is used to simulate the flow past these novel configurations in order to determine the flight characteristics of these vehicles

[235] Ashraf, M. A., Young, J., Lai, J.C.S., and Platzer, M. F., "Aerodynamic Analysis of Flapping-Wing Propellers For HALE Aircraft," AIAA Paper 2009-0092, Jan. 2009.

Keywords: 3-D, Numerical, HALE Aircraft

Abstract: In a paper presented at the 26th Congress of the International Council of the Aeronautical Sciences, we proposed to apply the flapping-wing propellers and turbines which we developed for micro air vehicles and hydropower generators to the development of high-altitude long-endurance (HALE) vehicles and flying electric generators. Aerodynamic analyses using Navier-Stokes calculations at a Reynolds number of 1,000,000 are presented here to assess the feasibility and advantages of using flapping-wing propellers for HALE aircraft. A range of values has been examined for various parameters including oscillation frequency, plunge amplitude, pitch amplitude, angle of incidence and separation between the main wing and the trailing airfoils. Results show that while a reasonable lift coefficient can be achieved with the main wing, the propulsive efficiency of a HALE aircraft with trailing airfoils executing pure plunge motion is only in the vicinity of 1 percent. By employing combined pitch-plunge motions for the trailing airfoils, the overall thrust and efficiency are increased by at least 10 times and 25 times respectively within the range of parameter values examined.

[236] Liu H., and Kawachi, K., "Leading-Edge Vortices of Flapping and Rotary Wings at Low Reynolds Number," *Fixed and Flapping Wing Aerodynamics for Micro Air Vehicles*, AIAA, Danvers, MA, 2001, pp. 275–285.

Keywords: 3-D, Numerical, Vortices, Flapping vs Rotary

[237] Blondeaux, P., Fornarelli, F., Guglielmini, L., Triantafyllou, M. S., and Verzicco, R., "Numerical Experiments on Flapping Foils Mimicking Fish-like Locomotion," *Physics of Fluids*, Vol. 17, No. 11, 2005, pp. 113601-1–113601-12.

Keywords: 3-D, Numerical, Vortices

Abstract: The results of numerical experiments aimed at investigating the topology of the vortex structures shed by an oscillating foil of finite span are described. The motion of the foil and its geometry are chosen to mimic the tail of a fish using the carangiform swimming. The numerical results have been compared with the flow visualizations of Freymuth [J. Fluids Eng.111, 217 (1989)] and those of von Ellenrieder *et al.* [J. Fluid Mech.490, 129 (2003)]. The results show that a vortex ring is shed by the oscillating foil every half a cycle. The dynamics of the vortex rings depends on the Strouhal number St. For relatively small values of St, the interaction between adjacent rings is weak and they are mainly convected downstream by the free stream. On the other hand, for relatively large values of St, a strong interaction among adjacent rings takes place and the present results suggest the existence of reconnection phenomena, which create pairs of longitudinal counter-rotating vortices.

[238] Chandar, D. D. J., and Damodaran, M., "Computation of Unsteady Low Reynolds Number Free-Flight Aerodynamics of Flapping Wings," *Journal of Aircraft*, Vol. 47, No. 1, 2010, pp. 141–150.

Keywords: 3-D, Numerical, Vortices

Abstract: The observation that thrust is produced when a wing flaps above a particular reduced frequency at low Reynolds numbers has been associated with the formation of a reverse Karman vortex street. Through experiments,

numerical computations, and analytical methods, scientists have been able to explain thrust generation in birds and insects. This has increased the interest in the development of micro aerial vehicles. There is, however, a paucity of experimental or computational studies that explain the basic mechanism of thrust generation from the viewpoint of the surrounding vortical structures and the effect of these vortices on free flight when the wing is accelerating in the direction of thrust. In the present work, three-dimensional free-flight computations are carried out on flapping wings that have rectangular planforms composed of NACA 0012 and an elliptical airfoil section, respectively, to demonstrate that thrust is generated as a result of vortex asymmetry. Based on the computed vortex dynamics, it is also shown that the relative convection rates of positive and negative vorticity are a key parameter involved in thrust generation. Numerical computations are performed using the unsteady three-dimensional Navier-Stokes solver composite grid incompressible Navier-Stokes, which is based on the Overture framework for overlapping grids. Comparative analysis with existing experimental/computational data is also presented.

[239] Harbig, R. R., Sheridan, J., and Thompson, M. C., "The Role of Advance Ratio and Aspect Ratio in Determining Leading-Edge Vortex Stability for Flapping Flight," *Journal of Fluid Mechanics*, Vol. 751, July 2014, pp. 71–105.

Keywords: 3-D, Numerical, Vortices

Abstract: The effects of advance ratio and the wing's aspect ratio on the structure of the leading-edge vortex (LEV) that forms on flapping and rotating wings under insect-like flight conditions are not well understood. However, recent studies have indicated that they could play a role in determining the stable attachment of the LEV. In this study, a numerical model of a flapping wing at insect Reynolds numbers is used to explore the effects of these parameters on the characteristics and stability of the LEV. The word 'stability' is used here to describe whether the LEV was attached throughout the stroke or if it was shed. It is demonstrated that increasing the advance ratio enhances vorticity production at the leading edge during the downstroke, and this results in more rapid growth of the LEV for non-zero advance ratios. Increasing the wing aspect ratio was found to have the effect of shortening the wing's chord length relative to the LEV's size. These two effects combined determine the stability of the LEV. For high advance ratios and large aspect ratios, the LEV was observed to quickly grow to envelop the entire wing during the early stages of the downstroke. Continued rotation of the wing resulted in the LEV being eventually shed as part of a vortex loop that peels away from the wing's tip. The shedding of the LEV for high-aspect-ratio wings at non-zero advance ratios leads to reduced aerodynamic performance of these wings, which helps to explain why a number of insect species have evolved to have low-aspect-ratio wings.

[240] Rayner, J. M. V., "A Vortex Theory of Animal Flight. Part 2. The Forward Flight of Birds," *Journal of Fluid Mechanics*, Vol. 91, Apr. 1979, pp. 731–763.

Keywords: 3-D, Numerical, Vortices

Abstract: The vortex wake of a bird in steady forward flight is modelled by a chain of elliptical vortex rings, each generated by a single downstroke. The shape and inclination of each ring are determined by the downstroke geometry, and the size of each ring by the wing circulation; the momentum of the ring must overcome parasitic and profile drags and the bird's weight for the duration of a stroke period. From the equation of motion it is possible to determine exactly the kinematics of the wing-stroke for any flight velocity. This approach agrees more readily with the nature of the wing-stroke than the classical actuator disk and momentum-jet theory; it also dispenses with lift and induced drag coefficients and is not bound by the constraints of steady-state aerodynamics. The induced power is calculated as the mean rate of increase of wake kinetic energy. The remaining components of the flight power (parasite and profile) are calculated by traditional methods; there is some consideration of different representations of body parasite drag. The lift coefficient required for flight is also calculated; for virtually all birds the lift coefficient in slow flight and hovering is too large to be consistent with steady-state aerodynamics. A bird is concerned largely to reduce its power consumption on all but the shortest flights. The model suggests that there are a number of ways in which power reduction can be achieved. These various strategies are in good agreement with observation.

[241] Shyy, W., Aono, H., Chimakurthi, S. K., Trizila, P., Kang, C. K., Cesnik, C. E. S., Liu, H., "Recent Progress in Flapping Wing Aerodynamics and Aeroelasticity," *Progress in Aerospace Sciences*, Vol. 46, No. 7, 2010, pp. 284–327.

Keywords: 3-D, Numerical, Vortices

Abstract: Micro air vehicles (MAVs) have the potential to revolutionize our sensing and information gathering capabilities in areas such as environmental monitoring and homeland security. Flapping wings with suitable wing kinematics, wing shapes, and flexible structures can enhance lift as well as thrust by exploiting large-scale vortical flow structures under various conditions. However, the scaling invariance of both fluid dynamics and structural

dynamics as the size changes is fundamentally difficult. The focus of this review is to assess the recent progress in flapping wing aerodynamics and aeroelasticity. It is realized that a variation of the Reynolds number (wing sizing, flapping frequency, etc.) leads to a change in the leading edge vortex (LEV) and spanwise flow structures, which impacts the aerodynamic force generation. While in classical stationary wing theory, the tip vortices (TiVs) are seen as wasted energy, in flapping flight, they can interact with the LEV to enhance lift without increasing the power requirements. Surrogate modeling techniques can assess the aerodynamic outcomes between two- and three-dimensional wing. The combined effect of the TiVs, the LEV, and jet can improve the aerodynamics of a flapping wing. Regarding aeroelasticity, chordwise flexibility in the forward flight can substantially adjust the projected area normal to the flight trajectory via shape deformation, hence redistributing thrust and lift. Spanwise flexibility in the forward flight creates shape deformation from the wing root to the wing tip resulting in varied phase shift and effective angle of attack distribution along the wing span. Numerous open issues in flapping wing aerodynamics are highlighted.

[242] Smith, M., Wilkin, P., and Williams, M., "The advantages of an unsteady panel method in modelling the aerodynamic forces on rigid flapping wings," *Journal of Experimental Biology*, Vol. 199, May 1996, pp. 1073–1083.

Keywords: 3-D, Numerical, Vortices

Abstract: This paper responds to research into the aerodynamics of flapping wings and to the problem of the lack of an adequate method which accommodates large-scale trailing vortices. A comparative review is provided of prevailing aerodynamic methods, highlighting their respective limitations as well as strengths. The main advantages of an unsteady aerodynamic panel method are then introduced and illustrated by modelling the flapping wings of a tethered sphingid moth and comparing the results with those generated using a quasi-steady method. The improved correlations of the aerodynamic forces and the resultant graphics clearly demonstrate the advantages of the unsteady panel method (namely, its ability to detail the trailing wake and to include dynamic effects in a distributed manner).

[243] Wang, X. X., and Wu, Z. N., "Stroke-Averaged Lift Forces Due to Vortex Rings and Their Mutual Interactions for a Flapping Flight Model," *Journal of Fluid Mechanics*, Vol. 654, July 2010, pp. 453–472.

Keywords: 3-D, Numerical, Vortices

Abstract: The stroke-averaged lift forces due to various vortex rings and their mutual interactions are studied using a flapping flight vortex model (Rayner, *J. Fluid Mech.*, vol. 91, 1979, p. 697; Ellington, *Phil. Trans. R. Soc. Lond.* B, vol. 305, 1984*b*, p. 115). The vortex system is decomposed into the wing plane (wing-linked) vortex ring, a loop closed by the bound vortex and (arc-shaped) trailing vortex and the wake (the vortex rings shed previously). Using the vorticity moment theory (Wu, *AIAA J.*, vol. 19, 1981, p. 432) we are able to identify the roles of vortex rings in lift production or reduction and express the lift as function of areal contraction or expansion of vortex rings. The wake vortex rings induce areal contraction of the trailing vortex, which should decrease the lift, but this decrease is exactly compensated by the inducing effect of the trailing arc on the wake. The wake reduces the lift through inducing a downwash velocity on the wing plane. The lift force is shown to drop to a minimum at the second half stroke, and then increases to an asymptotic value slightly below the lift at the first half stroke, in such a way following the experimental observation of Birch & Dickinson (*Nature*, vol. 412, 2001, p. 729). The existence of the negative peak of lift is due to the first shed vortex ring which, just at the second half stroke, lies in the close vicinity to the wing plane, leading to a peak of the wing plane downwash velocity.

[244] Zhu, Q., Wolfgang, M. J., Yue, D. K. P., and Triantafyllou, M. S., "Three-Dimensional Flow Structures and Vorticity Control in Fish-like Swimming," *Journal of Fluid Mechanics*, Vol. 468, Oct. 2002, pp. 1–28.

Keywords: 3-D, Numerical, Wake

Abstract: We employ a three-dimensional, nonlinear inviscid numerical method, in conjunction with experimental data from live fish and from a fish-like robotic mechanism, to establish the three-dimensional features of the flow around a fish-like body swimming in a straight line, and to identify the principal mechanisms of vorticity control employed in fish-like swimming. The computations contain no structural model for the fish and hence no recoil correction. First, we show the near-body flow structure produced by the travelling-wave undulations of the bodies of a tuna and a giant danio. As revealed in cross-sectional planes, for tuna the flow contains dominant features resembling the flow around a two-dimensional oscillating plate over most of the length of the fish body. For the giant danio, on the other hand, a mixed longitudinal–transverse structure appears along the hind part of the body. We also investigate the interaction of the body-generated vortices with the oscillating caudal fin and with tail-generated vorticity. Two distinct vorticity interaction modes are identified: the first mode results in high thrust and is generated by constructive pairing of body-generated vorticity with same-sign tail-generated vorticity, resulting in the formation of a strong thrust wake;

the second corresponds to high propulsive efficiency and is generated by destructive pairing of body-generated vorticity with opposite-sign tail-generated vorticity, resulting in the formation of a weak thrust wake.

[245] Vest, M., and Katz, J., "Unsteady Aerodynamic Model of Flapping Wings," *AIAA Journal*, Vol. 34, No. 7, 1996, pp. 1435–1440.

Keywords: 3-D, Numerical, Model

Abstract: Propulsive forces can be generated with flapping or heaving wing traveling through a fluid, as demonstrated in animal flight. To examine the flowfield around variable geometry bodies, with specific application to the unsteady flow associated with flapping wings, an unsteady, three-dimensional, incompressible, potential flow model was developed. The problem is formulated in an inertial reference frame such that the body moves through an otherwise quiescent fluid. Results were compared with the limited experimental results available and analytical methods. In one case the model was applied to a flapping wing in a wind tunnel at high advance ratios (J=4.31) where the computed average lift and thrust were within the error bounds of the experimental data. The model was also applied to high-frequency flapping flight (J=0.76) of a pigeon flying in a wind tunnel, where the predicted lift matched the weight of the bird.

[246] Liu, H., "Computational Biological Fluid Dynamics: Digitizing and Visualizing Animal Swimming and Flying," *Integrative and Comparative Biology*, Vol. 42, No. 5, 2002, pp. 1050–1059.

Keywords: 3-D, Numerical, Modeling

Abstract: Characterized by complex geometry and complicated dynamic process, biological fluid dynamics in swimming and flying is usually of large scale vortex flows with four-dimensional nature, namely, spatial three-dimensional and one-dimensional in time. Conventional theories for understanding power and energetics in swimming and flying rely exclusively on the consistent potential flow formulation in qualitatively analyzing the physics as well as the observations and measurements in visualizing the flows so as to support the theories. In the present paper we address a new paradigm of the so-called, *simulation-based biological fluid dynamics* that can digitize and visualize swimming and flying by using computational mechanical modeling of the biological fluid dynamics through faithful reconstruction of morphology and realistic representation of kinematics of an individual object. We demonstrate an integrated computational system as a baseline for the simulation-based biological fluid dynamics, which involves four subsystems of the morphological modeling, the kinematic modeling, the computational fluid dynamic modeling, and the post-processing for visualization. Applications of a realistic model of insect flapping flight and an extensive study on the Micro Air Vehicle are then presented and discussed.

[247] Brunton, S. L., Rowley, C. W., and Williams, D. R., "Reduced-Order Unsteady Aerodynamic Models at Low Reynolds Numbers," *Journal of Fluid Mechanics*, Vol. 724, June 2013, pp. 203–233.

Keywords: 2-D and 3-D, Numerical, Models

Abstract: In this paper we develop reduced-order models for the unsteady lift on a pitching and plunging aerofoil over a range of angles of attack. In particular, we analyze the pitching and plunging dynamics for two cases: a two-dimensional flat plate at Re= 100 using high-fidelity direct numerical simulations and a three-dimensional NACA 0006 aerofoil at Re= 65,000 using wind-tunnel measurements. Models are obtained at various angles of attack and they are verified against measurements using frequency response plots and large-amplitude maneuvers. These models provide a low-dimensional balanced representation of the relevant unsteady fluid dynamics. In simulations, flow structures are visualized using finite-time Lyapunov exponents. A number of phenomenological trends are observed, both in the data and in the models. As the base angle of attack increases, the boundary layer begins to separate, resulting in a decreased quasi-steady lift coefficient slope and a delayed relaxation to steady state at low frequencies. This extends the low-frequency range of motions that excite unsteady effects, meaning that the quasi-steady approximation is not valid until lower frequencies than are predicted by Theodorsen's classical inviscid model. In addition, at small angles of attack, the lift coefficient rises to the steady-state value after a step in angle, while at larger angles of attack, the lift coefficient relaxes down to the steady-state after an initially high lift state. Flow visualization indicates that this coincides with the formation and convection of vortices at the leading edge and trailing edge. As the angle of attack approaches the critical angle for vortex shedding, the poles and zeroes of the model approach the imaginary axis in the complex plane, and some zeroes cross into the right half plane. This has significant implications for active flow control, which are discussed. These trends are observed in both simulations and wind-tunnel data.

[248] Isogai, K., and Harino, Y., "Optimum Aeroelastic Design of a Flapping Wing," *Journal of Aircraft*, Vol. 44, No. 6, 2007, pp. 2040–2048.

Keywords: 3-D, Numerical, Design, Optimization

Abstract: A method is presented for the optimum aeroelastic design of a flapping wing employing a lifting-surface theory as an aerodynamic tool and the complex method as the optimization algorithm. The method is applied to the optimum design of a flapping wing of a Kite Hawk unmanned air vehicle and the optimum thickness distribution of the main spar is determined. As a result of the optimization, a high propulsive efficiency of 75% is attained considering only dihedral flapping of the main spar. By evaluating the viscous effect for this optimum design using a three-dimensional Navier-Stokes code, the effectiveness of the design is confirmed.

[249] Willis, D. J., and Persson, P. O., "Multiple-Fidelity Computational Framework for the Design of Efficient Flapping Wings," *AIAA Journal*, Vol. 52, No. 12, 2014, pp. 2840–2854.

Keywords: 3-D, Numerical, Design

Abstract: A multiple-fidelity computational framework is presented for designing energetically efficient flapping wings. The goal of this design process is to achieve specific aerodynamics characteristics, namely prescribed lift and thrust coefficients at low energetic cost. The wing kinematics (flapping frequency, flapping amplitude) and the resulting optimal wake-circulation distribution (wake circulation/vorticity strength and wake shape) are determined using a low-order, wake-only, energetics method. A quasi-inverse, doublet-lattice method is used to determine the detailed flapping-wing geometry corresponding to the optimal wake. Because of the efficiency of potential flow approximations, the wake-only method and quasi-inverse, doublet-lattice method tools can explore a large number of wing kinematics and wing-morphing strategies efficiently; however, only a handful of those wing designs will achieve the desired performance in the physical low-Reynolds-number, viscous-flow regime. Thus, a high-order, discontinuous Galerkin, Navier–Stokes method is employed at the end of the process to assess which candidate wing designs meet the original design criteria in real fluids.

[250] Hall, K. C., and Hall, S. R., "Minimum Induced Power Requirements for Flapping Flight," *Journal of Fluid Mechanics*, Vol. 323, Sep. 1996, pp. 285–315.

Keywords: 3-D, Numerical, Optimization, Circulation

Abstract: The Betz criterion for minimum induced loss is used to compute the optimal circulation distribution along the span of flapping wings in fast forward flight. In particular, we consider the case where flapping motion is used to generate both lift (weight support) and thrust. The Betz criterion is used to develop two different numerical models of flapping. In the first model, which applies to small-amplitude harmonic flapping motions, the optimality condition is reduced to a one-dimensional integral equation which we solve numerically. In the second model, which applies to large-amplitude periodic flapping motions, the optimal circulation problem is reduced to solving for the flow over an infinitely long wavy sheet translating through an inviscid fluid at rest at infinity. This three-dimensional flow problem is solved using a vortex-lattice technique. Both methods predict that the induced power required to produce thrust decreases with increasing flapping amplitude and frequency. Using the large-amplitude theory, we find that the induced power required to produce lift increases with flapping amplitude and frequency. Therefore, an optimum flapping amplitude exists when the flapping motion of wings must simultaneously produce lift and thrust.

[251] Rozhdestvensky, K. V., and Ryzhov, V. A., "Aerohydrodynamics of Flapping-wing Propulsors," *Progress in Aerospace Sciences*, Vol. 39, No. 8, 2003, pp. 585–633.

Keywords: 3-D, Numerical, Summary

Abstract: It is the objective of this survey to review research and development results of flapping-wing propulsors and of vehicles equipped with them. Given the complex and multi-disciplinary character of the problem, a wide range of questions is considered in order to provide a general idea of the state-of-the-art. The main attention is directed at the aerohydrodynamics of flapping-wing propulsors. The major relevant mathematical models and the corresponding numerical results are presented together with the experimental data obtained up to the present time. Also, the physical and the design factors are discussed, which affect the aerohydrodynamic characteristics of flapping wings and that therefore have to be accounted for in the modern mathematical models. Experimental data and numerical modeling results are compared to determine domains of validity of the latter for the aerohydrodynamic design of full-scale air and marine vehicles. Also, existing engineering solutions for vehicles with flapping-wing propulsors are presented and prospective directions for future investigations are outlined.

[252] Phillips, W. F., and Snyder, D. O., "Modern Adaptation of Prandtl's Classic Lifting-Line Theory," *Journal of Aircraft*, Vol. 37, No. 4, 2000, pp. 662–670.

Keywords: 3-D, Numerical, Lifting-line

Abstract: The classical solution to Prandtl"s well-known lifting-line theory applies only to a single lifting surface with no sweep and no dihedral. However, Prandtl's original model of a finite lifting surface has much broader applicability. A general numerical lifting-line method based on Prandtl's model is presented. Whereas classical lifting-line theory is based on applying the two-dimensional Kutta-Joukowski law to a three-dimensional flow, the present method is based on a fully three-dimensional vortex lifting law. The method can be used for systems of lifting surfaces with arbitrary camber, sweep, and dihedral. The accuracy realized from this method is shown to be comparable to that obtained from numerical panel methods and inviscid computational fluid dynamics solutions, but at a small fraction of the computational cost.

[253] Phillips, W. F., Fugal, S. R., and Spall, R. E., "Minimizing Induced Drag with Wing Twist, Computational-Fluid-Dynamics Validation," *Journal of Aircraft*, Vol. 43, No. 2, 2006, pp. 437–444.

Keywords: 3-D, Numerical, Lifting-line

Abstract: A more practical analytical solution for the effects of wing twist on the performance of a finite wing of arbitrary planform has recently been presented. This infinite series solution is based on Prandtl's classical lifting-line theory, and the Fourier coefficients are presented in a form that depends only on wing geometry. Except for the special case of an elliptic planform, this solution shows that, if properly chosen, wing twist can be used to reduce the induced drag for a wing producing finite lift. A relation for the optimum twist distribution on a wing of arbitrary planform was presented. If this optimum twist distribution is used, the new solution predicts that a wing of any planform can be designed for a given lift coefficient to produce induced drag at the same minimum level as an elliptic wing having the same aspect ratio and no twist. In the present paper, results predicted from this new lifting-line solution are compared with results predicted from computational-fluid-dynamics (CFD) solutions. In all cases, the CFD solutions showed that the drag reduction achieved with optimum twist was equal to or greater than that predicted by lifting-line theory.

[254] Moore, M. N. J., "Analytical Results on the Role of Flexibility in Flapping Propulsion," *Journal of Fluid Mechanics*, Vol. 757, Oct. 2014, pp. 599–612.

Keywords: 3-D, Numerical and Experimental, Flexibility

Abstract: Wing or fin flexibility can dramatically affect the performance of flying and swimming animals. Both laboratory experiments and numerical simulations have been used to study these effects, but analytical results are notably lacking. Here, we develop small-amplitude theory to model a flapping wing that pitches passively due to a combination of wing compliance, inertia and fluid forces. Remarkably, we obtain a class of exact solutions describing the wing's emergent pitching motions, along with expressions for how thrust and efficiency are modified by compliance. The solutions recover a range of realistic behaviors and shed new light on how flexibility can aid performance, the importance of resonance, and the separate roles played by wing and fluid inertia. The simple robust estimates afforded by our theory may prove valuable even in situations where details of the flapping motion and wing geometry differ.

[255] Spagnolie, S. E., Moret, L., Shelley, M. J., and Zhang, J., "Surprising Behaviors in Flapping Locomotion with Passive Pitching," *Physics of Fluids*, Vol. 22, No. 4, 2010, pp. 041903-1–041903-20.

Keywords: 3-D, Numerical and Experimental, Flexibility

Abstract: To better understand the role of wing and fin flexibility in flapping locomotion, we study through experiment and numerical simulation a freely moving wing that can "pitch" passively as it is actively heaved in a fluid. We observe a range of flapping frequencies corresponding to large horizontal velocities, a regime of underperformance relative to a clamped (nonpitching) flapping wing, and a surprising, hysteretic regime in which the flapping wing can move horizontally in either direction (despite left/right symmetry being broken by the specific mode of pitching). The horizontal velocity is shown to peak when the flapping frequency is near the immersed system's resonant frequency. Unlike for the clamped wing, we find that locomotion is achieved by vertically flapped symmetric wings with even the slightest pitching flexibility, and the system exhibits a continuous departure from the Stokesian regime. The phase difference between the vertical heaving motion and consequent pitching changes continuously with the flapping frequency, and the direction reversal is found to correspond to a critical phase relationship. Finally, we show a transition from coherent to chaotic motion by increasing the wing's aspect ratio, and then a return to coherence for flapping bodies with circular cross section.

[256] Jones, K. D., Castro, B. M., Mahmoud, O., and Platzer, M. F., "A Numerical and Experimental Investigation of Flapping Wing Propulsion in Ground Effect," AIAA Paper 2002-0866, Jan. 2002.

Keywords: 3-D, Numerical and Experimental, Ground Effect

Abstract: An experimental and numerical investigation of flapping-wing propulsion in ground effect is undertaken. Flying in ground effect is shown to have substantial performance advantages both in thrust and efficiency. To gain the performance advantage without requiring flight in the proximity of the ground, a bi-plane configuration is designed, providing increased performance as well as inherent balanced mechanical and aerodynamic loading. A high aspect-ratio experimental model is tested both qualitatively and quantitatively, using a smoke-wire for flow visualization, laser Doppler velocimetry for unsteady flow measurements, and a direct approach for thrust measurement. The configuration is simulated numerically using a two-dimensional, unsteady, inviscid panel code with a deforming wake model, and a two-dimensional, unsteady, compressible Navier-Stokes solver. The Navier-Stokes solver is used with a three-block, deforming grid, and it is run on a Beowulf Linux parallel cluster. Direct comparisons of thrust are made, as well as qualitative comparisons of the vortical wake structures produced by the wing-flapping. A strong Reynolds-number dependence is shown, reducing or eliminating the benefits of wake-interference at Reynolds numbers on the order of 10,000.

[257] Isaac, K. M., Rolwes, J., and Colozza, A., "Aerodynamics of a Flapping and Pitching Wing Using Simulations and Experiments," *AIAA Journal*, Vol. 46, No. 6, 2008, pp. 1505–1515.

Keywords: 3-D, Numerical and Experimental, Flat Plate

Abstract: Computational fluid dynamics simulation results for a thin cambered plate airfoil, and flow visualization and force measurements from experiments conducted in water on a flapping-and-pitching thin flat-plate wing of semi-elliptic planform at low Reynolds numbers are reported. Time-varying force data, measured using a force transducer, provide a means to understand the mechanisms that lead to enhanced performance observed in insect flight compared with fixed-wing aerodynamics. Experimental uncertainties associated with low-level (~1 N) fluid dynamic force measurements on flapping-and-pitching wings, including inertia effects, are addressed. A previously proposed pitching mode in which the leading-edge and trailing-edge switch roles to allow using cambered airfoils is shown to be feasible. A vortex-trapping model is proposed to explain the aerodynamic advantages of switching. The present results also support the authors' proposed idea that an optimum reduced flapping frequency might exist. The study has applications in micro air vehicle development.

[258] Jones, K. D., Lund, T. C., and Platzer, M. F., "Experimental and Computational Investigation of Flapping Wing Propulsion for Micro Air Vehicles," *Fixed and Flapping Wing Aerodynamics for Micro Air Vehicles*, AIAA, Danvers, MA, 2001, pp. 307–339.

Keywords: 3-D, Numerical and Experimental, Summary

[259] Alben, S., "Optimal Flexibility of a Flapping Appendage in an Inviscid Fluid," *Journal of Fluid Mechanics*, Vol. 614, Nov. 2008, pp. 355–380.

Keywords: 3-D, Numerical and Analytical, Flexibility

Abstract: We present a new formulation of the motion of a flexible body with a vortex-sheet wake and use it to study propulsive forces generated by a flexible body pitched periodically at the leading edge in the small-amplitude regime. We find that the thrust power generated by the body has a series of resonant peaks with respect to rigidity, the highest of which corresponds to a body flexed upwards at the trailing edge in an approximately one-quarter-wavelength mode of deflection. The optimal efficiency approaches 1 as rigidity becomes small and decreases to 30–50% (depending on pitch frequency) as rigidity becomes large. The optimal rigidity for thrust power increases from approximately 60 for large pitching frequency to ∞ for pitching frequency 0.27. Subsequent peaks in response have power-law scalings with respect to rigidity and correspond to higher-wavenumber modes of the body. We derive the power-law scalings by analyzing the fin as a damped resonant system. In the limit of small driving frequency, solutions are self-similar at the leading edge. In the limit of large driving frequency, we find that the distribution of resonant rigidities $\sim k^{-5}$, corresponding to fin shapes with wavenumber k. The input power and output power are proportional to rigidity (for small-to-moderate rigidity) and to pitching frequency (for moderate-to-large frequency). We compare these results with the range of rigidity and flapping frequency for the hawkmoth forewing and the bluegill sunfish pectoral fin.

[260] Orchini, A., Mazzino, A., Guerrero, J., Festa, R., and Boragno, C., "Flapping States of an Elastically Anchored Plate in a Uniform Flow with Applications to Energy Harvesting by Fluid-Structure Interaction," *Physics of Fluids*, Vol. 25, No. 9, 2013, pp. 097105-1–097105-17.

Keywords: 3-D, Numerical and Analytical, Flat Plate

Abstract: Linear stability analysis of an elastically anchored flat plate in a uniform flow is investigated both analytically and numerically. The analytical formulation explicitly takes into account the effect of the wake on the plate

by means of Theodorsen's theory. Three different parameters non-trivially rule the observed dynamics: mass density ratio between plate and fluid, spring elastic constant, and distance between the plate center of mass and the spring anchor point on the plate. We found relationships between these parameters which rule the transition between stable equilibrium and fluttering. The shape of the resulting marginal curve has been successfully verified by high Reynolds number numerical simulations. Finally, the limiting case corresponding to a simply supported rigid rod is also analyzed and the resulting flapping instability traced back to a simple resonance condition. Our findings are of interest in applications related to energy harvesting by fluid-structure interaction, a problem that has recently attracted a great deal of attention. The main aim in that context is to identify the optimal physical/geometrical system configuration leading to large sustained motion, which is the source of energy one aims to extract.

[261] CD-adapco, "User Guide: Star-CCM+ Version 8.06," 2013, pp. 1–13268.

Keywords: CFD

[262] Alley, N. R., Phillips, W. F., and Spall, R. E., "Predicting Maximum Lift Coefficient for Twisted Wings Using Computational Fluid Dynamics," *Journal of Aircraft*, Vol. 44, No. 3, pp. 911–917.

Keywords: CFD, Twist

Abstract: A method is presented that allows one to predict the maximum lift coefficient for a finite wing from knowledge of wing geometry and maximum airfoil section lift coefficient. This approach applies to wings of arbitrary planform and includes the effects of twist and sweep. The method uses a correlation obtained from grid-resolved computational fluid dynamics solutions for 25 different wing geometries. These wings had aspect ratios ranging from 4 to 20, taper ratios from 0.5 to 1.0, quarter-chord sweep angles from 0 to 30 deg, and linear geometric washout ranging from 0 to 8 deg. For this range of parameters, the ratio of maximum wing lift coefficient to maximum airfoil section lift coefficient varied from about 0.70 to 0.98, with high-aspect-ratio tapered wings producing the highest values and low-aspect-ratio wings with washout and sweep producing the lowest values.

[263] Richardson, L.F., "The Approximate Arithmetical Solution by Finite Differences of Physical Problems Involving Differential Equations, with an Application to the Stresses in a Masonry Dam," *Philosophical Transactions of the Royal Society A*, Vol. 210, Jan. 1911, pp. 307–357.

Keywords: 3-D, Numerical and Analytical, Richardson Extrapolation

Abstract: The object of this paper is to develop methods whereby the differential equations of physics may be applied more freely than hitherto in the approximate form of difference equations to problems concerning irregular bodies.

APPENDIX D

TABLES OF DATA USED FOR PLOTTING

Table 17 Data Used to Create Figure 20

Angle of Attack	Coarse Grid	Medium Grid	Fine Grid	Richardson Extrapolation	Exact Solution
-4	0.198844737	0.164328605	0.128062865	-0.29124951	0.123207501
-3	0.284253681	0.263272244	0.249186297	0.219325849	0.246377472
-2	0.391582551	0.379087117	0.371129953	0.356736847	0.369472394
-1	0.501704388	0.495990689	0.493283117	0.490807121	0.492454772
0	0.61105882	0.61463145	0.615532119	0.615835718	0.615287142
1	0.713524042	0.733767847	0.73785432	0.738887951	0.737932091
2	0.818623901	0.849541883	0.859448506	0.864125006	0.860352258
3	0.919778415	0.961488063	0.979515528	0.99329624	0.982510353
4	0	1.07020671	1.099188994	1.100005509	1.104369167

Table 18 Data Used to Create Figure 21

Angle of Attack	Coarse Grid	Medium Grid	Fine Grid	Richardson Extrapolation	Exact Solution
-4	0.184164878	0.141775344	0.127285452	0.119760015	0.123207501
-3	0.283965154	0.257390317	0.248830726	0.244763804	0.246377472
-2	0.388702698	0.375808657	0.370761929	0.367516301	0.369472394
-1	0.498332116	0.495173137	0.493029918	0.488507791	0.492454772
0	0.60924072	0.614786963	0.615367896	0.615435864	0.615287142
1	0.717252852	0.733914618	0.73732534	0.738203236	0.737932091
2	0.826889562	0.851222664	0.858787836	0.862201007	0.860352258
3	0.923283375	0.966340119	0.979467398	0.985225119	0.982510353
4	1.009884644	1.078051166	1.09879856	1.107876212	1.104369167

Table 19 Data Used to Create Figure 22

Angle of Attack	Coarse Grid	Medium Grid	Fine Grid	Richardson Extrapolation	Exact Solution
-5	0.130895251	0.030655507	0.006398202	-0.001345914	0
-4	0.184000442	0.141234468	0.126551872	0.118875492	0.123207501
-3	0.283987208	0.25698372	0.248283662	0.244148316	0.246377472
-2	0.389279931	0.375988971	0.370866955	0.367655396	0.369472394
-1	0.499274452	0.496069319	0.493857842	0.488935986	0.492454772
0	0.610560026	0.616097163	0.616692308	0.61676398	0.615287142
1	0.718482052	0.735117998	0.738637289	0.73958154	0.737932091
2	0.827010819	0.851418784	0.859212865	0.862869306	0.860352258
3	0.920172361	0.964454416	0.97777692	0.983509855	0.982510353
4	1.004468033	1.07249584	1.093348956	1.102566875	1.104369167

5	1.084108288	1.17405956	1.205868922	1.223271782	1.225891578

Table 20 Data Used to Create Figure 23

Angle of Attack	Coarse Grid	Medium Grid	Fine Grid	Richardson Extrapolation	Exact Solution
-5	0.122463826	0.03091994	0.006428571	-0.002517061	0
-4	0.183900485	0.141357622	0.126918408	0.119499765	0.123207501
-3	0.283853229	0.257211462	0.248666193	0.244631068	0.246377472
-2	0.389106723	0.376134546	0.371088019	0.367874727	0.369472394
-1	0.499238336	0.496052751	0.493912455	0.489530066	0.492454772
0	0.610560026	0.616097163	0.616692308	0.61676398	0.615287142
1	0.718617043	0.735301215	0.738741378	0.739634968	0.737932091
2	0.827733683	0.852098045	0.859710165	0.863169068	0.860352258
3	0.92278993	0.965905086	0.979081081	0.984879735	0.982510353
4	1.00726049	1.075302434	1.096078263	1.105210283	1.104369167
5	1.087911728	1.178508559	1.21057776	1.228149521	1.225891578

Table 21 Data Used to Create Figure 24

Angle of Attack	Coarse Grid	Medium Grid	Fine Grid	Richardson Extrapolation	Exact Solution
-5	0.122426065	0.03091994	0.006428571	-0.002522102	0
-4	0.183900485	0.141357622	0.126918408	0.119499765	0.123207501
-3	0.283853229	0.257211462	0.248666193	0.244631068	0.246377472
-2	0.389106723	0.376134546	0.371088019	0.367874727	0.369472394
-1	0.499238336	0.496052751	0.493912455	0.489530066	0.492454772
0	0.610560026	0.616097163	0.616692308	0.61676398	0.615287142
1	0.718617043	0.735301215	0.738741378	0.739634968	0.737932091
2	0.827733683	0.852098045	0.859710165	0.863169068	0.860352258
3	0.92278993	0.965905086	0.979081081	0.984879735	0.982510353
4	1.00726049	1.075302434	1.096078263	1.105210283	1.104369167
5	1.087911728	1.178508559	1.21057776	1.228149521	1.225891578

Table 22 Data Used to Create Figure 25

Angle of Attack	Rotate Grid	Rotate Freestream	Translate Grid
-5	0.001345914	0.002517061	0.002522102
-4	0.004332009	0.003707736	0.003707736
-3	0.002229156	0.001746404	0.001746404
-2	0.001816998	0.001597668	0.001597668
-1	0.003518786	0.002924706	0.002924706
0	-0.001476837	-0.001476837	-0.001476837
1	-0.001649449	-0.001702878	-0.001702878

2	-0.002517048	-0.002816811	-0.002816811
3	-0.000999501	-0.002369382	-0.002369382
4	0.001802292	-0.000841116	-0.000841116
5	0.002619796	-0.002257943	-0.002257943

Table 23 Data Used to Create Figure 26

Angle of Attack	j=89, i=25	j=89, i=33	j=89, i=17	j=97, i=25	j=81, i=25
-4	-0.00164436	-0.00297	0.00126	-0.00162	-0.00168
-3	-0.00048379	-0.00166	0.002496	-0.00054	-0.00058
-2	-0.00026521	-0.00102	0.002766	-0.0002	-0.00023
-1	1.52286E-05	-0.00092	0.002261	-7.8E-05	-0.00011
0	-0.0008792	-0.0014	0.00072	-0.00098	-0.00094
1	-0.00125681	-0.00153	-0.00035	-0.00138	-0.00143
2	-0.0025204	-0.00186	-0.00224	-0.0024	-0.0025
3	-0.00260331	-0.0017	-0.00371	-0.0027	-0.00287
4	-0.00283714	-0.00087	-0.00659	-0.00267	-0.003
3	-0.00163275	-0.00072	-0.00221	-0.00146	-0.00156
2	-0.0010199	-0.0009	-0.00056	-0.00095	-0.00102
1	-0.00045626	-0.00077	-0.00049	-0.00041	-0.00048
0	-0.00033924	-0.00068	0.001076	-0.0003	-0.00035
-1	0.000279398	-0.00064	0.001633	0.000303	0.000266
-2	0.00021425	-0.00092	0.003046	0.000217	0.00022
-3	-0.00045464	-0.00169	0.002706	-0.00041	-0.00043

Table 24 Data Used to Create Figure 27

Angle of Attack	Coarse Grid	Medium Grid	Fine Grid	Richardson Extrapolation	Exact Solution
-4	0.180325	0.139166	0.124852	0.11722	0.123208
-3	0.278333	0.254987	0.246861	0.242523	0.246377
-2	0.383523	0.374036	0.369738	0.366176	0.369472
-1	0.496868	0.492806	0.49244	0.492403	0.492455
0	0.607382	0.614677	0.616166	0.616548	0.615287
1	0.71879	0.733762	0.739189	0.742275	0.737932
2	0.825602	0.854021	0.862873	0.866877	0.860352
3	0.925071	0.970963	0.985114	0.991423	0.98251
4	1.018486	1.086525	1.107206	1.116238	1.104369
3	0.926227	0.970579	0.984143	0.990119	0.98251
2	0.829979	0.853953	0.861372	0.864696	0.860352
1	0.713433	0.734526	0.738388	0.739254	0.737932

0	0.603197	0.613424	0.615626	0.616231	0.615287
-1	0.492378	0.49383	0.492175	0.4803	0.492455
-2	0.387183	0.374358	0.369258	0.365891	0.369472
-3	0.278336	0.255182	0.246832	0.242122	0.246377

Table 25 Data Used to Create Figure 28

Angle of Attack	Coarse Grid	Medium Grid	Fine Grid	Richardson Extrapolation	Exact Solution
-4	0.010845	0.002215	0.000385	-0.00011	0
-3	0.008471	0.001639	0.000282	-5.5E-05	0
-2	0.006616	0.001296	0.00023	-3.6E-05	0
-1	0.005247	0.001194	0.000215	-9.7E-05	0
0	0.005033	0.001059	0.000221	-4E-06	0
1	0.005093	0.001248	0.000275	-5.4E-05	0
2	0.006182	0.001391	0.000338	4.09E-05	0
3	0.007791	0.001886	0.0005	7.49E-05	0
4	0.009747	0.002464	0.000594	-5.3E-05	0
3	0.007691	0.001868	0.000463	1.67E-05	0
2	0.005959	0.001312	0.00032	5.05E-05	0
1	0.005218	0.001171	0.00025	-2.2E-05	0
0	0.004948	0.001132	0.000205	-9.2E-05	0
-1	0.005348	0.001148	0.000205	-6.7E-05	0
-2	0.006515	0.001272	0.000228	-3.1E-05	0
-3	0.007966	0.001675	0.0003	-8.6E-05	0

Table 26 Data Used to Create Figure 29

Angle of Attack	Coarse Grid	Medium Grid	Fine Grid	Richardson Extrapolation
-4	-0.0148	-0.00332	-0.0005	0.000525
-3	-0.01013	-0.00209	-0.00031	0.000257
-2	-0.0071	-0.00145	-0.00024	0.000151
-1	-0.00532	-0.0012	-0.00021	9.78E-05
0	-0.00503	-0.00106	-0.00022	4.02E-06
1	-0.00543	-0.00132	-0.00025	0.00013
2	-0.00739	-0.00161	-0.00025	0.000187
3	-0.01079	-0.00249	-0.00036	0.000392
4	-0.01571	-0.0037	-0.00039	0.000881
3	-0.01063	-0.00249	-0.00038	0.000382
2	-0.00702	-0.00153	-0.00028	0.000101
1	-0.00565	-0.00123	-0.00024	4.49E-05

0	-0.00495	-0.00113	-0.00021	9.2E-05
-1	-0.00535	-0.00117	-0.0002	0.000279
-2	-0.00713	-0.00144	-0.00022	0.000156
-3	-0.00963	-0.00213	-0.00032	0.000308

Table 27 Data Used to Create Figure 30

Angle of Attack	Coarse Grid	Medium Grid	Fine Grid	Richardson Extrapolation
-4	-0.05622	-0.01576	-0.00161	0.005966
-3	-0.03147	-0.00851	-0.00047	0.003847
-2	-0.01381	-0.00452	-0.00026	0.003293
-1	-0.00432	-0.00033	1.9E-05	4.98E-05
0	0.007905	0.00061	-0.00088	-0.00126
1	0.01905	0.004148	-0.00126	-0.00434
2	0.034513	0.006279	-0.00253	-0.00652
3	0.056953	0.011433	-0.00263	-0.0089
4	0.084994	0.017629	-0.00287	-0.01184
3	0.055803	0.011818	-0.00165	-0.0076
2	0.030147	0.006349	-0.00103	-0.00434
1	0.024405	0.003385	-0.00046	-0.00132
0	0.012091	0.001863	-0.00034	-0.00094
-1	0.00017	-0.00135	0.000283	0.012152
-2	-0.01747	-0.00484	0.000222	0.003578
-3	-0.0315	-0.0087	-0.00044	0.004245

Table 28 128 Time Steps Data Used to Create Figure 31 – 32

Angle of Attack	Power Coefficient	Thrust Coefficient
-4.27954	-0.01147	-0.00222
-4.26413	-0.01138	-0.00223
-4.23848	-0.01129	-0.00181
-4.20265	-0.01121	-0.00195
-4.15674	-0.01118	-0.00175
-4.10083	-0.01117	-0.00155
-4.03507	-0.0112	-0.00186
-3.95961	-0.01121	-0.00155
-3.87463	-0.01127	-0.00185
-3.78032	-0.0113	-0.00176
-3.67691	-0.01132	-0.00192
-3.56464	-0.01139	-0.00207

-3.44377	-0.0114	-0.00206
-3.31459	-0.01142	-0.00242
-3.17741	-0.01139	-0.00243
-3.03256	-0.01133	-0.00258
-2.88037	-0.01123	-0.00291
-2.72121	-0.01108	-0.00291
-2.55546	-0.01086	-0.00307
-2.38352	-0.01059	-0.00326
-2.20579	-0.01024	-0.00331
-2.02272	-0.0098	-0.00336
-1.83473	-0.00929	-0.00338
-1.64229	-0.00868	-0.0034
-1.44586	-0.00797	-0.00331
-1.24591	-0.00716	-0.00318
-1.04292	-0.00624	-0.00302
-0.8374	-0.00522	-0.00276
-0.62984	-0.00408	-0.00243
-0.42075	-0.00283	-0.00208
-0.21063	-0.00147	-0.00162
-3.7E-13	-2.7E-15	-0.0011
0.210631	0.00158	-0.0005
0.42075	0.003266	0.000174
0.629843	0.005055	0.000894
0.837403	0.006939	0.001775
1.042924	0.008914	0.002674
1.245906	0.010971	0.003625
1.445857	0.013104	0.004661
1.642292	0.015305	0.005783
1.834734	0.017563	0.006858
2.02272	0.019866	0.008185
2.205794	0.022197	0.009401
2.383515	0.024562	0.010775
2.555457	0.026934	0.011994
2.721206	0.029295	0.013434
2.880366	0.031644	0.014837
3.032556	0.033979	0.016161
3.177413	0.036244	0.017604
3.314592	0.038465	0.019023
3.443768	0.040627	0.020341
3.564635	0.042664	0.021755
3.676908	0.044699	0.02307

3.78032	0.046531	0.024382
3.874629	0.048268	0.02566
3.959613	0.04992	0.026667
4.035073	0.051331	0.027994
4.100832	0.052698	0.028732
4.156736	0.053816	0.029913
4.202654	0.054818	0.030936
4.23848	0.055665	0.031309
4.26413	0.056245	0.032318
4.279544	0.056752	0.032485
4.284686	0.056945	0.033151
4.279544	0.056997	0.033617
4.26413	0.056922	0.033554
4.23848	0.05657	0.034086
4.202654	0.056044	0.033679
4.156736	0.055377	0.033527
4.100832	0.054449	0.033431
4.035073	0.05341	0.032854
3.959613	0.052202	0.032441
3.874629	0.050769	0.032035
3.78032	0.049212	0.031152
3.676908	0.047541	0.030272
3.564635	0.045666	0.029381
3.443768	0.043696	0.028427
3.314592	0.041643	0.027181
3.177413	0.039463	0.026044
3.032556	0.037198	0.024854
2.880366	0.034859	0.023568
2.721206	0.03245	0.022101
2.555457	0.030013	0.020675
2.383515	0.02754	0.019207
2.205794	0.025039	0.017704
2.02272	0.022537	0.016176
1.834734	0.020046	0.0147
1.642292	0.017574	0.013202
1.445857	0.015143	0.011655
1.245906	0.012756	0.01016
1.042924	0.010427	0.008697
0.837403	0.008166	0.007253
0.629843	0.005985	0.005841
0.42075	0.003892	0.004512

0.210631	0.001894	0.003233
5.38E-13	4.7E-15	0.002006
-0.21063	-0.00178	0.00085
-0.42075	-0.00346	-0.00022
-0.62984	-0.00501	-0.00122
-0.8374	-0.00644	-0.00217
-1.04292	-0.00774	-0.00302
-1.24591	-0.00893	-0.00377
-1.44586	-0.00999	-0.00446
-1.64229	-0.01093	-0.00505
-1.83473	-0.01174	-0.00555
-2.02272	-0.01245	-0.00586
-2.20579	-0.01303	-0.00622
-2.38352	-0.01351	-0.00651
-2.55546	-0.0139	-0.00675
-2.72121	-0.01418	-0.00688
-2.88037	-0.01437	-0.00689
-3.03256	-0.01449	-0.0068
-3.17741	-0.01452	-0.00673
-3.31459	-0.0145	-0.00655
-3.44377	-0.01443	-0.00636
-3.56464	-0.01429	-0.00623
-3.67691	-0.0141	-0.00598
-3.78032	-0.01391	-0.00568
-3.87463	-0.01368	-0.0054
-3.95961	-0.01343	-0.00491
-4.03507	-0.01319	-0.0046
-4.10083	-0.01293	-0.00438
-4.15674	-0.01265	-0.00401
-4.20265	-0.01243	-0.00366
-4.23848	-0.01218	-0.00345
-4.26413	-0.01199	-0.0029
-4.27954	-0.01178	-0.00288
-4.28469	-0.0116	-0.00255

Table 29 256 Time Steps Data Used to Create Figure 31 – 32

Angle of Attack	Power Coefficient	Thrust Coefficient
-4.27312	-0.01144	-0.00234
-4.26413	-0.01136	-0.00212
-4.25258	-0.01134	-0.00196

-4.23848	-0.0113	-0.00182
-4.22183	-0.01124	-0.00191
-4.20265	-0.01124	-0.00201
-4.18095	-0.0112	-0.00178
-4.15674	-0.01119	-0.00173
-4.13002	-0.01117	-0.00157
-4.10083	-0.0112	-0.00162
-4.06918	-0.01121	-0.00196
-4.03507	-0.01119	-0.00165
-3.99855	-0.01122	-0.00161
-3.95961	-0.01122	-0.00158
-3.9183	-0.01125	-0.00175
-3.87463	-0.01129	-0.00191
-3.82863	-0.01128	-0.0017
-3.78032	-0.01131	-0.00178
-3.72974	-0.01132	-0.00178
-3.67691	-0.01134	-0.00207
-3.62186	-0.01138	-0.00202
-3.56464	-0.01139	-0.00197
-3.50526	-0.01141	-0.00206
-3.44377	-0.01141	-0.00205
-3.3802	-0.01142	-0.00234
-3.31459	-0.01143	-0.00241
-3.24698	-0.01141	-0.00235
-3.17741	-0.0114	-0.00244
-3.10592	-0.01138	-0.00251
-3.03256	-0.01134	-0.00264
-2.95736	-0.0113	-0.00283
-2.88037	-0.01124	-0.00281
-2.80163	-0.01117	-0.00286
-2.72121	-0.01109	-0.00293
-2.63913	-0.01099	-0.003
-2.55546	-0.01087	-0.0031
-2.47023	-0.01074	-0.00321
-2.38352	-0.0106	-0.00323
-2.29535	-0.01043	-0.00328
-2.20579	-0.01024	-0.0033
-2.1149	-0.01004	-0.00334
-2.02272	-0.00981	-0.00335
-1.92931	-0.00956	-0.00337
-1.83473	-0.00929	-0.00342

-1.73904	-0.009	-0.0034
-1.64229	-0.00868	-0.00337
-1.54454	-0.00834	-0.00335
-1.44586	-0.00797	-0.00331
-1.34629	-0.00758	-0.00325
-1.24591	-0.00716	-0.00321
-1.14476	-0.00672	-0.00309
-1.04292	-0.00625	-0.003
-0.94045	-0.00575	-0.00284
-0.8374	-0.00522	-0.00277
-0.73385	-0.00467	-0.00259
-0.62984	-0.00408	-0.00245
-0.52546	-0.00347	-0.00226
-0.42075	-0.00283	-0.00206
-0.31579	-0.00217	-0.00186
-0.21063	-0.00147	-0.00162
-0.10535	-0.00075	-0.00137
-3.1E-13	-2.3E-15	-0.00109
0.105348	0.000777	-0.0008
0.210631	0.001581	-0.0005
0.315787	0.002411	-0.00016
0.42075	0.003268	0.000175
0.525456	0.00415	0.000541
0.629843	0.005057	0.000942
0.733846	0.005988	0.001323
0.837403	0.006942	0.001774
0.940449	0.00792	0.002131
1.042924	0.008919	0.002707
1.144763	0.009938	0.003148
1.245906	0.010977	0.003674
1.346291	0.012034	0.004152
1.445857	0.01311	0.004688
1.544544	0.014201	0.005219
1.642292	0.01531	0.00578
1.739041	0.016432	0.006372
1.834734	0.017567	0.006966
1.929313	0.018714	0.007432
2.02272	0.019874	0.008176
2.114898	0.021036	0.00883
2.205794	0.02221	0.009399
2.29535	0.023382	0.010086

2.383515	0.024564	0.010766
2.470235	0.025751	0.011447
2.555457	0.026943	0.011956
2.639131	0.028128	0.012786
2.721206	0.029305	0.013466
2.801634	0.030484	0.014103
2.880366	0.031647	0.014866
2.957355	0.032814	0.015633
3.032556	0.033987	0.016051
3.105923	0.03513	0.016969
3.177413	0.036254	0.017603
3.246983	0.037372	0.018312
3.314592	0.038458	0.01912
3.3802	0.039566	0.01964
3.443768	0.040645	0.020317
3.505259	0.041667	0.021123
3.564635	0.042684	0.021686
3.621863	0.043666	0.022488
3.676908	0.044684	0.023131
3.729737	0.045652	0.023718
3.78032	0.046543	0.024409
3.828627	0.047421	0.024952
3.874629	0.048247	0.02573
3.9183	0.049127	0.0262
3.959613	0.049932	0.026674
3.998545	0.050651	0.027305
4.035073	0.051359	0.027903
4.069175	0.051998	0.028575
4.100832	0.052688	0.028765
4.130024	0.053305	0.029256
4.156736	0.053818	0.029895
4.180951	0.054334	0.030338
4.202654	0.05476	0.030993
4.221835	0.055311	0.031202
4.23848	0.055674	0.031276
4.252581	0.055961	0.031818
4.26413	0.056259	0.032169
4.273119	0.056481	0.032698
4.279544	0.056739	0.032524
4.2834	0.056896	0.032717
4.284686	0.056929	0.033164

4.2834	0.057019	0.033309
4.279544	0.056971	0.033762
4.273119	0.056986	0.033476
4.26413	0.056878	0.033608
4.252581	0.056791	0.033647
4.23848	0.056596	0.03408
4.221835	0.056292	0.033957
4.202654	0.056051	0.033782
4.180951	0.055704	0.033543
4.156736	0.055375	0.03349
4.130024	0.054935	0.03349
4.100832	0.054454	0.033268
4.069175	0.053927	0.033361
4.035073	0.053399	0.032789
3.998545	0.052804	0.032663
3.959613	0.052197	0.032403
3.9183	0.05149	0.032124
3.874629	0.050784	0.031912
3.828627	0.049987	0.031688
3.78032	0.049192	0.031216
3.729737	0.048385	0.03063
3.676908	0.047514	0.030285
3.621863	0.046631	0.02981
3.564635	0.045656	0.029359
3.505259	0.044694	0.02885
3.443768	0.043681	0.028332
3.3802	0.042669	0.027922
3.314592	0.041624	0.027147
3.246983	0.040553	0.026596
3.177413	0.039448	0.026013
3.105923	0.038326	0.025376
3.032556	0.037188	0.024762
2.957355	0.036023	0.024187
2.880366	0.03485	0.023521
2.801634	0.033655	0.022855
2.721206	0.032436	0.022117
2.639131	0.031228	0.021325
2.555457	0.030004	0.020665
2.470235	0.028765	0.019904
2.383515	0.027522	0.019207
2.29535	0.026283	0.018419

2.205794	0.025031	0.017686
2.114898	0.023779	0.016909
2.02272	0.022527	0.016147
1.929313	0.021283	0.015412
1.834734	0.02004	0.014619
1.739041	0.018798	0.013909
1.642292	0.017567	0.013152
1.544544	0.016345	0.012402
1.445857	0.015135	0.011654
1.346291	0.013934	0.010879
1.245906	0.012749	0.010131
1.144763	0.011577	0.009392
1.042924	0.01042	0.008652
0.940449	0.009281	0.007946
0.837403	0.008161	0.007221
0.733846	0.007062	0.006537
0.629843	0.005981	0.005828
0.525456	0.004924	0.005164
0.42075	0.003889	0.004485
0.315787	0.002878	0.003843
0.210631	0.001893	0.003205
0.105348	0.000933	0.002585
9.4E-13	8.2E-15	0.001988
-0.10535	-0.00091	0.001404
-0.21063	-0.00178	0.000837
-0.31579	-0.00263	0.000284
-0.42075	-0.00345	-0.00024
-0.52546	-0.00424	-0.00078
-0.62984	-0.005	-0.00125
-0.73385	-0.00573	-0.00175
-0.8374	-0.00643	-0.00218
-0.94045	-0.0071	-0.00262
-1.04292	-0.00774	-0.00301
-1.14476	-0.00834	-0.00342
-1.24591	-0.00892	-0.00379
-1.34629	-0.00947	-0.00414
-1.44586	-0.00998	-0.00447
-1.54454	-0.01047	-0.00477
-1.64229	-0.01092	-0.00505
-1.73904	-0.01134	-0.00532
-1.83473	-0.01173	-0.0055

-1.92931	-0.0121	-0.00569
-2.02272	-0.01243	-0.00586
-2.1149	-0.01274	-0.00607
-2.20579	-0.01302	-0.00624
-2.29535	-0.01327	-0.00638
-2.38352	-0.01351	-0.00655
-2.47023	-0.01371	-0.00665
-2.55546	-0.01388	-0.00672
-2.63913	-0.01404	-0.00677
-2.72121	-0.01417	-0.00698
-2.80163	-0.01427	-0.00686
-2.88037	-0.01436	-0.0068
-2.95736	-0.01443	-0.00686
-3.03256	-0.01447	-0.00678
-3.10592	-0.0145	-0.00677
-3.17741	-0.01451	-0.00674
-3.24698	-0.0145	-0.00667
-3.31459	-0.0145	-0.00649
-3.3802	-0.01446	-0.00648
-3.44377	-0.01442	-0.00636
-3.50526	-0.01435	-0.00633
-3.56464	-0.01428	-0.0062
-3.62186	-0.01418	-0.00613
-3.67691	-0.0141	-0.0059
-3.72974	-0.014	-0.00575
-3.78032	-0.01391	-0.00579
-3.82863	-0.01379	-0.00559
-3.87463	-0.01366	-0.00527
-3.9183	-0.01355	-0.00505
-3.95961	-0.01341	-0.00499
-3.99855	-0.01331	-0.00474
-4.03507	-0.01318	-0.00461
-4.06918	-0.01306	-0.00452
-4.10083	-0.01291	-0.00432
-4.13002	-0.01277	-0.00417
-4.15674	-0.01265	-0.004
-4.18095	-0.01255	-0.00378
-4.20265	-0.01242	-0.0037
-4.22183	-0.01231	-0.00358
-4.23848	-0.01216	-0.00344
-4.25258	-0.01209	-0.00299

-4.26413	-0.01199	-0.00302
-4.27312	-0.01186	-0.00293
-4.27954	-0.0118	-0.00288
-4.2834	-0.01168	-0.00264
-4.28469	-0.0116	-0.00257

Table 30 3 Cycles Steps Data Used to Create Figure 33 – 34

Angle of Attack	Power Coefficient	Thrust Coefficient
-4.27954	-0.01147	-0.00222
-4.26413	-0.01138	-0.00223
-4.23848	-0.01129	-0.00181
-4.20265	-0.01121	-0.00195
-4.15674	-0.01118	-0.00175
-4.10083	-0.01117	-0.00155
-4.03507	-0.0112	-0.00186
-3.95961	-0.01121	-0.00155
-3.87463	-0.01127	-0.00185
-3.78032	-0.0113	-0.00176
-3.67691	-0.01132	-0.00192
-3.56464	-0.01139	-0.00207
-3.44377	-0.0114	-0.00206
-3.31459	-0.01142	-0.00242
-3.17741	-0.01139	-0.00243
-3.03256	-0.01133	-0.00258
-2.88037	-0.01123	-0.00291
-2.72121	-0.01108	-0.00291
-2.55546	-0.01086	-0.00307
-2.38352	-0.01059	-0.00326
-2.20579	-0.01024	-0.00331
-2.02272	-0.0098	-0.00336
-1.83473	-0.00929	-0.00338
-1.64229	-0.00868	-0.0034
-1.44586	-0.00797	-0.00331
-1.24591	-0.00716	-0.00318
-1.04292	-0.00624	-0.00302
-0.8374	-0.00522	-0.00276
-0.62984	-0.00408	-0.00243
-0.42075	-0.00283	-0.00208
-0.21063	-0.00147	-0.00162
-3.7E-13	-2.7E-15	-0.0011

0.210631	0.00158	-0.0005
0.42075	0.003266	0.000174
0.629843	0.005055	0.000894
0.837403	0.006939	0.001775
1.042924	0.008914	0.002674
1.245906	0.010971	0.003625
1.445857	0.013104	0.004661
1.642292	0.015305	0.005783
1.834734	0.017563	0.006858
2.02272	0.019866	0.008185
2.205794	0.022197	0.009401
2.383515	0.024562	0.010775
2.555457	0.026934	0.011994
2.721206	0.029295	0.013434
2.880366	0.031644	0.014837
3.032556	0.033979	0.016161
3.177413	0.036244	0.017604
3.314592	0.038465	0.019023
3.443768	0.040627	0.020341
3.564635	0.042664	0.021755
3.676908	0.044699	0.02307
3.78032	0.046531	0.024382
3.874629	0.048268	0.02566
3.959613	0.04992	0.026667
4.035073	0.051331	0.027994
4.100832	0.052698	0.028732
4.156736	0.053816	0.029913
4.202654	0.054818	0.030936
4.23848	0.055665	0.031309
4.26413	0.056245	0.032318
4.279544	0.056752	0.032485
4.284686	0.056945	0.033151
4.279544	0.056997	0.033617
4.26413	0.056922	0.033554
4.23848	0.05657	0.034086
4.202654	0.056044	0.033679
4.156736	0.055377	0.033527
4.100832	0.054449	0.033431
4.035073	0.05341	0.032854
3.959613	0.052202	0.032441
3.874629	0.050769	0.032035

3.78032	0.049212	0.031152
3.676908	0.047541	0.030272
3.564635	0.045666	0.029381
3.443768	0.043696	0.028427
3.314592	0.041643	0.027181
3.177413	0.039463	0.026044
3.032556	0.037198	0.024854
2.880366	0.034859	0.023568
2.721206	0.03245	0.022101
2.555457	0.030013	0.020675
2.383515	0.02754	0.019207
2.205794	0.025039	0.017704
2.02272	0.022537	0.016176
1.834734	0.020046	0.0147
1.642292	0.017574	0.013202
1.445857	0.015143	0.011655
1.245906	0.012756	0.01016
1.042924	0.010427	0.008697
0.837403	0.008166	0.007253
0.629843	0.005985	0.005841
0.42075	0.003892	0.004512
0.210631	0.001894	0.003233
5.38E-13	4.7E-15	0.002006
-0.21063	-0.00178	0.00085
-0.42075	-0.00346	-0.00022
-0.62984	-0.00501	-0.00122
-0.8374	-0.00644	-0.00217
-1.04292	-0.00774	-0.00302
-1.24591	-0.00893	-0.00377
-1.44586	-0.00999	-0.00446
-1.64229	-0.01093	-0.00505
-1.83473	-0.01174	-0.00555
-2.02272	-0.01245	-0.00586
-2.20579	-0.01303	-0.00622
-2.38352	-0.01351	-0.00651
-2.55546	-0.0139	-0.00675
-2.72121	-0.01418	-0.00688
-2.88037	-0.01437	-0.00689
-3.03256	-0.01449	-0.0068
-3.17741	-0.01452	-0.00673
-3.31459	-0.0145	-0.00655

-3.44377	-0.01443	-0.00636
-3.56464	-0.01429	-0.00623
-3.67691	-0.0141	-0.00598
-3.78032	-0.01391	-0.00568
-3.87463	-0.01368	-0.0054
-3.95961	-0.01343	-0.00491
-4.03507	-0.01319	-0.0046
-4.10083	-0.01293	-0.00438
-4.15674	-0.01265	-0.00401
-4.20265	-0.01243	-0.00366
-4.23848	-0.01218	-0.00345
-4.26413	-0.01199	-0.0029
-4.27954	-0.01178	-0.00288
-4.28469	-0.0116	-0.00255

Table 31 4 Cycles Data Used to Create Figure 33 – 34

Angle of Attack	Power Coefficient	Thrust Coefficient
-4.27312	-0.01144	-0.00234
-4.26413	-0.01136	-0.00212
-4.25258	-0.01134	-0.00196
-4.23848	-0.0113	-0.00182
-4.22183	-0.01124	-0.00191
-4.20265	-0.01124	-0.00201
-4.18095	-0.0112	-0.00178
-4.15674	-0.01119	-0.00173
-4.13002	-0.01117	-0.00157
-4.10083	-0.0112	-0.00162
-4.06918	-0.01121	-0.00196
-4.03507	-0.01119	-0.00165
-3.99855	-0.01122	-0.00161
-3.95961	-0.01122	-0.00158
-3.9183	-0.01125	-0.00175
-3.87463	-0.01129	-0.00191
-3.82863	-0.01128	-0.0017
-3.78032	-0.01131	-0.00178
-3.72974	-0.01132	-0.00178
-3.67691	-0.01134	-0.00207
-3.62186	-0.01138	-0.00202
-3.56464	-0.01139	-0.00197
-3.50526	-0.01141	-0.00206

-3.44377	-0.01141	-0.00205
-3.3802	-0.01142	-0.00234
-3.31459	-0.01143	-0.00241
-3.24698	-0.01141	-0.00235
-3.17741	-0.0114	-0.00244
-3.10592	-0.01138	-0.00251
-3.03256	-0.01134	-0.00264
-2.95736	-0.0113	-0.00283
-2.88037	-0.01124	-0.00281
-2.80163	-0.01117	-0.00286
-2.72121	-0.01109	-0.00293
-2.63913	-0.01099	-0.003
-2.55546	-0.01087	-0.0031
-2.47023	-0.01074	-0.00321
-2.38352	-0.0106	-0.00323
-2.29535	-0.01043	-0.00328
-2.20579	-0.01024	-0.0033
-2.1149	-0.01004	-0.00334
-2.02272	-0.00981	-0.00335
-1.92931	-0.00956	-0.00337
-1.83473	-0.00929	-0.00342
-1.73904	-0.009	-0.0034
-1.64229	-0.00868	-0.00337
-1.54454	-0.00834	-0.00335
-1.44586	-0.00797	-0.00331
-1.34629	-0.00758	-0.00325
-1.24591	-0.00716	-0.00321
-1.14476	-0.00672	-0.00309
-1.04292	-0.00625	-0.003
-0.94045	-0.00575	-0.00284
-0.8374	-0.00522	-0.00277
-0.73385	-0.00467	-0.00259
-0.62984	-0.00408	-0.00245
-0.52546	-0.00347	-0.00226
-0.42075	-0.00283	-0.00206
-0.31579	-0.00217	-0.00186
-0.21063	-0.00147	-0.00162
-0.10535	-0.00075	-0.00137
-3.1E-13	-2.3E-15	-0.00109
0.105348	0.000777	-0.0008
0.210631	0.001581	-0.0005

0.315787	0.002411	-0.00016
0.42075	0.003268	0.000175
0.525456	0.00415	0.000541
0.629843	0.005057	0.000942
0.733846	0.005988	0.001323
0.837403	0.006942	0.001774
0.940449	0.00792	0.002131
1.042924	0.008919	0.002707
1.144763	0.009938	0.003148
1.245906	0.010977	0.003674
1.346291	0.012034	0.004152
1.445857	0.01311	0.004688
1.544544	0.014201	0.005219
1.642292	0.01531	0.00578
1.739041	0.016432	0.006372
1.834734	0.017567	0.006966
1.929313	0.018714	0.007432
2.02272	0.019874	0.008176
2.114898	0.021036	0.00883
2.205794	0.02221	0.009399
2.29535	0.023382	0.010086
2.383515	0.024564	0.010766
2.470235	0.025751	0.011447
2.555457	0.026943	0.011956
2.639131	0.028128	0.012786
2.721206	0.029305	0.013466
2.801634	0.030484	0.014103
2.880366	0.031647	0.014866
2.957355	0.032814	0.015633
3.032556	0.033987	0.016051
3.105923	0.03513	0.016969
3.177413	0.036254	0.017603
3.246983	0.037372	0.018312
3.314592	0.038458	0.01912
3.3802	0.039566	0.01964
3.443768	0.040645	0.020317
3.505259	0.041667	0.021123
3.564635	0.042684	0.021686
3.621863	0.043666	0.022488
3.676908	0.044684	0.023131
3.729737	0.045652	0.023718

3.78032	0.046543	0.024409
3.828627	0.047421	0.024952
3.874629	0.048247	0.02573
3.9183	0.049127	0.0262
3.959613	0.049932	0.026674
3.998545	0.050651	0.027305
4.035073	0.051359	0.027903
4.069175	0.051998	0.028575
4.100832	0.052688	0.028765
4.130024	0.053305	0.029256
4.156736	0.053818	0.029895
4.180951	0.054334	0.030338
4.202654	0.05476	0.030993
4.221835	0.055311	0.031202
4.23848	0.055674	0.031276
4.252581	0.055961	0.031818
4.26413	0.056259	0.032169
4.273119	0.056481	0.032698
4.279544	0.056739	0.032524
4.2834	0.056896	0.032717
4.284686	0.056929	0.033164
4.2834	0.057019	0.033309
4.279544	0.056971	0.033762
4.273119	0.056986	0.033476
4.26413	0.056878	0.033608
4.252581	0.056791	0.033647
4.23848	0.056596	0.03408
4.221835	0.056292	0.033957
4.202654	0.056051	0.033782
4.180951	0.055704	0.033543
4.156736	0.055375	0.03349
4.130024	0.054935	0.03349
4.100832	0.054454	0.033268
4.069175	0.053927	0.033361
4.035073	0.053399	0.032789
3.998545	0.052804	0.032663
3.959613	0.052197	0.032403
3.9183	0.05149	0.032124
3.874629	0.050784	0.031912
3.828627	0.049987	0.031688
3.78032	0.049192	0.031216

3.729737	0.048385	0.03063
3.676908	0.047514	0.030285
3.621863	0.046631	0.02981
3.564635	0.045656	0.029359
3.505259	0.044694	0.02885
3.443768	0.043681	0.028332
3.3802	0.042669	0.027922
3.314592	0.041624	0.027147
3.246983	0.040553	0.026596
3.177413	0.039448	0.026013
3.105923	0.038326	0.025376
3.032556	0.037188	0.024762
2.957355	0.036023	0.024187
2.880366	0.03485	0.023521
2.801634	0.033655	0.022855
2.721206	0.032436	0.022117
2.639131	0.031228	0.021325
2.555457	0.030004	0.020665
2.470235	0.028765	0.019904
2.383515	0.027522	0.019207
2.29535	0.026283	0.018419
2.205794	0.025031	0.017686
2.114898	0.023779	0.016909
2.02272	0.022527	0.016147
1.929313	0.021283	0.015412
1.834734	0.02004	0.014619
1.739041	0.018798	0.013909
1.642292	0.017567	0.013152
1.544544	0.016345	0.012402
1.445857	0.015135	0.011654
1.346291	0.013934	0.010879
1.245906	0.012749	0.010131
1.144763	0.011577	0.009392
1.042924	0.01042	0.008652
0.940449	0.009281	0.007946
0.837403	0.008161	0.007221
0.733846	0.007062	0.006537
0.629843	0.005981	0.005828
0.525456	0.004924	0.005164
0.42075	0.003889	0.004485
0.315787	0.002878	0.003843

0.210631	0.001893	0.003205
0.105348	0.000933	0.002585
9.4E-13	8.2E-15	0.001988
-0.10535	-0.00091	0.001404
-0.21063	-0.00178	0.000837
-0.31579	-0.00263	0.000284
-0.42075	-0.00345	-0.00024
-0.52546	-0.00424	-0.00078
-0.62984	-0.005	-0.00125
-0.73385	-0.00573	-0.00175
-0.8374	-0.00643	-0.00218
-0.94045	-0.0071	-0.00262
-1.04292	-0.00774	-0.00301
-1.14476	-0.00834	-0.00342
-1.24591	-0.00892	-0.00379
-1.34629	-0.00947	-0.00414
-1.44586	-0.00998	-0.00447
-1.54454	-0.01047	-0.00477
-1.64229	-0.01092	-0.00505
-1.73904	-0.01134	-0.00532
-1.83473	-0.01173	-0.0055
-1.92931	-0.0121	-0.00569
-2.02272	-0.01243	-0.00586
-2.1149	-0.01274	-0.00607
-2.20579	-0.01302	-0.00624
-2.29535	-0.01327	-0.00638
-2.38352	-0.01351	-0.00655
-2.47023	-0.01371	-0.00665
-2.55546	-0.01388	-0.00672
-2.63913	-0.01404	-0.00677
-2.72121	-0.01417	-0.00698
-2.80163	-0.01427	-0.00686
-2.88037	-0.01436	-0.0068
-2.95736	-0.01443	-0.00686
-3.03256	-0.01447	-0.00678
-3.10592	-0.0145	-0.00677
-3.17741	-0.01451	-0.00674
-3.24698	-0.0145	-0.00667
-3.31459	-0.0145	-0.00649
-3.3802	-0.01446	-0.00648
-3.44377	-0.01442	-0.00636

-3.50526	-0.01435	-0.00633
-3.56464	-0.01428	-0.0062
-3.62186	-0.01418	-0.00613
-3.67691	-0.0141	-0.0059
-3.72974	-0.014	-0.00575
-3.78032	-0.01391	-0.00579
-3.82863	-0.01379	-0.00559
-3.87463	-0.01366	-0.00527
-3.9183	-0.01355	-0.00505
-3.95961	-0.01341	-0.00499
-3.99855	-0.01331	-0.00474
-4.03507	-0.01318	-0.00461
-4.06918	-0.01306	-0.00452
-4.10083	-0.01291	-0.00432
-4.13002	-0.01277	-0.00417
-4.15674	-0.01265	-0.004
-4.18095	-0.01255	-0.00378
-4.20265	-0.01242	-0.0037
-4.22183	-0.01231	-0.00358
-4.23848	-0.01216	-0.00344
-4.25258	-0.01209	-0.00299
-4.26413	-0.01199	-0.00302
-4.27312	-0.01186	-0.00293
-4.27954	-0.0118	-0.00288
-4.2834	-0.01168	-0.00264
-4.28469	-0.0116	-0.00257

Table 32 CFD Data Used to Create Figures 35 – 38

t/τ	C_x	C_y	C_P	C_T
0.058443	0.009093	0.124521	-0.00871	-0.00888
0.126703	0.013201	0.246508	-0.01292	-0.01299
0.17283	0.013134	0.369504	-0.0129	-0.01292
0.212577	0.008809	0.492361	-0.00859	-0.0086
0.25	0.000221	0.616166	0	-7.7E-06
0.287423	-0.01263	0.739081	0.012901	0.012838
0.32717	-0.02978	0.862359	0.030114	0.029989
0.373297	-0.05106	0.98379	0.051558	0.05127
0.441557	-0.07664	1.104551	0.077238	0.076855
0.558443	-0.07664	1.104551	0.077238	0.076855

0.626703	-0.05104	0.982819	0.051507	0.051256
0.67283	-0.02974	0.860859	0.030062	0.029955
0.712577	-0.01264	0.73828	0.012887	0.01285
0.75	0.000205	0.615626	0	7.69E-06
0.787423	0.008795	0.492097	-0.00859	-0.00858
0.82717	0.013115	0.369025	-0.01289	-0.0129
0.873297	0.013217	0.246478	-0.01292	-0.013
0.941557	0.009093	0.124521	-0.00871	-0.00888

Table 33 Lifting-Line Data Used to Create Figures 35 – 38

$t/_{\tau}$	C_x	C_y	C_P	C_T
0.058443	0.008702	0.124447	-0.0087	-0.0087
0.068069	0.009319	0.136697	-0.00932	-0.00932
0.076556	0.009893	0.14895	-0.00989	-0.00989
0.08425	0.010425	0.161205	-0.01042	-0.01042
0.091354	0.010913	0.173462	-0.01091	-0.01091
0.097996	0.011359	0.185721	-0.01136	-0.01136
0.104266	0.011762	0.197982	-0.01176	-0.01176
0.110228	0.012123	0.210246	-0.01212	-0.01212
0.115931	0.01244	0.222511	-0.01244	-0.01244
0.121413	0.012715	0.234778	-0.01272	-0.01272
0.126703	0.012947	0.247046	-0.01295	-0.01295
0.131825	0.013136	0.259316	-0.01314	-0.01314
0.136799	0.013283	0.271587	-0.01328	-0.01328
0.141642	0.013386	0.28386	-0.01339	-0.01339
0.146367	0.013447	0.296134	-0.01345	-0.01345
0.150987	0.013465	0.308408	-0.01347	-0.01347
0.155513	0.013441	0.320684	-0.01344	-0.01344
0.159952	0.013373	0.33296	-0.01337	-0.01337
0.164313	0.013263	0.345238	-0.01326	-0.01326
0.168604	0.013109	0.357515	-0.01311	-0.01311
0.17283	0.012913	0.369794	-0.01291	-0.01291
0.176997	0.012675	0.382072	-0.01267	-0.01267
0.181111	0.012393	0.394351	-0.01239	-0.01239
0.185175	0.012069	0.40663	-0.01207	-0.01207
0.189195	0.011701	0.418909	-0.0117	-0.0117
0.193174	0.011291	0.431188	-0.01129	-0.01129
0.197116	0.010838	0.443467	-0.01084	-0.01084

0.201024	0.010342	0.455746	-0.01034	-0.01034
0.204901	0.009804	0.468024	-0.0098	-0.0098
0.208751	0.009222	0.480301	-0.00922	-0.00922
0.212577	0.008598	0.492578	-0.0086	-0.0086
0.21638	0.007931	0.504854	-0.00793	-0.00793
0.220163	0.007221	0.51713	-0.00722	-0.00722
0.223929	0.006468	0.529404	-0.00647	-0.00647
0.227681	0.005673	0.541677	-0.00567	-0.00567
0.231419	0.004834	0.553949	-0.00483	-0.00483
0.235148	0.003953	0.56622	-0.00395	-0.00395
0.238868	0.003029	0.578489	-0.00303	-0.00303
0.242582	0.002062	0.590757	-0.00206	-0.00206
0.246292	0.001052	0.603023	-0.00105	-0.00105
0.25	0	0.615287	0	0
0.253708	-0.0011	0.62755	0.001095	0.001095
0.257418	-0.00223	0.63981	0.002233	0.002233
0.261132	-0.00341	0.652068	0.003414	0.003414
0.264852	-0.00464	0.664325	0.004638	0.004638
0.268581	-0.0059	0.676578	0.005904	0.005904
0.272319	-0.00721	0.68883	0.007214	0.007214
0.276071	-0.00857	0.701079	0.008566	0.008566
0.279837	-0.00996	0.713325	0.009961	0.009961
0.28362	-0.0114	0.725568	0.011398	0.011398
0.287423	-0.01288	0.737809	0.012878	0.012878
0.291249	-0.0144	0.750046	0.014402	0.014402
0.295099	-0.01597	0.762281	0.015968	0.015968
0.298976	-0.01758	0.774512	0.017576	0.017576
0.302884	-0.01923	0.78674	0.019228	0.019228
0.306826	-0.02092	0.798964	0.020922	0.020922
0.310805	-0.02266	0.811185	0.022658	0.022658
0.314825	-0.02444	0.823402	0.024438	0.024438
0.318889	-0.02626	0.835616	0.02626	0.02626
0.323003	-0.02813	0.847825	0.028125	0.028125
0.32717	-0.03003	0.860031	0.030033	0.030033
0.331396	-0.03198	0.872232	0.031983	0.031983
0.335687	-0.03398	0.88443	0.033976	0.033976
0.340048	-0.03601	0.896622	0.036012	0.036012
0.344487	-0.03809	0.908811	0.03809	0.03809
0.349013	-0.04021	0.920995	0.040211	0.040211

0.353633	-0.04238	0.933174	0.042375	0.042375
0.358358	-0.04458	0.945348	0.044581	0.044581
0.363201	-0.04683	0.957518	0.04683	0.04683
0.368175	-0.04912	0.969682	0.049122	0.049122
0.373297	-0.05146	0.981842	0.051456	0.051456
0.378587	-0.05383	0.993996	0.053833	0.053833
0.384069	-0.05625	1.006145	0.056252	0.056252
0.389772	-0.05871	1.018288	0.058714	0.058714
0.395734	-0.06122	1.030426	0.061219	0.061219
0.402004	-0.06377	1.042558	0.063766	0.063766
0.408646	-0.06636	1.054684	0.066355	0.066355
0.41575	-0.06899	1.066805	0.068987	0.068987
0.423444	-0.07166	1.078919	0.071662	0.071662
0.431931	-0.07438	1.091027	0.074379	0.074379
0.441557	-0.07714	1.103129	0.077138	0.077138
0.453018	-0.07994	1.115225	0.07994	0.07994
0.468247	-0.08278	1.127314	0.082785	0.082785
0.475781	-0.08567	1.139397	0.085672	0.085672
0.49085	-0.0886	1.151473	0.088601	0.088601
0.50915	-0.0886	1.151473	0.088601	0.088601
0.524219	-0.08567	1.139397	0.085672	0.085672
0.531753	-0.08278	1.127314	0.082785	0.082785
0.546982	-0.07994	1.115225	0.07994	0.07994
0.558443	-0.07714	1.103129	0.077138	0.077138
0.568069	-0.07438	1.091027	0.074379	0.074379
0.576556	-0.07166	1.078919	0.071662	0.071662
0.58425	-0.06899	1.066805	0.068987	0.068987
0.591354	-0.06636	1.054684	0.066355	0.066355
0.597996	-0.06377	1.042558	0.063766	0.063766
0.604266	-0.06122	1.030426	0.061219	0.061219
0.610228	-0.05871	1.018288	0.058714	0.058714
0.615931	-0.05625	1.006145	0.056252	0.056252
0.621413	-0.05383	0.993996	0.053833	0.053833
0.626703	-0.05146	0.981842	0.051456	0.051456
0.631825	-0.04912	0.969682	0.049122	0.049122
0.636799	-0.04683	0.957518	0.04683	0.04683
0.641642	-0.04458	0.945348	0.044581	0.044581
0.646367	-0.04238	0.933174	0.042375	0.042375
0.650987	-0.04021	0.920995	0.040211	0.040211

0.655513	-0.03809	0.908811	0.03809	0.03809
0.659952	-0.03601	0.896622	0.036012	0.036012
0.664313	-0.03398	0.88443	0.033976	0.033976
0.668604	-0.03198	0.872232	0.031983	0.031983
0.67283	-0.03003	0.860031	0.030033	0.030033
0.676997	-0.02813	0.847825	0.028125	0.028125
0.681111	-0.02626	0.835616	0.02626	0.02626
0.685175	-0.02444	0.823402	0.024438	0.024438
0.689195	-0.02266	0.811185	0.022658	0.022658
0.693174	-0.02092	0.798964	0.020922	0.020922
0.697116	-0.01923	0.78674	0.019228	0.019228
0.701024	-0.01758	0.774512	0.017576	0.017576
0.704901	-0.01597	0.762281	0.015968	0.015968
0.708751	-0.0144	0.750046	0.014402	0.014402
0.712577	-0.01288	0.737809	0.012878	0.012878
0.71638	-0.0114	0.725568	0.011398	0.011398
0.720163	-0.00996	0.713325	0.009961	0.009961
0.723929	-0.00857	0.701079	0.008566	0.008566
0.727681	-0.00721	0.68883	0.007214	0.007214
0.731419	-0.0059	0.676578	0.005904	0.005904
0.735148	-0.00464	0.664325	0.004638	0.004638
0.738868	-0.00341	0.652068	0.003414	0.003414
0.742582	-0.00223	0.63981	0.002233	0.002233
0.746292	-0.0011	0.62755	0.001095	0.001095
0.75	0	0.615287	0	0
0.753708	0.001052	0.603023	-0.00105	-0.00105
0.757418	0.002062	0.590757	-0.00206	-0.00206
0.761132	0.003029	0.578489	-0.00303	-0.00303
0.764852	0.003953	0.56622	-0.00395	-0.00395
0.768581	0.004834	0.553949	-0.00483	-0.00483
0.772319	0.005673	0.541677	-0.00567	-0.00567
0.776071	0.006468	0.529404	-0.00647	-0.00647
0.779837	0.007221	0.51713	-0.00722	-0.00722
0.78362	0.007931	0.504854	-0.00793	-0.00793
0.787423	0.008598	0.492578	-0.0086	-0.0086
0.791249	0.009222	0.480301	-0.00922	-0.00922
0.795099	0.009804	0.468024	-0.0098	-0.0098
0.798976	0.010342	0.455746	-0.01034	-0.01034
0.802884	0.010838	0.443467	-0.01084	-0.01084

0.806826	0.011291	0.431188	-0.01129	-0.01129
0.810805	0.011701	0.418909	-0.0117	-0.0117
0.814825	0.012069	0.40663	-0.01207	-0.01207
0.818889	0.012393	0.394351	-0.01239	-0.01239
0.823003	0.012675	0.382072	-0.01267	-0.01267
0.82717	0.012913	0.369794	-0.01291	-0.01291
0.831396	0.013109	0.357515	-0.01311	-0.01311
0.835687	0.013263	0.345238	-0.01326	-0.01326
0.840048	0.013373	0.33296	-0.01337	-0.01337
0.844487	0.013441	0.320684	-0.01344	-0.01344
0.849013	0.013465	0.308408	-0.01347	-0.01347
0.853633	0.013447	0.296134	-0.01345	-0.01345
0.858358	0.013386	0.28386	-0.01339	-0.01339
0.863201	0.013283	0.271587	-0.01328	-0.01328
0.868175	0.013136	0.259316	-0.01314	-0.01314
0.873297	0.012947	0.247046	-0.01295	-0.01295
0.878587	0.012715	0.234778	-0.01272	-0.01272
0.884069	0.01244	0.222511	-0.01244	-0.01244
0.889772	0.012123	0.210246	-0.01212	-0.01212
0.895734	0.011762	0.197982	-0.01176	-0.01176
0.902004	0.011359	0.185721	-0.01136	-0.01136
0.908646	0.010913	0.173462	-0.01091	-0.01091
0.91575	0.010425	0.161205	-0.01042	-0.01042
0.923444	0.009893	0.14895	-0.00989	-0.00989
0.931931	0.009319	0.136697	-0.00932	-0.00932
0.941557	0.008702	0.124447	-0.0087	-0.0087

Table 34 CFD Data Used to Create Figures 39 – 42

t/τ	C_x	C_y	C_P	C_T
0	0.006465	0.07681	-0.00575	0.002159
0.007813	0.006494	0.077265	-0.00578	0.00213
0.015625	0.006583	0.078627	-0.00586	0.002042
0.023438	0.006728	0.080893	-0.006	0.001896
0.03125	0.006929	0.084056	-0.00618	0.001695
0.039063	0.007181	0.088108	-0.0064	0.001443
0.046875	0.007481	0.09304	-0.00667	0.001144
0.054688	0.007824	0.098849	-0.00697	0.0008
0.0625	0.008206	0.105519	-0.0073	0.000418
0.070313	0.008619	0.113029	-0.00766	5.49E-06

0.078125	0.009056	0.121359	-0.00802	-0.00043
0.085938	0.00951	0.130501	-0.00839	-0.00089
0.09375	0.009975	0.140448	-0.00875	-0.00135
0.101563	0.010441	0.151156	-0.0091	-0.00182
0.109375	0.010896	0.16257	-0.00942	-0.00227
0.117188	0.011334	0.174672	-0.0097	-0.00271
0.125	0.011748	0.187477	-0.00993	-0.00312
0.132813	0.012131	0.200969	-0.01011	-0.00351
0.140625	0.012471	0.215103	-0.01022	-0.00385
0.148438	0.012758	0.229813	-0.01026	-0.00413
0.15625	0.012984	0.245055	-0.0102	-0.00436
0.164063	0.01314	0.260811	-0.01005	-0.00452
0.171875	0.013222	0.277075	-0.00979	-0.0046
0.179688	0.01322	0.293781	-0.00941	-0.0046
0.1875	0.013127	0.310869	-0.00891	-0.0045
0.195313	0.012938	0.32831	-0.00829	-0.00431
0.203125	0.012649	0.346094	-0.00753	-0.00402
0.210938	0.012256	0.36416	-0.00663	-0.00363
0.21875	0.011754	0.382453	-0.00559	-0.00313
0.226563	0.011142	0.400939	-0.00441	-0.00252
0.234375	0.010419	0.419576	-0.00308	-0.00179
0.242188	0.009583	0.43831	-0.00161	-0.00096
0.25	0.008636	0.457105	1.47E-17	-1.2E-05
0.257813	0.00758	0.475919	0.00175	0.001044
0.265625	0.006418	0.494705	0.003633	0.002206
0.273438	0.005153	0.51341	0.005644	0.003471
0.28125	0.00379	0.531989	0.007776	0.004834
0.289063	0.002335	0.550394	0.01002	0.006289
0.296875	0.000796	0.568577	0.012366	0.007828
0.304688	-0.00082	0.586501	0.014803	0.009445
0.3125	-0.00251	0.604122	0.017321	0.011129
0.320313	-0.00425	0.621386	0.019905	0.012873
0.328125	-0.00604	0.638256	0.022542	0.014666
0.335938	-0.00787	0.6547	0.025217	0.016496
0.34375	-0.00973	0.670663	0.027916	0.018353
0.351563	-0.0116	0.686121	0.030622	0.020225
0.359375	-0.01347	0.701035	0.03332	0.022099
0.367188	-0.01534	0.715365	0.035993	0.023963
0.375	-0.01718	0.72907	0.038624	0.025805
0.382813	-0.01899	0.742122	0.041198	0.027612
0.390625	-0.02075	0.754491	0.043696	0.029372

0.398438	-0.02245	0.766146	0.046105	0.031073
0.40625	-0.02408	0.777053	0.048407	0.032703
0.414063	-0.02563	0.787185	0.050586	0.03425
0.421875	-0.02708	0.796521	0.05263	0.035702
0.429688	-0.02843	0.805037	0.054524	0.037051
0.4375	-0.02966	0.812715	0.056255	0.038285
0.445313	-0.03077	0.819535	0.057812	0.039396
0.453125	-0.03175	0.825477	0.059183	0.040376
0.460938	-0.03259	0.830529	0.06036	0.041218
0.46875	-0.03329	0.834679	0.061334	0.041915
0.476563	-0.03384	0.837918	0.062099	0.042462
0.484375	-0.03423	0.840238	0.062649	0.042856
0.492188	-0.03447	0.841631	0.06298	0.043094
0.5	-0.03455	0.842096	0.063091	0.043173
0.507813	-0.03447	0.841631	0.06298	0.043094
0.515625	-0.03423	0.840238	0.062649	0.042856
0.523438	-0.03384	0.837918	0.062099	0.042462
0.53125	-0.03329	0.834679	0.061334	0.041915
0.539063	-0.03259	0.830529	0.06036	0.041218
0.546875	-0.03175	0.825477	0.059183	0.040376
0.554688	-0.03077	0.819535	0.057812	0.039396
0.5625	-0.02966	0.812715	0.056255	0.038285
0.570313	-0.02843	0.805037	0.054524	0.037051
0.578125	-0.02708	0.796521	0.05263	0.035702
0.585938	-0.02563	0.787185	0.050586	0.03425
0.59375	-0.02408	0.777053	0.048407	0.032703
0.601563	-0.02245	0.766146	0.046105	0.031073
0.609375	-0.02075	0.754491	0.043696	0.029372
0.617188	-0.01899	0.742122	0.041198	0.027612
0.625	-0.01718	0.72907	0.038624	0.025805
0.632813	-0.01534	0.715365	0.035993	0.023963
0.640625	-0.01347	0.701035	0.03332	0.022099
0.648438	-0.0116	0.686121	0.030622	0.020225
0.65625	-0.00973	0.670663	0.027916	0.018353
0.664063	-0.00787	0.6547	0.025217	0.016496
0.671875	-0.00604	0.638256	0.022542	0.014666
0.679688	-0.00425	0.621386	0.019905	0.012873
0.6875	-0.00251	0.604122	0.017321	0.011129
0.695313	-0.00082	0.586501	0.014803	0.009445
0.703125	0.000796	0.568577	0.012366	0.007828
0.710938	0.002335	0.550394	0.01002	0.006289

0.71875	0.00379	0.531989	0.007776	0.004834
0.726563	0.005153	0.51341	0.005644	0.003471
0.734375	0.006418	0.494705	0.003633	0.002206
0.742188	0.00758	0.475919	0.00175	0.001044
0.75	0.008636	0.457105	-1E-17	-1.2E-05
0.757813	0.009583	0.43831	-0.00161	-0.00096
0.765625	0.010419	0.419576	-0.00308	-0.00179
0.773438	0.011142	0.400939	-0.00441	-0.00252
0.78125	0.011754	0.382453	-0.00559	-0.00313
0.789063	0.012256	0.36416	-0.00663	-0.00363
0.796875	0.012649	0.346094	-0.00753	-0.00402
0.804688	0.012938	0.32831	-0.00829	-0.00431
0.8125	0.013127	0.310869	-0.00891	-0.0045
0.820313	0.01322	0.293781	-0.00941	-0.0046
0.828125	0.013222	0.277075	-0.00979	-0.0046
0.835938	0.01314	0.260811	-0.01005	-0.00452
0.84375	0.012984	0.245055	-0.0102	-0.00436
0.851563	0.012758	0.229813	-0.01026	-0.00413
0.859375	0.012471	0.215103	-0.01022	-0.00385
0.867188	0.012131	0.200969	-0.01011	-0.00351
0.875	0.011748	0.187477	-0.00993	-0.00312
0.882813	0.011334	0.174672	-0.0097	-0.00271
0.890625	0.010896	0.16257	-0.00942	-0.00227
0.898438	0.010441	0.151156	-0.0091	-0.00182
0.90625	0.009975	0.140448	-0.00875	-0.00135
0.914063	0.00951	0.130501	-0.00839	-0.00089
0.921875	0.009056	0.121359	-0.00802	-0.00043
0.929688	0.008619	0.113029	-0.00766	5.49E-06
0.9375	0.008206	0.105519	-0.0073	0.000418
0.945313	0.007824	0.098849	-0.00697	0.0008
0.953125	0.007481	0.09304	-0.00667	0.001144
0.960938	0.007181	0.088108	-0.0064	0.001443
0.96875	0.006929	0.084056	-0.00618	0.001695
0.976563	0.006728	0.080893	-0.006	0.001896
0.984375	0.006583	0.078627	-0.00586	0.002042
0.992188	0.006494	0.077265	-0.00578	0.00213
1	0.006465	0.07681	-0.00575	0.002159

Table 35 Lifting-Line Data Used to Create Figures 39 – 42

t/τ	C_x	C_y	C_P	C_T
0	0.00507	0.065276	-0.00489	0.003906
0.007813	0.005103	0.065753	-0.00492	0.003873
0.015625	0.0052	0.067184	-0.00501	0.003776
0.023438	0.005359	0.069564	-0.00516	0.003616
0.03125	0.00558	0.072888	-0.00536	0.003396
0.039063	0.005858	0.077148	-0.00561	0.003118
0.046875	0.006189	0.082335	-0.0059	0.002787
0.054688	0.006568	0.088434	-0.00624	0.002408
0.0625	0.00699	0.095432	-0.00661	0.001986
0.070313	0.007447	0.103312	-0.007	0.001529
0.078125	0.007933	0.112054	-0.0074	0.001042
0.085938	0.00844	0.121639	-0.00782	0.000535
0.09375	0.00896	0.132041	-0.00823	1.52E-05
0.101563	0.009485	0.143238	-0.00862	-0.00051
0.109375	0.010004	0.155201	-0.00899	-0.00103
0.117188	0.010509	0.167901	-0.00932	-0.00153
0.125	0.010991	0.181309	-0.00961	-0.00202
0.132813	0.01144	0.195392	-0.00983	-0.00246
0.140625	0.011848	0.210116	-0.00999	-0.00287
0.148438	0.012204	0.225445	-0.01006	-0.00323
0.15625	0.012501	0.241342	-0.01005	-0.00353
0.164063	0.01273	0.25777	-0.00993	-0.00375
0.171875	0.012882	0.274689	-0.0097	-0.00391
0.179688	0.012951	0.292057	-0.00936	-0.00398
0.1875	0.01293	0.309834	-0.00888	-0.00395
0.195313	0.012813	0.327975	-0.00828	-0.00384
0.203125	0.012594	0.346439	-0.00753	-0.00362
0.210938	0.012269	0.365179	-0.00665	-0.00329
0.21875	0.011836	0.384151	-0.00561	-0.00286
0.226563	0.01129	0.403309	-0.00443	-0.00231
0.234375	0.010632	0.422608	-0.0031	-0.00166
0.242188	0.00986	0.442	-0.00162	-0.00088
0.25	0.008976	0.461438	-2.1E-18	-1.2E-18
0.257813	0.00798	0.480877	0.001768	0.000996
0.265625	0.006876	0.500269	0.003674	0.0021
0.273438	0.005668	0.519568	0.005712	0.003308
0.28125	0.00436	0.538726	0.007874	0.004616
0.289063	0.002959	0.557698	0.010153	0.006017
0.296875	0.00147	0.576438	0.012537	0.007505

0.304688	-9.7E-05	0.594902	0.015016	0.009073
0.3125	-0.00173	0.613043	0.017577	0.01071
0.320313	-0.00343	0.63082	0.020207	0.012408
0.328125	-0.00518	0.648188	0.022893	0.014157
0.335938	-0.00697	0.665107	0.025618	0.015946
0.34375	-0.00879	0.681534	0.028368	0.017764
0.351563	-0.01062	0.697432	0.031127	0.019598
0.359375	-0.01246	0.712761	0.033877	0.021438
0.367188	-0.01429	0.727485	0.036603	0.023269
0.375	-0.0161	0.741568	0.039286	0.025081
0.382813	-0.01788	0.754975	0.041911	0.026859
0.390625	-0.01962	0.767676	0.04446	0.028593
0.398438	-0.02129	0.779639	0.046917	0.03027
0.40625	-0.0229	0.790835	0.049265	0.031877
0.414063	-0.02443	0.801238	0.051489	0.033403
0.421875	-0.02586	0.810822	0.053575	0.034837
0.429688	-0.02719	0.819565	0.055508	0.036169
0.4375	-0.02841	0.827445	0.057275	0.037389
0.445313	-0.02951	0.834443	0.058863	0.038487
0.453125	-0.03048	0.840542	0.060263	0.039456
0.460938	-0.03131	0.845728	0.061464	0.040289
0.46875	-0.032	0.849989	0.062459	0.040979
0.476563	-0.03255	0.853313	0.06324	0.041521
0.484375	-0.03294	0.855693	0.063801	0.041911
0.492188	-0.03317	0.857124	0.06414	0.042146
0.5	-0.03325	0.857601	0.064253	0.042225
0.507813	-0.03317	0.857124	0.06414	0.042146
0.515625	-0.03294	0.855693	0.063801	0.041911
0.523438	-0.03255	0.853313	0.06324	0.041521
0.53125	-0.032	0.849989	0.062459	0.040979
0.539063	-0.03131	0.845728	0.061464	0.040289
0.546875	-0.03048	0.840542	0.060263	0.039456
0.554688	-0.02951	0.834443	0.058863	0.038487
0.5625	-0.02841	0.827445	0.057275	0.037389
0.570313	-0.02719	0.819565	0.055508	0.036169
0.578125	-0.02586	0.810822	0.053575	0.034837
0.585938	-0.02443	0.801238	0.051489	0.033403
0.59375	-0.0229	0.790835	0.049265	0.031877
0.601563	-0.02129	0.779639	0.046917	0.03027
0.609375	-0.01962	0.767676	0.04446	0.028593
0.617188	-0.01788	0.754975	0.041911	0.026859

0.625	-0.0161	0.741568	0.039286	0.025081
0.632813	-0.01429	0.727485	0.036603	0.023269
0.640625	-0.01246	0.712761	0.033877	0.021438
0.648438	-0.01062	0.697432	0.031127	0.019598
0.65625	-0.00879	0.681534	0.028368	0.017764
0.664063	-0.00697	0.665107	0.025618	0.015946
0.671875	-0.00518	0.648188	0.022893	0.014157
0.679688	-0.00343	0.63082	0.020207	0.012408
0.6875	-0.00173	0.613043	0.017577	0.01071
0.695313	-9.7E-05	0.594902	0.015016	0.009073
0.703125	0.00147	0.576438	0.012537	0.007505
0.710938	0.002959	0.557698	0.010153	0.006017
0.71875	0.00436	0.538726	0.007874	0.004616
0.726563	0.005668	0.519568	0.005712	0.003308
0.734375	0.006876	0.500269	0.003674	0.0021
0.742188	0.00798	0.480877	0.001768	0.000996
0.75	0.008976	0.461438	6.35E-18	3.52E-18
0.757813	0.00986	0.442	-0.00162	-0.00088
0.765625	0.010632	0.422608	-0.0031	-0.00166
0.773438	0.01129	0.403309	-0.00443	-0.00231
0.78125	0.011836	0.384151	-0.00561	-0.00286
0.789063	0.012269	0.365179	-0.00665	-0.00329
0.796875	0.012594	0.346439	-0.00753	-0.00362
0.804688	0.012813	0.327975	-0.00828	-0.00384
0.8125	0.01293	0.309834	-0.00888	-0.00395
0.820313	0.012951	0.292057	-0.00936	-0.00398
0.828125	0.012882	0.274689	-0.0097	-0.00391
0.835938	0.01273	0.25777	-0.00993	-0.00375
0.84375	0.012501	0.241342	-0.01005	-0.00353
0.851563	0.012204	0.225445	-0.01006	-0.00323
0.859375	0.011848	0.210116	-0.00999	-0.00287
0.867188	0.01144	0.195392	-0.00983	-0.00246
0.875	0.010991	0.181309	-0.00961	-0.00202
0.882813	0.010509	0.167901	-0.00932	-0.00153
0.890625	0.010004	0.155201	-0.00899	-0.00103
0.898438	0.009485	0.143238	-0.00862	-0.00051
0.90625	0.00896	0.132041	-0.00823	1.52E-05
0.914063	0.00844	0.121639	-0.00782	0.000535
0.921875	0.007933	0.112054	-0.0074	0.001042
0.929688	0.007447	0.103312	-0.007	0.001529
0.9375	0.00699	0.095432	-0.00661	0.001986

0.945313	0.006568	0.088434	-0.00624	0.002408
0.953125	0.006189	0.082335	-0.0059	0.002787
0.960938	0.005858	0.077148	-0.00561	0.003118
0.96875	0.00558	0.072888	-0.00536	0.003396
0.976563	0.005359	0.069564	-0.00516	0.003616
0.984375	0.0052	0.067184	-0.00501	0.003776
0.992188	0.005103	0.065753	-0.00492	0.003873
1	0.00507	0.065276	-0.00489	0.003906

Table 36 CFD Data Used to Create Figures 43 – 46

t/τ	C_x	C_y	C_P	C_T
0	0.007948	0.077209	-0.00723	0.000688
0.007813	0.007984	0.077664	-0.00726	0.000652
0.015625	0.008092	0.079025	-0.00737	0.000544
0.023438	0.00827	0.08128	-0.00753	0.000367
0.03125	0.008514	0.084427	-0.00775	0.000123
0.039063	0.00882	0.088459	-0.00804	-0.00018
0.046875	0.009184	0.093375	-0.00837	-0.00055
0.054688	0.009601	0.099171	-0.00874	-0.00097
0.0625	0.010063	0.105823	-0.00916	-0.00143
0.070313	0.010558	0.113285	-0.00959	-0.00192
0.078125	0.011081	0.121578	-0.01004	-0.00244
0.085938	0.011624	0.130707	-0.0105	-0.00299
0.09375	0.012176	0.140608	-0.01095	-0.00354
0.101563	0.012725	0.151286	-0.01138	-0.00409
0.109375	0.013256	0.162651	-0.01177	-0.00462
0.117188	0.01376	0.174721	-0.01212	-0.00512
0.125	0.014228	0.187492	-0.01242	-0.00559
0.132813	0.014649	0.200919	-0.01264	-0.00601
0.140625	0.015007	0.214923	-0.01277	-0.00637
0.148438	0.015298	0.229527	-0.0128	-0.00666
0.15625	0.015506	0.244695	-0.01273	-0.00687
0.164063	0.015625	0.26041	-0.01254	-0.00699
0.171875	0.015642	0.276636	-0.01221	-0.00701
0.179688	0.015548	0.293331	-0.01175	-0.00691
0.1875	0.015332	0.310483	-0.01113	-0.0067
0.195313	0.014989	0.32804	-0.01035	-0.00635
0.203125	0.014514	0.345867	-0.0094	-0.00588
0.210938	0.013898	0.363937	-0.00828	-0.00526
0.21875	0.013139	0.382248	-0.00698	-0.0045

0.226563	0.012235	0.400763	-0.00551	-0.0036
0.234375	0.011182	0.41944	-0.00385	-0.00255
0.242188	0.009981	0.438237	-0.00201	-0.00134
0.25	0.008636	0.457105	1.84E-17	0
0.257813	0.007141	0.47591	0.002187	0.001495
0.265625	0.00551	0.494694	0.004541	0.003127
0.273438	0.003744	0.513408	0.007055	0.004893
0.28125	0.00185	0.53201	0.00972	0.006786
0.289063	-0.00016	0.550448	0.012526	0.008799
0.296875	-0.00229	0.568668	0.01546	0.010922
0.304688	-0.00451	0.586654	0.018509	0.013142
0.3125	-0.00682	0.604435	0.021662	0.015455
0.320313	-0.00921	0.621821	0.024899	0.017843
0.328125	-0.01166	0.638801	0.028201	0.020293
0.335938	-0.01415	0.655294	0.03155	0.022789
0.34375	-0.01667	0.671201	0.034923	0.025309
0.351563	-0.01921	0.686637	0.038306	0.027842
0.359375	-0.02174	0.701472	0.041676	0.03038
0.367188	-0.02427	0.715791	0.045018	0.032908
0.375	-0.02677	0.729532	0.048311	0.035406
0.382813	-0.02922	0.742613	0.051531	0.037854
0.390625	-0.0316	0.755034	0.05466	0.040238
0.398438	-0.0339	0.766703	0.057673	0.042538
0.40625	-0.0361	0.77765	0.060555	0.044741
0.414063	-0.03819	0.7878	0.063282	0.046829
0.421875	-0.04015	0.797167	0.065841	0.048791
0.429688	-0.04198	0.805705	0.068211	0.050612
0.4375	-0.04364	0.813408	0.070379	0.052278
0.445313	-0.04514	0.82026	0.072328	0.05378
0.453125	-0.04647	0.82623	0.074046	0.055104
0.460938	-0.0476	0.831322	0.075522	0.056241
0.46875	-0.04855	0.835538	0.076746	0.057189
0.476563	-0.0493	0.838826	0.077707	0.057933
0.484375	-0.04983	0.841179	0.078399	0.058468
0.492188	-0.05015	0.842592	0.078815	0.058791
0.5	-0.05026	0.843063	0.078954	0.058899
0.507813	-0.05015	0.842592	0.078815	0.058791
0.515625	-0.04983	0.841179	0.078399	0.058468
0.523438	-0.0493	0.838826	0.077707	0.057933
0.53125	-0.04855	0.835538	0.076746	0.057189
0.539063	-0.0476	0.831322	0.075522	0.056241

0.546875	-0.04647	0.82623	0.074046	0.055104
0.554688	-0.04514	0.82026	0.072328	0.05378
0.5625	-0.04364	0.813408	0.070379	0.052278
0.570313	-0.04198	0.805705	0.068211	0.050612
0.578125	-0.04015	0.797167	0.065841	0.048791
0.585938	-0.03819	0.7878	0.063282	0.046829
0.59375	-0.0361	0.77765	0.060555	0.044741
0.601563	-0.0339	0.766703	0.057673	0.042538
0.609375	-0.0316	0.755034	0.05466	0.040238
0.617188	-0.02922	0.742613	0.051531	0.037854
0.625	-0.02677	0.729532	0.048311	0.035406
0.632813	-0.02427	0.715791	0.045018	0.032908
0.640625	-0.02174	0.701472	0.041676	0.03038
0.648438	-0.01921	0.686637	0.038306	0.027842
0.65625	-0.01667	0.671201	0.034923	0.025309
0.664063	-0.01415	0.655294	0.03155	0.022789
0.671875	-0.01166	0.638801	0.028201	0.020293
0.679688	-0.00921	0.621821	0.024899	0.017843
0.6875	-0.00682	0.604435	0.021662	0.015455
0.695313	-0.00451	0.586654	0.018509	0.013142
0.703125	-0.00229	0.568668	0.01546	0.010922
0.710938	-0.00016	0.550448	0.012526	0.008799
0.71875	0.00185	0.53201	0.00972	0.006786
0.726563	0.003744	0.513408	0.007055	0.004893
0.734375	0.00551	0.494694	0.004541	0.003127
0.742188	0.007141	0.47591	0.002187	0.001495
0.75	0.008636	0.457105	-1.3E-17	0
0.757813	0.009981	0.438237	-0.00201	-0.00134
0.765625	0.011182	0.41944	-0.00385	-0.00255
0.773438	0.012235	0.400763	-0.00551	-0.0036
0.78125	0.013139	0.382248	-0.00698	-0.0045
0.789063	0.013898	0.363937	-0.00828	-0.00526
0.796875	0.014514	0.345867	-0.0094	-0.00588
0.804688	0.014989	0.32804	-0.01035	-0.00635
0.8125	0.015332	0.310483	-0.01113	-0.0067
0.820313	0.015548	0.293331	-0.01175	-0.00691
0.828125	0.015642	0.276636	-0.01221	-0.00701
0.835938	0.015625	0.26041	-0.01254	-0.00699
0.84375	0.015506	0.244695	-0.01273	-0.00687
0.851563	0.015298	0.229527	-0.0128	-0.00666
0.859375	0.015007	0.214923	-0.01277	-0.00637

0.867188	0.014649	0.200919	-0.01264	-0.00601
0.875	0.014228	0.187492	-0.01242	-0.00559
0.882813	0.01376	0.174721	-0.01212	-0.00512
0.890625	0.013256	0.162651	-0.01177	-0.00462
0.898438	0.012725	0.151286	-0.01138	-0.00409
0.90625	0.012176	0.140608	-0.01095	-0.00354
0.914063	0.011624	0.130707	-0.0105	-0.00299
0.921875	0.011081	0.121578	-0.01004	-0.00244
0.929688	0.010558	0.113285	-0.00959	-0.00192
0.9375	0.010063	0.105823	-0.00916	-0.00143
0.945313	0.009601	0.099171	-0.00874	-0.00097
0.953125	0.009184	0.093375	-0.00837	-0.00055
0.960938	0.00882	0.088459	-0.00804	-0.00018
0.96875	0.008514	0.084427	-0.00775	0.000123
0.976563	0.00827	0.08128	-0.00753	0.000367
0.984375	0.008092	0.079025	-0.00737	0.000544
0.992188	0.007984	0.077664	-0.00726	0.000652
1	0.007948	0.077209	-0.00723	0.000688

Table 37 Lifting-Line Data Used to Create Figures 43 – 46

t/τ	C_x	C_y	C_P	C_T
0	0.006293	0.065276	-0.00611	0.002683
0.007813	0.006333	0.065753	-0.00615	0.002643
0.015625	0.006452	0.067184	-0.00626	0.002524
0.023438	0.006648	0.069564	-0.00644	0.002327
0.03125	0.006919	0.072888	-0.00669	0.002057
0.039063	0.007259	0.077148	-0.00701	0.001716
0.046875	0.007665	0.082335	-0.00738	0.001311
0.054688	0.008128	0.088434	-0.0078	0.000848
0.0625	0.008641	0.095432	-0.00826	0.000335
0.070313	0.009196	0.103312	-0.00875	-0.00022
0.078125	0.009784	0.112054	-0.00925	-0.00081
0.085938	0.010395	0.121639	-0.00977	-0.00142
0.09375	0.011017	0.132041	-0.01028	-0.00204
0.101563	0.01164	0.143238	-0.01077	-0.00266
0.109375	0.012251	0.155201	-0.01124	-0.00328
0.117188	0.012839	0.167901	-0.01165	-0.00386
0.125	0.013392	0.181309	-0.01201	-0.00442
0.132813	0.013898	0.195392	-0.01229	-0.00492
0.140625	0.014344	0.210116	-0.01248	-0.00537

0.148438	0.01472	0.225445	-0.01258	-0.00574
0.15625	0.015012	0.241342	-0.01256	-0.00604
0.164063	0.015212	0.25777	-0.01241	-0.00624
0.171875	0.015307	0.274689	-0.01213	-0.00633
0.179688	0.01529	0.292057	-0.01169	-0.00631
0.1875	0.015151	0.309834	-0.0111	-0.00618
0.195313	0.014882	0.327975	-0.01035	-0.00591
0.203125	0.014478	0.346439	-0.00942	-0.0055
0.210938	0.013931	0.365179	-0.00831	-0.00496
0.21875	0.013239	0.384151	-0.00702	-0.00426
0.226563	0.012399	0.403309	-0.00554	-0.00342
0.234375	0.011408	0.422608	-0.00388	-0.00243
0.242188	0.010267	0.442	-0.00203	-0.00129
0.25	0.008976	0.461438	-2.6E-18	-1.7E-18
0.257813	0.007538	0.480877	0.00221	0.001438
0.265625	0.005958	0.500269	0.004592	0.003018
0.273438	0.00424	0.519568	0.00714	0.004736
0.28125	0.002391	0.538726	0.009843	0.006584
0.289063	0.00042	0.557698	0.012691	0.008555
0.296875	-0.00166	0.576438	0.015671	0.01064
0.304688	-0.00385	0.594902	0.018769	0.012826
0.3125	-0.00613	0.613043	0.021971	0.015104
0.320313	-0.00848	0.63082	0.025259	0.01746
0.328125	-0.0109	0.648188	0.028616	0.01988
0.335938	-0.01338	0.665107	0.032023	0.022351
0.34375	-0.01588	0.681534	0.03546	0.024856
0.351563	-0.0184	0.697432	0.038909	0.02738
0.359375	-0.02093	0.712761	0.042347	0.029907
0.367188	-0.02344	0.727485	0.045754	0.03242
0.375	-0.02593	0.741568	0.049108	0.034902
0.382813	-0.02836	0.754975	0.052389	0.037337
0.390625	-0.03073	0.767676	0.055575	0.039708
0.398438	-0.03302	0.779639	0.058646	0.041999
0.40625	-0.03522	0.790835	0.061581	0.044193
0.414063	-0.0373	0.801238	0.064362	0.046275
0.421875	-0.03926	0.810822	0.066969	0.048231
0.429688	-0.04107	0.819565	0.069385	0.050046
0.4375	-0.04273	0.827445	0.071593	0.051707
0.445313	-0.04423	0.834443	0.073579	0.053203
0.453125	-0.04555	0.840542	0.075329	0.054522
0.460938	-0.04668	0.845728	0.07683	0.055655

0.46875	-0.04762	0.849989	0.078074	0.056594
0.476563	-0.04836	0.853313	0.079049	0.057331
0.484375	-0.04889	0.855693	0.079751	0.057861
0.492188	-0.04921	0.857124	0.080175	0.058181
0.5	-0.04931	0.857601	0.080316	0.058288
0.507813	-0.04921	0.857124	0.080175	0.058181
0.515625	-0.04889	0.855693	0.079751	0.057861
0.523438	-0.04836	0.853313	0.079049	0.057331
0.53125	-0.04762	0.849989	0.078074	0.056594
0.539063	-0.04668	0.845728	0.07683	0.055655
0.546875	-0.04555	0.840542	0.075329	0.054522
0.554688	-0.04423	0.834443	0.073579	0.053203
0.5625	-0.04273	0.827445	0.071593	0.051707
0.570313	-0.04107	0.819565	0.069385	0.050046
0.578125	-0.03926	0.810822	0.066969	0.048231
0.585938	-0.0373	0.801238	0.064362	0.046275
0.59375	-0.03522	0.790835	0.061581	0.044193
0.601563	-0.03302	0.779639	0.058646	0.041999
0.609375	-0.03073	0.767676	0.055575	0.039708
0.617188	-0.02836	0.754975	0.052389	0.037337
0.625	-0.02593	0.741568	0.049108	0.034902
0.632813	-0.02344	0.727485	0.045754	0.03242
0.640625	-0.02093	0.712761	0.042347	0.029907
0.648438	-0.0184	0.697432	0.038909	0.02738
0.65625	-0.01588	0.681534	0.03546	0.024856
0.664063	-0.01338	0.665107	0.032023	0.022351
0.671875	-0.0109	0.648188	0.028616	0.01988
0.679688	-0.00848	0.63082	0.025259	0.01746
0.6875	-0.00613	0.613043	0.021971	0.015104
0.695313	-0.00385	0.594902	0.018769	0.012826
0.703125	-0.00166	0.576438	0.015671	0.01064
0.710938	0.00042	0.557698	0.012691	0.008555
0.71875	0.002391	0.538726	0.009843	0.006584
0.726563	0.00424	0.519568	0.00714	0.004736
0.734375	0.005958	0.500269	0.004592	0.003018
0.742188	0.007538	0.480877	0.00221	0.001438
0.75	0.008976	0.461438	7.94E-18	5.11E-18
0.757813	0.010267	0.442	-0.00203	-0.00129
0.765625	0.011408	0.422608	-0.00388	-0.00243
0.773438	0.012399	0.403309	-0.00554	-0.00342
0.78125	0.013239	0.384151	-0.00702	-0.00426

0.789063	0.013931	0.365179	-0.00831	-0.00496
0.796875	0.014478	0.346439	-0.00942	-0.0055
0.804688	0.014882	0.327975	-0.01035	-0.00591
0.8125	0.015151	0.309834	-0.0111	-0.00618
0.820313	0.01529	0.292057	-0.01169	-0.00631
0.828125	0.015307	0.274689	-0.01213	-0.00633
0.835938	0.015212	0.25777	-0.01241	-0.00624
0.84375	0.015012	0.241342	-0.01256	-0.00604
0.851563	0.01472	0.225445	-0.01258	-0.00574
0.859375	0.014344	0.210116	-0.01248	-0.00537
0.867188	0.013898	0.195392	-0.01229	-0.00492
0.875	0.013392	0.181309	-0.01201	-0.00442
0.882813	0.012839	0.167901	-0.01165	-0.00386
0.890625	0.012251	0.155201	-0.01124	-0.00328
0.898438	0.01164	0.143238	-0.01077	-0.00266
0.90625	0.011017	0.132041	-0.01028	-0.00204
0.914063	0.010395	0.121639	-0.00977	-0.00142
0.921875	0.009784	0.112054	-0.00925	-0.00081
0.929688	0.009196	0.103312	-0.00875	-0.00022
0.9375	0.008641	0.095432	-0.00826	0.000335
0.945313	0.008128	0.088434	-0.0078	0.000848
0.953125	0.007665	0.082335	-0.00738	0.001311
0.960938	0.007259	0.077148	-0.00701	0.001716
0.96875	0.006919	0.072888	-0.00669	0.002057
0.976563	0.006648	0.069564	-0.00644	0.002327
0.984375	0.006452	0.067184	-0.00626	0.002524
0.992188	0.006333	0.065753	-0.00615	0.002643
1	0.006293	0.065276	-0.00611	0.002683

Table 38 CFD Data Used to Create Figures 47 – 50

t/τ	C_x	C_y	C_P	C_T
0	0.005473	0.076478	-0.00477	0.003151
0.007813	0.005498	0.076932	-0.0048	0.003126
0.015625	0.005573	0.078295	-0.00486	0.003051
0.023438	0.005697	0.080561	-0.00498	0.002927
0.03125	0.005868	0.083729	-0.00513	0.002756
0.039063	0.006084	0.087788	-0.00532	0.00254
0.046875	0.006342	0.092734	-0.00554	0.002282
0.054688	0.006638	0.098582	-0.0058	0.001986
0.0625	0.006968	0.105293	-0.00607	0.001657

0.070313	0.007325	0.112843	-0.00637	0.001299
0.078125	0.007705	0.121216	-0.00667	0.000919
0.085938	0.008102	0.130411	-0.00698	0.000523
0.09375	0.008508	0.140398	-0.00729	0.000116
0.101563	0.008918	0.151145	-0.00758	-0.00029
0.109375	0.009323	0.162605	-0.00785	-0.0007
0.117188	0.009715	0.17473	-0.00808	-0.00109
0.125	0.01009	0.187549	-0.00828	-0.00147
0.132813	0.010442	0.20103	-0.00843	-0.00182
0.140625	0.010763	0.215162	-0.00852	-0.00214
0.148438	0.011045	0.229865	-0.00855	-0.00242
0.15625	0.01128	0.245086	-0.0085	-0.00266
0.164063	0.011462	0.260798	-0.00837	-0.00284
0.171875	0.011585	0.277028	-0.00815	-0.00296
0.179688	0.011646	0.293742	-0.00784	-0.00302
0.1875	0.011637	0.310835	-0.00743	-0.00301
0.195313	0.011553	0.328275	-0.0069	-0.00293
0.203125	0.011391	0.34606	-0.00627	-0.00277
0.210938	0.011148	0.364132	-0.00552	-0.00252
0.21875	0.01082	0.382428	-0.00466	-0.0022
0.226563	0.010406	0.40092	-0.00367	-0.00178
0.234375	0.009903	0.419571	-0.00257	-0.00128
0.242188	0.009313	0.438297	-0.00134	-0.00069
0.25	0.008636	0.457105	1.22E-17	-1.2E-05
0.257813	0.007869	0.475864	0.001458	0.000755
0.265625	0.007018	0.494593	0.003027	0.001606
0.273438	0.006087	0.51324	0.004702	0.002537
0.28125	0.005078	0.531761	0.006477	0.003546
0.289063	0.003996	0.550113	0.008345	0.004628
0.296875	0.002846	0.568239	0.010299	0.005778
0.304688	0.001634	0.586102	0.012328	0.00699
0.3125	0.000368	0.603664	0.014423	0.008256
0.320313	-0.00095	0.620885	0.016574	0.009572
0.328125	-0.0023	0.637713	0.018769	0.010927
0.335938	-0.00369	0.654016	0.020992	0.012313
0.34375	-0.00509	0.669809	0.023234	0.013716
0.351563	-0.00651	0.68514	0.025482	0.015132
0.359375	-0.00793	0.699932	0.027723	0.016553
0.367188	-0.00935	0.714195	0.029945	0.017971
0.375	-0.01075	0.727828	0.032132	0.019374
0.382813	-0.01213	0.740822	0.034271	0.020753

0.390625	-0.01347	0.75315	0.036349	0.022099
0.398438	-0.01478	0.764763	0.038351	0.023401
0.40625	-0.01603	0.775638	0.040265	0.024652
0.414063	-0.01722	0.785733	0.042078	0.025839
0.421875	-0.01833	0.795045	0.043777	0.026954
0.429688	-0.01937	0.803537	0.045352	0.02799
0.4375	-0.02032	0.811212	0.046792	0.028939
0.445313	-0.02117	0.818006	0.048086	0.029796
0.453125	-0.02193	0.823957	0.049228	0.030552
0.460938	-0.02258	0.829036	0.050209	0.031201
0.46875	-0.02311	0.833196	0.051021	0.031737
0.476563	-0.02353	0.836433	0.051657	0.032156
0.484375	-0.02384	0.83876	0.052116	0.03246
0.492188	-0.02402	0.840146	0.052391	0.032642
0.5	-0.02408	0.840608	0.052483	0.032703
0.507813	-0.02402	0.840146	0.052391	0.032642
0.515625	-0.02384	0.83876	0.052116	0.03246
0.523438	-0.02353	0.836433	0.051657	0.032156
0.53125	-0.02311	0.833196	0.051021	0.031737
0.539063	-0.02258	0.829036	0.050209	0.031201
0.546875	-0.02193	0.823957	0.049228	0.030552
0.554688	-0.02117	0.818006	0.048086	0.029796
0.5625	-0.02032	0.811212	0.046792	0.028939
0.570313	-0.01937	0.803537	0.045352	0.02799
0.578125	-0.01833	0.795045	0.043777	0.026954
0.585938	-0.01722	0.785733	0.042078	0.025839
0.59375	-0.01603	0.775638	0.040265	0.024652
0.601563	-0.01478	0.764763	0.038351	0.023401
0.609375	-0.01347	0.75315	0.036349	0.022099
0.617188	-0.01213	0.740822	0.034271	0.020753
0.625	-0.01075	0.727828	0.032132	0.019374
0.632813	-0.00935	0.714195	0.029945	0.017971
0.640625	-0.00793	0.699932	0.027723	0.016553
0.648438	-0.00651	0.68514	0.025482	0.015132
0.65625	-0.00509	0.669809	0.023234	0.013716
0.664063	-0.00369	0.654016	0.020992	0.012313
0.671875	-0.0023	0.637713	0.018769	0.010927
0.679688	-0.00095	0.620885	0.016574	0.009572
0.6875	0.000368	0.603664	0.014423	0.008256
0.695313	0.001634	0.586102	0.012328	0.00699
0.703125	0.002846	0.568239	0.010299	0.005778

0.710938	0.003996	0.550113	0.008345	0.004628
0.71875	0.005078	0.531761	0.006477	0.003546
0.726563	0.006087	0.513239	0.004702	0.002537
0.734375	0.007018	0.494593	0.003027	0.001606
0.742188	0.007869	0.475864	0.001458	0.000755
0.75	0.008636	0.457105	-8.7E-18	-1.2E-05
0.757813	0.009313	0.438297	-0.00134	-0.00069
0.765625	0.009903	0.419571	-0.00257	-0.00128
0.773438	0.010406	0.40092	-0.00367	-0.00178
0.78125	0.01082	0.382428	-0.00466	-0.0022
0.789063	0.011148	0.364132	-0.00552	-0.00252
0.796875	0.011391	0.34606	-0.00627	-0.00277
0.804688	0.011553	0.328275	-0.0069	-0.00293
0.8125	0.011637	0.310835	-0.00743	-0.00301
0.820313	0.011646	0.293742	-0.00784	-0.00302
0.828125	0.011585	0.277028	-0.00815	-0.00296
0.835938	0.011462	0.260798	-0.00837	-0.00284
0.84375	0.01128	0.245086	-0.0085	-0.00266
0.851563	0.011045	0.229865	-0.00855	-0.00242
0.859375	0.010763	0.215162	-0.00852	-0.00214
0.867188	0.010442	0.20103	-0.00843	-0.00182
0.875	0.01009	0.187549	-0.00828	-0.00147
0.882813	0.009715	0.17473	-0.00808	-0.00109
0.890625	0.009323	0.162605	-0.00785	-0.0007
0.898438	0.008918	0.151145	-0.00758	-0.00029
0.90625	0.008508	0.140398	-0.00729	0.000116
0.914063	0.008102	0.130411	-0.00698	0.000523
0.921875	0.007705	0.121216	-0.00667	0.000919
0.929688	0.007325	0.112843	-0.00637	0.001299
0.9375	0.006968	0.105293	-0.00607	0.001657
0.945313	0.006638	0.098582	-0.0058	0.001986
0.953125	0.006342	0.092734	-0.00554	0.002282
0.960938	0.006084	0.087788	-0.00532	0.00254
0.96875	0.005868	0.083729	-0.00513	0.002756
0.976563	0.005697	0.080561	-0.00498	0.002927
0.984375	0.005573	0.078295	-0.00486	0.003051
0.992188	0.005498	0.076932	-0.0048	0.003126
1	0.005473	0.076478	-0.00477	0.003151

Table 39 Lifting-Line Data Used to Create Figures 47 – 50

t/τ	C_x	C_y	C_P	C_T
0	0.004255	0.065276	-0.00408	0.004721
0.007813	0.004283	0.065753	-0.0041	0.004693
0.015625	0.004365	0.067184	-0.00417	0.004611
0.023438	0.0045	0.069564	-0.0043	0.004476
0.03125	0.004687	0.072888	-0.00446	0.004288
0.039063	0.004923	0.077148	-0.00467	0.004052
0.046875	0.005205	0.082335	-0.00492	0.003771
0.054688	0.005528	0.088434	-0.0052	0.003447
0.0625	0.005889	0.095432	-0.0055	0.003087
0.070313	0.006281	0.103312	-0.00583	0.002695
0.078125	0.006699	0.112054	-0.00617	0.002276
0.085938	0.007138	0.121639	-0.00651	0.001838
0.09375	0.00759	0.132041	-0.00685	0.001386
0.101563	0.008048	0.143238	-0.00718	0.000928
0.109375	0.008506	0.155201	-0.00749	0.00047
0.117188	0.008956	0.167901	-0.00777	2E-05
0.125	0.00939	0.181309	-0.008	-0.00041
0.132813	0.009802	0.195392	-0.00819	-0.00083
0.140625	0.010183	0.210116	-0.00832	-0.00121
0.148438	0.010527	0.225445	-0.00838	-0.00155
0.15625	0.010827	0.241342	-0.00837	-0.00185
0.164063	0.011075	0.25777	-0.00827	-0.0021
0.171875	0.011265	0.274689	-0.00808	-0.00229
0.179688	0.011392	0.292057	-0.0078	-0.00242
0.1875	0.011449	0.309834	-0.0074	-0.00247
0.195313	0.011433	0.327975	-0.0069	-0.00246
0.203125	0.011338	0.346439	-0.00628	-0.00236
0.210938	0.011161	0.365179	-0.00554	-0.00219
0.21875	0.0109	0.384151	-0.00468	-0.00192
0.226563	0.010551	0.403309	-0.00369	-0.00158
0.234375	0.010115	0.422608	-0.00259	-0.00114
0.242188	0.009589	0.442	-0.00135	-0.00061
0.25	0.008976	0.461438	-1.8E-18	-8.2E-19
0.257813	0.008275	0.480877	0.001473	0.000701
0.265625	0.007488	0.500269	0.003061	0.001487
0.273438	0.00662	0.519568	0.00476	0.002356
0.28125	0.005672	0.538726	0.006562	0.003303
0.289063	0.004651	0.557698	0.00846	0.004325
0.296875	0.00356	0.576438	0.010447	0.005416

0.304688	0.002406	0.594902	0.012513	0.00657
0.3125	0.001195	0.613043	0.014647	0.00778
0.320313	-6.5E-05	0.63082	0.016839	0.00904
0.328125	-0.00137	0.648188	0.019077	0.010342
0.335938	-0.0027	0.665107	0.021348	0.011677
0.34375	-0.00406	0.681534	0.02364	0.013036
0.351563	-0.00543	0.697432	0.025939	0.01441
0.359375	-0.00682	0.712761	0.028231	0.015791
0.367188	-0.00819	0.727485	0.030502	0.017169
0.375	-0.00956	0.741568	0.032739	0.018533
0.382813	-0.0109	0.754975	0.034926	0.019874
0.390625	-0.01221	0.767676	0.03705	0.021183
0.398438	-0.01347	0.779639	0.039097	0.02245
0.40625	-0.01469	0.790835	0.041054	0.023666
0.414063	-0.01585	0.801238	0.042908	0.024821
0.421875	-0.01693	0.810822	0.044646	0.025908
0.429688	-0.01794	0.819565	0.046256	0.026918
0.4375	-0.01887	0.827445	0.047729	0.027843
0.445313	-0.0197	0.834443	0.049053	0.028677
0.453125	-0.02044	0.840542	0.050219	0.029413
0.460938	-0.02107	0.845728	0.05122	0.030045
0.46875	-0.02159	0.849989	0.052049	0.030569
0.476563	-0.02201	0.853313	0.0527	0.030981
0.484375	-0.0223	0.855693	0.053168	0.031278
0.492188	-0.02248	0.857124	0.05345	0.031456
0.5	-0.02254	0.857601	0.053544	0.031516
0.507813	-0.02248	0.857124	0.05345	0.031456
0.515625	-0.0223	0.855693	0.053168	0.031278
0.523438	-0.02201	0.853313	0.0527	0.030981
0.53125	-0.02159	0.849989	0.052049	0.030569
0.539063	-0.02107	0.845728	0.05122	0.030045
0.546875	-0.02044	0.840542	0.050219	0.029413
0.554688	-0.0197	0.834443	0.049053	0.028677
0.5625	-0.01887	0.827445	0.047729	0.027843
0.570313	-0.01794	0.819565	0.046256	0.026918
0.578125	-0.01693	0.810822	0.044646	0.025908
0.585938	-0.01585	0.801238	0.042908	0.024821
0.59375	-0.01469	0.790835	0.041054	0.023666
0.601563	-0.01347	0.779639	0.039097	0.02245
0.609375	-0.01221	0.767676	0.03705	0.021183
0.617188	-0.0109	0.754975	0.034926	0.019874

0.625	-0.00956	0.741568	0.032739	0.018533
0.632813	-0.00819	0.727485	0.030502	0.017169
0.640625	-0.00682	0.712761	0.028231	0.015791
0.648438	-0.00543	0.697432	0.025939	0.01441
0.65625	-0.00406	0.681534	0.02364	0.013036
0.664063	-0.0027	0.665107	0.021348	0.011677
0.671875	-0.00137	0.648188	0.019077	0.010342
0.679688	-6.5E-05	0.63082	0.016839	0.00904
0.6875	0.001195	0.613043	0.014647	0.00778
0.695313	0.002406	0.594902	0.012513	0.00657
0.703125	0.00356	0.576438	0.010447	0.005416
0.710938	0.004651	0.557698	0.00846	0.004325
0.71875	0.005672	0.538726	0.006562	0.003303
0.726563	0.00662	0.519568	0.00476	0.002356
0.734375	0.007488	0.500269	0.003061	0.001487
0.742188	0.008275	0.480877	0.001473	0.000701
0.75	0.008976	0.461438	5.29E-18	2.46E-18
0.757813	0.009589	0.442	-0.00135	-0.00061
0.765625	0.010115	0.422608	-0.00259	-0.00114
0.773438	0.010551	0.403309	-0.00369	-0.00158
0.78125	0.0109	0.384151	-0.00468	-0.00192
0.789063	0.011161	0.365179	-0.00554	-0.00219
0.796875	0.011338	0.346439	-0.00628	-0.00236
0.804688	0.011433	0.327975	-0.0069	-0.00246
0.8125	0.011449	0.309834	-0.0074	-0.00247
0.820313	0.011392	0.292057	-0.0078	-0.00242
0.828125	0.011265	0.274689	-0.00808	-0.00229
0.835938	0.011075	0.25777	-0.00827	-0.0021
0.84375	0.010827	0.241342	-0.00837	-0.00185
0.851563	0.010527	0.225445	-0.00838	-0.00155
0.859375	0.010183	0.210116	-0.00832	-0.00121
0.867188	0.009802	0.195392	-0.00819	-0.00083
0.875	0.00939	0.181309	-0.008	-0.00041
0.882813	0.008956	0.167901	-0.00777	2E-05
0.890625	0.008506	0.155201	-0.00749	0.00047
0.898438	0.008048	0.143238	-0.00718	0.000928
0.90625	0.00759	0.132041	-0.00685	0.001386
0.914063	0.007138	0.121639	-0.00651	0.001838
0.921875	0.006699	0.112054	-0.00617	0.002276
0.929688	0.006281	0.103312	-0.00583	0.002695
0.9375	0.005889	0.095432	-0.0055	0.003087

0.945313	0.005528	0.088434	-0.0052	0.003447
0.953125	0.005205	0.082335	-0.00492	0.003771
0.960938	0.004923	0.077148	-0.00467	0.004052
0.96875	0.004687	0.072888	-0.00446	0.004288
0.976563	0.0045	0.069564	-0.0043	0.004476
0.984375	0.004365	0.067184	-0.00417	0.004611
0.992188	0.004283	0.065753	-0.0041	0.004693
1	0.004255	0.065276	-0.00408	0.004721

Table 40 CFD Data Used to Create Figures 51 – 54

t/τ	C_x	C_y	C_P	C_T
0.005208	0.007641	0.095441	-0.00715	0.000983
0.010417	0.007557	0.094858	-0.00709	0.001067
0.015625	0.007471	0.094356	-0.00704	0.001153
0.020833	0.007498	0.094715	-0.00704	0.001126
0.026042	0.007497	0.095298	-0.00704	0.001127
0.03125	0.007509	0.095914	-0.00705	0.001115
0.036458	0.007526	0.097368	-0.0071	0.001098
0.041667	0.007584	0.099029	-0.00717	0.00104
0.046875	0.007672	0.100953	-0.00724	0.000952
0.052083	0.007789	0.103377	-0.00733	0.000835
0.057292	0.007896	0.106265	-0.00745	0.000728
0.0625	0.00804	0.109393	-0.00757	0.000584
0.067708	0.008212	0.112929	-0.00771	0.000412
0.072917	0.008384	0.116808	-0.00785	0.00024
0.078125	0.008577	0.121093	-0.008	4.74E-05
0.083333	0.008786	0.125739	-0.00816	-0.00016
0.088542	0.009016	0.130693	-0.00832	-0.00039
0.09375	0.009234	0.135966	-0.00847	-0.00061
0.098958	0.009477	0.141682	-0.00863	-0.00085
0.104167	0.00973	0.147621	-0.00877	-0.00111
0.109375	0.009932	0.154017	-0.00892	-0.00131
0.114583	0.010229	0.160577	-0.00905	-0.0016
0.119792	0.010465	0.167602	-0.00916	-0.00184
0.125	0.010704	0.174793	-0.00926	-0.00208
0.130208	0.010925	0.182457	-0.00934	-0.0023
0.135417	0.0112	0.190305	-0.0094	-0.00258
0.140625	0.011383	0.198455	-0.00943	-0.00276
0.145833	0.011603	0.20681	-0.00943	-0.00298
0.151042	0.011805	0.215556	-0.00941	-0.00318

0.15625	0.011991	0.224418	-0.00934	-0.00337
0.161458	0.012078	0.233673	-0.00924	-0.00345
0.166667	0.012308	0.243091	-0.00911	-0.00368
0.171875	0.012374	0.252769	-0.00893	-0.00375
0.177083	0.012465	0.262683	-0.0087	-0.00384
0.182292	0.012464	0.272739	-0.00843	-0.00384
0.1875	0.012553	0.283039	-0.00812	-0.00393
0.192708	0.012548	0.293575	-0.00775	-0.00392
0.197917	0.012501	0.304287	-0.00733	-0.00388
0.203125	0.012393	0.315117	-0.00685	-0.00377
0.208333	0.012277	0.326068	-0.00632	-0.00365
0.213542	0.012094	0.337195	-0.00574	-0.00347
0.21875	0.011905	0.348451	-0.00509	-0.00328
0.223958	0.011685	0.359851	-0.00439	-0.00306
0.229167	0.011434	0.371371	-0.00363	-0.00281
0.234375	0.011105	0.382982	-0.00281	-0.00248
0.239583	0.010726	0.394665	-0.00193	-0.0021
0.244792	0.010308	0.40642	-0.001	-0.00168
0.25	0.009849	0.418228	-4.5E-15	-0.00122
0.255208	0.009343	0.430078	0.001054	-0.00072
0.260417	0.00879	0.441957	0.002166	-0.00017
0.265625	0.008194	0.453844	0.003333	0.00043
0.270833	0.007553	0.465742	0.004555	0.001071
0.276042	0.006862	0.477632	0.005829	0.001762
0.28125	0.00613	0.489512	0.007155	0.002494
0.286458	0.005347	0.501341	0.008529	0.003277
0.291667	0.004522	0.513138	0.00995	0.004102
0.296875	0.003674	0.524896	0.011416	0.00495
0.302083	0.002788	0.536568	0.012922	0.005836
0.307292	0.001877	0.548153	0.014466	0.006747
0.3125	0.000919	0.559699	0.016047	0.007705
0.317708	-4.8E-05	0.571065	0.017658	0.008672
0.322917	-0.0011	0.582343	0.019297	0.00972
0.328125	-0.00215	0.593526	0.020962	0.010778
0.333333	-0.00325	0.604515	0.022646	0.011878
0.338542	-0.00428	0.615297	0.024343	0.012901
0.34375	-0.0054	0.626061	0.026059	0.014025
0.348958	-0.00658	0.636512	0.027777	0.0152
0.354167	-0.00769	0.64691	0.029505	0.016312
0.359375	-0.00884	0.656957	0.031225	0.017468
0.364583	-0.01002	0.666892	0.032944	0.018642

0.369792	-0.01116	0.676564	0.034651	0.01978
0.375	-0.01233	0.686074	0.036347	0.020951
0.380208	-0.0135	0.695194	0.038015	0.022127
0.385417	-0.01465	0.704234	0.039669	0.023278
0.390625	-0.01576	0.712879	0.041287	0.024385
0.395833	-0.01694	0.721323	0.042875	0.025565
0.401042	-0.01803	0.729376	0.044419	0.026652
0.40625	-0.01911	0.737323	0.045932	0.027732
0.411458	-0.02021	0.744873	0.047391	0.028834
0.416667	-0.02125	0.752068	0.048797	0.029869
0.421875	-0.02224	0.758989	0.05015	0.030868
0.427083	-0.02323	0.765607	0.051445	0.031851
0.432292	-0.02419	0.771891	0.052676	0.032809
0.4375	-0.02507	0.777758	0.053835	0.033695
0.442708	-0.02591	0.783235	0.05492	0.034529
0.447917	-0.02676	0.788581	0.055946	0.035382
0.453125	-0.02751	0.793438	0.056886	0.036132
0.458333	-0.02821	0.797886	0.057742	0.036833
0.463542	-0.02887	0.801995	0.058517	0.037496
0.46875	-0.02952	0.805914	0.05922	0.038144
0.473958	-0.03013	0.809188	0.059816	0.038753
0.479167	-0.03054	0.812189	0.06033	0.039164
0.484375	-0.03087	0.814743	0.060748	0.039492
0.489583	-0.0314	0.817259	0.061099	0.04002
0.494792	-0.03161	0.819108	0.061336	0.040235
0.5	-0.03191	0.820134	0.061446	0.040539
0.505208	-0.03206	0.821867	0.061543	0.040688
0.510417	-0.03215	0.82207	0.061459	0.040773
0.515625	-0.03218	0.822412	0.06132	0.040804
0.520833	-0.03222	0.822951	0.061129	0.040848
0.526042	-0.03215	0.822019	0.060764	0.040774
0.53125	-0.03195	0.820912	0.060322	0.040569
0.536458	-0.03172	0.820233	0.059848	0.04034
0.541667	-0.03155	0.818277	0.059218	0.040169
0.546875	-0.03106	0.816423	0.058534	0.039688
0.552083	-0.03078	0.813921	0.057744	0.039408
0.557292	-0.03023	0.811207	0.056881	0.038854
0.5625	-0.02972	0.80775	0.055911	0.038339
0.567708	-0.02914	0.804671	0.054913	0.037762
0.572917	-0.02856	0.80038	0.053782	0.03718
0.578125	-0.02771	0.796271	0.052614	0.036329

0.583333	-0.0271	0.791547	0.051359	0.035725
0.588542	-0.02623	0.786572	0.050044	0.034854
0.59375	-0.02535	0.781237	0.048667	0.033976
0.598958	-0.02453	0.775514	0.047229	0.033157
0.604167	-0.02351	0.769377	0.045731	0.03213
0.609375	-0.02258	0.76302	0.04419	0.031207
0.614583	-0.02158	0.756336	0.042604	0.030199
0.619792	-0.02046	0.749274	0.040972	0.029085
0.625	-0.01944	0.742023	0.039311	0.028064
0.630208	-0.01832	0.734171	0.037601	0.026941
0.635417	-0.01722	0.726403	0.035884	0.025846
0.640625	-0.016	0.717877	0.034121	0.02462
0.645833	-0.01487	0.709555	0.032362	0.023499
0.651042	-0.0137	0.700674	0.030577	0.022321
0.65625	-0.0125	0.691639	0.028789	0.021122
0.661458	-0.0113	0.682116	0.026987	0.01992
0.666667	-0.0101	0.672773	0.025203	0.018723
0.671875	-0.0089	0.662974	0.023415	0.01752
0.677083	-0.00771	0.652939	0.021636	0.016335
0.682292	-0.00654	0.642731	0.019874	0.015162
0.6875	-0.00535	0.632194	0.018126	0.013975
0.692708	-0.00416	0.621561	0.016404	0.012782
0.697917	-0.00304	0.61089	0.014712	0.011659
0.703125	-0.00191	0.60001	0.013049	0.010539
0.708333	-0.00078	0.588863	0.011419	0.009406
0.713542	0.000253	0.577661	0.009828	0.008371
0.71875	0.001327	0.566347	0.008278	0.007297
0.723958	0.002333	0.554895	0.006772	0.006292
0.729167	0.003329	0.543342	0.005313	0.005295
0.734375	0.004273	0.531645	0.003904	0.004351
0.739583	0.005181	0.519908	0.002548	0.003443
0.744792	0.006055	0.508092	0.001246	0.002569
0.75	0.006886	0.496239	3.01E-15	0.001738
0.755208	0.007677	0.484347	-0.00119	0.000947
0.760417	0.00843	0.472427	-0.00231	0.000194
0.765625	0.009139	0.46051	-0.00338	-0.00051
0.770833	0.009802	0.448544	-0.00439	-0.00118
0.776042	0.010424	0.436642	-0.00533	-0.0018
0.78125	0.010966	0.424735	-0.00621	-0.00234
0.786458	0.011482	0.412857	-0.00702	-0.00286
0.791667	0.011903	0.40103	-0.00778	-0.00328

0.796875	0.01234	0.389156	-0.00846	-0.00372
0.802083	0.012702	0.377466	-0.00909	-0.00408
0.807292	0.013017	0.365962	-0.00966	-0.00439
0.8125	0.013348	0.354467	-0.01016	-0.00472
0.817708	0.013587	0.343096	-0.01061	-0.00496
0.822917	0.013769	0.331892	-0.011	-0.00514
0.828125	0.013939	0.320653	-0.01132	-0.00531
0.833333	0.013956	0.30972	-0.0116	-0.00533
0.838542	0.01408	0.298988	-0.01183	-0.00546
0.84375	0.014123	0.288289	-0.012	-0.0055
0.848958	0.014123	0.27789	-0.01213	-0.0055
0.854167	0.014057	0.267608	-0.01221	-0.00543
0.859375	0.013944	0.257622	-0.01224	-0.00532
0.864583	0.013908	0.247666	-0.01223	-0.00528
0.869792	0.013725	0.238256	-0.0122	-0.0051
0.875	0.013592	0.228731	-0.01212	-0.00497
0.880208	0.013366	0.219641	-0.01201	-0.00474
0.885417	0.013181	0.210832	-0.01188	-0.00456
0.890625	0.012975	0.202239	-0.01171	-0.00435
0.895833	0.012675	0.193908	-0.01153	-0.00405
0.901042	0.012456	0.18588	-0.01132	-0.00383
0.90625	0.012159	0.178135	-0.0111	-0.00353
0.911458	0.0119	0.170648	-0.01086	-0.00328
0.916667	0.01161	0.163589	-0.01061	-0.00299
0.921875	0.011238	0.156763	-0.01036	-0.00261
0.927083	0.011075	0.150275	-0.0101	-0.00245
0.932292	0.010657	0.144053	-0.00983	-0.00203
0.9375	0.010421	0.13838	-0.00958	-0.0018
0.942708	0.01012	0.132809	-0.00931	-0.0015
0.947917	0.009855	0.12772	-0.00906	-0.00123
0.953125	0.009525	0.122884	-0.00881	-0.0009
0.958333	0.009349	0.118572	-0.00858	-0.00073
0.963542	0.009002	0.114324	-0.00834	-0.00038
0.96875	0.008815	0.110971	-0.00815	-0.00019
0.973958	0.008604	0.10738	-0.00794	2.03E-05
0.979167	0.008357	0.104348	-0.00775	0.000267
0.984375	0.008186	0.102116	-0.00761	0.000438
0.989583	0.008058	0.099729	-0.00746	0.000566
0.994792	0.00784	0.097984	-0.00734	0.000784
1	0.007821	0.096503	-0.00723	0.000803

Table 41 CFD Data Used to Create Figures 55 – 58

t/τ	C_x	C_y	C_P	C_T
0.005208	0.007864	0.099074	-0.00742	0.00076
0.010417	0.00771	0.098395	-0.00736	0.000914
0.015625	0.007773	0.097856	-0.0073	0.000851
0.020833	0.007716	0.09802	-0.00728	0.000908
0.026042	0.007644	0.098417	-0.00728	0.00098
0.03125	0.007609	0.09903	-0.00728	0.001015
0.036458	0.007735	0.100387	-0.00732	0.000889
0.041667	0.007747	0.101941	-0.00738	0.000877
0.046875	0.007808	0.103821	-0.00744	0.000816
0.052083	0.007902	0.106025	-0.00752	0.000722
0.057292	0.008032	0.108696	-0.00762	0.000592
0.0625	0.008142	0.111842	-0.00774	0.000482
0.067708	0.008303	0.115177	-0.00786	0.000321
0.072917	0.008459	0.118987	-0.008	0.000165
0.078125	0.008641	0.123101	-0.00813	-1.7E-05
0.083333	0.008833	0.127593	-0.00828	-0.00021
0.088542	0.009056	0.132424	-0.00843	-0.00043
0.09375	0.009258	0.13763	-0.00857	-0.00063
0.098958	0.009486	0.143117	-0.00872	-0.00086
0.104167	0.009737	0.148977	-0.00886	-0.00111
0.109375	0.009955	0.155141	-0.00899	-0.00133
0.114583	0.010204	0.161648	-0.00911	-0.00158
0.119792	0.010452	0.16847	-0.00921	-0.00183
0.125	0.010645	0.175652	-0.00931	-0.00202
0.130208	0.010923	0.183008	-0.00937	-0.0023
0.135417	0.011143	0.19074	-0.00942	-0.00252
0.140625	0.011328	0.198729	-0.00945	-0.0027
0.145833	0.011577	0.207	-0.00944	-0.00295
0.151042	0.011709	0.215571	-0.00941	-0.00308
0.15625	0.011953	0.224352	-0.00934	-0.00333
0.161458	0.012009	0.233398	-0.00923	-0.00339
0.166667	0.012233	0.242665	-0.00909	-0.00361
0.171875	0.012287	0.252179	-0.00891	-0.00366
0.177083	0.012422	0.26196	-0.00868	-0.0038
0.182292	0.01242	0.271901	-0.00841	-0.0038
0.1875	0.012496	0.282014	-0.00809	-0.00387
0.192708	0.012446	0.292385	-0.00772	-0.00382
0.197917	0.012406	0.302933	-0.0073	-0.00378
0.203125	0.012396	0.313627	-0.00682	-0.00377

0.208333	0.012266	0.324469	-0.00629	-0.00364
0.213542	0.012105	0.335482	-0.00571	-0.00348
0.21875	0.011908	0.346666	-0.00507	-0.00328
0.223958	0.011697	0.357904	-0.00437	-0.00307
0.229167	0.011395	0.369228	-0.00361	-0.00277
0.234375	0.011089	0.380652	-0.0028	-0.00246
0.239583	0.010726	0.392193	-0.00192	-0.0021
0.244792	0.010316	0.40379	-0.00099	-0.00169
0.25	0.009878	0.415436	-2.6E-15	-0.00125
0.255208	0.009393	0.427136	0.001047	-0.00077
0.260417	0.008848	0.438886	0.002151	-0.00022
0.265625	0.008268	0.450673	0.00331	0.000356
0.270833	0.007663	0.462472	0.004523	0.000961
0.276042	0.006968	0.47428	0.005788	0.001656
0.28125	0.006296	0.486049	0.007104	0.002328
0.286458	0.005537	0.49782	0.008469	0.003087
0.291667	0.004734	0.509505	0.00988	0.00389
0.296875	0.003887	0.521158	0.011334	0.004737
0.302083	0.003086	0.532741	0.01283	0.005538
0.307292	0.002152	0.544208	0.014362	0.006472
0.3125	0.001208	0.555689	0.015932	0.007416
0.317708	0.000262	0.566995	0.017532	0.008362
0.322917	-0.00081	0.578168	0.019159	0.009434
0.328125	-0.00176	0.589301	0.020813	0.010387
0.333333	-0.00288	0.600223	0.022485	0.011505
0.338542	-0.00386	0.610985	0.024173	0.012479
0.34375	-0.00505	0.621619	0.025874	0.013676
0.348958	-0.00609	0.632065	0.027583	0.014714
0.354167	-0.00727	0.642331	0.029296	0.015891
0.359375	-0.00834	0.652411	0.031009	0.016963
0.364583	-0.00954	0.662312	0.032718	0.01816
0.369792	-0.01067	0.671956	0.034415	0.019299
0.375	-0.0118	0.681334	0.036095	0.020421
0.380208	-0.01298	0.690529	0.03776	0.021599
0.385417	-0.01409	0.699486	0.039401	0.022712
0.390625	-0.01523	0.708104	0.04101	0.023856
0.395833	-0.01636	0.716511	0.042589	0.024985
0.401042	-0.01745	0.724725	0.044136	0.026069
0.40625	-0.01853	0.732504	0.045631	0.027159
0.411458	-0.0196	0.740021	0.047083	0.028226
0.416667	-0.02062	0.747275	0.048486	0.029244

0.421875	-0.02166	0.754237	0.049836	0.030287
0.427083	-0.02261	0.760815	0.051123	0.031236
0.432292	-0.02355	0.76709	0.052349	0.032173
0.4375	-0.02443	0.772916	0.0535	0.033055
0.442708	-0.02533	0.778678	0.054601	0.033954
0.447917	-0.02612	0.783936	0.055617	0.034747
0.453125	-0.02689	0.788839	0.056556	0.035511
0.458333	-0.02765	0.793329	0.057412	0.036274
0.463542	-0.02832	0.797339	0.058177	0.036941
0.46875	-0.02884	0.801709	0.058911	0.037469
0.473958	-0.02949	0.804956	0.059503	0.038111
0.479167	-0.02999	0.807675	0.059995	0.038611
0.484375	-0.03046	0.810379	0.060423	0.039081
0.489583	-0.03071	0.813428	0.060813	0.039331
0.494792	-0.0311	0.815028	0.061031	0.039719
0.5	-0.03141	0.816191	0.06115	0.040036
0.505208	-0.03154	0.818091	0.06126	0.040168
0.510417	-0.03171	0.818205	0.06117	0.040335
0.515625	-0.03169	0.818934	0.06106	0.040314
0.520833	-0.03165	0.819206	0.060851	0.040275
0.526042	-0.03183	0.818527	0.060506	0.040457
0.53125	-0.03148	0.81819	0.060122	0.040105
0.536458	-0.03134	0.81645	0.059572	0.039968
0.541667	-0.03109	0.81556	0.059021	0.039714
0.546875	-0.03083	0.813333	0.058312	0.039459
0.552083	-0.03033	0.811214	0.057552	0.038953
0.557292	-0.02996	0.808334	0.05668	0.038587
0.5625	-0.02945	0.805641	0.055765	0.038075
0.567708	-0.02889	0.801752	0.054714	0.037513
0.572917	-0.02818	0.798355	0.053646	0.036807
0.578125	-0.02762	0.794139	0.052473	0.036241
0.583333	-0.02688	0.789523	0.051227	0.035503
0.588542	-0.02598	0.784774	0.04993	0.0346
0.59375	-0.02531	0.7795	0.048559	0.033929
0.598958	-0.02434	0.773944	0.047133	0.032962
0.604167	-0.02342	0.768172	0.04566	0.032043
0.609375	-0.02251	0.76178	0.044119	0.031137
0.614583	-0.02151	0.755344	0.042548	0.03013
0.619792	-0.02041	0.748296	0.040919	0.029034
0.625	-0.01943	0.741171	0.039265	0.028059
0.630208	-0.01831	0.733641	0.037574	0.026939

0.635417	-0.01721	0.725944	0.035861	0.025831
0.640625	-0.01605	0.71769	0.034112	0.02467
0.645833	-0.01495	0.709482	0.032359	0.023569
0.651042	-0.01374	0.700663	0.030577	0.022366
0.65625	-0.0126	0.69189	0.028799	0.021228
0.661458	-0.0114	0.682643	0.027008	0.020029
0.666667	-0.01019	0.673202	0.025219	0.018813
0.671875	-0.00903	0.663711	0.023441	0.01765
0.677083	-0.00784	0.653759	0.021664	0.016463
0.682292	-0.00666	0.643801	0.019907	0.015287
0.6875	-0.00551	0.633499	0.018163	0.014132
0.692708	-0.00434	0.623006	0.016442	0.012966
0.697917	-0.00319	0.612266	0.014745	0.011812
0.703125	-0.00208	0.601568	0.013083	0.010704
0.708333	-0.00097	0.590633	0.011453	0.009591
0.713542	0.000103	0.579624	0.009861	0.008521
0.71875	0.001142	0.568415	0.008308	0.007482
0.723958	0.002163	0.557096	0.006799	0.006461
0.729167	0.003166	0.545677	0.005336	0.005458
0.734375	0.00412	0.534129	0.003922	0.004504
0.739583	0.005039	0.522565	0.002561	0.003585
0.744792	0.005916	0.510902	0.001252	0.002708
0.75	0.006755	0.499172	5.55E-15	0.001869
0.755208	0.007553	0.487395	-0.00119	0.001071
0.760417	0.008306	0.475593	-0.00233	0.000318
0.765625	0.009013	0.463793	-0.00341	-0.00039
0.770833	0.009678	0.451922	-0.00442	-0.00105
0.776042	0.010311	0.440085	-0.00537	-0.00169
0.78125	0.010881	0.428247	-0.00626	-0.00226
0.786458	0.011352	0.416454	-0.00709	-0.00273
0.791667	0.011832	0.404694	-0.00785	-0.00321
0.796875	0.012283	0.393018	-0.00855	-0.00366
0.802083	0.012665	0.381519	-0.00919	-0.00404
0.807292	0.013035	0.369926	-0.00976	-0.00441
0.8125	0.013335	0.358528	-0.01028	-0.00471
0.817708	0.013619	0.34721	-0.01074	-0.005
0.822917	0.013781	0.336152	-0.01114	-0.00516
0.828125	0.013951	0.324996	-0.01148	-0.00533
0.833333	0.014025	0.314112	-0.01177	-0.0054
0.838542	0.014167	0.303315	-0.012	-0.00554
0.84375	0.014216	0.292742	-0.01219	-0.00559

0.848958	0.014188	0.282474	-0.01233	-0.00556
0.854167	0.014215	0.272121	-0.01241	-0.00559
0.859375	0.014065	0.262187	-0.01246	-0.00544
0.864583	0.01404	0.252295	-0.01246	-0.00542
0.869792	0.013889	0.242814	-0.01244	-0.00526
0.875	0.013783	0.233456	-0.01237	-0.00516
0.880208	0.013526	0.224375	-0.01227	-0.0049
0.885417	0.013382	0.215459	-0.01214	-0.00476
0.890625	0.013174	0.206963	-0.01199	-0.00455
0.895833	0.012912	0.19853	-0.0118	-0.00429
0.901042	0.012676	0.190533	-0.0116	-0.00405
0.90625	0.012435	0.18283	-0.01139	-0.00381
0.911458	0.012059	0.175365	-0.01116	-0.00343
0.916667	0.011875	0.168216	-0.01091	-0.00325
0.921875	0.011591	0.161289	-0.01066	-0.00297
0.927083	0.011197	0.154819	-0.0104	-0.00257
0.932292	0.011032	0.148739	-0.01015	-0.00241
0.9375	0.010658	0.142704	-0.00988	-0.00203
0.942708	0.0104	0.137346	-0.00963	-0.00178
0.947917	0.010078	0.132075	-0.00937	-0.00145
0.953125	0.009888	0.127374	-0.00913	-0.00126
0.958333	0.009553	0.122644	-0.00888	-0.00093
0.963542	0.009284	0.11896	-0.00868	-0.00066
0.96875	0.009078	0.11477	-0.00843	-0.00045
0.973958	0.008914	0.111606	-0.00825	-0.00029
0.979167	0.008546	0.108522	-0.00806	7.8E-05
0.984375	0.008487	0.10586	-0.00789	0.000137
0.989583	0.008303	0.103799	-0.00776	0.000321
0.994792	0.008074	0.101761	-0.00762	0.00055
1	0.008067	0.100233	-0.00751	0.000557

Table 42 CFD Data Used to Create Figures 59 – 62

t/τ	C_x	C_y	C_P	C_T
0.005208	0.008054	0.102307	-0.00766	0.00057
0.010417	0.007901	0.10167	-0.0076	0.000723
0.015625	0.008019	0.100972	-0.00753	0.000605
0.020833	0.007834	0.100937	-0.0075	0.00079
0.026042	0.007765	0.101296	-0.00749	0.000859
0.03125	0.007888	0.102197	-0.00751	0.000736
0.036458	0.007882	0.102874	-0.00751	0.000742

0.041667	0.007827	0.104508	-0.00756	0.000797
0.046875	0.007938	0.106488	-0.00763	0.000686
0.052083	0.008051	0.108583	-0.0077	0.000573
0.057292	0.008131	0.111109	-0.00779	0.000493
0.0625	0.008257	0.114013	-0.00789	0.000367
0.067708	0.008379	0.11744	-0.00801	0.000245
0.072917	0.00854	0.121045	-0.00813	8.42E-05
0.078125	0.008705	0.125115	-0.00827	-8.1E-05
0.083333	0.008917	0.129482	-0.0084	-0.00029
0.088542	0.009104	0.134146	-0.00853	-0.00048
0.09375	0.009307	0.139259	-0.00868	-0.00068
0.098958	0.009522	0.144639	-0.00881	-0.0009
0.104167	0.009748	0.150404	-0.00894	-0.00112
0.109375	0.009955	0.156467	-0.00906	-0.00133
0.114583	0.010215	0.162852	-0.00917	-0.00159
0.119792	0.010446	0.169521	-0.00927	-0.00182
0.125	0.010651	0.176566	-0.00935	-0.00203
0.130208	0.010905	0.18385	-0.00942	-0.00228
0.135417	0.0111	0.191484	-0.00946	-0.00248
0.140625	0.01132	0.199377	-0.00948	-0.0027
0.145833	0.011507	0.20747	-0.00946	-0.00288
0.151042	0.011728	0.215874	-0.00942	-0.0031
0.15625	0.011851	0.224578	-0.00935	-0.00323
0.161458	0.012021	0.233443	-0.00924	-0.0034
0.166667	0.012161	0.242644	-0.00909	-0.00354
0.171875	0.012235	0.25205	-0.0089	-0.00361
0.177083	0.012391	0.261658	-0.00867	-0.00377
0.182292	0.012354	0.271478	-0.00839	-0.00373
0.1875	0.012407	0.281536	-0.00807	-0.00378
0.192708	0.012451	0.291729	-0.0077	-0.00383
0.197917	0.012402	0.30216	-0.00728	-0.00378
0.203125	0.012294	0.312732	-0.0068	-0.00367
0.208333	0.012259	0.323439	-0.00627	-0.00364
0.213542	0.012069	0.334351	-0.00569	-0.00344
0.21875	0.011883	0.345354	-0.00505	-0.00326
0.223958	0.011655	0.356469	-0.00435	-0.00303
0.229167	0.0114	0.367743	-0.0036	-0.00278
0.234375	0.011095	0.379071	-0.00278	-0.00247
0.239583	0.010765	0.390487	-0.00191	-0.00214
0.244792	0.010354	0.401967	-0.00099	-0.00173
0.25	0.009927	0.413522	-7.8E-16	-0.0013

0.255208	0.009449	0.425134	0.001042	-0.00082
0.260417	0.008905	0.436788	0.00214	-0.00028
0.265625	0.008358	0.448466	0.003293	0.000266
0.270833	0.007753	0.460134	0.0045	0.000871
0.276042	0.007117	0.471841	0.005759	0.001507
0.28125	0.006416	0.483479	0.007067	0.002208
0.286458	0.005666	0.495103	0.008423	0.002958
0.291667	0.004858	0.506759	0.009827	0.003766
0.296875	0.00413	0.518348	0.011273	0.004494
0.302083	0.003225	0.529823	0.01276	0.005399
0.307292	0.002334	0.541246	0.014284	0.00629
0.3125	0.001462	0.552545	0.015842	0.007163
0.317708	0.000515	0.563825	0.017434	0.008109
0.322917	-0.00056	0.574939	0.019052	0.009182
0.328125	-0.00148	0.585957	0.020695	0.010106
0.333333	-0.00256	0.596793	0.022356	0.011184
0.338542	-0.0036	0.607545	0.024037	0.012224
0.34375	-0.00464	0.618061	0.025726	0.013262
0.348958	-0.00581	0.62854	0.02743	0.01443
0.354167	-0.00687	0.638741	0.029133	0.015495
0.359375	-0.00801	0.648694	0.030832	0.016639
0.364583	-0.0091	0.658572	0.032533	0.017728
0.369792	-0.01027	0.668173	0.034221	0.018898
0.375	-0.01139	0.677521	0.035893	0.020011
0.380208	-0.01253	0.68668	0.037549	0.021156
0.385417	-0.01365	0.695558	0.03918	0.022271
0.390625	-0.01478	0.704243	0.040786	0.023405
0.395833	-0.01588	0.712622	0.042358	0.024502
0.401042	-0.01699	0.72069	0.04389	0.025617
0.40625	-0.01804	0.728508	0.045382	0.026663
0.411458	-0.01911	0.736091	0.046833	0.027737
0.416667	-0.02016	0.743328	0.04823	0.02878
0.421875	-0.02114	0.750241	0.049572	0.02976
0.427083	-0.0221	0.756833	0.050855	0.030722
0.432292	-0.02302	0.762987	0.052069	0.031644
0.4375	-0.02394	0.769121	0.053237	0.032569
0.442708	-0.02481	0.774742	0.054325	0.033438
0.447917	-0.02566	0.780009	0.055338	0.03428
0.453125	-0.02634	0.784798	0.056266	0.034965
0.458333	-0.02703	0.789445	0.057131	0.035658
0.463542	-0.02784	0.793904	0.057927	0.036468

0.46875	-0.02849	0.797531	0.058604	0.037114
0.473958	-0.02883	0.801393	0.05924	0.037456
0.479167	-0.02948	0.804057	0.059726	0.038103
0.484375	-0.03007	0.806827	0.060158	0.038698
0.489583	-0.03017	0.809789	0.060541	0.038798
0.494792	-0.03063	0.81157	0.060772	0.039253
0.5	-0.03097	0.812748	0.060892	0.039594
0.505208	-0.03101	0.81467	0.061004	0.039639
0.510417	-0.03139	0.81508	0.060936	0.040019
0.515625	-0.03118	0.815775	0.060825	0.039804
0.520833	-0.03133	0.815677	0.060589	0.039951
0.526042	-0.03131	0.816068	0.060324	0.039931
0.53125	-0.03124	0.814694	0.059865	0.039864
0.536458	-0.03092	0.813927	0.059388	0.039544
0.541667	-0.03076	0.812447	0.058796	0.03938
0.546875	-0.03048	0.810868	0.058136	0.039104
0.552083	-0.0301	0.808416	0.057353	0.03872
0.557292	-0.02959	0.80607	0.056521	0.038218
0.5625	-0.02918	0.802881	0.055574	0.037805
0.567708	-0.02863	0.799941	0.054591	0.037251
0.572917	-0.02801	0.795876	0.053479	0.036631
0.578125	-0.02731	0.791965	0.052329	0.035931
0.583333	-0.02665	0.787869	0.05112	0.035275
0.588542	-0.02596	0.782814	0.049805	0.03458
0.59375	-0.02501	0.777745	0.04845	0.033636
0.598958	-0.02418	0.772465	0.047043	0.032802
0.604167	-0.02336	0.766512	0.045561	0.031988
0.609375	-0.02236	0.760488	0.044044	0.030989
0.614583	-0.02136	0.75408	0.042477	0.029987
0.619792	-0.02042	0.747284	0.040863	0.029042
0.625	-0.01935	0.740265	0.039217	0.027976
0.630208	-0.01826	0.732798	0.037531	0.026879
0.635417	-0.01717	0.725176	0.035823	0.025793
0.640625	-0.01608	0.717151	0.034086	0.024705
0.645833	-0.01493	0.708953	0.032335	0.02355
0.651042	-0.01379	0.700488	0.030569	0.022416
0.65625	-0.01258	0.69162	0.028788	0.021201
0.661458	-0.01146	0.682612	0.027007	0.02008
0.666667	-0.01029	0.673463	0.025228	0.018918
0.671875	-0.00907	0.663819	0.023445	0.017692
0.677083	-0.00793	0.654215	0.021679	0.016552

0.682292	-0.00676	0.644235	0.01992	0.015386
0.6875	-0.00561	0.634091	0.01818	0.01423
0.692708	-0.00441	0.623659	0.016459	0.013035
0.697917	-0.00331	0.613308	0.01477	0.011931
0.703125	-0.0022	0.602661	0.013107	0.010825
0.708333	-0.00108	0.591829	0.011476	0.009708
0.713542	-1.9E-05	0.58087	0.009882	0.008643
0.71875	0.001067	0.569818	0.008329	0.007557
0.723958	0.002044	0.558649	0.006818	0.00658
0.729167	0.003044	0.547313	0.005352	0.00558
0.734375	0.003992	0.535899	0.003935	0.004632
0.739583	0.004904	0.52442	0.00257	0.00372
0.744792	0.005785	0.512852	0.001257	0.002839
0.75	0.00663	0.501224	1.91E-15	0.001994
0.755208	0.007436	0.489545	-0.0012	0.001188
0.760417	0.008198	0.477843	-0.00234	0.000426
0.765625	0.008917	0.466133	-0.00342	-0.00029
0.770833	0.009595	0.454404	-0.00444	-0.00097
0.776042	0.010248	0.44266	-0.0054	-0.00162
0.78125	0.010786	0.431001	-0.0063	-0.00216
0.786458	0.011353	0.419319	-0.00713	-0.00273
0.791667	0.01182	0.407688	-0.00791	-0.0032
0.796875	0.012263	0.396045	-0.00861	-0.00364
0.802083	0.012633	0.384479	-0.00926	-0.00401
0.807292	0.012967	0.37317	-0.00985	-0.00434
0.8125	0.013337	0.36171	-0.01037	-0.00471
0.817708	0.013571	0.350525	-0.01084	-0.00495
0.822917	0.013838	0.339347	-0.01124	-0.00521
0.828125	0.01396	0.328532	-0.0116	-0.00534
0.833333	0.014159	0.317532	-0.0119	-0.00553
0.838542	0.014195	0.30688	-0.01214	-0.00557
0.84375	0.014223	0.296372	-0.01234	-0.0056
0.848958	0.014316	0.285977	-0.01248	-0.00569
0.854167	0.014261	0.275858	-0.01258	-0.00564
0.859375	0.014246	0.265926	-0.01264	-0.00562
0.864583	0.01413	0.256091	-0.01265	-0.00551
0.869792	0.014016	0.246598	-0.01263	-0.00539
0.875	0.013878	0.237259	-0.01257	-0.00525
0.880208	0.013747	0.228234	-0.01248	-0.00512
0.885417	0.013518	0.219291	-0.01235	-0.00489
0.890625	0.013345	0.210747	-0.01221	-0.00472

0.895833	0.013093	0.202573	-0.01204	-0.00447
0.901042	0.012834	0.194429	-0.01184	-0.00421
0.90625	0.012569	0.186714	-0.01163	-0.00394
0.911458	0.012407	0.179302	-0.01141	-0.00378
0.916667	0.012009	0.171994	-0.01116	-0.00339
0.921875	0.011745	0.165273	-0.01092	-0.00312
0.927083	0.011531	0.158778	-0.01067	-0.00291
0.932292	0.011174	0.152421	-0.0104	-0.00255
0.9375	0.010911	0.146709	-0.01015	-0.00229
0.942708	0.010581	0.141033	-0.00989	-0.00196
0.947917	0.010384	0.135997	-0.00965	-0.00176
0.953125	0.010066	0.130929	-0.00939	-0.00144
0.958333	0.009769	0.126548	-0.00916	-0.00114
0.963542	0.009541	0.122451	-0.00893	-0.00092
0.96875	0.009359	0.118601	-0.00872	-0.00074
0.973958	0.009047	0.114955	-0.0085	-0.00042
0.979167	0.008839	0.112297	-0.00834	-0.00021
0.984375	0.008655	0.109238	-0.00814	-3.1E-05
0.989583	0.008586	0.107128	-0.00801	3.84E-05
0.994792	0.008231	0.105185	-0.00788	0.000393
1	0.008288	0.103511	-0.00776	0.000336

Table 43 CFD Data Used to Create Figures 63 – 66

t/τ	C_x	C_y	C_P	C_T
0.007812	0.008509	0.110001	-0.00823	0.000115
0.015625	0.008374	0.109047	-0.00813	0.00025
0.023437	0.008221	0.10869	-0.00806	0.000403
0.03125	0.008266	0.109572	-0.00805	0.000358
0.039062	0.00825	0.111024	-0.00807	0.000374
0.046875	0.008329	0.113311	-0.00812	0.000295
0.054687	0.008386	0.116538	-0.00822	0.000238
0.0625	0.008534	0.120446	-0.00834	9E-05
0.070312	0.008722	0.125143	-0.00848	-9.8E-05
0.078125	0.008931	0.13075	-0.00864	-0.00031
0.085937	0.009169	0.137087	-0.00881	-0.00055
0.09375	0.009444	0.144187	-0.00898	-0.00082
0.101562	0.009752	0.152051	-0.00915	-0.00113
0.109375	0.010048	0.160595	-0.0093	-0.00142
0.117187	0.01036	0.169931	-0.00943	-0.00174
0.125	0.010684	0.179937	-0.00953	-0.00206

0.132812	0.010988	0.190567	-0.00959	-0.00236
0.140625	0.011289	0.201883	-0.0096	-0.00266
0.148437	0.011551	0.213744	-0.00954	-0.00293
0.15625	0.011789	0.226282	-0.00942	-0.00316
0.164062	0.012007	0.23926	-0.00922	-0.00338
0.171875	0.012183	0.252852	-0.00893	-0.00356
0.179687	0.012232	0.266933	-0.00855	-0.00361
0.1875	0.012355	0.281488	-0.00807	-0.00373
0.195312	0.012315	0.296407	-0.00748	-0.00369
0.203125	0.012235	0.311783	-0.00678	-0.00361
0.210937	0.012096	0.327484	-0.00596	-0.00347
0.21875	0.011822	0.343541	-0.00502	-0.0032
0.226562	0.011491	0.359815	-0.00396	-0.00287
0.234375	0.011099	0.376338	-0.00276	-0.00247
0.242187	0.010581	0.393067	-0.00145	-0.00196
0.25	0.009993	0.409971	-3.9E-15	-0.00137
0.257812	0.009309	0.427003	0.00157	-0.00068
0.265625	0.008499	0.444094	0.003261	0.000125
0.273437	0.007636	0.461211	0.00507	0.000988
0.28125	0.006653	0.478333	0.006992	0.001971
0.289062	0.005559	0.495462	0.00902	0.003065
0.296875	0.004454	0.512459	0.011145	0.00417
0.304687	0.003207	0.529352	0.013361	0.005417
0.3125	0.001874	0.546005	0.015655	0.006751
0.320312	0.000557	0.562534	0.01802	0.008067
0.328125	-0.00095	0.57877	0.020441	0.009571
0.335937	-0.00244	0.594753	0.022908	0.01106
0.34375	-0.00397	0.610311	0.025404	0.01259
0.351562	-0.00556	0.625668	0.027924	0.014179
0.359375	-0.0072	0.640482	0.030442	0.015829
0.367187	-0.00883	0.654987	0.032955	0.017451
0.375	-0.01048	0.668881	0.035436	0.019103
0.382812	-0.01212	0.682346	0.037879	0.020744
0.390625	-0.01376	0.695276	0.040267	0.022389
0.398437	-0.01541	0.707608	0.042582	0.02403
0.40625	-0.01695	0.719331	0.044811	0.025579
0.414062	-0.01848	0.730407	0.046938	0.027105
0.421875	-0.01999	0.740852	0.048952	0.028614
0.429687	-0.02142	0.750689	0.050843	0.030043
0.4375	-0.02274	0.759737	0.052588	0.031361
0.445312	-0.024	0.767999	0.054176	0.032629

0.453125	-0.02521	0.77546	0.055597	0.033837
0.460937	-0.02629	0.782534	0.056872	0.034912
0.46875	-0.02721	0.788456	0.057937	0.035834
0.476562	-0.02792	0.793604	0.058815	0.036545
0.484375	-0.0288	0.798215	0.059516	0.03742
0.492187	-0.02929	0.801869	0.060005	0.037915
0.5	-0.0298	0.804168	0.06025	0.038426
0.507812	-0.03017	0.806596	0.060359	0.038792
0.515625	-0.03016	0.807493	0.060207	0.038788
0.523437	-0.03026	0.80765	0.059855	0.038888
0.53125	-0.0303	0.807294	0.059322	0.038922
0.539062	-0.02989	0.805997	0.058577	0.038515
0.546875	-0.02956	0.803255	0.05759	0.038184
0.554687	-0.02908	0.800601	0.056476	0.037703
0.5625	-0.02841	0.796452	0.055129	0.037037
0.570312	-0.02756	0.791631	0.053616	0.036185
0.578125	-0.02676	0.786346	0.051958	0.035386
0.585937	-0.02566	0.779671	0.050104	0.034288
0.59375	-0.02452	0.772649	0.048132	0.033142
0.601562	-0.02332	0.76489	0.046029	0.031943
0.609375	-0.02203	0.756078	0.043788	0.030659
0.617187	-0.02047	0.746808	0.041458	0.029098
0.625	-0.01914	0.736732	0.03903	0.027761
0.632812	-0.0175	0.725976	0.036527	0.026124
0.640625	-0.01589	0.714604	0.033965	0.024509
0.648437	-0.01426	0.702589	0.031357	0.022886
0.65625	-0.01256	0.689993	0.02872	0.021184
0.664062	-0.01085	0.676838	0.02607	0.019473
0.671875	-0.0091	0.663078	0.023418	0.017724
0.679687	-0.00744	0.64897	0.020789	0.016064
0.6875	-0.00567	0.63424	0.018184	0.01429
0.695312	-0.004	0.619188	0.015629	0.012625
0.703125	-0.00235	0.60379	0.013132	0.010975
0.710937	-0.00073	0.587961	0.010704	0.009355
0.71875	0.000847	0.571778	0.008357	0.007777
0.726562	0.002341	0.555389	0.006106	0.006283
0.734375	0.003783	0.53875	0.003956	0.004841
0.742187	0.005149	0.521905	0.001919	0.003475
0.75	0.006426	0.50491	4.74E-15	0.002198
0.757812	0.00762	0.4878	-0.00179	0.001004
0.765625	0.008726	0.470621	-0.00346	-0.0001

0.773437	0.009734	0.453425	-0.00498	-0.00111
0.78125	0.010634	0.436251	-0.00638	-0.00201
0.789062	0.011464	0.419056	-0.00763	-0.00284
0.796875	0.012219	0.402027	-0.00874	-0.0036
0.804687	0.012799	0.385202	-0.00972	-0.00417
0.8125	0.013323	0.368486	-0.01056	-0.0047
0.820312	0.013761	0.351932	-0.01127	-0.00514
0.828125	0.01402	0.335747	-0.01186	-0.0054
0.835937	0.01429	0.319755	-0.01232	-0.00567
0.84375	0.014408	0.30418	-0.01266	-0.00578
0.851562	0.014497	0.288956	-0.0129	-0.00587
0.859375	0.014434	0.27407	-0.01303	-0.00581
0.867187	0.014356	0.259731	-0.01307	-0.00573
0.875	0.014237	0.24584	-0.01302	-0.00561
0.882812	0.013903	0.232487	-0.01291	-0.00528
0.890625	0.013776	0.219642	-0.01272	-0.00515
0.898437	0.013367	0.207333	-0.01248	-0.00474
0.90625	0.01301	0.195773	-0.0122	-0.00439
0.914062	0.012704	0.184787	-0.01187	-0.00408
0.921875	0.012249	0.174326	-0.01152	-0.00363
0.929687	0.011815	0.16476	-0.01116	-0.00319
0.9375	0.01147	0.155829	-0.01079	-0.00285
0.945312	0.011011	0.147443	-0.0104	-0.00239
0.953125	0.010576	0.140294	-0.01006	-0.00195
0.960937	0.010229	0.133231	-0.00968	-0.0016
0.96875	0.009881	0.127475	-0.00937	-0.00126
0.976562	0.009472	0.122538	-0.00908	-0.00085
0.984375	0.009209	0.117962	-0.0088	-0.00058
0.992187	0.008935	0.114689	-0.00858	-0.00031
1	0.008764	0.111847	-0.00838	-0.00014

Table 44 CFD Data Used to Create Figures 67 – 70

t/τ	C_x	C_y	C_P	C_T
0.007812	0.008747	0.114038	-0.00853	-0.00012
0.015625	0.008593	0.113013	-0.00843	3.07E-05
0.023437	0.008473	0.11251	-0.00834	0.000151
0.03125	0.008474	0.113352	-0.00833	0.00015
0.039063	0.008461	0.114787	-0.00834	0.000163
0.046875	0.008521	0.116687	-0.00837	0.000103
0.054687	0.008537	0.119894	-0.00846	8.74E-05

0.0625	0.008679	0.12378	-0.00857	-5.5E-05
0.070312	0.008843	0.128417	-0.0087	-0.00022
0.078125	0.009071	0.133799	-0.00884	-0.00045
0.085938	0.00928	0.140043	-0.009	-0.00066
0.09375	0.009523	0.146962	-0.00915	-0.0009
0.101562	0.009825	0.15468	-0.00931	-0.0012
0.109375	0.01011	0.163086	-0.00945	-0.00149
0.117187	0.010417	0.172204	-0.00956	-0.00179
0.125	0.010698	0.182052	-0.00964	-0.00207
0.132813	0.010998	0.19251	-0.00969	-0.00237
0.140625	0.011276	0.203661	-0.00968	-0.00265
0.148437	0.011552	0.215326	-0.00961	-0.00293
0.15625	0.011785	0.227655	-0.00948	-0.00316
0.164062	0.011979	0.240449	-0.00926	-0.00335
0.171875	0.012119	0.253867	-0.00897	-0.00349
0.179688	0.012247	0.267718	-0.00858	-0.00362
0.1875	0.012277	0.282021	-0.00809	-0.00365
0.195312	0.012301	0.296812	-0.00749	-0.00368
0.203125	0.012192	0.311956	-0.00678	-0.00357
0.210937	0.012008	0.327469	-0.00596	-0.00338
0.21875	0.011797	0.343272	-0.00502	-0.00317
0.226563	0.011491	0.359384	-0.00395	-0.00287
0.234375	0.011101	0.375732	-0.00276	-0.00248
0.242187	0.0106	0.392259	-0.00144	-0.00198
0.25	0.010012	0.408965	-9.4E-16	-0.00139
0.257812	0.009327	0.42579	0.001565	-0.0007
0.265625	0.008546	0.442666	0.003251	7.8E-05
0.273438	0.007697	0.459608	0.005053	0.000927
0.28125	0.00675	0.476535	0.006965	0.001874
0.289062	0.005721	0.493426	0.008983	0.002903
0.296875	0.004564	0.510245	0.011097	0.00406
0.304687	0.003348	0.526923	0.0133	0.005276
0.3125	0.002096	0.543479	0.015582	0.006528
0.320313	0.000719	0.559763	0.017931	0.007905
0.328125	-0.00068	0.575819	0.020337	0.009301
0.335937	-0.00216	0.591693	0.02279	0.010783
0.34375	-0.00371	0.607109	0.02527	0.01233
0.351562	-0.00524	0.622332	0.027775	0.013862
0.359375	-0.00683	0.63698	0.030276	0.015458
0.367188	-0.00847	0.651307	0.03277	0.017089
0.375	-0.01005	0.665134	0.035237	0.018678

0.382812	-0.01172	0.678494	0.037665	0.020345
0.390625	-0.01332	0.691338	0.040039	0.021946
0.398437	-0.01492	0.703543	0.042337	0.023544
0.40625	-0.01644	0.715216	0.044554	0.025068
0.414063	-0.01801	0.726218	0.046668	0.026633
0.421875	-0.0195	0.736721	0.048679	0.028124
0.429687	-0.02086	0.746288	0.050545	0.029488
0.4375	-0.02216	0.755285	0.05228	0.030788
0.445312	-0.02341	0.763557	0.053863	0.032031
0.453125	-0.02467	0.771345	0.055302	0.033295
0.460937	-0.0257	0.778025	0.056544	0.034327
0.46875	-0.02662	0.783953	0.057606	0.03524
0.476562	-0.02736	0.789216	0.058489	0.035989
0.484375	-0.02824	0.793951	0.059198	0.036863
0.492187	-0.02872	0.797546	0.059681	0.037346
0.5	-0.02925	0.799918	0.059931	0.037875
0.507812	-0.02955	0.802585	0.060059	0.038179
0.515625	-0.02971	0.80321	0.059888	0.038333
0.523437	-0.02976	0.803616	0.059557	0.038388
0.53125	-0.02966	0.803677	0.059056	0.038288
0.539062	-0.02957	0.801737	0.058267	0.038198
0.546875	-0.02907	0.799615	0.057329	0.037692
0.554687	-0.02857	0.796924	0.056217	0.037195
0.5625	-0.02809	0.792951	0.054887	0.03671
0.570312	-0.02718	0.788454	0.053401	0.035808
0.578125	-0.02633	0.782728	0.051719	0.034959
0.585937	-0.02538	0.77697	0.04993	0.034009
0.59375	-0.02424	0.769682	0.047947	0.032861
0.601562	-0.023	0.761903	0.045849	0.031629
0.609375	-0.02174	0.75379	0.043656	0.030359
0.617187	-0.02042	0.74434	0.041321	0.029045
0.625	-0.01883	0.734444	0.038909	0.027455
0.632812	-0.01732	0.72404	0.03643	0.025945
0.640625	-0.01581	0.712696	0.033874	0.024439
0.648437	-0.01413	0.700987	0.031286	0.022754
0.65625	-0.01246	0.688552	0.02866	0.021086
0.664062	-0.01077	0.675627	0.026023	0.019399
0.671875	-0.00911	0.662127	0.023385	0.017737
0.679687	-0.00737	0.648187	0.020763	0.015991
0.6875	-0.0057	0.633738	0.01817	0.014325
0.695312	-0.00399	0.618827	0.015619	0.012613

0.703125	-0.00238	0.603625	0.013128	0.011
0.710937	-0.00079	0.588057	0.010705	0.009414
0.71875	0.000783	0.572133	0.008363	0.007841
0.726562	0.002309	0.555879	0.006111	0.006315
0.734375	0.003731	0.539518	0.003962	0.004893
0.742187	0.005096	0.522921	0.001922	0.003528
0.75	0.006379	0.506124	4.45E-15	0.002245
0.757812	0.007579	0.489196	-0.0018	0.001045
0.765625	0.008686	0.472245	-0.00347	-6.2E-05
0.773437	0.009697	0.455278	-0.005	-0.00107
0.78125	0.010634	0.438222	-0.00641	-0.00201
0.789062	0.011451	0.42127	-0.00767	-0.00283
0.796875	0.01215	0.404425	-0.0088	-0.00353
0.804687	0.012751	0.38771	-0.00979	-0.00413
0.8125	0.013339	0.371121	-0.01064	-0.00471
0.820312	0.013727	0.354799	-0.01137	-0.0051
0.828125	0.014115	0.338705	-0.01196	-0.00549
0.835937	0.01433	0.322905	-0.01244	-0.00571
0.84375	0.014459	0.307413	-0.0128	-0.00583
0.851562	0.014573	0.292279	-0.01304	-0.00595
0.859375	0.014546	0.277724	-0.0132	-0.00592
0.867187	0.01446	0.263337	-0.01325	-0.00584
0.875	0.014292	0.249619	-0.01322	-0.00567
0.882812	0.014202	0.236345	-0.01312	-0.00558
0.890625	0.013826	0.223473	-0.01294	-0.0052
0.898437	0.013552	0.211467	-0.01273	-0.00493
0.90625	0.013276	0.199846	-0.01245	-0.00465
0.914062	0.012847	0.188814	-0.01213	-0.00422
0.921875	0.012459	0.178635	-0.0118	-0.00383
0.929687	0.012069	0.168942	-0.01144	-0.00345
0.9375	0.011722	0.160013	-0.01108	-0.0031
0.945312	0.01119	0.151717	-0.0107	-0.00257
0.953125	0.01088	0.144492	-0.01036	-0.00226
0.960937	0.010532	0.137585	-0.01	-0.00191
0.96875	0.010027	0.13164	-0.00967	-0.0014
0.976562	0.009794	0.126702	-0.00939	-0.00117
0.984375	0.009485	0.122273	-0.00912	-0.00086
0.992187	0.009146	0.11876	-0.00889	-0.00052
1	0.009018	0.11596	-0.00869	-0.00039

Table 45 CFD Data Used to Create Figures 71 – 74

t/τ	C_x	C_y	C_P	C_T
0.007812	0.009384	0.125318	-0.00938	-0.00076
0.015625	0.009157	0.12433	-0.00927	-0.00053
0.023437	0.009223	0.123689	-0.00917	-0.0006
0.03125	0.008997	0.12411	-0.00912	-0.00037
0.039062	0.008961	0.125358	-0.00911	-0.00034
0.046875	0.009063	0.12758	-0.00915	-0.00044
0.054687	0.009067	0.129955	-0.00917	-0.00044
0.0625	0.009091	0.133861	-0.00927	-0.00047
0.070312	0.009318	0.138245	-0.00936	-0.00069
0.078125	0.009409	0.1433	-0.00947	-0.00078
0.085937	0.009588	0.149208	-0.00959	-0.00096
0.09375	0.009855	0.155765	-0.0097	-0.00123
0.101562	0.010062	0.163081	-0.00981	-0.00144
0.109375	0.01031	0.171246	-0.00992	-0.00169
0.117187	0.010553	0.179911	-0.00999	-0.00193
0.125	0.010859	0.189342	-0.01003	-0.00223
0.132812	0.011069	0.199355	-0.01003	-0.00244
0.140625	0.011331	0.21004	-0.00998	-0.00271
0.148437	0.01159	0.221233	-0.00987	-0.00297
0.15625	0.011719	0.233089	-0.0097	-0.00309
0.164062	0.011963	0.245428	-0.00945	-0.00334
0.171875	0.012052	0.258287	-0.00912	-0.00343
0.179687	0.012172	0.271635	-0.0087	-0.00355
0.1875	0.012182	0.285485	-0.00819	-0.00356
0.195312	0.012182	0.299666	-0.00756	-0.00356
0.203125	0.01208	0.314283	-0.00684	-0.00346
0.210937	0.011941	0.32923	-0.00599	-0.00332
0.21875	0.011699	0.344489	-0.00504	-0.00307
0.226562	0.011413	0.360037	-0.00396	-0.00279
0.234375	0.011033	0.375812	-0.00276	-0.00241
0.242187	0.010542	0.391779	-0.00144	-0.00192
0.25	0.009996	0.407907	-4.4E-15	-0.00137
0.257812	0.009356	0.424155	0.001559	-0.00073
0.265625	0.008601	0.440486	0.003235	2.28E-05
0.273437	0.007785	0.456865	0.005022	0.000839
0.28125	0.006908	0.473247	0.006917	0.001716
0.289062	0.005908	0.489602	0.008913	0.002716
0.296875	0.00486	0.505888	0.011002	0.003764
0.304687	0.003661	0.522062	0.013177	0.004963

0.3125	0.002483	0.538029	0.015426	0.006141
0.320312	0.00116	0.553895	0.017743	0.007464
0.328125	-0.00016	0.569451	0.020112	0.008785
0.335937	-0.00159	0.58477	0.022524	0.010212
0.34375	-0.00299	0.599795	0.024966	0.011612
0.351562	-0.00455	0.614515	0.027426	0.013175
0.359375	-0.00604	0.628802	0.029887	0.014667
0.367187	-0.00756	0.642751	0.03234	0.016184
0.375	-0.00916	0.656155	0.034762	0.017784
0.382812	-0.01067	0.669139	0.037146	0.019298
0.390625	-0.01223	0.681484	0.039468	0.020852
0.398437	-0.01377	0.693598	0.041739	0.022398
0.40625	-0.0153	0.704984	0.043917	0.023929
0.414062	-0.01673	0.715656	0.04599	0.025355
0.421875	-0.01815	0.725841	0.04796	0.02677
0.429687	-0.01956	0.735247	0.049797	0.028185
0.4375	-0.02073	0.743956	0.051496	0.029359
0.445312	-0.0221	0.752569	0.053088	0.03072
0.453125	-0.02322	0.759635	0.054462	0.031843
0.460937	-0.0241	0.766657	0.055718	0.032724
0.46875	-0.02514	0.772224	0.056745	0.033763
0.476562	-0.02613	0.777435	0.057616	0.034751
0.484375	-0.02655	0.782392	0.058336	0.035172
0.492187	-0.02726	0.785845	0.058806	0.035884
0.5	-0.02781	0.788234	0.059056	0.036434
0.507812	-0.02799	0.790951	0.059188	0.036609
0.515625	-0.02848	0.791846	0.059041	0.037106
0.523437	-0.02822	0.792393	0.058725	0.036843
0.53125	-0.02831	0.791836	0.058186	0.036937
0.539062	-0.02811	0.791362	0.057513	0.036736
0.546875	-0.02794	0.788686	0.056545	0.036568
0.554687	-0.02731	0.786434	0.055477	0.035935
0.5625	-0.02679	0.782289	0.054149	0.035419
0.570312	-0.02604	0.778551	0.05273	0.034667
0.578125	-0.0254	0.773155	0.051086	0.034024
0.585937	-0.02429	0.76739	0.049314	0.032917
0.59375	-0.02326	0.760702	0.047388	0.031885
0.601562	-0.0222	0.753237	0.045328	0.030819
0.609375	-0.02093	0.745461	0.043173	0.029558
0.617187	-0.0196	0.736507	0.040886	0.02822
0.625	-0.01826	0.726911	0.03851	0.026884

0.632813	-0.01668	0.716975	0.036074	0.025308
0.640625	-0.01525	0.706374	0.033574	0.023872
0.648437	-0.01372	0.694867	0.031012	0.022342
0.65625	-0.01211	0.682987	0.028429	0.020732
0.664062	-0.01043	0.670584	0.025829	0.019049
0.671875	-0.00877	0.657679	0.023228	0.017391
0.679687	-0.00717	0.644221	0.020636	0.015791
0.6875	-0.00558	0.630342	0.018073	0.014204
0.695313	-0.00386	0.616026	0.015549	0.012489
0.703125	-0.00229	0.601379	0.013079	0.010912
0.710937	-0.00073	0.586376	0.010675	0.009357
0.71875	0.000797	0.570986	0.008346	0.007827
0.726562	0.002273	0.555337	0.006105	0.006352
0.734375	0.003673	0.539535	0.003962	0.004951
0.742187	0.005022	0.523452	0.001924	0.003602
0.75	0.006289	0.507242	3.72E-15	0.002335
0.757812	0.007478	0.490905	-0.0018	0.001146
0.765625	0.008594	0.474483	-0.00348	3E-05
0.773438	0.009611	0.458095	-0.00504	-0.00099
0.78125	0.010554	0.44161	-0.00645	-0.00193
0.789062	0.0114	0.425168	-0.00774	-0.00278
0.796875	0.012163	0.408862	-0.00889	-0.00354
0.804687	0.012775	0.392741	-0.00991	-0.00415
0.8125	0.013387	0.376633	-0.0108	-0.00476
0.820312	0.013814	0.360781	-0.01156	-0.00519
0.828125	0.014105	0.345146	-0.01219	-0.00548
0.835938	0.014437	0.3298	-0.0127	-0.00581
0.84375	0.014663	0.314828	-0.0131	-0.00604
0.851563	0.014831	0.300192	-0.0134	-0.00621
0.859375	0.014759	0.285706	-0.01358	-0.00613
0.867187	0.014696	0.271995	-0.01369	-0.00607
0.875	0.01471	0.258572	-0.0137	-0.00609
0.882812	0.014505	0.245586	-0.01363	-0.00588
0.890625	0.014262	0.233126	-0.0135	-0.00564
0.898438	0.014044	0.221345	-0.01332	-0.00542
0.90625	0.013651	0.209934	-0.01308	-0.00503
0.914063	0.013401	0.199314	-0.01281	-0.00478
0.921875	0.013105	0.1892	-0.0125	-0.00448
0.929688	0.012608	0.179614	-0.01216	-0.00398
0.9375	0.01222	0.17126	-0.01185	-0.0036
0.945312	0.011914	0.162789	-0.01148	-0.00329

0.953125	0.011586	0.155616	-0.01116	-0.00296
0.960937	0.011044	0.148844	-0.01082	-0.00242
0.96875	0.01076	0.143319	-0.01053	-0.00214
0.976563	0.010431	0.137872	-0.01022	-0.00181
0.984375	0.010223	0.13369	-0.00997	-0.0016
0.992188	0.009749	0.130206	-0.00974	-0.00112
1	0.009703	0.127296	-0.00954	-0.00108

Table 46 CFD Data Used to Create Figures 75 – 78

t/τ	C_x	C_y	C_P	C_T
0.007813	0.009937	0.135736	-0.01016	-0.00131
0.015625	0.009771	0.134692	-0.01004	-0.00115
0.023438	0.009718	0.134222	-0.00995	-0.00109
0.03125	0.009525	0.134339	-0.00987	-0.0009
0.039063	0.009584	0.135848	-0.00987	-0.00096
0.046875	0.009399	0.137626	-0.00987	-0.00078
0.054688	0.009605	0.140549	-0.00991	-0.00098
0.0625	0.00949	0.143632	-0.00994	-0.00087
0.070313	0.009766	0.148163	-0.01003	-0.00114
0.078125	0.009746	0.152923	-0.0101	-0.00112
0.085938	0.00996	0.158825	-0.01021	-0.00134
0.09375	0.010138	0.16508	-0.01028	-0.00151
0.101563	0.010301	0.172233	-0.01036	-0.00168
0.109375	0.010558	0.179974	-0.01042	-0.00193
0.117188	0.01075	0.188426	-0.01046	-0.00213
0.125	0.010986	0.197539	-0.01047	-0.00236
0.132813	0.011193	0.207327	-0.01043	-0.00257
0.140625	0.011425	0.217575	-0.01034	-0.0028
0.148438	0.011608	0.228486	-0.0102	-0.00298
0.15625	0.011798	0.239947	-0.00999	-0.00317
0.164063	0.011894	0.251868	-0.0097	-0.00327
0.171875	0.012063	0.264314	-0.00933	-0.00344
0.179688	0.012087	0.277267	-0.00888	-0.00346
0.1875	0.012133	0.290625	-0.00833	-0.00351
0.195313	0.012097	0.304396	-0.00768	-0.00347
0.203125	0.011981	0.318528	-0.00693	-0.00336
0.210938	0.011808	0.332991	-0.00606	-0.00318
0.21875	0.011582	0.347799	-0.00508	-0.00296
0.226563	0.011303	0.362833	-0.00399	-0.00268
0.234375	0.01092	0.378093	-0.00278	-0.0023
0.242188	0.010446	0.393565	-0.00145	-0.00182

0.25	0.009924	0.409181	2.48E-15	-0.0013
0.257813	0.009311	0.424927	0.001562	-0.00069
0.265625	0.008585	0.440772	0.003237	3.9E-05
0.273438	0.007791	0.456593	0.005019	0.000833
0.28125	0.006944	0.472434	0.006905	0.00168
0.289063	0.005994	0.488286	0.008889	0.00263
0.296875	0.004952	0.504028	0.010962	0.003672
0.304688	0.003834	0.519695	0.013117	0.00479
0.3125	0.002656	0.535191	0.015345	0.005968
0.320313	0.001447	0.550469	0.017633	0.007177
0.328125	0.00015	0.565639	0.019977	0.008474
0.335938	-0.00117	0.580458	0.022358	0.009797
0.34375	-0.0026	0.595002	0.024766	0.011222
0.351563	-0.00404	0.609231	0.02719	0.012668
0.359375	-0.00545	0.623047	0.029613	0.014072
0.367188	-0.00697	0.636437	0.032022	0.015591
0.375	-0.00844	0.649581	0.034413	0.017063
0.382813	-0.00996	0.662174	0.036759	0.018587
0.390625	-0.01145	0.674285	0.039051	0.020069
0.398438	-0.01292	0.685746	0.041267	0.021547
0.40625	-0.01434	0.696869	0.043411	0.022962
0.414063	-0.01581	0.707055	0.045437	0.024436
0.421875	-0.01708	0.71711	0.047383	0.025709
0.429688	-0.01852	0.725951	0.049167	0.027144
0.4375	-0.01969	0.735253	0.050893	0.02831
0.445313	-0.02097	0.742555	0.052381	0.029594
0.453125	-0.02189	0.750255	0.05379	0.03051
0.460938	-0.02304	0.7561	0.054951	0.031662
0.46875	-0.02383	0.762272	0.056013	0.032456
0.476563	-0.02487	0.767342	0.056868	0.033497
0.484375	-0.02529	0.771754	0.057543	0.033917
0.492188	-0.02597	0.775385	0.058023	0.034593
0.5	-0.02656	0.777545	0.058255	0.035184
0.507813	-0.02668	0.779943	0.058364	0.035307
0.515625	-0.02716	0.781508	0.05827	0.035782
0.523438	-0.0271	0.781317	0.057904	0.035726
0.53125	-0.02695	0.781504	0.057426	0.035575
0.539063	-0.02692	0.780042	0.056691	0.035546
0.546875	-0.02659	0.77885	0.05584	0.035214
0.554688	-0.02635	0.775448	0.054702	0.034973
0.5625	-0.02559	0.772668	0.053483	0.034211
0.570313	-0.02499	0.767728	0.051997	0.033613

0.578125	-0.02422	0.763305	0.050435	0.032842
0.585938	-0.0233	0.757692	0.048691	0.031928
0.59375	-0.02247	0.751152	0.046793	0.03109
0.601563	-0.02121	0.744007	0.044773	0.029832
0.609375	-0.02006	0.736446	0.042651	0.028685
0.617188	-0.01878	0.727619	0.040392	0.027401
0.625	-0.01751	0.718602	0.03807	0.026138
0.632813	-0.0161	0.709116	0.035679	0.024722
0.640625	-0.01457	0.698545	0.033202	0.023197
0.648437	-0.01312	0.687608	0.030688	0.02174
0.65625	-0.01161	0.67593	0.028135	0.020238
0.664063	-0.00994	0.664087	0.025579	0.018567
0.671875	-0.00836	0.651536	0.023011	0.016979
0.679688	-0.00679	0.63863	0.020457	0.015418
0.6875	-0.00521	0.625217	0.017926	0.013839
0.695312	-0.00363	0.611301	0.015429	0.012256
0.703125	-0.0021	0.597142	0.012987	0.010726
0.710938	-0.00056	0.582613	0.010606	0.009183
0.71875	0.000951	0.567746	0.008298	0.007673
0.726563	0.002405	0.552579	0.006075	0.006219
0.734375	0.003776	0.53727	0.003945	0.004848
0.742187	0.005092	0.521763	0.001918	0.003532
0.75	0.006351	0.506058	-3.6E-15	0.002273
0.757813	0.007533	0.490246	-0.0018	0.001091
0.765625	0.008629	0.474407	-0.00348	-5.3E-06
0.773438	0.009645	0.45851	-0.00504	-0.00102
0.78125	0.010603	0.442523	-0.00647	-0.00198
0.789062	0.011463	0.426641	-0.00777	-0.00284
0.796875	0.012263	0.410851	-0.00894	-0.00364
0.804688	0.012849	0.395251	-0.00998	-0.00422
0.8125	0.013437	0.379539	-0.01088	-0.00481
0.820312	0.013839	0.364174	-0.01167	-0.00521
0.828125	0.014249	0.349086	-0.01233	-0.00562
0.835937	0.01456	0.334171	-0.01287	-0.00594
0.84375	0.014869	0.319755	-0.01331	-0.00625
0.851563	0.014986	0.305437	-0.01363	-0.00636
0.859375	0.01498	0.291644	-0.01386	-0.00636
0.867187	0.015002	0.278035	-0.01399	-0.00638
0.875	0.014974	0.265145	-0.01405	-0.00635
0.882813	0.014769	0.252562	-0.01402	-0.00614
0.890625	0.014586	0.240425	-0.01392	-0.00596
0.898438	0.014438	0.229059	-0.01378	-0.00581

0.90625	0.014189	0.21802	-0.01358	-0.00557
0.914062	0.01378	0.207506	-0.01333	-0.00516
0.921875	0.013439	0.197833	-0.01307	-0.00482
0.929688	0.013166	0.18892	-0.0128	-0.00454
0.9375	0.01279	0.179943	-0.01246	-0.00417
0.945313	0.012521	0.172418	-0.01216	-0.0039
0.953125	0.011962	0.165064	-0.01183	-0.00334
0.960937	0.01167	0.159006	-0.01156	-0.00305
0.96875	0.011353	0.152828	-0.01123	-0.00273
0.976563	0.011067	0.148257	-0.01099	-0.00244
0.984375	0.010716	0.143761	-0.01072	-0.00209
0.992188	0.010351	0.140483	-0.01051	-0.00173
1	0.010314	0.137647	-0.01031	-0.00169

Table 47 CFD Data Used to Create Figures 79 – 82

t/τ	C_x	C_y	C_P	C_T
0.007812	0.010386	0.144752	-0.01083	-0.00176
0.015625	0.010385	0.143882	-0.01073	-0.00176
0.023437	0.010003	0.14344	-0.01063	-0.00138
0.03125	0.010164	0.143781	-0.01057	-0.00154
0.039062	0.009825	0.144785	-0.01052	-0.0012
0.046875	0.010055	0.147079	-0.01054	-0.00143
0.054687	0.009792	0.14958	-0.01055	-0.00117
0.0625	0.010063	0.153232	-0.01061	-0.00144
0.070312	0.009938	0.157037	-0.01064	-0.00131
0.078125	0.010247	0.162016	-0.01071	-0.00162
0.085937	0.010147	0.167636	-0.01077	-0.00152
0.09375	0.01047	0.173951	-0.01084	-0.00185
0.101562	0.010514	0.18093	-0.01089	-0.00189
0.109375	0.010764	0.188466	-0.01092	-0.00214
0.117187	0.010927	0.196769	-0.01092	-0.0023
0.125	0.011108	0.205551	-0.01089	-0.00248
0.132812	0.011353	0.215156	-0.01083	-0.00273
0.140625	0.011486	0.225136	-0.0107	-0.00286
0.148437	0.011673	0.235769	-0.01052	-0.00305
0.15625	0.011801	0.246993	-0.01028	-0.00318
0.164062	0.011929	0.258633	-0.00996	-0.00331
0.171875	0.012017	0.270773	-0.00956	-0.00339
0.179687	0.01203	0.283342	-0.00908	-0.00341
0.1875	0.012093	0.29641	-0.0085	-0.00347

0.195312	0.012007	0.309818	-0.00782	-0.00338
0.203125	0.011902	0.323578	-0.00704	-0.00328
0.210937	0.01171	0.33765	-0.00615	-0.00309
0.21875	0.011481	0.352014	-0.00515	-0.00286
0.226562	0.011164	0.366671	-0.00403	-0.00254
0.234375	0.01081	0.381498	-0.0028	-0.00219
0.242187	0.01036	0.396554	-0.00146	-0.00174
0.25	0.009819	0.411745	-1.5E-15	-0.00119
0.257812	0.009197	0.427032	0.00157	-0.00057
0.265625	0.008513	0.442403	0.003249	0.000111
0.273437	0.007763	0.457781	0.005033	0.000861
0.28125	0.006904	0.473212	0.006917	0.00172
0.289062	0.005992	0.488572	0.008894	0.002632
0.296875	0.004974	0.503837	0.010958	0.00365
0.304687	0.003932	0.519082	0.013102	0.004692
0.3125	0.002743	0.534095	0.015313	0.005881
0.320312	0.001617	0.548952	0.017585	0.007007
0.328125	0.000347	0.563562	0.019904	0.008277
0.335937	-0.00096	0.577969	0.022262	0.009579
0.34375	-0.00231	0.591967	0.02464	0.010934
0.351562	-0.00367	0.605891	0.027041	0.012293
0.359375	-0.00512	0.619349	0.029438	0.013749
0.367187	-0.00658	0.632232	0.03181	0.015207
0.375	-0.00794	0.645073	0.034174	0.016567
0.382812	-0.00944	0.657038	0.036474	0.018068
0.390625	-0.01084	0.668912	0.03874	0.019462
0.398437	-0.01229	0.679931	0.040917	0.020912
0.40625	-0.01371	0.690579	0.04302	0.022335
0.414062	-0.01499	0.700648	0.045025	0.023614
0.421875	-0.01648	0.71011	0.04692	0.025099
0.429687	-0.01763	0.71947	0.048728	0.026256
0.4375	-0.01895	0.727237	0.050338	0.027575
0.445312	-0.01991	0.735423	0.051878	0.028531
0.453125	-0.02117	0.741605	0.05317	0.02979
0.460937	-0.02193	0.74841	0.054392	0.030551
0.46875	-0.02312	0.753271	0.055352	0.031746
0.476562	-0.02363	0.759369	0.056277	0.032251
0.484375	-0.02456	0.7625	0.056853	0.033188
0.492187	-0.02476	0.766758	0.057378	0.033382
0.5	-0.02543	0.76866	0.057589	0.034056
0.507812	-0.02588	0.770421	0.057652	0.0345

0.515625	-0.02602	0.772513	0.057599	0.034641
0.523437	-0.0262	0.772013	0.057214	0.034826
0.53125	-0.02588	0.772017	0.056729	0.034505
0.539062	-0.02592	0.770638	0.056007	0.034549
0.546875	-0.02556	0.768922	0.055128	0.034183
0.554687	-0.02519	0.766721	0.054086	0.033814
0.5625	-0.02491	0.762678	0.052791	0.033533
0.570312	-0.02399	0.759001	0.051406	0.032614
0.578125	-0.02332	0.754187	0.049833	0.031944
0.585937	-0.0225	0.748021	0.04807	0.031127
0.59375	-0.02144	0.742328	0.046243	0.030065
0.601562	-0.02043	0.735366	0.044253	0.029056
0.609375	-0.01944	0.727727	0.042146	0.028061
0.617187	-0.0181	0.719226	0.039927	0.026722
0.625	-0.01679	0.71047	0.037639	0.025418
0.632812	-0.01541	0.701068	0.035274	0.024035
0.640625	-0.01399	0.690726	0.03283	0.022619
0.648437	-0.0126	0.679968	0.030347	0.021223
0.65625	-0.01106	0.669034	0.027848	0.019682
0.664062	-0.00955	0.657426	0.025322	0.01817
0.671875	-0.00795	0.64505	0.022782	0.01657
0.679687	-0.00641	0.632505	0.020261	0.015037
0.6875	-0.00488	0.619427	0.01776	0.0135
0.695312	-0.00337	0.605879	0.015293	0.011993
0.703125	-0.00181	0.59198	0.012875	0.010438
0.710937	-0.00032	0.577957	0.010521	0.008945
0.71875	0.001169	0.563504	0.008236	0.007455
0.726562	0.002571	0.548761	0.006033	0.006053
0.734375	0.003942	0.533874	0.003921	0.004682
0.742187	0.005238	0.51877	0.001907	0.003386
0.75	0.00647	0.503534	2.52E-15	0.002154
0.757812	0.007632	0.488178	-0.00179	0.000992
0.765625	0.008721	0.472744	-0.00347	-9.7E-05
0.773437	0.009744	0.457295	-0.00503	-0.00112
0.78125	0.010672	0.441779	-0.00646	-0.00205
0.789062	0.011541	0.42638	-0.00776	-0.00292
0.796875	0.0123	0.411178	-0.00894	-0.00368
0.804687	0.012979	0.395884	-0.00999	-0.00435
0.8125	0.013537	0.38076	-0.01092	-0.00491
0.820312	0.013965	0.365882	-0.01172	-0.00534
0.828125	0.014439	0.351207	-0.0124	-0.00581

0.835937	0.014711	0.336656	-0.01297	-0.00609
0.84375	0.014996	0.322591	-0.01343	-0.00637
0.851562	0.015172	0.308872	-0.01379	-0.00655
0.859375	0.015175	0.295337	-0.01404	-0.00655
0.867187	0.015181	0.282201	-0.0142	-0.00656
0.875	0.015224	0.269767	-0.01429	-0.0066
0.882812	0.015164	0.257638	-0.0143	-0.00654
0.890625	0.014937	0.245827	-0.01424	-0.00631
0.898437	0.014685	0.234619	-0.01412	-0.00606
0.90625	0.014424	0.224051	-0.01396	-0.0058
0.914062	0.014155	0.214294	-0.01377	-0.00553
0.921875	0.013957	0.20443	-0.01351	-0.00533
0.929687	0.013532	0.195587	-0.01325	-0.00491
0.9375	0.013348	0.187559	-0.01298	-0.00472
0.945312	0.012757	0.179801	-0.01268	-0.00413
0.953125	0.01245	0.173166	-0.01242	-0.00383
0.960937	0.012221	0.166846	-0.01213	-0.0036
0.96875	0.011815	0.161299	-0.01185	-0.00319
0.976562	0.011573	0.156732	-0.01162	-0.00295
0.984375	0.011144	0.152547	-0.01137	-0.00252
0.992187	0.010999	0.149263	-0.01117	-0.00237
1	0.010705	0.146399	-0.01097	-0.00208

Table 48 CFD Data Used to Create Figures 83 – 86

t/τ	C_x	C_y	C_P	C_T
0.007812	0.010841	0.153322	-0.01147	-0.00222
0.015625	0.010851	0.152568	-0.01138	-0.00223
0.023437	0.010436	0.152395	-0.01129	-0.00181
0.03125	0.010577	0.152595	-0.01121	-0.00195
0.039062	0.010369	0.153852	-0.01118	-0.00175
0.046875	0.01017	0.155829	-0.01117	-0.00155
0.054687	0.010488	0.158757	-0.0112	-0.00186
0.0625	0.010171	0.162017	-0.01121	-0.00155
0.070312	0.010477	0.166385	-0.01127	-0.00185
0.078125	0.010381	0.171027	-0.0113	-0.00176
0.085937	0.010548	0.176199	-0.01132	-0.00192
0.09375	0.010698	0.182872	-0.01139	-0.00207
0.101562	0.010689	0.189483	-0.0114	-0.00206
0.109375	0.011047	0.197143	-0.01142	-0.00242
0.117187	0.01105	0.205188	-0.01139	-0.00243

0.125	0.011202	0.213908	-0.01133	-0.00258
0.132812	0.011531	0.223241	-0.01123	-0.00291
0.140625	0.011531	0.233039	-0.01108	-0.00291
0.148437	0.011695	0.243406	-0.01086	-0.00307
0.15625	0.011888	0.254324	-0.01059	-0.00326
0.164062	0.011933	0.265778	-0.01024	-0.00331
0.171875	0.011989	0.277613	-0.0098	-0.00336
0.179687	0.012001	0.289883	-0.00929	-0.00338
0.1875	0.012021	0.302596	-0.00868	-0.0034
0.195312	0.011929	0.315723	-0.00797	-0.00331
0.203125	0.011809	0.329149	-0.00716	-0.00318
0.210937	0.011643	0.342872	-0.00624	-0.00302
0.21875	0.01138	0.356916	-0.00522	-0.00276
0.226562	0.01105	0.37116	-0.00408	-0.00243
0.234375	0.010705	0.385573	-0.00283	-0.00208
0.242187	0.010247	0.400206	-0.00147	-0.00162
0.25	0.009724	0.414969	-2.7E-15	-0.0011
0.257812	0.009123	0.429837	0.00158	-0.0005
0.265625	0.00845	0.444801	0.003266	0.000174
0.273437	0.00773	0.459788	0.005055	0.000894
0.28125	0.006849	0.474766	0.006939	0.001775
0.289062	0.00595	0.489666	0.008914	0.002674
0.296875	0.005	0.504445	0.010971	0.003625
0.304687	0.003964	0.519167	0.013104	0.004661
0.3125	0.002842	0.533802	0.015305	0.005783
0.320312	0.001766	0.548272	0.017563	0.006858
0.328125	0.000439	0.562485	0.019866	0.008185
0.335937	-0.00078	0.576284	0.022197	0.009401
0.34375	-0.00215	0.590088	0.024562	0.010775
0.351562	-0.00337	0.603492	0.026934	0.011994
0.359375	-0.00481	0.616356	0.029295	0.013434
0.367187	-0.00621	0.628919	0.031644	0.014837
0.375	-0.00754	0.641379	0.033979	0.016161
0.382812	-0.00898	0.652885	0.036244	0.017604
0.390625	-0.0104	0.664154	0.038465	0.019023
0.398437	-0.01172	0.675121	0.040627	0.020341
0.40625	-0.01313	0.684871	0.042664	0.021755
0.414062	-0.01445	0.695566	0.044699	0.02307
0.421875	-0.01576	0.704213	0.046531	0.024382
0.429687	-0.01704	0.712674	0.048268	0.02566
0.4375	-0.01804	0.721195	0.04992	0.026667

0.445312	-0.01937	0.727671	0.051331	0.027994
0.453125	-0.02011	0.735023	0.052698	0.028732
0.460937	-0.02129	0.740486	0.053816	0.029913
0.46875	-0.02231	0.746005	0.054818	0.030936
0.476562	-0.02269	0.751103	0.055665	0.031309
0.484375	-0.02369	0.754346	0.056245	0.032318
0.492187	-0.02386	0.758393	0.056752	0.032485
0.5	-0.02453	0.760059	0.056945	0.033151
0.507812	-0.02499	0.76167	0.056997	0.033617
0.515625	-0.02493	0.763427	0.056922	0.033554
0.523437	-0.02546	0.763318	0.05657	0.034086
0.53125	-0.02505	0.762686	0.056044	0.033679
0.539062	-0.0249	0.761965	0.055377	0.033527
0.546875	-0.02481	0.759444	0.054449	0.033431
0.554687	-0.02423	0.757142	0.05341	0.032854
0.5625	-0.02382	0.754156	0.052202	0.032441
0.570312	-0.02341	0.749597	0.050769	0.032035
0.578125	-0.02253	0.744792	0.049212	0.031152
0.585937	-0.02165	0.739803	0.047541	0.030272
0.59375	-0.02076	0.733058	0.045666	0.029381
0.601562	-0.0198	0.726113	0.043696	0.028427
0.609375	-0.01856	0.719026	0.041643	0.027181
0.617187	-0.01742	0.710877	0.039463	0.026044
0.625	-0.01623	0.702145	0.037198	0.024854
0.632812	-0.01494	0.692829	0.034859	0.023568
0.640625	-0.01348	0.682735	0.03245	0.022101
0.648437	-0.01205	0.672471	0.030013	0.020675
0.65625	-0.01058	0.661624	0.02754	0.019207
0.664062	-0.00908	0.650077	0.025039	0.017704
0.671875	-0.00755	0.638118	0.022537	0.016176
0.679687	-0.00608	0.625779	0.020046	0.0147
0.6875	-0.00458	0.612966	0.017574	0.013202
0.695312	-0.00303	0.599941	0.015143	0.011655
0.703125	-0.00154	0.586498	0.012756	0.01016
0.710937	-7.3E-05	0.572778	0.010427	0.008697
0.71875	0.001371	0.558694	0.008166	0.007253
0.726562	0.002783	0.544395	0.005985	0.005841
0.734375	0.004112	0.529923	0.003892	0.004512
0.742187	0.005391	0.515238	0.001894	0.003233
0.75	0.006618	0.500418	4.7E-15	0.002006
0.757812	0.007774	0.485488	-0.00178	0.00085

0.765625	0.008843	0.470481	-0.00346	-0.00022
0.773437	0.009843	0.455475	-0.00501	-0.00122
0.78125	0.010797	0.440392	-0.00644	-0.00217
0.789062	0.011646	0.425354	-0.00774	-0.00302
0.796875	0.01239	0.410505	-0.00893	-0.00377
0.804687	0.013082	0.395673	-0.00999	-0.00446
0.8125	0.013675	0.381122	-0.01093	-0.00505
0.820312	0.014174	0.366577	-0.01174	-0.00555
0.828125	0.014488	0.352392	-0.01245	-0.00586
0.835937	0.014841	0.338333	-0.01303	-0.00622
0.84375	0.015137	0.324608	-0.01351	-0.00651
0.851562	0.015374	0.311364	-0.0139	-0.00675
0.859375	0.015504	0.298402	-0.01418	-0.00688
0.867187	0.015509	0.285683	-0.01437	-0.00689
0.875	0.015425	0.273435	-0.01449	-0.0068
0.882812	0.015355	0.261573	-0.01452	-0.00673
0.890625	0.015178	0.2504	-0.0145	-0.00655
0.898437	0.014986	0.239834	-0.01443	-0.00636
0.90625	0.014855	0.229432	-0.01429	-0.00623
0.914062	0.014601	0.219422	-0.0141	-0.00598
0.921875	0.014307	0.210561	-0.01391	-0.00568
0.929687	0.014024	0.202007	-0.01368	-0.0054
0.9375	0.013533	0.193957	-0.01343	-0.00491
0.945312	0.013222	0.18698	-0.01319	-0.0046
0.953125	0.013002	0.180312	-0.01293	-0.00438
0.960937	0.012634	0.174038	-0.01265	-0.00401
0.96875	0.012287	0.169201	-0.01243	-0.00366
0.976562	0.012076	0.164406	-0.01218	-0.00345
0.984375	0.011529	0.160846	-0.01199	-0.0029
0.992187	0.0115	0.157441	-0.01178	-0.00288
1	0.011178	0.154819	-0.0116	-0.00255

Table 49 Lifting-Line Data Used to Create Figures 51 – 86

t/τ	C_x	C_y	C_P	C_T
0	0.00507	0.065276	-0.00489	0.003906
0.007813	0.005103	0.065753	-0.00492	0.003873
0.015625	0.0052	0.067184	-0.00501	0.003776
0.023438	0.005359	0.069564	-0.00516	0.003616
0.03125	0.00558	0.072888	-0.00536	0.003396
0.039063	0.005858	0.077148	-0.00561	0.003118

0.046875	0.006189	0.082335	-0.0059	0.002787
0.054688	0.006568	0.088434	-0.00624	0.002408
0.0625	0.00699	0.095432	-0.00661	0.001986
0.070313	0.007447	0.103312	-0.007	0.001529
0.078125	0.007933	0.112054	-0.0074	0.001042
0.085938	0.00844	0.121639	-0.00782	0.000535
0.09375	0.00896	0.132041	-0.00823	1.52E-05
0.101563	0.009485	0.143238	-0.00862	-0.00051
0.109375	0.010004	0.155201	-0.00899	-0.00103
0.117188	0.010509	0.167901	-0.00932	-0.00153
0.125	0.010991	0.181309	-0.00961	-0.00202
0.132813	0.01144	0.195392	-0.00983	-0.00246
0.140625	0.011848	0.210116	-0.00999	-0.00287
0.148438	0.012204	0.225445	-0.01006	-0.00323
0.15625	0.012501	0.241342	-0.01005	-0.00353
0.164063	0.01273	0.25777	-0.00993	-0.00375
0.171875	0.012882	0.274689	-0.0097	-0.00391
0.179688	0.012951	0.292057	-0.00936	-0.00398
0.1875	0.01293	0.309834	-0.00888	-0.00395
0.195313	0.012813	0.327975	-0.00828	-0.00384
0.203125	0.012594	0.346439	-0.00753	-0.00362
0.210938	0.012269	0.365179	-0.00665	-0.00329
0.21875	0.011836	0.384151	-0.00561	-0.00286
0.226563	0.01129	0.403309	-0.00443	-0.00231
0.234375	0.010632	0.422608	-0.0031	-0.00166
0.242188	0.00986	0.442	-0.00162	-0.00088
0.25	0.008976	0.461438	-2.1E-18	-1.2E-18
0.257813	0.00798	0.480877	0.001768	0.000996
0.265625	0.006876	0.500269	0.003674	0.0021
0.273438	0.005668	0.519568	0.005712	0.003308
0.28125	0.00436	0.538726	0.007874	0.004616
0.289063	0.002959	0.557698	0.010153	0.006017
0.296875	0.00147	0.576438	0.012537	0.007505
0.304688	-9.7E-05	0.594902	0.015016	0.009073
0.3125	-0.00173	0.613043	0.017577	0.01071
0.320313	-0.00343	0.63082	0.020207	0.012408
0.328125	-0.00518	0.648188	0.022893	0.014157
0.335938	-0.00697	0.665107	0.025618	0.015946
0.34375	-0.00879	0.681534	0.028368	0.017764
0.351563	-0.01062	0.697432	0.031127	0.019598
0.359375	-0.01246	0.712761	0.033877	0.021438

0.367188	-0.01429	0.727485	0.036603	0.023269
0.375	-0.0161	0.741568	0.039286	0.025081
0.382813	-0.01788	0.754975	0.041911	0.026859
0.390625	-0.01962	0.767676	0.04446	0.028593
0.398438	-0.02129	0.779639	0.046917	0.03027
0.40625	-0.0229	0.790835	0.049265	0.031877
0.414063	-0.02443	0.801238	0.051489	0.033403
0.421875	-0.02586	0.810822	0.053575	0.034837
0.429688	-0.02719	0.819565	0.055508	0.036169
0.4375	-0.02841	0.827445	0.057275	0.037389
0.445313	-0.02951	0.834443	0.058863	0.038487
0.453125	-0.03048	0.840542	0.060263	0.039456
0.460938	-0.03131	0.845728	0.061464	0.040289
0.46875	-0.032	0.849989	0.062459	0.040979
0.476563	-0.03255	0.853313	0.06324	0.041521
0.484375	-0.03294	0.855693	0.063801	0.041911
0.492188	-0.03317	0.857124	0.06414	0.042146
0.5	-0.03325	0.857601	0.064253	0.042225
0.507813	-0.03317	0.857124	0.06414	0.042146
0.515625	-0.03294	0.855693	0.063801	0.041911
0.523438	-0.03255	0.853313	0.06324	0.041521
0.53125	-0.032	0.849989	0.062459	0.040979
0.539063	-0.03131	0.845728	0.061464	0.040289
0.546875	-0.03048	0.840542	0.060263	0.039456
0.554688	-0.02951	0.834443	0.058863	0.038487
0.5625	-0.02841	0.827445	0.057275	0.037389
0.570313	-0.02719	0.819565	0.055508	0.036169
0.578125	-0.02586	0.810822	0.053575	0.034837
0.585938	-0.02443	0.801238	0.051489	0.033403
0.59375	-0.0229	0.790835	0.049265	0.031877
0.601563	-0.02129	0.779639	0.046917	0.03027
0.609375	-0.01962	0.767676	0.04446	0.028593
0.617188	-0.01788	0.754975	0.041911	0.026859
0.625	-0.0161	0.741568	0.039286	0.025081
0.632813	-0.01429	0.727485	0.036603	0.023269
0.640625	-0.01246	0.712761	0.033877	0.021438
0.648438	-0.01062	0.697432	0.031127	0.019598
0.65625	-0.00879	0.681534	0.028368	0.017764
0.664063	-0.00697	0.665107	0.025618	0.015946
0.671875	-0.00518	0.648188	0.022893	0.014157
0.679688	-0.00343	0.63082	0.020207	0.012408

0.6875	-0.00173	0.613043	0.017577	0.01071
0.695313	-9.7E-05	0.594902	0.015016	0.009073
0.703125	0.00147	0.576438	0.012537	0.007505
0.710938	0.002959	0.557698	0.010153	0.006017
0.71875	0.00436	0.538726	0.007874	0.004616
0.726563	0.005668	0.519568	0.005712	0.003308
0.734375	0.006876	0.500269	0.003674	0.0021
0.742188	0.00798	0.480877	0.001768	0.000996
0.75	0.008976	0.461438	6.35E-18	3.52E-18
0.757813	0.00986	0.442	-0.00162	-0.00088
0.765625	0.010632	0.422608	-0.0031	-0.00166
0.773438	0.01129	0.403309	-0.00443	-0.00231
0.78125	0.011836	0.384151	-0.00561	-0.00286
0.789063	0.012269	0.365179	-0.00665	-0.00329
0.796875	0.012594	0.346439	-0.00753	-0.00362
0.804688	0.012813	0.327975	-0.00828	-0.00384
0.8125	0.01293	0.309834	-0.00888	-0.00395
0.820313	0.012951	0.292057	-0.00936	-0.00398
0.828125	0.012882	0.274689	-0.0097	-0.00391
0.835938	0.01273	0.25777	-0.00993	-0.00375
0.84375	0.012501	0.241342	-0.01005	-0.00353
0.851563	0.012204	0.225445	-0.01006	-0.00323
0.859375	0.011848	0.210116	-0.00999	-0.00287
0.867188	0.01144	0.195392	-0.00983	-0.00246
0.875	0.010991	0.181309	-0.00961	-0.00202
0.882813	0.010509	0.167901	-0.00932	-0.00153
0.890625	0.010004	0.155201	-0.00899	-0.00103
0.898438	0.009485	0.143238	-0.00862	-0.00051
0.90625	0.00896	0.132041	-0.00823	1.52E-05
0.914063	0.00844	0.121639	-0.00782	0.000535
0.921875	0.007933	0.112054	-0.0074	0.001042
0.929688	0.007447	0.103312	-0.007	0.001529
0.9375	0.00699	0.095432	-0.00661	0.001986
0.945313	0.006568	0.088434	-0.00624	0.002408
0.953125	0.006189	0.082335	-0.0059	0.002787
0.960938	0.005858	0.077148	-0.00561	0.003118
0.96875	0.00558	0.072888	-0.00536	0.003396
0.976563	0.005359	0.069564	-0.00516	0.003616
0.984375	0.0052	0.067184	-0.00501	0.003776
0.992188	0.005103	0.065753	-0.00492	0.003873
1	0.00507	0.065276	-0.00489	0.003906

Table 50 CFD Data Used to Create Figures 87 – 90

t/τ	C_x	C_y	C_P	C_T
0.007812	0.012161	0.129973	-0.01216	-0.00354
0.015625	0.011906	0.128309	-0.01196	-0.00328
0.023437	0.011726	0.127472	-0.01181	-0.0031
0.03125	0.011681	0.127054	-0.01167	-0.00306
0.039062	0.011528	0.127801	-0.01161	-0.0029
0.046875	0.011529	0.128968	-0.01156	-0.00291
0.054687	0.011547	0.131273	-0.01158	-0.00292
0.0625	0.011614	0.134087	-0.0116	-0.00299
0.070312	0.0117	0.137887	-0.01167	-0.00308
0.078125	0.011843	0.142452	-0.01177	-0.00322
0.085937	0.012041	0.147618	-0.01186	-0.00342
0.09375	0.012249	0.153498	-0.01195	-0.00362
0.101562	0.012465	0.16028	-0.01206	-0.00384
0.109375	0.012699	0.167706	-0.01214	-0.00408
0.117187	0.012956	0.175819	-0.0122	-0.00433
0.125	0.013201	0.184537	-0.01222	-0.00458
0.132812	0.013423	0.193981	-0.0122	-0.0048
0.140625	0.013627	0.20408	-0.01212	-0.005
0.148437	0.013793	0.214751	-0.01198	-0.00517
0.15625	0.013977	0.226011	-0.01176	-0.00535
0.164062	0.01405	0.237808	-0.01145	-0.00543
0.171875	0.014118	0.250132	-0.01104	-0.00549
0.179687	0.014043	0.262943	-0.01053	-0.00542
0.1875	0.014015	0.276326	-0.0099	-0.00539
0.195312	0.013804	0.290058	-0.00915	-0.00518
0.203125	0.013592	0.304244	-0.00827	-0.00497
0.210937	0.0132	0.318812	-0.00725	-0.00458
0.21875	0.012729	0.333688	-0.0061	-0.00411
0.226562	0.0122	0.348851	-0.00479	-0.00358
0.234375	0.011565	0.364309	-0.00334	-0.00294
0.242187	0.010816	0.380033	-0.00175	-0.00219
0.25	0.009917	0.395893	-7.3E-16	-0.00129
0.257812	0.008921	0.41193	0.001893	-0.0003
0.265625	0.007809	0.428068	0.003929	0.000815
0.273437	0.006562	0.444316	0.006106	0.002062
0.28125	0.005245	0.460533	0.008414	0.003379
0.289062	0.003819	0.476805	0.01085	0.004805
0.296875	0.0023	0.493016	0.013403	0.006324
0.304687	0.000623	0.509173	0.016065	0.008001

0.3125	-0.00112	0.52524	0.018824	0.009746
0.320312	-0.00294	0.541039	0.021664	0.011564
0.328125	-0.00481	0.556784	0.02458	0.013434
0.335937	-0.00675	0.572158	0.027548	0.015371
0.34375	-0.00878	0.587346	0.03056	0.017407
0.351562	-0.01087	0.60227	0.0336	0.019492
0.359375	-0.01294	0.616805	0.036646	0.021563
0.367187	-0.01503	0.630969	0.039683	0.023658
0.375	-0.0172	0.644689	0.042693	0.025826
0.382812	-0.01926	0.658031	0.045662	0.027883
0.390625	-0.02141	0.670738	0.048557	0.030035
0.398437	-0.02347	0.683139	0.051387	0.032093
0.40625	-0.02549	0.694939	0.054114	0.034113
0.414062	-0.02748	0.706064	0.056717	0.0361
0.421875	-0.02938	0.716595	0.059186	0.038007
0.429687	-0.03106	0.726654	0.061519	0.039679
0.4375	-0.03291	0.735999	0.063681	0.041533
0.445312	-0.03449	0.744752	0.06567	0.043113
0.453125	-0.03596	0.752318	0.067422	0.044589
0.460937	-0.03733	0.759761	0.069021	0.045956
0.46875	-0.03857	0.766586	0.070413	0.047189
0.476562	-0.03953	0.77207	0.071523	0.048153
0.484375	-0.04047	0.777179	0.072434	0.049098
0.492187	-0.04125	0.780724	0.073028	0.049879
0.5	-0.0418	0.785186	0.073534	0.050423
0.507812	-0.04213	0.787807	0.073691	0.050752
0.515625	-0.04238	0.789284	0.073562	0.051007
0.523437	-0.04257	0.790582	0.073238	0.051197
0.53125	-0.04217	0.790888	0.072645	0.050798
0.539062	-0.0419	0.790049	0.071772	0.050524
0.546875	-0.04167	0.789391	0.070745	0.050295
0.554687	-0.04072	0.786962	0.069392	0.049343
0.5625	-0.03986	0.783423	0.067784	0.048489
0.570312	-0.03898	0.780737	0.066098	0.047607
0.578125	-0.03776	0.775374	0.064041	0.046385
0.585937	-0.03627	0.770542	0.061896	0.044894
0.59375	-0.03506	0.764388	0.059522	0.043684
0.601562	-0.03324	0.757795	0.057003	0.041861
0.609375	-0.0316	0.74987	0.054286	0.040221
0.617187	-0.02967	0.742039	0.051491	0.038291
0.625	-0.02784	0.733174	0.048552	0.036465

0.632812	-0.02574	0.723307	0.045491	0.034361
0.640625	-0.02354	0.71324	0.042375	0.032165
0.648437	-0.0215	0.702619	0.039198	0.030124
0.65625	-0.01925	0.690956	0.035951	0.027875
0.664062	-0.01697	0.679145	0.032699	0.025591
0.671875	-0.01467	0.666557	0.029427	0.023293
0.679687	-0.01244	0.653676	0.026174	0.021066
0.6875	-0.01013	0.640064	0.022939	0.018752
0.695312	-0.00792	0.626355	0.019762	0.016548
0.703125	-0.00567	0.611962	0.016637	0.014289
0.710937	-0.00349	0.597218	0.01359	0.012112
0.71875	-0.00144	0.582295	0.010639	0.01006
0.726562	0.00063	0.567051	0.007792	0.007994
0.734375	0.002621	0.55133	0.005061	0.006003
0.742187	0.004487	0.535608	0.002461	0.004137
0.75	0.006252	0.519678	4.37E-15	0.002372
0.757812	0.007931	0.503553	-0.00231	0.000693
0.765625	0.009477	0.487337	-0.00447	-0.00085
0.773437	0.010918	0.471047	-0.00647	-0.00229
0.78125	0.012241	0.454719	-0.00831	-0.00362
0.789062	0.013432	0.438436	-0.00998	-0.00481
0.796875	0.014516	0.422193	-0.01148	-0.00589
0.804687	0.015406	0.406005	-0.01281	-0.00678
0.8125	0.016212	0.389909	-0.01397	-0.00759
0.820312	0.016915	0.374078	-0.01498	-0.00829
0.828125	0.017483	0.358447	-0.01582	-0.00886
0.835937	0.017928	0.343019	-0.01652	-0.0093
0.84375	0.018318	0.327848	-0.01706	-0.00969
0.851562	0.018442	0.313098	-0.01747	-0.00982
0.859375	0.018576	0.298569	-0.01774	-0.00995
0.867187	0.018598	0.284533	-0.0179	-0.00997
0.875	0.018599	0.270861	-0.01794	-0.00997
0.882812	0.018326	0.257737	-0.01788	-0.0097
0.890625	0.018242	0.244916	-0.01773	-0.00962
0.898437	0.017849	0.232889	-0.01752	-0.00922
0.90625	0.01749	0.221122	-0.01722	-0.00887
0.914062	0.017191	0.210174	-0.01688	-0.00857
0.921875	0.016721	0.199646	-0.01649	-0.0081
0.929687	0.016246	0.189762	-0.01607	-0.00762
0.9375	0.015822	0.180653	-0.01563	-0.0072
0.945312	0.015355	0.172094	-0.01517	-0.00673

0.953125	0.014841	0.164217	-0.01472	-0.00622
0.960937	0.014413	0.157179	-0.01428	-0.00579
0.96875	0.0139	0.150771	-0.01385	-0.00528
0.976562	0.013535	0.145239	-0.01345	-0.00491
0.984375	0.013092	0.140034	-0.01305	-0.00447
0.992187	0.012789	0.136022	-0.01272	-0.00417
1	0.012479	0.133034	-0.01246	-0.00386

Table 51 CFD Data Used to Create Figures 91 – 94

t/τ	C_x	C_y	C_P	C_T
0.007812	0.015223	0.172001	-0.01609	-0.0066
0.015625	0.015047	0.170727	-0.01591	-0.00642
0.023437	0.014752	0.169665	-0.01572	-0.00613
0.03125	0.014525	0.169961	-0.01561	-0.0059
0.039062	0.01441	0.170193	-0.01546	-0.00579
0.046875	0.014288	0.171136	-0.01534	-0.00566
0.054687	0.014246	0.173124	-0.01527	-0.00562
0.0625	0.013953	0.175989	-0.01523	-0.00533
0.070312	0.014231	0.179104	-0.01516	-0.00561
0.078125	0.014018	0.182964	-0.01511	-0.00539
0.085937	0.014135	0.187534	-0.01506	-0.00551
0.09375	0.014133	0.192939	-0.01502	-0.00551
0.101562	0.014144	0.19866	-0.01494	-0.00552
0.109375	0.014316	0.205035	-0.01484	-0.00569
0.117187	0.014243	0.212218	-0.01473	-0.00562
0.125	0.01441	0.219835	-0.01456	-0.00579
0.132812	0.014388	0.228174	-0.01435	-0.00576
0.140625	0.01443	0.236948	-0.01408	-0.00581
0.148437	0.014473	0.246344	-0.01374	-0.00585
0.15625	0.014413	0.256125	-0.01333	-0.00579
0.164062	0.014362	0.266374	-0.01283	-0.00574
0.171875	0.014291	0.27716	-0.01224	-0.00567
0.179687	0.014095	0.288383	-0.01155	-0.00547
0.1875	0.013944	0.30001	-0.01075	-0.00532
0.195312	0.013611	0.312032	-0.00984	-0.00499
0.203125	0.013267	0.324354	-0.00882	-0.00464
0.210937	0.012856	0.337097	-0.00767	-0.00423
0.21875	0.012383	0.350093	-0.0064	-0.00376
0.226562	0.011769	0.363325	-0.00499	-0.00314
0.234375	0.011056	0.376822	-0.00346	-0.00243

0.242187	0.010342	0.390401	-0.00179	-0.00172
0.25	0.009482	0.404244	-3E-15	-0.00086
0.257812	0.008539	0.418187	0.001922	8.49E-05
0.265625	0.007507	0.432253	0.003968	0.001117
0.273437	0.006374	0.446358	0.006134	0.00225
0.28125	0.005161	0.460503	0.008414	0.003463
0.289062	0.00385	0.474699	0.010802	0.004774
0.296875	0.002511	0.488849	0.01329	0.006113
0.304687	0.000948	0.502866	0.015866	0.007676
0.3125	-0.00054	0.516754	0.01852	0.009168
0.320312	-0.00217	0.530495	0.021242	0.010792
0.328125	-0.00387	0.543991	0.024016	0.012497
0.335937	-0.00555	0.557617	0.026847	0.014174
0.34375	-0.00733	0.570966	0.029708	0.015953
0.351562	-0.0091	0.583658	0.032561	0.017727
0.359375	-0.01106	0.596165	0.035419	0.019682
0.367187	-0.0129	0.608691	0.038282	0.021523
0.375	-0.01461	0.620779	0.041109	0.02323
0.382812	-0.01645	0.632109	0.043863	0.025079
0.390625	-0.01867	0.643111	0.046557	0.027292
0.398437	-0.02	0.654202	0.04921	0.028627
0.40625	-0.02195	0.66402	0.051706	0.030573
0.414062	-0.02382	0.673684	0.054116	0.032443
0.421875	-0.02512	0.683216	0.056429	0.033746
0.429687	-0.02715	0.691452	0.058539	0.035771
0.4375	-0.02838	0.699989	0.060565	0.037005
0.445312	-0.02983	0.707555	0.06239	0.038453
0.453125	-0.03129	0.714045	0.063992	0.039914
0.460937	-0.03205	0.720841	0.065485	0.040672
0.46875	-0.03369	0.726019	0.066687	0.042311
0.476562	-0.03419	0.731348	0.067751	0.042817
0.484375	-0.03518	0.735154	0.068517	0.043802
0.492187	-0.03592	0.738684	0.069096	0.044546
0.5	-0.03623	0.742414	0.069529	0.044851
0.507812	-0.0368	0.74496	0.069683	0.045424
0.515625	-0.03681	0.746501	0.069575	0.045434
0.523437	-0.03701	0.746984	0.069199	0.045631
0.53125	-0.03682	0.747218	0.068634	0.04544
0.539062	-0.03659	0.746968	0.067859	0.045211
0.546875	-0.03639	0.745692	0.066828	0.045012
0.554687	-0.03555	0.743971	0.065601	0.044177

0.5625	-0.0348	0.741354	0.064144	0.043423
0.570312	-0.03398	0.737707	0.062455	0.0426
0.578125	-0.03288	0.734051	0.060628	0.041509
0.585937	-0.03174	0.729831	0.058626	0.040363
0.59375	-0.0309	0.724536	0.056419	0.039526
0.601562	-0.02904	0.718227	0.054026	0.037666
0.609375	-0.02756	0.712122	0.051553	0.036187
0.617187	-0.02586	0.704416	0.048881	0.034479
0.625	-0.02432	0.696592	0.04613	0.032942
0.632812	-0.0224	0.688833	0.043323	0.031019
0.640625	-0.02058	0.68014	0.040409	0.029209
0.648437	-0.01869	0.670346	0.037398	0.027313
0.65625	-0.01673	0.66038	0.03436	0.025356
0.664062	-0.01464	0.650284	0.031309	0.023268
0.671875	-0.01255	0.639175	0.028218	0.021172
0.679687	-0.01044	0.627881	0.025141	0.019068
0.6875	-0.00838	0.616312	0.022088	0.017009
0.695312	-0.00642	0.604326	0.019067	0.015043
0.703125	-0.00442	0.591553	0.016082	0.013047
0.710937	-0.00237	0.578918	0.013174	0.010991
0.71875	-0.00039	0.565981	0.010341	0.009013
0.726562	0.001503	0.552699	0.007595	0.007121
0.734375	0.003345	0.539214	0.00495	0.005279
0.742187	0.005159	0.525456	0.002415	0.003465
0.75	0.006819	0.511577	4.69E-15	0.001805
0.757812	0.008405	0.49761	-0.00229	0.000219
0.765625	0.009941	0.483449	-0.00444	-0.00132
0.773437	0.011343	0.469352	-0.00645	-0.00272
0.78125	0.01267	0.455117	-0.00832	-0.00405
0.789062	0.013867	0.440945	-0.01003	-0.00524
0.796875	0.014902	0.426882	-0.01161	-0.00628
0.804687	0.015964	0.412729	-0.01302	-0.00734
0.8125	0.016857	0.398671	-0.01429	-0.00823
0.820312	0.017636	0.384981	-0.01542	-0.00901
0.828125	0.018259	0.371333	-0.01639	-0.00964
0.835937	0.018843	0.357878	-0.01723	-0.01022
0.84375	0.019194	0.344929	-0.01795	-0.01057
0.851562	0.019535	0.331833	-0.01851	-0.01091
0.859375	0.019796	0.319208	-0.01896	-0.01117
0.867187	0.020082	0.306889	-0.0193	-0.01146
0.875	0.020191	0.294963	-0.01953	-0.01157

0.882812	0.020096	0.283847	-0.0197	-0.01147
0.890625	0.019983	0.272596	-0.01973	-0.01136
0.898437	0.019948	0.261704	-0.01969	-0.01132
0.90625	0.019588	0.251946	-0.01962	-0.01096
0.914062	0.019278	0.242167	-0.01945	-0.01065
0.921875	0.019293	0.232846	-0.01923	-0.01067
0.929687	0.018811	0.224613	-0.01902	-0.01019
0.9375	0.018474	0.21635	-0.01872	-0.00985
0.945312	0.018235	0.208751	-0.01841	-0.00961
0.953125	0.017647	0.202461	-0.01814	-0.00902
0.960937	0.017299	0.195747	-0.01778	-0.00867
0.96875	0.01697	0.190163	-0.01747	-0.00835
0.976562	0.016611	0.185728	-0.01721	-0.00799
0.984375	0.016262	0.180869	-0.01686	-0.00764
0.992187	0.015868	0.177884	-0.01664	-0.00724
1	0.015599	0.174732	-0.01636	-0.00697

Table 52 Lifting-Line Data Used to Create Figures 87 – 94

t/τ	C_x	C_y	C_P	C_T
0	0.006293	0.065276	-0.00611	0.002683
0.007813	0.006333	0.065753	-0.00615	0.002643
0.015625	0.006452	0.067184	-0.00626	0.002524
0.023438	0.006648	0.069564	-0.00644	0.002327
0.03125	0.006919	0.072888	-0.00669	0.002057
0.039063	0.007259	0.077148	-0.00701	0.001716
0.046875	0.007665	0.082335	-0.00738	0.001311
0.054688	0.008128	0.088434	-0.0078	0.000848
0.0625	0.008641	0.095432	-0.00826	0.000335
0.070313	0.009196	0.103312	-0.00875	-0.00022
0.078125	0.009784	0.112054	-0.00925	-0.00081
0.085938	0.010395	0.121639	-0.00977	-0.00142
0.09375	0.011017	0.132041	-0.01028	-0.00204
0.101563	0.01164	0.143238	-0.01077	-0.00266
0.109375	0.012251	0.155201	-0.01124	-0.00328
0.117188	0.012839	0.167901	-0.01165	-0.00386
0.125	0.013392	0.181309	-0.01201	-0.00442
0.132813	0.013898	0.195392	-0.01229	-0.00492
0.140625	0.014344	0.210116	-0.01248	-0.00537
0.148438	0.01472	0.225445	-0.01258	-0.00574
0.15625	0.015012	0.241342	-0.01256	-0.00604

0.164063	0.015212	0.25777	-0.01241	-0.00624
0.171875	0.015307	0.274689	-0.01213	-0.00633
0.179688	0.01529	0.292057	-0.01169	-0.00631
0.1875	0.015151	0.309834	-0.0111	-0.00618
0.195313	0.014882	0.327975	-0.01035	-0.00591
0.203125	0.014478	0.346439	-0.00942	-0.0055
0.210938	0.013931	0.365179	-0.00831	-0.00496
0.21875	0.013239	0.384151	-0.00702	-0.00426
0.226563	0.012399	0.403309	-0.00554	-0.00342
0.234375	0.011408	0.422608	-0.00388	-0.00243
0.242188	0.010267	0.442	-0.00203	-0.00129
0.25	0.008976	0.461438	-2.6E-18	-1.7E-18
0.257813	0.007538	0.480877	0.00221	0.001438
0.265625	0.005958	0.500269	0.004592	0.003018
0.273438	0.00424	0.519568	0.00714	0.004736
0.28125	0.002391	0.538726	0.009843	0.006584
0.289063	0.00042	0.557698	0.012691	0.008555
0.296875	-0.00166	0.576438	0.015671	0.01064
0.304688	-0.00385	0.594902	0.018769	0.012826
0.3125	-0.00613	0.613043	0.021971	0.015104
0.320313	-0.00848	0.63082	0.025259	0.01746
0.328125	-0.0109	0.648188	0.028616	0.01988
0.335938	-0.01338	0.665107	0.032023	0.022351
0.34375	-0.01588	0.681534	0.03546	0.024856
0.351563	-0.0184	0.697432	0.038909	0.02738
0.359375	-0.02093	0.712761	0.042347	0.029907
0.367188	-0.02344	0.727485	0.045754	0.03242
0.375	-0.02593	0.741568	0.049108	0.034902
0.382813	-0.02836	0.754975	0.052389	0.037337
0.390625	-0.03073	0.767676	0.055575	0.039708
0.398438	-0.03302	0.779639	0.058646	0.041999
0.40625	-0.03522	0.790835	0.061581	0.044193
0.414063	-0.0373	0.801238	0.064362	0.046275
0.421875	-0.03926	0.810822	0.066969	0.048231
0.429688	-0.04107	0.819565	0.069385	0.050046
0.4375	-0.04273	0.827445	0.071593	0.051707
0.445313	-0.04423	0.834443	0.073579	0.053203
0.453125	-0.04555	0.840542	0.075329	0.054522
0.460938	-0.04668	0.845728	0.07683	0.055655
0.46875	-0.04762	0.849989	0.078074	0.056594
0.476563	-0.04836	0.853313	0.079049	0.057331

0.484375	-0.04889	0.855693	0.079751	0.057861
0.492188	-0.04921	0.857124	0.080175	0.058181
0.5	-0.04931	0.857601	0.080316	0.058288
0.507813	-0.04921	0.857124	0.080175	0.058181
0.515625	-0.04889	0.855693	0.079751	0.057861
0.523438	-0.04836	0.853313	0.079049	0.057331
0.53125	-0.04762	0.849989	0.078074	0.056594
0.539063	-0.04668	0.845728	0.07683	0.055655
0.546875	-0.04555	0.840542	0.075329	0.054522
0.554688	-0.04423	0.834443	0.073579	0.053203
0.5625	-0.04273	0.827445	0.071593	0.051707
0.570313	-0.04107	0.819565	0.069385	0.050046
0.578125	-0.03926	0.810822	0.066969	0.048231
0.585938	-0.0373	0.801238	0.064362	0.046275
0.59375	-0.03522	0.790835	0.061581	0.044193
0.601563	-0.03302	0.779639	0.058646	0.041999
0.609375	-0.03073	0.767676	0.055575	0.039708
0.617188	-0.02836	0.754975	0.052389	0.037337
0.625	-0.02593	0.741568	0.049108	0.034902
0.632813	-0.02344	0.727485	0.045754	0.03242
0.640625	-0.02093	0.712761	0.042347	0.029907
0.648438	-0.0184	0.697432	0.038909	0.02738
0.65625	-0.01588	0.681534	0.03546	0.024856
0.664063	-0.01338	0.665107	0.032023	0.022351
0.671875	-0.0109	0.648188	0.028616	0.01988
0.679688	-0.00848	0.63082	0.025259	0.01746
0.6875	-0.00613	0.613043	0.021971	0.015104
0.695313	-0.00385	0.594902	0.018769	0.012826
0.703125	-0.00166	0.576438	0.015671	0.01064
0.710938	0.00042	0.557698	0.012691	0.008555
0.71875	0.002391	0.538726	0.009843	0.006584
0.726563	0.00424	0.519568	0.00714	0.004736
0.734375	0.005958	0.500269	0.004592	0.003018
0.742188	0.007538	0.480877	0.00221	0.001438
0.75	0.008976	0.461438	7.94E-18	5.11E-18
0.757813	0.010267	0.442	-0.00203	-0.00129
0.765625	0.011408	0.422608	-0.00388	-0.00243
0.773438	0.012399	0.403309	-0.00554	-0.00342
0.78125	0.013239	0.384151	-0.00702	-0.00426
0.789063	0.013931	0.365179	-0.00831	-0.00496
0.796875	0.014478	0.346439	-0.00942	-0.0055

0.804688	0.014882	0.327975	-0.01035	-0.00591
0.8125	0.015151	0.309834	-0.0111	-0.00618
0.820313	0.01529	0.292057	-0.01169	-0.00631
0.828125	0.015307	0.274689	-0.01213	-0.00633
0.835938	0.015212	0.25777	-0.01241	-0.00624
0.84375	0.015012	0.241342	-0.01256	-0.00604
0.851563	0.01472	0.225445	-0.01258	-0.00574
0.859375	0.014344	0.210116	-0.01248	-0.00537
0.867188	0.013898	0.195392	-0.01229	-0.00492
0.875	0.013392	0.181309	-0.01201	-0.00442
0.882813	0.012839	0.167901	-0.01165	-0.00386
0.890625	0.012251	0.155201	-0.01124	-0.00328
0.898438	0.01164	0.143238	-0.01077	-0.00266
0.90625	0.011017	0.132041	-0.01028	-0.00204
0.914063	0.010395	0.121639	-0.00977	-0.00142
0.921875	0.009784	0.112054	-0.00925	-0.00081
0.929688	0.009196	0.103312	-0.00875	-0.00022
0.9375	0.008641	0.095432	-0.00826	0.000335
0.945313	0.008128	0.088434	-0.0078	0.000848
0.953125	0.007665	0.082335	-0.00738	0.001311
0.960938	0.007259	0.077148	-0.00701	0.001716
0.96875	0.006919	0.072888	-0.00669	0.002057
0.976563	0.006648	0.069564	-0.00644	0.002327
0.984375	0.006452	0.067184	-0.00626	0.002524
0.992188	0.006333	0.065753	-0.00615	0.002643
1	0.006293	0.065276	-0.00611	0.002683

Table 53 CFD Data Used to Create Figures 95 – 98

t/τ	C_x	C_y	C_P	C_T
0.007812	0.006788	0.103687	-0.00647	0.001836
0.015625	0.006718	0.103215	-0.00641	0.001906
0.023437	0.006692	0.103477	-0.00639	0.001933
0.03125	0.00666	0.104586	-0.0064	0.001964
0.039062	0.00667	0.106453	-0.00645	0.001954
0.046875	0.006721	0.109368	-0.00653	0.001903
0.054688	0.006831	0.112967	-0.00664	0.001793
0.0625	0.007003	0.117476	-0.00678	0.001621
0.070313	0.0072	0.122677	-0.00692	0.001424
0.078125	0.0074	0.128785	-0.00709	0.001224
0.085938	0.007642	0.135618	-0.00726	0.000983

0.09375	0.007912	0.14324	-0.00744	0.000712
0.101563	0.008228	0.151603	-0.0076	0.000396
0.109375	0.008501	0.160711	-0.00776	0.000123
0.117188	0.00882	0.170585	-0.00789	-0.0002
0.125	0.009147	0.181073	-0.00799	-0.00052
0.132813	0.009482	0.1923	-0.00806	-0.00086
0.140625	0.009784	0.204069	-0.00808	-0.00116
0.148438	0.010087	0.216471	-0.00805	-0.00146
0.15625	0.010337	0.229488	-0.00796	-0.00171
0.164063	0.010618	0.242997	-0.0078	-0.00199
0.171875	0.010798	0.25711	-0.00757	-0.00217
0.179688	0.011005	0.271609	-0.00725	-0.00238
0.1875	0.011134	0.286652	-0.00685	-0.00251
0.195313	0.011218	0.30204	-0.00635	-0.00259
0.203125	0.011209	0.31786	-0.00576	-0.00259
0.210938	0.01119	0.334	-0.00507	-0.00257
0.21875	0.011106	0.350447	-0.00427	-0.00248
0.226563	0.010943	0.367156	-0.00336	-0.00232
0.234375	0.01071	0.384067	-0.00235	-0.00209
0.242188	0.010391	0.40117	-0.00123	-0.00177
0.25	0.01	0.4184	1.75E-15	-0.00138
0.257813	0.009519	0.435722	0.001335	-0.00089
0.265625	0.008993	0.453101	0.002773	-0.00037
0.273438	0.00838	0.470499	0.00431	0.000244
0.28125	0.007692	0.487856	0.005942	0.000932
0.289063	0.00692	0.505159	0.007663	0.001704
0.296875	0.00606	0.522333	0.009467	0.002564
0.304688	0.005167	0.539388	0.011345	0.003457
0.3125	0.004189	0.556212	0.013289	0.004435
0.320313	0.003158	0.572769	0.01529	0.005466
0.328125	0.002078	0.589188	0.017341	0.006546
0.335938	0.000918	0.605155	0.019424	0.007706
0.34375	-0.00022	0.620806	0.021534	0.008849
0.351563	-0.00145	0.63604	0.023656	0.010072
0.359375	-0.00271	0.650918	0.025782	0.011334
0.367188	-0.00394	0.665253	0.027893	0.012568
0.375	-0.00525	0.679181	0.029984	0.013871
0.382813	-0.00651	0.692519	0.032037	0.015137
0.390625	-0.00778	0.705292	0.034039	0.016405
0.398438	-0.00905	0.717418	0.035977	0.017672
0.40625	-0.01027	0.728876	0.037838	0.018899

0.414063	-0.01151	0.739932	0.039625	0.02013
0.421875	-0.01267	0.750081	0.041301	0.02129
0.429688	-0.01375	0.75945	0.042864	0.022372
0.4375	-0.01482	0.768224	0.044313	0.023444
0.445313	-0.0159	0.776603	0.045653	0.024526
0.453125	-0.01679	0.783613	0.046818	0.02541
0.460938	-0.01761	0.789862	0.047837	0.026234
0.46875	-0.01836	0.795819	0.048732	0.026987
0.476563	-0.01906	0.80064	0.049447	0.027682
0.484375	-0.01964	0.804612	0.049994	0.028267
0.492188	-0.02018	0.807937	0.050383	0.028804
0.5	-0.02057	0.810633	0.050612	0.029199
0.507813	-0.02079	0.811593	0.05061	0.029412
0.515625	-0.02098	0.812459	0.050481	0.029602
0.523438	-0.02101	0.812509	0.05018	0.029634
0.53125	-0.02108	0.811347	0.049683	0.029705
0.539063	-0.02082	0.809212	0.049009	0.029448
0.546875	-0.02051	0.806709	0.048198	0.029135
0.554688	-0.02031	0.803067	0.047208	0.028935
0.5625	-0.01967	0.798672	0.046069	0.028293
0.570313	-0.01918	0.793284	0.044773	0.027805
0.578125	-0.0185	0.787558	0.043365	0.027126
0.585938	-0.01772	0.780317	0.041788	0.026344
0.59375	-0.01686	0.772882	0.040122	0.025481
0.601563	-0.01594	0.764535	0.03834	0.02456
0.609375	-0.01498	0.755225	0.036449	0.0236
0.617188	-0.01386	0.745577	0.034491	0.022483
0.625	-0.01269	0.734809	0.03244	0.021316
0.632813	-0.0116	0.723693	0.030343	0.020225
0.640625	-0.01029	0.711773	0.028192	0.018914
0.648438	-0.00909	0.699359	0.026011	0.017711
0.65625	-0.00777	0.686161	0.023801	0.016399
0.664063	-0.0065	0.67262	0.02159	0.015124
0.671875	-0.00515	0.658451	0.019379	0.013772
0.679688	-0.00388	0.643808	0.017186	0.012501
0.6875	-0.00255	0.628694	0.015021	0.011175
0.695313	-0.00129	0.613221	0.012898	0.009915
0.703125	-3.7E-05	0.597365	0.010827	0.008661
0.710938	0.001188	0.581069	0.008815	0.007436
0.71875	0.002395	0.564593	0.006877	0.006229
0.726563	0.003529	0.547859	0.005019	0.005095

0.734375	0.004607	0.530849	0.003249	0.004017
0.742188	0.005633	0.513695	0.001574	0.002991
0.75	0.00659	0.496389	-4.8E-15	0.002034
0.757813	0.007475	0.478985	-0.00147	0.001149
0.765625	0.008291	0.461574	-0.00282	0.000333
0.773438	0.009028	0.444042	-0.00407	-0.0004
0.78125	0.009696	0.426621	-0.0052	-0.00107
0.789063	0.010261	0.409289	-0.00621	-0.00164
0.796875	0.010755	0.392057	-0.00711	-0.00213
0.804688	0.0112	0.374966	-0.00789	-0.00258
0.8125	0.011548	0.358138	-0.00856	-0.00292
0.820313	0.011845	0.341489	-0.00912	-0.00322
0.828125	0.012007	0.325138	-0.00957	-0.00338
0.835938	0.012139	0.309066	-0.00992	-0.00351
0.84375	0.012183	0.29345	-0.01018	-0.00356
0.851563	0.012191	0.278204	-0.01035	-0.00357
0.859375	0.012101	0.263313	-0.01043	-0.00348
0.867188	0.011939	0.249024	-0.01044	-0.00331
0.875	0.011868	0.23523	-0.01038	-0.00324
0.882813	0.011524	0.221813	-0.01026	-0.0029
0.890625	0.011289	0.209274	-0.0101	-0.00266
0.898438	0.011028	0.197034	-0.00988	-0.0024
0.90625	0.010683	0.185487	-0.00963	-0.00206
0.914063	0.010322	0.174732	-0.00936	-0.0017
0.921875	0.009979	0.164595	-0.00906	-0.00135
0.929688	0.009673	0.155014	-0.00875	-0.00105
0.9375	0.009228	0.146497	-0.00845	-0.0006
0.945313	0.008876	0.138501	-0.00814	-0.00025
0.953125	0.008585	0.131414	-0.00785	3.89E-05
0.960938	0.008193	0.124844	-0.00756	0.000431
0.96875	0.007928	0.119375	-0.00731	0.000696
0.976563	0.007644	0.114765	-0.00709	0.00098
0.984375	0.007356	0.110536	-0.00687	0.001268
0.992188	0.007184	0.107559	-0.00671	0.00144
1	0.006981	0.105313	-0.00658	0.001643

Table 54 CFD Data Used to Create Figures 99 – 102

t/τ	C_x	C_y	C_P	C_T
0.007812	0.008331	0.139806	-0.00872	0.000293
0.015625	0.008307	0.139194	-0.00865	0.000318

0.023437	0.008183	0.13926	-0.0086	0.000441
0.03125	0.007959	0.14046	-0.0086	0.000665
0.039062	0.008075	0.14194	-0.0086	0.000549
0.046875	0.007933	0.144202	-0.00862	0.000691
0.054687	0.00802	0.147691	-0.00868	0.000604
0.0625	0.008085	0.15121	-0.00872	0.000539
0.070312	0.008062	0.155908	-0.0088	0.000562
0.078125	0.008315	0.161455	-0.00889	0.000309
0.085937	0.008289	0.167261	-0.00896	0.000335
0.09375	0.008567	0.174301	-0.00905	5.71E-05
0.101562	0.008709	0.18162	-0.00911	-8.5E-05
0.109375	0.008822	0.189694	-0.00916	-0.0002
0.117187	0.009205	0.198493	-0.00918	-0.00058
0.125	0.009289	0.207811	-0.00917	-0.00067
0.132812	0.009483	0.217754	-0.00913	-0.00086
0.140625	0.009814	0.228245	-0.00904	-0.00119
0.148437	0.009985	0.239389	-0.0089	-0.00136
0.15625	0.010141	0.25095	-0.0087	-0.00152
0.164062	0.010333	0.263054	-0.00844	-0.00171
0.171875	0.010548	0.27561	-0.00811	-0.00192
0.179687	0.010652	0.288651	-0.00771	-0.00203
0.1875	0.010754	0.302098	-0.00722	-0.00213
0.195312	0.010827	0.315892	-0.00664	-0.0022
0.203125	0.010841	0.330064	-0.00598	-0.00222
0.210937	0.010802	0.344479	-0.00523	-0.00218
0.21875	0.010754	0.359169	-0.00437	-0.00213
0.226562	0.01063	0.374116	-0.00343	-0.00201
0.234375	0.010444	0.389243	-0.00238	-0.00182
0.242187	0.010213	0.404564	-0.00124	-0.00159
0.25	0.009904	0.419995	-2.5E-15	-0.00128
0.257812	0.009551	0.435538	0.001334	-0.00093
0.265625	0.009145	0.451154	0.002761	-0.00052
0.273437	0.008623	0.466719	0.004276	1.33E-06
0.28125	0.00806	0.482263	0.005874	0.000564
0.289062	0.007468	0.497752	0.007551	0.001156
0.296875	0.006794	0.513121	0.0093	0.00183
0.304687	0.006039	0.528422	0.011115	0.002586
0.3125	0.005298	0.543619	0.012989	0.003326
0.320312	0.004382	0.558431	0.014907	0.004242
0.328125	0.003534	0.573118	0.016868	0.00509
0.335937	0.002604	0.587653	0.018862	0.00602

0.34375	0.001558	0.601639	0.020869	0.007066
0.351562	0.000602	0.615247	0.022882	0.008022
0.359375	-0.0004	0.628748	0.024904	0.009028
0.367187	-0.00154	0.64157	0.0269	0.010161
0.375	-0.00261	0.653926	0.02887	0.011231
0.382812	-0.0036	0.666059	0.030813	0.012224
0.390625	-0.00483	0.677378	0.032692	0.013449
0.398437	-0.00591	0.688887	0.034546	0.014534
0.40625	-0.00695	0.699158	0.036295	0.015571
0.414062	-0.00805	0.708716	0.037953	0.016671
0.421875	-0.00891	0.718267	0.03955	0.017532
0.429687	-0.01005	0.726478	0.041003	0.018676
0.4375	-0.01095	0.734705	0.042379	0.019575
0.445312	-0.01184	0.741828	0.043608	0.020463
0.453125	-0.01299	0.748804	0.044738	0.021614
0.460937	-0.01332	0.754517	0.045696	0.021941
0.46875	-0.01426	0.759385	0.046501	0.022887
0.476562	-0.01487	0.764365	0.047206	0.023494
0.484375	-0.01551	0.768084	0.047724	0.024137
0.492187	-0.01602	0.77086	0.04807	0.02464
0.5	-0.01637	0.773911	0.048319	0.024999
0.507812	-0.01683	0.774416	0.048292	0.025459
0.515625	-0.01688	0.774875	0.048146	0.025505
0.523437	-0.01708	0.776124	0.047933	0.025709
0.53125	-0.01714	0.774273	0.047413	0.02576
0.539062	-0.01705	0.773126	0.046823	0.025677
0.546875	-0.0169	0.771011	0.046065	0.025524
0.554687	-0.01678	0.767356	0.045109	0.025402
0.5625	-0.01647	0.764032	0.044071	0.025089
0.570312	-0.01588	0.759295	0.042855	0.024505
0.578125	-0.01545	0.753806	0.041506	0.024071
0.585937	-0.01491	0.747792	0.040046	0.023531
0.59375	-0.01415	0.741246	0.03848	0.022773
0.601562	-0.01336	0.733694	0.036793	0.021988
0.609375	-0.01266	0.725801	0.035029	0.021281
0.617187	-0.01184	0.717009	0.03317	0.020462
0.625	-0.01076	0.707537	0.031236	0.019386
0.632812	-0.0098	0.69774	0.029255	0.018426
0.640625	-0.00877	0.687108	0.027215	0.017395
0.648437	-0.00769	0.676123	0.025147	0.016318
0.65625	-0.00657	0.664321	0.023043	0.015192

0.664062	-0.00546	0.652234	0.020935	0.014087
0.671875	-0.00431	0.639646	0.018826	0.012934
0.679687	-0.00317	0.626746	0.016731	0.01179
0.6875	-0.00201	0.613272	0.014653	0.01063
0.695312	-0.00084	0.599453	0.012609	0.009465
0.703125	0.000287	0.585322	0.010608	0.008337
0.710937	0.001425	0.570879	0.00866	0.0072
0.71875	0.002509	0.556108	0.006774	0.006115
0.726562	0.003553	0.54115	0.004958	0.005071
0.734375	0.004578	0.525955	0.003219	0.004046
0.742187	0.005543	0.510608	0.001564	0.003081
0.75	0.006472	0.495095	3.79E-15	0.002153
0.757812	0.007324	0.479512	-0.00147	0.0013
0.765625	0.008147	0.463863	-0.00284	0.000477
0.773437	0.008919	0.448128	-0.00411	-0.00029
0.78125	0.009588	0.432522	-0.00527	-0.00096
0.789062	0.010223	0.41688	-0.00632	-0.0016
0.796875	0.010784	0.40151	-0.00728	-0.00216
0.804687	0.011267	0.386092	-0.00812	-0.00264
0.8125	0.011643	0.370864	-0.00886	-0.00302
0.820312	0.011914	0.355954	-0.0095	-0.00329
0.828125	0.012243	0.341216	-0.01004	-0.00362
0.835937	0.012493	0.326875	-0.01049	-0.00387
0.84375	0.012665	0.312685	-0.01085	-0.00404
0.851562	0.012825	0.298969	-0.01112	-0.0042
0.859375	0.012721	0.28554	-0.01131	-0.0041
0.867187	0.01271	0.272394	-0.01142	-0.00409
0.875	0.012632	0.26	-0.01148	-0.00401
0.882812	0.012458	0.248298	-0.01149	-0.00383
0.890625	0.012341	0.236432	-0.01141	-0.00372
0.898437	0.012246	0.225308	-0.0113	-0.00362
0.90625	0.011925	0.215248	-0.01117	-0.0033
0.914062	0.011758	0.205103	-0.01098	-0.00313
0.921875	0.011296	0.195991	-0.01079	-0.00267
0.929687	0.011079	0.187284	-0.01057	-0.00246
0.9375	0.010821	0.179423	-0.01035	-0.0022
0.945312	0.010462	0.172141	-0.01012	-0.00184
0.953125	0.010209	0.165692	-0.0099	-0.00159
0.960937	0.009893	0.15976	-0.00968	-0.00127
0.96875	0.009561	0.154391	-0.00945	-0.00094
0.976562	0.00935	0.150111	-0.00927	-0.00073

0.984375	0.009048	0.146501	-0.0091	-0.00042
0.992187	0.008753	0.143487	-0.00895	-0.00013
1	0.008674	0.141532	-0.00884	-5E-05

Table 55 Lifting-Line Data Used to Create Figures 95 – 102

t/τ	C_x	C_y	C_P	C_T
0	0.004255	0.065276	-0.00408	0.004721
0.007813	0.004283	0.065753	-0.0041	0.004693
0.015625	0.004365	0.067184	-0.00417	0.004611
0.023438	0.0045	0.069564	-0.0043	0.004476
0.03125	0.004687	0.072888	-0.00446	0.004288
0.039063	0.004923	0.077148	-0.00467	0.004052
0.046875	0.005205	0.082335	-0.00492	0.003771
0.054688	0.005528	0.088434	-0.0052	0.003447
0.0625	0.005889	0.095432	-0.0055	0.003087
0.070313	0.006281	0.103312	-0.00583	0.002695
0.078125	0.006699	0.112054	-0.00617	0.002276
0.085938	0.007138	0.121639	-0.00651	0.001838
0.09375	0.00759	0.132041	-0.00685	0.001386
0.101563	0.008048	0.143238	-0.00718	0.000928
0.109375	0.008506	0.155201	-0.00749	0.00047
0.117188	0.008956	0.167901	-0.00777	2E-05
0.125	0.00939	0.181309	-0.008	-0.00041
0.132813	0.009802	0.195392	-0.00819	-0.00083
0.140625	0.010183	0.210116	-0.00832	-0.00121
0.148438	0.010527	0.225445	-0.00838	-0.00155
0.15625	0.010827	0.241342	-0.00837	-0.00185
0.164063	0.011075	0.25777	-0.00827	-0.0021
0.171875	0.011265	0.274689	-0.00808	-0.00229
0.179688	0.011392	0.292057	-0.0078	-0.00242
0.1875	0.011449	0.309834	-0.0074	-0.00247
0.195313	0.011433	0.327975	-0.0069	-0.00246
0.203125	0.011338	0.346439	-0.00628	-0.00236
0.210938	0.011161	0.365179	-0.00554	-0.00219
0.21875	0.0109	0.384151	-0.00468	-0.00192
0.226563	0.010551	0.403309	-0.00369	-0.00158
0.234375	0.010115	0.422608	-0.00259	-0.00114
0.242188	0.009589	0.442	-0.00135	-0.00061
0.25	0.008976	0.461438	-1.8E-18	-8.2E-19
0.257813	0.008275	0.480877	0.001473	0.000701

0.265625	0.007488	0.500269	0.003061	0.001487
0.273438	0.00662	0.519568	0.00476	0.002356
0.28125	0.005672	0.538726	0.006562	0.003303
0.289063	0.004651	0.557698	0.00846	0.004325
0.296875	0.00356	0.576438	0.010447	0.005416
0.304688	0.002406	0.594902	0.012513	0.00657
0.3125	0.001195	0.613043	0.014647	0.00778
0.320313	-6.5E-05	0.63082	0.016839	0.00904
0.328125	-0.00137	0.648188	0.019077	0.010342
0.335938	-0.0027	0.665107	0.021348	0.011677
0.34375	-0.00406	0.681534	0.02364	0.013036
0.351563	-0.00543	0.697432	0.025939	0.01441
0.359375	-0.00682	0.712761	0.028231	0.015791
0.367188	-0.00819	0.727485	0.030502	0.017169
0.375	-0.00956	0.741568	0.032739	0.018533
0.382813	-0.0109	0.754975	0.034926	0.019874
0.390625	-0.01221	0.767676	0.03705	0.021183
0.398438	-0.01347	0.779639	0.039097	0.02245
0.40625	-0.01469	0.790835	0.041054	0.023666
0.414063	-0.01585	0.801238	0.042908	0.024821
0.421875	-0.01693	0.810822	0.044646	0.025908
0.429688	-0.01794	0.819565	0.046256	0.026918
0.4375	-0.01887	0.827445	0.047729	0.027843
0.445313	-0.0197	0.834443	0.049053	0.028677
0.453125	-0.02044	0.840542	0.050219	0.029413
0.460938	-0.02107	0.845728	0.05122	0.030045
0.46875	-0.02159	0.849989	0.052049	0.030569
0.476563	-0.02201	0.853313	0.0527	0.030981
0.484375	-0.0223	0.855693	0.053168	0.031278
0.492188	-0.02248	0.857124	0.05345	0.031456
0.5	-0.02254	0.857601	0.053544	0.031516
0.507813	-0.02248	0.857124	0.05345	0.031456
0.515625	-0.0223	0.855693	0.053168	0.031278
0.523438	-0.02201	0.853313	0.0527	0.030981
0.53125	-0.02159	0.849989	0.052049	0.030569
0.539063	-0.02107	0.845728	0.05122	0.030045
0.546875	-0.02044	0.840542	0.050219	0.029413
0.554688	-0.0197	0.834443	0.049053	0.028677
0.5625	-0.01887	0.827445	0.047729	0.027843
0.570313	-0.01794	0.819565	0.046256	0.026918
0.578125	-0.01693	0.810822	0.044646	0.025908

0.585938	-0.01585	0.801238	0.042908	0.024821
0.59375	-0.01469	0.790835	0.041054	0.023666
0.601563	-0.01347	0.779639	0.039097	0.02245
0.609375	-0.01221	0.767676	0.03705	0.021183
0.617188	-0.0109	0.754975	0.034926	0.019874
0.625	-0.00956	0.741568	0.032739	0.018533
0.632813	-0.00819	0.727485	0.030502	0.017169
0.640625	-0.00682	0.712761	0.028231	0.015791
0.648438	-0.00543	0.697432	0.025939	0.01441
0.65625	-0.00406	0.681534	0.02364	0.013036
0.664063	-0.0027	0.665107	0.021348	0.011677
0.671875	-0.00137	0.648188	0.019077	0.010342
0.679688	-6.5E-05	0.63082	0.016839	0.00904
0.6875	0.001195	0.613043	0.014647	0.00778
0.695313	0.002406	0.594902	0.012513	0.00657
0.703125	0.00356	0.576438	0.010447	0.005416
0.710938	0.004651	0.557698	0.00846	0.004325
0.71875	0.005672	0.538726	0.006562	0.003303
0.726563	0.00662	0.519568	0.00476	0.002356
0.734375	0.007488	0.500269	0.003061	0.001487
0.742188	0.008275	0.480877	0.001473	0.000701
0.75	0.008976	0.461438	5.29E-18	2.46E-18
0.757813	0.009589	0.442	-0.00135	-0.00061
0.765625	0.010115	0.422608	-0.00259	-0.00114
0.773438	0.010551	0.403309	-0.00369	-0.00158
0.78125	0.0109	0.384151	-0.00468	-0.00192
0.789063	0.011161	0.365179	-0.00554	-0.00219
0.796875	0.011338	0.346439	-0.00628	-0.00236
0.804688	0.011433	0.327975	-0.0069	-0.00246
0.8125	0.011449	0.309834	-0.0074	-0.00247
0.820313	0.011392	0.292057	-0.0078	-0.00242
0.828125	0.011265	0.274689	-0.00808	-0.00229
0.835938	0.011075	0.25777	-0.00827	-0.0021
0.84375	0.010827	0.241342	-0.00837	-0.00185
0.851563	0.010527	0.225445	-0.00838	-0.00155
0.859375	0.010183	0.210116	-0.00832	-0.00121
0.867188	0.009802	0.195392	-0.00819	-0.00083
0.875	0.00939	0.181309	-0.008	-0.00041
0.882813	0.008956	0.167901	-0.00777	2E-05
0.890625	0.008506	0.155201	-0.00749	0.00047
0.898438	0.008048	0.143238	-0.00718	0.000928

0.90625	0.00759	0.132041	-0.00685	0.001386
0.914063	0.007138	0.121639	-0.00651	0.001838
0.921875	0.006699	0.112054	-0.00617	0.002276
0.929688	0.006281	0.103312	-0.00583	0.002695
0.9375	0.005889	0.095432	-0.0055	0.003087
0.945313	0.005528	0.088434	-0.0052	0.003447
0.953125	0.005205	0.082335	-0.00492	0.003771
0.960938	0.004923	0.077148	-0.00467	0.004052
0.96875	0.004687	0.072888	-0.00446	0.004288
0.976563	0.0045	0.069564	-0.0043	0.004476
0.984375	0.004365	0.067184	-0.00417	0.004611
0.992188	0.004283	0.065753	-0.0041	0.004693
1	0.004255	0.065276	-0.00408	0.004721

Table 56 CFD Data Used to Create Figures 103 – 107 $\hat{\alpha}_y = 0.0$

ω_x	Mean C_x	Mean C_y	Mean C_P	Mean C_T	Mean Efficiency
0.383276	0.000738	0.457668	0.011337	0.007886	0.695616
0.335366	0.000385	0.457688	0.011656	0.008239	0.706847
0.291623	-8.2E-08	0.45772	0.011993	0.008624	0.71908
0.24842	-0.00046	0.457766	0.012387	0.009088	0.73366
0.206379	-0.00098	0.457815	0.012819	0.009602	0.749024
0.191638	-0.00117	0.45783	0.012975	0.00979	0.754525
0.161622	-0.00154	0.457861	0.013294	0.010167	0.764774
0.149052	-0.00169	0.457859	0.01342	0.010317	0.768759
0.134147	-0.00186	0.457871	0.013564	0.010485	0.773005
0	-0.00271	0.456819	0.014269	0.011332	0.794133

Table 57 CFD Data Used to Create Figures 103 – 107 $\hat{\alpha}_y = 0.2$

ω_x	Mean C_x	Mean C_y	Mean C_P	Mean C_T	Mean Efficiency
0	-0.006267	0.458548	0.017940	0.014903	0.830743
0.479095	-0.001123	0.458149	0.013289	0.009747	0.733442
0.257974	-0.003302	0.458289	0.015269	0.011926	0.781036

Table 58 CFD Data Used to Create Figures 103 – 107 $\hat{\alpha}_y = -0.2$

ω_x	Mean C_x	Mean C_y	Mean C_P	Mean C_T	Mean Efficiency
0	-0.000334	0.457753	0.011928	0.008958	0.751055
0.319397	0.002145	0.457397	0.009864	0.006479	0.656826
0.171983	0.000749	0.457571	0.011009	0.007875	0.715345

Table 59 Lifting- Line Data Used to Create Figures 103 – 107 $\hat{\alpha}_y = 0.0$

ω_x	Mean C_x	Mean C_y	Mean C_P	Mean C_T	Mean Efficiency
0	-0.00256	0.461438	0.014841	0.011533	0.777101
0.5	-0.00256	0.461438	0.014841	0.011533	0.777101

Table 60 Lifting- Line Data Used to Create Figures 103 – 107 $\hat{\alpha}_y = 0.2$

ω_x	Mean C_x	Mean C_y	Mean C_P	Mean C_T	Mean Efficiency
0	-0.006267054	0.461438	0.018551	0.015243	0.821681
0.5	-0.006267054	0.461438	0.018551	0.015243	0.821681

Table 61 Lifting- Line Data Used to Create Figures 103 – 107 $\hat{\alpha}_y = -0.2$

ω_x	Mean C_x	Mean C_y	Mean C_P	Mean C_T	Mean Efficiency
0	-8.3488E-05	0.461438	0.012367	0.009059	0.732522
0.5	-8.3488E-05	0.461438	0.012367	0.009059	0.732522